

LEVEL

AGARD-CP-275

AGARD-CP-275

AGARD

ADVISORY GROUP FOR AEROSPACE RESEARCH & DEVELOPMENT

7 RUE AVOUELE 92285 NEUILLY SUR SEINE FRANCE

ADA 086707

AGARD CONFERENCE PROCEEDINGS No. 275

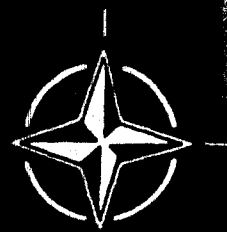
## Combustor Modelling

**DISTRIBUTION STATEMENT A**

Approved for public release;  
Distribution Unlimited

SEP 10 1980  
A

NORTH ATLANTIC TREATY ORGANIZATION



IDC FILE COPY

DISTRIBUTION AND AVAILABILITY  
ON BACK COVER

80 7 10 00 8

14 AGARD-CP-275

NORTH ATLANTIC TREATY ORGANIZATION  
ADVISORY GROUP FOR AEROSPACE RESEARCH AND DEVELOPMENT  
(ORGANISATION DU TRAITE DE L'ATLANTIQUE NORD)

11 Feb 80 12 382

9 AGARD Conference Proceedings No. 275  
6 COMBUSTOR MODELLING

SERIALIZED JUL 10 1980 A

Accession For	
NTIS G.W.&I	<input checked="checked" type="checkbox"/>
DDC TAB	<input type="checkbox"/>
Unannounced	<input type="checkbox"/>
Justification	
By	
Distribution/	
Availability Codes	
Dist	Avail and/or special
A	

Papers presented at the Propulsion and Energetics Panel 54th (B) Specialists' Meeting, held at DFVLR, Cologne, Germany, on 3-5 October 1979.

4000043 Ym

## THE MISSION OF AGARD

The mission of AGARD is to bring together the leading personalities of the NATO nations in the fields of science and technology relating to aerospace for the following purposes:

- Exchanging of scientific and technical information;
- Continuously stimulating advances in the aerospace sciences relevant to strengthening the common defence posture;
- Improving the co-operation among member nations in aerospace research and development;
- Providing scientific and technical advice and assistance to the North Atlantic Military Committee in the field of aerospace research and development;
- Rendering scientific and technical assistance, as requested, to other NATO bodies and to member nations in connection with research and development problems in the aerospace field;
- Providing assistance to member nations for the purpose of increasing their scientific and technical potential;
- Recommending effective ways for the member nations to use their research and development capabilities for the common benefit of the NATO community.

The highest authority within AGARD is the National Delegates Board consisting of officially appointed senior representatives from each member nation. The mission of AGARD is carried out through the Panels which are composed of experts appointed by the National Delegates, the Consultant and Exchange Programme and the Aerospace Applications Studies Programme. The results of AGARD work are reported to the member nations and the NATO Authorities through the AGARD series of publications of which this is one.

Participation in AGARD activities is by invitation only and is normally limited to citizens of the NATO nations.

The content of this publication has been reproduced  
directly from material supplied by AGARD or the authors.

Published February 1980

Copyright © AGARD 1980  
All Rights Reserved

ISBN 92-835-0260 4



*Printed by Technical Editing and Reproduction Ltd  
Harford House, 7-9 Charlotte St, London, W1P 1HD*

## PROPULSION AND ENERGETICS PANEL

**CHAIRMAN:** Dr J.Dunham  
National Gas Turbine Establishment  
Pyestock  
Farnborough  
Hants GU14 OLS, UK

**DEPUTY CHAIRMAN:** Professor E.E.Covert  
Department of Aeronautics and Astronautics  
Massachusetts Institute of Technology  
Cambridge, Mass 02139

## PROGRAM COMMITTEE

M.l'Ing. en Chef M.Pianko (Chairman)  
Coordinateur des Recherches en Turbo-  
Machines – ONERA  
29 Avenue de la Division Leclerc  
92320 Châtillon sous Bagneux, France

M. le Professeur Ch.Hirsch  
Vrije Universiteit Brussel  
Dept. de Mécanique des Fluides  
Pleinlaan 2  
1050 Bruxelles, Belgique

Professor F.J.Bayley  
Dean of the School of Engineering  
and Applied Sciences  
The University of Sussex  
Falmer, Brighton BN1 9QT, UK

Dr D.K.Hennecke  
Motoren und Turbinen Union GmbH  
Abt. EW  
Dachauerstrasse 665  
D-8000 München 50, Germany

Professor F.E.C.Culick  
Professor of Engineering and Applied  
Physics  
California Institute of Technology  
Pasadena, California 91125, US

Professor R.Monti  
Istituto di Aerodinamica  
Università degli Studi  
Piazzale Tecchio 80  
80125 Napoli, Italy

## HOST NATION COORDINATOR

Professor Dr Ing.G.Winterfeld  
DFVLR  
Institut für Antriebstechnik  
Postfach 90 60 58  
D-5000 Köln 90, Germany

## PANEL EXECUTIVE

Dr Ing.E.Riester

## ACKNOWLEDGEMENT

The Propulsion and Energetics Panel wishes to express its thanks to the German National Delegates to AGARD for the invitation to hold its 54th Meeting in Cologne, and for the personnel and facilities made available for this meeting.



# V CONTENTS

	Page
PROPULSION AND ENERGETICS PANEL	iii
	Reference
<u>SESSION I – SURVEY</u>	
MODELISATION DES FOYERS DE TURBOREACTEURS: POINT DE VUE D'UN MOTORISTE par Ph.Gastebois	1
FUNDAMENTAL MODELLING OF MIXING, EVAPORATION AND KINETICS IN GAS TURBINE COMBUSTORS by J.Swithenbank, A.Turan, P.G.Felton and D.B.Spalding	2
Paper 3 not presented	
<u>SESSION II – BASIC PHENOMENA (PART I)</u>	
MATHEMATICAL MODELLING OF GAS-TURBINE COMBUSTION CHAMBERS by W.P.Jones and J.J.McGuirk	4
A PREDICTION MODEL FOR TURBULENT DIFFUSION FLAMES INCLUDING NO-FORMATION by J.Janicka and W.Kollmann	5
TURBULENT REACTION AND TRANSPORT PHENOMENA IN JET FLAMES by H.Eickhoff, K.Grethe and F.Thiele	6
ON THE PREDICTION OF TEMPERATURE PROFILES AT THE EXIT OF ANNULAR COMBUSTORS by O.M.F.Elbahar and S.L.K.Wittig	7
Paper 8 not presented	
SECOND-ORDER CLOSURE MODELING OF TURBULENT MIXING AND REACTING FLOWS by A.K.Varma, G.Sandri and C.duP.Donaldson	9
COMBUSTOR MODELLING FOR SCRAMJET ENGINES by J.P.Drummond, R.C.Rogers and J.S.Evans	10
<u>SESSION II – BASIC PHENOMENA (PART II)</u>	
DEVELOPMENT AND VERIFICATION OF RADIATION MODELS by H.Bartelds	11
ASSESSMENT OF AN APPROACH TO THE CALCULATION OF THE FLOW PROPERTIES OF SPRAY-FLAMES by Y.El Bahawy and J.H.Whitelaw	12
FUNDAMENTAL CHARACTERIZATION OF ALTERNATIVE FUEL EFFECTS IN CONTINUOUS COMBUSTION SYSTEMS by R.B.Edelman, A.Turan, P.T.Harsha, E.Wong and W.S.Blazowski	13
CHEMICAL KINETIC MODELLING FOR COMBUSTION APPLICATION by F.L.Dryer and C.K.Westbrook	14
COALESCENCE/DISPERSION MODELLING OF GAS TURBINE COMBUSTORS by D.T.Pratt	15

## CONTENTS :

### PROPULSION AND ENERGETICS PANEL

Page

iii

Reference

#### SESSION I - SURVEY :

##### MODELISATION DES FOYERS DE TURBOREACTEURS: POINT DE VUE D'UN MOTORISTE

par Ph.Gastebois

1

##### FUNDAMENTAL MODELLING OF MIXING, EVAPORATION AND KINETICS IN GAS TURBINE COMBUSTORS

by J.Swithenbank, A.Turan, P.G.Felton and D.B.Spalding

2

Paper 3 not presented

#### SESSION II - BASIC PHENOMENA (PART I)

##### MATHEMATICAL MODELLING OF GAS-TURBINE COMBUSTION CHAMBERS

by W.P.Jones and J.J.McGuirk

4

##### A PREDICTION MODEL FOR TURBULENT DIFFUSION FLAMES INCLUDING NO-FORMATION

by J.Janicka and W.Kollmann

5

##### TURBULENT REACTION AND TRANSPORT PHENOMENA IN JET FLAMES

by H.Eickhoff, K.Grethe and F.Thiele

6

##### ON THE PREDICTION OF TEMPERATURE PROFILES AT THE EXIT OF ANNULAR COMBUSTORS

by O.M.F.Elbahar and S.L.K.Wittig

7

Paper 8 not presented

##### SECOND-ORDER CLOSURE MODELING OF TURBULENT MIXING AND REACTING FLOWS

by A.K.Varma, G.Sandri and C.duP.Donaldson

9

##### COMBUSTOR MODELLING FOR SCRAMJET ENGINES

by J.P.Drummond, R.C.Rogers and J.S.Evans

10

#### SESSION II - BASIC PHENOMENA (PART II)

##### DEVELOPMENT AND VERIFICATION OF RADIATION MODELS

by H.Bartelds

11

##### ASSESSMENT OF AN APPROACH TO THE CALCULATION OF THE FLOW PROPERTIES OF SPRAY-FLAMES

by Y.El Banhawy and J.H.Whitelaw

12

##### FUNDAMENTAL CHARACTERIZATION OF ALTERNATIVE FUEL EFFECTS IN CONTINUOUS COMBUSTION SYSTEMS

by R.B.Edelman, A.Turan, P.T.Harsha, E.Wong and W.S.Blazowski

13

##### CHEMICAL KINETIC MODELLING FOR COMBUSTION APPLICATION

by F.L.Dryer and C.K.Westbrook

14

##### COALESCENCE/DISPERSION MODELLING OF GAS TURBINE COMBUSTORS

by D.T.Pratt

15

→ SESSION III – TRANSIENT PHENOMENA AND INSTABILITIES

**MODELISATION DE ZONES DE COMBUSTION EN REGIME INSTATIONNAIRE**

par F.Hirsinger et H.Tichtinsky

16

**ANALYSIS OF LOW-FREQUENCY DISTURBANCES IN AFTERBURNERS**

by F.E.Marble, M.V.Subbaiah and S.M.Candel

17

↓  
SESSION IV – FURNACES AND BOILERS

**SURVEY ON PREDICTION PROCEDURES FOR THE CALCULATION OF FURNACE PERFORMANCE**

by J.B.Michel, S.Michelfelder and R.Payne

18

**NUMERICAL ANALYSIS AND EXPERIMENTAL DATA IN A CONTINUOUS FLOW COMBUSTION CHAMBER: A COMPARISON**

by F.Gamma, C.Casci, A.Coghe and U.Ghezzi

19

**MODELISATION DES FOURS ALIMENTES A L'AIR ENRICHI EN OXYGENE**

par R.Guenot, A.Ivernel, F.C.Lockwood et A.P.Salooja

20

**AN EFFECTIVE PROBABILISTIC SIMULATION OF THE TURBULENT FLOW AND COMBUSTION IN AXISYMMETRIC FURNACES**

by Th.T.A.Paauw, A.J.Stroo and C.W.J.Van Koppen

21

**MODELISATION MATHEMATIQUE DU FONCTIONNEMENT DES CHAUDIERES DE CHAUFFAGE**

par E.Perthuis

22

↓  
SESSION V – GAS TURBINE COMBUSTORS AND R/H SYSTEMS ←

**A CHEMICAL REACTOR MODEL AND ITS APPLICATION TO A PRACTICAL COMBUSTOR**

by W.Krockow, B.Simon and E.C.Parnell

23

**SEMI-EMPIRICAL CORRELATIONS FOR GAS TURBINE EMISSIONS, IGNITION, AND FLAME STABILIZATION**

by A.M.Mellor

24

**COMBUSTION MODELLING WITHIN GAS TURBINE ENGINES, SOME APPLICATIONS AND LIMITATIONS**

by J.Odgers

25

**ETUDE DE L'AERODYNAMIQUE D'UNE CHAMBRE DE COMBUSTION EN VUE D'UNE MODELISATION SEMI-EMPIRIQUE**

par P.Hebrard et P.Magre

26

## MODELISATION DES FOYERS DE TURBOREACTEURS : POINT DE VUE D'UN MOTORISTE

Ph. GASTEBOIS  
Chef du Département "COMBUSTION"

S.N.E.C.M.A  
Centre de Villaroche  
77550 MOISSY CRAMAYEL - FRANCE

0 - RESUME

La modélisation des foyers de turboréacteurs doit répondre à deux objectifs :

- d'une part l'optimisation des foyers orientée à l'heure actuelle vers la réduction des émissions polluantes mais qui peut s'orienter vers l'optimisation des performances de stabilité ou de réallumage, et qui doit considérer les caractéristiques du système d'injection, de la zone primaire et de la dilution.
- d'autre part la prévision des performances des foyers en projet qui doit permettre de prévoir les caractéristiques des températures de sortie, des températures de paroi et des émissions polluantes.

Pour répondre à ces deux objectifs, le motoriste souhaite deux types de modélisation, l'une simplifiée pour estimer les performances, l'autre plus approfondie pour optimiser l'architecture des foyers.

Dans les deux cas une meilleure connaissance des phénomènes physiques (rayonnement, transferts, cinétique chimique), grâce à des mesures perfectionnées est indispensable.

1 - INTRODUCTION

La conception des foyers de turboréacteurs est restée pendant de nombreuses années un "art" pour lequel l'ingénieur mettait à profit l'expérience acquise et la réflexion fondée sur des idées simples pour approcher les résultats recherchés par étapes et modifications successives.

Néanmoins, il est apparu assez rapidement la nécessité de prévoir les performances des chambres de combustion en projet. Des études nombreuses ont été entreprises pour tenter par exemple de prévoir le profil radial des températures de sortie, le rendement de combustion ou les températures de paroi du foyer en utilisant des modèles aérodynamiques et thermiques simples.

Cette tendance s'est accrue d'autant plus que le coût des essais partiels s'est élevé avec l'augmentation des niveaux de pression et de température à l'entrée des foyers.

La recherche du compromis nécessaire pour tenir compte simultanément des contraintes de performances classiques et des contraintes de pollution a conduit en outre à rechercher à priori une optimisation de l'architecture des foyers grâce à une modélisation de l'ensemble du tube à flamme faisant intervenir des modèles plus perfectionnés intégrant les phénomènes de cinétique chimique et de turbulence.

2 - OPTIMISATION DES FOYERS GRACE A LA MODELISATION

Les contraintes de réduction des émissions d'espèces polluantes par les chambres de combustion principales des turboréacteurs ont conduit, soit à reconsidérer l'architecture des foyers classiques en vue d'optimiser la répartition de l'air entre les différentes zones du foyer et d'utiliser au mieux le volume disponible, soit à concevoir des foyers à injection étagée ou à géométrie variable pour lesquels il importe de connaître la meilleure répartition de l'air et du carburant - Fig. 1.

La modélisation des foyers s'est révélée être l'instrument indispensable à une telle optimisation.

Les difficultés rencontrées pour modéliser les foyers de turboréacteurs proviennent de la nécessité de tenir compte simultanément des phénomènes de mélange turbulent et des évolutions chimiques.

De plus, il faut en outre pour s'approcher des foyers réels décrire la répartition spatiale et l'évaporation du combustible.

Une première étape, simple et néanmoins déjà très utile pour le motoriste, consiste à supposer que les temps de mélange et de vaporisation sont négligeables par rapport au temps chimique. Le foyer peut alors être modélisé par un assemblage de foyers homogènes (Ref. 1, 2). On pourra concevoir par exemple d'une part une modélisation de la zone primaire permettant de connaître l'évolution des indices d'émission à la sortie de la zone primaire en fonction des paramètres aérothermodynamiques et de la richesse de fonctionnement et d'autre part une modélisation de la zone de dilution qui joue un rôle essentiel dans le processus de combustion même dans les conditions du régime ralenti ou se forme la majeure partie du monoxyde de carbone et des hydrocarbures imbrûlés.

La zone primaire est modélisée par un assemblage de foyers homogènes en introduisant une recirculation de gaz brûlés dans au moins un des foyers homogènes (PSR) encore appelés, foyers parfaitement mélangés.

Toutefois pour mieux approcher les performances du foyer, il est souhaitable d'inclure un "réacteur piston" (PFR) pour modéliser l'évolution des gaz recirculants.

La zone de dilution est représentée par un réacteur piston qui peut, d'ailleurs également être simulé par une suite de réacteurs homogènes de faible volume unitaire - Fig. 2 et 3.

S'il est vrai que l'amélioration de la qualité de la pulvérisation par adoption d'injecteurs aérodynamiques a permis de se rapprocher sensiblement du cas où les temps de mélange et de vaporisation sont faibles, les phénomènes de mélange ne peuvent être complètement négligés et nous pensons que la notion de foyers "bien mélangés" (W.S.R) dans lesquels le carburant et l'air sont mélangés rapidement mais pas instantanément constitue une étape susceptible d'apporter des améliorations notables (Ref. 3, 4, 5).

L'un des avantages de ces modèles, hormis une certaine simplicité est que l'ingénieur peut à partir de considérations physiques simples, d'estimations ou de mesures du temps de séjour dans le foyer, déterminer les volumes de chacun des foyers homogènes entrant dans le modèle ; il contrôle donc relativement bien l'exactitude des hypothèses d'entrée dans le modèle.

Dans le but d'optimiser l'architecture des foyers, l'introduction des paramètres relatifs à l'injection et notamment ceux relatifs à la répartition du carburant dans la zone primaire n'est sans doute pas fondamentale dans une première étape. Néanmoins, si l'on veut par exemple s'intéresser aux hydrocarbures imbrûlés ou à la formation des fumées, il faudra, nous semble-t-il tenir compte effectivement de ces paramètres et modéliser alors de façon détaillée les processus de mélange, d'évaporation du combustible ainsi que les premières étapes de décomposition et de combustion du carburant.

La schématisation par foyers homogènes "parfaitement mélangés" ou même "bien mélangés" sera alors insuffisante et une modélisation tridimensionnelle plus complète sera alors nécessaire. Le degré de complexité auquel on est alors conduit rend ces méthodes, à notre avis, d'un emploi systématique difficile dans l'industrie.

L'optimisation des foyers de rechauffe qui constitue également un objectif essentiel pour le motoriste est accessible par une modélisation appropriée de la zone de recirculation créée par l'accroche-flamme, et de la propagation du front de flamme turbulent se développant en aval de l'accroche-flamme - Voir Fig. 4.

Cette modélisation doit permettre d'optimiser le nombre d'accroche-flammes afin d'obtenir le rendement de rechauffe demandé avec une longueur de canal minimale tout en satisfaisant aux critères de stabilité et de perte de charge.

Là encore, deux stades de complexité peuvent être considérés, d'une part un modèle de combustion où l'on fait l'hypothèse que l'air et le carburant sont prémélangés en amont des accroche-flammes, d'autre part un modèle plus sophistiqué où l'on prend en compte les phénomènes de mélange et d'évaporation du combustible.

Les méthodes de calculs complètes couplant les modèles aérodynamiques turbulents aux modèles de cinétique chimiques sont sans doute les seules dans ce cas susceptibles de permettre cette optimisation.

### 3 - MODELISATION DES FOYERS EN PROJET

L'architecture générale du foyer étant définie, soit à partir de l'expérience antérieure, soit à partir de l'optimisation par le calcul, il reste au motoriste à préciser le dimensionnement du foyer et à calculer grâce à des modèles appropriés les performances du foyer, telles que :

- répartition de l'air dans les différentes zones,
- pertes de charge,
- températures de paroi dans divers cas de fonctionnement,
- performances de stabilité,
- répartition des températures de sortie,
- estimation des performances de pollution.

Pour chacun de ces modèles, le motoriste est confronté à deux problèmes ; d'une part il doit choisir le niveau de complexité auquel il va s'arrêter pour rendre compte avec un degré de confiance satisfaisant des performances du foyer ; d'autre part, il doit dans tout modèle rentrer un certain nombre de données initiales ou de coefficients empiriques qu'il est parfois difficile de connaître a priori.

Pour exemple, dans le calcul de la répartition des débits d'air dans le tube à flamme, outre la géométrie du tube à flamme et des orifices on pourra ou non tenir compte des profils de vitesse et de pression à la sortie du diffuseur, on pourra calculer ou non l'écoulement autour de la tête de chambre pour introduire les profils de pression et de vitesse entre tube à flamme et carters, etc. mais il faudra dans tous les cas entrer les coefficients de débit des orifices et parfois les profils initiaux s'ils sont pris en compte.

Ce programme pourra être couplé avec un modèle de combustion plus ou moins simplifié afin de calculer la répartition des débits d'air en combustion.

L'expérience acquise nous a montré que des variations géométriques de détail pouvaient avoir des conséquences importantes sur telle ou telle performance et ceci nous incite à penser que, même des modèles très sophistiqués auront beaucoup de peine à permettre des prévisions quantitatives très précises.

C'est donc, même au niveau du développement du foyer, principalement pour prévoir l'effet d'une variation de tel ou tel paramètre, le résultat de telle ou telle modification, ou rechercher quelle modification permettrait d'atteindre tel objectif, que le constructeur utilisera la modélisation des foyers.

Citons par exemple l'importance relative des échanges par rayonnement et convection dans l'équilibre thermique des parois du foyer, la modification du profil radial d'un foyer par modification des perçages de dilution etc.

Une méthode séduisante permettant d'aboutir au degré de complexité minimal, consiste à partir d'une modélisation très sophistiquée, prenant en compte dans la mesure du possible, tous les phénomènes aérothermochimiques, puis à rechercher quelles simplifications peuvent être réalisées sans remettre en cause le résultat final.

Cette technique est employée dans la modélisation des phénomènes de cinétique chimique pour lesquels l'ingénieur peut reconnaître sans difficultés les réactions très rapides des réactions lentes et établir des modèles "à équilibre partiel" ou "à état quasi stationnaire".

Son emploi sera certainement utile dans les modèles aérothermodynamiques tridimensionnels pour lesquels les temps de calculs sont très longs et peu compatibles avec une utilisation fréquente comme peut en avoir besoin le constructeur.

La connaissance des valeurs initiales des variables d'entrée dans les problèmes de combustion turbulente d'un mélange air-carburant liquide reste un des problèmes importants ; en effet, plus la modélisation des phénomènes de mélange turbulent est poussée plus l'accès aux paramètres d'entrée est difficile. Ceci est d'autant plus vrai que l'on s'éloigne des montages expérimentaux de recherche pour s'intéresser aux foyers réels des turbomachines.

Un effort particulier doit donc être porté sur les techniques de mesure, d'une part pour acquérir expérimentalement les données de base nécessaires au calcul mais aussi d'autre part pour n'introduire dans les modèles que des paramètres auxquels on sait avoir accès ou dont l'ordre de grandeur est suffisamment bien connu.

Le motoriste est évidemment très méfiant devant des modèles très élaborés pour lesquels certaines "variables" sont choisies en fonction de chaque cas d'application pour que le calcul recoupe l'expérience sans que les lois ou les règles définissant ces variables soient bien connues.

#### 4 - ETAT ACTUEL A LA SNECMA

Nous ne décrirons pas ici le contenu des modélisations utilisées à la SNECMA mais tenterons plutôt de décrire le processus de conception et de mise au point des foyers pour mettre en évidence les réussites et les lacunes des modèles proposés ainsi que l'énorme travail qui reste à faire.

Connaissant les conditions de fonctionnement et les performances du foyer recherchées, le motoriste va, à partir d'un certain nombre de critères déduits soit de l'expérience antérieure soit des résultats des études d'optimisation dont nous avons parlé, se fixer une répartition des débits d'air dans la zone primaire, la zone de dilution, les films de refroidissement, le système d'injection ...

Un modèle de calcul aérothermodynamique, avec un schéma de combustion simplifié va permettre de calculer les perçages du tube à flamme pour obtenir les caractéristiques recherchées.

Un programme de calcul inverse, permettant à partir de données géométriques du tube à flamme de calculer la répartition des débits d'air dans chacune des zones du foyer ainsi que sa perte de charge sert de base aux modifications éventuelles sur celui-ci.

Des modèles de calcul de "performances" peuvent être alors utilisés. Ceux que nous présentons sont soit opérationnels, soit en cours de mise au point, soit objet de recherches en vue de leur élaboration.

Un modèle de calcul des températures de paroi des foyers refroidis par convection, film-cooling ou multiperforation permet de prévoir les températures de paroi en fonction des diverses conditions de fonctionnement et de s'assurer de la tenue thermique et de la durée de vie du tube à flamme. Toute recherche aboutissant à une meilleure connaissance des caractéristiques de rayonnement des flammes ainsi que la description des phénomènes d'interaction couche-limite-jets transversaux permettra de perfectionner ce type de modélisation.

Un modèle de calcul de la répartition des températures de sortie du foyer est particulièrement utile au motoriste puisqu'il lui permet d'adapter la répartition des perçages de dilution du tube à flamme afin d'obtenir le profil radial nécessaire à la tenue thermique de la turbine. Les études portant sur le mélange des jets turbulents et sur les méthodes de calcul tridimensionnelles permettront d'affiner les modèles existants.

Enfin, essentiellement dans le domaine des moteurs civils, la prévision des niveaux de pollution peut être effectuée grâce à un modèle de calcul faisant appel soit à l'assemblage de foyers homogènes, soit à une modélisation globale tridimensionnelle. Dans ce domaine les recherches fondamentales concernant la formation des polluants (CO, HC, NOx, fumées) sont indispensables concurremment avec le développement des techniques de calcul, afin d'une part de mieux décrire les étapes de combustion du produit complexe qu'est le kérosène, d'autre part de mieux connaître les constantes de vitesse de réaction dans une large gamme de température.

Nous pensons qu'une modélisation basée sur l'assemblage de foyers homogènes (PSR) ou bien mélangés (WSR), constitue une base de départ intéressante puisqu'elle permet d'envisager des assemblages dont la complexité ira croissant au fur-et-à-mesure que le besoin s'en fera sentir et que la connaissance de l'aérodynamique du foyer et de la répartition du carburant dans le foyer s'amélioreront.

## CONCLUSION

La modélisation des foyers est un outil très utile au motoriste pour la mise au point des foyers, d'autant plus que le coût des essais partiels s'accroît avec l'élévation du taux de compression des moteurs. L'intérêt porté aux problèmes de pollution a accru le besoin en modèles comportant aussi bien une modélisation des phénomènes aérodynamiques et thermiques qu'une modélisation des évolutions chimiques.

Le constructeur souhaite disposer de deux types de modèles :

- d'une part une modélisation globale du foyer permettant d'optimiser les répartitions d'air et de carburant entre les différentes zones du foyer, pour utiliser le volume minimal tout en assurant un niveau de performances satisfaisant. Ces modèles tout en restant assez simples pour être utilisables industriellement devront à l'avenir tenir compte de manière plus approfondie des paramètres liés à l'injection.
- d'autre part des modèles permettant à partir de l'optimisation précédente de définir les données géométriques du foyer et d'en estimer avec une bonne précision les principales performances. Dans ce but des modèles élémentaires spécifiques et simplifiés se révèlent très utiles pour le motoriste au cours du développement du foyer.

Cependant dans les deux cas la prévision ou l'optimisation des niveaux de pollution amènent à envisager des modèles dont le degré de sophistication ira croissant en même temps que la modélisation détaillée des processus aérothermochimiques progressera.

En tous cas le motoriste insiste sur la nécessité de connaître a priori ou par l'expérience antérieure tous les paramètres d'entrée figurant dans ces modèles. Il nous paraît donc indispensable que les moyens de diagnostic et de mesures progressent en parallèle avec les moyens de calcul.

## REFERENCES

- 1 - BORGHI R.  
Etude théorique de l'optimisation de la combustion dans les foyers de turbomachines  
Acta Astronautica Vol 1 - 1974 - pp 667-685
- 2 - HAMMOND D.C Inr et MELLOR A.n  
Analytical calculations for the performance and pollutant emissions of gas turbine combustors  
AIAA Paper 71-711
- 3 - OSGERBY I.T  
Literature review of turbine combustor modeling and emissions  
AIAA journal Vol 12 N° 6 Juin 1974
- 4 - BEER J.M - LEE K.B  
The effect of residence time distribution on the performance and efficiency of combustor  
10th International Symposium on Combustion 1965 - pp 1187-1262
- 5 - SWITENBANK, J, POLL, I., VINCENT, M.W. et WRIGHT, D.D  
Combustor Design Fundamentals - 14th Symposium (International) on Combustion 1972 - p 627

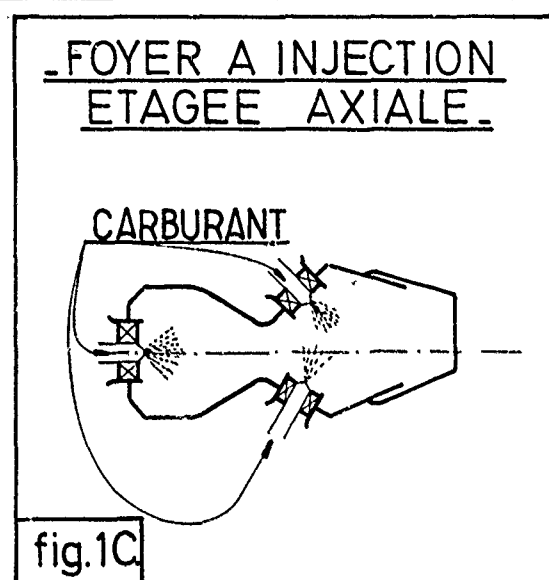
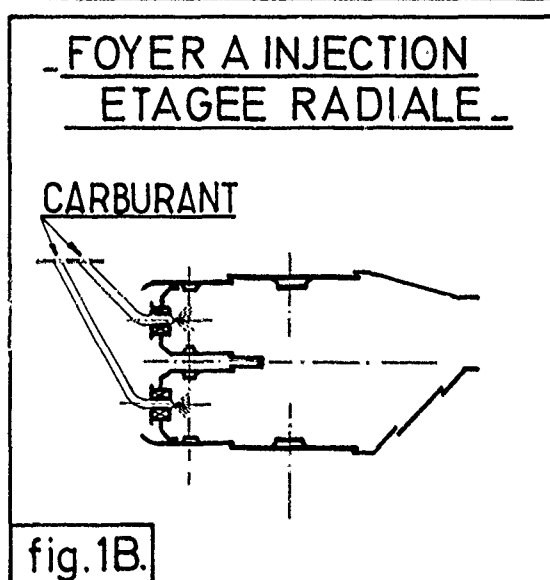
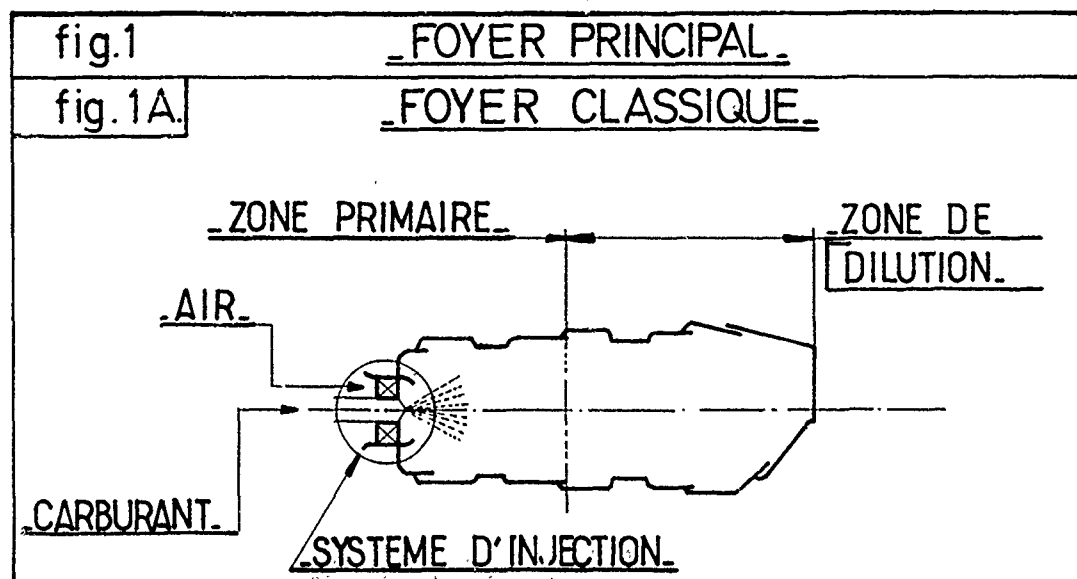
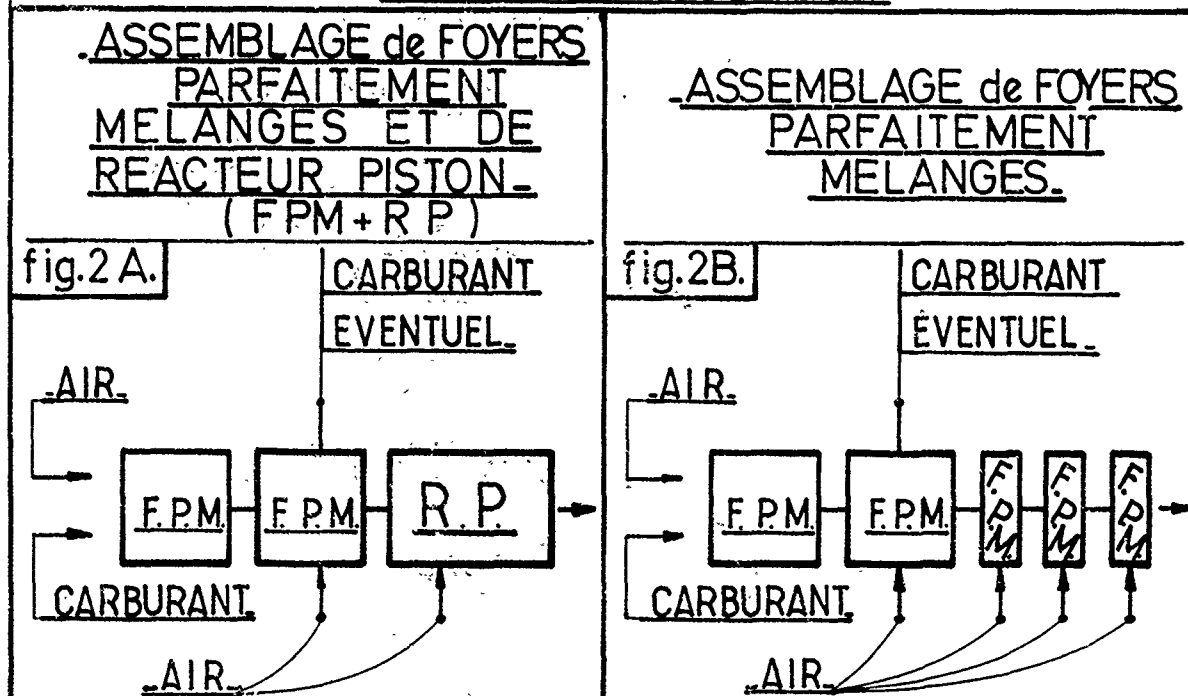
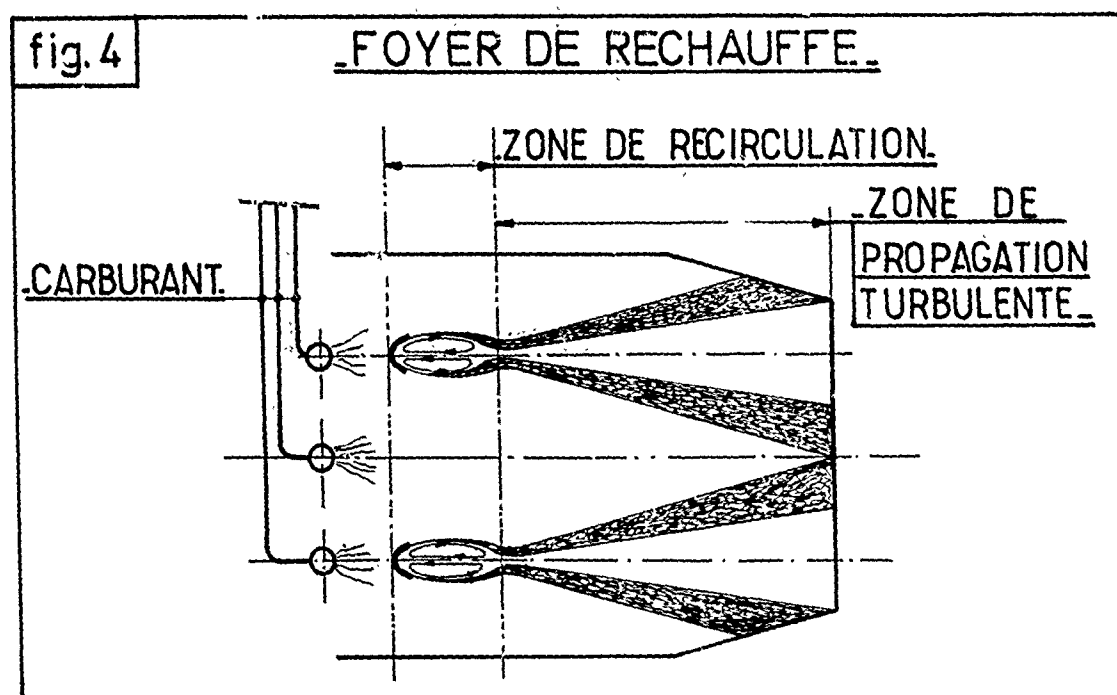
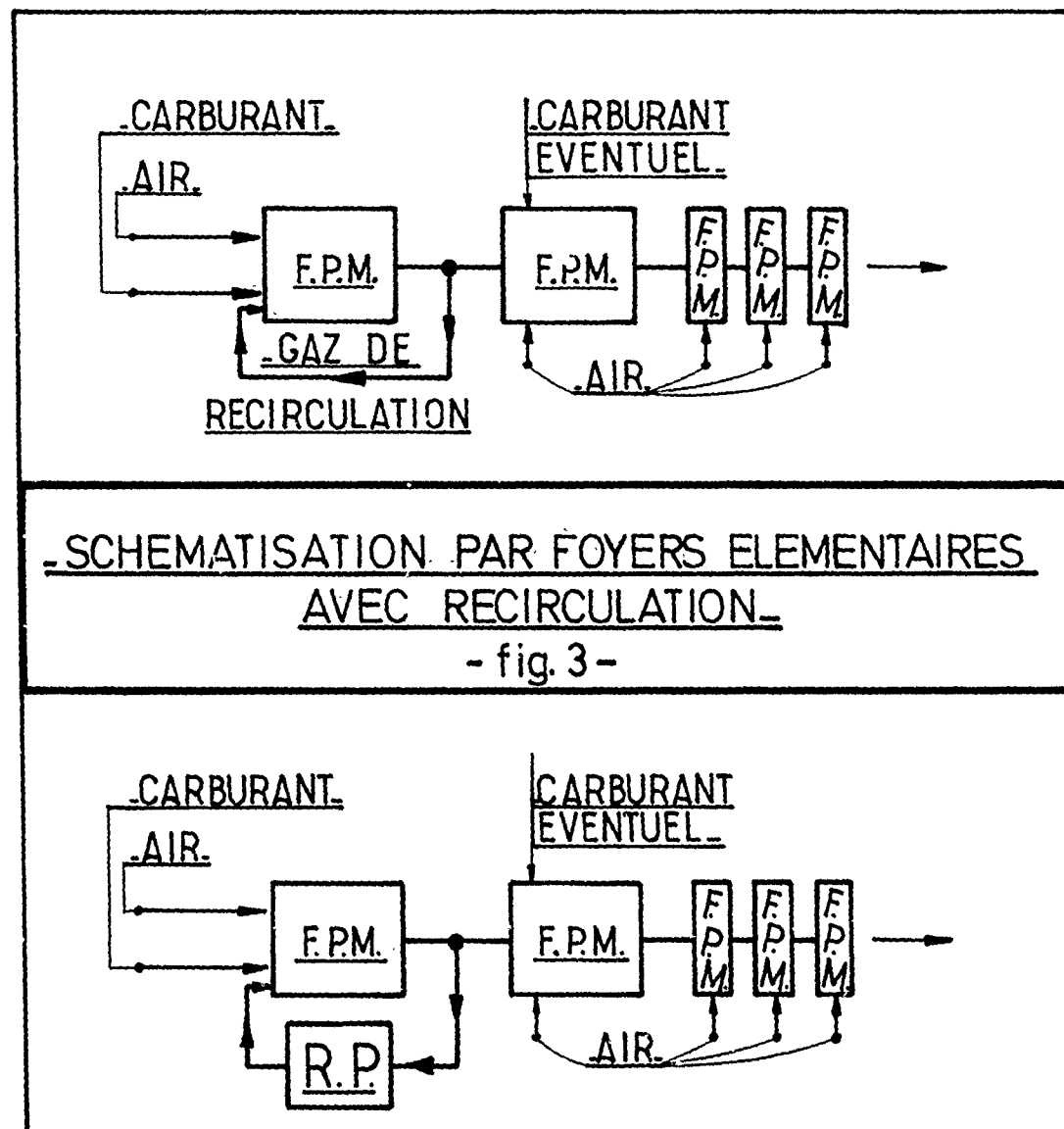
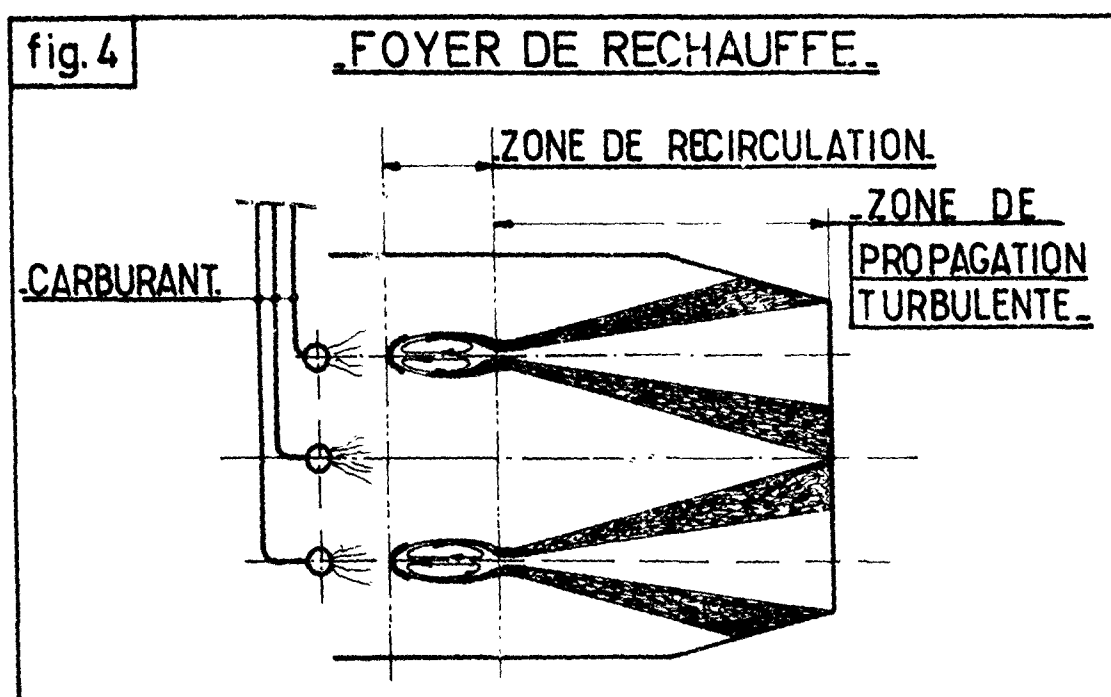
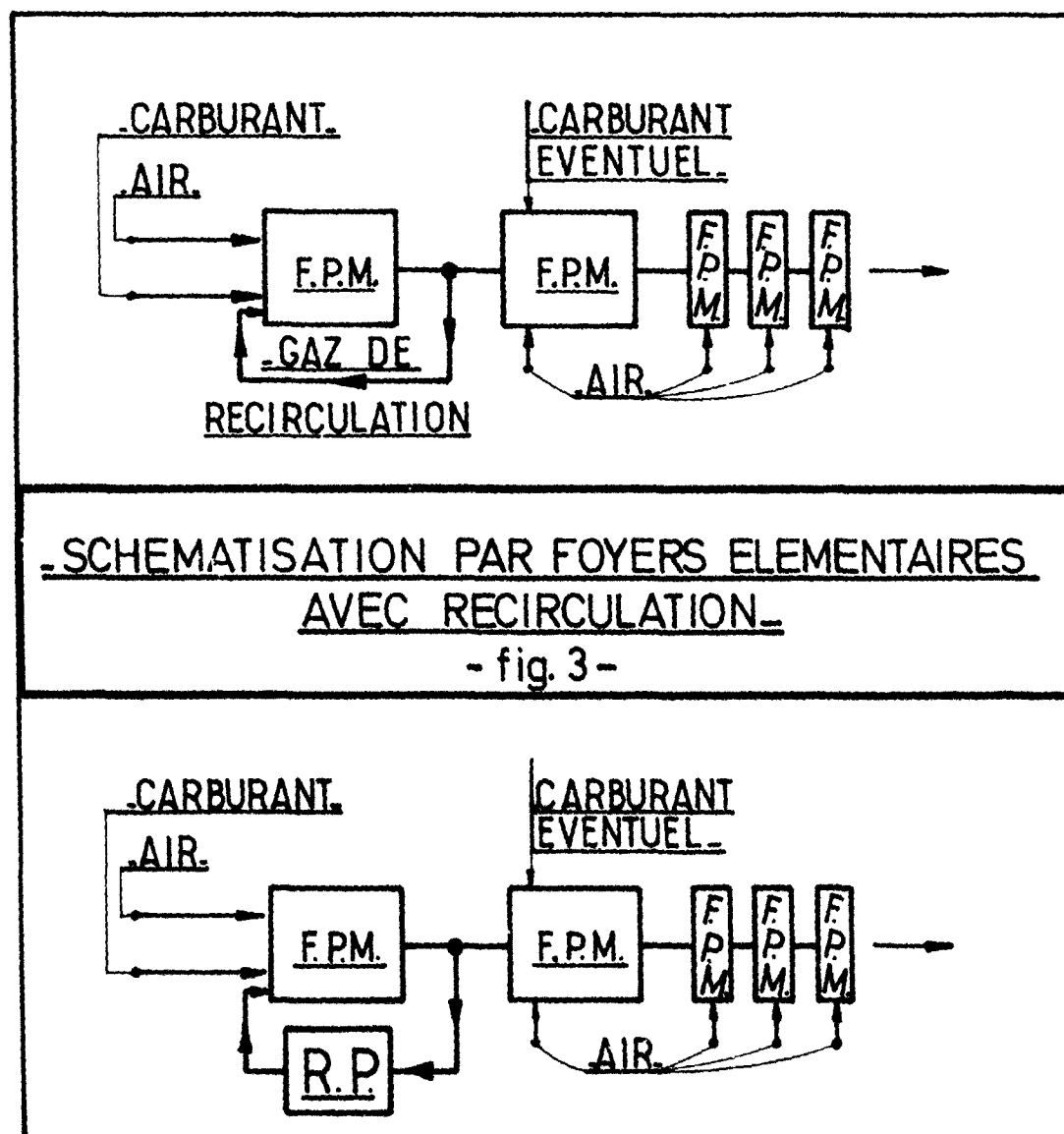


fig.2 \_SCHEMATISATION PAR FOYERS ELEMENTAIRES SANS RECIRCULATION\_









## DISCUSSION

C.Hirsch, Be

- (1) Quel est le contenu (degré de complexité, variables entrée-sortie, représentation de la turbulence, . . .) des modèles partiels utilisés (FPM: foyer parfaitement mélangé; RP: réacteur piston)?
- (2) Sur quels critères sont basés le choix du nombre de modèles partiels entrant dans la modélisation d'un foyer?

Réponse d'Auteur

- (1) En ce qui concerne les foyers homogènes (FPM) nous utilisons une cinétique simplifiée en ce qu'elle comporte une réaction global de décomposition du carburant, les données de cinétique chimique nous sont fournies par des organismes de recherches, comme l'ONERA par exemple. En ce qui concerne les modèles utilisés dans les réacteurs pistons (RP) nous utilisons des constantes de cinétique déduites de nos essais partiels ou de la littérature.
- (2) Le choix du nombre et de la nature des foyers élémentaires résulte d'essais partiels décrivant les différentes zones, les temps de séjour et les volumes de chacune de ces zones; le débit d'air entrant dans chacun de ces foyers résulte du calcul global de la répartition des débits d'air et des données précédentes.

M.Pianko, Fr

A t'on des preuves expérimentales, que dans les foyers des turbo-réacteurs, le temps physique est nettement inférieur au temps chimique?

Réponse d'Auteur

Nous avons comparé les résultats expérimentaux obtenus avec un foyer représentant une zone primaire seule et les résultats de calcul en assimilant cette zone à un foyer homogène. L'accord qualitatif entre ces résultats lorsque l'injection est du type aérodynamique est assez bon pour justifier cette hypothèse en première approximation.

M.Pianko, Fr

Quels sont, de façon précise, les besoins d'amélioration des techniques et procédés de mesure?

Réponse d'Auteur

Il ne suffit pas de vérifier que les résultats de la modélisation sont en accord avec ceux obtenus à la sortie du foyer, il nous paraît indispensable de comparer les répartitions de vitesse, les intensités de turbulence, les fluctuations de température et de concentrations obtenues par le calcul avec les valeurs mesurées dans les foyers. C'est dans le domaine des mesures optiques des vitesses, température et concentrations au sein des foyers en combustion que doit, à notre avis, être porté l'effort.

N.Peters, Ge

Je crois à l'avenir des méthodes traitant de l'interaction turbulence-réactions chimiques. Pour la turbulence on dispose des modèles à deux équations  $k - \epsilon$  ou du type longueur de mélange. Pour la cinétique chimique des réactions à température d'activation élevée on peut utiliser les méthodes de développement asymptotique qui ont donné de bons résultats pour la prédiction de l'allumage d'une flamme de diffusion et la prédiction des oxydes d'azote. En général ces problèmes ne sont pas couplés (écoulement turbulents non réactifs ou flammes laminares). Pouvez-vous commenter ces nouvelles méthodes de calcul?

Réponse d'Auteur

Nous sommes très intéressés par ces nouvelles méthodes; mais comme vous le dites elles ne sont applicables qu'à des flammes simples alors que nous traitons, dans nos foyers, d'écoulements tridimensionnels avec injection de carburant liquide.

## FUNDAMENTAL MODELLING OF MIXING, EVAPORATION AND KINETICS IN GAS TURBINE COMBUSTORS

J. Swithenbank\*, A. Turan<sup>+</sup>, P.G. Felton\* and D.B. Spalding<sup>#</sup>

\* Department of Chemical Engineering and Fuel Technology, University of Sheffield, Sheffield, S1 3JD.

<sup>+</sup> Science Applications, Inc., Woodland Hills, California, 91364, U.S.A.<sup>#</sup> Department of Mechanical Engineering, Imperial College, Kensington, London. S.W.7.

## SUMMARY

The objective of this review is to highlight past achievements, current status and future prospects of combustor modelling. The past achievements largely consists of detailed studies of idealized flames which have given an understanding of the relevant fundamental processes. However, gas turbine combustor computations must include the simultaneous interacting processes of three-dimensional two-phase turbulent flow, evaporating droplets, mixing, radiation and chemical kinetics. At the present time numerical prediction algorithms are becoming available which can model all these processes to compute the hydrodynamic, thermodynamic and chemical quantities throughout a three-dimensional field. Complementary stirred reactor network algorithms permit the prediction of minor constituents (pollutants), again including such effects as droplet evaporation and unmixedness. Experimental verification of these various predictions reveals remarkably good agreement between measured and predicted values of all parameters in spite of the physical and mathematical assumptions currently used. Future problems include: more accurate modelling of turbulence/kinetic interactions, numerical procedure optimization and detailed measurements of residence time distribution and two-phase parameters in real, hot combustors.

## 1. INTRODUCTION - PAST ACHIEVEMENTS

Presently the aviation industry produces a wide variety of engine designs, ranging from simple lift engines to sophisticated multispool by-pass engines. In so doing the combustion engineer has the important task of selecting the combustor design which yields maximum overall efficiency, while minimizing the emission of pollutants.

Gas turbine combustors involve the simultaneous processes of three-dimensional turbulent flow, two-phase evaporating droplets, mixing, radiation and chemical kinetics. The complexity of these interacting processes is such that most current gas turbine combustor design methods depend largely on empirical correlations. However, current pressures to minimize pollutant formation, together with the foreseeable requirement to use more aromatic fuels, and even synthetic shale or coal derived fuels, suggest that the initial stages of combustor design would be greatly facilitated by a comprehensive mathematical model based on fundamental principles.

Fortunately, the past achievements in combustion science, which large consist of detailed studies of simple laminar/turbulent, pre-mixed/diffusion, and single droplet flames, have given an understanding of the relevant fundamental processes. In modelling combustors, the problem is to write down a set of governing differential equations, which correctly, or at least adequately, model interactions such as those between turbulence and chemical kinetics, whose solution is within the capability of present computers.

It is beyond the scope of this paper to present all the models which have been developed, and the approach used is to present some modelling procedures which are typical of the current 'state of the art'. A key feature of this presentation is a critical comparison of the results of the prediction procedures with experiment. Whilst this does not necessarily prove the validity of the mathematical models used, it does indicate the present capability, and future potential and promise of the techniques.

Previous studies of turbulent flow fields have predominantly considered two-dimensional isothermal flow. Simplifying assumptions which are made in the mathematical and physical stages of modelling will certainly introduce errors and it has been demonstrated that the inherent constants used in the equations cannot claim true universalism. Nevertheless, although there are uncertainties associated with their use, many studies have shown that isothermal flow fields can be predicted with sufficient accuracy to be of practical value.

Models of turbulence employed in combustion situations have, on the other hand, frequently assumed extended forms of the isothermal cases, the flame/turbulence interaction being represented by simple expressions lacking rigorous formulation. Turbulence models are required because it is not possible to solve the unsteady versions of the transport equations analytically, and their numerical evaluation is well beyond the capabilities of present computers. Since we normally only require the time averaged flow for engineering purposes, the problem reduces to the representation of the statistical correlation terms, which appear in the time averaged versions of the transport equations, in terms of known quantities. In the first part of this paper, the two equation ( $k, \epsilon$ ) model of turbulence has been used although its validity in hot reacting flows has not yet been firmly established. Whilst higher order models would probably be required for strongly swirling flows for example, in the present case the two equation model was considered to be the lowest level of closure which would give adequate accuracy.

In the second part of the paper, contrary to the rigorous description employed in the finite difference modelling by partial differential equations of heat, mass and momentum transfer, the "Chemical Reactor Modelling" approach concentrates on the representation of the combustor flow field in terms of interconnected partially stirred and plug flow reactors. This approach has the advantage that the complex, time-consuming solution of the equations is replaced by simple flow models and the computational requirements are generally minimum. These features enable the attractiveness of chemical reactor modelling to be exploited during the development phase of combustor design.

## 2. FINITE DIFFERENCE PROCEDURE FOR AERODYNAMIC AND THERMAL PREDICTIONS

The finite difference procedure employed in this work is derived from the pioneering work at Imperial College, (1,2,3,4,5). It uses the cylindrical polar system of coordinates to predict the complex three-dimensional swirling and reacting flow inside a combustor.

The numerical scheme for solving the governing non-linear equations with arbitrary boundary conditions coupled with mathematical models of turbulence and combustion has the pressure and velocities as the main flow variables; facilities exist to treat both physically-controlled and kinetically controlled combustion. The latter can be formulated in terms of either one or two steps.

The present algorithm is also capable of predicting the local distribution of droplets in any specified number of distinct size ranges for the investigation of two-phase combustion. Means are provided to account for the vaporization-plus-combustion processes around the droplets if required, however no significant interphase drag and consequent modification of the evaporation rate has been considered. Techniques developed to overcome this limitation in the near field of the injector are discussed below. Radiation effects are incorporated by means of a six flux model.

(a) Equations of Continuity and Momentum

$$\frac{1}{r} \frac{\partial}{\partial r} (\rho r v) + \frac{1}{r} \frac{\partial}{\partial \theta} (\rho w) + \frac{\partial}{\partial x} (\rho u) = 0 \quad (1)$$

X - momentum:-

$$\rho \left\{ v \frac{\partial u}{\partial r} + \frac{w}{r} \frac{\partial u}{\partial \theta} + u \frac{\partial u}{\partial x} \right\} = - \frac{\partial p}{\partial x} + \frac{1}{r} \frac{\partial}{\partial r} \left( r \mu \left\{ \frac{\partial u}{\partial r} + \frac{\partial v}{\partial x} \right\} \right) + \frac{1}{r} \frac{\partial}{\partial \theta} \left( \mu \left\{ \frac{\partial u}{r \partial \theta} + \frac{\partial w}{\partial x} \right\} \right) + \frac{\partial}{\partial x} \left( 2 \mu \frac{\partial u}{\partial x} \right) \quad (2)$$

r - momentum:

$$\rho \left\{ v \frac{\partial v}{\partial r} + \frac{w}{r} \frac{\partial v}{\partial \theta} + u \frac{\partial v}{\partial x} - \frac{w^2}{r} \right\} = - \frac{\partial p}{\partial r} + \frac{1}{r} \frac{\partial}{\partial r} \left( 2 r \mu \frac{\partial v}{\partial r} \right) + \frac{1}{r} \frac{\partial}{\partial \theta} \left( \mu \left\{ r \frac{\partial}{\partial r} \left( \frac{w}{r} \right) + \frac{1}{r} \frac{\partial v}{\partial \theta} \right\} \right) - 2 \frac{\mu}{r} \left( \frac{\partial w}{r \partial \theta} + \frac{v}{r} \right) + \frac{\partial}{\partial x} \left( \mu \left\{ \frac{\partial u}{\partial r} + \frac{\partial v}{\partial x} \right\} \right) \quad (3)$$

$\theta$  - momentum

$$\rho \left\{ v \frac{\partial w}{\partial r} + \frac{w}{r} \frac{\partial w}{\partial \theta} + u \frac{\partial w}{\partial x} + \frac{v w}{r} \right\} = - \frac{1}{r} \frac{\partial p}{\partial \theta} + \frac{1}{r} \frac{\partial}{\partial r} \left( r \mu \left\{ r \frac{\partial (w/r)}{\partial r} + \frac{1}{r} \frac{\partial v}{\partial \theta} \right\} \right) + \frac{\mu}{r} \left\{ r \frac{\partial}{\partial r} \left( \frac{w}{r} \right) + \frac{1}{r} \frac{\partial v}{\partial \theta} \right\} + \frac{1}{r} \frac{\partial}{\partial \theta} \left( \mu \left\{ \frac{2}{r} \frac{\partial w}{\partial \theta} + \frac{2v}{r} \right\} \right) + \frac{\partial}{\partial x} \left( \mu \left\{ \frac{\partial w}{\partial x} + \frac{1}{r} \frac{\partial u}{\partial \theta} \right\} \right) \quad (4)$$

For turbulent flows which are generally encountered in combustion studies, it shall be assumed that the same equations are also valid provided that all the flow variables and fluid properties are represented by the corresponding time-mean values and  $\mu$  is now the effective viscosity which is the molecular viscosity augmented by the turbulent contribution. The local variation of the latter is assumed to be of the following form:

$$\mu_t = C_D \rho k^2 / \epsilon \quad (5)$$

where  $C_D$  is a universal constant.

The hydrodynamic turbulence model adopted here is a two-equation model of turbulence known as the  $k \sim \epsilon$  model. (2) It entails the solution of two transport equations for turbulence characteristics, namely that of  $k$ , the local energy of the fluctuating motion and  $\epsilon$ , the energy dissipation rate. Knowledge of  $k$  and  $\epsilon$  allows the length scale to be determined and also the effective viscosity (as above) from which the turbulent shear stresses can be evaluated.

The differential transport equations for  $k$  and  $\epsilon$  are expressed as:

$$\rho \left( v \frac{\partial k}{\partial r} + \frac{w}{r} \frac{\partial k}{\partial \theta} + u \frac{\partial k}{\partial x} \right) = \frac{1}{r} \frac{\partial}{\partial r} \left( r \Gamma_k \frac{\partial k}{\partial r} \right) + \frac{1}{r} \frac{\partial}{\partial \theta} \left( \Gamma_k \frac{\partial k}{\partial \theta} \right) + \frac{\partial}{\partial x} \left( \Gamma_k \frac{\partial k}{\partial x} \right) - G_k - \rho \epsilon \quad (6)$$

$$\rho \left( v \frac{\partial \epsilon}{\partial r} + \frac{w}{r} \frac{\partial \epsilon}{\partial \theta} + u \frac{\partial \epsilon}{\partial x} \right) = \frac{1}{r} \frac{\partial}{\partial r} \left( r \Gamma_\epsilon \frac{\partial \epsilon}{\partial r} \right) + \frac{1}{r} \frac{\partial}{\partial \theta} \left( \Gamma_\epsilon \frac{\partial \epsilon}{\partial \theta} \right) + \frac{\partial}{\partial x} \left( \Gamma_\epsilon \frac{\partial \epsilon}{\partial x} \right) + C_1 \frac{\epsilon}{k} G_k - C_2 \frac{\rho \epsilon^2}{k} \quad (7)$$

In the above equations the generation term for  $K, G_k$  is given by:

$$G_k = \mu_t \left\{ 2 \left( \frac{\partial u}{\partial x} \right)^2 + 2 \left( \frac{\partial v}{\partial r} \right)^2 + 2 \left( \frac{\partial w}{r \partial \theta} + \frac{v}{r} \right)^2 + \left( \frac{\partial u}{\partial r} + \frac{\partial v}{\partial x} \right)^2 + \left( \frac{\partial w}{\partial x} + \frac{\partial u}{r \partial \theta} \right)^2 + \left( \frac{\partial v}{r \partial \theta} + \frac{\partial w}{\partial r} - \frac{w}{r} \right)^2 \right\} \quad (8)$$

In equations (6) and (7),  $\Gamma_k$  and  $\Gamma_\epsilon$  are taken to be the effective exchange coefficients;  $C_1$  and  $C_2$  are assumed to be constants.

Recommended values for the above constants are:

$$\begin{array}{ccc} C_D & C_1 & C_2 \\ 0.09 & 1.43 & 1.92 \end{array} \quad (9)$$

(b) Reaction Models

Conservation Equation for a Chemical Species J:-

$$\rho \left\{ v \frac{\partial m_J}{\partial r} + \frac{w}{r} \frac{\partial m_J}{\partial \theta} + u \frac{\partial m_J}{\partial x} \right\} = R_J + \frac{1}{r} \frac{\partial}{\partial r} \left( r \Gamma_J \frac{\partial m_J}{\partial r} \right) + \frac{1}{r} \frac{\partial}{\partial \theta} \left( \Gamma_J \frac{\partial m_J}{r \partial \theta} \right) + \frac{\partial}{\partial x} \left( \Gamma_J \frac{\partial m_J}{\partial x} \right) \quad (10)$$

In a multi-component system, simplifications can be introduced through the use of the concept of a simple chemically reacting system. This assumes fuel and oxidant react chemically in a unique proportion. Furthermore, the effective diffusivities of all the chemical species are taken to be equal and the reaction is a single step with no intermediate compounds.

These suppositions enable various concentrations to be determined by solving only one equation for the mixture fraction variable  $f$  (Fig. 1.), defined as the mass fraction of fuel in any form, for diffusion flames. Treatment of kinetically influenced flames is affected via equations for the variables  $f$  and  $m_{fu}$ , where  $m_{fu}$  is the mass fraction of fuel. Thus the evaluation of  $m_{ox}$  in kinetically influenced flames is achieved via:

$$m_{ox} = \left[ m_{fu} - \left( \frac{f - f_s}{1 - f_{st}} \right) \right] S_t \quad \text{where } S_t \text{ is the stoichiometric constant.} \quad (11)$$

The influence of turbulence on reaction rates is taken into account by employing the eddy break up model of Spalding (3). The reaction rate in this case is taken to be the smaller of the two expressions given by the familiar Arrhenius formulation and the eddy break-up model. The latter is conveniently described as:

$$R_{fu,EBU} = - C_R \phi g^{\frac{1}{2}} \epsilon / k \quad (12)$$

where  $C_R$  is a constant and  $g$  represents the local mean square concentration fluctuations.

#### (c) Two-step Kinetic Model

Predictions of the local mass fractions of fuel,  $CO_2$ ,  $CO$ ,  $H_2O$ ,  $O_2$  and  $N_2$  are provided by a slightly more sophisticated kinetic scheme proceeding via the following steps:



Three differential transport equations are solved for the species  $f$ ,  $m_{fu}$  and  $CO$  employing the partial equilibrium model of Morr and Heywood for concentrations of  $CO$ . In addition algebraic equations for the atomic balance of  $C$ ,  $H$ , and  $O$  together with a trivial relation involving the total sum of the species mass fractions completely specify the problem.

Manipulation of the algebraic expressions involving the individual element mass fractions, and the inherent assumption that the effective turbulent exchange coefficients for all the species are equal throughout the field, yield  $m_{ox}$ ,  $m_{H_2O}$  and  $m_{CO_2}$  as:

$$m_{ox} = \frac{576}{168} m_{fu} + \frac{16}{28} m_{CO} + 0.232 - \left( 0.232 + \frac{576}{168} \right) f - 0.232 \sum_{J=1}^K m_{d,J} \quad (15)$$

$$m_{H_2O} = \frac{216}{168} (f - m_{fu}) \quad (16)$$

$$m_{CO_2} = \frac{22}{7} (f - m_{fu}) - \frac{44}{28} m_{CO} \quad (17)$$

In the above,  $\sum_{J=1}^K m_{d,J}$  is the liquid fuel mass fraction prevailing in the field.  $m_{N_2}$  is found from

$$m_{fu} + m_{CO} + m_{CO_2} + m_{H_2O} + m_{ox} + m_{N_2} + \sum_{J=1}^K m_{d,J} = 1 \quad (18)$$

#### (d) Treatment of droplet (particle) combustion

Assumptions involved in the analysis:

- (1) In the course of diminution of size by vaporization, the heat absorbed is proportional to the mass of material changing phase.
- (2) The specific heat of the liquid phase fuel is taken as identical with that of the vapour-phase.
- (3) It is presumed that the droplets are small enough in size for Reynolds number of relative motion between phases to be negligible (N.B. see later discussion).
- (4) Under turbulent conditions, the mode of diffusion for droplets is taken to be identical to that of the gaseous phase; however relative dispersion effects for near-dynamic equilibrium cases can be incorporated without much difficulty (6).
- (5) The temperature and concentration fields surrounding the droplets are spherically symmetric. (Forced convection effects are neglected in this analysis).
- (6) The droplets are of uniform density and spherical in shape.
- (7) The mode of mass transfer depends on either:  
The driving force due to a temperature difference between the local gas mixture and the presumed droplet surface temperature.

or:

The oxygen concentration in the local mixture.

The above restrictions are convenient rather than necessary and can be removed should the extra computational effort and cost be justifiable.

In the following analysis, the size of a particle is characterised by  $S$ , which is identified with the square of the particle radius. Choice of  $S$  as the size parameter offers considerable simplification in that the rate of change of size with time emerges as a constant independent of  $S$ .

" $n$ " defines the number of particles in unit volume having sizes between  $S$  and  $S+dS$ ;  $M$  is the mass of a single droplet in this size range, while  $m$  signifies the mass of droplets in this size range per unit volume. Finally,  $f_j$  denotes the mass of particles in the size range  $S_{j+1}$  to a larger size  $S_j$  per unit mass of local gas-droplet mixture.

A control volume analysis for a balance of droplets entering, leaving and changing size together with hypotheses, about the interphase mass transfer yields the following governing equation for  $f_j$ : (7).

$$\frac{d}{dt} (\rho f_j) = \dot{S} \left\{ (m_j - m_{j+1}) - \int_{S_{j+1}}^{S_j} \frac{3}{2} \frac{m}{S} dS \right\} \quad (19)$$

This study employs the commonly used supposition that the mass transfer rate from the condensed phase to the gaseous phase per unit surface area is expressible in the form:

$$\dot{m}'' = \frac{\Gamma}{r} \ln (1+B) \quad (20)$$

For distillate fuels, B is evaluated from:

$$B = \left( \int_{T_{ref}}^{T_g} C_{pd} T - \int_{T_{ref}}^{T_s} C_{pd} T \right) / L \quad (21)$$

Even though the actual  $m$ 's variation of a two-phase mixture can only be described by a smooth curve, it suffices for purposes of this study to discretize this distribution. Arrangement of the droplet sizes is in such a manner that  $J=1$  signifies the largest size and  $J=K$  the smallest. This is done for the considerable simplification that this arrangement offers in the linearization of the source terms. The final equations are expressed in the following form:

$$\frac{d}{dt} (\rho f_j) = \frac{\rho \Gamma}{\rho_p} \ln (1+B) \left\{ \frac{f_{j-1}}{S_{j-1} - S_j} - \frac{f_j}{S_j - S_{j+1}} - \frac{3}{2} \frac{f_j}{S_j} \right\} \quad \text{for } J < K \quad (22)$$

$$\frac{d}{dt} (\rho f_1) = - \frac{\rho \Gamma}{\rho_p} \ln (1+B) \left\{ \frac{f_1}{S_1 - S_2} + \frac{3}{2} \frac{f_1}{S_1} \right\} \quad \text{for } J = 1 \quad (23)$$

$$\frac{d}{dt} (\rho f_K) = \frac{\rho \Gamma}{\rho_p} \ln (1+B) \left\{ \frac{f_{K-1}}{S_{K-1} - S_K} - \frac{3}{2} \frac{f_K}{S_K} \right\} \quad \text{for } J = K \quad (24)$$

In view of the fact that the concentration of droplets in an intermediate size range is influenced only by the behaviour of larger droplets, not of the smaller ones, (equations (22) to (24)), a specific droplets treatment can be devised. This offers extremely economical use of storage while permitting an extremely sophisticated representation of the droplet size distributions. The essential feature is stated as follows:

It suffices to provide storage for just one droplet concentration array. The computation is so arranged that the integration proceeds through the droplet size distribution from large size to small, overwriting the contents of each concentration store as it does so. This is particularly valuable when storage is a near prohibitive factor.

The incorporation of the droplet size distribution equations and the corresponding source term manipulations are discussed in great detail in Reference (7).

#### (e) Radiation effects

The effect of radiation in the mathematical model are accounted for, by reference to the six flux model of radiation. The differential equations describing the variations of the fluxes are:

$$\frac{d}{dr} (rI) = r \left\{ -(a+S_c)I + \frac{J}{r} + aE + \frac{S_c}{6} (I + J + K + L + M + N) \right\} \quad (25)$$

$$\frac{d}{dr} (rJ) = r \left\{ (a+S_c)J + \frac{J}{r} - aE - \frac{S_c}{6} (I + J + K + L + M + N) \right\} \quad (26)$$

$$\frac{d}{dx} (K) = -(a+S_c)K + aE + \frac{S_c}{6} (I + J + K + L + M + N) \quad (27)$$

$$\frac{d}{dx} (L) = (a+S_c)L - aE - \frac{S_c}{6} (I + J + K + L + M + N) \quad (28)$$

$$\frac{d(M)}{rd} = -(a+S_c)M + aE + \frac{S_c}{6} (I + J + K + L + M + N) \quad (29)$$

$$\frac{d(N)}{rd\theta} = (a+S_c)N - aE - \frac{S_c}{6} (I + J + K + L + M + N) \quad (30)$$

The composite fluxes defined as:

$$R^y = \frac{1}{2} (I + J) \quad (31)$$

$$R^x = \frac{1}{2} (K + L) \quad (32)$$

$$R^z = \frac{1}{2} (M + N) \quad (33)$$

are employed to eliminate I, J, K, L, M and N from the previous equations to yield three second-order ordinary differential equations.

The recent radiation model developed by Lockwood and co-workers (8) where the inherent grey gas assumption of the above formulation is relaxed by employing a pseudo-grey approximation for the local emissivity, could be used for improved radiation predictions.

#### (f) Solution Procedure

The previous governing partial differential equations for mass, momentum, energy, droplet and species are all elliptic in nature and can be conveniently presented in the general form:

$$\text{div}(\vec{\sigma}^n - \vec{\tau}_n \text{grad } \phi) = S_n \quad (34)$$

The equations are first reduced to finite difference equations by integrating over finite control volumes (5) and then solved by a procedure described in detail in Reference (1) for three-dimensional flows.

It will be sufficient for the purposes of this paper to summarize the pertinent features of the solution procedure.

The numerical scheme is a semi-implicit, iterative one which starts from given initial conditions for all the variables and converges to the correct solution on the completion of a number of iterations.

Each iteration performs the following steps:

- (i) The u, v and w momentum equations are solved sequentially with guessed pressures.
- (ii) Since the velocities at this stage do not satisfy the continuity equation locally, a "Poisson-type" equation is derived from the continuity equation and the three linearised momentum equations. This pressure-correction equation is then solved for corrections to the pressure field and consequent corrections of the velocity components are established.
- (iii) The "Sectional balance" (7) technique is applied to the velocity field before and after the solution of the pressure correction equation.
- (iv) The k and ε equations are then solved using the most recent values of the velocities.
- (v) The iteration is completed upon solution of the droplet, species concentration and all the remaining equations.

One point to note here is the implementation of the cyclic boundary condition in the θ direction compatible with the nature of the swirling flows.

#### (g) Current physical modelling limitations and future improvements

Some of the problems facing the mathematical modeller have already been indicated above. Primarily, the flame-turbulence interaction, represented in the first part of this study by the tentative eddy break-up model, needs to be critically assessed. It should be emphasised that the adopted eddy break-up expression falls short of a probabilistic description for the temporal variation of the turbulence energy and dissipation, i.e. the delay time associated with the break-up of eddies to provide adequate interfaces with the hot gas, as a consequence of the processes initiated by the turbulence energy, seems to have been neglected. A cross-correlation analysis might be profitably adopted for this purpose.

The local Reynolds number insensitivity of the model, together with the fixed eddy states presumed in the derivation have already been pointed out by Spalding (3). However, the latter influence can probably be accounted by reference to a differential equation which has as the dependent variable the root mean-square fluctuation of reactiveness.

The solution of a concentration fluctuation equation, especially for diffusion flames, should be viewed as a problem of utmost urgency. The implications of employing a particular waveform for the instantaneous variation of the composite mass fraction needs to be explored in detail. The treatment of "unmixedness" for premixed flames can be developed via a similar approach.

It is the authors' belief that in predicting turbulent combustor flow situations recourse has to be made to more fundamental approaches, initially free from all the obstructive sophistications one could envisage. Recently there appeared in the literature a number of encouraging attempts aimed at fulfilling this task (e.g. Ref. 9.) Chemical reactor modelling formulated in terms of a "population balance" coupled with a "mechanistic" approach to predict the gross profiles could yet initiate a new era in modern combustion research. It is then a relatively simple matter to introduce gradually any desired level of complexity.

Space precludes a detailed discussion of potential improvements in numerical methods. However, issues related to grid optimization, delineation of two and three-dimensional combustor zones, effective "restart" procedures, devising of convergence-promoting features without changing the basic structure of the algorithm, should be considered to achieve a computationally more "attractive" model. Further recommendations for improvements are to be found in Reference (7).

### 3. THREE-DIMENSIONAL FINITE DIFFERENCE ANALYSIS. RESULTS OF THEORY AND EXPERIMENTS

In order to assess the prediction algorithm specified above, a simple 70 mm dia. gas turbine can combustor shown in Fig. 2. was tested experimentally and modelled analytically. The experimental tests were carried out at atmospheric pressure using a total air flow rate of 0.1275 kg/s both cold and at overall air/fuel ratios of 30 and 40. The computations were carried out using the grid network of over 3000 nodes as shown in Figs. 3 and 4, both cold and with overall air/fuel ratios of 68 and 40. The flow was divided as follows: swirler 7.8% (swirl No. 0.8), primary jets 25.5% (6 jets), secondary jets 29.9% (6 jets), dilution 36.8% (6 jets). The cold flow computations were carried out first yielding the radial, axial and tangential velocity profiles including the recirculation zone, as shown in Figs. 4, 5 and 6. Good agreement was found between the measured and predicted profiles as illustrated in Fig. 7. Computations were then carried out with diffusive combustion using the cold flow pattern to initiate the iteration procedure. This case was simulated experimentally using rich premixed propane/air mixture introduced through the swirler. As a relatively severe test of the modelling procedure, the exit turbulence levels were measured with a photon correlation laser anemometer with the results shown in Fig. 8. Again the agreement is remarkably good considering the difficulty of the experiment and the complexity of the prediction, however the results suggest that the model slightly overestimates the turbulence intensity.

The more complex computational procedure including the droplet spray and two stage kinetics was then tested, using the previous results to start the iterations. In both the computations and experiments the liquid fuel was introduced as a spray of 80° included angle from the axially located fuel nozzle. The droplet size distribution used for the analysis was divided into 10 size ranges as shown in Fig. 9. Although it would be preferable to use about 20 size increments, considerable saving in computer time is



achieved by a more modest model at this stage. The problem of representing the upper 'tail' of the size distribution curve is met by placing all the larger droplets in the upper size band. In practice, these droplets would usually impinge on the combustor wall and evaporate there as indicated in Fig. 10 (Ref. 10). The associated study reported in Ref. 9. is based on the fact, shown clearly in Fig. 11, that the flow in the vicinity of the fuel injector is 2-dimensional even though the main combustor flow is 3-dimensional. The detailed spray trajectories can therefore be analysed in detail by the 2-dimensional computation. It can be seen that, for the relative initial droplet/air velocity ratios associated with conventional atomizers, the droplets tend to travel in straight lines. In general, as a droplet becomes small enough to be deflected by the hot gas flow, its life is so short that it quickly vanishes. The dashed lines in Fig. 10 show that the inclusion of finite droplet heat-up time in the computations only contributes about 10% to the droplet range. Thus, the evaporation constant B should be adjusted to compensate for the relative velocity of the droplets and their actual shorter residence time in each grid cell.

The predictions of the droplet concentration distribution is shown in Fig. 12, whilst Fig. 13 illustrates the mass fraction of fuel evaporated but unburned assuming kinetic control of the reaction. Such information would be invaluable to a designer concerned with quenching and the minimization of unburned hydrocarbon formation at engine idle conditions. Our experiments indicated about 0.1% unburned hydrocarbons near the wall at the combustor exit, and were thus consistent with the predictions although detailed quenching mechanisms were not modelled in this study.

When the fuel spray and two-stage kinetics are included in the model, the computation is close to the limits of present day computers, both with regard to fast memory capacity and speed. The approach of the computational iteration to convergence can be monitored by the normalized error in the sum of the modulus of the mass sources as shown in Fig. 14. Although the figure shows that there is little improvement in this error after about 80 iterations, it was found that the temperatures and associated concentrations were still evolving slightly even after 240 iterations. Fortunately, the trends were clearly established and it was not economic to continue the computation to its ultimate precision. The results for exit velocity and temperature are given in Fig. 15 and 16 respectively where it can be seen that the predicted and experimental values are in remarkably good agreement. The hot exit velocity profile should be compared with the cold case shown in Fig. 7. The true exit temperature would be slightly higher than shown, since the experimental results are not corrected for radiation, and the computation would have finally converged on a slightly higher profile. Nevertheless, it is considered that the prediction of pattern factor would be most useful to a combustor designer.

The predicted and measured exit concentration profiles of oxygen, CO and CO<sub>2</sub> at an air/fuel ratio of 40 are shown in Fig. 17. Again, allowing for the fact that the kinetic part of the computations have not completely converged the concentration profiles are in good agreement. The agreement between the measured and predicted profiles at the exit from the primary zone is illustrated in Fig. 18, where the large radial changes are again apparent. In the experimental studies it was found that the fuel nozzle gave a slightly skew distribution which precluded a valid comparison of the predicted and measured circumferential variations in concentration.

The location of the highly stirred regions within the combustor may be obtained from the predictions of the turbulence dissipation rate since mixing occurs by the movement of molecules between adjacent eddies which simultaneously dissipates the velocity difference between the eddies. The major stirred reactor regions can be clearly identified on Fig. 19.

#### 4. STIRRED REACTOR MODELLING

This second stage of the calculation consists of a procedure which represents the combustor as a network of interconnected stirred and plug flow reactors and includes a detailed kinetic scheme for the chemical species to be considered. A model of the fuel evaporation and mixing rate is also built into this part of the computation since only the fuel which has evaporated and mixed with the air can take part in the chemical reaction. The objective of this stage of the computation is to quickly predict the combustion efficiency and pollution levels produced by the particular combustor design. As with the 3-dimensional modelling, an important aspect of the procedure is that it should be capable of predicting the trend of dependence. For example, it is important to be able to predict the effect which a finer fuel spray may be expected to have on the production of nitric oxide at some particular combustor throughput.

To set up the network of stirred reactors, we require a sub-model for a well stirred reactor which includes the internal processes of fuel evaporation, mixing and complex chemical kinetics. In addition, to model the sections of the flowfield where no mixing is taking place, a plug flow reactor is required. This can be achieved as a sequence of differentially small well stirred reactors or in some cases as a larger poorly stirred reactor.

Previous stirred reactor models of combustors have been mainly confined to homogeneous combustion with "global" reaction kinetics, and encouraging results were obtained within the limitations of this approach (11). Evaporation effects were later included with some success (12).

Although the three processes of evaporation, mixing and reaction must occur simultaneously in a combustor it is convenient to consider that in a steady state condition these processes occur in series. This approach allows us to calculate the reactor gaseous phase composition after evaporation and mixing have taken place, this constitutes the homogeneous feed to the reactor. A general combustion scheme which summarizes this is shown in Table 1. (13)

The feedstream to, or product stream from any reactor is assumed to be composed of any or all of the eight species in the above scheme. Fig. 19 shows the composition of the general two phase steady state reactor with the liquid phase shown coalesced for convenience. Transfer from the liquid phase to the gas phase is represented by the mean fuel evaporation rate,  $\overline{F}_E$ . In addition it is assumed that the mean residence time of each phase in the reactor is the same. This assumption is incompatible with the existence of a relative velocity between the gas and the fuel droplets but greatly simplifies the analysis and calculation of fuel distribution around any particular reactor network. It is not essential to assume this however, and the analysis could be modified to incorporate unequal phase residence times. Transfer of fluid from the unmixed state to the mixed state is assumed to take place at the rate (mass of unmixed fluid)/ $\tau_D$ , where  $\tau_D$  is the characteristic turbulence dissipation time.

$$\text{Total reactor mass} = m + \epsilon$$

achieved by a more modest model at this stage. The problem of representing the upper 'tail' of the size distribution curve is met by placing all the larger droplets in the upper size band. In practice, these droplets would usually impinge on the combustor wall and evaporate there as indicated in Fig. 10 (Ref. 10). The associated study reported in Ref. 9. is based on the fact, shown clearly in Fig. 11, that the flow in the vicinity of the fuel injector is 2-dimensional even though the main combustor flow is 3-dimensional. The detailed spray trajectories can therefore be analysed in detail by the 2-dimensional computation. It can be seen that, for the relative initial droplet/air velocity ratios associated with conventional atomizers, the droplets tend to travel in straight lines. In general, as a droplet becomes small enough to be deflected by the hot gas flow, its life is so short that it quickly vanishes. The dashed lines in Fig. 10 show that the inclusion of finite droplet heat-up time in the computations only contributes about 10% to the droplet range. Thus, the evaporation constant B should be adjusted to compensate for the relative velocity of the droplets and their actual shorter residence time in each grid cell.

The predictions of the droplet concentration distribution is shown in Fig. 12, whilst Fig. 13 illustrates the mass fraction of fuel evaporated but unburned assuming kinetic control of the reaction. Such information would be invaluable to a designer concerned with quenching and the minimization of unburned hydrocarbon formation at engine idle conditions. Our experiments indicated about 0.1% unburned hydrocarbons near the wall at the combustor exit, and were thus consistent with the predictions although detailed quenching mechanisms were not modelled in this study.

When the fuel spray and two-stage kinetics are included in the model, the computation is close to the limits of present day computers, both with regard to fast memory capacity and speed. The approach of the computational iteration to convergence can be monitored by the normalized error in the sum of the modulus of the mass sources as shown in Fig. 14. Although the figure shows that there is little improvement in this error after about 80 iterations, it was found that the temperatures and associated concentrations were still evolving slightly even after 240 iterations. Fortunately, the trends were clearly established and it was not economic to continue the computation to its ultimate precision. The results for exit velocity and temperature are given in Fig. 15 and 16 respectively where it can be seen that the predicted and experimental values are in remarkably good agreement. The hot exit velocity profile should be compared with the cold case shown in Fig. 7. The true exit temperature would be slightly higher than shown, since the experimental results are not corrected for radiation, and the computation would have finally converged on a slightly higher profile. Nevertheless, it is considered that the prediction of pattern factor would be most useful to a combustor designer.

The predicted and measured exit concentration profiles of oxygen, CO and CO<sub>2</sub> at an air/fuel ratio of 40 are shown in Fig. 17. Again, allowing for the fact that the kinetic part of the computations have not completely converged the concentration profiles are in good agreement. The agreement between the measured and predicted profiles at the exit from the primary zone is illustrated in Fig. 18, where the large radial changes are again apparent. In the experimental studies it was found that the fuel nozzle gave a slightly skew distribution which precluded a valid comparison of the predicted and measured circumferential variations in concentration.

The location of the highly stirred regions within the combustor may be obtained from the predictions of the turbulence dissipation rate since mixing occurs by the movement of molecules between adjacent eddies which simultaneously dissipates the velocity difference between the eddies. The major stirred reactor regions can be clearly identified on Fig. 19.

#### 4. STIRRED REACTOR MODELLING

This second stage of the calculation consists of a procedure which represents the combustor as a network of interconnected stirred and plug flow reactors and includes a detailed kinetic scheme for the chemical species to be considered. A model of the fuel evaporation and mixing rate is also built into this part of the computation since only the fuel which has evaporated and mixed with the air can take part in the chemical reaction. The objective of this stage of the computation is to quickly predict the combustion efficiency and pollution levels produced by the particular combustor design. As with the 3-dimensional modelling, an important aspect of the procedure is that it should be capable of predicting the trend of dependence. For example, it is important to be able to predict the effect which a finer fuel spray may be expected to have on the production of nitric oxide at some particular combustor throughput.

To set up the network of stirred reactors, we require a sub-model for a well stirred reactor which includes the internal processes of fuel evaporation, mixing and complex chemical kinetics. In addition, to model the sections of the flowfield where no mixing is taking place, a plug flow reactor is required. This can be achieved as a sequence of differentially small well stirred reactors or in some cases as a larger poorly stirred reactor.

Previous stirred reactor models of combustors have been mainly confined to homogeneous combustion with "global" reaction kinetics, and encouraging results were obtained within the limitations of this approach (11). Evaporation effects were later included with some success (12).

Although the three processes of evaporation, mixing and reaction must occur simultaneously in a combustor it is convenient to consider that in a steady state condition these processes occur in series. This approach allows us to calculate the reactor gaseous phase composition after evaporation and mixing have taken place, this constitutes the homogeneous feed to the reactor. A general combustion scheme which summarizes this is shown in Table 1. (13)

The feedstream to, or product stream from any reactor is assumed to be composed of any or all of the eight species in the above scheme. Fig. 19 shows the composition of the general two phase steady state reactor with the liquid phase shown coalesced for convenience. Transfer from the liquid phase to the gas phase is represented by the mean fuel evaporation rate, FE. In addition it is assumed that the mean residence time of each phase in the reactor is the same. This assumption is incompatible with the existence of a relative velocity between the gas and the fuel droplets but greatly simplifies the analysis and calculation of fuel distribution around any particular reactor network. It is not essential to assume this however, and the analysis could be modified to incorporate unequal phase residence times. Transfer of fluid from the unmixed state to the mixed state is assumed to take place at the rate (mass of unmixed fluid)/ $\tau_D$ , where  $\tau_D$  is the characteristic turbulence dissipation time.

$$\text{Total reactor mass} = m + c$$

$$\tau_s = m/\dot{m}_2 = \epsilon/\dot{\epsilon}_2 \quad (36)$$

$$\text{Using (35) } \tau_s = V/(\dot{m}_2/\rho_G + \dot{\epsilon}_2/\rho_2) \quad (37)$$

$$\text{Gaseous phase mass balance } \dot{m}_1 - \dot{m}_2 + FE = dm/dt \quad (38)$$

$$\text{Liquid phase mass balance } \dot{\epsilon}_1 - \dot{\epsilon}_2 - FE = dc/dt \quad (39)$$

Mass balance on the unmixed fluid in the gaseous phase

$$d(m\phi_u)/dt = \dot{m}_1\phi'_m - \dot{m}_2\phi_u - \dot{m}\phi_u/\tau_D + FE, \therefore m \frac{d\phi_u}{dt} + \phi_u \frac{dm}{dt} = \dot{m}_1\phi'_u - \dot{m}_2\phi_u - \frac{m\phi_u}{\tau_D} + FE \quad (40)$$

$$\text{Using (41) } m \frac{d\phi_u}{dt} = \dot{m}_1(\phi'_u - \phi_u) - \frac{m\phi_u}{\tau_D} + FE(1 - \phi_u)$$

$$\text{At the steady state } \frac{dm}{dt} = \frac{d\phi_u}{dt} = 0$$

$$\text{Thus } \frac{m}{\dot{m}_1} = \frac{m}{(\dot{m}_2 - FE)} = \frac{m/\dot{m}_2}{(1 - FE/\dot{m}_2)} = \frac{\tau_s}{(1 - \beta)} \quad (41), \text{ where } \beta = FE/\dot{m}_2 \quad (42), \therefore \phi_u = \frac{\phi'_u(1 - \beta) + \beta}{(1 + \tau_{SD})} \quad (43)$$

where  $\tau_{SD} = \tau_s/\tau_D$  (unmixedness parameter)

Thus for a given  $FE$ ,  $\tau_{SD}$  and feed conditions (43) defines the proportion of the steady state reactor gas phase which is unmixed. Therefore the reactor composition prior to reaction may be expressed as follows:

$$C_x^* = \phi_u \omega_x + (1 - \phi_u) \gamma_x^* \quad (\text{where } x = f, O_2 \text{ or } N_2), \quad C_{CS}^* = (1 - \phi_u) \gamma_{CS}^*$$

$$\text{N.B. } \omega_f + \omega_{O_2} + \omega_{N_2} = \gamma_f^* + \gamma_{O_2}^* + \gamma_{N_2}^* + \gamma_{CS}^* = 1 \quad (44)$$

The concentrations of the unmixed species can be obtained by performing the relevant species mass balances. For example, unmixed fuel vapour mass balance is as follows:

$$\frac{d(m\phi_u \omega_f)}{dt} = \dot{m}_1\phi'_u \omega'_f - \dot{m}_2\phi_u \omega_f + FE - \frac{m\phi_u \omega_f}{\tau_D} \quad (45)$$

$$\text{At the steady state } d(m\phi_u \omega_f)/dt = 0, \therefore m\phi_u \frac{d\omega_f}{dt} + m\omega_f \frac{d\phi_u}{dt} + \phi_u \omega_f \frac{dm}{dt} = 0$$

$$\text{As } d\omega_f/dt = 0, \quad (1 - \beta)\phi'_u \omega'_f - \phi_u \omega_f + \beta - \phi_u \omega_f \tau_{SD} = 0$$

$$\therefore \omega_f = \frac{\phi'_u(1 - \beta)\omega'_f + \beta}{\phi_u(1 + \tau_{SD})} = \frac{\phi'_u(1 - \beta)\omega'_f + \beta}{\phi'_u(1 - \beta) + \beta} \quad (46)$$

using (43).

The expressions for the intermediate concentrations of the mixed reactants and combustion products are obtained by performing similar mass balances on the mixed portion of the reactor gas phase.

$$\therefore \gamma_f^* = ((1 - \beta)(1 - \phi'_u)\gamma'_f + \phi_u \omega_f \tau_{SD}) / (1 - \phi_u)$$

Using (43) and (46)

$$\gamma_f^* = ((1 - \beta)(1 - \phi'_u)(1 + \tau_{SD})\gamma'_f + \tau_{SD}(\phi'_u(1 - \beta)\omega'_f + \beta)) / ((1 - \beta)(1 - \phi'_u) + \tau_{SD}) \quad (47)$$

Similarly:

$$\gamma_x^* = ((1 - \beta)(1 - \phi'_u)(1 + \tau_{SD})\phi'_x + \tau_{SD}\phi'_u(1 - \beta)\omega'_x) / ((1 - \beta)(1 - \phi'_u) + \tau_{SD})$$

Having defined the intermediate composition of the gaseous phase, i.e. after mixing and evaporation, two further balances must be made to determine the final reactor composition. These are the species and energy balances for the PSR for the steady state. During the reaction stage the mixed gaseous phase concentrations,  $\gamma^*$ , are transformed to the final concentration  $\gamma$ ; the unmixed gas phase concentrations,  $\omega$ , do not change of course although they do contribute to the physical properties of enthalpy, specific heat and density.

Chemical reaction, mixed species mass balance:-

$$\frac{\dot{m}_2}{\rho_G V W_i} (\gamma_i^* - \gamma_i)(1 - \phi_u) + \dot{p}_i = 0, \quad (48), \text{ where } i = 1, MT. \quad MT = \text{total number of mixed gaseous species.}$$

Chemical reaction, gas phase energy balance:-

$$\frac{\dot{m}_2}{\rho_G V W_i} \sum_{i=1}^{MT} (\gamma_i^* h_i^* - \gamma_i h_i)(1 - \phi_u) + \frac{\dot{m}_2}{\rho_G V W_i} \sum_{i=1}^{NT} \omega_i (h_i^* - h_i) \phi_u = \dot{H}_L \quad (49)$$

$\dot{H}_L = 0$  for adiabatic operation.

$$\text{The species kinetic production term is given by: } \dot{p}_i = \sum_{j=1}^{NR} (\alpha_{ij} - \delta_{ij})(F_j - B_j) \quad (50)$$

The forward and backward reaction rates are related to the reactor gas phase species concentrations by the following:

$$F_j = f_j X_j^{\sigma_j} \prod_{i=1}^{MT} (\rho_G (1 - \phi_u) \gamma_i / W_i)^{\delta_{ij}} \quad (51), \quad B_j = b_j X_j^{\sigma_j} \prod_{i=1}^{MT} (\rho_G (1 - \phi_u) \gamma_i / W_i)^{\alpha_{ij}} \quad (52)$$

where  $X_j$  is a third body in a dissociation reaction.

$$X_j = \sum_{i=1}^{MT} d_{ij} ((1 - \phi_u) \gamma_i / W_i), \quad (53), \quad \text{The forward reaction rate constants are: } f_j = A_j T^{n_j} \exp(-E_j/RT) \quad (54)$$

The backward reaction rate constants are fixed by the equilibrium constants:-

$$b_j = f_j K_j \sum_{i=1}^{MT} (\delta_{ij} - \alpha_{ij}), \quad (55) \quad K_j = \exp(-\sum_{i=1}^{MT} (\alpha_{ij} - \delta_{ij}) F_i^0 / RT) \quad (56)$$

The system of equations is completed with the equation of state:-

$$P = \rho_G \frac{R}{W} T = \rho_G RT \sum_{i=1}^{MT} (1 - \phi_u) \frac{\gamma_i}{W_i} + \rho_G RT \sum_{i=1}^{NT} (\phi_u \frac{\omega_i}{W_i}) \quad (57)$$

The final reactor gas phase composition has thus been defined and the final overall concentrations may be expressed as:

$$C_f = \phi_u \omega_f + (1 - \phi_u) \gamma_f \quad (58)$$

and similarly for the other species.

The complete set of equations characterises a heterogeneous stirred reactor in steady state operation, they reduce to the equations for the homogeneous case if  $\beta$  is set to zero. These equations are very non-linear due to the exponential dependence of the reaction rates in temperature, additionally FE is a complex function of temperature and staytime,  $\tau_s$ , hence the WSR equations must be solved iteratively.

The technique which we have used previously is the numerical method of PSR solution developed by Osgerby (14), in which a Newton-Raphson correction procedure is employed to converge onto the solution from an initial guess. An alternative method of solution due to Pratt (15) has several advantages and is now preferred. This method uses Newton-Raphson correction equations in terms of the 128 variables and a self-adjusting under relaxation technique suggested by Gordon & McBride (16) which gives improved convergence and stability. The data required for the solution are a kinetic scheme, rate data, thermodynamic data and feed conditions. An initial guess is provided by an equilibrium calculation.

Fuel evaporation rates are obtained by numerically integrating the two simultaneous differential equations describing single droplet evaporation and viscous drag on a droplet. The spray is assumed to consist of a number (usually 20) of size intervals, each of which is represented by the interval mean diameter. The spray mean evaporation rate is obtained by integrating the equations over the staytime of the reactor to obtain the total fuel evaporated in the reactor and dividing by the staytime. Initially the droplets have a velocity relative to the gas stream, however, as the drag forces acting on the droplets are inversely proportional to the diameter, the small droplets rapidly assume the local gas velocity whereas the larger droplets tend to retain their own velocity. There are two modes of combustion possible for an evaporating fuel droplet; droplet diffusion flames and droplet wake flames. The wake flames are generally blue due to good mixing prior to combustion whereas diffusion flames are typically yellow due to soot formation. The velocity necessary to cause a transition from diffusional to wake burning is a strong function of the local oxygen concentration and falls to zero at oxygen concentrations in the range 14 - 16%, thus at such oxygen levels a diffusion flame cannot exist. This is generally the case in gas-turbine combustion. Using the evaporation model of Wise et al. (17), we can derive the static evaporation rate:

$$\dot{m}_E = \frac{4 \pi \lambda r_L}{C_p} \ln(1 + B_{ev}); \text{ where } B_{ev} = \bar{C}_p (T_\infty - T_L)/L \text{ and } \lambda = 1.432 \times 10^{-5} \bar{C}_p (T - 44.67)^{2/3} \text{ W m}^{-1} \text{ K}^{-1} \quad (59)$$

To allow for the effects of droplet dynamics an empirical correlation of the type suggested by Frossling is used (18):-

$$\dot{m}_{E,F} = \dot{m}_E (1 + 0.244 \text{Re}^{1/2}), \quad (60); \quad \text{where } \text{Re} = \frac{2 v_{rel} r \rho_G}{\mu_G} \quad (61)$$

In order to incorporate drag effects into the model an expression is required for the acceleration experienced by an individual droplet, the expression derived by Vincent (19) is used:-

$$\frac{d v_{rel}}{dt} = \frac{3 C_D \rho_a v_{rel}^2}{8 r \rho_l} \quad \text{where } C_D = 0.48 + 28/\text{Re}^{0.85} \quad (62)$$

The only information needed to allow calculation of the evaporation rate is the initial droplet size distribution and the droplet initial velocity, these are normally provided by correlations derived experimentally for the atomizer in use. In our studies, we use the laser diffraction drop size distribution meter which we have developed, to characterize the spray accurately (20).

Before vaporized fuel and oxidant can react, the respective molecules must be brought into intimate contact, the physical processes involved are termed mixing. Mixing is important under combustion conditions since it is usually the rate determining step, however it is the most difficult process to model mathematically. The principle source of mixing energy in a gas turbine combustor is the pressure loss across the turbulence generator, that is the combustion can. Since the velocity and concentration fluctuations decay simultaneously it is proposed that the degree of mixing is equal to the degree of turbulence dissipation within the flow system. An energy balance is performed:

$$\text{Pressure drop across baffle} = \text{Energy "held" in flow velocity profile} + \text{turbulence kinetic} + \text{dissipation} \\ \Delta P/q = \frac{KE_{av}}{q} + \frac{\text{energy}}{3(u'/U)^2} + \frac{\text{energy}}{D/q} \quad (63)$$

It is proposed that a characteristic dissipation time  $\tau_D = C^* \lambda_e / u'_{max}$ , where  $C^*$  = constant (unity),  $\lambda_e$  = mean size of energy containing eddies (0.2Y),  $u'_{max}$  = maximum value of the r.m.s. velocity fluctuations, But  $\tau_s = X/\bar{U}$  ( $X=10Y$ )  $\therefore \tau_{SD} = 50 (u'/\bar{U})_{max}$ , thus using the energy balance (62), this yields  $\tau_{SD} = 50(\Delta P/3q)^{1/2}$

Thus the unmixedness parameter,  $\tau_{SD}$ , used from equation (43) onwards can be related to the system geometry. This parameter has high values for good mixing ( $> 200$ ) and low values ( $< 5$ ) cause "blowout" due to inadequate mixing (fig. 20). A mathematical model of each process has now been described and these are combined using the equations derived earlier (35 + 58). The equations are solved in the following way, firstly a gas temperature is estimated so that an initial evaporation rate for the reactor can be calculated. Then using the above equations the homogeneous feed to a reactor can be calculated and an equilibrium calculation performed to generate the starting values for the iterative calculation. Several iterations of the chemical species equations are performed until the mass convergence test is satisfied, then the energy convergence test is applied. If this is not satisfied then the temperature is corrected by  $(H' - H)/C_p$  followed by recalculation of the fuel evaporation rate and homogeneous feed condition, after which the Newton-Raphson scheme for solving the chemical species equations is re-entered. This decoupling of the energy equation is used to avoid oscillating non-convergence caused by the non-linearity of the temperature terms. Pratt (15) suggests that a more efficient procedure is to solve the fully coupled set of equations and if oscillating non-convergence occurs to partially decouple the energy equation, that is, variations of temperature do not affect the distribution of species concentrations, but concentration changes are allowed to affect the temperature, by setting the appropriate terms in the correction equations to zero. It was found that if the fuel evaporation rate was recalculated every time the temperature was corrected then a slight instability is introduced into the iteration; therefore the evaporation rate is only calculated for the first ten iterations by which time the correction is less than 5K.

We have now derived a method for solving an individual reactor:- we have to devise a sequence of reactors to represent the combustor under consideration. There are several methods which can be used to determine these sequences:- a) Qualitative observations of combustor performance, e.g. for a typical gas turbine combustor this leads to a series model consisting essentially of a stirred reactor followed by a plug flow reactor.

b) The distribution of "macro scale mixing", derived from theoretical and experimental tracer response functions (e.g. water modelling and Argon tracer studies.) c) The distribution of 'micro mixing' energy within the flow; in this method the stirred reactors are placed in the flow regions where high levels of turbulence energy exist. As already discussed above, the 3-D finite difference procedure is used to determine flow patterns and turbulent energy distribution and hence derive the volumes, flow rates and inter-connections of the appropriate stirred reactor network. An example of a gas turbine combustor is shown in fig. 21.

As a simple illustration of the stirred reactor network approach we will discuss its application to a novel design of "blue flame", low pollution burner built at Sheffield (fig. 22). Air is added via a Coanda ejector, which causes controlled recirculation of combustion products thus reducing the oxygen concentration in the vicinity of the spray leading to wake burning. WSR1 is the main flame zone, its volume is set equal to that of the truncated cone bounded by the dotted line (240 cm<sup>3</sup>). The unmixedness parameter,  $\tau_{sp}$ , for this reactor was estimated to be 300, i.e. virtually perfect mixing. The secondary flame zone is represented by a poorly mixed WSR2 (volume 280 cm<sup>3</sup>), this WSR2 was estimated to have  $\tau_{sp}$  of 10, (fig. 22). A cooling of the recirculation flow around the narrow coanda unit annulus is to be expected and was apparent from temperature measurements carried out. Consequently a heat exchanger unit was incorporated into the recycle path to take account of this (fig. 23). The kinetic scheme used for the calculations is shown in table 2, the rate of reaction 1 is given by :-

$$-\frac{d[C_{12}H_{24}]}{dt} = 5.52 \times 10^8 \cdot \exp(-12900/T) \cdot [C_{12}H_{24}]^{\frac{1}{2}} \cdot [O_2] \cdot P^{-0.825} \quad (64)$$

In the experimental system water was condensed in the sampling system therefore for comparison purposes the predicted water concentration was reduced by a factor of 10 and all other concentrations adjusted accordingly. The initial droplet size distribution was described by the Rosin-Rammler expression based on our own experimental results. The spray initial velocity was calculated using discharge coefficients based on Tipler's results (21), assuming that all the droplets were projected with the same initial velocity.

## 6. RESULTS AND DISCUSSION OF THE STIRRED REACTOR ANALYSIS

The predicted values of NO and CO at the burner exit (after WSR2) are plotted against airflow rate (and hence  $\phi$ ) for a given set of operating conditions (Figs. 24 and 25) together with the corresponding experimental values. The effect of fuel pressure on NO emissions is shown in Fig. 26 and in all cases good agreement for both trend and magnitude was obtained.

We have described a program capable of predicting the performance of any sequence of reactors using a detailed evaporation model, the  $\tau_{sp}$  mixing model and a detailed chemical kinetic scheme which may be extended as is necessary. However, several difficulties remain, these are mainly associated with the data available rather than with the computational method. The principal problem is concerned with the chemical kinetic schemes available. The kinetic model currently in use involves a global initiation reaction :

$C_xH_y + \frac{x}{2} O_2 \rightarrow x CO + \frac{y}{2} H_2$  using the rate constant due to Edelman et al (22) eqn. (64) followed by a set of radical reactions leading to complete reaction. This rate constant has recently been revised (Edelman & Harsha 23) the previous value being too fast by several orders of magnitude. This approach deals well with the lean combustion situation but rich combustion still presents a problem as hydrocarbon fragments, radicals and oxygenated species are produced and must be accounted for in the kinetic scheme. In summary there is a need for kinetic information concerning the break-up of higher hydrocarbons ( $x \approx 10$ ) under both rich and lean conditions. In spite of these difficulties, on the lean side of stoichiometric the program works well. Other areas of improvement involve refinement of the model as follows :

- The evaporation model. At present, this is the Wise et al (17) model with a correction for droplet dynamic effects. Further refinements to this model based on the work of W. Sirignano (24), together with reliable data on transport properties and thermodynamic properties at the temperatures of interest for higher hydrocarbons are the hoped for developments in this area.
- In the mixing field, studies of the interaction of reaction and turbulence and how this is related to combustor design are needed.
- A further weakness of the stirred reactor program is that it cannot, at present, predict the formation and agglomeration of soot. This problem can be approached from two directions. In the first, we assume that soot is an undesirable product from gas turbine combustors, and the foregoing design procedure may therefore be used to avoid the local rich conditions under which soot is formed. In the second, an appropriate set of rate equations for soot formation, such as those advocated by Magnussen must be used, and these equations may then be incorporated into the existing computer program with a simple change in the input data. If the fuel to be employed were residual oil or coal which burn with a more complex process than simple evaporation, then the appropriate module of both the computer programs would have to be modified. However, the modular nature of the programs and simple physical form of the variables allow such changes to be made relatively easily.
- At this point, a brief discussion of the relationship between the  $\tau_{sp}$  stirred reactor mixing parameter concepts used above and the coalescence/dispersion micromixing model of Curl (26) is relevant. Curl's model regards the reacting mass as being typically made up of a large number of equally sized 'eddies' behaving as small batch reactors. Eddies undergo collision from time to time and equalize concentrations when this happens. The model does not claim to be an exact description of the processes occurring in a stirred reactor, but predicts a decay in concentration of the same exponential form as that known to exist in stirred systems. The general form of the equation for the rate of change of the concentration probability density function  $p(c)$ , is given by Pratt (27)

$$\frac{d}{dt} p(c) = \alpha[p_0(c) - p(c)] - \frac{d}{dt} [x p(c)] + 8\beta \int_0^c p(c') p(c - c') dc' - 2\beta p(c) \quad (65)$$

where  $\alpha = 1/(\text{mean residence time})$  and  $\beta$  is one half of the fractional number of cells coalescing per second. This equation has normally been solved using Monte Carlo methods, however, in well stirred systems the method of Katz et al (28) may also be used conveniently to compare the predictions of the coalescence/dispersion model with those of the Vulis (29)  $\tau_{sp}$  model used here. For a single stirred reactor the results are

conveniently expressed as the degree of completeness of combustion  $(1 - \psi)$  vs temperature and a typical result is shown in Fig. 27 (see Ref. 30 for further details). It is quite clear from this figure that the same results are obtained with either method. The  $\tau_{SD}$  method has two advantages however: (a) it is much quicker and simpler to calculate, and (b) the asymptotic value of combustion efficiency, limited by unmixedness is simply  $1/(1 + 1/\tau_{SD})$ .

It may be argued that the Monte Carlo methods are more advantageous for predicting the effect of local (fluctuating) high temperatures in producing high  $NO_x$  due to the high activation energy of the reaction. However, to make these predictions, the joint probabilities of the concentrations and temperatures are required and these are not yet available. We must therefore judge by results, and for the situations shown in Figs 24 and 26 it appears that the method used here gives acceptable results. Indeed, if the rate constants for the reactions are obtained in well stirred reactors, then the errors may be self compensating. (There is a similar anomaly in the use of mean temperatures to evaluate the radiant heat flux from flames. Whilst the temperature fluctuations should exaggerate the heat flux due to averaging the non-linear  $T^4$  term, however, it is well known that results acceptable for engineering purposes may be obtained neglecting this effect.) The value of a dimensionless time mixing parameter in assessing gas turbine combustor designs has been demonstrated by Mellor (31). In the preceding discussion it is suggested that  $\tau_{SD} \sim (\Delta P/q)$ . A related expression is given by the eddy break-up model Eq. 12, whilst Pratt (27) suggests that the local mixing intensity  $\beta \sim \epsilon/k$ . Due to the computational simplicity of reactor network modelling and hence its complementary role to finite difference models, more effort is required to evaluate a mixing parameter  $\tau_p$  (or  $\beta$ ) and residence time  $\tau_r$  (or  $1/\alpha$ ), and to define the interconnections within a network. It is also possible that the statistical variations in micromixed  $\tau_{SD}$  between macromixed regions could be represented by a larger number of cells in the network. This approach would then allow for the limitations of the simple  $\tau_{SD}$  model. The advantage of this approach compared to that proposed by Pratt (27) is that it eliminates the computer generated random selection procedure required by the coalescence/dis-persion approach and is therefore much more efficient in the use of computer time.

Evangelista (32) suggested an interesting experimental method of estimating the mixing intensity factor  $\beta$  based on the variance of the response to a step function tracer. A new technique is presented in the next section to determine the residence time distribution in a complex geometry. This allows the size of each sub-reactor and their interconnections (network) to be determined, and by a relatively simple extension would also permit a micromixing intensity factor  $\tau_p$  (or  $\beta$ ) to be determined for each sub-reactor.

## 6. IDENTIFICATION OF STIRRED REACTOR NETWORKS

Mixing in combustion systems is clearly of prime importance since it is usually the rate-limiting step. It is also one of the most difficult processes to model mathematically since present day theories cannot deal with the behaviour of individual molecules. The value of the residence time distribution (RTD) analysis, presented in this section, can be appreciated fully when use is made of such practices in the ultimate refining of the inherent mixing hypotheses of a finite difference formulation.

The link between the finite difference and reactor modelling consists of identifying the appropriate reactor network from the computed flow pattern. The field distribution of turbulence dissipation obtained by the solution of equation (7) is utilized to define possible stirred and plug flow regions with the degree of stirring or mixing rate being determined from the total dissipation within the reactor. Previous work by Swithenbank et al (11) can be utilized extensively in such an analysis. The finite difference part of the predictions can also supply the local flow rates, temperatures and interconnections between the reactors forming the network.

Once an appropriate reactor sequence with associated initial and boundary conditions is decided upon, the full complexity of kinetics, evaporation, mixing and other phenomena are introduced. Thus this "piecewise" approach to predicting turbulent combustion circumvents the conventional problems encountered in physical and mathematical modelling areas and computational requirements. The overall model can be said to share in principle, several aspects of the currently available "refined" models.

Due to our limited understanding of the reactor network and turbulence/kinetics interactions, an experimental technique which can be applied to the complex three-dimensional flows in gas turbine combustors, is plainly required to investigate the phenomena. Water flow visualization has been used extensively as a qualitative method of studying the reaction zones, mixing zones and the interconnecting flows (but not at present, the micromixing parameter  $\tau_p$ ). Clearly this method is related to the concept of the stirred reactor network discussed above. One important difference between water models (or air models) and hot combustor flows is that the former are isothermal. If geometrical similarity is maintained and Reynolds Numbers are chosen to ensure that the model flow is turbulent, then as a result of the well known jet similarity characteristics, the flow patterns in the water model and prototype will be closely related. Using "partial modelling" (33) methods in which the diameters of the holes in the combustor are increased in proportion to the square root of the cold jet to hot chamber gas density ratio, the relative velocities and flow patterns are even more closely modelled. The technique is not able to take full account of the effect of heat release on the turbulence structure, nor the effect of the turbulent fluctuations on the local heat release rate. Nevertheless water (or air) modelling has proved to be an invaluable tool for the combustor designer, and Clarke (34), for example, was able to predict quantitatively the component pressure losses, flow distributions and, with the introduction of a chemical tracer, the exhaust temperature profile.

Theoretical analyses by Dankwerts (35) and Zweitering (36) showed how departures from the assumptions of perfect mixing and ideal plug flow, could be explained in terms of distribution functions for residence times. Novel hypotheses about segregation, hold-up, dead-space, macro and micro-mixedness and age distributions were introduced and related rigorously to reactor performance.

In the present experimental studies, highly specialized identification techniques have been used to investigate their applicability to gas turbine combustor design. These methods are based on correlation and generalized least squares parameter estimation techniques and associated diagnostic tests. In a different context these techniques have been used by Cummins, Briggs and Eykhoff (37) to estimate the dynamic system response of a heat exchanger and a distillation column.

The method is based on the introduction of a tracer in a pseudo-random binary sequence of pulses. In the experiments described below, the tracer was saturated salt solution introduced through a hypodermic needle into a water model of the gas turbine combustor. The response of the system was measured by means of a conductivity probe which could be traversed throughout the chamber. The experiments could be conducted



similarly with a hot or cold combustor using tracers such as mercury vapour (38) or helium (39). Similarly, by modulating the fuel flow, (or air flow), an infra-red measurement of the CO and CO<sub>2</sub> could be used to investigate the dynamics of the kinetic processes. Since only the a.c. response signals are required, a simple I.R. emission or absorption signal would suffice.

The interpretation of the measurements is carried out as follows:- The output signal from a practical system is almost invariably corrupted with inherent micro-mixing noise in the system. Assuming the validity of linearity, application of superposition yields:

$$Z(t) = y(t) + n(t) \quad (66)$$

where  $Z(t)$ ,  $y(t)$  and  $n(t)$  represent the output signal, response signal and noise respectively. The mathematical expression relating the process response and the applied input,  $i(t)$ , is the familiar convolution integral, i.e.

$$y(t) = \int_0^{\infty} h(t_1) i(t-t_1) dt_1 \quad (67)$$

Here  $h(t)$  is the weighting function (or impulse response) of the process.

Combining equations 66 and 67 the measurable output to an arbitrary input signal is given by: (inputs occurring at times greater than  $T_s$  in the past are assumed to have no effect on the present output):

$$Z(t) = \int_0^{T_s} h(t_1) i(t-t_1) dt_1 + n(t) \quad (68)$$

The deconvolution of the above when a short duration pulse is used yields:

$$Z(t) \approx K_1 h(t) + n(t) \quad (69)$$

where  $K_1$  is a constant determined by the energy in the input pulse. The approximation becomes more accurate as the pulse duration becomes shorter. A step function input yields the step response which is the integral of the impulse response. The effect of noise on the system dynamics represented by  $n(t)$  in the above equation can be substantially reduced via correlation techniques.

It can be shown that (40) a relationship exists between the input-output cross-correlation function (ccf) and the input auto-correlation function (acf), i.e.

$$R_{iz}(\tau) = \int_0^{T_s} h(t_1) R_{ii}(\tau - t_1) dt_1 + R_{in}(\tau) \quad (70)$$

(c.f. equation 9)

where  $R_{iz}(\tau)$ ,  $R_{ii}(\tau)$  and  $R_{in}(\tau)$  represent respectively the input-output ccf, input acf and the input-noise ccf. Assuming  $R_{ii}(\tau)$  can be represented by a delta function for random inputs, equation (70) reduces to the following simple form:

$$R_{iz}(\tau) = h(\tau)$$

The practical implementation of a random signal as used in system analysis and identification is a pseudo-random binary signal, PRBS.

The PRBS approximates a truly random signal due to the properties of its acf. For a periodic PRBS, this can be shown to comprise a series of triangular spikes of width  $2t$  where  $t$  denotes the bit interval. Furthermore, due to its constant spectral density the PRBS is persistently exciting - a desired quality of the input signal for parameter estimation and identification studies, as the variance of the estimated system parameters is generally proportional to the inverse of the power input.

Amongst the generally available identification techniques including correlation methods, instrumental variables, maximum likelihood, etc, the generalised least square, GLS, algorithm has proven to be statistically sufficient and is linear in its formulation. The algorithm can provide unbiased estimates, a desirable feature, as data acquired for the formulation of simple dynamic models is almost always corrupted with correlated noise and the need to evaluate unbiased estimates of the process model and of the noise becomes apparent. Additionally, means exist to apply various diagnostic checks.

The algorithm is applied to discrete input/output data sequences  $i_t$ ,  $Z_t$  ( $t=1 \dots N$ ) to produce optimal models of the form:

$$Z_t = \frac{W^{-k} B(W^{-1})}{V^p A(W^{-1})} i_t + \frac{D(W^{-1})}{V^p C(W^{-1})} \xi_t \quad (72)$$

where  $p$  is the number of integrations in the system and noise models.  $W$  represents the forward shift operator and  $k$  is the system time delay.  $V$  is identified as the differencing operator  $(1-W^{-1})$  and  $A, B, C$  and  $D$  are taken to be polynomials of the form:

$$\begin{aligned} A(W^{-1}) &\equiv 1 + a_1 W^{-1} + \dots + a_n W^{-n}; B(W^{-1}) \equiv b_1 W^{-1} + \dots + b_n W^{-n} \\ C(W^{-1}) &\equiv 1 + c_1 W^{-1} + \dots + c_m W^{-m}; D(W^{-1}) \equiv 1 + d_1 W^{-1} + \dots + d_m W^{-m} \end{aligned} \quad (73)$$

In equation 72 the rational transfer function driven by the uncorrelated sequence  $\xi_t$  comprises the entire extraneous behaviour.

Equation 72 can be re-expressed upon removal of the system integrations by data differencing in the following convenient form:

$$AZ_t = W^{-k} Bi_t + \frac{AD}{C} \xi_t \quad (74)$$

It is worth noting that unless  $ADC^{-1} \equiv 1$ , the process parameter estimates will be biased. Hence the GLS aims to transform the term  $ADC^{-1}\xi_t$  iteratively to an uncorrelated sequence  $\xi_t$  via the following steps:

- i) The process parameters ( $a_i, b_i$ ) are initially estimated by an ordinary least squares.
- ii) The residuals, viz,

$$e_t = \hat{AZ}_t - W^{-1} \hat{Bi}_t \quad (75)$$

( $\hat{\phantom{x}}$  denotes estimated values)

are analysed to be subsequently transformed by autoregression.

$$\hat{F} e_t = \xi_t$$

- iii) The process input and output are filtered with the autoregression  $\hat{F}$  to yield:

$$Z_t^F = \hat{F} Z_t \quad (76)$$

$$i_t^F = \hat{F} i_t \quad (77)$$

iv) if  $\hat{F}$  and  $Z$  are modified by a new least squares fit to commence another iteration cycle proceeding from step ii. The final model is expressed in the form:

$$\hat{A}(\hat{F}Z_t) = W^{-k} \hat{B}(\hat{F}i_t) + \xi_t \quad (78)$$

The validity of the estimated process and noise models given by the GLS algorithm have to be established by diagnostic checks for the statistical properties of the models. Currently available diagnostic algorithms utilize model order tests including determinant-ratio test, F-ratio test, loss function analysis, pole-zero cancellation and tests for independence. In addition, auto-correlations of the residuals and cross-correlations of the input and the residuals can be employed to reveal the adequacy of the fitted model.

Tentative values for the time delay and model order can be obtained via the impulse response evaluated directly by cross-correlation of the input and output for white inputs, equation (69). An alternative means of extracting the same information is to use the determinant ratio tests (41). The test is especially valuable in that it limits the number of possible model orders and associated time delays prior to parameter estimation if the signal to noise ratio is reasonably high.

Loss function analysis and the associated F-ratio test are employed once the process and noise models have been derived by the GLS algorithm. They are primarily concerned with the behaviour of the error function in the neighbourhood of  $N_0$ , taken to correspond to the actual system order.

Additionally, residual manipulation in terms of acf's provides a critical assessment of the structure and order of the estimated model. The acf of the residuals is employed to yield an indication of the measure of the whiteness of the residuals. The ccf, on the other hand establishes the statistical independence of the residuals and the process input.

The above ideas have been applied using the salt solution injection tracer technique to study the isothermal residence time distributions in a water model of the Lycoming combustor with the objective of quantifying the stirred and plug flow reactor locations. The predicted aerodynamic patterns yielded by the finite difference procedures are utilized in conjunction with the GLS algorithm to determine the local mixing history. A detailed description of the experimental set up and the measuring environment is given in (7).

The investigation employed PRBS and step signals respectively as the system mode of excitation for parameter estimation purposes. The particular PRBS adopted comprises a period 15, bit interval 1.1 sec which was fed to a solenoid valve introducing the tracer. A number of measuring stations, representative of the distinct mixing zones in the combustor, were chosen for identification and parameter estimation. A typical sequence of operational steps adopted in such an analysis is summarized as follows:

A determinant ratio test was employed to limit the number of possible model orders for the range of time delays suggested by the deconvoluted impulse response. GLS parameter estimation was then applied for varying model orders and time delays. The optimum value for the latter was taken as that which minimized the sum of squared residuals. Typically noise model orders of 10-15 were adopted in an iterative scheme of 5-10 steps. The loss function was recorded for all the different cases tried.

Diagnostic checks comprising mainly the evaluation of the acf of the residuals, ccf between the input sequence and the residuals and pole-zero cancellation were applied for varying model orders and time delays. Parameter estimation and subsequent validation was carried out in a strict iterative manner. Finally the impulse response function corresponding to the estimated model was computed and this was compared with the original weighting sequence obtained from the cross-correlation analysis of the input/output data.

Measurements were made at locations marked on Fig.2 using both the conventional step response method and the p.r.b.s. technique. The results obtained using step changes in salt concentration are illustrated in Fig. 28. The sharp cut off at station 2 within the primary jets is clearly demonstrated. The recirculation in the primary zone which behaves as a stirred reactor is illustrated by the response at stations 1, 7 and 8. The time constant of the exponential decay together with the known primary flow rate of 0.075 l/s indicates an effective primary volume of 0.2 l which is consistent with the anticipated value. The secondary zone response is indicated by the results at station 12. Correcting the measured time constant for the effect of the primary zone and the additional secondary flow gives the volume of the secondary stirred reactor as 0.15 l.

Turning next to the p.r.b.s technique, some of the results obtained are given as follows:-

Station	Location	Order	Time Delay	$a_1$	$a_2$	$b_1$	$b_2$
7	Primary	1	2	- 0.5718	-	- 112.9	-
13	Primary	2	1	- 0.7527	- 0.1171	3.157	- 116.5
9	Secondary	2	3	- 0.2929	- 0.2929	- 78.34	- 61.83
14	Dilution	2	4	- 0.3389	- 0.5284	- 17.14	- 112.3

The corresponding response curves (together with Station 14 integral) are shown in Fig. 29, which represent the fitted value of the cross correlation function. Integrating these curves gives a representation of the step response which can be used to determine the residence time distribution as discussed above, however it appears that the p.r.b.s. method gives greater resolution as can be seen by comparing the response at Station 14 with its integral. The experimentally determined cross-correlation (pulse response) at station 19 is particularly interesting since this point is on the opposite side of the axis to the trace injector. The response at this point is therefore due to turbulent transport rather than convection. The fact that it is about identical to that above the axis shows the large scale of the turbulent transport, and this is responsible for the fact that the primary zone behaves as one large stirred reactor rather than as six small reactors. The effect of the reactor size is to increase the throughput at blow-off (i.e. large stability loop) as discussed in Ref. 11.

In principle the value of the mixing parameter  $\beta$  (or  $\tau_p$ ) can be crudely obtained from the location of the maximum of the variance of the step response (see Ref. 27), however in well stirred systems such as this, the location of the maximum is so close to zero that it cannot be clearly distinguished. This characteristic is easily demonstrated by inserting representative values of  $t_s^{-1}$  and  $\beta$  in Evangelista's Equation  $t_{|<y(t)>>\max} = (1/(\beta - t_s^{-1})) \ln((\beta + t_s^{-1})/2 t_s^{-1})$  (79).

Thus, taking a residence time  $t_s = 1$  sec and  $\beta > 100$  gives the time of the maximum variance  $t_{|<y(t)>>0.04}$  seconds. Fortunately in highly stirred systems such as gas turbine combustors the results are insensitive to the exact value of  $\tau_p$  (or  $\beta$ ). In fact, the combustion efficiency is more significantly influenced by the uniformity of the fuel distribution and the production of  $NO_x$  may be more influenced by the



joint probability distribution of concentrations and temperature (which is at present unknown), than by the exact value of  $\tau_p$ . Since probability distributions tend towards gaussian when they depend on the combination of several other probability distributions, almost whatever the shape of the separate distributions, it is likely that any effects of the p.d.f. on pollutant formation can be represented by a maximum of five parallel stirred reactors (with recycle) in the model, the size and operating of each weighted according to a portion of the gaussian curve.

If an accurate value of  $\tau_p$  were required to determine the ultimate combustion efficiency achievable by any given combustor  $\eta_{\max} = 1/(1 + 1/\tau_{SD})$  then it is believed that the noise term in Eq. 72 could be used to obtain this parameter quite accurately, however we have not yet investigated this possibility.

## 7. CONCLUSION

An overall modelling procedure has been described, and by comparison with experiment it has been demonstrated that all the key physical and chemical factors controlling the behaviour of a real gas turbine combustor were predicted with sufficient accuracy to be of engineering value. It is therefore considered that progress is being made in this complex and rapidly evolving subject.

## 8. ACKNOWLEDGEMENT

Financial support for this work has been received from the Science Research Council and USAF grant No. . This support is gratefully acknowledged.

## NOMENCLATURE

### i) Finite difference equations

a	Absorption coefficient for radiation.
B	Driving force for mass transfer (dimensionless).
$C_1, C_2, C_D$	Constants in the turbulence model.
$C_p$	Specific heat.
$C_R$	Constant in the eddy break-up model.
E	Black body emissive power.
g	Mean square concentration fluctuation of fuel species.
$G_K$	Quantity in the generation term for k.
$H_{fu}$	Heat of combustion.
I, J, K, L, M, N	Radiation fluxes in the r, x and $\theta$ directions.
k	Kinetic energy of turbulence.
$\lambda$	Length scale of turbulence.
L	Latent heat of vapourization.
$m_J$	Mass fraction of a species J, mass fraction in size range J.
$m_{fu}, m_{ox}, m_{pr}$	Mass reactions of fuel, oxygen and product respectively.
$\dot{m}$	Mass transfer rate.
$\dot{m}'''$	Rate of fuel injection per unit volume.
M	Mass of a single droplet.
p	Pressure.
$Q^x, Q^y, Q^z$	Net radiative transfer in the coordinate directions.
$R_J$	Mass rate of creation of species J by chemical reaction.
$R^x, R^y, R^z$	A dependent variable for radiation fluxes in the three coordinate directions.
r	Distance from axis of symmetry, instantaneous drop radius.
s	Stoichiometric mass ratio.
S	Square of droplet radius.
$S_c$	Scattering coefficient for radiation.
$S_\phi$	Source term.
T	Absolute temperature.
$T_g$	Local gas phase temperature.
$T_s$	Droplet surface temperature.
t	Time.
u, v, w	Velocity components in the x, r and z (or $\theta$ ) direction.
$\vec{v}$	Velocity vector.
x, z	coordinate distances.
$\Gamma$	Diffusion coefficient, gas phase transport property.
$\Gamma_{J,eff}$	Effective exchange coefficient for J.
$\Delta V$	Injection cell volume.
$\epsilon$	Dissipation rate of turbulence.
$\mu$	Viscosity.
$\rho$	Density.
$\sigma$	Stefan-Boltzman constant.
$\phi$	General dependent variable.
$\phi_{inj}$	Contribution of the injected mass to the variable
$\phi$	Coordinate in the cylindrical-polar system.

### ii) Stirred Reactor equations

$A_j$	Pre-exponential factor of the jth reaction.
$B_j$	Reverse reaction rate of the jth reaction.
$b_j$	Rate constant of the reverse of reaction j.
$B_{ev}$	Transfer number in evaporation rate equation $[\bar{C}_p(T - T_L)/L]$

joint probability distribution of concentrations and temperature (which is at present unknown), than by the exact value of  $\tau_p$ . Since probability distributions tend towards gaussian when they depend on the combination of several other probability distributions, almost whatever the shape of the separate distributions, it is likely that any effects of the p.d.f. on pollutant formation can be represented by a maximum of five parallel stirred reactors (with recycle) in the model, the size and operating of each weighted according to a portion of the gaussian curve.

If an accurate value of  $\tau_p$  were required to determine the ultimate combustion efficiency achievable by any given combustor  $\eta_{\max} = 1/(1 + 1/\tau_{\text{SP}})$  then it is believed that the noise term in Eq. 72 could be used to obtain this parameter quite accurately, however we have not yet investigated this possibility.

## 7. CONCLUSION

An overall modelling procedure has been described, and by comparison with experiment it has been demonstrated that all the key physical and chemical factors controlling the behaviour of a real gas turbine combustor were predicted with sufficient accuracy to be of engineering value. It is therefore considered that progress is being made in this complex and rapidly evolving subject.

## 8. ACKNOWLEDGEMENT

Financial support for this work has been received from the Science Research Council and USAF grant No. . This support is gratefully acknowledged.

## NOMENCLATURE

### i) Finite difference equations

a	Absorption coefficient for radiation.
B	Driving force for mass transfer (dimensionless).
$C_1, C_2, C_D$	Constants in the turbulence model.
$C_p$	Specific heat.
$C_R$	Constant in the eddy break-up model.
E	Black body emissive power.
g	Mean square concentration fluctuation of fuel species.
$G_K$	Quantity in the generation term for k.
$H_{fu}$	Heat of combustion.
I, J, K, L, M, N	Radiation fluxes in the r, x and $\theta$ directions.
k	Kinetic energy of turbulence.
l	Length scale of turbulence.
L	Latent heat of vapourization.
$m_J$	Mass fraction of a species J, mass fraction in size range J.
$m_{fu}, m_{ox}, m_{pr}$	Mass reactions of fuel, oxygen and product respectively.
$\dot{m}'$	Mass transfer rate.
$\dot{m}'''$	Rate of fuel injection per unit volume.
M	Mass of a single droplet.
p	Pressure.
$Q^x, Q^y, Q^z$	Net radiative transfer in the coordinate directions.
$R_J$	Mass rate of creation of species J by chemical reaction.
$R^x, R^y, R^z$	A dependent variable for radiation fluxes in the three coordinate directions.
r	Distance from axis of symmetry, instantaneous drop radius.
s	Stoichiometric mass ratio.
S	Square of droplet radius.
$S_c$	Scattering coefficient for radiation.
$S_\phi$	Source term.
T	Absolute temperature.
$T_g$	Local gas phase temperature.
$T_s$	Droplet surface temperature.
t	Time.
u, v, w	Velocity components in the x, r and z (or $\theta$ ) direction.
$\vec{v}$	Velocity vector.
x, z	coordinate distances.
$\Gamma$	Diffusion coefficient, gas phase transport property.
$\Gamma_{J,eff}$	Effective exchange coefficient for J.
$\Delta V$	Injection cell volume.
$\epsilon$	Dissipation rate of turbulence.
$\mu$	Viscosity.
$\rho$	Density.
$\sigma$	Stefan-Boltzman constant.
$\phi$	General dependent variable.
$\phi_{inj}$	Contribution of the injected mass to the variable
$\phi$	Coordinate in the cylindrical-polar system.

### ii) Stirred Reactor equations

$A_j$	Pre-exponential factor of the jth reaction.
$B_j$	Reverse reaction rate of the jth reaction.
$b_j$	Rate constant of the reverse of reaction j.
$B_{ev}$	Transfer number in evaporation rate equation $[\bar{C}_p(T-T_L)/L]$

$C_i$	Overall gas phase mass fraction of ith species.
$\bar{C}_p$	Mean heat capacity of gas phase.
$C_D$	Droplet drag coefficient.
$D$	Dissipation energy term.
$d_{ij}$	Third body efficiency of species i in reaction j. (usually assumed to be 1).
$E_j$	Activation energy of the jth reaction.
$\dot{E}$	Fuel evaporation rate.
$F_j$	Forward reaction rate of reaction j.
$F_i^0$	Standard molar free energy of species i.
$f_j$	Forward rate constant of reaction j.
$\dot{H}_L$	Rate of enthalpy loss from the reactor.
$h_i$	Specific enthalpy of species i.
$K_j$	Equilibrium constant of jth reaction.
$KE_{av}$	Mean kinetic energy.
MT	Total number of mixed gaseous species.
m	Mass of reactor gas phase.
NR	Total number of reactions.
NT	Total number of gaseous species.
$n_j$	Temperature exponent in modified Arrhenius equation.
P	Pressure.
$p(c)$	Concentration probability density function.
$\dot{P}_i$	Rate of production of species i by chemical reaction.
q	Dynamic head.
R	Universal gas constant.
Re	Reynold's number of droplet.
r	Reaction rate.
$r_L$	Droplet radius.
T	Temperature.
$T_L$	Temperature of droplet surface.
U	Mean velocity.
$u'$	Fluctuation velocity.
V	Reactor volume.
$v_{rel}$	Velocity relative to droplet.
$W_i$	Molecular weight of species i.
$X_j$	Third body concentration in a dissociation reaction j.
$\alpha$	Reciprocal mean residence time.
$\alpha_{ij}$	Stoichiometric coefficient of species i as a product, in reaction j.
$\beta$	$\dot{E}/\dot{m}$ , non-dimensionalized evaporation rate. Mixing intensity factor.
$\gamma_i$	Mass fraction of species i in reactor mixed gas phase.
$\delta_{ij}$	Stoichiometric coefficient of species i as a reactant in reaction j.
$\epsilon$	Mass of reactor liquid phase.
$\lambda$	Mean thermal conductivity of gas phase.
$\mu$	Viscosity.
$\rho$	Density.
$\sigma_j$	Index to indicate whether the third body participates.
$\tau_D$	Characteristic dissipation time.
$\tau_s$	Reactor residence time.
$\tau_{SD}$	$\tau_s/\tau_D$ , unmixedness parameter.
$\phi_u$	Proportion of gas phase which is unmixed.
$\omega_i$	Mass fraction of species i in reactor unmixed gas phase.
Superscripts	
*	Feed conditions.
	Intermediate value (i.e. after mixing and evaporation).
Subscripts	
1	Reactor inlet.
2	Reactor outlet.
G	Gas phase.
L	Liquid phase.
f	Fuel.
$N_2$	Nitrogen.
$O_2$	Oxygen.
cs	General combustion species.
i	Chemical species identifier.
j	Chemical reaction identifier.
E	Evaporation.
E,F	Forced evaporation.

## REFERENCES

1. Patankar, S.V. and Spalding, D.B. "A calculation procedure for heat, mass and momentum transfer in three-dimensional parabolic flows", *Int. J. Heat and Mass Transfer*, 15, pp. 1787 - 1806, 1972.
2. Launder, B.E. and Spalding, D.B. "The numerical computation of turbulent flows", *Computer Methods in Applied Mechanics and Engineering*, Vol. 3, pp. 269-289, 1974.
3. Spalding D.B. "Mixing and Chemical reaction in steady confined turbulent flames", 13th (Int.) Symposium on Combustion, 1971.
4. Gosman, A.D. and Lockwood, F.C. "Incorporation of a flux model for radiation into a finite difference procedure for furnace calculation", 14th (Int.) Symposium on Combustion, pp. 661-671, 1973.
5. Gosman, A.D. and Pun, M.W. Lecture Notes for course entitled "Calculation of Recirculating Flows", Imperial College of Science and Technology, December, 1973.
6. Edelman, R.B., Schmotolocha, S. and Slutsky, S. "Combustion of liquid hydrocarbons in a high-speed airstream", *AIAA Journal*, Vol. 9, No.7, 1971.
7. Turan, A. "A three-dimensional mathematical model for gas turbine combustors", Ph.D. Thesis, University of Sheffield, 1978.
8. Lockwood, F.C. and Shah, N.G. "An improved model for the calculation of radiation heat transfer in combustion chambers", *Proceedings of ASME-AICHE National Heat Transfer Conference*, 1975.
9. Bray, K.N.C. "The interaction between turbulence and combustion", 17th. Symp (Intl.) on Combustion. The Combustion Institute, Pittsburgh, 1979.
10. Boysan, F. and Swithenbank, J. "Spray Evaporation in Recirculating Flow", 17th. Int. Symp. on Comb. The Combustion Institute, 1979.
11. Swithenbank, J., I. Poll, D.D. Wright & M.W. Vincent, "Combustion Design Fundamentals", 14th. Combustion (Int.) Symposium, Pennsylvania, p.627, 1973.
12. Poll, I., Payne, R., Swithenbank, J. and Vincent, M.W. Second International Symposium on Air Breathing Engines, Sheffield, 1974.
13. Prior, D.S., "Pollutant Minimization by Blue Flame Staged Combustion", Ph.D. Thesis. Sheffield University, 1976.
14. Osgerby, I.T., "An efficient numerical method for stirred reactor calculations", A.E.D.C. Report No. TR-72-164.
15. Pratt, D.T. and Wormeck, J.J., "CREK, A computer program for calculation of Combustion Reaction Equilibrium and Kinetics in laminar or turbulent flow", Washington State University, Report No. WSU-ME-TEL-76-1, March, 1976.
16. Gordon S., and McBride, B., "Computer program for calculation of complex chemical equilibrium compositions, NASA SP-273 (1971).
17. Wise, H. et al, 5th. Combustion (Int.) Symposium, p.32, 1955.
18. Frössling, N. "The evaporation of falling drops", *Gerlands Beitrage Zur Geophysik*, 52, p.170, 1938.
19. Vincent, M.W., "Fuel spray evaporation in gas turbine combustors", Ph.D. thesis, Sheffield University, 1973.
20. Swithenbank, J. et al., "A laser diagnostic for the measurement of droplet and particle size distribution", A.I.A.A. Paper No. 76-69. Now published in "Experimental Diagnostics in Gas Phase Combustion Systems", *Progress in Astronautics and Aeronautics*, ed. B.T. Zinn, vol. 53, pp. 421, 1977.
21. Tipler, W. "The measurement and significance of fuel spray momentum", Shell Technical Report No. APD 202/62M, 1962.
22. Edelman, R.B. and Fortune, O., "A quasi-global chemical kinetic model for the finite rate combustion of hydrocarbon fuels", *AIAA paper* 69-86, 1969.
23. Edelman, R.B. and Harsha, P.T. "Some observations on turbulent mixing with chemical reactions", *Progress in Astronautics and Aeronautics*, vol. 58, Ed. L.A. Kennedy, pp.55, (1978).
24. Sirignano, W.A., "Theory of Multicomponent Fuel Droplet Vaporization", presented at Vth International Symposium on Combustion Processes, Sept. 1977, Krakow, Poland, to be published in *Archives of Thermodynamics and Combustion*.
25. Magnussen, B.F. and Hertager, B.H. "On Mathematical Modelling of Turbulent Combustion with Special Emphasis on Soot Formation and Combustion", 16th International Symposium on Combustion, p. 719, 1977.
26. Curl, R.L. A.I.Ch.E. J. 9, 175 (1963).
27. Pratt, D.T. "Mixing and Chemical Reaction in Continuous Combustion", *Prog. in Energy and Comb. Sci.* Vol. 1. No. 2/3 (1976).
28. Katz, S., Evangelista, J.J. and Shinnar, R. "Scale-up criteria for stirred tank reactors", New York University, City College, 1967.
29. Vulis, L.A. "Thermal Regimes of Combustion", McGraw Hill, 1961.
30. Dixon, G.T., "Fundamentals of Gas Burner Design", Ph.D. Thesis, Sheffield University, 1970.
31. Mellor, A.M., "Gas Turbine Engine Pollution", *Progress in Energy and Comb. Sci.*, Vol. 1. Pergamon Press, 1976.
32. Evangelista, J.J., Shinnar, R.R., and Katz, S., "Effect of Imperfect Mixing on Stirred Combustion Reactors", 12th. Symposium (Intl.) on Comb. The Combustion Institute, p.901, 1969.
33. Spalding, D.B. "The Art of Partial Modelling", 9th. Symp. (Int.) on Comb. The Combustion Institute, p.833, 1962.
34. Clarke, A.E., Gerard, A.J. and Holliday, L.A. "Some Experiences in Gas Turbine Combustion Practice Using Water Flow Visualization Techniques" 9th. Symp. (Intl) on Comb. The Combustion Institute, p.878, 1962.
35. Dankwerts, P.V. "The Effect of Incomplete Mixing on Homogeneous Reactions", *Ch.Eng. Sci.* Vol 11, 1, 1959.
36. Zweitering, T.N. "The Degree of Mixing in Continuous Flow Systems", *Ch. Eng. Sci.* Vol.11, 1, 1959.
37. Eykhoff, P., (Ed.) "Identification and System Parameter Estimation", Part 1. *Int. Fed. of Automatic Control*, Elsevier, 1973.
38. Topps, J.E.C., "An Optical Technique for the Investigation of Flow in Gas Turbine Combustors", 17th Symp (Int.) on Comb. The Combustion Institute, 1978.
39. Tilston, J.R. and Stoner, J.R. "An Investigation of the Internal Flow Mechanisms in a Pegasus 6 Combustion Chamber Using A Gaseous Tracer Technique" NGTE Note No. NT 957, 1975.
40. Lee, Y.W., "Statistical Theory of Communication", John Wiley & Sons, 341, 1960.
41. Billings, S.A., Ph.D. Thesis, Sheffield University, 1975.

Table 1. WSR COMBUSTION SCHEME

(1) Liquid fuel	+	Evaporated fuel (unmixed)	EVAPORATION
(2) Evaporated fuel (unmixed)	+	Evaporated fuel (mixed)	
Oxygen (unmixed)	+	Oxygen (mixed)	MIXING
Nitrogen (unmixed)	+	Nitrogen (mixed)	
(3) Evaporated fuel (mixed)	)		
+	)		
Oxygen (mixed)	)		
Oxygen (mixed)	)		
+	)		
Nitrogen (mixed)	)		
	+	Combustion products	CHEMICAL REACTION

Table 2. Kerosine Combustion, Reaction Mechanism

Reaction step	Forward reaction rate data $A_j$	$E_j$ (cal/mole)	$n_j$
$C_{12}H_{24} + 6 O_2 + 12 H_2 + 12 CO$			
$CO + OH \rightleftharpoons CO_2 + H$	$0.56 \times 10^{12}$	544	0
$H + O_2 \rightleftharpoons OH + O$	$0.22 \times 10^{15}$	8450	0
$O + H_2 \rightleftharpoons OH + H$	$0.18 \times 10^{11}$	4480	1
$OH + H_2 \rightleftharpoons H_2O + H$	$0.219 \times 10^{14}$	2592	0
$OH + OH \rightleftharpoons H_2O + O$	$0.575 \times 10^{13}$	393	0
$H + O + M \rightleftharpoons OH + M$	$0.53 \times 10^{16}$	-2780	0
$H + OH + M \rightleftharpoons H_2O + M$	$0.14 \times 10^{24}$	0	-2
$H + H + M \rightleftharpoons H_2 + M$	$0.30 \times 10^{16}$	0	0
$O + O + M \rightleftharpoons O_2 + M$	$0.47 \times 10^{16}$	0	-0.28
$N + O_2 \rightleftharpoons NO + O$	$0.64 \times 10^{10}$	3150	1
$N_2 + O \rightleftharpoons NO + N$	$0.76 \times 10^{14}$	38000	0
$N + OH \rightleftharpoons NO + H$	$0.32 \times 10^{14}$	0	0
$N_2 + O + M \rightleftharpoons N_2O + M$	$0.162 \times 10^{12}$	1601	0
$N_2O + O \rightleftharpoons NO + NO$	$0.458 \times 10^{14}$	12130	0
$N_2O + O \rightleftharpoons N_2 + O_2$	$0.381 \times 10^{14}$	12130	0
$N_2O + H \rightleftharpoons N_2 + OH$	$0.295 \times 10^{14}$	5420	0

(Backward reaction rates evaluated from equilibrium constants obtained from free energy function).

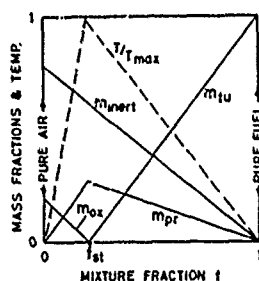


Fig. 1. Mass fractions and temperature v's mixture fraction.

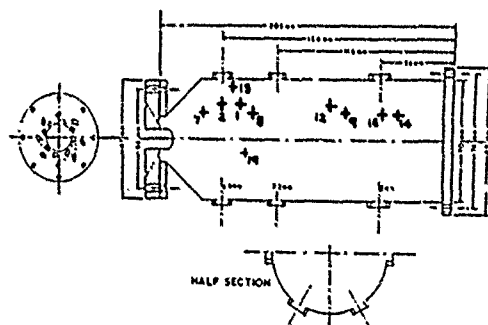


Fig. 2. Gas turbine combustor can.

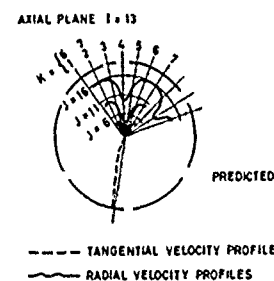


Fig. 4. Cold flow radial and tangential velocity profiles.

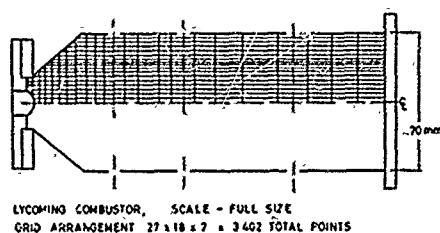


Fig. 3. Finite difference grid.

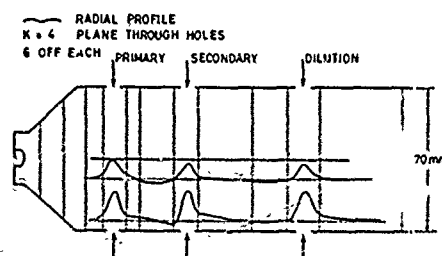


Fig. 5. Cold flow radial velocity profiles.

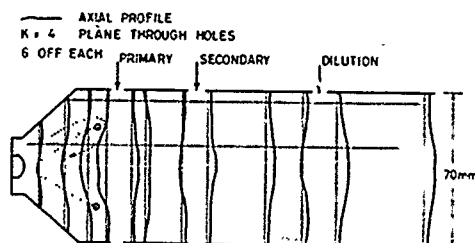


Fig. 6. Cold flow axial velocity profiles.

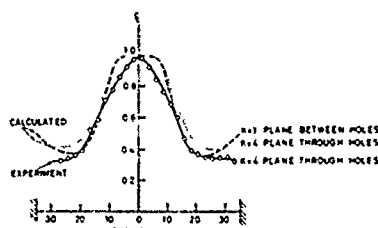


Fig. 7. Cold flow axial exit velocity-predicted and measured.

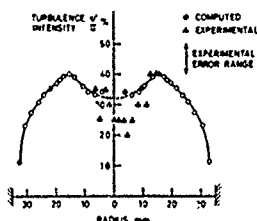


Fig. 8. Exit turbulence intensity profile with combustion.

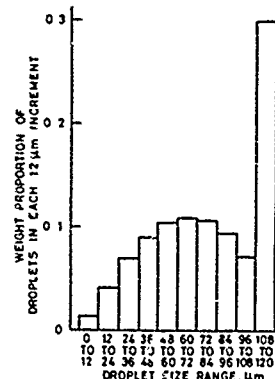


Fig. 9. Droplet size distribution.

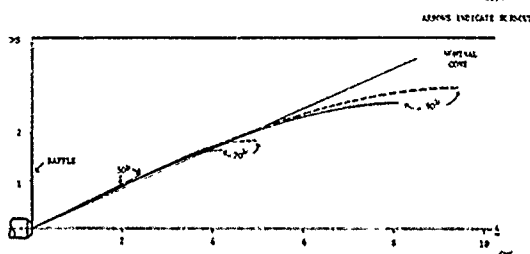


Fig. 10. Predicted droplet trajectories with and without heat-up time.

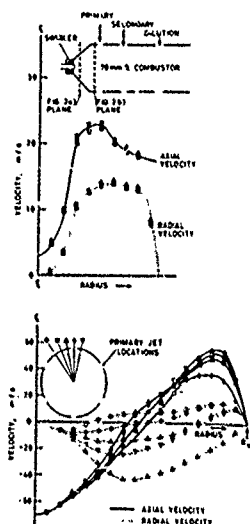


Fig. 11. Axial and radial velocity distributions in primary zone.  
 a) 19 mm downstream of full nozzle.  
 b) 6 mm upstream of primary jets.

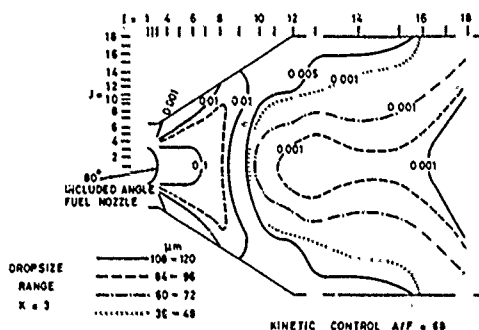


Fig. 12. Predicted droplet concentration distribution.

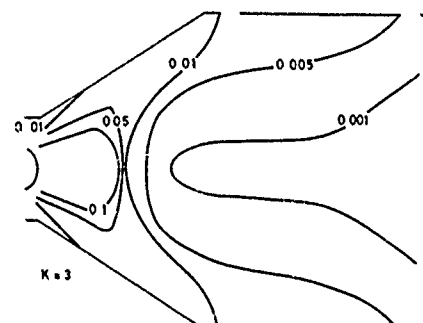


Fig. 13. Mass fraction of fuel evaporated but unburned.

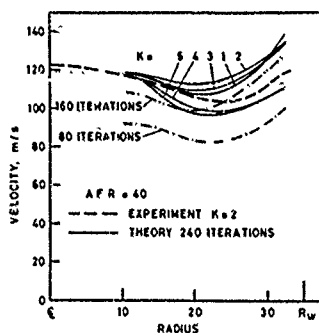


Fig. 15. Predicted and measured exit velocity profile with combustion.

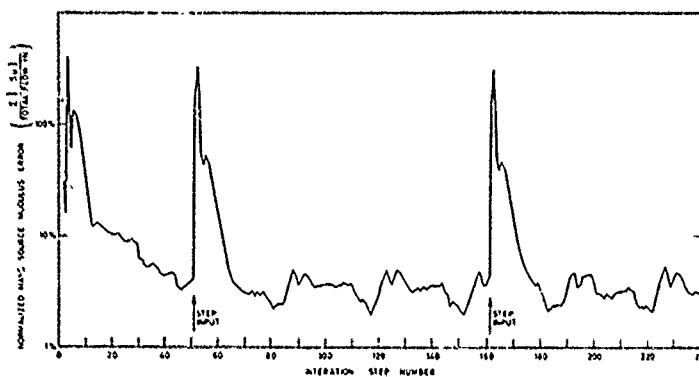


Fig. 14. Mass source convergence criterion v's iteration step number.

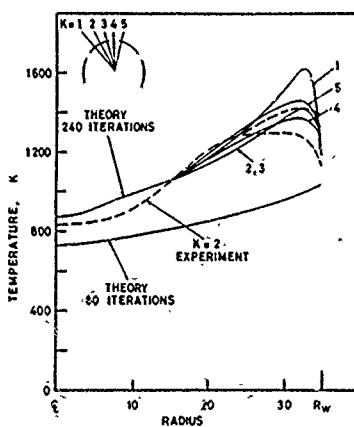


Fig. 16. Predicted and measured exit temperature profile with combustion.

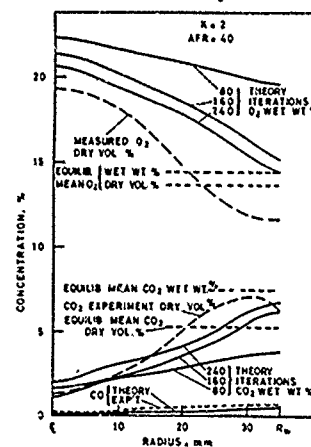


Fig. 17. Predicted and measured exit concentration profiles.

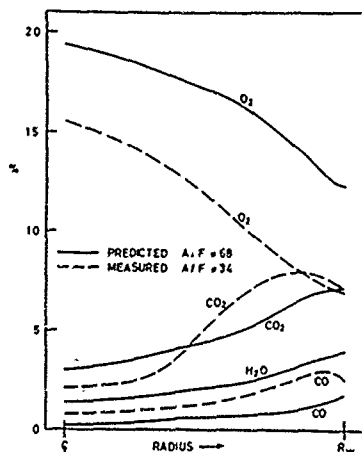


Fig. 18. Predicted and measured concentrations 20 mm downstream of primary jets.

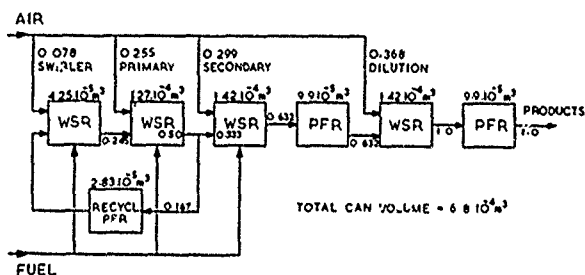


Fig. 21. Reactor network model.

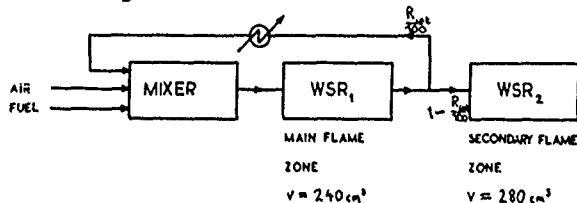


Fig. 23. Blue flame burner stirred reactor network.

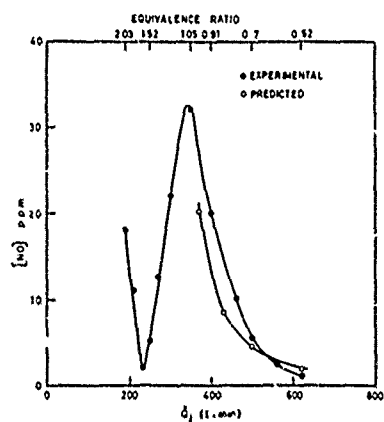


Fig. 24. Predicted and measured NO concentrations.

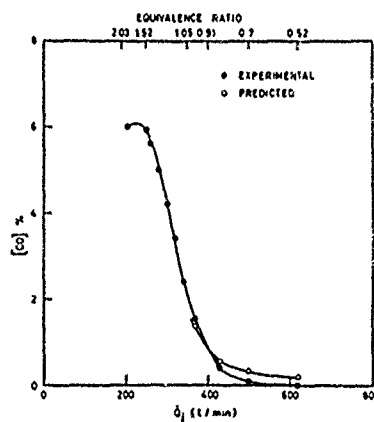


Fig. 25. Predicted and measured CO concentrations.

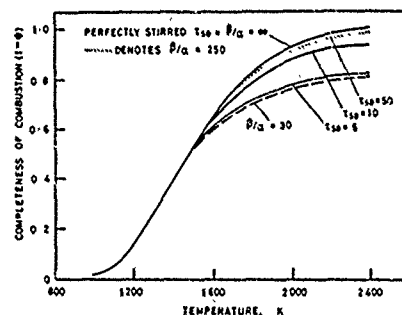


Fig. 27. Comparison of  $\tau_{sp}$  and  $\beta/\alpha$  methods for computing partially stirred reactor performance.

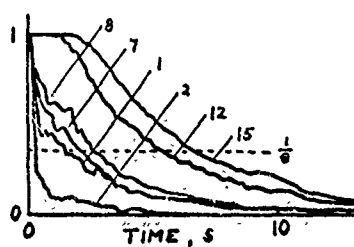


Fig. 28. Variation of concentration with time for step input.

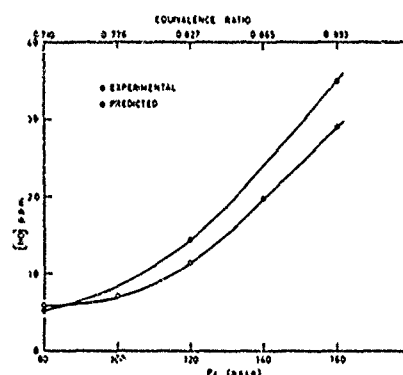


Fig. 26. Effect of fuel pressure (flowrate and drops size) on NO.

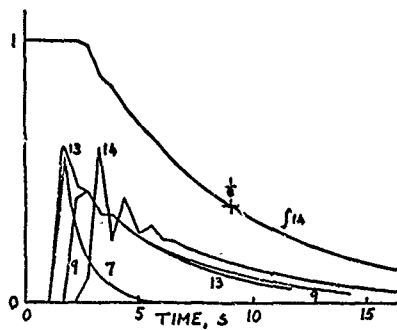


Fig. 29. Impulse response computed P.R.B.S. input.

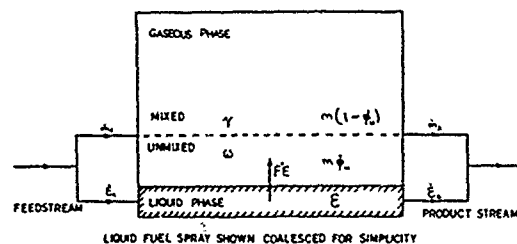


Fig. 19. General steady state well stirred reactor model.

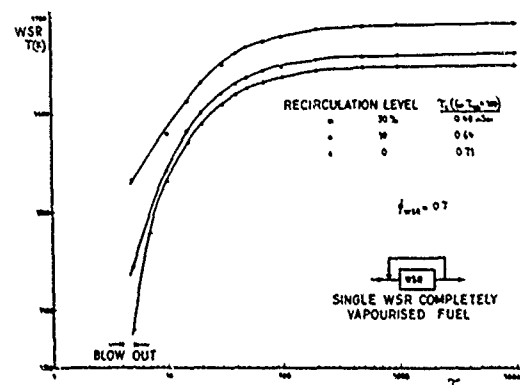


Fig. 20. Effect of mixing parameter  $\tau_{sp}$  on WSR temperature.

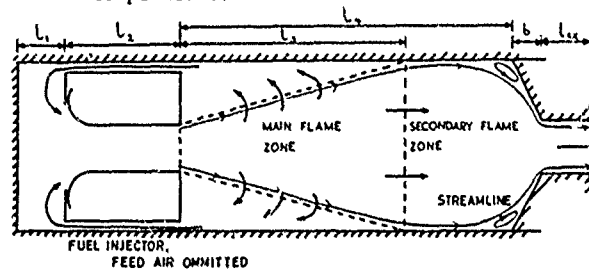


Fig. 22. Schematic representation of blue flame burner zones.

## DISCUSSION

A.M.Mellor, US

Have you made any in situ spray drop size distribution measurements with the forward scattering apparatus? This is actually desired for input conditions for the reacting finite difference code.

Author's Reply

Using the laser diffraction droplet size distribution meter, we have carried out some measurements in emulsified fuel flames and steam assisted atomizer flames, but not yet in gas turbine combustors. The effect of ambient temperature and pressure on droplet size distribution should be investigated urgently.

The input to the computations also requires the droplet velocity distribution. I would like to emphasize that most current methods of obtaining spray information yield spatial rather than temporal size distribution and it is now becoming important that we take account of the difference. At Sheffield we are measuring the droplet velocities by two techniques. In the first a modified laser doppler system is used, whilst the second employs a double flash ruby laser to obtain a time lapse hologram of the spray. The diffraction pattern of the hologram yields the spray velocity distribution directly.

J.H.Whitelaw, UK

Professor Swithenbank said that he would prefer to have 20 droplet size ranges in his finite difference calculations. Our experience, in the Fluids Section at Imperial College, suggests that many fewer will be required with the range of diameters discussed in the presentation.

The phrase "all trends have been correctly predicted", used in the presentation can be misleading to the designer. In this connection, the comparison of calculated mean velocity profiles, normalized with a centreline velocity in a confined flow, can hide important discrepancies. The phrase is probably best avoided and the presentation of comparisons, by the calculating community at large, requires greater consideration of the designers' requirements.

Author's Reply

My proposal that 20 droplet size ranges is generally satisfactory is based on spray evaporation computations which we carried out, (M.W.Vincent Ph.D. Thesis 1976), in which we used 6, 20 and 40 size ranges at typical gas turbine combustor operating conditions. The results for 20 and 40 droplet sizes were identical whilst that at 6 sizes showed significant errors.

With respect to predicted velocity profiles, I would suggest that both computational and experimental mass balance requirements ensure that the weighted mean values will agree. It is interesting to note in our results that the mass flow distribution does not change much with heat addition and the velocity profiles largely reflect the change in temperature distribution. If this were a general trend it could be used to help speed up the convergence of the equations.

A.Sotheran, UK

The processes which determine the various performance aspects of a combustor are known in most cases and empirical correlations are already adequate to ensure that new designs achieve, for instance, specification light up characteristics, idling efficiency. . . whilst  $\text{NO}_x$  emissions are similarly predictable. Whilst modelling seems unlikely to improve design techniques in these respects, at least in the short term they can instruct the designer on how to engineer new concepts like staging. There are new problems and possibilities on which present background experience is sparse or irrelevant and modelling might best concentrate on these. They include soot and particle formation, changing fuel properties and their effects, liner temperature and life prediction with increasingly arduous conditions and so on. Models which ignore the major unknowns are seriously incomplete.

Author's Reply

I disagree with your claim that current correlations are adequate for all purposes. For example, the airlines find that light-up reliability is far from ideal and scheduled flights are regularly delayed by light-up problems. Similarly, the idle efficiency of many engines still leaves much to be desired. I also expect the modelling techniques will help to optimize staging, indeed the very concept of staging derives from a model of the combustion process. However, I agree that modelling techniques are not yet fully developed and my paper aimed to indicate the current state of the "science". With respect to soot and particle formation, the paper by Edelman et al. at this meeting shows how progress is being made in deriving a sub-model for this process which can be readily incorporated in the overall combustor models which were presented.

I welcome your comments on the importance of liner temperature and life. The important feature to predict is the peak liner temperature and in most cases this is associated with non-uniformities in the spray distribution. There is relatively little *fundamental* work on the atomization process and the factors which affect the variability of the spray and mixture distribution and I certainly advocate more work in this area.



Comment by R.B.Edeiman, US

I will be talking tomorrow about the work that we are arguing in expanding the steps higher up in the mechanisms to include pyrolysis and partial oxidation particularly relevant to the question of soot formation.

C.M.Coats, UK

How sensitive are the stirred reactor models you have described to uncertainties in the assumed reaction scheme, particularly the representation of the hydrocarbon chemistry by a single global reaction.

Author's Reply

The rate constants of the semi-global reaction are determined from stirred reactor experiments so the prediction of stability loops, etc. is quite accurate. It is difficult to assess the accuracy of the assumed reaction scheme at a wide range of conditions, although the results of network calculations carried out to date appear reasonably satisfactory.

D.T.Pratt, US

- (1) With respect to Figure 27: of course, both solutions agree, as they are both *asymptotic* solutions to the problem; however, in poorly-mixed regions, they may not agree with the actual physics, much less with the Monte Carlo solution.
- (2) The statement on p.2-10, § 2, "However, to make . . . are not yet available" is categorically wrong. On the contrary, the joint PDF's of C and T are *predicted*; that is in fact the object of doing the calculation!

Author's Reply

I agree with these points and believe that in principle much more can be extracted from stirred reactor modelling concepts than has been achieved to date. Much more experimental and theoretical work is needed in this area.

D.C.Dryburgh, UK

There is a large loss of resolution when one goes from a 3-D finite difference model with about 30 000 grid points to a network of 6 or 7 well stirred or plug flow reactors. What is the advantage of using a reactor network instead of the detailed 3D calculation?

Author's Reply

There are two main advantages of the reactor network approach: Firstly, it is possible to include highly complex chemical kinetic schemes which would not be possible with our present 3-D scheme.

Secondly, the computer time required for our reactor network programme is very small. Other important advantages of the concept are discussed in detail in Prof. Pratt's paper in this conference.

J.McGuirk, UK

I would like to question your claim that the 3D numerical solution you have obtained is converged. From the residual source variation you show in Figure 14, if the procedure is converging at all, it seems to be converging to a solution with a mass source of about 2% - do you not find this disturbing? If the finite-difference solution ought to do anything, it ought to obey overall mass conservation.

Author's Reply

It is made clear in the paper that the 3-D computation was not continued to ultimate convergence, nor were the relaxation parameters optimized, as this would have consumed an unjustified amount of computer time. I guess it's a case of the common engineering approach of achieving 95% of the results with 5% of the effort.

J.P.Patureau, Fr

- (1) Did you account for radiation heat transfer in the WSR computer model?
- (2) How many iterations are required (on the average) for convergence of the WSR computer model?

Author's Reply

- (1) Heat transfer was included in the blue flame burner reactor network presented in the paper although in this case it was convective loss rather than radiation. There would be no difficulty in including a simplified zone method of radiative heat transfer.
- (2) There are various iterations carried out in the subroutines of the WSR network computation. I can best answer your question by saying that the overall computation only requires two or three minutes on a medium size computer.

**H. Wilhelmi, Ge**

The equations for the computation or modelling of combustors became more and more complicated in the course of the years, as there is a tendency to include additional parameters. It was mentioned in the presentation of the paper that the time required for the solution of the procedure described is about six hours on a high speed computer. How is this in accordance with the statement that it will be possible in the near future to perform the same calculations on a minicomputer without any simplifying assumptions in the basic equations but merely using convergence promoting features, grid optimisation etc.

**Author's Reply**

The possibility stems from the fact that whilst bulk storage (e.g. a disc) is necessary for the large number of variables involved, with appropriate manipulations only a small number are actually required in "core" for computation at any one time. In spite of the fact that the *full* computation would require a relatively long time on a mini-computer with (FPP) the situation would be preferable to that at present where, at Sheffield, we can only obtain one turn-around per week on a larger machine.

With respect to future developments, the problem of the slow "diffusion of information" across a fine grid can probably be solved by the super-position of coarser grids (the multi-grid approach). This would give about a three fold increase in speed. A further factor of about two could emerge from the hybrid grid technique. The optimization of the relaxation parameters could give a further two-fold increase in speed. The use of logarithmic values of the concentration should make the composition equations more linear and further speed-up the convergence. I therefore see about an order of magnitude increase in speed in the longer term.

## Mathematical Modelling of Gas-Turbine Combustion Chambers

W.P. Jones and J.J. McGuirk

Department of Chemical Engineering and Chemical Technology  
Imperial College  
London SW 7

## SUMMARY

A mathematical model for predicting the performance of gas turbine combustion chambers is described. The model is based on the finite difference solution of the averaged forms of the governing partial differential conservation equations and turbulent transport is approximated via a variable density form of the  $k-\epsilon$  turbulence model. The reactions associated with heat release are assumed sufficiently fast for chemical equilibrium to prevail on an instantaneous basis; and the influence of local turbulent fluctuations in mixture strength accounted for by a  $\beta$ -probability density function. Liquid fuel sprays are represented by a transport equation for the probability density function describing the variation of droplet mass fraction with droplet radius. Computations of 2-d axisymmetric and 3-d flows are compared with experimental results and an assessment made of the adequacy of the various submodels embodied in the prediction procedure.

## INTRODUCTION

The majority of gas turbine combustion chamber designs in current use have evolved over many years of largely empirical development. Whilst this approach has been relatively successful in the past, current interest and legislation concerning the reduction of combustion generated pollutant emissions has imposed additional constraints, so that large departures from conventional design practice are becoming necessary. In this case existing conventional design information is of restricted value and the development of low emission combustion chambers is thus an expensive and time-consuming process. In fact it is unlikely that the necessary reductions in pollutant emission levels can be achieved by purely traditional methods while at the same time maintaining the no less important requirements concerning such features as re-light, stability, combustor exit temperature pattern and durability; a more fundamental approach is needed. In such circumstances the contributions which could be made by theoretical procedures for predicting combustor performance are potentially substantial. The provision of such prediction procedures represents an area of great current interest and is the subject of the present paper.

## PREVIOUS WORK

Mathematical models for predicting combustion chamber performance can be considered in general terms to fall within two groups: methods based on a modular approach and those based on finite difference solution of the appropriate partial differential conservation equations. The primary objective of the former approach is in most cases the prediction of pollutant emission levels whereas in the latter wider objectives may be considered (e.g. prediction of outlet temperature profiles). In the modular approach spatial variations in dependent variables such as velocity and temperature are largely ignored and no attempt is made at calculating the local detailed features of the flow and reaction, except insofar as complex kinetic schemes may be included. Instead the combustor is divided up into a number of regions each of which is modelled globally using stirred and plug flow reactor concepts. Exhaustive reviews of such methods have already been provided elsewhere, Mellor (1 & 2), and we will concern ourselves here only with their general features, by way of illustration of which we may consider one of the more sophisticated models, namely that described by Fletcher, Siegel and Battress (3) and Fletcher and Heywood (4). In this model the combustor primary zone is modelled by a partially stirred reactor with assumed AFR and residence time distributions and 'unmixedness' described via a single mixing parameter, the value of which must be assigned. The primary zone is followed by a one-dimensional plug flow reactor in which dilution air on entry is assumed to instantaneously distribute itself across the combustor. Thus in addition to the essential arbitrariness involved in assigning the various reactor volumes and residence times, for any particular combustion chamber, a value of the mixing parameter must be chosen. The model parameters depend strongly on the geometric and other details of the particular combustor being considered. They are invariably chosen so as to reproduce some measured emission level: the only quantity which the model is capable of predicting. It should be appreciated that the above features are not peculiar to the model of Fletcher et al; the deficiencies are common to all reactor network models. In practice the use of such models appears to be restricted to interpolation along the operating curve of individual combustors for which some measured pollutant emission level data is available and which can be used as a basis for selecting the model parameters. Even in this case it is often not possible to use fixed model parameters if it is desired to encompass conditions from idle to full power. e.g. see Mellor (5).

An alternative and much more powerful approach is that based on use and finite difference solution of the averaged forms of the partial differential conservation equations for momentum, mass, chemical species and energy. This approach is however also not without its difficulties as in the averaging process information is lost so that the resulting equations are not closed. Approximations must be introduced for unknown terms representing turbulent 'diffusive' transport and the ensemble averaged values of net formation rate of the various species before solution is possible. However in contrast to modular approaches approximations have to be introduced at a much more fundamental and soundly based physical level. In the conservation equation approach approximation is introduced to relate well defined physical (i.e. directly measurable) quantities whereas in modular approaches the model parameters invariably relate somewhat nebulous and ill defined global quantities, e.g. reactor mixedness. Whilst requiring a large computer the provision of calculation methods for practical combustion systems based on finite difference solution of the 3-dimensional

forms of the conservation equations has in the past few years become viable. An assessment of the appropriate models required is given, for example, by Jones and Whitelaw (6) and Bray (7) and the approach has been used to predict the flow and combustion in gas turbine combustors by Jones et al (8), Serag-Eldin and Spalding (9), Reynolds et al (10) and Jones and Priddin (11). The approaches are generally similar with some not inconsequential differences occurring in the modelling of reaction. Such techniques are beginning to be used as design aids by industry and in our view are the only ones profitable to pursue.

Some authors have attempted to combine reactor models with finite difference flow solutions. For example, Mosier, Roberts and Henderson (12) modelled the combustor primary zone recirculation with a well stirred reactor and the remaining flow region was approximated by a set of reacting co-annular one-dimensional stream tubes which exchange momentum, mass and energy. Such modelling implies that the combustor flow (excepting the primary zone recirculation) is two-dimensional with a preferred flow direction and no recirculation. Clearly whether or not this is an acceptable approximation will depend on the particular combustor being considered. However in our view the mass and velocity of air entering the combustor through dilution holes will in the vast majority of designs be sufficiently large to ensure that the combustor flow is three-dimensional and elliptic, i.e. downstream influences make themselves felt upstream over most of the combustor. Perhaps the most sophisticated attempt to combine reactor network models and finite difference solutions is that of Swithenbank, Turan and Felton (13). A computer code and prediction method developed by Spalding and co-workers was used to obtain a full three-dimensional solution to the velocity and temperature fields within the combustor, albeit with a combustion model making no allowance for fluctuations in mixture fraction. The velocity and turbulent solutions were then used to select the volumes and distribution of the various interconnected stirred and plug flow reactors. The selection of the reactor network is now less arbitrary than in a straight modular approach, though it still depends on a subjective interpretation of the finite difference solutions. In common with other reactor models, the technique allows only the calculation of total pollutant emission levels and the problems in assigning individual reactor parameters remain. For example Swithenbank et al modelled a low pollution combustor with an isothermal mixer followed by two well stirred reactors. These two stirred reactors were assigned unmixedness parameter values as widely separated as 300 and 10 - the basis for these values was not given - and the model then used to obtain prediction of NO and CO emission levels in quite good agreement with measured values over a range of operating conditions. This was achieved in spite of the fact that the rate constant for the global fuel breakdown reaction was too large by several orders of magnitude. In general there can be no rational way of estimating the values of the unmixedness parameters and they will in any case vary from combustor to combustor and also with the precise reactor network chosen. Thus in the case of, say, a new or novel combustor design one might well question whether one would be any better off guessing values for mixedness parameters rather than estimating the pollutant emission levels directly after a careful examination of the finite difference solution.

#### PRESENT CONTRIBUTION

The purpose of the present paper is to describe the work being undertaken by the authors towards developing a computational procedure for predicting combustion chamber performance. As stated above this is based on the finite-difference solution of the averaged conservation equations governing the transport of mass, momentum and energy within the combustor. The computational aspects of the procedure (e.g. finite-difference formulation, solution algorithms and techniques for handling irregular shaped geometries) are not discussed here, rather emphasis is laid on describing the physical models used to approximate the turbulent transport processes and chemical reaction; this forms the topic of the next section. Examples of predictions in two and three-dimensional flows are then presented so that some assessment may be made of the models currently in use. Finally, the concluding section contains some suggestions for possible improvements.

#### MATHEMATICAL MODEL

The problems associated with devising a mathematical model based on solution of the averaged forms of the governing transport equations for practical combustion systems are many and varied. In general it may be necessary to provide models for a large number of separate but inter-related phenomena. Typically models may be required to describe turbulent transport in variable density situations, to evaluate the time (or ensemble) average of the net formation rate of each of the chemical species being considered, and to describe radiative heat transfer, and multi-phase phenomena including the formation and consumption of particulate matter including soot and liquid fuel sprays. In the case of gas turbine combustion chambers not all of the above phenomena are of equal importance. For example the heat loss to the surrounds by radiative heat transfer is rarely greater than 1% of the heat release by reaction and so its influence on the combustor flow, heat release and pollutant formation processes can be considered negligible. Of course if the calculation of combustor wall temperature is an objective then radiative heat transfer must be included, but this can be performed after completion of the main flow calculation. Also neglected in the present formulation is the formation and consumption of soot particles. Here it may be presumed that the amounts present, especially in the newer combustor designs, are sufficiently small for their neglect to introduce little error. In principle there appears no reason why the presence of soot particles could not be included in the formulation but, as far as the authors are aware, at the present time there does not appear to be available a tractable scheme for describing soot formation. The determination of the mean formation rates of chemical species represents perhaps the central and unresolved difficulty in developing prediction methods for turbulent reacting flows. Essentially the problem arises because the formation rates are invariably highly non linear functions of temperature and species mass fractions. Knowledge of the mean values of these latter quantities (to be obtained from the solution of the appropriate transport equations) is insufficient to determine the mean value of formation rate. Fortunately however the reactions associated with the high temperature oxidation of hydrocarbons usually have time scales very short compared with those characteristic of the transport processes and the assumption of (instantaneous) chemical equilibrium thus provides a reasonable approximation under many circumstances. Of course it cannot be

appropriate under all circumstances. In particular the calculation of the formation and emission levels of pollutants such as carbon monoxide, unburnt fuel and nitric oxide all require consideration of finite rate reactions as do ignition and extinction phenomena. Nevertheless the assumption does allow the prediction of many of the major features of combustor operation. If in addition to the assumption of fast reaction the diffusion coefficients for all species and heat are taken to be equal - an accurate assumption in turbulent flow - and the heat loss to the surrounds is negligible, then the instantaneous thermodynamic state of the gas is determinable as a nonlinear function of a strictly conserved scalar variable. All the relevant conserved scalar quantities are linearly related and any one can be chosen: here we select a mixture fraction,  $f$ , defined as the mass fraction of fuel present both burnt and unburnt. Alternative choices would be the mass fraction of any element present or fuel-air ratio. With the fast reaction assumption described above the averaged forms of the appropriate conservation equations for high Reynolds number turbulent stationary flows can be written \* :-

$$\text{Mass} \quad \frac{\partial \bar{\rho} \tilde{u}_i}{\partial x_i} = 0 \quad (1)$$

$$\text{Momentum} \quad \frac{\partial \bar{\rho} \tilde{u}_i \tilde{u}_j}{\partial x_j} = \frac{\partial \bar{p}}{\partial x_i} - \frac{\partial \bar{\rho}}{\partial x_j} \tilde{u}_i'' \tilde{u}_j'' \quad (2)$$

$$\text{Mixture fraction} \quad \frac{\partial \bar{\rho} \tilde{u}_j \tilde{f}}{\partial x_j} = - \frac{\partial \bar{\rho} \tilde{u}_j'' \tilde{f}''}{\partial x_j} \quad (3)$$

For liquid fuelled systems the fuel droplets are described by :-

$$\frac{\partial \bar{\rho} \tilde{u}_j \tilde{b}}{\partial x_j} = - s^3 \frac{\partial}{\partial s} \left\{ \frac{\tilde{\rho} \tilde{b}}{s^3} \right\} - \frac{\partial \bar{\rho}}{\partial x_j} \tilde{u}_j'' \tilde{b}'' \quad (4)$$

where  $b(s)ds$  represents the mass fraction of droplets in the droplet radius range  $s$  to  $s + ds$  and where  $\dot{s}$  is the rate of change of droplet radius by a process such as evaporation. Amongst the approximations implied by equation (4) is the assumption that the relative velocity between the droplets and surrounding fluid is zero. While this is unlikely to be a good approximation for large droplets any improvements are likely to bring with them very considerable increases in complexity.

The averaged equations (1) to (4) are the forms resulting from a density weighted decomposition and subsequent averaging of the dependent variables where tildes represent density weighted averages and over-bars conventional averages. It should be noted that equations (1) to (4) are similar to their constant density counterparts. In contrast if conventional averaging were to be used then additional unknown correlations involving the fluctuating component of density would appear. Further details of both averaging processes and their relative merits is given by Bilger (14), Jones and Whitelaw (6) and Jones (15).

Before solution of equations (1) to (4) is possible approximations are necessary. The unknown terms involving the fluctuating component of velocity must be related to known quantities as must the mean values of  $\rho$  and  $\dot{s}$ . The models to be described in the following section are essentially those used by Jones and Priddin (11) though there are here some differences in detail.

#### TURBULENCE MODEL

Equations (2) to (4) contain turbulent fluxes of momentum and the scalar quantities  $f$  and  $b$  which are here approximated via a version of the two equation  $k - \epsilon$  turbulence model introduced by Jones (16) and Jones and Launder (27) and cast in density weighted form.

The density weighted Reynolds stress is obtained from :-

$$\bar{\rho} \tilde{u}_i'' \tilde{u}_j'' = \frac{2}{3} \delta_{ij} k - \mu_T \left\{ \frac{\partial \tilde{u}_i}{\partial x_j} + \frac{\partial \tilde{u}_j}{\partial x_i} - \frac{2}{3} \delta_{ij} \frac{\partial \tilde{u}_k}{\partial x_k} \right\} \quad (5)$$

and the scalar fluxes given by :-

$$\bar{\rho} \tilde{u}_j'' \tilde{f}'' = - \frac{\mu_T}{\sigma_f} \frac{\partial \tilde{f}}{\partial x_j}; \quad \bar{\rho} \tilde{u}_j'' \tilde{b}'' = - \frac{\mu_T}{\sigma_b} \frac{\partial \tilde{b}}{\partial x_j} \quad (6)$$

\* In order to obtain the results to be described the equations were cast in a cylindrical polar coordinate system: for brevity they are here written using Cartesian tensor notation.

The turbulent viscosity is expressed as :-

$$\mu_T = C_\mu \bar{\rho} k^2 / \epsilon \quad (7)$$

where  $k$  and  $\epsilon$  are the density weighted turbulence kinetic energy and dissipation rate of turbulence energy, the values of which are obtained from the solution of the transport equations :-

$$\bar{\rho} \tilde{U}_j \frac{\partial k}{\partial x_j} = \frac{\partial}{\partial x_j} \left\{ \frac{\mu_T}{\sigma_k} \frac{\partial k}{\partial x_j} \right\} - \bar{\rho} \overline{u_i'' u_j''} \frac{\partial \tilde{U}_i}{\partial x_j} - \frac{\mu_T}{\bar{\rho}^2} \frac{\partial \bar{p}}{\partial x_i} \frac{\partial \bar{p}}{\partial x_i} - \bar{\rho} \epsilon \quad (8)$$

$$\bar{\rho} \tilde{U}_j \frac{\partial \epsilon}{\partial x_j} = \frac{\partial}{\partial x_j} \left\{ \frac{\mu_T}{\sigma_\epsilon} \frac{\partial \epsilon}{\partial x_j} \right\} - C_1 \frac{\epsilon}{k} \left\{ \bar{\rho} \overline{u_i'' u_j''} \frac{\partial \tilde{U}_i}{\partial x_j} + \frac{\mu_T}{\bar{\rho}^2} \frac{\partial \bar{p}}{\partial x_i} \frac{\partial \bar{p}}{\partial x_i} \right\} - C_2 \frac{\bar{\rho} \epsilon^2}{k} \quad (9)$$

Equations (8) and (9) differ from their constant density counterparts in that a term involving the product of the mean density and pressure gradients appears. An exact term comprising the product of a fluctuating density-velocity correlation and the mean pressure gradient arises in the density weighted turbulence energy equation. For this an approximation which can be inferred from Jones (15) has been used. A similar term has also been added to the  $\epsilon$ -equation. Strictly both terms should be multiplied by a constant of order unity. The remaining constants were assigned the following values, found to give good agreement in a wide range of 2D shear flows (see e.g. Launder and Spalding (25)).

$$C_\mu = .09 ; C_1 = 1.44 ; C_2 = 1.92 ; \sigma_k = 1.0 ; \sigma_\epsilon = 1.3 \text{ and } \sigma_T = 0.9$$

#### COMBUSTION MODEL

With the 'fast' reaction assumption outlined previously the instantaneous chemical equilibrium gas composition, temperature and density can in the case of gaseous fuelled systems be determined as a non-linear function of the mixture fraction  $f$ . For hydrocarbons explicit expressions relating the species mass fractions, temperature and density to  $f$  cannot be obtained and the instantaneous thermodynamic state was obtained as a function of  $f$  from equilibrium calculations performed with the computer programme described by Gordon and McBride (18). For computational convenience the results were then curve fitted via least squares orthogonal polynomials. Now at any location  $f$  will fluctuate with time and so knowledge of the mean value,  $\bar{f}$ , is insufficient to determine the local mean values of species mass fraction, mean temperature or mean fluid density and it is necessary to know the probability density function (p.d.f.) for  $f$  (or some equivalent information). Following many workers we here chose to specify a two parameter form of the p.d.f. in terms of the mean  $\bar{f}$  and the variance  $\tilde{f}''^2$ . The former is to be obtained from solution of equation (3) whereas  $\tilde{f}''^2$  is to be obtained from :-

$$\bar{\rho} \tilde{U}_j \frac{\partial \tilde{f}''^2}{\partial x_j} = \frac{\partial}{\partial x_j} \left\{ \frac{\mu_T}{\sigma_T} \frac{\partial \tilde{f}''^2}{\partial x_j} \right\} + 2 \frac{\mu_T}{\sigma_T} \left\{ \frac{\partial \tilde{f}}{\partial x_i} \right\}^2 - C_D \bar{\rho} \frac{\epsilon}{k} \tilde{f}''^2 \quad (10)$$

Following Spalding (19) the constant  $C_D$  was assigned the value 2.0.

The p.d.f. introduced is a density weighted quantity and the definition allows the determination of both density weighted and conventional averaged quantities :

$$\text{e.g. } \tilde{\phi} = \int_0^1 \phi(f) p(f) df \quad (11)$$

$$\text{and } \bar{\phi} = \bar{\rho} \int_0^1 \frac{\phi(f)}{\bar{\rho}(f)} p(f) df$$

where  $\phi$  can represent any quantity uniquely related to  $f$  including species mass fraction or temperature. The mean fluid density can be obtained via the p.d.f. definition :-

$$\bar{\rho} = \left\{ \int_0^1 \frac{p(f)}{\bar{\rho}(f)} df \right\}^{-1} \quad (12)$$

Various forms of the p.d.f. have in the past been proposed. A rectangular wave variation of  $f$  corresponding to a double Dirac  $\delta$ -function p.d.f. was suggested by Spalding (19) and used by Gosman and Lockwood (20) and Serag-Eldin and Spalding (9). The  $\delta$ -function form has the attribute of simplicity rather than physical realism and more realistic forms have been proposed and used. In the present work we will utilise the  $\beta$ -p.d.f. first suggested by Richardson, Howard and Smith (21) and used by Jones and Priddin (11). It can be written :-

$$p(f) = \frac{f^{a-1}(1-f)^{b-1}}{\int_0^1 f^{a-1}(1-f)^{b-1} df} \quad 0 \leq f \leq 1 \quad (13)$$

where

$$a = \tilde{f} \left\{ \frac{\tilde{f}(1-\tilde{f})}{\tilde{f}^{n^2}} - 1 \right\}; \quad b = \frac{(1-\tilde{f})a}{\tilde{f}}$$

For liquid fuels it is envisaged that the fuel droplets evaporate to form gaseous fuel which on mixing with air reacts in a similar manner to that assumed for gaseous fuels. However the mixture fraction  $f$  previously defined now includes fuel present both in liquid and gas phases. In order to determine the equilibrium state of the gas mixture it is thus necessary to know the mass fraction of fuel (burnt and unburnt) present in gaseous phase. In order to do this it is necessary to establish some instantaneous relationship between the mass fractions present in liquid and gaseous phases. Here possibly the simplest assumption is made, namely that the ratio of mass fraction of gaseous fuel (burnt + unburnt) to the mass fraction of fuel (burnt + unburnt) in both liquid and gaseous phases does not fluctuate with time. The gas phase mixture fraction can then be obtained from :-

$$f_g = \frac{\left\{ 1 - \frac{\int_0^{\infty} b ds}{\tilde{f}} \right\} f}{1 - f \frac{\int_0^{\infty} b ds}{\tilde{f}}} \quad (14)$$

Equations (11) and (12) now refer only to the gas phase and the mixture fraction appearing therein must therefore be interpreted as the gas phase mixture fraction. This quantity is also used for the evaluation of the chemical equilibrium state.

For two phase mixtures the total fluid density is given by :-

$$\rho = \frac{\rho_g}{1 - \int_0^{\infty} b ds + \frac{\rho_g}{\rho_L} \int_0^{\infty} b ds} \quad (15)$$

where  $\rho_g$  and  $\rho_L$  are the densities of the gas and liquid phases respectively.

Finally to complete the formulation, following Williams (22) the instantaneous rate of change of droplet size through evaporation is taken to be given by :-

$$\dot{s} = - \frac{\mu_g}{\rho_L s Pr} \ln \left\{ 1 + \frac{h_g - h_L}{\Delta h_{fg}} \right\} \quad (16)$$

where  $Pr$  is gas phase molecular Prandtl number and  $\Delta h_{fg}$  is the latent heat.

The instantaneous gas phase enthalpy  $h_g$  and viscosity,  $\mu_g$  are then expressed as a function of mixture fraction and equation (11) then used to evaluate the mean value,  $\bar{s}$ .

#### COMPUTATIONAL DETAILS

The closed set of differential equations outlined in the previous section has been solved by finite-difference techniques for both two- and three-dimensional, reacting and non-reacting problems. The finite-difference formulation uses central differencing except in regions where mean flow convection dominates diffusive processes in which case donor cell differencing is used. The computational scheme is cast in terms of the primitive variables, velocity and pressure and a guess-and-correct procedure is used to obtain the pressure field, see e.g. Chorin (23) and Patankar and Spalding (24). Lack of space prevents a detailed description of the boundary conditions used for each individual problem, but wherever possible these were deduced from the experimental measurements. To avoid the necessity of using fine grids near wall boundaries the finite-difference solutions were patched onto fully turbulent local equilibrium wall-law profiles, see e.g. Launder and Spalding (25). Information on the grid fineness and disposition is given in the next section for each problem discussed, as is the computer time and storage requirements where this is deemed relevant. The number of equations solved obviously varies from problem to problem; for the most complicated case - a liquid fuelled flame in a 3D combustor - a total of 13 differential equations must be solved, namely: continuity, 3 momentum equations, 2 turbulence model equations ( $k, \epsilon$ ), equations for mean mixture fraction  $\bar{f}$  and its variance  $\bar{f}''^2$  and 5 equations to represent the droplet size distribution. These latter equations were obtained from equation (4) by integrating over a given size range  $s_i$  to  $s_{i+1}$  to



obtain an equation for the mass fraction of droplets within this size range. From information on the droplet size distribution produced by the fuel injector considered, 5 size range bands were judged sufficient.

#### RESULTS AND DISCUSSION

As an example of predictions obtained in isothermal flow in a two-dimensional model combustor geometry, the measurements of Owen (26) are first considered. The flow configuration consists of a central air jet surrounded by a faster-moving co-axial annular air stream, both streams exhausting into a circular duct of slightly larger diameter - the flow is therefore axisymmetric. At high velocity ratios (annulus/jet velocity) the central air stream is rapidly entrained by the annular jet and a recirculation region is formed on the duct centre-line; a further negative velocity region is observed near the outer wall caused by the sudden expansion of the duct radius. In Figure 1 the predictions obtained using the two-equation  $k-\epsilon$  model are compared with the measurements of Owen (1975). The Figure shows the predicted and measured position of the separation streamlines which enclose the two recirculation regions described above for a velocity ratio of 12; the predictions were obtained with a fairly fine grid (40 axial x 20 radial grid nodes) and are believed to be grid independent. The agreement is good although both radial and axial dimensions of the central recirculation are under-predicted, a feature which other authors have also observed in calculation of free recirculation regions with two-equation turbulence models.

Measurements have also been made of reacting flow in the same geometry by Spadacini, Owen and Bowman (27); in this case the central air jet was replaced by a jet of natural gas, and the possibility of introducing swirl into the annular air stream was included. The flow field which results under burning conditions is shown in Figure 2 in terms of predicted and measured axial velocity contours. The velocity ratio (air/fuel velocity) in this instance was 21, the overall equivalence ratio 0.9, combustor pressure 3.8 atmospheres and the air and fuel inlet temperatures 750°K and 300°K respectively. Figure 2(a) shows results where the air stream had zero swirl velocity and Figure 2(b) gives the predictions and measurements for the case where the annular air stream also entered with a swirl component of velocity (The swirl No for the run considered was 0.3 (Swirl No = tangential momentum flux/axial momentum flux x effective annulus diameter)). In the first case a central, spheroidal recirculation region is measured as in the isothermal flow, and Figure 2(a) shows that this is also what is predicted. Again the size of the central negative velocity region (shown shaded) is underpredicted. In the reacting flow case the strength of the backflow is in addition found to be too weak, the maximum negative velocities being only about half of those measured. Further the acceleration of the fluid along the centre-line is too slow, particularly in the swirling flow case. The qualitative effect of swirl is however reproduced correctly in that the central negative velocity region changes in shape from spheroidal to toroidal, although again its volume and strength are underpredicted. These calculations were made with a 20 x 20 finite-difference grid, and finer grid solutions are being obtained to check the results. While it is possible that the discrepancies result from numerical error a much more likely possibility is that the inlet conditions used (uniform axial velocity and zero radial component in both streams) are incorrect as the data clearly indicated significant intermittent penetration of the flame into the fuel injector; extension of the calculation domain upstream into the fuel jet and annular air ducts is also being investigated. Comparison of the development of the swirl velocity is shown in Figure 3 which presents profiles across the duct at three axial stations, the agreement is quite good in the outer half of the duct but discrepancies exist near the centre-line at larger downstream distances. The accuracy of the experimental data must also be questioned however as measurements along two radii (open and closed symbols) show large asymmetries.

It can be seen from the above figures that large changes in the flow pattern occur in the immediate vicinity of the fuel injector; the measurements of temperature and species mole fractions were also concentrated in this region and Figures 4 - 7 present comparisons for the same two sets of conditions as outlined above. Figure 4 presents predicted and measured temperature contours and indicates that the introduction of swirl does not change the temperature pattern strongly from that typical of a turbulent diffusion flame with high temperatures occurring in the annular mixing region. Slightly higher temperatures and larger axial gradients occur in the swirling flow case and this effect is reproduced by the predictions, although the radial gradients are much steeper in the calculations than in the data, indicating a too slow rate of mixing. The most noticeable discrepancy occurs in the region near the centre-line where the predictions show the cold fuel jet penetrating far downstream whereas the data show high temperatures very close to the injector. Again, this is attributable to too slow mixing, possibly pointing to a turbulence model inaccuracy; however, the penetration of air up into the fuel jet would also lead to reaction and higher temperatures in this initial region, and as noted earlier, the inlet conditions used did not allow this. In our view this latter explanation is the more probable and, as can be seen, its consequences have far reaching effects on all predicted quantities over large regions of the flow.

The effect of swirl on unburnt hydrocarbon and CO concentration levels in the first 5 combustor diameters is unfortunately not predicted correctly. Once more the slow mixing is in evidence since the UHC contours penetrate too far downstream; however, when swirl is introduced (Figure 5(b)) the measured reduction in unburnt fuel concentration and increase in CO levels (see Figure 6(b)) is not observed. If anything UHC contours are shifted downstream, as is the location of the high CO levels, in complete contrast to the measurements. This behaviour is consistent with the predicted velocity fields for, although the correct influence of swirl was predicted near the inlet, qualitative discrepancies in velocities were evident further downstream. The measurements show swirl to increase the rate of recovery (of velocity) downstream of the recirculation whereas the predictions indicate little change. As a consequence the effect of swirl on the turbulent exchange coefficients for scalar transport is also not reproduced. Similar discrepancies occur in the CO<sub>2</sub> contours, although here the tendency for higher levels to appear at the downstream stations with the introduction of swirl is reproduced by the calculation. The predicted contour map is more complicated than the measured, indicating relative maxima along the centre line. This results from the simplified equilibrium analysis used for the 2D natural gas/air calculations, which is slightly inaccurate for mixtures with equivalence ratio greater than about 15.

The calculation of 2D reacting flows such as that described in the previous paragraphs is, it is believed, essential to the development of the mathematical model. Only in such relatively simple geometries can the detailed measurements be made which are so important if the weak links in the mathematical model are to be isolated; additionally, for 2D recirculating flows the possibility of obtaining fine-grid solutions



not marred by numerical errors is feasible, whereas this is very difficult with present core-store limitations for 3D recirculating flows. It is still worthwhile however to apply the mathematical model to 3D flows as useful information can be gained. The model described earlier is at present being applied to the combustor in Figure 8; at the time the calculations were performed not all details concerning the fuel injector were known, so only preliminary results are presented here. The combustor is basically cylindrical in shape with eight rows of air holes, the first containing 4 (regularly spaced) holes and all others containing 8 holes. The symmetry properties of the geometry meant therefore that only a 90° sector had to be considered if cyclic boundary conditions were used on the two extreme circumferential planes. Four separate air feeds enable the air supply to each row of holes to be calculated, and also that to the vaned swirler (the protrusion of the swirler into the combustor was neglected). Liquid kerosene fuel was injected using a swirl atomiser which in the experiments produced a spray angle of 95° with a mean droplet diameter of about 50  $\mu$ m; finally the cooling air temperature was set at 500° K and the swirl Number at 0.38 (30° vane angle). The calculation was performed using a 25 x 15 x 10 grid (axial x radial x circumferential) which meant that details to the flow through the swirler and the dilution holes could not be resolved accurately. Computational time and storage requirements were approximately 28 minutes CPU time per 100 iterations and 150 K words central memory (IBM 360/195).

Figure 9 shows the predicted and measured temperature fields on a circumferential plane displaced 22.5° from the vertical plane of the combustor as it is sketched in Figure 8; this plane contains neither the dilution air holes, nor the gaps between the swirler vanes, but these are indicated in the figure for reference purposes. In the measurements the high temperatures in the primary zone extend right out to the liner wall, indicating complete penetration of the fuel, probably with impingement of some fuel droplets on the outer wall. At present the predictions display a quite different behaviour resulting from a much too shallow spray angle; the droplets evaporate too slowly and show little spread causing local equivalence ratios to be everywhere much richer than measured. Accordingly the temperature is everywhere too low and the existence of fuel in the vicinity of the centre-line right to the exit of the combustor is qualitatively incorrect. Some high temperatures are predicted in the outer regions interspersed with cool areas near the dilution air entries, but, in the initial part of the combustor, these are caused by recirculation of burned products from downstream between the air jets, and the observation that the fuel does not penetrate into the outer areas remains valid. Predictions of UHC and CO concentrations display similarly incorrect features when compared with measurements. The reasons for the completely incorrect spray angle are at present under investigation; it may be that the conditions assumed at the injector exit are inaccurate or that the method of inputting the spray angle is inadequate. Alternatively the assumption that the droplets follow the instantaneous gas velocity may be at fault - further calculations are being undertaken to isolate the cause of error.

#### CONCLUSION

The paper has given a description of the work being undertaken towards developing a mathematical model for gas-turbine combustion chambers based on finite-difference solution of the averaged equations governing the transport of mass, momentum and heat. The models for approximating turbulent transport and chemical reaction are being tested by calculating isothermal and reacting flows in 2D combustor geometries, and the application of the present scheme to a more realistic 3D combustor is under way, although only preliminary results could be shown here; a complete report of the performance of the model in this 3D geometry will be presented elsewhere. The predictions for the 2D gaseous-fuelled combustor indicate that the presently used models are capable of calculating the flow pattern and heat release fairly well, although lack of knowledge concerning inlet conditions often makes definite conclusions difficult to make. Whilst this uncertainty in the inlet conditions can account for a large part of any discrepancy between measured and predicted quantities, there are also some indications of a failure of the k- $\epsilon$  turbulence model to provide a sufficiently accurate representation of turbulent transport. This is particularly so in the case of flows with swirl. If these inlet condition and turbulence model uncertainties could be removed then a substantial improvement in the prediction of, say, the temperature and species concentration fields would undoubtedly result. It appears likely that the combustion model used here would then be adequate as far as the calculation of major species, temperature and heat release is concerned. However, the accurate prediction of pollutant emissions will undoubtedly necessitate some improvement in the present scheme. For example, although the primary zone CO levels are quite well predicted, combustor CO emission levels under idle power conditions would certainly be in error with the present equilibrium model. The first improvement would be to allow for the finite-rate oxidation of CO to CO<sub>2</sub>; this will involve the inclusion of an assumed form for a two-dimensional joint pdf and the solution of additional differential equations for the mean and the variance of the CO mass fraction and for the CO and mixture fraction covariance. Other extensions to the present model planned are to include the prediction of nitric oxide emissions using the model outlined in Jones (15) and to apply the 2D calculation procedure to the liquid-fuelled flames measured by Spaducini et al (29) in the same axi-symmetric combustor as investigated here; this will enable the droplet model to be adequately tested.

#### REFERENCES

- 1). A.M. Mellor : Current kinetic modelling techniques for continuous flow combustors. Proc. of Symp. on Emissions from Continuous Combustion Systems, Plenum Press (1972)
- 2). A.M. Mellor : Gas turbine engine pollution. Prog. Energy Combust. Sci. 1, 111 (1976)
- 3). R.S. Fletcher, R.D. Siegel & E.K. Battress : The control of oxides of nitrogen emissions from aircraft gas turbines. FAA report FAA-RD-111-2 (1971)
- 4). R.S. Fletcher & J.B. Heywood : A model for nitric oxide emissions from aircraft gas turbine engines. AIAA Paper No. 71-123 (1971)
- 5). A.M. Mellor : Turbulent-combustion interaction models for practical high intensity combustors. XVII Symposium (Int.) on Combustion (1978)
- 6). W.P. Jones & J.H. Whitelaw : Coupling of turbulence and chemical reaction. Proc. of Workshop on Modelling of Combustion and Practical Systems. Los Angeles (1978)
- 7). K.N.C. Bray : The interaction between turbulence and combustion. XVII Symposium (Int.) on Combustion (1978)

- 8). W.P. Jones, W.C. Clifford, C.H. Priddin & R. De Chair : A comparison between predicted and measured species concentrations and velocities in a research combustor. Proc. AGARD 50th Meeting, Turkey (1977)
- 9). M.A. Serag-Eldin & D.B. Spalding : Computations of three-dimensional gas turbine combustion chamber flows. ASME 23rd Int. Gas Turbine Conference. London (1978)
- 10). R.S. Reynolds, T.E. Kuhn & H.C. Mongia : An advanced combustor analytical design procedure and its application in the design and development testing of a premix/prevaporized combustion system. U.S. Section, Combustion Inst. (1977)
- 11). W.P. Jones & C.H. Priddin : Predictions of the flow field and local gas composition in gas turbine combustors. XVII Symposium (Int.) on Combustion (1978)
- 12). S.A. Mosier, R. Roberts & R.E. Henderson : Development and verification of an analytic model for predicting emissions from gas turbine engine combustor during low-power operation. AGARD Proc. 125 (1973)
- 13). J. Swithenbank, A. Turan & P.G. Felton : 3-Dimensional 2-phase mathematical modelling of gas turbine combustors. Project SQUID (ONR) Workshop on "Gas Turbine Combustor design problems" Purdue (1978)
- 14). R.W. Bilger : Turbulent jet diffusion flames. Prog. Energy Combust. Sci. 1, 87 (1976)
- 15). W.P. Jones : Prediction methods for turbulent flows; models for turbulent flows with variable density and combustion (1979) ; to be published by Hemisphere Pub. Co.
- 16). W.P. Jones : Laminarisation in strongly accelerated boundary layers. Ph. D. thesis, Univ. of London (1971)
- 17). W.P. Jones & B.E. Launder : The prediction of laminarisation with a two-equation model of turbulence. Int. J. Heat Mass Trans. 15 (1972)
- 18). S. Gordon & B.J. McBride : Computer programme for the calculation of complex chemical equilibrium compositions. NASA SP 273 (1971)
- 19). D.B. Spalding : Concentration fluctuations in a round turbulent free jet. Chem. Eng. Sci. 26, 95 (1971)
- 20). A.D. Gosman & F.C. Lockwood : Prediction of the influence of turbulent fluctuations on flow and heat transfer in furnaces. Imperial College, Mech. Eng. Rep. HTS/75/53 (1973)
- 21). J.N. Richardson, H.C. Howard & R.W. Smith. IV Symposium (Int.) on Combustion (1953)
- 22). A. Williams : Combustion of sprays of liquid fuels. ELEK Science 1976.
- 23). A.J. Chorin : Numerical solution of the Navier-Stokes equations. Math. Comp. 22, 745 (1968)
- 24). S.V. Patankar & D.B. Spalding : A calculation procedure for heat, mass and momentum transfer in three-dimensional parabolic flows. Int. J. Heat Mass Trans. 10, 1787 (1972)
- 25). B.E. Launder & D.B. Spalding : The numerical computation of turbulent flows. Computer Methods in Appl. Mech. & Engrg, 3 (1974)
- 26). F.K. Owen : Measurements and observations of turbulent recirculating jet flows. AIAA Journal 14, No. 11 (1976)
- 27). L.J. Spadacini, F.K. Owen & C.T. Bowman : Influence of aerodynamic phenomena on pollutant formation in combustion. U.S. Environmental Protection Agency Rep. EPA-600/2-76-247a (1976)
- 28). M. Katsuki, Y. Mizutani & K. Shibuya : An experimental study on the emissions of a model gas turbine combustor. Comb. Sci. & Tech. 17, 11 (1977)
- 29). L.J. Spadacini, J.B. McVey, J.B. Kennedy, F.K. Owen, C.T. Bowman, A. Vranos & A.S. Kesten : Influence of aerodynamic phenomena on pollutant formation in combustion. Phase II - Liquid Fuels. Proceedings of the 2nd Stationary Source Combustion Symposium, 1977. Vol. IV - Fundamental Combustion Research. J.S. Bowen, R.E. Hall (Editors).

#### ACKNOWLEDGEMENTS

The work reported here has been performed under a contract sponsored by Rolls-Royce Ltd. Computing facilities were provided by the Imperial College Computing Centre and the Science Research Council Rutherford Laboratory.

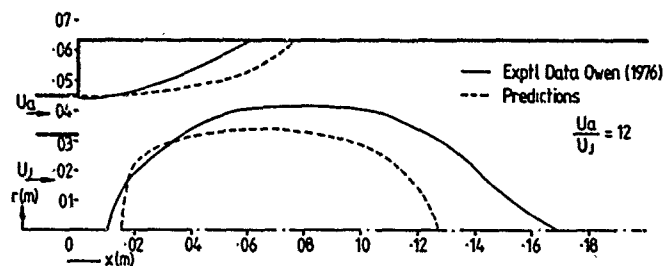


Figure 1 Isothermal co-axial confined jet flow - separation streamlines

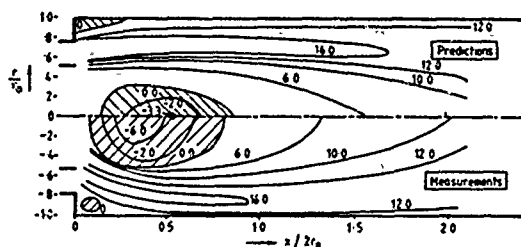


Figure 2(a) Axial velocity contours  
zero air swirl.

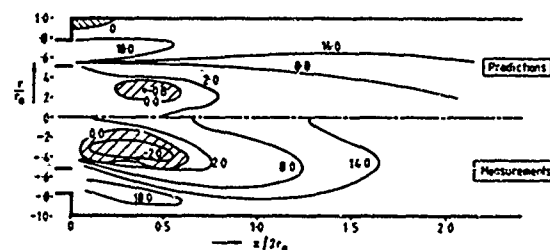


Figure 2(b) Axial velocity contours  
annulus air swirl number = 0.3

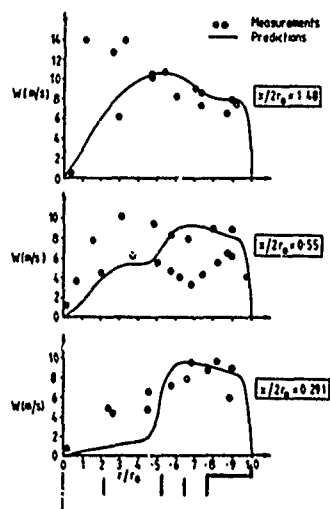


Figure 3 Swirl velocity profiles in reacting flow  
swirl number = 0.3

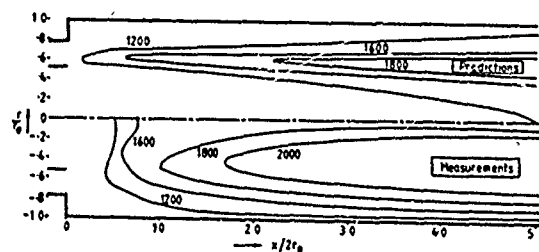


Figure 4(a) Temperature contours ( $^{\circ}\text{K}$ ), zero swirl

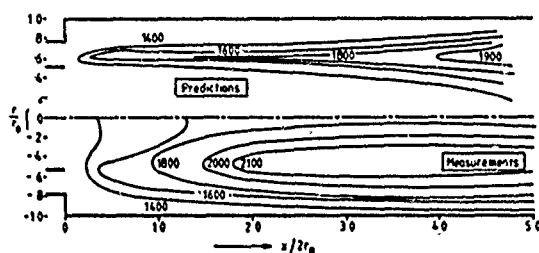


Figure 4(b) Temperature contours ( $^{\circ}\text{K}$ )  
swirl number = 0.3

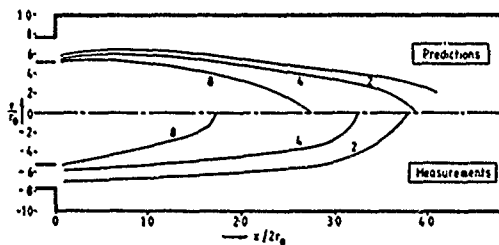


Figure 5(a) Unburnt hydrocarbon contours  
(mole fraction %), zero swirl

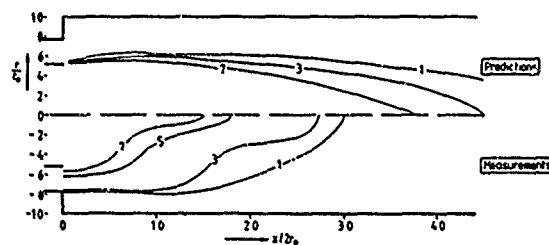


Figure 5(b) Unburnt hydrocarbon contours  
(mole fraction %), swirl number = 0.3

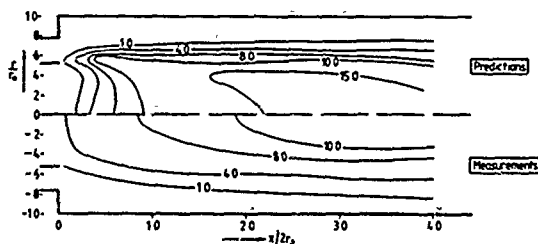


Figure 6(a) CO mole fraction (%), zero swirl

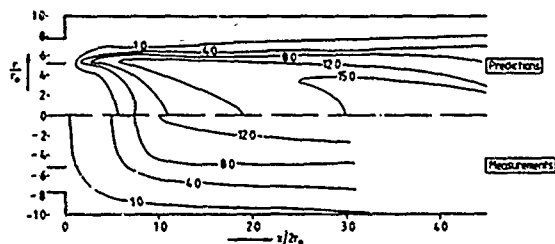


Figure 6(b) CO mole fraction (%)  
swirl number = 0.3

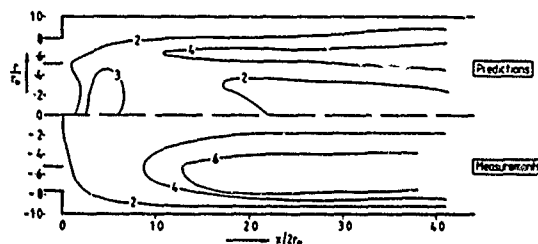


Figure 7(a) CO<sub>2</sub> mole fraction (%), zero swirl

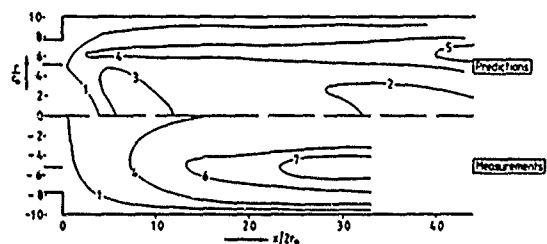


Figure 7(b) CO<sub>2</sub> mole fraction (%)  
swirl number = 0.3

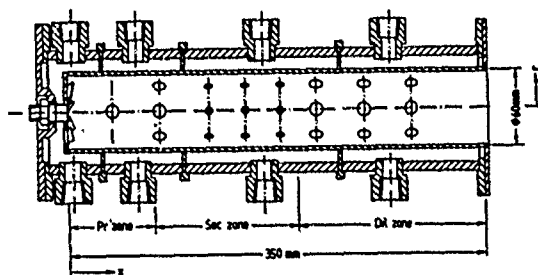


Figure 8 3D combustor geometry

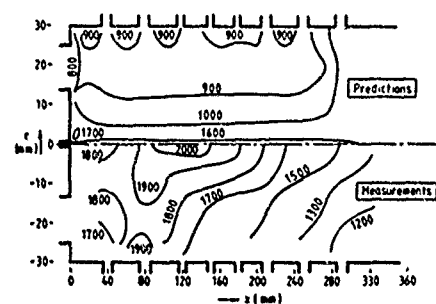


Figure 9 Temperature contours  
3D combustor

## DISCUSSION

**D.T.Pratt, US**

On p.2, you overstate the case when you state "in general, there can be no rational way" etc. . . This is true of Fletcher and Heywood parameter which is really a standard deviation of a Gaussian (F/A) ratio distribution.

However, Swithenbank's  $\beta$  (or  $\tau_{SD}$ ) is easily estimated by  $\sim\sqrt{\Delta P}$  or  $\epsilon/k$ ; the former of course from experimental measurement, the latter perhaps from such a model as you propose.

**Author's Reply**

In our view the construction of stirred reactor models necessarily involves a very large number of essentially arbitrary and ad hoc assumptions related to the selection of reactor volumes, and their locations, residence time and 'mixedness' parameters. At what stage the maximum uncertainty arises will in general depend on the particular model being considered. However to turn to the 'mixedness' parameter  $\tau_{SD}$  to which Professor Pratt refers I am afraid that I simply do not agree that there is a rational basis for selecting its value. Relating  $\tau_{SD}$  to  $\sqrt{\Delta P}$  involves a number of what appear to be extremely dubious assumptions which, for example, take no explicit account of the system geometry. In any case one is still left with the problem of determining the constant of proportionality and how one does this while still leaving something to predict is not at all clear. The alternative suggestion of relating  $\tau_{SD}$  to the local turbulence time scale  $k/\epsilon$  which could be extracted from a finite difference solution does not remove the difficulty. The turbulence time scale is a local quantity which will have different values at each spatial location. However for a stirred reactor model some average single value appropriate to the total reactor volume is required – but how precisely is this average to be formed? This is in addition to the arbitrariness introduced via the estimation of mean residence time.

**J.H.Whitelaw, UK**

It is possible that, in the comparisons which you presented the turbulence model is more at fault at a swirl number of 0.3 than at higher or lower values? Our experience\* with a swirl number of 0.23 and a similar geometry, suggests that there is a region of flow with swirl numbers which give rise to small regions of central recirculation, where the eddy viscosity model gives rise to more significant errors than at higher or lower swirl numbers.

**\*M.Habib and J.H.Whitelaw**

Measured velocity characteristics of confined coaxial jets with and without swirl. To be published in J. Fluid Eng.

**Author's Reply**

The experiments quoted by Professor Whitelaw certainly confirm our contention that, as in the comparisons shown in our paper for reacting flow, a two-equation turbulence model does not adequately account for the effect of swirl on the turbulent transport as the swirl number is increased from zero to an intermediate value of 0.2–0.3. Other calculations we have performed at a higher swirl number (0.6) also indicate the same inadequacies, and, as far as we are aware, there is no evidence that the turbulence model performs any better at even higher swirl numbers.

**R.B.Edelman, US**

Do you establish grid independence and convergence of your solution? What was the grid network you used?

**Author's Reply**

We have grid independent solutions and convergent solutions in 2-D calculations. In 3-D calculations, I think it's not generally possible to establish whether or not a good independent solution is obtained. Indeed I think it's unlikely that you can get a true good independent solution. We used a mesh of  $25 \times 10 \times 15$ . We used about 150 words in the central memory. We did not use any secondary storage. The calculation time was 28 minutes. Good independent solutions in 3-D calculations are a major problem.

## A PREDICTION MODEL FOR TURBULENT DIFFUSION

## FLAMES INCLUDING NO - FORMATION

J. JANICKA

Lehrstuhl für Techn. Thermodynamik, RWTH Aachen,  
D-51 Aachen, Schinkelstr. 8, Germany

W. KOLLMANN

von Karman Institute for Fluid Dynamics,  
Ch. de Waterloo, 72, B-1640 Rhode St Genèse, BelgiumAbstract

A prediction model for turbulent diffusion flames burning gaseous fuels is developed and applied to  $H_2$ -air flames. In the (simplified) system of chemical reactions the fast reactions are assumed in partial equilibrium whereas three-body recombinations are treated in non-equilibrium. For the  $H_2$ -air flames this assumption leads to a description of the reacting system with only two variables  $f$  and  $r$ . Two methods of treating such a system in a turbulent flow are discussed: (1) modelling and solving transport equations for first and second order moments of these variables and prescribing the form of the pdf of  $f$  and  $r$  as a function of the selected moments, or (2) modelling and solving the equation for the pdf of  $f$  and  $r$ . Both sets of equations are complemented with a modified version of the  $k$ - $\epsilon$  turbulence model. The NO-formation in such flames can be calculated using the non-equilibrium values (mean values and covariances) of the O and H radicals. The results obtained with both models are compared with experiments and show good agreement.

LIST OF SYMBOLS

$A_n$	coefficient of pdf	O	oxygen
$A_{\alpha,i}$	Arrhenius coefficient	P	probability density function
$c$	mass fraction	p	pressure
$c_D, c_{\epsilon_1}, c_{\epsilon_2}, c_{\epsilon_3}$	} turbulence model constants	$P$	transition probability
$c_{\epsilon_4}, c_{\rho u_1}, c_{\rho v_1}, c_{\rho v_2}$		q	a priori probability
$c_{\tau_1}, c_{\tau_2}$		R	gas constant
D	nozzle diameter	r	reaction variable
$D_{\alpha,i}$	Arrhenius coefficient	Re	Reynolds number
E	entropy	S	source term
$F_{\alpha,j}$	Arrhenius coefficient	Sc	Schmidt number
$f$	mixture fraction	s	value of r
$g_\alpha$	acceleration of gravity	T	temperature
g	variance of mixture fraction	t	time
H	hydrogen	u	longitudinal velocity component
h	enthalpy	$v_\alpha$	velocity vector
$K_{\alpha,i}$	reaction rate expression	v	radial velocity component
k	kinetic energy of turbulence	w	kinetic source term
L	number of statistical moments	$X_i$	component symbol
M	inert component	$x_\alpha$	Cartesian coordinate
$M_i$	molar mass	x	longitudinal coordinate
m	number of scalar variables	y	radial coordinate
N	nitrogen	z	atomic mass fraction, value of f
n	number of components in mixture		

Greek symbols

$\alpha$	Arrhenius exponent (forward step), exponent of beta-function	$\phi$	flow variable
$\beta$	Arrhenius exponent (backward step), exponent of beta-function	$\pi$	product
$\gamma$	coefficient of pdf	$\rho$	density
$\delta$	Dirac pseudofunction	$\sigma$	Prandtl/Schmidt number
$\delta_{\alpha\beta}$	Kronecker symbol	$\mu$	dynamic viscosity
$\epsilon$	dissipation rate	$\mu_n$	statistical moment of order n
$\Gamma$	molecular transport coefficient	$\nu$	kinematic viscosity
$\chi$	source term of r-equation	$\tau$	time scale
$\psi$	concentration	$\langle \cdot \rangle$	ensemble average

Superscripts

o	nozzle exit	-	instantaneous
∞	ambient	u	unburnt
-	unweighted mean value	v	burnt
'	fluctuating part		

Subscripts

b	backward	j	component in mixture
D	turbulent viscosity	z	component in mixture
e	equilibrium, ambient	o	reference value
f	forward	t	turbulent
i	component in mixture	α	Cartesian component
J	jet pipe exit	β	Cartesian component

1. INTRODUCTION

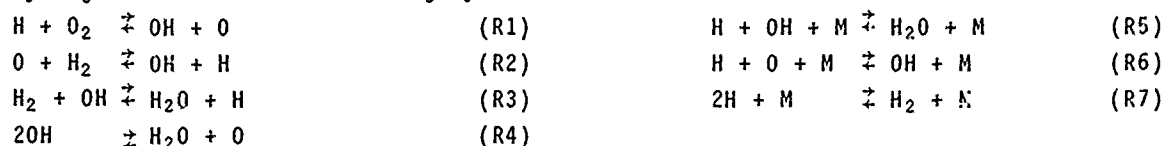
The prediction of the turbulent and chemically reacting flow in gas turbine combustors is an extremely complex problem and far from a satisfactory solution. The investigation of turbulent diffusion flames is a step in gaining predictive capabilities for such complex phenomena. Diffusion flames contain all the important physical and chemical processes but are structurally simpler than combustors. The mathematical treatment of turbulent diffusion flames leads to the well-known closure problem for moment equations which is aggravated by an increased number of fluctuating field variables due to the heat release and different molar masses of mixture components. For this reason the complete prediction model is built up from : the thermo-chemical model describing in a reasonably simplified way the instantaneous transfer of mass and energy, the turbulence model describing the turbulent fluxes of mass, momentum and energy, the coupling model which links thermo-chemical and turbulence model by providing the information about the probability density function of the scalars in the thermo-chemical model that are described by differential transport equations. The pdf plays a central role in this model because it is essential for the calculation of the mean thermodynamic state of the flame at any point of the flow field. The thermo-chemical model for H<sub>2</sub>-air diffusion flames is based on a simplified (Ref. 30) reaction mechanism for H<sub>2</sub>-combustion and assumes partial equilibrium for fast reactions but treats the slow three-body recombinations kinetically (Ref. 5). The turbulent model is based on the k-ε model of Jones and Launder (Ref. 18) and is written in terms of unweighted statistics. To include properly density fluctuations the modelled equations for the density-velocity correlations are added to it. For the coupling model two different approaches to obtain the (two-dimensional) pdf are discussed and the computationally most efficient method is chosen for the current prediction model. The model is then applied to several H<sub>2</sub>-air diffusion flames, for which experimental data including NO-formation are available, to evaluate its properties.

2. THE CLOSURE MODEL

The flow in turbulent flames burning fossile fuels is extremely complex and a complete mathematical description involves an infinite set of nonlinear partial differential equations. This complexity is due to the turbulent nature of the flow and the complicated set of chemical reactions essential to the description of the instantaneous transfer of mass and energy in gaseous systems. Consequently, the development of a closure model will consist of two parts, one devoted to the thermo-chemical processes and the other to the turbulent fluxes. The link between them will be provided by the pdf of certain scalar variables which will be constructed from a small set of statistical moments.

2.1 The thermo-chemical model

The assumptions concerning the instantaneous transfer mechanisms for mass and energy are loosely termed thermo-chemical model. The dispersion of liquid fuel in sprays and its vaporization will not be considered here and attention will be restricted to the gaseous phase. The following assumptions are put forward : all participants in the turbulent and combustible mixture are assumed ideal gases with possibly temperature dependent thermal and caloric coefficients. Thermal equilibrium will be assumed locally and Soret/Dufour effects as well as volume forces and volume viscosity will be neglected. The molecular diffusion in the multi-component mixture will be treated crudely by relations of the Fick-law type. In addition, the diffusivities for all components and energy will be considered equal. Radiative energy transfer will not be taken into account and the Mach number will be significantly smaller than unity. The set of these simplifications is usually referred to as Shvab-Zeldovich assumptions (Ref. 1) and has found frequent application to the mathematical analysis of flames. For the description of the combustion of hydrogen with air the following system of reactions is considered :



This mechanism was suggested by several authors (Refs. 2, 3, 4) as a reasonable description of diffusion flame kinetics. Its range of validity was estimated (Ref. 5) in laminar test calculation and it was found to be a good approximation of the  $H_2$ -air kinetics for temperatures  $T > 1200$  K and conditions close to stoichiometric. In this range the reactions (R1)-(R4) are much faster than the relatively slow three-body recombination reactions (R5)-(R7). This leads to the hypothesis (see Refs. 2, 6) that the fast reactions (R1)-(R4) are in partial equilibrium. The slow reactions (R5)-(R7) are in general not in equilibrium and have to be treated by means of rate equations. In order to make efficient use of this hypothesis combined variables are introduced according to Dixon-Lewis et al. (Ref. 2), in such a way that the kinetic source terms of the new variables do not contain contributions from the fast reactions (R1)-(R4). They are given by

$$C_{O_2}^* = C_{O_2} + \frac{1}{2} \frac{M_{O_2}}{M_{OH}} C_{OH} + \frac{M_{O_2}}{M_O} C_O + \frac{1}{2} \frac{M_{O_2}}{M_H} C_H \quad (1)$$

$$C_{H_2}^* = C_{H_2} + \frac{1}{2} \frac{M_{H_2}}{M_{OH}} C_{OH} + \frac{M_{H_2}}{M_O} C_O + \frac{3}{2} \frac{M_{H_2}}{M_H} C_H \quad (2)$$

$$C_{H_2O}^* = C_{H_2O} - \frac{M_{H_2O}}{M_O} C_O - \frac{M_{H_2O}}{M_H} C_H \quad (3)$$

The instantaneous transport equations for them contain the kinetic source terms

$$w_{H_2O}^* = 2M_{H_2O} (w_5 + w_6 + w_7) \quad (4)$$

$$\frac{1}{M_{O_2}} w_{O_2}^* = - \frac{1}{2} \frac{1}{M_{H_2O}} w_{H_2O}^* \quad (5)$$

$$\frac{1}{M_{H_2}} w_{H_2}^* = - \frac{1}{M_{H_2O}} w_{H_2O}^* \quad (6)$$

The system of eight equations describing the mass and energy transfer can be assembled as follows: four partial differential equations for the atomic mass fractions  $z_O, z_H$  of the elements O and H, the combined fuel  $C_{H_2}^*$  and the static enthalpy (defined by eq. 8), together with conservation of total mass, the linear relations between atomic and molecular mass fractions and three linearly independent equilibrium conditions as four local equations (see Ref. 5). Note that only the equations for the combined variable  $C_{H_2}^*$  and the enthalpy contain source terms. This set of equations applies to flows in the main reaction zone of combustors if a general character of partially premixed/diffusive conditions prevails and the source terms in the energy equation are not neglected. For diffusion flames further simplifications can be made. Normalizing the element mass fractions and the enthalpy with the values at the jet pipe exit and the ambient value the variable  $f$  (mixture fraction; Refs. 7, 8), can be defined

$$f \equiv \frac{\phi - \phi_\infty}{\phi_0 - \phi_\infty}, \quad \phi = z_H, z_O, z_N, h \quad (7)$$

Neglecting the source terms in the equation for the enthalpy  $h$

$$h = \sum_{i=1}^n \left[ h_{0i} + C_i \int_{T_0}^T dT c_{p_i}(T) \right] \quad (8)$$

allows indeed the application of (7) to  $h$ . The system of equations for diffusion flames is now reduced to two partial differential equations for  $f$  and  $C_{H_2}^*$ :

$$\rho \frac{\partial f}{\partial t} + \rho v_\alpha \frac{\partial f}{\partial x_\alpha} = \frac{\partial}{\partial x_\alpha} \left( \frac{\mu}{Sc} \frac{\partial f}{\partial x_\alpha} \right) \quad (9)$$

$$\text{and} \quad \rho \frac{\partial C_{H_2}^*}{\partial t} + \rho v_\alpha \frac{\partial C_{H_2}^*}{\partial x_\alpha} = \frac{\partial}{\partial x_\alpha} \left( \frac{\mu}{Sc} \frac{\partial C_{H_2}^*}{\partial x_\alpha} \right) + w_{H_2}^* \quad (10)$$

with source term given by (6) and the local relations where (2) expresses the combined variable  $C_{H_2}^*$  in terms of mass fractions and the equilibrium relations for (R1)-(R4)



$$C_0 = M_0 \cdot K_{e,1} \cdot K_{e,3} \cdot \frac{C_{H_2}}{M_{H_2}} \cdot \frac{C_{O_2}}{M_{O_2}} \cdot \left( \frac{C_{H_2O}}{M_{H_2O}} \right)^{-1} \quad (11)$$

$$C_H = M_H \cdot K_{e,1}^{1/2} \cdot K_{e,3}^{3/2} \cdot \left( \frac{C_{H_2}}{M_{H_2}} \right)^{3/2} \cdot \left( \frac{C_{O_2}}{M_{O_2}} \right)^{1/2} \cdot \left( \frac{C_{H_2O}}{M_{H_2O}} \right)^{-1} \quad (12)$$

$$C_{OH} = M_{OH} \cdot K_{e,1}^{1/2} \cdot K_{e,3}^{1/2} \cdot K_{e,4}^{-1/2} \cdot \left( \frac{C_{H_2}}{M_{H_2}} \right)^{1/2} \cdot \left( \frac{C_0}{M_0} \right)^{1/2} \quad (13)$$

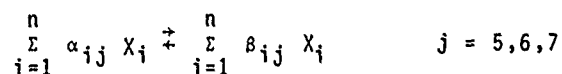
plus the four linear equations (7). The temperature follows from (8) and the density  $\rho$  from the thermal equation of state

$$\rho = \frac{p}{T \sum_{i=1}^n R_i C_i} \quad (14)$$

with known pressure  $p$ . The kinetic source terms  $w_i$  ( $i = 5, 6, 7$ ) are of Arrhenius type expressions

$$w_i = M_i \cdot \left[ \sum_{j=1}^n (\beta_{ij} - \alpha_{ij}) \left( \frac{k_{fj}}{\prod_{\ell=1}^n M_{\ell}^{\alpha_{\ell j}}} \prod_{\ell=1}^n (\rho C_{\ell})^{\alpha_{\ell j}} - \frac{k_{bj}}{\prod_{\ell=1}^n M_{\ell}^{\beta_{\ell j}}} \prod_{\ell=1}^n (\rho C_{\ell})^{\beta_{\ell j}} \right) \right] \quad i=5,6,7 \quad (15)$$

where the reaction is denoted by



The local relations allow the representation of the  $w_i$  as functions of  $f$  and  $C_{H_2}^*$  only.

The domain of possible states in the  $f$ - $C_{H_2}^*$  plane is bounded by the lines for pure mixing (no reaction) and chemical equilibrium (reactions completed) forming a triangular shaped area. For easier coupling of the thermo-chemical model with the turbulence model via pdf's the variable  $C_{H_2}^*$  is transformed into a reaction variable  $r$  defined by

$$r = \frac{C_{H_2}^* - C_{H_2}^u}{C_{H_2}^* - C_{H_2}^v} \quad (16)$$

where the superscripts  $u$  and  $v$  denote unburnt and completely burnt (i.e. equilibrium) mixture. The domain of possible states is now the unit quadrangle in the  $f$ - $r$  plane. All quantities (density, temperature, mass fractions) can be represented as local functions of  $f$  and  $r$ . Figure 1 and figure 2 show temperature and OH-radical mass fraction as functions of  $f$  and  $r$ .

#### Nitric-Oxide formation

The thermo-chemical model described above allows the inclusion of NO-formation without making the assumption of unconstrained chemical equilibrium. Measurements in flames (Refs. 9, 19, 11, 12) have shown that the NO-concentration is significantly lower than its equilibrium value and is very small compared with stable components. Therefore the influence of NO-formation on the flow field can be neglected and no change of the thermo-chemical model is called for. For the  $H_2$ -air flames considered here, the NO-formation is governed by the extended Zeldovich-mechanism (Ref. 13).



"Prompt" NO-formation involving fuel-N does not play a role in  $H_2$ -air flames unless N-containing components are mixed to the  $H_2$ -fuel (Ref. 14). The thermo-chemical model allows nonequilibrium values for the radical concentrations O, H, OH. In particular, for the O-radical there exists indirect experimental evidence (Ref. 8) that super-equilibrium concentration values can be expected. Two partial differential equations for the mass fractions of N and NO are added to the thermo-chemical model. They are of the form

$$\rho \frac{\partial \phi}{\partial t} + \rho v_{\alpha} \frac{\partial \phi}{\partial x_{\alpha}} = \frac{\partial}{\partial x_{\alpha}} \left( \frac{\mu}{Sc} \frac{\partial \phi}{\partial x_{\alpha}} \right) + w_{\phi} \quad \phi = C_N, C_{NO} \quad (17)$$

The source terms  $w_i$  are represented (see Refs. 5, 6) as a sum of four contributions. For NO this is denoted by

$$w_{NO} = M_{NO} (S_1 + C_{NO} S_2 + C_N S_3 + C_{NO} C_N S_4) \quad (18)$$

and similarly for N

$$w_N = M_N (S_1 - C_{NO} S_2 - C_N S_3 + C_{NO} C_N S_4) \quad (19)$$

It is important to notice that the  $S_i$  are independent of the new variables  $C_{NO}$  and  $C_N$ . They are given by

$$S_1 = \rho^2 K_{f,9} \frac{C_{N_2} C_O}{M_{N_2} M_O} \quad (20)$$

$$S_2 = - \frac{\rho^2}{M_{NO}} (K_{b,8} \frac{C_O}{M_O} + K_{b,10} \frac{C_H}{M_H}) \quad (21)$$

$$S_3 = \frac{\rho^2}{M_N} (K_{f,8} \frac{C_{O_2}}{M_{O_2}} + K_{f,10} \frac{C_{OH}}{M_{OH}}) \quad (22)$$

$$S_4 = - \frac{\rho^2 K_{b,9}}{M_{NO} M_N} \quad (23)$$

as special cases of (15) and can be represented as functions of  $f$  and  $r$  alone. This dependence is shown in figure 3 for the dominant term  $S_1$ . The rate and equilibrium constants are summarized in table 2.

## 2.2 Turbulence model

In turbulent flames with high heat release rates strong fluctuations of density are encountered. Two kinds of statistics can be applied to the description of such flows: Density-weighted (Favre, Ref. 15) or unweighted statistics. In particular Favre-statistics have been advocated for flame calculations (Refs. 8, 16) recently because of the attractive simplicity of the resulting moment equations. Here unweighted statistics will be used for the following reasons. Unweighted quantities can easily be compared with experimental results (laser-doppler measurements) and, as a consequence of extensive comparison of Favre- and unweighted calculation models (Refs. 6, 17), it is plausible that modelling assumptions for unweighted quantities cannot simply be carried over to density-weighted variables. The model suggested here is an improved version of the four-equation model developed in reference 19, which is based on the  $k$ - $\epsilon$  model of Jones and Launder (Ref. 18). The main modelling assumptions for (unweighted) turbulent fluxes are (Ref. 6) :

$$-\overline{\rho \overline{v'_\alpha v'_\beta}} = \mu_t \left( \frac{\partial \overline{v}_\alpha}{\partial x_\beta} + \frac{\partial \overline{v}_\beta}{\partial x_\alpha} \right) - \frac{2}{3} \delta_{\alpha\beta} \overline{\rho k} \quad (24)$$

and

$$-\overline{\rho \overline{v'_\alpha \phi}} = \frac{\mu_t}{\sigma_\phi} \frac{\partial \overline{\phi}}{\partial x_\alpha} \quad (25)$$

where the eddy viscosity  $\mu_t$  is defined by

$$\mu_t = C_D \overline{\rho} \frac{k^2}{\epsilon} \quad \nu_t = \frac{1}{\overline{\rho}} \mu_t \quad (26)$$

and  $\sigma_\phi$  is a turbulent Prandtl/Schmidt number. The kinetic energy of turbulence  $k$  and its dissipation rate  $\epsilon$  are determined as solutions of transport equations, which assume for stationary axisymmetric and parabolic flows the form given below :

$$(\overline{\rho \bar{u}} + \overline{\rho' \bar{u}'}) \frac{\partial k}{\partial x} + (\overline{\rho \bar{v}} + \overline{\rho' \bar{v}'}) \frac{\partial k}{\partial y} = \frac{1}{y} \frac{\partial}{\partial y} \left[ y \left( \mu + \frac{\mu_t}{\sigma_k} \right) \frac{\partial k}{\partial y} \right] + \mu_t \left( \frac{\partial \bar{u}}{\partial y} \right)^2 + \frac{\nu_t}{\sigma_{\rho u}} \frac{\partial \bar{u}}{\partial y} \frac{\partial}{\partial y} \overline{\rho' \bar{u}'} + \overline{\rho' \bar{u}'} g_x - \overline{\rho \epsilon} \quad (27)$$

and

$$\begin{aligned} (\overline{\rho \bar{u}} + \overline{\rho' \bar{u}'}) \frac{\partial \epsilon}{\partial x} + (\overline{\rho \bar{v}} + \overline{\rho' \bar{v}'}) \frac{\partial \epsilon}{\partial y} = \frac{1}{y} \frac{\partial}{\partial y} \left[ y \left( \mu + \frac{\mu_t}{\sigma_\epsilon} \right) \frac{\partial \epsilon}{\partial y} \right] + \frac{\epsilon}{k} \left[ C_{\epsilon 1} \mu_t \left( \frac{\partial \bar{u}}{\partial y} \right)^2 + C_{\epsilon 2} \frac{\nu_t}{\sigma_{\rho u}} \frac{\partial \bar{u}}{\partial y} \frac{\partial}{\partial y} \overline{\rho' \bar{u}'} \right. \\ \left. + C_{\epsilon 3} \overline{\rho' \bar{u}'} g_x - C_{\epsilon 4} \overline{\rho \epsilon} \right] \end{aligned} \quad (28)$$

These equations for  $k$  and  $\epsilon$  are supplemented by the modelled transport equations for the density-velocity correlations

$$\begin{aligned} (\overline{\rho \bar{u}} + \overline{\rho' \bar{u}'}) \frac{\partial}{\partial x} \overline{\rho' \bar{u}'} + (\overline{\rho \bar{v}} + \overline{\rho' \bar{v}'}) \frac{\partial}{\partial y} \overline{\rho' \bar{u}'} = \frac{1}{y} \frac{\partial}{\partial y} \left[ y \left( \mu + \frac{\mu_t}{\sigma_{\rho u}} \right) \frac{\partial}{\partial y} \overline{\rho' \bar{u}'} \right] - \\ - \overline{\rho \overline{\rho' \bar{v}'}} \frac{\partial \bar{u}}{\partial y} + \mu_t \frac{\partial \bar{u}}{\partial y} \frac{\partial \overline{\rho}}{\partial y} + \overline{\rho' \bar{u}'} \frac{\partial}{\partial y} \overline{\rho' \bar{v}'} - C_{\rho u 1} \overline{\rho \overline{\rho' \bar{u}'}} \frac{\epsilon}{k} \end{aligned} \quad (29)$$

and

$$(\bar{\rho}\bar{u} + \bar{\rho}'u') \frac{\partial}{\partial x} \bar{\rho}'v' + (\bar{\rho}\bar{v} + \bar{\rho}'v') \frac{\partial}{\partial y} \bar{\rho}'v' = \frac{1}{y} \frac{\partial}{\partial y} \left( y(\mu + \frac{\mu_t}{\sigma_{\rho v}}) \frac{\partial}{\partial y} \bar{\rho}'v' \right) - c_{\rho v_1} \bar{\rho} k \frac{\partial \bar{\rho}}{\partial y} + \frac{\nu_t}{\sigma_{\rho v}} \frac{\partial \bar{\rho}}{\partial y} \frac{\partial}{\partial y} \bar{\rho}'v' + \bar{\rho}'v' \frac{\partial}{\partial y} \bar{\rho}'v' - c_{\rho v_2} \bar{\rho} \frac{\epsilon}{k} \bar{\rho}'v' \quad (30)$$

In modelling the exact equations for  $k$ ,  $\epsilon$ ,  $\bar{\rho}'u'$ ,  $\bar{\rho}'v'$ , the expressions (24) and (25) and the case of high turbulent Re-numbers was assumed. From the latter follows in particular that the correlation between quantities determined by different parts of their spectra is negligible. Finally, the averaged mass and momentum equations are given by

$$\frac{\partial}{\partial x} (\bar{\rho}\bar{u} + \bar{\rho}'u') + \frac{1}{y} \frac{\partial}{\partial y} y(\bar{\rho}\bar{v} + \bar{\rho}'v') = 0 \quad (31)$$

and

$$(\bar{\rho}\bar{u} + \bar{\rho}'u') \frac{\partial \bar{u}}{\partial x} + (\bar{\rho}\bar{v} + \bar{\rho}'v') \frac{\partial \bar{u}}{\partial y} = \frac{1}{y} \frac{\partial}{\partial y} \left( y(\mu + \mu_t) \frac{\partial \bar{u}}{\partial y} \right) - \frac{\partial \bar{p}}{\partial x} + \bar{\rho} g_x \quad (32)$$

The constants for the turbulence model are given in table 1.

### 2.3 Probability density functions

Average values of the thermodynamic quantities can be calculated if the statistical characteristics of the variables in the thermo-chemical model are known. It would be sufficient to provide first and second order statistical moments of the variables  $f$  and  $r$  (or  $CH_2$ ) if the local relations would be close to linear. But the strongly non-linear character of  $\rho(f,r)$ ,  $T(f,r)$ ,  $c_i(f,r)$  requires the knowledge of the pdf (probability density function) of  $f$  and  $r$ . Two different approaches to construct such pdf's will be discussed.

#### Method I

The pdf of the scalar variables  $f$  and  $r$  is constructed on the basis of a selected set of statistical moments. The general idea is to prescribe the functional dependence of the pdf on these moments. The crucial modelling assumption is obviously the explicit form of this dependence. Two different ways of establishing such forms will be considered.

In the first method the analogy between the pdf of fluctuating scalars in cold and non-reacting flows and the pdf of the reacting species in the diffusion controlled limit (Ref. 20) is used to infer qualitatively the form of the pdf from measurements in incompressible flows. This was applied to the case of a single conserved scalar (Ref. 8) called mixture fraction for the description of turbulent diffusion flames using the flame-sheet model. The measured pdf's (Refs. 21, 22) show strongly non-Gaussian features such as singular contributions reflecting the intermittent character of free shear flows and non-zero skewness. A reasonable fit with the experiments (Ref. 23) can be obtained if the functional dependence of single scalar pdf's on mean and variance is prescribed as beta-function.

$$P(x_\alpha, z) = \frac{z^{\alpha-1} (1-z)^{\beta-1}}{\int_0^1 dz z^{\alpha-1} (1-z)^{\beta-1}} \quad (33)$$

where the exponents are given in terms of mean  $\bar{f}$  and variance  $g \equiv (\bar{f}-\bar{f})^2$  as

$$\alpha = \bar{f} \left( \frac{\bar{f}(1-\bar{f})}{g} - 1 \right) \quad (34)$$

and

$$\beta = (1-\bar{f}) \left( \frac{\bar{f}(1-\bar{f})}{g} - 1 \right) \quad (35)$$

The variable  $z$  denotes in (33) a possible value of the random variable  $f(x_\alpha, t)$ . This function, however, is not able to represent pdf's with relative maxima, which can be expected in the outer part of free shear layers (Refs. 21, 22). Other forms that have been suggested are the clipped Gaussian and combinations of Dirac-pseudofunctions (Ref. 24). For the two dimensional pdf required here the following form of  $P(z,s)$  where  $s$  denotes a possible value of the reaction variable  $r(x_\alpha, t)$ , is put forward. First it is assumed that mixture fraction  $f$  and reaction variable  $r$  are statistically independent. Hence

$$P(z,s) = P(z) \cdot P(s) \quad (36)$$

Note that this does not imply statistical independence of  $f$  and  $CH_2^*$ . For  $P(z)$  the representation (33) as betafunction and for  $P(s)$  three Dirac-functions at  $r = 0, 1, \bar{r}$  are used leading to

$$P(z,s) = \frac{z^{\alpha-1} (1-z)^{\beta-1}}{\int_0^1 dz z^{\alpha-1} (1-z)^{\beta-1}} \left( \gamma_1 \delta(s) + \gamma_2 \delta(s-\bar{r}) + \gamma_3 \delta(s-1) \right) \quad (37)$$

The exponents  $\alpha$  and  $\beta$  are determined by  $\bar{f}$  and  $\bar{g}$  according to (34) and (35). The nonnegative coefficients  $\gamma_1, \gamma_2, \gamma_3$  depend on  $\bar{f}$  and  $\bar{r}^{1/2}$  as follows

$$\gamma_1 = \frac{\bar{r}^{1/2}}{\bar{f}} \quad (38)$$

$$\gamma_2 = 1 - \frac{\bar{r}^{1/2}}{\bar{f}(1-\bar{f})} \quad (39)$$

$$\gamma_3 = \frac{\bar{r}^{1/2}}{1-\bar{f}} \quad (40)$$

At each point in the flow field the pdf  $P(z, s)$  is therefore determined by the four moments  $\bar{f}, \bar{g}, \bar{r}, \bar{r}^{1/2}$  for which modelled transport equations have to be solved (equations (45)-(48) below).

A second method was devised by Pope (Ref. 25) which relies solely on the information provided by statistical moments. The statistically most-likely distribution of a scalar  $f$  given the first  $L$  moments  $\mu_n$  is

$$P_L(z) = q(z) \exp \left( \sum_{k=0}^L A_k z^k \right) \quad (41)$$

where  $q(z)$  is the a priori probability of the samples of  $f(x_\alpha, t)$ . It can be shown that  $q(z)$  is constant for strictly conserved scalars and for scalars  $f$  obeying a transport equation with source term  $\rho S(f)$  it can be estimated for dominant  $S(f)$  by (Ref. 25)

$$q(z) = 1 + \frac{\tau}{\sqrt{g}} S(z) \quad (42)$$

where  $\tau$  is the time scale of dissipation of  $f$ . The coefficients  $A_n$  are determined by making the information entropy  $E$

$$E \equiv - \int_0^1 dz P_L(z) \ln \frac{P_L(z)}{q(z)} \quad (43)$$

maximal under the side conditions

$$\int_0^1 dz z^n P_L(z) = \mu_n \quad n = 0, (1), L \quad (44)$$

of the available moments  $\mu_n$ . This approach can be extended to any number of scalars. Calculations by Pope (Ref. 25) show that good agreement with experimental data for passive scalars can be achieved for  $L > 3$ . For the case of two scalars this would require at least nine moment equations.

#### Moment equations

The four moment equations for the pdf in the form (37) can be obtained from (9) and (10) together with (16) by applying the usual manipulations and averaging. The details of the closure operation are described in reference 26. For the  $f$  and  $g$  equations, the modelling follows closely the manipulations of the turbulence model described above. The resulting equations are

$$(\bar{\rho} \bar{u} + \bar{\rho}' u') \frac{\partial \bar{f}}{\partial x} + (\bar{\rho} \bar{v} + \bar{\rho}' v') \frac{\partial \bar{f}}{\partial y} = \frac{1}{y} \frac{\partial}{\partial y} \left( y \left( \frac{\mu}{Sc} + \frac{\mu_t}{\sigma_f} \right) \frac{\partial \bar{f}}{\partial y} \right) \quad (45)$$

and

$$\begin{aligned} (\bar{\rho} \bar{u} + \bar{\rho}' u') \frac{\partial \bar{g}}{\partial x} + (\bar{\rho} \bar{v} + \bar{\rho}' v') \frac{\partial \bar{g}}{\partial y} &= \frac{1}{y} \frac{\partial}{\partial y} \left( y \left( \frac{\mu}{Sc} + \frac{\mu_t}{\sigma_g} \right) \frac{\partial \bar{g}}{\partial y} \right) + 2 \frac{\mu_t}{\sigma_f} \left( \frac{\partial \bar{f}}{\partial y} \right)^2 + \\ &+ 2 \frac{\nu_t}{\sigma_{\rho f}} \frac{\partial \bar{f}}{\partial y} \frac{\partial}{\partial y} \frac{\bar{\rho}}{\rho' f} - \frac{\nu_t}{\sigma_g} \frac{\partial \bar{g}}{\partial y} \frac{\partial \bar{\rho}}{\partial y} - \tau \frac{\epsilon}{k} \bar{\rho} g \end{aligned} \quad (46)$$

The derivation and modelling of the equations for  $\bar{r}$  and  $\bar{r}^{1/2}$  is more complex (Refs. 6, 26) and requires the consideration of the interaction between reactions and turbulent mixing. The result can be stated as follows:

$$(\bar{\rho} \bar{u} + \bar{\rho}' u') \frac{\partial \bar{r}}{\partial x} + (\bar{\rho} \bar{v} + \bar{\rho}' v') \frac{\partial \bar{r}}{\partial y} = \frac{1}{y} \frac{\partial}{\partial y} \left( y \left( \frac{\mu}{Sc} + \frac{\mu_t}{\sigma_r} \right) \frac{\partial \bar{r}}{\partial y} \right) + \bar{S}_r + \frac{1}{2} \bar{\rho} \tau \frac{\epsilon}{k} \bar{X} \cdot \bar{r} g \quad (47)$$

and

$$\begin{aligned} (\bar{\rho} \bar{u} + \bar{\rho}' u') \frac{\partial \bar{r}^{1/2}}{\partial x} + (\bar{\rho} \bar{v} + \bar{\rho}' v') \frac{\partial \bar{r}^{1/2}}{\partial y} &= \frac{1}{y} \frac{\partial}{\partial y} \left( y \left( \frac{\mu}{Sc} + \frac{\mu_t}{\sigma_{r^2}} \right) \frac{\partial \bar{r}^{1/2}}{\partial y} \right) + 2 \frac{\mu_t}{\sigma_r} \left( \frac{\partial \bar{r}}{\partial y} \right)^2 + 2 \frac{\nu_t}{\sigma_{\rho r}} \frac{\partial \bar{r}}{\partial y} \frac{\partial}{\partial y} \frac{\bar{\rho}}{\rho' r} \\ &- \frac{\nu_t}{\sigma_{r^2}} \frac{\partial \bar{r}^{1/2}}{\partial y} \frac{\partial \bar{\rho}}{\partial y} + 2 \bar{r}^{1/2} \bar{S}_r - \bar{\rho} \tau \frac{\epsilon}{k} \bar{r}^{1/2} (1 - g \bar{X}) \end{aligned} \quad (48)$$

where using (6) (see Ref. 26)

$$S_r = \frac{w_{H_2}^*}{w} \quad (49)$$

and  $w \equiv C_{H_2}^{*v} - C_{H_2}^{*u}$  denotes the denominator of (16), and

$$X \equiv \frac{1}{w} \frac{\partial^2 w}{\partial f^2} \quad (50)$$

Noting that both quantities are functions of  $z$  and  $s$  we can evaluate their statistical moments by integration using the pdf  $P(z, s)$ .

For the calculation of the mean NO-mass fraction two additional partial differential equations must be modelled. Averaging (17) for  $\phi = C_{NO}$  and  $\phi = C_N$  and applying (25) leads to

$$(\bar{\rho} \bar{u} + \bar{\rho} \bar{u}') \frac{\partial \bar{\phi}}{\partial x} + (\bar{\rho} \bar{v} + \bar{\rho} \bar{v}') \frac{\partial \bar{\phi}}{\partial y} = \frac{1}{y} \frac{\partial}{\partial y} \left[ y \left( \frac{\mu}{Sc} + \frac{\mu_t}{\sigma_\phi} \right) \frac{\partial \bar{\phi}}{\partial y} \right] + \bar{w}_\phi \quad (51)$$

where only the mean kinetic source terms  $\bar{w}_{NO}$  and  $\bar{w}_N$  require special considerations. First we note that the terms  $S_i$ ,  $i = 1, \dots, 4$  in (18) and (19) can be represented as local functions of  $z$  and  $s$  only, because they are a function of  $\rho$ ,  $T$ ,  $C_O$ ,  $C_H$ ,  $C_{OH}$ ,  $C_{N_2}$ ,  $C_{O_2}$  which in turn are functions of  $f$  and  $r$  via the local relations. Hence we can evaluate the moments of  $w_{NO}$  and  $w_N$  simply by integration using  $P(z, s)$ . But the averaged source term

$$\begin{aligned} \bar{w}_{NO} = M_{NO} (\bar{S}_1 + \bar{C}_{NO} \bar{S}_2 + \bar{C}_N \bar{S}_3 + \bar{C}_{NO} \bar{C}_N \bar{S}_4 + \bar{C}_{NO} \bar{S}_2 + \bar{C}_N \bar{S}_3 + \bar{C}_{NO} \bar{C}_N \bar{S}_4 + \bar{C}_{NO} \bar{S}_4 + \bar{C}_{NO} \bar{S}_4 \bar{C}_N \\ + \bar{C}_N \bar{S}_4 \bar{C}_{NO} + \bar{C}_{NO} \bar{C}_N \bar{S}_4) \end{aligned}$$

contains several correlations that cannot be calculated by integration. Remembering that  $S_1$  is the dominant source term and the fact that the mass fractions  $C_{NO}$  and  $C_N$  are small compared with the stable components, it is reasonable to neglect (for the NO-formation) these correlations. Then the equations (51) are closed with mean kinetic source terms given by

$$\bar{w}_{NO} = M_{NO} (\bar{S}_1 + \bar{C}_{NO} \bar{S}_2 + \bar{C}_N \bar{S}_3 + \bar{C}_{NO} \bar{C}_N \bar{S}_4) \quad (52)$$

and

$$\bar{w}_N = M_N (\bar{S}_1 - \bar{C}_{NO} \bar{S}_2 - \bar{C}_N \bar{S}_3 + \bar{C}_{NO} \bar{C}_N \bar{S}_4) \quad (53)$$

The time scale ratio  $\tau$  appearing in (46) and (48) was estimated on the basis of recent measurements (Ref. 36) for a passive scalar in incompressible shear flows as

$$\tau \cong C_{\tau_2} \ln \bar{\phi}^2 + C_{\tau_2}, \quad \phi = f, r$$

The values for  $C_{\tau_1}$  and  $C_{\tau_2}$  are given in table 1.

This completes the coupling of the thermo-chemical model with the turbulence model using the method I for the construction of the pdf.

#### Method II

The second method avoids the explicit construction of the pdf  $P(z, s)$  in terms of statistical moments by making use of the transport equation for  $P(z, s)$ . Consider a set of  $m$  scalar variables  $\phi_i(x, t)$  satisfying transport equations of the form (17). The one-point pdf  $P$  of the values  $z_i$  of the  $\phi_i(x_\alpha, t)$  can be defined by

$$\hat{P}(\phi_i, z_i) = \prod_{i=1}^m \delta(\phi_i(x_\alpha, t) - z_i)$$

and

$$P(z_i, x_\alpha, t) = \langle \hat{P} \rangle$$

where the angular brackets denote ensemble averaging. The transport equation for  $P$  follows according to Lundgren (Ref. 27) as

$$\frac{\partial}{\partial t} \rho P + \frac{\partial}{\partial x_\alpha} \rho v_\alpha P = - \frac{\partial}{\partial x_\alpha} \langle \rho v'_\alpha \hat{P} \rangle - \frac{\partial}{\partial z_i} (\rho S_i P) + \frac{\partial}{\partial x_\alpha} (\rho \Gamma \frac{\partial P}{\partial x_\alpha}) - \frac{\partial^2}{\partial z_i \partial z_j} \langle \rho \Gamma \frac{\partial \phi_i}{\partial x_\alpha} \frac{\partial \phi_j}{\partial x_\alpha} \hat{P} \rangle \quad (54)$$

where the density and the sources  $S_i$  are assumed to be local functions of the  $\phi_i$  (hence  $\rho = \rho(z_i)$  and  $S_j = S_j(z_i)$  in (54)) and the molecular transport coefficients  $\rho \Gamma_i$  are constant and equal for all  $i = 1(1)m$  (Smagorinsky-Zeldovich assumption). Equation (54) poses two modelling problems (see Ref. 28): the turbulent flux term and the scalar dissipation term. On the other hand, the nonlinear sources  $S_i$  produce a closed term in the equation

for the pdf  $P$ . This property is the main advantage of the transport equation (54). For the case of a single scalar variable ( $m=1$ ) closure models (Refs. 28, 32, 33) have been suggested. In particular, the turbulent flux term can be modelled by reference 32.

$$-\langle \rho v'_\alpha \tilde{P} \rangle \cong \frac{\rho v_t}{\sigma_p} \frac{\partial P}{\partial x_\alpha} \quad (55)$$

This expression produces gradient-flux models for all higher correlations with the velocity. For the scalar dissipation term several stochastic models have been constructed. The integral model suggested in reference 28

$$-\frac{\partial^2}{\partial z^2} \langle \rho \Gamma \frac{\partial \phi}{\partial x_\alpha} \frac{\partial \phi}{\partial x_\alpha} \tilde{P} \rangle = \rho \frac{\epsilon}{k} \tau \Gamma_0 \left[ \int_0^z dz' \int_z^1 dz'' P(z') P(z'') \mathcal{R}(z', z'', z) - P \right] \quad (56)$$

$$\text{where } \mathcal{R}(z', z'', z) = \begin{cases} \frac{2}{z'' - z'} & \text{for } 0 \leq z' \leq z \leq z'' \leq 1 \\ 0 & \text{otherwise} \end{cases}$$

has been applied to flame calculations on the basis of the flame-sheet model (Ref. 34) and gave satisfactory results. For two-scalar case considered here, the question of modelling the cross-correlation

$$-\frac{\partial^2}{\partial z \partial s} \langle \rho \Gamma \frac{\partial f}{\partial x_\alpha} \frac{\partial r}{\partial x_\alpha} \tilde{P} \rangle$$

is still not settled. Closure can easily be achieved using (55) and (56) if this term is neglected, but  $r$  is a transformed variable containing information about mixture fraction and therefore the usual argument of statistical independence at high turbulent Reynolds numbers does not apply. Further work on this problem is under way.

### 3. APPLICATION TO H<sub>2</sub>-AIR DIFFUSION FLAMES

The closure model developed in the previous chapter was applied to several turbulent H<sub>2</sub>-air diffusion flames for which experimental results including NO-formation (Refs. 9, 10, 11) are available. The discretization and numerical solution of the set of parabolic differential equations was performed with standard methods (Ref. 35).

Flame 1 (Refs. 11, 12).

Kent and Bilger performed extensive measurements in several turbulent diffusion flames. The horizontal flame simulated in our calculations is characterized by the mean nozzle

exit velocity  $U_j = 150 \frac{m}{s}$  of H<sub>2</sub> and  $\frac{U_j}{U_e} = 10$ ,  $Re = 11700$  (at nozzle exit) where  $U_e$  denotes

the velocity of the outer air stream. The initial conditions for the calculations are given by the measured profiles for mean velocity and turbulence energy. The initial distributions of mean mass fractions can easily be inferred from the nozzle conditions and the dissipation rate is calculated from the condition of production equals dissipation in the turbulence kinetic energy equation with prescribed turbulent viscosity. The results of the calculations are compared in figures 4 to 8 with the measurements. The agreement between the mean concentrations of the stable components and the mean temperature in experiment and computation is very satisfactory. In the initial region for  $\frac{x}{D} < 80$  the calculated profiles are spreading more rapidly than the experimental values (Figs. 4 and 5), whereas the axial development is very well represented in figure 6. Several reasons can be given for this overprediction of the spreading. The turbulent Schmidt/Prandtl numbers are constant in the calculation, but values inferred from experiments show a variation from 0.4 to 1.0, furthermore are free shear flows highly intermittent and consequently the unconditional statistics of any flow quantity are highly non-Gaussian in the outer part which cannot be described adequately by first and second order moments. The calculated profiles for the mean NO-concentration in figures 7 and 8 show that in axial direction (Fig. 8) NO is underpredicted in the region  $\frac{x}{D} < 60$ , very well predicted in the medium range  $60 < \frac{x}{D} < 120$  and overpredicted further downstream. In radial direction (Fig. 7), the profile for  $\frac{x}{D} = 80$  is qualitatively correct but gives too small values in the core region due to the slightly larger spreading rate of the calculated jet.

Flame 2 (Ref. 10)

Lavoie and Schlader performed measurements in a vertical H<sub>2</sub>-air diffusion flame with mean nozzle exit velocity of  $U_j = 200 \frac{m}{s}$ . The fuel H<sub>2</sub> issues into still air and  $Re = 4500$  at the nozzle exit. The results of the calculations (Figs. 9 to 14) show the same agreement between experiment and computation as flame 1 for stable components in figures 9 and 10. The mean NO-concentration is again underpredicted for  $\frac{x}{D} < 80$  and very well predicted for  $\frac{x}{D} > 80$  as the axial development in figure 13 proves. The same figure contains in addition the results for a flame with  $U_j = 130 \frac{m}{s}$  giving good agreement for  $\frac{x}{D} > 80$  as well. The radial profiles in figures 11 and 12 reflect the axial underprediction at  $\frac{x}{D} = 40$  and the good agreement for  $\frac{x}{D} = 80$  and  $\frac{x}{D} = 120, 160$ .

#### Flame 3 (Ref. 9)

The vertical flame measured by Takagi and Ogasawara has a mean exit velocity of  $U_j = 108 \frac{m}{s}$  and  $Re = 2200$  and the fuel  $H_2$  issues into still air. The comparison of the concentrations of the stable components at  $\frac{x}{D} = 50$  shows the good agreement between experiment and calculation as flames 1 and 2. The NO-formation in this low  $Re$  number flame shows a much slower decay of the mean NO-concentration along the axis than the previous flames and the calculated values are smaller than the experimental concentration for  $\frac{x}{D} > 160$  (Fig. 17). In the medium range the agreement is very good and the initial region is underpredicted as for flames 1 and 2. The calculated radial profiles in figure 15 are too small in the core region for  $\frac{x}{D} < 80$  but agree well in the outer part whereas for  $\frac{x}{D} > 80$  in figure 16 the core region is well represented.

#### 4. CONCLUSIONS

A prediction model for turbulent  $H_2$ -air diffusion flames was developed that allows a certain degree of chemical non-equilibrium providing kinetic values for the O, H, OH radicals that determine the NO-formation in such flames. The results obtained with this model were compared with experiments in three different flames and lead to the following conclusions:

1. Stable components and temperature are well predicted. NO-formation is well predicted in the medium range of the flames, but underpredicted in the initial region and overpredicted (except for flame 3) far downstream.
2. NO-formation (calculated according to the extended Shvab-Zeldovich mechanism) is within the framework of this model very sensitive toward changes in the mean mixture fraction and the mean reaction variable and in particular their variances. Those four quantities determine the mean NO production rate via the pdf  $P(z,s)$ . It could be expected that the form of the pdf has a strong influence on NO-formation. But figure 3 shows that NO-formation is restricted to a small part of the  $r$ - $f$  rectangle and hence does the form of the pdf not play a decisive role in the determination of mean NO-concentrations. This was supported by numerical tests using different pdf forms (Ref. 6).
3. Comparison of the two methods for constructing the pdf shows two distinct advantages of the more elaborate transport equation approach. First is the modelling of moment equations avoided, which could lead to inconsistent solutions because the closure assumptions considered here do not guarantee the fulfillment of realizability conditions such as (references 5, 8):

$$g < \bar{f}(1-\bar{f}) \quad \text{etc}$$

which are a consequence of boundedness of  $f$  and  $r$ . Second, the treatment of reaction kinetic source terms is straightforward and does not produce closure problems. On the other hand, the transport equation (54) poses different closure problems and its numerical solution requires for more than two scalars excessive computing times. Hence the second method should be considered a research tool to check and ease constructing pdf's as functions of few moments.

#### REFERENCES

1. WILLIAMS, F.A.: Combustion theory. Addison Wesley 1965.
2. DIXON-LEWIS, G.; GOLDSWORTHY, F.A.; GREENBERG, J.B.: Flame structure and flame reaction kinetics. Proc. Roy. Soc. London, A346, 1975, pp 261-278.
3. DIXON-LEWIS, G. & RHODES, P.: Properties and kinetic mechanism in hydrogen-flames. 2nd European Combustion Symp., 1975, pp 473-478.
4. STEPHENSON, P.L. & TAYLOR, R.G.: Luminar flame propagation in hydrogen, oxygen, nitrogen mixtures. Comb. Flame, 20, 1973, pp 231-244.
5. JANICKA, J. & KOLLMANN, W.: A two variables formalism for the treatment of chemical reactions in turbulent  $H_2$ -air diffusion flames. 17th Symp. (Int.) Comb., 1978, to appear.
6. JANICKA, J.: Berechnung turbulenter Wassenstoff-Luft-Diffusionsflammen. Ph.D. Thesis, 1979, RWTH, Aachen, Germany.
7. SPALDING, D.B.: Concentration fluctuations in a round turbulent free jet. Chem. Eng. Sci. 26, 1971, pp 95-107.
8. BILGER, R.W.: Turbulent jet diffusion flames. Prog. Energy Comb. Sci., 1, 1976, pp 87-109.
9. TAKAGI, T. & OGASAWARA, M.: A study of nitric oxide formation in turbulent diffusion flames. 15th Symp. (Int.) Comb., 1975, pp 1051-1060.
10. LAVOIE, G.A. & SCHLADER, A.F.: A scaling study of NO-formation in turbulent diffusion flames of hydrogen in air. Comb. Sci. Technol., 8, 1974, pp 215-234.
11. KENT, J.H. & BILGER, R.W.: Turbulent diffusion flames. 14th Symp. (Int.) Comb., 1973, pp 615-625.
12. BILGER, R.W. & KENT, R.E.: Further experiments on turbulent jet diffusion flames. 15th Symp. (Int.) Comb., 1974, pp 541-551.
13. DOWMAN, C.T.: Kinetics of nitric oxide formulation in combustion processes. 14th Symp. (Int.) Comb., 1973, pp 729-738.
14. FENIMORE, C.P.: Effects of diluents and mixing on nitric oxide from fuel-nitrogen species in diffusion flames. 16th Symp. (Int.) Comb., 1976, pp 1065-1070.
15. FAVRE, A.: Equations des gaz turbulents compressibles. Part II. J. de Mécanique, 4, 1965, pp 391-421.
16. JONES, W.P. & PRIDDIN, C.H.: Prediction of the flow field and local gas composition in gas turbine combustion chambers. 17th Symp. (Int.) Comb., 1978, to appear.

17. JANICKA, J. ; KOLLMANN, W.; SAETRAN, L.; VANDROMME, D.: The modelling of turbulent fluxes in variable density flows. VKI, in preparation.
18. JONES, W.P. & LAUNDER, B.E.: The calculation of low Reynolds number phenomena with a two-equation model of turbulence. Int. J. Heat & Mass Transfer, 16, 1973, pp 1119-1130.
19. KOLBE, W. & KOLLMANN, W.: Prediction of turbulent diffusion flames with a four equation turbulence model. Paper submitted to Acta Astronautica, 1979.
20. LIU, C-H & O'BRIEN, E.E.: Turbulent shear flow mixing and rapid chemical reactions : an analogy. J. Fluid Mechanics, 64, 1974, pp 195-206.
21. LaRUE, J. & LIBBY, P.A.: Temperature fluctuations in the plane turbulent wake. Physics of Fluids, 17, 1974, pp 1956-1967.
22. BATT, R.G.: Turbulent mixing of passive and chemically reacting species in a low speed shear layer. J. Fluid Mechanics, 82, 1977, pp 53-95.
23. RHODES, R.P.: A probability distribution function for turbulent flows. in Turbulent Mixing in Nonreactive and Reactive Flows, Plenum Press, 1974, pp 235-241.
24. JONES, W.P.: Models for turbulent flow with variable density and combustion. VKI Lecture Series 1979-2.
25. POPE, S.B.: Probability distributions of scalars in turbulent shear flows. Proc. 2nd Symp. Turbulent Shear Flows, London 1979, pp 3.1-3.6.
26. JANICKA, J. & KOLLMANN, W.: Turbulence closure for flows with chemical reactions; in preparation, 1979.
27. LUNDGREN, T.S.: Distribution functions in the statistical theory of turbulence. Phys. Fluids, 10, 1967, pp 969-975.
28. JANICKA, J.; KOLBE, W.; KOLLMANN, W.: Closure of the transport equation for the pdf of turbulent scalar fields. J. Nonequil. Thermodyn., 4, 1979, pp 47-66.
29. HAY, J.H. & SICHEL, M.: Theoretical analysis of NO-formation near the primary reaction zone in methane combustion. Comb. Flame, 26, 1976, pp 1-15.
30. TSATSARONIS, G.: Vereinfachung des Methan/Sauerstoff Reaktionsmechanismus. Brenn.-Wärme-Kraft, 30, 1978, pp 249-255.
31. BAULCH, D.L.; DRYSDALE, D.D.; HORNE, D.G.: Evaluated kinetic data for high temperature reactions. Butterworths, London, 1973.
32. POPE, S.B.: The probability approach to the modelling of turbulent reacting flows. Comb. Flame, 27, 1976, pp 299-312.
33. DOPAZO, C.: Relaxation of initial probability density functions in the turbulent convection of scalar fields. Physics of Fluids, 22, 1979, pp 20-30.
34. JANICKA, J.; KOLBE, W.; KOLLMANN, W.: The solution of a pdf-transport equation for turbulent diffusion flames. Proc. 1978 Heat Transfer Fluid Mech. Inst., Stanford U. Press, 1978, pp 296-312.
35. PATANKAR, S.V. & SPALDING, D.B.: Heat and mass transfer in boundary layers. Intertext, London, 1970.
36. WARHAFT, Z. & LUMLEY, J.L. : An experimental study of the decay of temperature fluctuations in grid generated turbulence. J. Fluid Mechanics, 88, 1978, pp. 659-684.



TABLE 1 - CONSTANTS FOR THE CLOSURE MODEL

## TURBULENCE MODEL

$C_D$	$C_{\epsilon_1}$	$C_{\epsilon_2}$	$C_{\epsilon_3}$	$C_{\epsilon_4}$	$C_{\rho u_1}$
0.09	1.44	2.00	2.00	1.9	1.5
$C_{\rho v_1}$	$C_{\rho v_2}$	$\sigma_k$	$\sigma_\epsilon$	$\sigma_{\rho u}$	$\sigma_{\rho v}$
0.66	1.5	1.0	1.3	1.5	1.5

## COUPLING EQUATIONS

$\sigma_f$	$\sigma_g$	$\sigma_r$	$\sigma_{r_2}$	$\sigma_{\rho f}$	$\sigma_{\rho r}$
0.85	0.7	0.85	0.7	0.7	0.7
$\sigma_{NO}$	$\sigma_N$	$Sc$	$C_{\tau_1}$	$C_{\tau_2}$	
0.85	0.85	0.7	4.0	0.4	

TABLE 2 - CONSTANTS FOR THE THERMO-CHEMICAL MODEL

(References 29, 30, 31)

Rate constants :  $K_{\alpha,j} = A_{\alpha,j} \left(\frac{T}{T_0}\right)^{D_{\alpha,j}} \exp\left(\frac{F_{\alpha,j}}{T}\right)$ ,  $\alpha = f(\text{orward}), e(\text{quilibrium})$

Reaction	$A_{f,j}$	$D_{f,j}$	$F_{f,j}$	$A_{e,j}$	$D_{e,j}$	$F_{e,j}$
R1	1.42E+11	0.0	-8.248E+3	5.23E+2	-0.439	-8.7E+3
R2	1.8E+7	1.0	-4.479E+3	1.39E+0	-0.06	-8.86E+2
R3	1.17E+6	1.3	-1.825E+3	2.97E-2	0.2436	7.873E+3
R4	5.75E+9	0.0	-3.897E+2	2.13E-2	0.1835	8.762E+3
R5	9.77E+11	-0.71	0.0	3.82E-5	0.0476	6.009E+4
R6	6.2E+10	-0.6	0.0	1.79E-3	-0.1358	5.133E+4
R7	9.2E+10	-0.6	0.0	1.29E-3	-0.196	5.221E+4
R8	6.4E+6	1.0	3.14E+3	1.14E+9	-0.106	-1.593E+4
R9	7.6E+10	0.0	-3.8E+4	1.166E+0	0.1186	-3.767E+4
R10	3.2E+10	0.0	0.0	2.18E-2	0.3338	2.463E+4

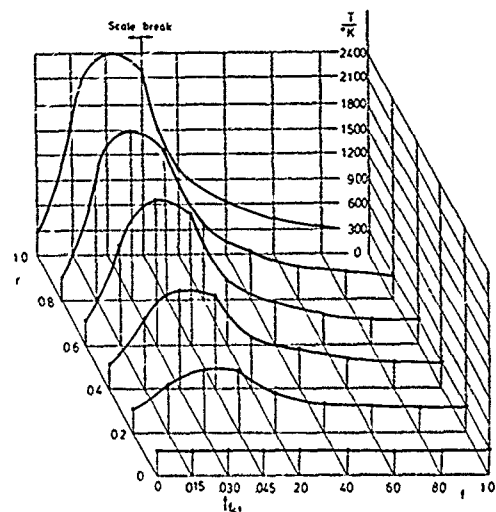


Fig. 1. Temperature as function of mixture fraction  $f$  and reaction variable  $r$ .

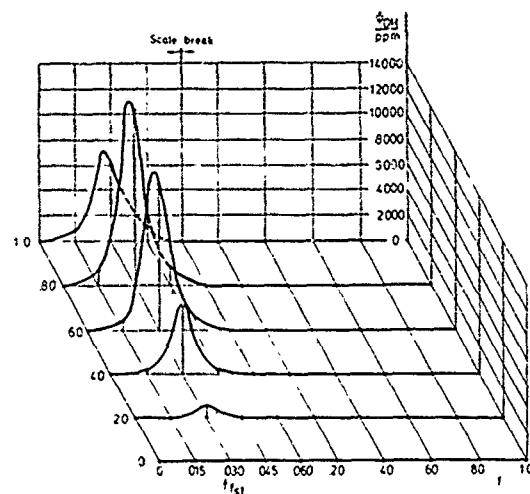


Fig. 2. Molar concentration of OH as function of  $f$  and  $r$ .

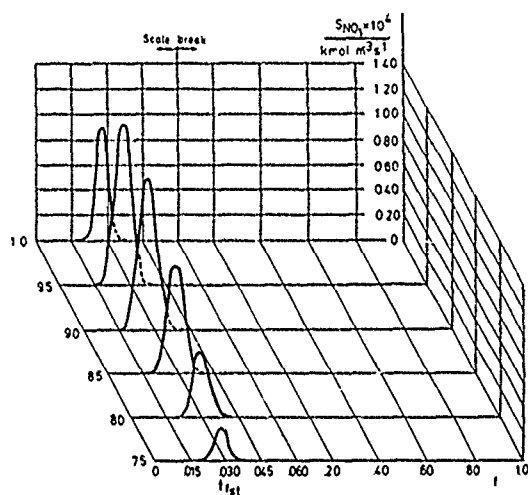


Fig. 3. Dominant source term of NO - production as function of  $f$  and  $r$ .

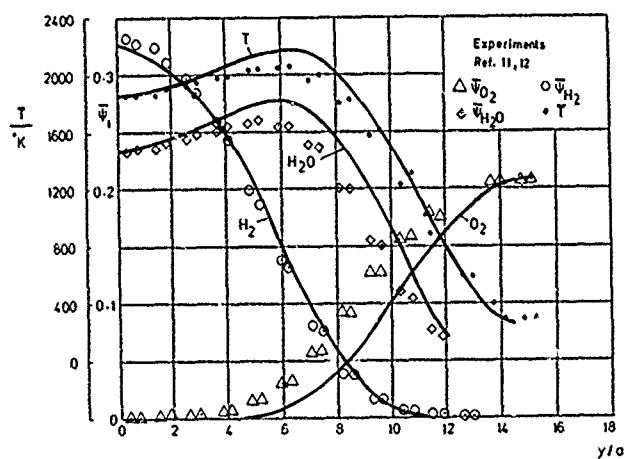


Fig. 5. Radial distribution of mean temperature and mean molar concentrations at  $x/D = 80$  for flame 1.

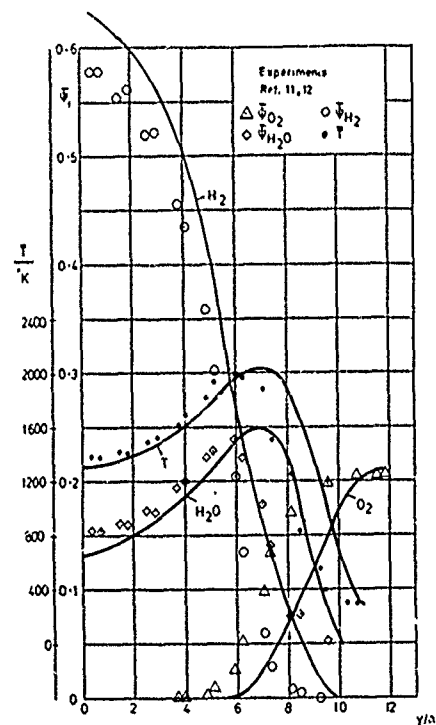


Fig. 4. Radial distribution of mean temperature and mean molar concentration at  $x/D = 40$  for flame 1.

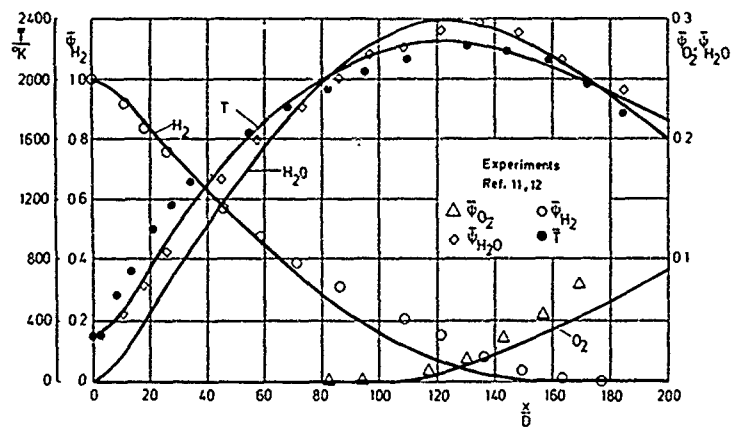


Fig. 6. Axial distribution of mean temperature and mean molar concentration for flame 1.

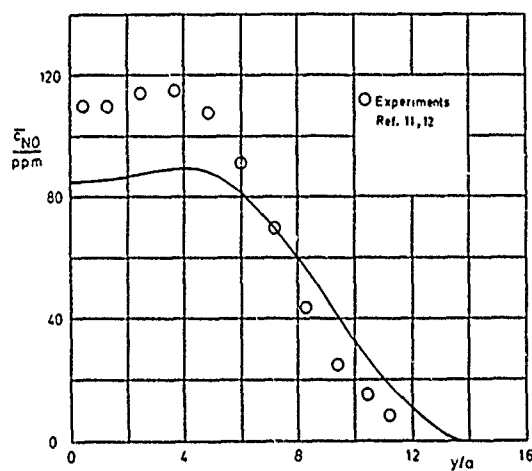


Fig. 7. Radial distribution of mean NO - mass fraction at  $x/D = 80$  for flame 1.

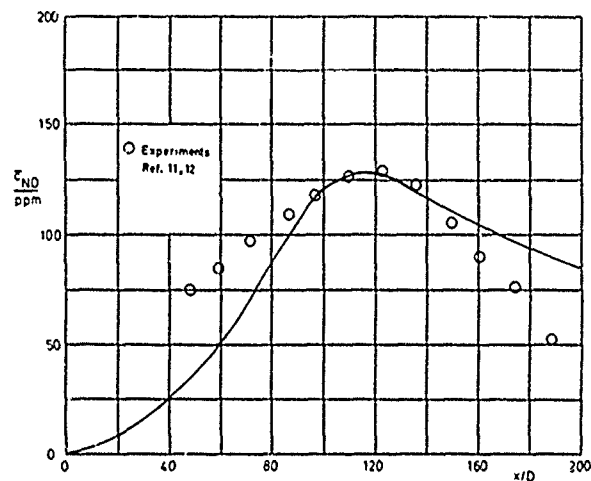


Fig. 8. Axial distribution of mean NO - mass fraction for flame 1.

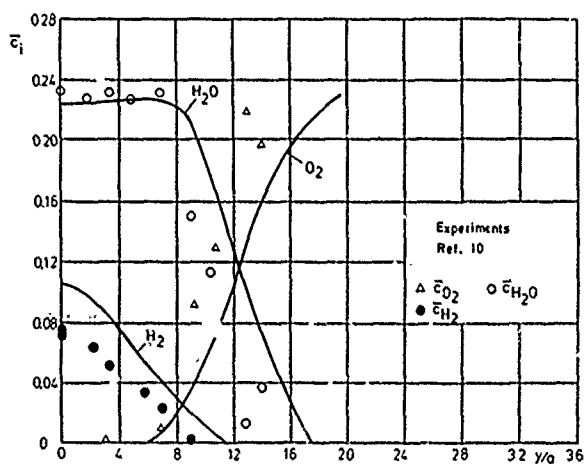


Fig. 9. Radial distribution of mean mass fractions at  $x/D = 40$  for flame 2.

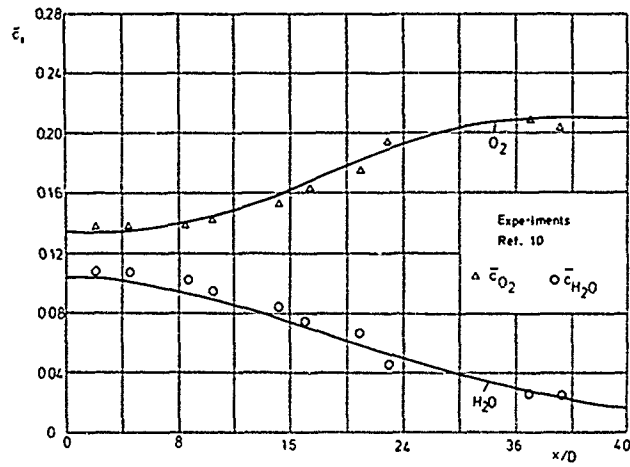


Fig. 10. Radial distribution of mean mass fractions at  $x/D = 160$  for flame 2.

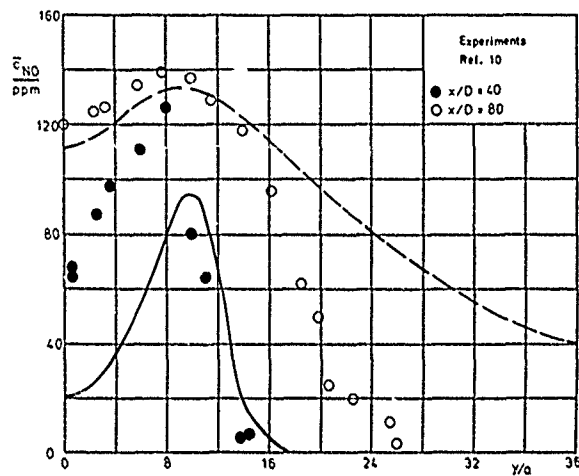


Fig. 11. Radial distribution of mean NO - mass fraction at  $x/D = 40, 80$  for flame 2.

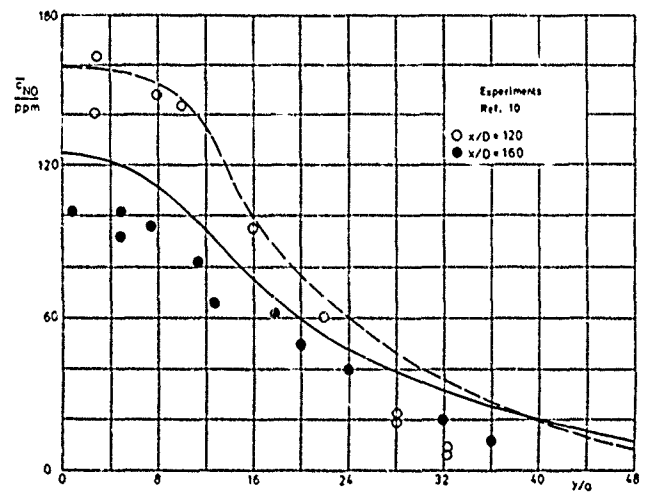


Fig. 12. Radial distribution of mean NO - mass fraction at  $x/D = 120, 160$  for flame 2.

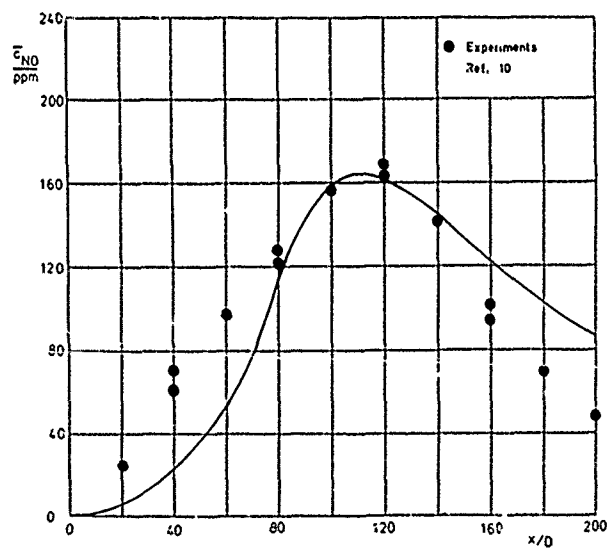


Fig. 13. Axial distribution of mean NO - fraction for flame 2.

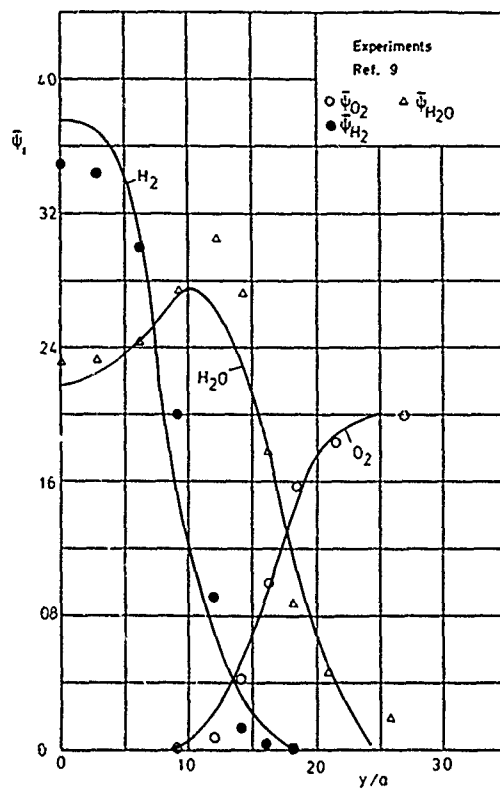


Fig. 14. Radial distribution of mean molar concentrations at  $x/D = 25, 50$  for flame 3.

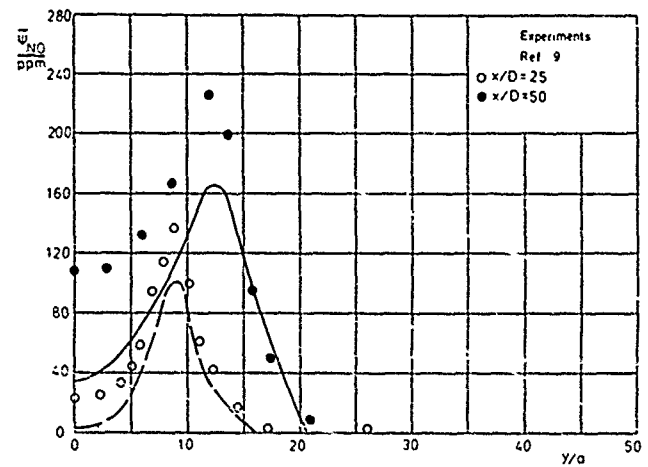


Fig. 15. Radial distribution of mean NO - concentration at  $x/D = 25, 50$  for flame 3.

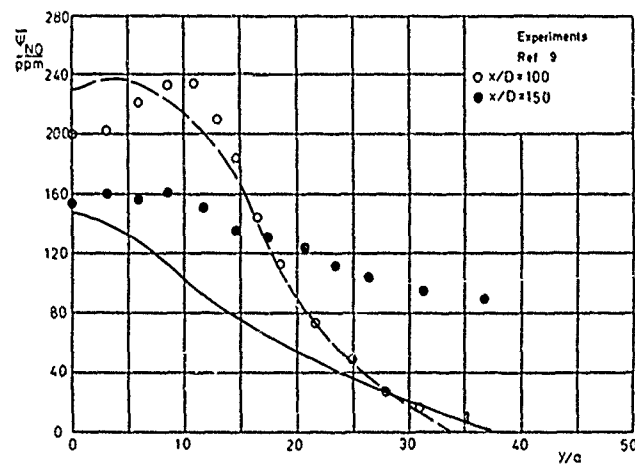


Fig. 16. Radial distribution of mean NO - concentration at  $x/D = 100, 150$  for flame 3.

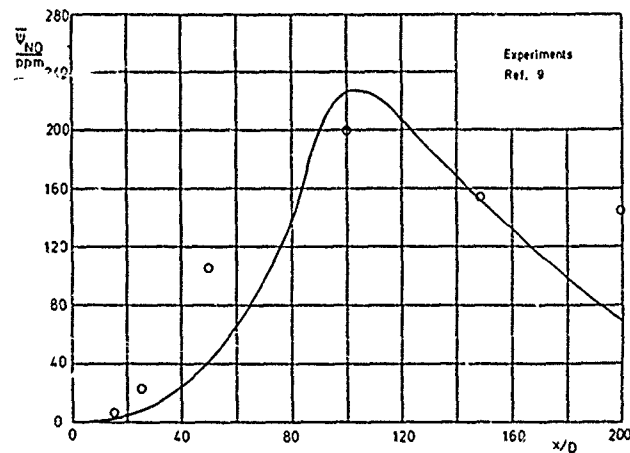


Fig. 17. Axial distribution of mean NO - concentration for flame 3.

## DISCUSSION

N.Peters, Ge

In a recent study [1] of the first author with myself we could show that the local NO-formation does depend on the scalar variance, the total NO-formation does not.

By evaluating the mean turbulent NO reaction rates in the limit of large NO-activation-energies we could decouple the influence of turbulence from that of the kinetics. We found that higher variances of the mixture fractions would spread the NO-production over a larger volume and into the fuel rich part of the flame but that its integral over the flame volume would not change considerably.

- [1] J.Janicha                      *Evaluation of the Turbulent NO-Production Rate in the Limit of Large Activation Energies*, submitted to Combustion, Science and Technology.  
N.Peters

Author's Reply

That superstates my own conclusion.

F.C.Lockwood, UK

- (1) It seems to me that the overall reaction in the flames you have examined must be largely turbulence rate controlled. In this respect how would your calculations compare with those assuming an infinitely fast reaction rate?
- (2) Can you offer any physical arguments in support of your three Dirac function assumption for  $P(s)$ ? The one at  $F$  would seem least satisfactory.

Author's Reply

- (1) Infinitely fast reactions can easily be simulated in our program by setting the reaction variable to unity. There is little influence on mean density, temperature and concentrations of stable components. The mean radical and NO concentrations show marked difference to the complete model.
- (2) A physically more satisfactory form of the pdf could be obtained by solving the pdf-transport equation as pointed out in the paper. For the current calculations the form of  $r(s)$  was chosen that seemed appropriate with respect to the dependence of the NO-source term  $S$ , on  $f$  and  $r$ .

A.K.Varma, US

Once a model for the pdf has been established, it is of course possible to calculate all the turbulence/chemistry interaction correlations in the equations for  $\bar{r}$ ,  $\bar{f}$ ,  $\bar{r}^2$  etc. Did you include all these terms — specially third-order correlations — in the source terms in the transport equations?

Author's Reply

All correlations of functions of mixture fractions  $f$  and reaction variable  $r$  were of course evaluated by integration using the pdf.

C.H.Priddin, UK

The applicability of your joint PDF depends strongly on the assumption of Equation (36) that the PDF is separable into two parts (covariance of  $Z$  and  $S$  zero). Do you have any information to indicate how good this assumption is?

Author's Reply

Since there is no experimental information for the simultaneous pdf  $P(f, r)$  available the computationally most efficient form was adopted. Numerical tests using different forms of the one-dimensional pdf's constituting  $P(f, r)$  showed little influence on the mean NO-profiles (see Reference 6). More general pdf's  $P(f, r)$  are currently investigated.

## TURBULENT REACTION AND TRANSPORT PHENOMENA IN JET FLAMES

BY

H. EICKHOFF, Institut für Antriebstechnik, DFVLR, Linder Höhe, 5000 Köln 90, W.Germany

K. GRETHE, Lehrstuhl für Feuerungstechnik, Universität Karlsruhe,  
Richard-Willstätter-Allee, 7500 Karlsruhe, W.GermanyF. THIELE, Hermann-Föttinger-Institut, Technische Universität Berlin,  
Straße des 17. Juni 135, 1000 Berlin 12

## SUMMARY

A new reaction model accounting for intermediate species was applied in connection with the  $k$ - $\epsilon$ -model to predict different free and enclosed turbulent natural gas flames. The reaction model is based on the assumption of a quasilaminar flame substructure of a turbulent diffusion flame and a probability density distribution of fuel-atom-concentration. It is assumed, that the quasilaminar flames are in local chemical equilibrium within zones of finite thickness.

The influence of variable density on the mixing process was studied for different jets and jet flames. In the parabolic flow cases it was found necessary to account for variable density which was done by a mixing length relation. Different numerical procedures were applied for the parabolic and elliptic flow fields

## LIST OF SYMBOLS

$c$	mass fraction
$c_A$	mass fraction of fuel atoms
$d$	nozzle-diameter
$f$	transformed stream function
$k$	kinetic energy of turbulence
$l$	mixing length
$P$	probability density function
$Q$	general variable, Eq.(3.5)
$S_\phi$	source term
$T$	temperature
$u, v$	velocity components
$x, r$	coordinates
$z$	similarity parameter
$\alpha$	intermittancy
$\epsilon$	dissipation
$\xi, \eta$	transformed coordinates
$\psi$	stream function
$\rho$	density
$\tau_t$	turbulent shear stress
$\mu_t$	effective viscosity
$\phi$	general variable, Eq.(3.1)
$\Gamma_\phi$	general transport coefficient

Subscripts

$\infty$	outer boundary
$c$	centerline

## 1. INTRODUCTION

The main problem in modelling turbulent combustion for engineering applications is to develop appropriate simplifications for the complex phenomena of chemical reactions and turbulent transport.

As a simple and useful way to account for the influence of turbulence on chemical reactions, the flame sheet assumption was introduced and coupled with a probability density distribution of the concentration of fuel atoms.

As in fuel rich regions of hydrocarbon flames especially the existence of carbon monoxide cannot be neglected the flame sheet model was extended [1].

## 2. THE REACTION MODEL

The instantaneous gas composition in the flame sheet approximation, with reactions taking place only in an infinitely thin layer, is a mixture of stoichiometric reaction products and either fuel or oxidant in the fuel rich and fuel-lean regions, respectively. In the present model it is assumed that the turbulent diffusion flame exists of a brush of quasilaminar flames in local chemical equilibrium within zones of finite thickness and a frozen flow outside.

In Fig. 1 as an example the instantaneous CO-concentration and temperature are shown as function of the mass fraction of fuel atoms  $c_A$ . To define the boundaries of the equilibrium zone it would be necessary to know the characteristic flow and chemical times.

For reasons of simplicity we introduce a critical temperature at  $c_{A1}$  in the fuel rich region below which the reactions freeze, as it was first done by Libby [2] for a laminar boundary layer combustion.

Since the concentrations of intermediate species are close to zero at the reaction zone boundary on the fuel lean side, equilibrium can be assumed throughout the fuel lean region. If the flame approximately can be assumed to be adiabatic with respect to its surrounding then it is not necessary to solve an energy balance equation to calculate the temperature and gas composition, which are obtained from an adiabatic equilibrium calculation if the fuel mass fraction  $c_A$  is known.

Otherwise a non adiabatic equilibrium calculation has to be performed and in addition the energy equation has to be solved.

To calculate the equilibrium-zone composition and temperature, a computer program of Pratt and Wormeck [3] was used. In the fuel rich region I, Fig. 1, our crude assumption is that the gas is a mixture of unreacted fuel and an averaged concentration of products of the equilibrium zone.

The steps of the temperature and concentrations at the freezing boundary  $c_{A1}$  of cause are physically unrealistic because of finite reaction rates and molecular diffusion. But as we are dealing with a highly turbulent flow this simplifying assumption may be adapted.

To account for the influence of turbulent fluctuations we introduce a probability density function for the mass fraction of fuel atoms  $P(c_A)$ . It is a modified Gaussian function and was derived by Haberdad [4], based on experiments.

Mean values of the flow variables are obtained, if the instantaneous values  $\phi(c_A)$  of the flame zone approximation, Fig. 1, are introduced from the relation, [4]:

$$\bar{\phi}(c_A) = \alpha \int_0^1 \phi(c_A) P(c_A) dc_A + (1 - \alpha) \phi_\infty \quad (2.1)$$

with  $\alpha$  as the intermittency factor being a function of the turbulence intensity of the concentration fluctuations.



### 3. BASIC EQUATIONS

The conservation equations for two-dimensional flows can be written in the general form

$$\frac{\partial(\rho u \phi)}{\partial x} + \frac{1}{r} \frac{\partial(r \rho v \phi)}{\partial r} - \frac{\partial}{\partial x} \left( \Gamma_{\phi} \frac{\partial \phi}{\partial x} \right) - \frac{1}{r} \frac{\partial}{\partial r} \left( r \Gamma_{\phi} \frac{\partial \phi}{\partial r} \right) = S_{\phi} \quad (3.1)$$

with

$$\phi = u, v, c_A, k, \epsilon, c_A'^2.$$

The set of equations given by Eq.(3.1), the equation of state and Eq.(2.1) including the flame zone approximation, Fig.1, determine the problem.

#### 3.1 Jet Flames of Boundary Layer Type

For jet flames of boundary layer type Eq.(3.1) in terms of the x-momentum equation becomes after an order of magnitude analysis for large density fluctuations

$(\frac{\rho'}{\rho} \sim 1)$ , as derived by Bray [5]

$$\frac{\partial(\bar{\rho} \bar{u}^2)}{\partial x} + \frac{1}{r} \frac{\partial(r \bar{\rho} \bar{v} \bar{u})}{\partial r} + \frac{\partial}{\partial r} (\bar{\rho} \overline{u'v'} + \bar{\rho}' \overline{u'v'} + \bar{v} \overline{\rho'u'}) = S_u \quad (3.2)$$

with  $S_u$  for the buoyancy term.

Introducing a stream function  $\psi$  by

$$\frac{\partial \psi}{\partial x} = -(\bar{\rho} \bar{v}), \quad \frac{\partial \psi}{\partial r} = \bar{\rho} \bar{u} \quad (3.3)$$

and neglecting the term  $\bar{v} \overline{\rho'u'}$  of the turbulent shear stress in Eq.(3.2) only the triple correlation  $\overline{\rho'u'v'}$  remains which has to be modelled for variable density flows of boundary layer type in addition to incompressible flows.

Here we introduce the simple assumption

$$-\overline{\rho'u'v'} = c_{\rho} \overline{u'v'} l \frac{\partial \rho}{\partial r} \quad (3.4)$$

where  $c_{\rho}$  is an empirical constant which has to be determined from experiments and  $l$  is a mixing length.

The term  $\overline{u'v'}$  is given by the known k- $\epsilon$ -model

$$-\overline{u'v'} = c_{D,r} \frac{k^2}{\epsilon} \frac{\partial u}{\partial r} \quad (3.5)$$

where  $c_{D,r}$  is an empirical expression.

With Eqs.(3.4) and (3.5) the turbulent shear stress becomes

$$\tau_t = -\mu_t \frac{\partial \bar{u}}{\partial r} = (\bar{\rho} + c_{\rho} l \frac{\partial \rho}{\partial r}) c_{D,r} \frac{k^2}{\epsilon} \frac{\partial \bar{u}}{\partial r} \quad (3.6)$$

### 4. NUMERICAL PROCEDURE

For free burning jet flames of boundary layer type a numerical procedure is applied which has been derived by Thiele [6]. The numerical procedure for predicting the elliptic flow field was taken from [7].

Before the parabolic differential equations according to Eq.(3.2) are solved numerically, the following similarity transformation [8] is applied

$$\xi = \int (\rho \mu_t)_c dx, \quad \eta = \int \rho r dr / \xi^{2\kappa} \quad (4.1)$$

with the transformed stream function

$$f(\xi, \eta) = \psi/\xi^K \quad (4.2)$$

The value of  $\kappa$  is equal to zero in the initial jet region  $u_c = u_0$  and 1 further downstream. With this transformation the x-momentum becomes

$$zf_{\eta\eta\eta} + \{z_\eta + \xi^K f_\xi + \kappa f\} f_{\eta\eta} + (\kappa f_\eta - \xi^K f_{\eta\xi}) f_\eta = S_u \quad (4.3)$$

with

$$z \equiv 2 \rho u_c / (\rho u_c)_c \cdot d\eta/\rho \quad (4.4)$$

If the value of  $z$  is a function of  $\eta$  only (for constant density and eddy viscosity  $z = 2 \eta$ ) then a similarity solution is obtained from Eq.(4.3) and accordingly from the other balance equations. Although there are deviations from similarity in turbulent jet flames, the "similarity"-transformation is useful if the equations are to be solved numerically as the flow variables vary slowly in the main flow direction.

The transformed differential equations can be written in the general form

$$a Q_{\eta\eta\eta} + b Q_{\eta\eta} + c Q_\eta + d Q_\xi + e Q_{\eta\xi} = g \quad (4.5)$$

where  $Q$  represents the stream function, element mass fraction etc. By applying the well known backward finite-differences in  $\xi$ -direction the parabolic differential equation is reduced to an ordinary differential equation. This equation is solved by the finite-difference method of Hermitian type. The high accuracy of the method results from the fact that the grid point values of the function and the first derivative are used for the approximation of the higher derivatives. Thus we get a considerable reduction in the number of grid points used. Furthermore, for the momentum equation which is of third order and the element mass fraction equation which is of second order the finite-difference approximation yields a  $2 \times 2$  block-tridiagonal system of finite difference equations which can be solved by a Gaussian elimination procedure. Due to the transformation only few iterations are necessary to solve the nonlinear momentum equation. An additional advantage of the transformation is that boundary conditions  $u(\eta_\infty) \geq 0$  can be satisfied without difficulties.

The system of conservation equation (4.5) of the unknowns  $f$ ,  $c_A$ ,  $c_A'^2$ ,  $k$  and  $\epsilon$  has been solved with the constants of the closure assumptions as given in Table 1 and the additional empirical relations discussed below.

Table 1 (Symbols as defined in [7]).

$c_1$	$c_2$	$c_D$	$\sigma_k$	$\sigma_\epsilon$	$c_{g1}$	$c_{g2}$	$\sigma_c$	$\sigma_g$
1,43	1,92	0,09	1,0	1,3	2,8	2,0	0,7	0,9

The influence of the value of the empirical constant  $c_p$  in Eq.(3.6) was studied numerically and was found to be approximately 1.5.

As known from Rodi's investigations [9] on free turbulent shear flows there exists no universal set of constants. To get agreement of prediction with experiment for round jets the value of  $c_D$  was modified [9]. Other proposals have been made also [10].

To account for the curvature effect in a round jet we prefer for simplicity and physical plausibility the following modification of  $c_D$  for round jets

$$c_{D,r} = c_D \frac{r + c_r l_c}{r + l} \quad (4.6)$$

where  $c_r$  is an additional empirical constant, which was found to be 0.78.

The mixing length  $l$  in Eqs.(3.6) and (4.6) is given by  $k$  and  $\epsilon$  through the relation  $l = k^{3/2}/\epsilon$ .

## 5. RESULTS

The influence of the additional constants  $c_p$  and  $c_r$  accounting for variable density and curvature effects were investigated systematically for parabolic flows.

First investigations concerned different non reacting jets with density differences due to the mixing of two different gases ( $H_2$ -air and  $CO_2$ -air).

Results are shown in Fig.2, where predictions are compared to experimental values [11, 12].

The larger spreading rate of the hydrogen jet in terms of  $(\rho u^2)_0/(\rho u^2)_c$  is rather well predicted with the constants  $c_r = 0.78$  and  $c_p = 1.5$ .

The strong influence of the constant  $c_p$  is demonstrated in Fig.3 where in addition to  $(\rho u^2)_0/(\rho u^2)_c$  the reciprocal value  $c_o/c_c$  of the mass fraction is shown.

In the next Fig.4 predictions of the axial temperature profile of a free burning natural gas flame are shown. There is a remarkable influence of  $c_r$  as well as of  $c_p$ .

The experimental data are rather well predicted with those values of the empirical constants  $c_r = 0,78$  and  $c_p = 1,5$  which have been fitted for the non reacting turbulent jets.

The influence of the constants  $c_r$  and  $c_p$  on the spreading rate is shown in Fig.5.

From predicted axial and radial profiles of species concentration in Figures 6 and 7 it can be seen, that the present reaction model yields satisfying results. The deviations of CO- and CO<sub>2</sub>-concentrations around  $x/d = 60$  in Fig.6 are due to the step of the instantaneous distributions in the flame zone approximation, Fig.1.

The flame zone model also has been used for the prediction of the same natural gas flame but enclosed in a combustion chamber. The flame data are listed in Table 2.

Table 2 flame data:

nozzle diameter	$d = 8 \text{ mm,}$
chamber diameter	$D = 450 \text{ mm}$
fuel velocity	$u_o = 71 \text{ m/s}$
equivalence ratio	$0,9$

Applying the numerical procedure of [7] preliminary results were obtained. Axial profiles of temperature  $T$  and velocity ratio  $u/u_o$  are shown in Fig.8 and radial profiles of temperature and CO-concentrations at two different cross sections  $X/d = 60$  and  $90$ , in Fig.9. The calculations of the elliptic flow field have been performed with  $c_r$  and  $c_p$  both equal to zero, but recently we found still some influence of the number of grid points used in the numerical scheme. Present investigations therefore concern further investigations on the influence of these constants.

## CONCLUSIONS

Numerical investigations on free turbulent jet flames have shown that it is necessary to account for variable density in the closure approximation of the  $k-\epsilon$ -model. Further investigations concerning the influence of variable density in elliptic flow fields are necessary.

The flame zone model was found to be appropriate for the prediction of intermediate species in the fuel rich region, where CO exists to a large extent. This comparatively simple model, based on the mass fraction of fuel atoms overcomes the disadvantages of the flame sheet model.

As far as the emission of carbonmonoxide as a pollutant is concerned, the model would be extended to include the CO- + OH-reaction kinetic for fuel lean regions.

As the finite-difference method of Hermitian type proved to be advantageous for parabolic flows it is being extended to predict elliptic flows also.

## REFERENCES

1. H. Eickhoff, K. Grethe, "A Flame Zone Model for Turbulent Hydrocarbon Diffusion flames." To appear in: Combustion and Flame (1979).
2. P.A. Libby, C. Economos, "A Flame Zone Model for Chemical Reaction in a Laminar Boundary Layer with Application to the Injection of Hydrogen-Oxygen-Mixtures." Int.J.Heat Mass Transf.6, 113-128 (1963).
3. D.T. Pratt, J.J. Wormeck, "A Computer Program for Calculation of Combustion Reaction Equilibrium and Kinetics in Laminar or Turbulent Flow." Report WSU-ME-TEL-76-1, Washington State Univ.
4. F. Haberda, "Die Berechnung turbulenter Diffusionsflammen unter Berücksichtigung von Konzentrationsschwankungen." Thesis, Univ.Karlsruhe (1977).
5. K.N.C. Bray, "Equations of Turbulent Combustion. I Fundamental Equations of Reacting Flow." AASU Report No.330 (1973).
6. F. Thiele, "Accurate Numerical Solutions of Boundary Layer Flows by the Finite-Difference Method of Hermitian Type." J.of Comp.Phys.Vol.27, No.1, (1978).

7. W.M. Pun, D.B. Spalding, "A General Computer Program for Two-Dimensional Elliptic Flows,". Report HTS/76/2, Imperial College of Science and Techn., Mech.Eng.Dep. London.
8. F. Thiele, "Die numerische Berechnung turbulenter rotationssymmetrischer Freistrahlen und Freistrahldiffusionsflammen." Thesis, Univ.Karlsruhe (1975).
9. W. Rodi, "The Prediction of Free Turbulent Boundary Layers by Use of a Two-Equation Model of Turbulence." Thesis, Univ.of London (1972).
10. S.B. Pope, "An Explanation of the Turbulent Round-Jet/Plane - Jet Anomaly. AIAA-Journal, Vol.16, No.3 (1978).
11. B. Lenze, R. Gunther, "Ausbrand und Wärmeentwicklung in Erdgas-Diffusionsflammen." Brennstoff-Wärme-Kraft, 17:387-394 (1975)
12. Engler-Bunte-Institut der Universität Karlsruhe (T.H.), Bereich Feuerungstechnik, Prof.R.Gunther (private communication).

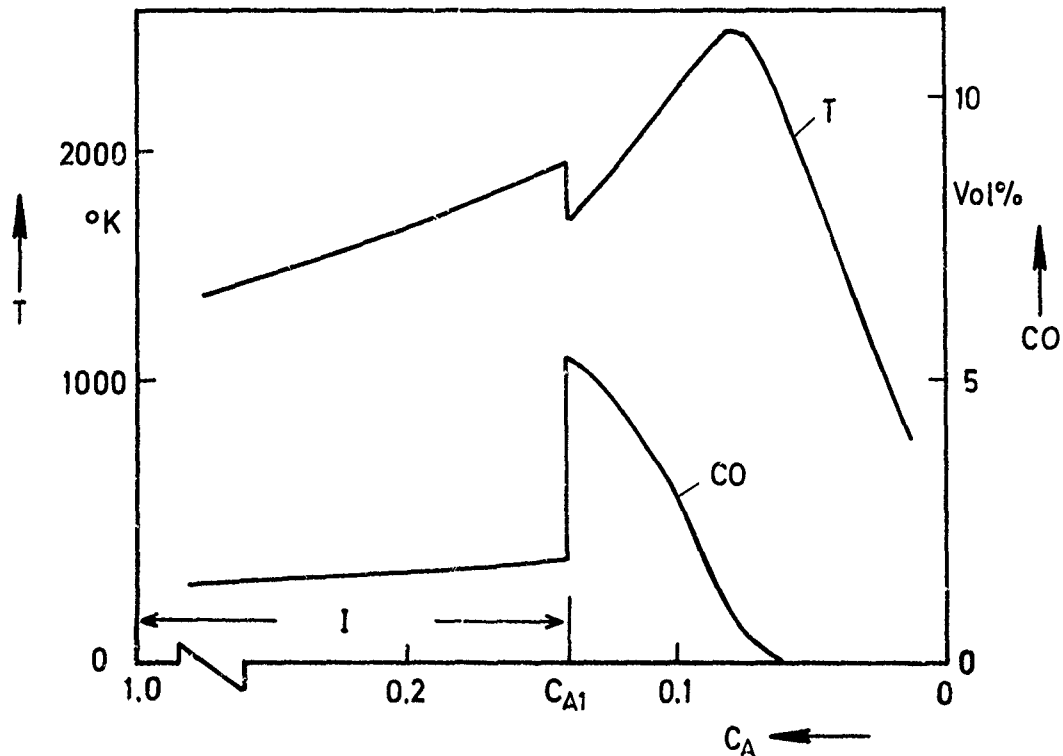


Fig. 1: Instantaneous temperature and CO-concentration as function of mass fraction of fuel atoms  $c_A$

7. W.M. Pun, D.B. Spalding, "A General Computer Program for Two-Dimensional Elliptic Flows,". Report HTS/76/2, Imperial College of Science and Techn., Mech.Eng.Dep. London.
8. F. Thiele, "Die numerische Berechnung turbulenter rotationssymmetrischer Freistrahlen und Freistrahldiffusionsflammen." Thesis, Univ.Karlsruhe (1975).
9. W. Rodi, "The Prediction of Free Turbulent Boundary Layers by Use of a Two-Equation Model of Turbulence." Thesis, Univ.of London (1972).
10. S.B. Pope, "An Explanation of the Turbulent Round-Jet/Plane - Jet Anomaly." AIAA-Journal, Vol.16, No.3 (1978).
11. B. Lenze, R. Gunther, "Ausbrand und Wärmeentwicklung in Erdgas-Diffusionsflammen." Brennstoff-Wärme-Kraft, 17:387-394 (1975)
12. Engler-Bunte-Institut der Universität Karlsruhe (T.H.), Bereich Feuerungstechnik, Prof.R.Gunther (private communication).

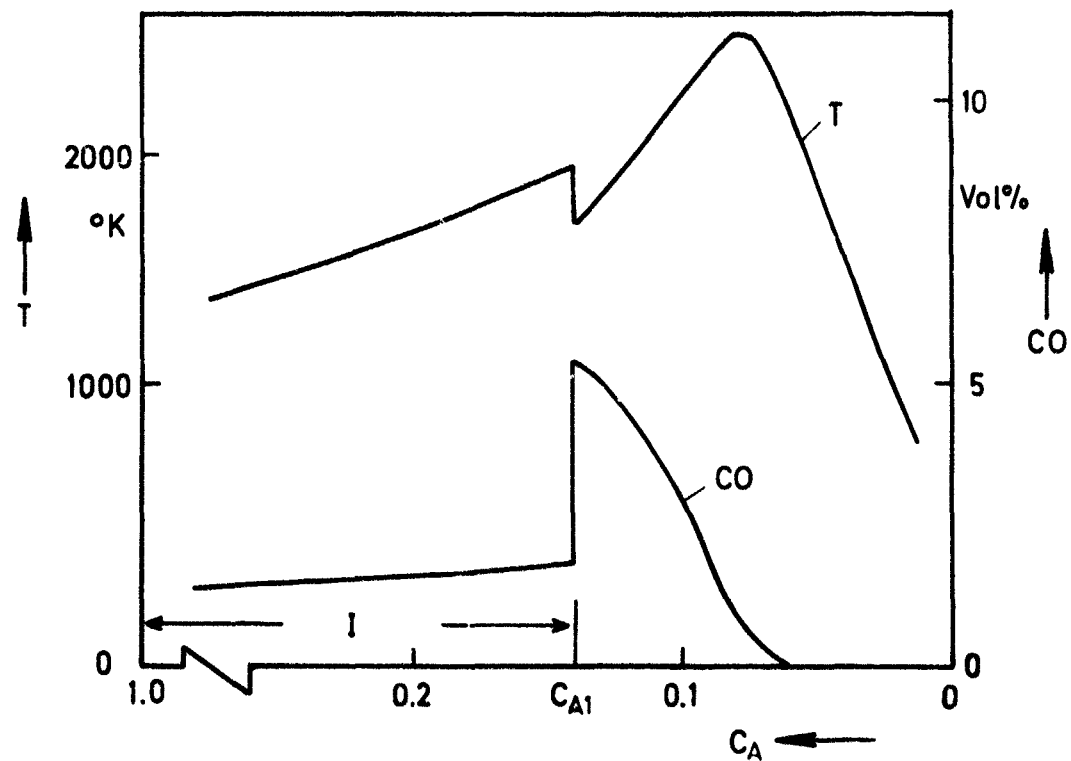


Fig. 1: Instantaneous temperature and CO-concentration as function of mass fraction of fuel atoms  $c_A$

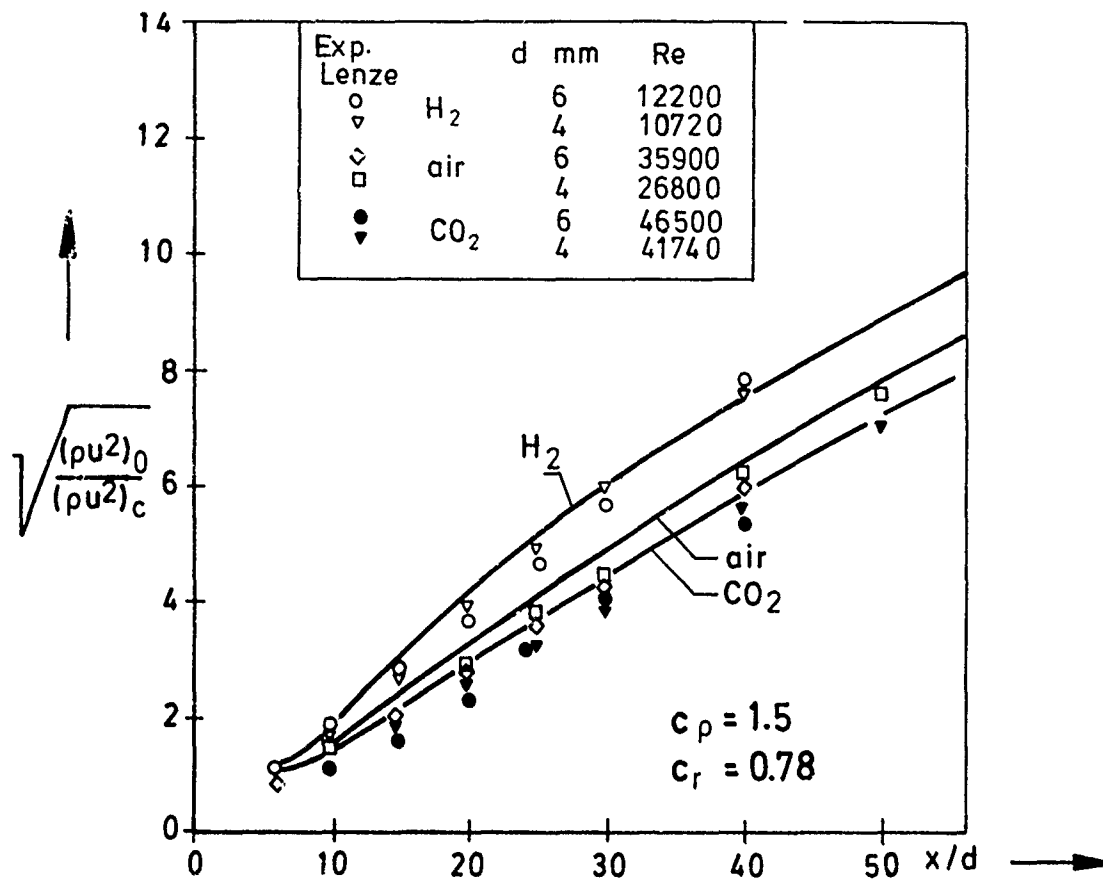


Fig. 2: Spreading rate of different turbulent gas jets. Comparison of prediction with experiments

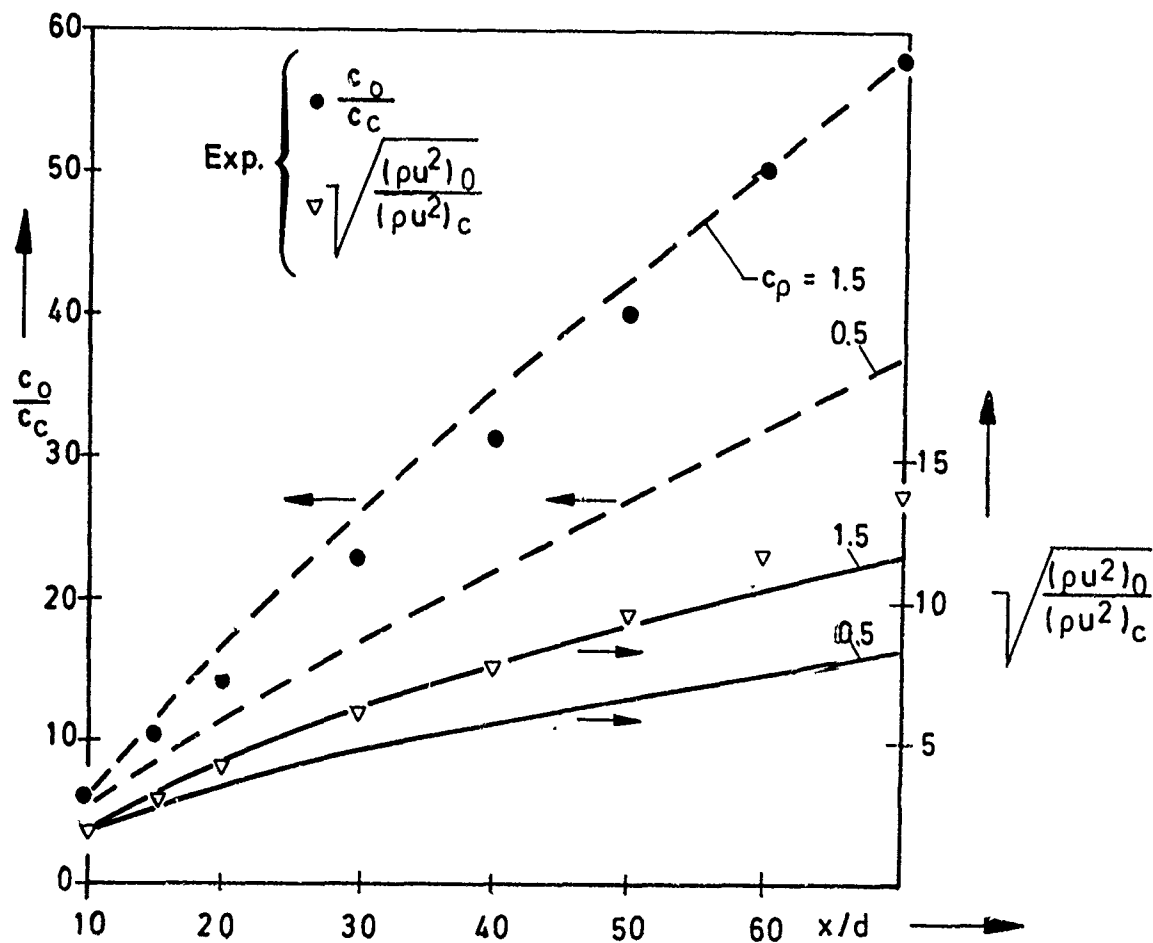


Fig. 3: Influence of the constant  $c_p$  on the spreading rate and axial concentration of a  $H_2$ -air jet

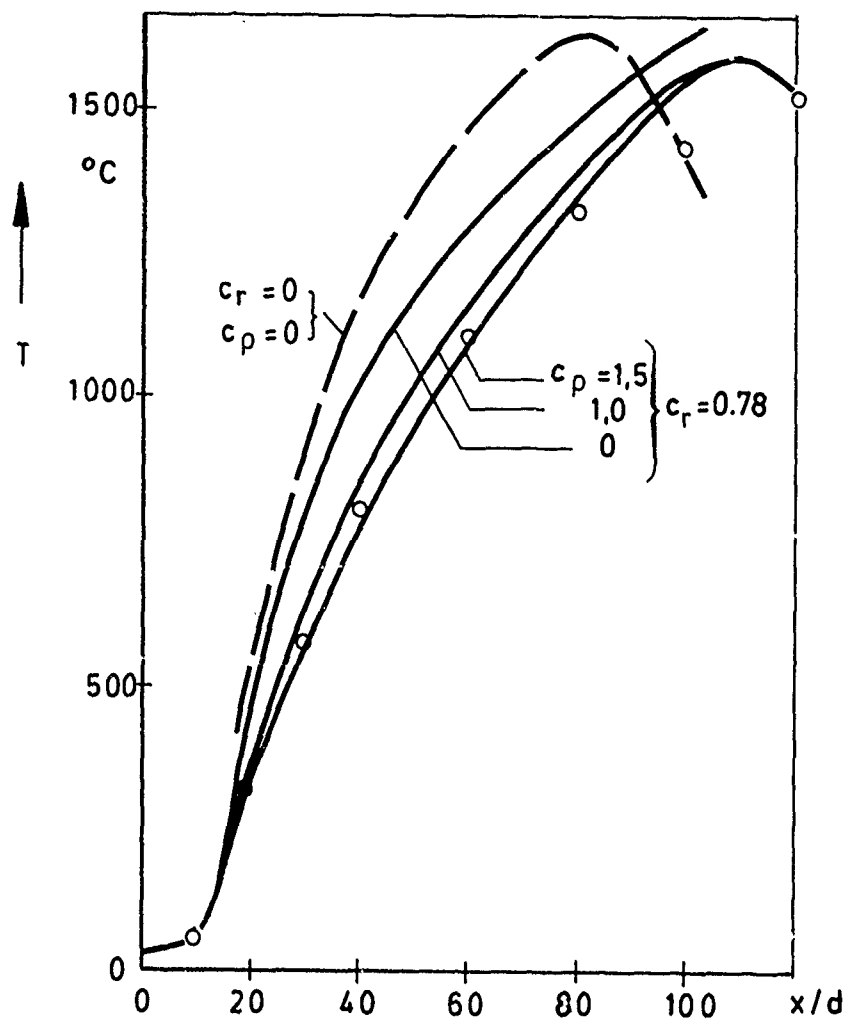


Fig. 4:  
Influence of the constants  $c_p$  and  $c_r$  on the axial temperature profile in a free natural gas flame

— prediction  
○ experiment

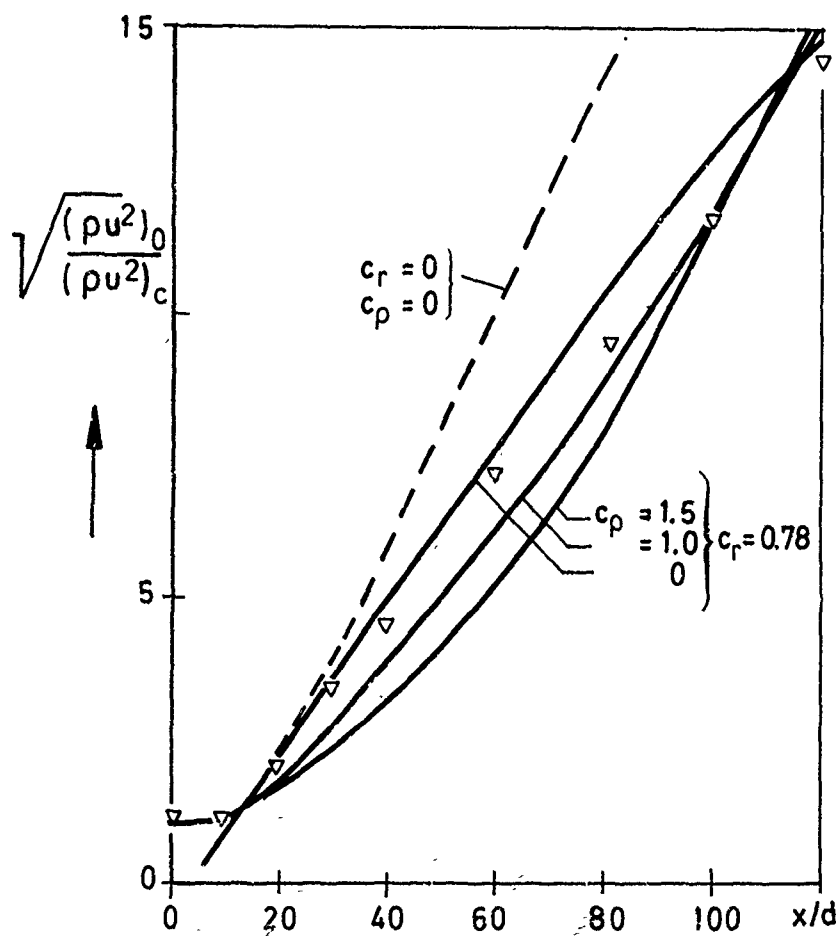


Fig. 5:  
Influence of the constants  $c_p$  and  $c_r$  on the spreading rate in a free jet natural gas flame

— prediction  
▽ experiment

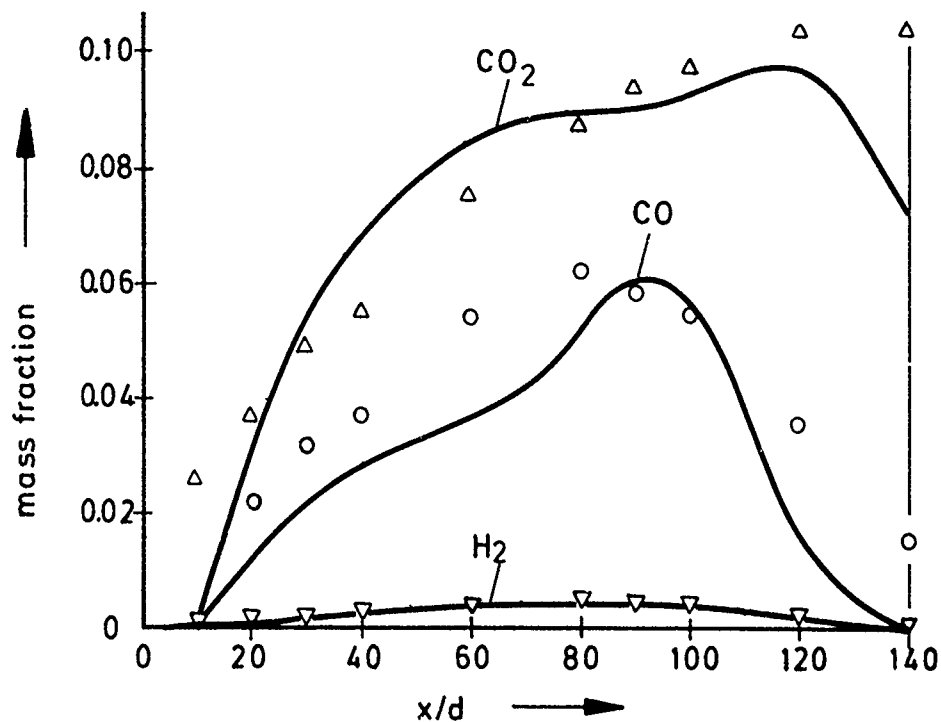


Fig. 6: Axial distributions of  $\text{CO}$ - and  $\text{CO}_2$ -concentrations in a free jet natural gas flame

— prediction  
 $\nabla \Delta \circ$  experiment

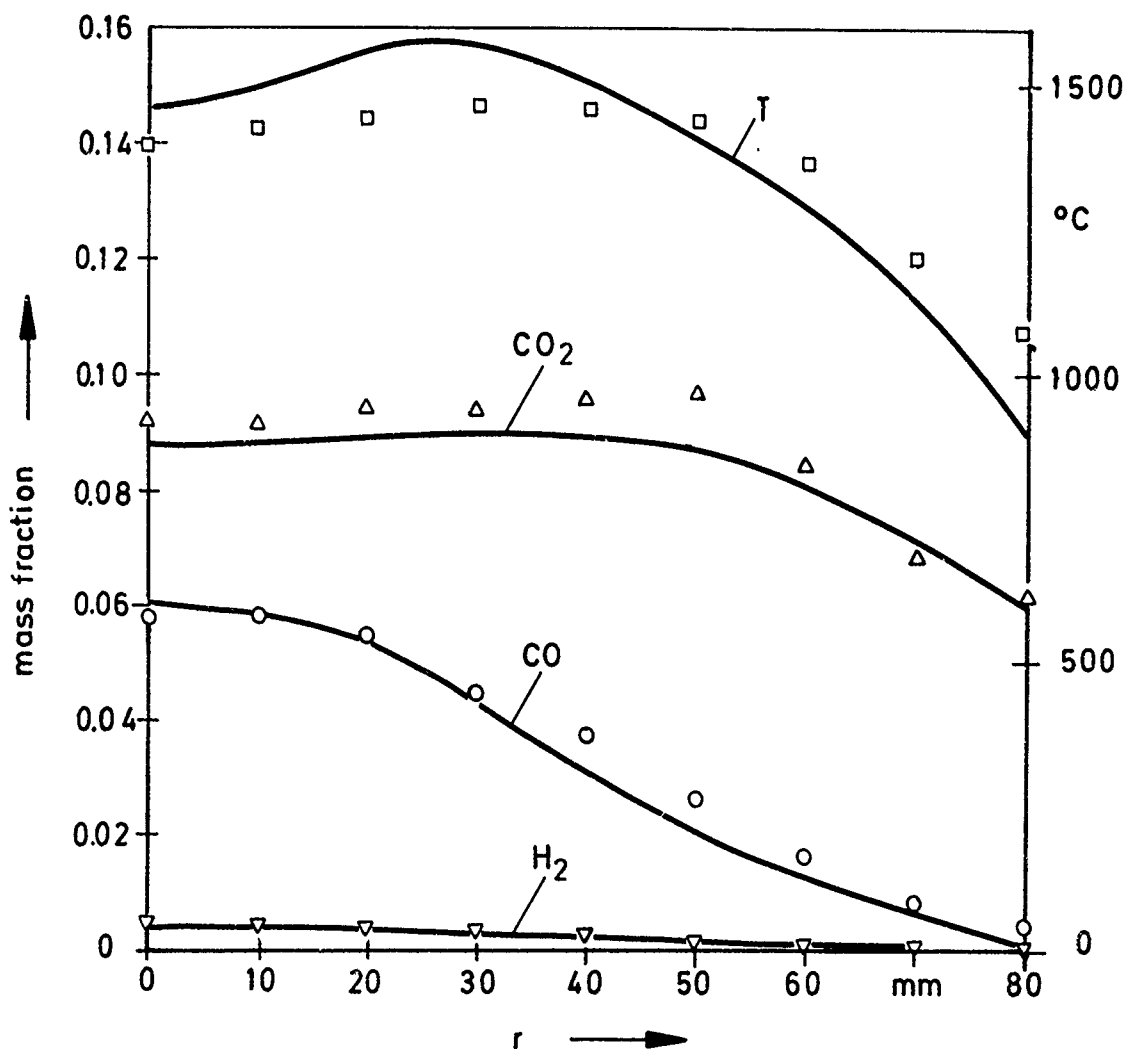


Fig. 7: Radial profiles of  $\text{H}_2$ -,  $\text{CO}$ -,  $\text{CO}_2$ -concentrations and temperature in a free jet natural gas flame at cross-section  $x/d = 90$



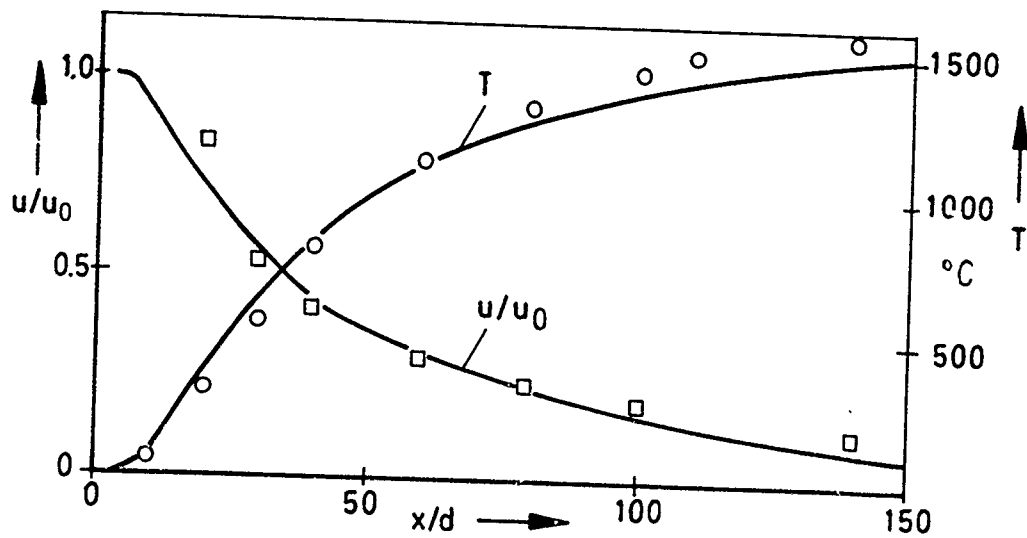


Fig. 8: Axial temperature  $T$  and velocity  $u/u_0$  in an enclosed natural gas flame

— prediction  
 □ ○ experiment

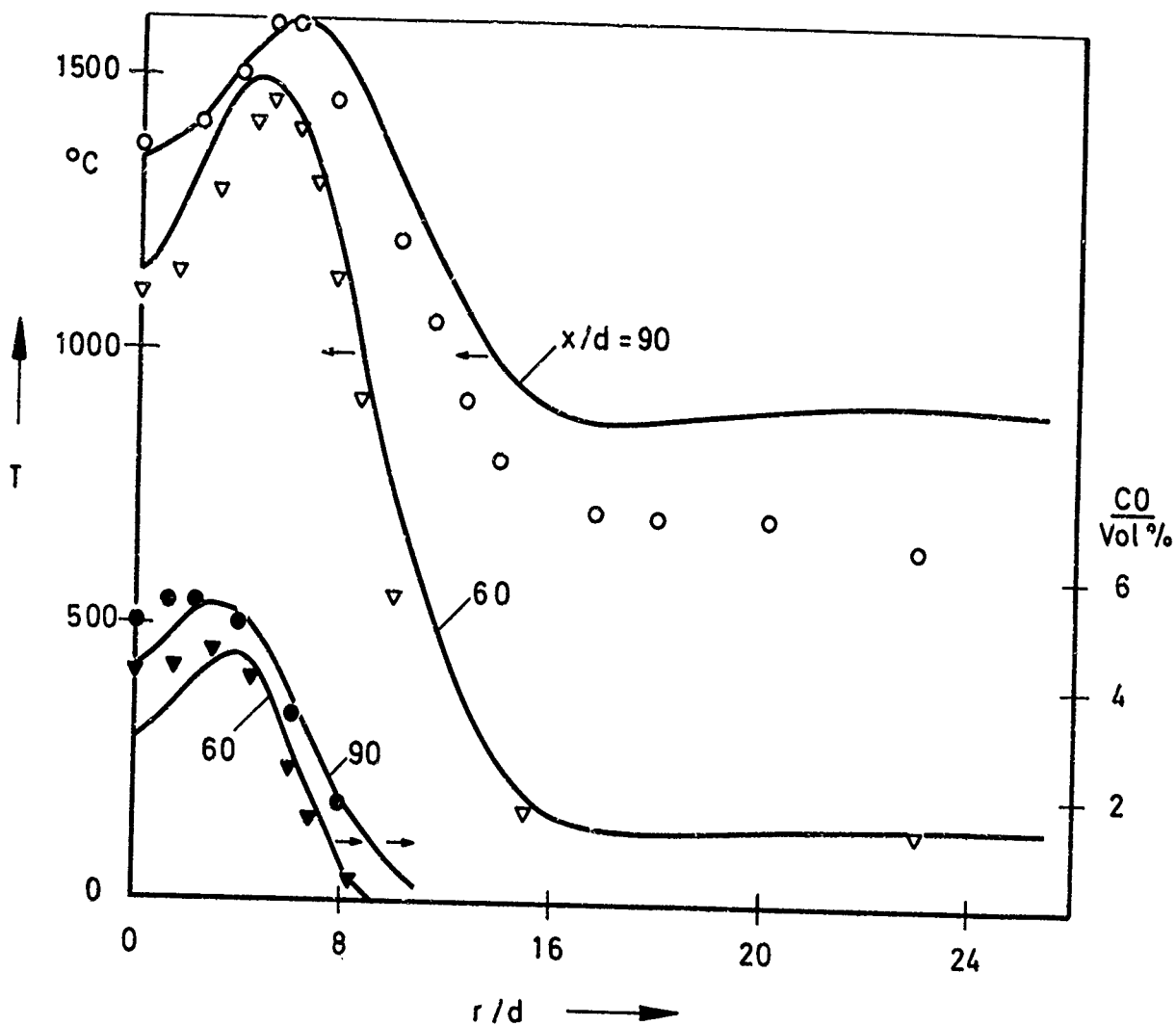


Fig. 9: Radial profiles of temperature  $T$  and CO-concentration in an enclosed natural gas flame

— prediction  
 ▽ ▴ ○ ● experiment

## DISCUSSION

J.H. Whitelaw, UK

It is likely that the round-jet anomaly does not occur in the sense that the  $k-\epsilon$  model can calculate the plane jet and not the round jet. It is more likely that the  $k-\epsilon$  cannot predict the spreading rate of either, if "flapping" and "room draughts" are present. Bradshaw has shown that the spreading rate of the flame jet, with its far-down stream measurements, is increased by the low frequency effects of flapping and draughts and that, without these phenomena, the spreading rate would be the same as for the round jet. Our own measurements show that flapping does not occur in round jets.

### Author's Reply

We agree that the  $k-\epsilon$  model cannot predict the spreading rate of jets if flapping is not taken into account. But in our opinion the gradient diffusion approximation for a transported quantity  $\phi$  in its' usual form:

$$\overline{\phi'v'} = \frac{\nu t}{\sigma \phi} \frac{\partial \phi}{\partial \pi}$$

should be modified in order to account for the influence of curvature, see also Spalding (‡)

(‡) Spalding, D.B. *Turbulent Mixing in Nonreactive and Reactive Flows*, ed. by S.N.B. Murthy, p.102, (1975).

A.K. Varma, US

Earlier in Paper 5 we saw good results obtained for Hydrogen-Air flames by the use of a turbulence model that used the basic  $k-\epsilon$  model unchanged but added equations for  $\rho'u'$  and  $\rho'v'$ . Can you reconcile your modifications of the  $k-\epsilon$  model for the effects of density variation with the results of Kollman?

### Author's Reply

Kollman and our approach are different but it cannot be excluded that they yield similar results. We demonstrated in our presentation the effect of  $\rho'u'$  modification of the  $k-\epsilon$  model and it would be interesting to see the effect of using additional equations for  $\rho'u'$  and  $\rho'v'$  as Kollman did it.

From our own investigations we know that the influence of variable density in turbulent hydrogen flames is less than in hydrocarbon flames.

N. Peters, Ge

I would like to point out the difference between the flame zone model of Libby and Economos and your model. In the flame zone model freezing at a certain temperature results in a jump of the slope of the temperature and concentration profiles while your model assumes the jump of the value itself. The flame zone model was shown to correspond to the large activation energy limit for a one-step reversible reaction<sup>1</sup>. I doubt that a jump condition for the values of the dependent variables can be justified in a rational way.

1. Peters, N. *Premixed Burning in Diffusion Flames - the Flame Zone Model of Libby and Economos*. Int. J. of Heat and Mass Transfer, Vol.22, pp.691-703, (1979).

### Author's Reply

In principle you agree with our statement in Chapter 2.

Th.T.A. Paaw, Ne

Did you measure oxygen concentrations on the centre-line of your natural gas flame, and if so, have you compared this with your predictions?

### Author's Reply

Yes we compared our predictions to the measurements of  $O_2$  in the natural gas flame. We obtained in general satisfying agreement except at the beginning of the flame where we had an underprediction of oxygen. This is due to the fact, that there have been problems with flame stabilisation. This has not been taken into account in our prediction.

# ON THE PREDICTION OF TEMPERATURE PROFILES AT THE EXIT OF ANNULAR COMBUSTORS

Osama M.F. Elbahar and Sigmar L.K. Wittig  
Institut für Thermische Strömungsmaschinen  
Universität Karlsruhe (TH), Kaiserstr. 12  
D-7500 Karlsruhe 1

## SUMMARY

Despite their inherent limitations, two-dimensional prediction procedures based on solving the basic equations and incorporating the  $k-\epsilon$  model of turbulence are shown to be effective tools in designing annular combustors. In comparing the results it is found that predictions from available jet mixing correlation data within certain limitations will represent measurements from single row injection more accurately. Detailed calculations, however, will be more effective in predicting opposite wall cooling air injection, multiple row jet mixing, heat transfer, film cooling and the effects of converging combustor exit. Because of its relative simplicity, the prediction procedure is particularly suited for design parameter studies.

## LIST OF SYMBOLS

B	slot width
$C_d$	hole discharge coefficient
$C_\mu$	a constant in the turbulence model
D	hole diameter
H	duct or combustor height
h	enthalpy of fluid
J	momentum flux ratio
k	Kinetic energy of turbulence
$\dot{m}$	mass flow rate
S	spacing between the centerlines of two adjacent holes
$S_\phi$	source term in the conservation equation of the variable $\phi$
T	absolute temperature
u	x-component of velocity
v	y-component of velocity
W	width
x	distance in flow direction
y	distance in direction perpendicular to x
z	distance in direction perpendicular to both x and y
$\Gamma_\phi$	exchange coefficient for the variable $\phi$
$\mu$	fluid viscosity
$\rho$	density
$\theta$	dimensionless temperature ratio
$\epsilon$	dissipation of turbulence energy
$\phi$	general notation of a dependent variable

## Subscripts

c	jet centerline
eff	effective
j	related to the cooling air jet
min	minimum
t	turbulent
w	wall
$\phi$	related to the variable $\phi$
1/2	half quantity
$\infty$	related to mainstream

## Superscripts

+	plus side, or side away from jet entrance wall
-	minus side, or side toward jet entrance wall

## 1. INTRODUCTION

Recent attempts to increase the specific power or thrust and to reduce the specific fuel consumption of jet engines as well as of stationary gas turbines necessitates operation under high turbine inlet temperatures. Elevated inlet temperatures imply increasingly stringent limitations upon the temperature profile at the entrance to the turbine, i.e. exit of the combustor. Hot gas temperature profiles must be matched carefully to turbine blade stress levels if long turbine life is to be attained. For this reason, prediction techniques for the temperature profile at the combustor exit have become of primary importance.

The development of the temperature profiles depends primarily on the mixing process between the cooling air and the hot gas flow in the mixing (dilution) zone of the combustor<sup>1</sup>. In addition to providing a suitable temperature profile, rapid mixing of the dilution air with the hot gases exiting the primary and secondary zones will lead to the desired reduction in combustor length and to a generally preferred uniform rapid quench of continuing high temperature chemical reactions. The penetration and mixing characteristics of rows of cooling jets injected into hot confined crossflow, therefore, have been the subject of several experimental investigations<sup>2,3</sup>. The results reported by Holdeman et al.<sup>4</sup> and by Walker and Kors<sup>3</sup> were used in modeling the penetration and mixing characteristics of multiple cooling jets. Walker and Eberhardt<sup>5</sup> developed a model for the temperature field. Data of selected tests from Reference 3 were used by Cox<sup>6</sup> and Holdeman and Walker<sup>7</sup> to generate empirical models for predicting the temperature distribution downstream of a row of dilution jets injected normal to a hot confined cross flow as illustrated in Figure 1a.

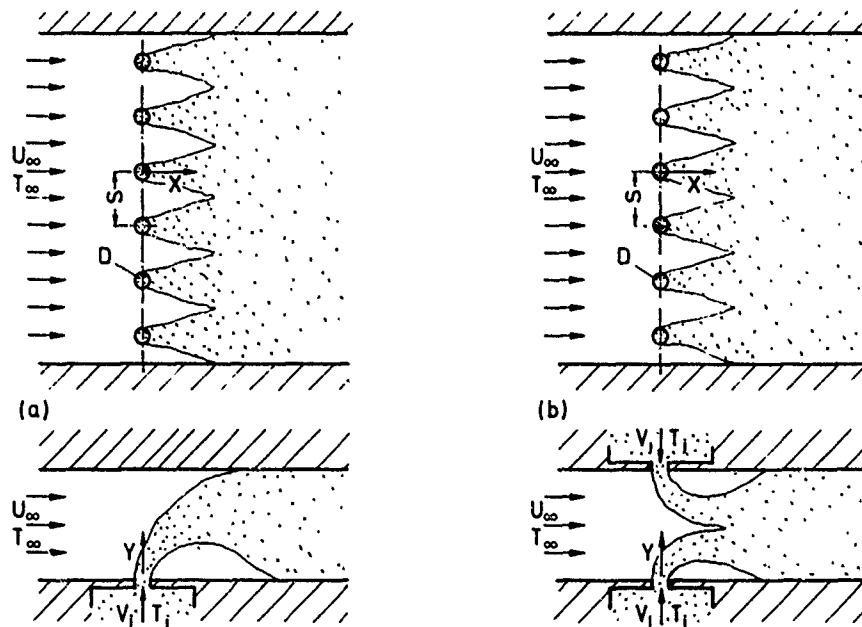


Fig. 1 Schematic of multiple-jet mixing process:  
a) single-wall cooling air introduction  
b) opposite-wall cooling air introduction

The results for the temperature field are presented as profiles of the dimensionless temperature difference ratio  $\theta$  where

$$\theta = \frac{T_{\infty} - T}{T_{\infty} - T_j} \quad (1)$$

and  $T$  is the local total temperature. Because  $T > T_j$ , the highest values of  $\theta$  in any profile correspond to the coolest region of the flow.

The empirical model used in the correlations<sup>6,7</sup> is based on the assumption that the properly nondimensionalized vertical temperature profiles in the flowfield can be expressed in a self-similar form, where six scaling parameters are required to completely define the vertical temperature profile. These scaling parameters, shown in Figure 2, are:

1.  $\theta_c$ , the jet-centerline dimensionless temperature difference ratio;
2.  $\theta_{\min}^{\pm}$ , the minimum dimensionless temperature difference ratio on the jet-minus side (the side toward the wall from which the jet enters) and plus-side (the side away from the jet entrance wall);
3.  $W_{1/2}^{\pm}/D$ , the normalized jet half-width (the location where  $\theta_{1/2}^{\pm} = (\theta_c + \theta_{\min}^{\pm})/2$ ) on the jet plus-side and minus-side;
4.  $y_c/D$ , the normalized location of the jet centerline (where  $\theta = \theta_c$ ).

The form of the self-similar solution is nearly Gaussian. The similarity equation is

$$\frac{\theta - \theta_{\min}^{\pm}}{\theta_c - \theta_{\min}^{\pm}} = \exp \left[ - \ln 2 \left( \frac{W/D}{W_{1/2}^{\pm}/D} \right)^2 \right] \quad (2)$$

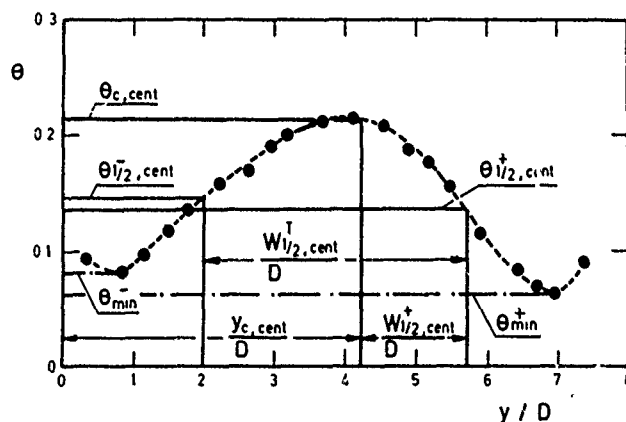


Fig. 2 Typical jet center plane of symmetry vertical-temperature profile showing similarity scaling parameters (see Reference 6)

The line defined by the locus of  $y_c$  as a function of the downstream distance  $x$  at the jet center-plane of symmetry ( $z = 0$ ), Figure 1a, is the jet thermal trajectory. Because the flow is confined, and the profiles are not symmetrical about the centerline, the half width  $W_{1/2}$  and the temperature difference ratios are different for the plus-side and the minus-side of the profiles. The correlations<sup>6,7</sup> have been developed for each of the scaling parameters in terms of the independent variables  $J$ ,  $S/D$ ,  $H/D$ ,  $x/H$  and  $z/S$ . The resulting temperature profiles for selected conditions are compared with measurements in Figures 4, 5 and 6. It is obvious that the predictions obtained from the correlations of Reference 7 deviate slightly from those obtained from the correlations of Reference 6. This is due to some additional simplifications in the form of the correlations equations reported in Reference 7.

Despite their usefulness, major shortcomings limit the applicability of the jet mixing correlations to design analysis. Because of their origin, i.e. derivation from single row injection, accurate predictions of the effects of multiple row, nonsymmetric opposite wall jet mixing, of heat transfer with the flame tube's walls, geometrical variations such as a convergent combustor exit as well as the profiled inlet velocity and temperature are impossible.

The present study is concerned with the development of a prediction procedure to be used in the design analysis of the temperature profile in the mixing zone of an annular combustor. Primary zone effects are not considered. The conservation equations of mass, momentum and energy are solved by means of a finite difference method including the two-equation  $k-\epsilon$  model of turbulence. The accuracy of the model is tested with available measurements.

## 2. PREDICTION PROCEDURE

The numerical description of turbulent flows by now is well established and a prediction of the mixing processes in the dilution zone of a combustor is possible. The method depends on the solution of the time-averaged conservation equations of mass, momentum and energy together with a model of turbulence. The flow in the mixing zone of a combustor is three-dimensional elliptic. However, a computer program for solving such a system of equations, although available in principle, cannot be considered as a design tool, owing to the huge storage capacity and the excessive computing times required. Furthermore, many aspects of the three-dimensional codes are not yet well tested. These problems are simplified in the present study by assuming that in order to predict the average radial temperature profile at the exit of the combustor it is sufficient under certain conditions to consider the flow to be two-dimensional. Results of the computations subsequently can be compared with measurements and predictions from available correlations.

The problem considered is that of the injection of one or more rows of cooling jets in a hot, confined crossflow either from one side, Figure 1a, or from both sides, Figure 1b. This is a typical case of three-dimensional and recirculating flow which will, however, be approximated, as mentioned before, to a two-dimensional one by assuming that each row of jets could be modeled by a slot of equivalent area, so that the momentum flux ratio and the mass flow ratio, defined respectively as

$$J = \left( \frac{\rho_j}{\rho_\infty} \right) \left( \frac{v_j}{u_\infty} \right)^2 \quad (3)$$

$$\frac{\dot{m}_j}{\dot{m}_\infty} = \frac{\pi}{4} C_d \sqrt{(\rho_j/\rho_\infty)} \sqrt{J} / (H/D)(S/D) \quad (4)$$

remain unchanged. It has been shown that the momentum flux ratio  $J$  is the most important parameter of the jet mixing processes<sup>6</sup>.

The approximated model of the flow was then tested by comparing the resulting predictions of the temperature profiles with those of the jet mixing correlations of References 6 and 7 and with the measurements reported in Reference 6. The predicted as well as the measured temperature profiles represent average values, in a transverse direction, of all the temperatures at a given vertical location, i.e. certain value of  $x/H$ .

For a steady flow, the time-averaged conservation equations of mass, momentum and energy can all be cast in the following form:

$$\frac{\partial}{\partial x_i} (\rho u_i \phi) = \frac{\partial}{\partial x_i} (r_{\phi, \text{eff}} \frac{\partial \phi}{\partial x_i}) + S_\phi, \quad (5)$$

where  $\phi$  stands for any of the dependent variables, and  $S_\phi$  is a "source term". Setting  $\phi = 1$  in the above equation, one gets the mass conservation equation; whereas for  $\phi = u$  and  $v$  one gets the momentum equations in  $x$  and  $y$  directions, respectively. The equation for  $\phi = h$  represents the conservation of the stagnation enthalpy; it is derived from the first law of thermodynamics under some simplifying assumptions. The local temperature can be easily obtained upon solving the  $h$ -equation. Further information on the above mentioned system of equations may be found, for instance, in References 8 and 9.

For the estimation of  $S_\phi$  and  $r_\phi$  it is necessary to know the local values of the effective viscosity,  $\mu_{\text{eff}}$ , defined as

$$\mu_{\text{eff}} = \mu_t + \mu \quad (6)$$

In order to calculate the distribution in the field of the turbulent viscosity  $\mu_t$ , a turbulence model must be included. The model applied here is the so-called  $k-\epsilon$  model<sup>10</sup>; it involves two transport equations for two turbulence characteristics. One of the equations governs the distribution in the field of  $k$ , the kinetic energy of the fluctuating motion; the other determines the turbulence energy dissipation  $\epsilon$ . The differential equations for  $k$  and  $\epsilon$  are of the form of equation (5). The turbulent viscosity  $\mu_t$  can then be calculated from

$$\mu_t = \rho C_\mu k^2 / \epsilon \quad (7)$$

The turbulence model constants were chosen following Reference 11.

The solution procedure chosen to solve the above system of equations is an iterative finite difference one<sup>12</sup>. The solution follows at specified points in the integration domain. A 25 x 25 grid was found to be suitable for performing the calculations. A well-converged solution was obtained after approximately 300 iterations.

To complete the mathematical formulation of the problem, it is necessary to specify the boundary conditions along the boundaries of the integration domain. The jet-to-mainstream velocity and temperature ratio as well as the mass flow ratio were set equal to those of the experimental conditions. The values of  $k$  and  $\epsilon$  at the inlet plane were calculated in a similar way as in Reference 11, whereas gradients of the dependent variables in the mainstream direction were set equal to zero at the exit plane. To avoid the need for detailed calculations in the regions close to the solid walls, the so-called wall-function approach was used<sup>10</sup>. It employs algebraic relations for the near-wall grid nodes, which have to be spaced at such a distance from the neighbouring walls that they lie within the so-called logarithmic layer.

Furthermore, for the present study the Reynolds analogy was used to calculate the heat exchange with the walls from the calculated value of the local wall shear stress. However, the boundary conditions for  $T$ , and accordingly  $h$ , could also be given through the specification of the gradient or the heat flux at the wall.

### 3. RESULTS AND DISCUSSION

The present prediction model is an attempt to approximate an originally three-dimensional flow to a two-dimensional one. Despite its limitations, it shows several advantages compared to the jet mixing correlations:

1. It can be easily developed to include calculations under complex geometries; e.g. the converging end of the annular combustor to the turbine inlet.
2. Despite the expected discrepancies in the temperature predictions, the model is sensitive to the heat transfer between the gases and the combustor walls, whereas the predicted wall temperatures from the jet mixing correlations are completely independent therefrom. Figure 3 shows the pronounced effect of the predicted temperature profile. The figure includes the predictions of correlations as well as the measurements and the predictions of the present procedure under two assumptions; the first case, curve (1), represents predictions obtained by setting the boundary conditions via the wall heat flux as previously explained, whereas curve (2) represents the predicted profile under the same conditions except for the bottom wall, Figure 1a, where the boundary conditions were specified by setting the temperature gradient at the wall equal to zero. A comparison shows clearly that changing the conditions of heat transfer with the walls does not only affect the local value of temperature, Figure 3, but also affects the shape of the predicted profile itself.
3. In general the cooling-air jets are introduced from both walls, as schematically shown in Figure 1b. The jet-mixing correlations cannot predict this case accurately, especially for nonsymmetric geometries.

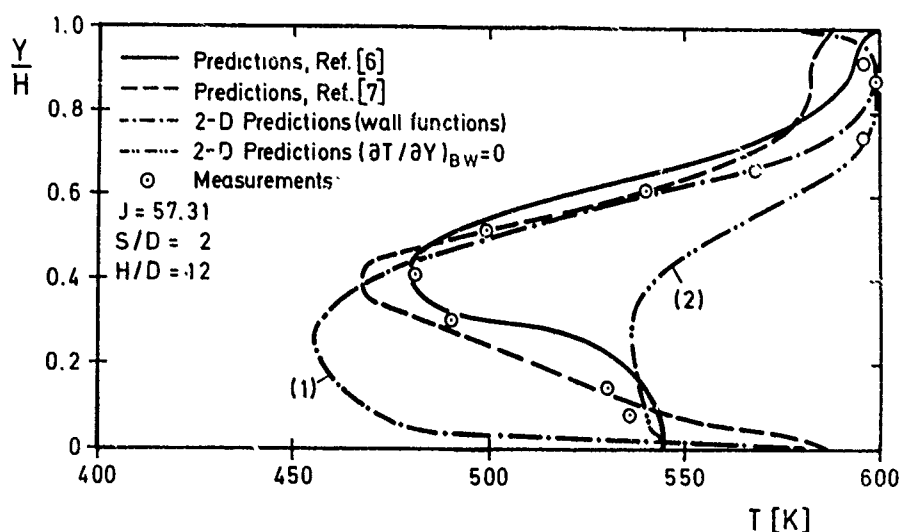


Fig. 3 Effect of boundary conditions on the predicted temperature profiles,  $x/H = 0.5$ .

Figure 4 shows a comparison between the results of the present predictions with available measurements and correlations for a test case with  $S/D = 2$ . The profiles from the correlations of References 6 and 7 as well as the measurements are averages, in a transverse direction, between two planes of symmetry, of all the temperature values at the considered axial location  $x/H$ . Here, the predictions were carried out for three axial

locations,  $x/H = 0.25, 0.5$  and  $1.0$ . Thus, the ability of the procedure to predict the temperature profiles, even close to the jet-injection plane, was tested. The results are in relatively good agreement with the measurements, even at low values of  $x/H$ .

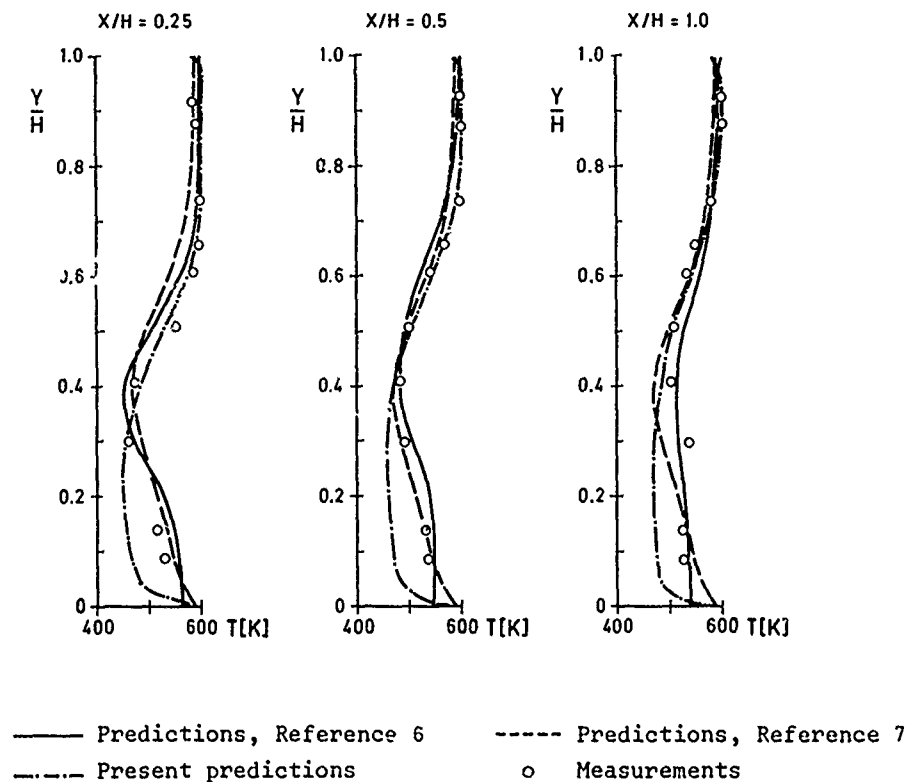
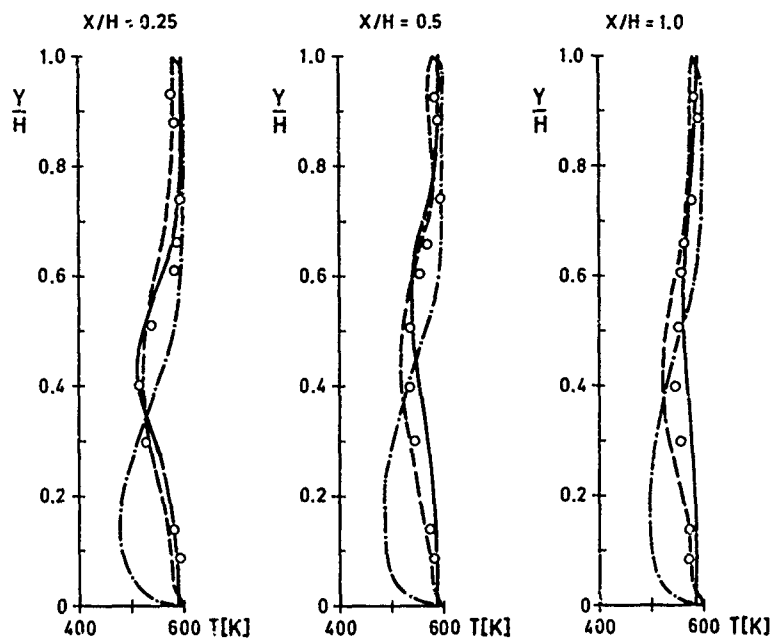


Fig. 4 Comparison of measured and predicted average-temperature profiles:  $J = 57.31$ ,  $S/D = 2$ ,  $d/D = 12$ .

Figure 5 illustrates the effects of an increase in spacing to  $S/D = 4$ . Here, as expected, predictions and measurements do not agree quite as well, the location of the point of minimum temperature is shifted towards the bottom, i.e. injection wall. This is due to two reasons: firstly, for the same mass flow ratio, the value of  $H/B$  is considerably higher than  $H/D$  and hence the penetration of the cooling jets will be drastically reduced<sup>6</sup>; secondly, as the value of  $S/D$  increases, the distance between each two cooling jets increases allowing more flow of hot gases in the gaps between the jets and resulting in some heating of the region near the bottom wall. However, Figure 5 shows clearly that present predictions are in good qualitative agreement with the measurements; the minimum temperature increases and the profile is flattened with increasing distance downstream the injection plane, i.e. increasing  $x/H$ . As  $S/D$  is found in the range between 3 and 4 for the new generation of annular combustors, the present prediction method is suitable for preliminary analysis in combustor design.

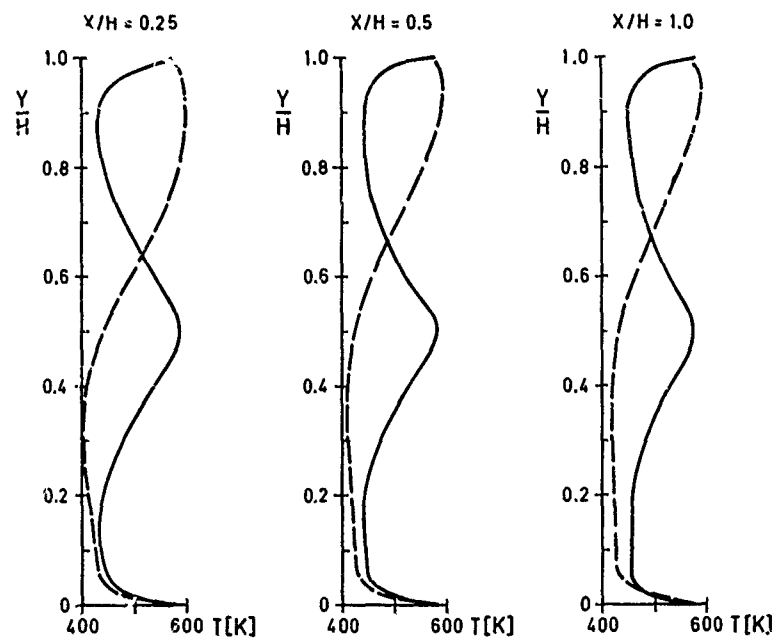
As previously mentioned, the major advantage of the present prediction procedure compared to the correlations approach is the possibility of its use under complex flow and geometrical conditions. Opposite-wall cooling air injection is a characteristic of the mixing zone of annular combustors. Especially for non-symmetric injection the application of available correlations is questionable. Figure 6 shows predictions of the present procedure for a typical test case with opposite-wall cooling air injection. Predicted are the temperature profiles at three axial locations:  $x/H = 0.25, 0.5$  and  $1.0$ . The dotted profiles are those for the case of single-wall injection but with all other boundary conditions kept constant, e.g. mass-flow ratio, temperature ratio .. etc. The rapid increase of the minimum temperature and the flattening of the profile with increasing  $x/H$  points out that the mixing under such conditions is considerably faster than that for single-wall injection. This is expected and can be explained if one imagines that for each row of jets in the opposite-wall case the effective duct height is smaller due to the existence of the opposite row of jets, and hence the mixing should be faster. Using the present procedure, calculations under more complex geometrical and flow conditions, e.g. converging end of the combustor, double-row opposite-wall cooling air injection etc. are possible<sup>13</sup>.





— Predictions, Reference 6      - - - Predictions, Reference 7  
 - · - Present predictions      o Measurements

Fig. 5 Comparison of measured and predicted average-temperature profiles;  $J = 60.34$ ,  $S/D = 4$ ,  $H/D = 12$ .



— one row of holes on each wall  
 - - - one row of holes on the bottom wall  
 $J = 57$ ,  $\dot{m}_j/\dot{m}_\infty = 0.48$ ,  $T_j = 290$  K,  $T_\infty = 600$  K

Fig. 6 Effect of cooling air introduction from both walls on the temperature profile

#### 4. CONCLUSIONS

The present prediction procedure for the calculation of the average radial temperature profiles in annular combustors was compared with experimental measurements and with two different jet mixing correlations. Despite the crude assumption of two-dimensional flow, the agreement between predicted temperature profiles and the measurements is sufficient, for use as a preliminary design tool for complex geometries as originally intended. Although the jet mixing correlations give better predictions of those measurements from which they were developed - as expected - the present procedure represents a better design technique; as it can be easily developed to include the effects of heat transfer with the combustor outer casing, the converging combustor exit (turbine inlet), the effects of film-cooling and opposite-wall cooling-air injection. The use as a design tool to show the effects of changing the design parameters of the combustor seems to bear considerable advantages. The final design decision, however, should be based on a more detailed analysis, i.e. three-dimensional calculation. Presently detailed experimental studies are under way for a verification of two-dimensional and three-dimensional codes under hot gas conditions.

#### REFERENCES

1. Lefebvre, A.H.  
Norster, E.R.      The Design of Tubular Gas Turbine Combustion Chambers for Optimum Mixing Performance.  
Proc. Institution of Mech. Engrs., Vol. 183, p. 150, 1968.
2. Norgen, C.T.  
Humenik, F.M.      Dilution Jet Mixing Study for Gas Turbine Combustors.  
NASA TN D-4695, 1968.
3. Walker, R.E.  
Kors, D.L.      Multiple Jet Study.  
NASA CR-121217, 1973.
4. Holdeman, J.D.  
Walker, R.E.  
Kors, D.L.      Mixing of Multiple Dilution Jets with a Hot Primary Airstream for Gas Turbine Combustors.  
AIAA Paper 73-1249, Las Vegas, Nev., 1973.
5. Walker, R.E.  
Eberhardt, R.G.      Multiple Jet Study Data Correlations.  
NASA CR 134795, June, 1975.
6. Cox, J.B., Jr.      Multiple Jet Correlations for Gas Turbine Engine Combustor Design.  
ASME Paper 75-GT-45, Houston, Tex., 1975.
7. Holdeman, J.D.  
Walker, R.E.      Mixing of a Row of Jets with a Confined Crossflow.  
AIAA Journal, Vol. 15, p. 243, Feb., 1977.
8. Spalding, D.B.      Basic Equations of Fluid Mechanics and Heat and Mass Transfer and Procedures for Their Solution.  
Report HTS/76/6, Imperial College, London, 1976.
9. Elghobashi, S.  
Pratt, D.T.  
Spalding, D.B.  
Srivatsa, S.K.      Unsteady Combustion of Fuels in Jet Engine Afterburners.  
Third International Symposium on Air Breathing Engines, DGLR-Fachband Nr. 6, Munich, 1976.
10. Launder, B.E.  
Spalding, D.B.      The Numerical Computation of Turbulent Flows.  
Computer Methods in Applied Mechanics and Engineering, Vol. 3, p. 269, 1974.
11. Khalil, E.E.  
Spalding, D.B.  
Whitelaw, J.H.      The Calculation of Local Flow Properties in Two-Dimensional Furnaces.  
Int. J. of Heat and Mass Transfer, Vol. 18, p. 775, 1975.
12. Caretto, L.S.  
Gosman, A.D.  
Patankar, S.V.  
Spalding, D.B.      Two Calculation Procedures for Steady, Three-Dimensional Flows with Recirculation.  
Proceedings of the Third Int. Conference on Numerical Methods in Fluid Mechanics, Vol. II, p. 60, 1973.
13. Wittig, S.L.K.  
Elbahar, O.      Zum Einfluß der Mischzone auf die Temperaturprofilentwicklung am Austritt von Gasturbinenbrennkammern.  
Festschrift zum 70. Geburtstag von Prof. R. Friedrich, Universität Karlsruhe, p. 131, 1979.

#### ACKNOWLEDGEMENTS

Thanks are due to Dr. D. Hennecke and Dr. B. Simon, Motoren- und Turbinen-Union (MTU) München, for their helpful discussions.

## DISCUSSION

**J. McGuirk, UK**

I would like to comment on your explanation of the fact that your predicted minimum temperature is closer to the injection wall than was measured. I think your reasoning, which highlighted the physical differences between 2D calculations and 3D measurements, may be correct, but even if you compared with proper 2D (plane) measurements, I think you would discover the same discrepancy. Calculations we have made at Imperial College for only 2D (i.e. plane) slot jets in cross flow show that, particularly for the high momentum flux ratios you are considering, the recirculation length downstream of injection is too short, hence the jet trajectory curves too quickly back to the injection plane, and the same discrepancy as you observe is obtained.

**Author's Reply**

Your comment is quite true. Earlier today we have seen similar effects for more detailed calculations. We feel we can introduce simple correction terms to account for this effect. However, this is an inadequate procedure and we preferred to present the uncorrected results for comparison. The basic problem — and you certainly have a better feeling for it than we do — probably stems from the turbulence model. In our experimental study we are planning to investigate this point in more detail.

**P. Magre, Fr**

Can you predict the effects of the inhomogeneities at the exit of the primary zone on the temperature profile at the exit of the burner.

**Author's Reply**

The computer program is certainly able to account for non-homogeneous flow and temperature distributions. However, they must be specified as boundary conditions at the inlet plane into the mixing zone.

As I already mentioned, we have not yet incorporated detailed primary zone calculations discussed earlier today into the present version of the computer program.

**D.C. Dryburgh, UK**

Experience with practical combustors indicates that there are large random effects in the dilution zone. Why these should exist is not known with certainty but it may be due to unstable flows in the annulus feeding of the dilution holes, to manufacturing tolerances and irregularities in the dilution holes and so on. This appears to imply that progress will require the use of fundamental models — possibly of finite difference type — and that to understand the random effects we may have to consider regions with 2 or 3 jets, rather than a region with half a jet and half a space with symmetry conditions. Could the author comment on this viewpoint?

**Author's Reply**

I agree basically with your assessment of the general problem. These questions were actually one of the dominant reasons for us to initiate the present study. We were interested in evaluating the effects of various parameters, i.e. wall temperature, momentum flux ratio, non-symmetric jet arrangement etc. At present, however, our program will not be applicable to unsteady mixing flows. These will be considered later. The present goal is to check on the limitations of available correlations and to provide the designer with a relatively simple tool in developing a combustor.

**A. Sotheran, UK**

I just make a point that I think practical. Randomness begins in the compressor, and in the diffuser. You just tried to find it in the dilution zone. These are more realistic models than all of them with CO, NO<sub>x</sub> predictions in the primary zone.

**Author's Reply**

I agree.

## DISCUSSION

**J. McGuirk, UK**

I would like to comment on your explanation of the fact that your predicted minimum temperature is closer to the injection wall than was measured. I think your reasoning, which highlighted the physical differences between 2D calculations and 3D measurements, may be correct, but even if you compared with proper 2D (plane) measurements, I think you would discover the same discrepancy. Calculations we have made at Imperial College for only 2D (i.e. plane) slot jets in cross flow show that, particularly for the high momentum flux ratios you are considering, the recirculation length downstream of injection is too short, hence the jet trajectory curves too quickly back to the injection plane, and the same discrepancy as you observe is obtained.

**Author's Reply**

Your comment is quite true. Earlier today we have seen similar effects for more detailed calculations. We feel we can introduce simple correction terms to account for this effect. However, this is an inadequate procedure and we preferred to present the uncorrected results for comparison. The basic problem – and you certainly have a better feeling for it than we do – probably stems from the turbulence model. In our experimental study we are planning to investigate this point in more detail.

**P. Magre, Fr**

Can you predict the effects of the inhomogeneities at the exit of the primary zone on the temperature profile at the exit of the burner.

**Author's Reply**

The computer program is certainly able to account for non-homogeneous flow and temperature distributions. However, they must be specified as boundary conditions at the inlet plane into the mixing zone.

As I already mentioned, we have not yet incorporated detailed primary zone calculations discussed earlier today into the present version of the computer program.

**D.C. Dryburgh, UK**

Experience with practical combustors indicates that there are large random effects in the dilution zone. Why these should exist is not known with certainty but it may be due to unstable flows in the annulus feeding of the dilution holes, to manufacturing tolerances and irregularities in the dilution holes and so on. This appears to imply that progress will require the use of fundamental models – possibly of finite difference type – and that to understand the random effects we may have to consider regions with 2 or 3 jets, rather than a region with half a jet and half a space with symmetry conditions. Could the author comment on this viewpoint?

**Author's Reply**

I agree basically with your assessment of the general problem. These questions were actually one of the dominant reasons for us to initiate the present study. We were interested in evaluating the effects of various parameters, i.e. wall temperature, momentum flux ratio, non-symmetric jet arrangement etc. At present, however, our program will not be applicable to unsteady mixing flows. These will be considered later. The present goal is to check on the limitations of available correlations and to provide the designer with a relatively simple tool in developing a combustor.

**A. Sotheran, UK**

I just make a point that I think practical. Randomness begins in the compressor, and in the diffuser. You just tried to find it in the dilution zone. These are more realist models than all of them with CO, NO<sub>x</sub> predictions in the primary zone.

**Author's Reply**

I agree.

## SECOND-ORDER CLOSURE MODELING OF TURBULENT MIXING AND REACTING FLOWS

Ashok K. Varma  
Guido Sandri  
Coleman duP. Donaldson

Aeronautical Research Associates of Princeton, Inc.  
50 Washington Road  
Princeton, N.J. 08540

Models for the scalar probability density function (pdf) have to be developed to achieve closure of turbulent transport equations for mixing and reacting flows. A delta function "typical eddy" model has been developed for the joint pdf of the scalar variables. It has been demonstrated that delta functions are a necessary part of pdf's in order to attain the extremums of the statistical constraints on the moments. The statistical bounds on a number of moments of interest for two and three species flows have been derived. It has been proven that a rational pdf composed of a set of delta functions alone can always be constructed at any point within the statistically valid moment space. The model provides a good representation of actual pdf's in two-species, variable-density mixing flows. The model has been directly compared to experimental pdf measurements and good agreement for higher-order moments has been demonstrated. It can be shown that the delta function pdf model is significantly simpler than other proposed pdf models and is more than adequate for the closure of the transport equations.

### NOMENCLATURE

$f, g$	arbitrary variables
$H$	arbitrary function
$p$	pressure
$P, P_1, P_2$	probability functions
$R$	universal gas constant
$T$	temperature
$u$	flow velocity
$W_\alpha, W_\beta, W_\gamma$	molecular weights of species
$x^\alpha$	coordinate in flow direction
$y$	coordinate normal to flow direction

### Greek Symbols

$\alpha, \beta, \gamma$	species mass fractions
$\alpha_3$	model parameter
$\delta_3(\alpha-\lambda)$	delta function located at $\alpha = \lambda$
$\Delta$	$1 - \frac{W_\beta}{W_\alpha}$
$\epsilon$	cell sizes in "typical eddy" model
$\eta$	entropy of mixing
$\kappa$	model parameter
$\lambda$	arbitrary constant
$\rho$	density
$\rho_*$	normalized density

### Superscripts

$\bar{\phantom{x}}, \langle \phantom{x} \rangle$	time average
$\bar{\phantom{x}}'$	fluctuation about mean value

### INTRODUCTION

Mixing and chemical reactions under turbulent flow conditions are a basic feature of the energy release processes in gas turbine combustors and other propulsion systems, and any predictive modeling of the flowfield has to properly account for the effects of the turbulence of the flow and its interactions with various physical and chemical processes. There are significant interaction effects of the turbulence on combustion and of the combustion on the turbulence, which are important in determining combustion efficiency, pollutant formation, combustion noise, heat transfer, etc. Second-order closure modeling of turbulent flows provides a convenient framework for studying these interactions and holds promise of providing a reliable predictive computational tool for the design of new systems and improvement of existing combustion systems.

The presence of finite-rate chemical reactions in a turbulent flow introduces the problem of proper modeling of many higher-order correlations involving scalar variables such as concentration, density and temperature. The transport equations for the mean variables and the second-order correlations are solved in a second-order closure procedure and these equations and especially the chemical reaction source terms contain many third-order and higher-order correlations, such as  $\overline{\rho^2 \alpha}$ ,  $\overline{\rho \alpha^2}$ , etc. These correlations have to be modeled in terms of the lower-order moments to close the system of transport equations. A convenient procedure for modeling these scalar correlations is to model or

calculate the probability density function (pdf) for the scalars. This procedure is being used at A.R.A.P., as well as by Rhodes, et al., (1) Bray and Moss, (2) Lockwood and Naguib (3), Libby (4), Bonniot (5) and Kewley (6).

A number of the above approaches require a number of simplifying assumptions and deal only with one-dimensional pdf's. Most of them are also restricted to fast chemistry and cannot handle finite-rate chemical reactions. The A.R.A.P. model, called the delta function "typical eddy" model is designed to be applicable to finite rate chemical reactions and models the joint pdf for all the scalars in a turbulent reacting flow. The basic model has been discussed by Donaldson (7) and Donaldson and Varma (8). Kewley (6) is using the A.R.A.P. model with some modifications and has reported good results on modeling of reacting flows.

Efforts are also being made to avoid the assumptions regarding the shape of the pdf, by directly solving transport equations for the pdf (9, 10, 11). However, these equations have only been solved for very simple flowfields and there appear to be serious modeling problems for some of the terms in the equations. Spalding (12) has recently proposed an alternate approach that involves the calculation of the pdf by following the age history of various eddies.

The paper discusses the statistical behavior of scalar variables in turbulent flows. Constraints on two and three species systems have been derived. The delta function "typical eddy" pdf model has been carefully tested against pdf measurements in a two-species, variable-density mixing layer and good results have been obtained.

### STATISTICAL CONSTRAINTS ON CORRELATIONS

Basic statistical principles can be used to develop a set of constraint conditions on correlations of various variables in a turbulent flowfield. The procedure is quite general and can be applied to scalar or vector variables, but at the present time, we are mainly interested in the constraints on scalar moments--specifically those for the species mass and/or molar concentration variables.

The constraint conditions are useful in a number of ways. The statistical constraints on first and second-order correlations are important in the question of "realizability" of second-order closure turbulence models. The lower-order moments are calculated by the solution of a set of modeled partial differential equations. It is possible that the modeled equations may not have solutions that are consistent with the independently derived statistical constraints, and this will require appropriate corrections to the models used in the equations. The statistical constraints on the third-order and higher-order moments are also useful in formulating models for these correlations. They are also useful in determining model sensitivity and the error-bounds of the modeling procedure.

### BASIC THEOREMS

#### Cauchy-Schwarz Inequality

The statistical constraints on various moments of the fluctuations are basically derived from conservation conditions and the Cauchy-Schwarz inequality. The Cauchy-Schwarz condition for arbitrary variables  $f$  and  $g$  is

$$\overline{f^2} \cdot \overline{g^2} \geq \overline{fg}^2 \quad (1)$$

The equality holds if and only if,

$$f = \lambda g \quad (2)$$

In principle, with suitable choices of  $f$  and  $g$ , one can derive all the required statistical constraints. In practice, this is not easy. A very useful short-cut is the use of a "Renormalization Theorem." If we have proven that,

$$\int_0^1 \overline{f^2}(A) P_1(A) dA \int_0^1 \overline{g^2}(A) P_1(A) dA \geq \left( \int_0^1 \overline{fg} P_1(A) dA \right)^2 \quad (3)$$

then it can be proven that for  $H(A) \geq 0$

$$\int_0^1 H \overline{f^2}(A) P_1(A) dA \int_0^1 H \overline{g^2}(A) P_1(A) dA \geq \left( \int_0^1 H \overline{fg} P_1(A) dA \right)^2 \quad (4)$$

The proof is simple. Since Eqn. 3 is valid for all  $P_1$ , one can select  $P_1$  of the special form  $HP_2$  for any  $P_2$ . Then Eqn. 4 follows. Note that the reverse passage from Eqn. 4 to Eqn. 3 is not valid in general.

Two other inequalities are useful.

#### Jensen's Inequality

If  $f(a)$  is convex ( $f'' > 0$  throughout the domain of interest,  $0 \leq a \leq 1$ ) then,

$$\overline{f(a)} \geq f(\overline{a}) \quad (5)$$

### Tchebycheff's Inequality

If  $f$  and  $g$  are similar functions, that is, they both increase or both decrease in the interval,  $0 \leq a \leq 1$ , then

$$\overline{fg} \geq \overline{f} \overline{g} \quad (6)$$

### STATISTICAL CONSTRAINTS FOR TWO SPECIES

Consider a two species flow with constant pressure and temperature,  $\alpha$  and  $\beta$  are the mass fractions of the species. Assume  $W_\alpha > W_\beta$ .  $\rho_*$  is a normalized density,

$$\rho_* = \rho / W_\beta \overline{p} / RT \quad p' = T' = 0 \quad (7)$$

define

$$\Delta = 1 - \frac{W_\beta}{W_\alpha} \quad 0 \leq \Delta \leq 1 \quad (8)$$

then

$$\rho_* = 1 / (1 - \Delta \alpha) \quad (9)$$

A simple conservation constraint on  $\alpha$  is

$$\alpha + \beta = 1$$

$$\text{or} \quad 0 \leq \alpha \leq 1$$

$$\text{then} \quad \boxed{0 \leq \overline{\alpha} \leq 1}$$

$$\text{and} \quad \overline{\alpha^2} \leq \overline{\alpha}$$

Consider  $f = \alpha$ ,  $g = 1$  in the Cauchy-Schwarz inequality

$$\overline{\alpha^2} \overline{1} \geq \overline{\alpha}^2 \quad (11)$$

Therefore, the bounds on the second moment  $\overline{\alpha^2}$  are

$$\boxed{\overline{\alpha}^2 \leq \overline{\alpha^2} \leq \overline{\alpha}} \quad (12)$$

Using the renormalization theorem with  $H(\alpha) = \alpha$ , Eqn. 11 becomes,

$$\overline{\alpha^3} \geq \frac{\overline{\alpha^2}^2}{\overline{\alpha}} \quad (13)$$

Using the renormalization theorem with  $H(\alpha) = 1 - \alpha$ , Eqn. 11 becomes,

$$\overline{\alpha^2(1-\alpha)} \geq \frac{\overline{\alpha(1-\alpha)}^2}{1-\overline{\alpha}}$$

$$\text{or} \quad \overline{\alpha^3} \leq \overline{\alpha^2} - \frac{(\overline{\alpha} - \overline{\alpha^2})^2}{1-\overline{\alpha}} \quad (14)$$

Therefore, the bounds on the third moment  $\overline{\alpha^3}$  for given  $\overline{\alpha}$  and  $\overline{\alpha^2}$  are,

$$\boxed{\frac{\overline{\alpha^2}^2}{\overline{\alpha}} \leq \overline{\alpha^3} \leq \overline{\alpha^2} - \frac{(\overline{\alpha} - \overline{\alpha^2})^2}{1-\overline{\alpha}}} \quad (15)$$

The bounds on the third moment given only  $\overline{\alpha}$  can be derived in a similar manner with the help of Jensen's Inequality for the lower bound

$$\overline{\alpha^3} \leq \overline{\alpha^2} \leq \overline{\alpha} \quad (16)$$

It is an interesting exercise to compare the bounds on  $\overline{\alpha^3}$  given by the two Eqns. 15 and 16. The results are shown in Figure 1. The dotted lines are the bounds on  $\overline{\alpha^3}$  for given  $\overline{\alpha}$ . For given  $\overline{\alpha}$ , we now pick  $\overline{\alpha^2}$  to correspond to the middle of its allowed range, that is  $\overline{\alpha^2} = \frac{\overline{\alpha} + \overline{\alpha}^2}{2}$ . Then, the solid lines indicate the bounds on  $\overline{\alpha^3}$  for specified  $\overline{\alpha}$  and  $\overline{\alpha^2}$ . The important point to be noted is that the bounds on  $\overline{\alpha^3}$  when two lower-order moments are specified are significantly narrower than the bounds when only one lower-order moment is specified. This is quite significant and leads to a very important conclusion for our approach to the modeling of the scalar probability density function.

The statistical constraints on  $\overline{\rho_* \alpha}$  and  $\overline{\rho_*^2}$  have also been derived by a similar procedure. The result for  $\overline{\rho_* \alpha}$  is,

$$\frac{\bar{\alpha}^2}{\bar{\alpha} - \Delta \bar{\alpha}^2} \leq \frac{\bar{\alpha}}{\rho_{\alpha} \bar{\alpha}} \leq \frac{1}{1 - \Delta} \frac{\bar{\alpha}(1 - \bar{\alpha}) - \Delta(\bar{\alpha} - \bar{\alpha}^2)}{(1 - \bar{\alpha}) - \Delta(\bar{\alpha} - \bar{\alpha}^2)} \quad (17)$$

Further details of the procedures are discussed by Varma, et al. (13). For a two species system, we have obtained the complete set of constraints on all moments up to the third-order for prescribed lower-order moments.

#### PDF STRUCTURE FOR EXTREMUM VALUES OF MOMENTS

The extremum values of the statistical bounds can only be realized by discrete probability density functions, that is, pdf's composed of delta functions. Consider the bounds on  $\bar{\alpha}^2$ . At the upper bound,  $\bar{\alpha}^2 = \bar{\alpha}$  and the pdf can be shown to correspond to two delta functions located at  $\alpha = 0$  and 1. This can be proven as follows:

$$\bar{\alpha}^2 = \bar{\alpha}$$

or

$$\int_0^1 (\alpha - \alpha^2) P(\alpha) d\alpha = 0$$

For nonzero  $P(\alpha)$ ,  $\alpha - \alpha^2 = 0$  or  $\alpha = 0$  and  $\alpha = 1$  are the only solutions. This corresponds to

$$P(\alpha) = (1 - \bar{\alpha}) \delta(\alpha) + \bar{\alpha} \delta(\alpha - 1) \quad (18)$$

as the pdf at the upper bound.

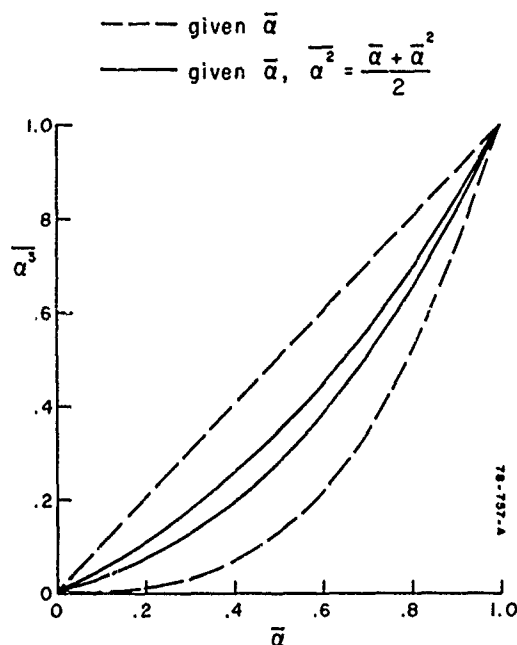


FIGURE 1 - Comparison of the statistical bounds on  $\bar{\alpha}^2$  for specified lower-order moments.

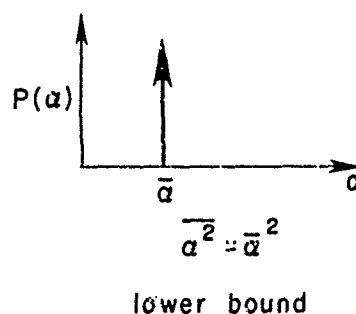
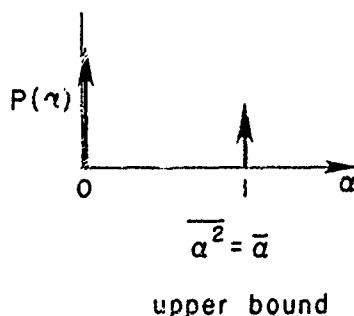
Similarly, at the lower bound,  $\bar{\alpha}^2 = \bar{\alpha}^2$ , the pdf can be shown to be

$$\rho(\alpha) = \delta(\alpha - \bar{\alpha}) \quad (19)$$

The two limiting pdf's are illustrated in the sketch. A popular model for the pdf is a clipped Gaussian (3). For small fluctuations, this model does approach the limiting pdf corresponding to the lower bound on  $\bar{\alpha}^2$ . However, it cannot attain the upper bound pdf corresponding to maximal fluctuations.

The same result can be proven for the upper and lower bounds of all the other moments. Delta functions are a necessary component of the pdf's.

Continuous pdf's alone cannot be valid over the entire moment space. Ideally, a pdf composed of delta functions and continuous functions will be desirable. However, we have demonstrated that a pdf composed of delta functions alone can always be constructed at every point in the statistically valid moment space, that these pdf's are simpler to construct than other proposed models, and that they provide sufficient accuracy for closure of the transport equations. This is discussed later in this paper.





# STATISTICAL CONSTRAINTS FOR THREE SPECIES

Consider a three species flow with constant pressure and temperature.  $\alpha$ ,  $\beta$ , and  $\gamma$  represent the mass fractions of the species.

## Given $\bar{\alpha}$ Only

We first assume that only  $\bar{\alpha}$  is specified. Conservation relations and the use of the renormalization theorem lead to the following inequalities.

$$0 \leq \bar{\alpha} \leq 1 \quad (20)$$

$$0 \leq \bar{\beta} \leq 1 - \bar{\alpha} \quad (21)$$

$$\boxed{\bar{\alpha}^2 \leq \alpha^2 \leq \bar{\alpha}} \quad (23)$$

$$0 \leq \bar{\alpha}\bar{\beta} \leq \bar{\alpha} - \bar{\alpha}^2 \quad (24)$$

$$0 \leq \bar{\beta}^2 \leq \bar{\beta} - \bar{\alpha}\bar{\beta} \quad (25)$$

$$\boxed{\bar{\alpha}^3 \leq \alpha^3 \leq \bar{\alpha}} \quad (26)$$

$$0 \leq \bar{\alpha}\bar{\beta}^2 \leq \bar{\alpha} - 2\bar{\alpha}^2 + \bar{\alpha}^3 \quad (27)$$

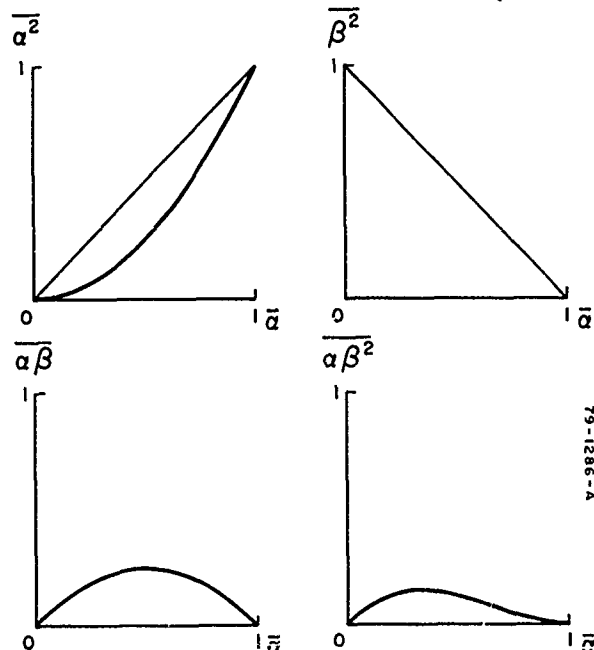
Given just  $\bar{\alpha}$ , Eqns. (23) and (26) represents the tightest bounds on  $\alpha^2$  and  $\alpha^3$ . Substituting the  $\alpha^2$  and  $\alpha^3$  bounds in Eqns. (24), (25), and (27) leads to,

$$0 \leq \bar{\alpha}\bar{\beta} \leq \bar{\alpha}(1 - \bar{\alpha}) \quad (27)$$

$$0 \leq \bar{\beta}^2 \leq 1 - \bar{\alpha} \quad (28)$$

$$0 \leq \bar{\alpha}\bar{\beta}^2 \leq \bar{\alpha} - 2\bar{\alpha}^2 + \bar{\alpha}^3 \quad (29)$$

These bounds on the moments are plotted in Figure 2.



## Given $\bar{\alpha}$ and $\bar{\beta}$

The bounds on  $\alpha^2$  and  $\beta^2$  have been derived to be the following:

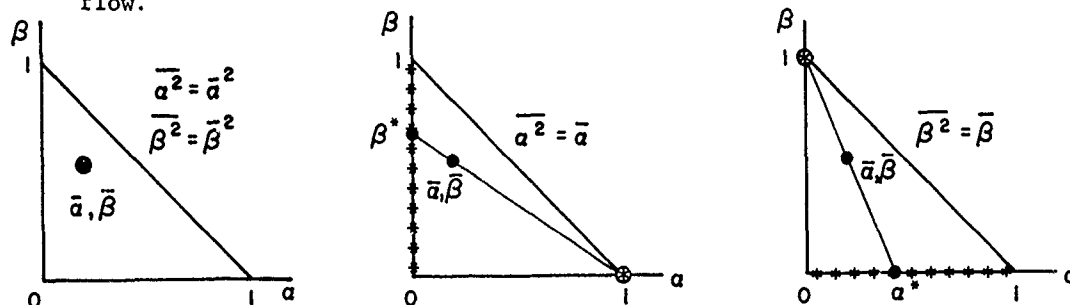
$$\boxed{\bar{\alpha}^2 \leq \alpha^2 \leq \bar{\alpha}} \quad (30)$$

$$\boxed{\bar{\beta}^2 \leq \beta^2 \leq \bar{\beta}} \quad (31)$$

PDF's can be constructed that attain these extremum values, and therefore, the above represent the best bounds on the second-order moments.

For a three species system, the allowed phase space region for the pdf is represented by a triangle as shown below. The specification of  $\bar{\alpha}$  and  $\bar{\beta}$  corresponds to defining the location of the centroid. The lower bounds on  $\alpha^2$  and  $\beta^2$  are attained if the pdf corresponds to all the mass distribution concentrated at the centroid. The upper bounds are attained by the two pdf's shown on the right. In these sketches, the mass locations are depicted by stars. Note that the mass distributions along the lines  $\alpha = 0$  or  $\beta = 0$  must be such that the mean of the distribution is located on the line joining the vertex and the centroid.

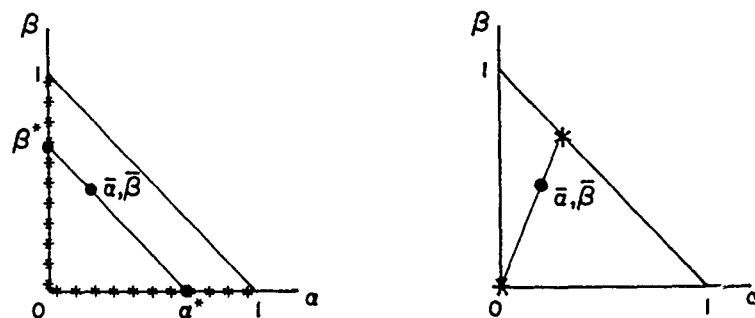
FIGURE 2 - Statistical constraints on moments for specified  $\bar{\alpha}$  in a three species flow.



The bounds on  $\bar{\alpha}\bar{\beta}$  are more interesting. We have derived the upper bound on  $\bar{\alpha}\bar{\beta}$  by the method of induction and considering an arbitrarily large number of point masses (14). The bounds are

$$0 \leq \overline{\alpha\beta} \leq \frac{\overline{\alpha} \overline{\beta}}{\overline{\alpha} + \overline{\beta}} \quad (32)$$

The lower bound is attained by mass distributions that are restricted to the lines  $\alpha = 0$  and  $\beta = 0$ . The upper bound is realized by the pdf on the right.



The bounds on  $\overline{\alpha\beta^2}$  are the smaller of the following three

$$0 \leq \overline{\alpha\beta^2} \leq \frac{\overline{\alpha} \overline{\beta}}{\overline{\alpha} + \overline{\beta}} \quad (32)$$

$$0 \leq \overline{\alpha\beta^2} \leq \overline{\alpha} - 2\overline{\alpha}^2 + \overline{\alpha}^3 \quad (29)$$

$$0 \leq \overline{\alpha\beta^2} \leq \overline{\beta}(1-\overline{\beta}) \quad (33)$$

The best bounds on the correlations in  $(\overline{\alpha}, \overline{\beta})$  space are shown in Figure 3. It should be noted that very small regions of the unit cube are allowed.

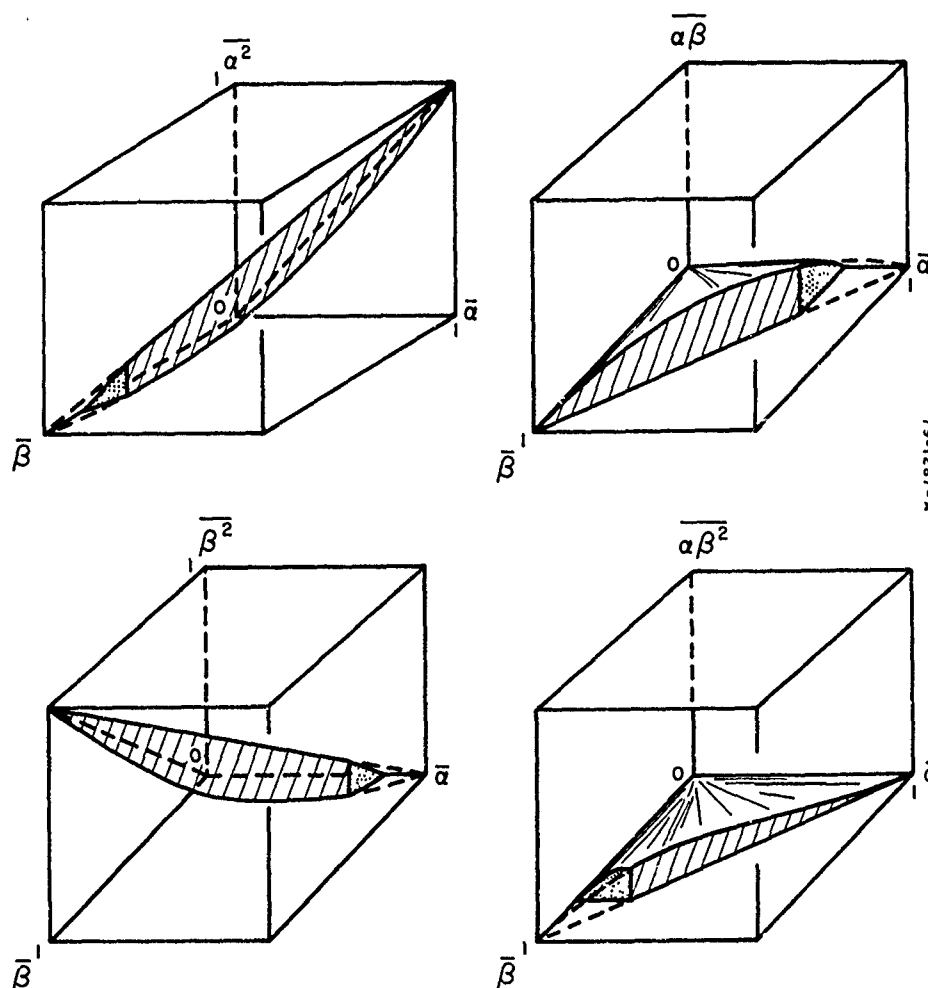
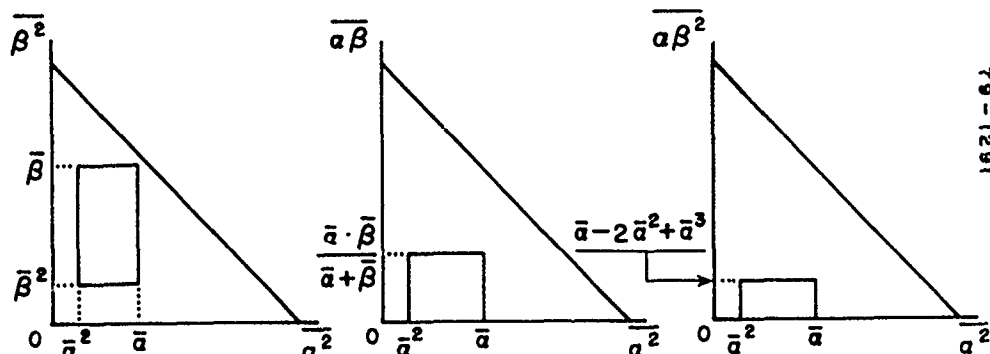


FIGURE 3 - Statistical constraints on moments for specified  $\overline{\alpha}$  and  $\overline{\beta}$  in a three species flow.

Given  $\bar{\alpha}$ ,  $\bar{\beta}$ , and  $\bar{\alpha}^2$

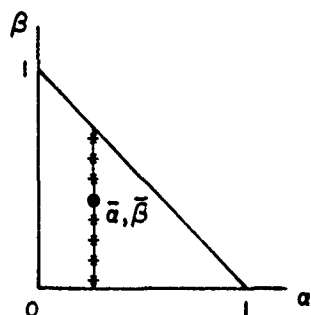
Following very similar procedures, we have determined the allowed regions for  $\bar{\beta}^2$ ,  $\bar{\alpha}\bar{\beta}$  and  $\bar{\alpha}\bar{\beta}^2$  in  $\bar{\alpha}^2$  space for specified  $\bar{\alpha}$  and  $\bar{\beta}$ . The procedure is illustrated below by one example; further details are available in (14).

The independent bounds on  $\bar{\alpha}^2$  and  $\bar{\beta}^2$  (Eqns. 30, 31) define a rectangle in  $(\bar{\alpha}^2, \bar{\beta}^2)$  space. However, there are regions within the rectangle that must be excluded. Similarly, there are excluded regions in  $(\bar{\alpha}^2, \bar{\alpha}\bar{\beta})$  and  $(\bar{\alpha}^2, \bar{\alpha}\bar{\beta}^2)$  spaces.



Consider  $\bar{\alpha}^2 = \bar{\alpha}^2$ :

The minimal value of  $\bar{\alpha}^2$  is attained by the following distribution.

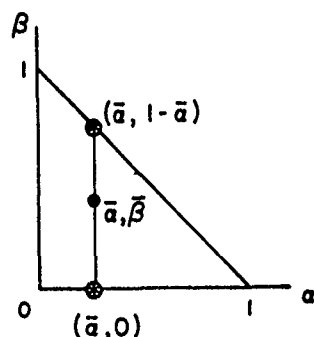


$$P(\alpha, \beta) = P_2(\beta) \delta(\alpha - \bar{\alpha})$$

$$\bar{\beta} = \int \beta P_2(\beta) d\beta$$

$$\bar{\beta}^2 = \int \beta^2 P_2(\beta) d\beta$$

For simplicity, consider  $P_2(\beta)$  to be a two delta function distribution with the delta functions located on the sides of the triangle (sketch below).



$$P_2(\beta) = (1-w)\delta(\beta) + w\delta[\beta - (1-\bar{\alpha})]$$

$$\bar{\beta} = w(1-\bar{\alpha})$$

$$w = \frac{\bar{\beta}}{1-\bar{\alpha}}$$

$$\bar{\beta}^2 = \bar{\beta}(1-\bar{\alpha}) \quad (34)$$

It is postulated that  $\bar{\beta}^2$  cannot be larger than this value for other general mass distributions  $P_2(\beta)$  that are located in the interior region of the triangle. Similarly, for  $\bar{\beta}^2 = \bar{\beta}^2$ , the largest allowed  $\bar{\alpha}^2$  is

$$\bar{\alpha}^2 = \bar{\alpha}(1-\bar{\beta}) \quad (35)$$

Using the general distribution,

$$\begin{aligned} \bar{\alpha}\bar{\beta} &= \int \alpha \beta \delta(\alpha - \bar{\alpha}) P_2(\beta) d\beta d\alpha \\ &= \bar{\alpha} \bar{\beta} \end{aligned} \quad (36)$$

Similarly,

$$\bar{\alpha}\bar{\beta}^2 = \bar{\alpha} \bar{\beta}^2$$

The allowed values of  $\bar{\beta}^2$  range from  $\bar{\beta}^2$  to  $\bar{\beta}(1-\bar{\alpha})$  and therefore,

$$\bar{\beta}^2 \leq \bar{\alpha}\bar{\beta}^2 \leq \bar{\beta}(1-\bar{\alpha}) \quad (37)$$

The allowed bounds on the correlations for other limiting values of  $\bar{\alpha}^2$ ,  $\bar{\alpha}\bar{\beta}$ , etc., have been similarly calculated. The shapes of the connecting curves between the allowed points have been determined by considering a series of two delta function pdf's, with the

delta functions located on the sides of the triangle. Some of the curves still have to be calculated, but their expected behavior is shown by dotted lines in the figures. There are some indications that these represent the best bounds on the moments but we have not yet completed the proof for more general mass distributions.

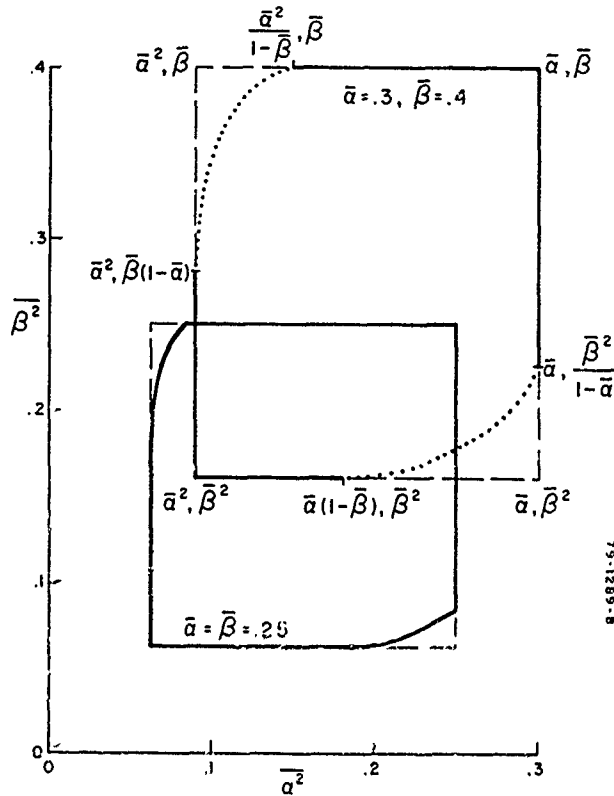


Figure 4 shows the results for the bounds in  $(\bar{\alpha}^2, \bar{\beta}^2)$  space for two sets of values for  $\bar{\alpha}$  and  $\bar{\beta}$ . Figures 5 and 6 show the corresponding results for the allowed regions in  $(\bar{\alpha}^2, \bar{\alpha}\bar{\beta})$  and  $(\bar{\alpha}^2, \bar{\alpha}\bar{\beta}^2)$  space. As in the case of the bounds on the third moment for two species system, the important feature to note here is the tightness of the constraint. For specified lower-order moments,  $\bar{\alpha}, \bar{\beta}$  and  $\bar{\alpha}^2, \bar{\alpha}\bar{\beta}^2$  has a maximum value of order 0.1. For three species, we have not yet investigated the constraints when second-order moments involving the density are also specified, but this will lead to further tightening of the bounds on the third-order moments of interest.

FIGURE 4 - Statistical bounds on  $\bar{\beta}^2$  and  $\bar{\alpha}^2$  for specified  $\bar{\alpha}$  and  $\bar{\beta}$  in a three species system.

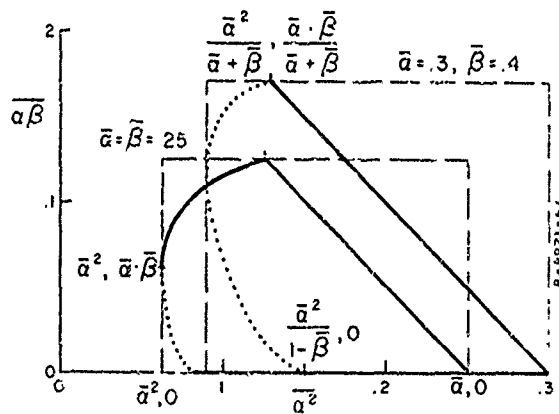


FIGURE 5 - Statistical bounds on  $\bar{\alpha}\bar{\beta}$  and  $\bar{\alpha}^2$  for specified  $\bar{\alpha}$  and  $\bar{\beta}$  in a three species system.

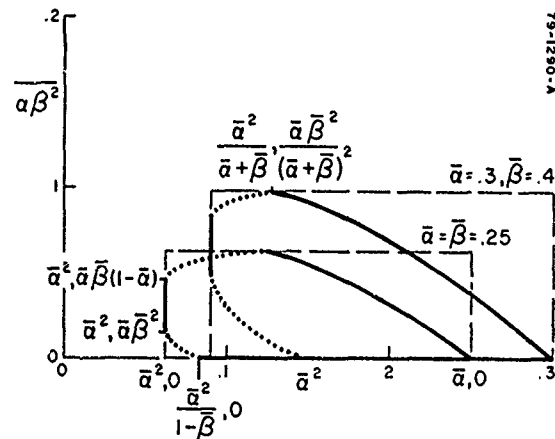


FIGURE 6 - Statistical bounds on  $\bar{\alpha}\bar{\beta}^2$  and  $\bar{\alpha}^2$  for specified  $\bar{\alpha}$  and  $\bar{\beta}$  in a three species system.

The "typical eddy" model is an attempt to define the joint pdf for the scalar variables by using all the available information from a second-order closure analysis. The model may consist of combinations of delta functions and continuous functions but we have extensively studied a model composed of delta functions alone. The model parameters are determined by matching the moments of the model to the values of the correlations obtained from the solution of the transport equations. The procedure is detailed in (13).

In a two-species, variable density flow, the pdf model consists of 4 delta functions. The model has one free parameter, designated  $\alpha_3$ , and we have demonstrated (13) that the allowed range of  $\alpha_3$  corresponds directly to the statistical bounds on the third-order moments  $\overline{\alpha^3}$  or  $\overline{\alpha\beta^2}$ . With the parameter  $\alpha_3$  selected at any point within its allowed range, we have also shown that a physically correct pdf model composed solely of delta functions can be constructed at every point in the statistically valid moment space. We will now demonstrate that these models provide sufficient accuracy for closure of the transport equations for turbulent flows.

#### Comparison with Experiments

Konrad (15) has made a series of detailed measurements of the pdf in three shear layer flowfields. The measurements have been made in (i) a He-N<sub>2</sub> shear layer with a velocity ratio  $u_2/u_1 = 0.38$  and a density ratio  $\rho_2/\rho_1 = 7.0$ . (ii) a uniform density He+Ar-N<sub>2</sub> shear layer with velocity ratio of  $u_2/u_1 = 0.38$  and (iii) a wake flow in which the gases have equal free-stream velocities and a density ratio of 7. All the flows are low speed and two-dimensional. The measurements consist of mean velocity, mean concentration, concentration fluctuation correlations, species intermittency functions and the species pdf's. The latter two parameters are used for the direct model comparison. Only the results for the first flowfield are discussed in this paper. Further studies and comparisons are available in (13).

The pdf measurements are used to determine the values of the four lower-order moments-- $\overline{\alpha}$ ,  $\overline{\alpha^2}$ ,  $\overline{\alpha\rho_x}$  and  $\overline{\rho_x^2}$ --that are needed to construct the two-species variable-density "typical eddy" model. The measured pdf is also used to calculate experimental values of a number of third-order correlations of interest, such as  $\overline{\alpha\beta^2}$  and  $\overline{\alpha^2\beta}$ . The third-order moments are also computed from the model and the results compared to the measurements. The valid range of the free parameter  $\alpha_3$ , corresponds to the upper and lower bounds on the third moments.

Figure 7 presents the results for the third moment  $\overline{\alpha\beta^2}$  for the He-N<sub>2</sub> shear layer. The ordinate of the figure is  $\overline{\alpha\beta^2}_{\text{model}} / \overline{\alpha\beta^2}_{\text{expt}}$ . The abscissa is the normalized coordinate across the shear layer. The dotted lines show the upper and lower bounds on the third moment when only two lower-order moments are used for the model construction. In this case  $\overline{\alpha\beta^2}_{\text{model}}$  has a large range of possible values and some models within the statistical range can lead to significant errors compared to the experiments. However, when 4 lower-order moments are specified, the model values of  $\overline{\alpha\beta^2}$  are tightly constrained as shown by the solid lines. For the "typical eddy" model, the solid lines correspond to the entire valid range of the parameter  $\alpha_3$ . It can be seen that with any choice of  $\alpha_3$  within this range, it is possible to predict  $\overline{\alpha\beta^2}$  (and other third-order moments) to better than 10% accuracy. This is significantly better accuracy than the expected error bounds on experimental measurements of third-order moments. Further, such accuracy is expected to be quite adequate for closure of the transport equations for the means and second-order correlations.

It must be noted that the statistical constraints on the moments are independent of the pdf model. The "typical eddy" model with end-choices of the parameter  $\alpha_3$  matches the bounds on the third moment. Any and all statistically valid pdf models that match the given values for the lower order moments will predict values for the third moment within these same bounds. These other models will typically be more difficult to construct and may not lead to significantly better prediction of third-order moments. Better accuracy in the prediction of third-order moments does not appear to be necessary as far as closure of the equations is concerned. The delta function "typical eddy" model can be used to provide better accuracy by empirically selecting the parameter  $\alpha_3$  at the middle of its allowed range, as shown in the figure. The third moment can now be predicted to better than 2% accuracy across the entire flowfield.

Konrad has also measured the species intermittency function or the probability of finding pure species at various points across the flowfield. A comparison of the model predictions to the data is shown in Figures 8 and 9. The theoretical predictions use a cutoff value of 0.9, that is, a delta function located at  $\alpha > 0.9$  is considered to be pure species  $\alpha$ . This is an arbitrary, but reasonable criterion. The results in Figure 8 are for  $\alpha_3$  equal to the maximum value within its allowed range. This also corresponds to a pdf structure with minimum mixedness or minimum entropy of mixing. The entropy of mixing is defined as,

$$\eta = \sum_i \epsilon_i \left( -\rho_i \alpha_i \ln \rho_i \alpha_i - \rho_i \beta_i \ln \rho_i \beta_i \right)$$

Figure 9 shows the results for  $\alpha_3$  at midrange and  $\alpha_3$  equal to the minimum value allowed. It is clear that the empirical choice of  $\alpha_3$  maximum leads to significantly better agreement

with the experimental data. Further arguments in support of this choice of  $\alpha_3$  that corresponds to minimum entropy of mixing are discussed in (13). A qualitative comparison of the delta function pdf for maximum  $\alpha_3$  and the measured pdf is shown in

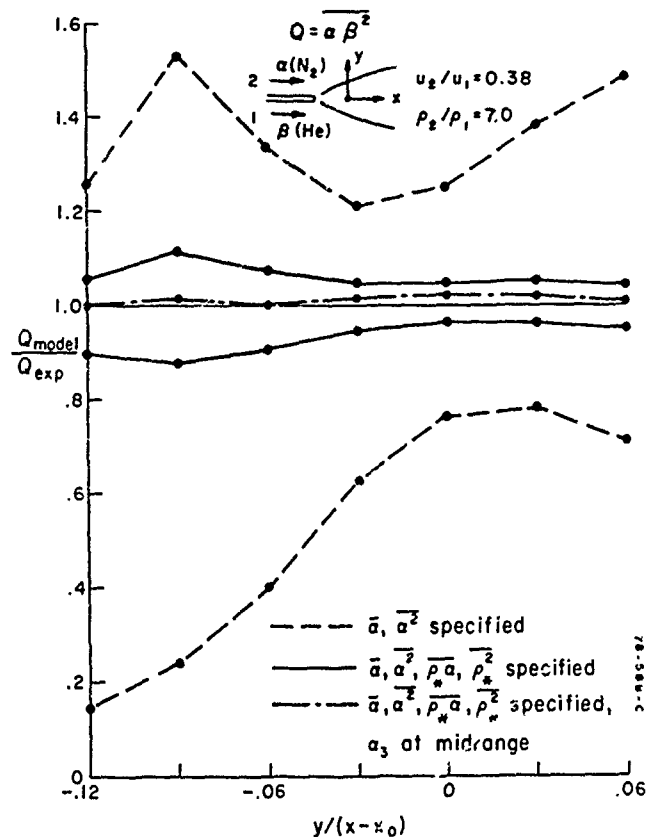


FIGURE 7 - Comparison of model predictions and experiments for the third moment  $\alpha\beta^2$ . He-N<sub>2</sub> shear layer.

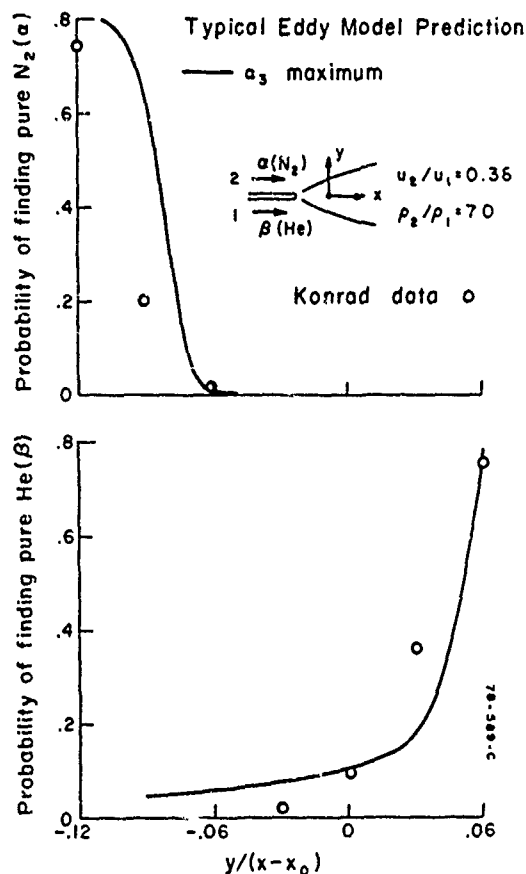


FIGURE 8 - Comparison of model predictions with experiments for the probability of finding pure species.  $\alpha_3$  maximum model. He-N<sub>2</sub> shear layer.

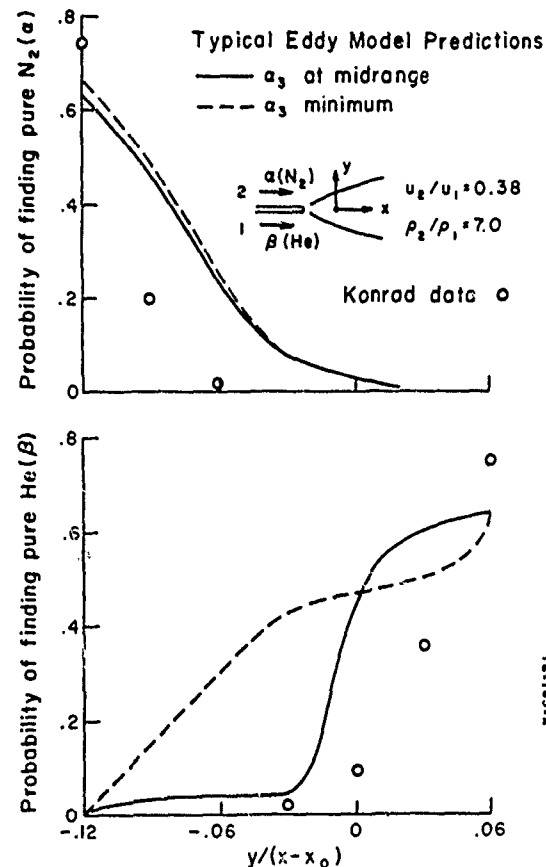


Figure 9 - Comparison of model predictions with experiments for the probability of finding pure species.  $\alpha_3$  at midrange and  $\alpha_3$  minimum models. He-N<sub>2</sub> shear layer.

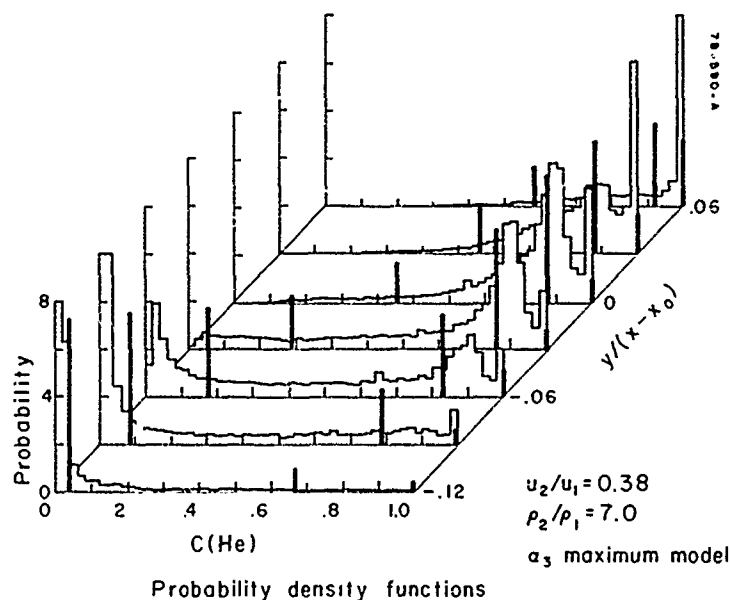


FIGURE 10 - Comparison of delta function pdf with measured pdf.

Figure 10. The experimental pdf is reproduced from the report by Konrad (15). The delta functions in the model are shown at their correct locations in the concentration space and the relative strengths of the delta functions are correct. The absolute magnitude of the strength of the delta functions cannot be directly plotted on this graph and we have selected a convenient scale for depicting the delta functions. The delta function representation of the pdf seems to be capable of capturing the important features of the experimental pdf structure.

This limited comparison with detailed pdf measurements indicates that the choice of  $\alpha_3$  maximum shows the best overall agreement with data for a two species variable density mixing flow. It will be desirable to compare the model to other data for different flow conditions for further model evaluation. Further, similar comparisons of the model for three species to measurements in simple reacting flows have to be carried out. However, it appears that the delta function pdf model is capable of predicting higher-order moments to sufficient accuracy for closure of the transport equations.

#### CONCLUSIONS

The direct comparison of the delta function "typical eddy" model for two species with pdf measurements has demonstrated that this simple model is quite adequate for achieving closure of the transport equations. The complete set of statistical constraints on correlations for two species flows have been derived. The constraints have been used to prove that delta functions are a necessary part of pdf in order to attain the extremum values of the moments. A rational pdf composed of a set of delta functions alone can always be constructed anywhere within the statistically valid moment space. A pdf of this type when constructed using all the available information in a second-order closure calculation, can predict higher order correlations to an accuracy better than they can be measured. It, therefore, appears unnecessary to construct more complex pdf's for the purpose of closure of the turbulence equations.

A number of the important statistical constraints for three species systems have been derived, and these indicate that the third-order correlations are quite tightly constrained. Therefore, it appears likely that the conclusions arrived at for two species mixing flows will also be applicable to simple reacting flows.

#### REFERENCES

1. Rhodes, R.P., Harsha, P.T., and Peters, C.E.: Turbulent Kinetic Energy Analyses of Hydrogen-Air Diffusion Flames. *Acta Astronautica*, Vol. 1, 1974, pp. 443-70.
2. Bray, K.N.C. and Moss, J.B., University of Southampton, "A Unified Statistical Model of the Premixed Turbulent Flame, 1974, AASU Report No. 335.
3. Lockwood, F.C. and Naguib, A.S., The Prediction of the Fluctuations in the Properties of Free, Round-Jet, Turbulent, Diffusion Flames, *Combustion and Flame*, Vol. 24, 1975, p. 109.
4. Libby, P.A., On Turbulent Flows with Fast Chemical Reactions, III, Two-Dimensional Mixing with Highly Dilute Reactants, *Combustion Science and Technology* (Special Issue on Turbulent Reactive Flows), Vol. 13, Nos. 1-6, 1976, pp. 79-98.

5. Bonniot, J.C., Borghi, R., and Magre, P., "Turbulent Combustion in a Stirred Combustor," in Turbulent Combustion, Vol. 58, AIAA Progress in Astronautics and Aeronautics Series, 1977.
6. Kewley, D.J., Development of a Second-Order Closure Model for Turbulent Reacting Flows, Presented at the 6th Australasian Hydraulics and Fluid Mechanics Conference, December 5-9, 1977, Adelaide, Australia.
7. Donaldson, C. duP., On the Modeling of the Scalar Correlations Necessary to Construct a Second-Order Closure Description of Turbulent Reacting Flows, Turbulent Mixing in Nonreactive and Reactive Flows, Plenum Press, New York, 1975, pp. 131-62.
8. Donaldson, C. duP. and Varma, A.K., Remarks on the Construction of a Second-Order Closure Description of Turbulent Reacting Flows, Combustion Science and Technology (Special Issue on Turbulent Reactive Flows), Vol. 13, Nos. 1-6, 1976, pp. 55-78.
9. Dopazo, C. and O'Brien, E.E., Statistical Treatment of Non-Isothermal Chemical Reactions in Turbulence, Combustion Science and Technology (Special Issue on Turbulent Reactive Flows), Vol. 13, Nos. 1-6, 1976, pp. 99-122.
10. Bonniot, J.C. and Borghi, R., Sur la Densite de Probabilite des Fluctuations D'Especes Reactives Dans la Combustion Turbulente, Communication presentee au 6e Colloque International sur la Dynamique des Gas et Explosion et des Systemes Reactifs, August 22-26, 1977, Stockholm, Sweden.
11. Pope, S.B., The Probability Approach to the Modeling of Turbulent Reacting Flows, Combustion and Flame, Vol. 27, 1976, p. 299.
12. Spalding, D.B., A General Theory of Turbulent Combustion, the LaGrangian Aspects, AIAA Paper No. 77-141, 1977.
13. Varma, A.K., Sandri, G., and Mansfield, P.J., A.R.A.P., Inc., "Modeling of Scalar Probability Density Functions in Turbulent Flows," Project SQUID Technical Report ARAP-1-PU., 1978.
14. Varma, A.K., Mansfield, P.J., and Sandri, G., A.R.A.P., Inc., "Second-order Closure Modeling of Variable Density Turbulent Flows," Project SQUID Technical Report ARAP-2-PU, 1979.
15. Konrad, J.H., California Institute of Technology, An Experimental Investigation of Mixing in Two-Dimensional Turbulent Shear Flows with Applications to Diffusion-Limited Chemical Reactions, Project SQUID Technical Report CIT-8-PU., 1976.

#### ACKNOWLEDGEMENTS

This research effort has been supported by the Office of Naval Research under Contract Nos. N0014-75-C-1143 (Project SQUID) and N0014-79-C-0335. Some support from the Air Force Office of Scientific Research under Contract No. F44620-76-C-0048 is also gratefully acknowledged. The authors wish to acknowledge the close involvement of Dr. P.J. Mansfield in the derivation of the statistical bounds.



## DISCUSSION

N.Peters, Ge

Let me congratulate you for the systematic investigation of the statistical constraints for higher order moments. However, let me comment that I do not believe that delta-function pdf's will be useful for the calculation of mean reaction rates in combustion situations. Laminar production rates plotted over the mixture fraction or a progress variable (for instance temperature) peak very sharply close to the stoichiometric mixture and at the upper adiabatic temperature limit. A delta function will give a zero mean reaction rate if it lies out of the peak and the laminar value if it falls on it.

Author's Reply

Please also see the reply to the question of Dr Jones.

The strong dependence of the reaction rate on the temperature is well-known and follows from the Arrhenius rate expression. We are hopeful that our delta function joint pdf model consisting of 7 delta functions for reacting flows will result in the placement of a number of delta functions in the high temperature end of the temperature spaces and will predict the correct average reaction rate.

W.P.Jones, UK

As I recall the experiments with which you compared your calculations were isothermal – or nearly so. My feeling is that if you were to apply your model to a flame, then the results – in particular the temperature profiles – would be much more sensitive to the selected p.d.f. and that forms constructed from Dirac  $\delta$ -functions will not be adequate. My reasons for holding this view are that in calculating  $H_2$ -air turbulent diffusion flames using various p.d.f. forms I found that the Dirac  $\delta$ -function form generated double peaked radial temperature profiles<sup>1</sup>. Would you like to comment on this result and the implications for your model?

1. Jones, W.P. *Turbulence Models for Turbulent Flow with Variable Density and Combustion*. To be published by Hemisphere Pub. Co., VKI Lecture Series, 1979.

Author's Reply

The results in the paper demonstrate that the delta function pdf model appears to be adequate for mixing flows. We are now working on extending the pdf model to reacting flows. We are aware of the referenced results of Dr Jones and are concerned about the problem of greater sensitivity of reacting flow calculations to the form of the pdf. For simple reacting flows involving 3 species our model for the joint pdf of all the scalars will consist of 7 delta functions and we are hopeful that this will lead to more satisfactory results. The main argument for the delta function model is its simplicity of construction compared to other pdf models but if the model does not prove satisfactory, it is conceptually straight-forward to use our procedure for constructing continuous type joint pdf's.

C.H.Priddin, UK

Your model shows clearly how closely the third-order moments are bounded for correlations between species which are themselves bounded by the values 0 and 1. However, to calculate reaction rates one also needs to evaluate correlations involving fluctuating reaction rate or temperature, which are not bounded to such an extent. How can your model cope with these terms?

Author's Reply

We are currently examining the constraints on temperature related correlations. Bounds on the temperature variable that can be used are the initial temperature and the adiabatic flame temperature, and these can be suitably normalized to range between 0 and 1. We are hopeful that this approach will enable us to derive the desired constraints on temperature correlations.

## COMBUSTOR MODELLING FOR SCRAMJET ENGINES

J. Philip Drummond, R. Clayton Rogers, and John S. Evans  
Aerospace Engineers

NASA Langley Research Center  
Hampton, Virginia 23665  
U.S.A.

## SUMMARY

Combustor flow fields found in hydrogen fueled scramjets are quite complex and, therefore, difficult to analyze. Analyses that adequately model the combustor must not only consider highly turbulent and reacting flows with complex wave structure, but also must cope with the possibility of embedded subsonic regions and recirculation within a predominantly supersonic flow. Conventional analytic approaches to scramjet analysis and design have been global in nature or have been restricted to all-supersonic flow; they must therefore be extended to realistically describe actual combustor flow fields. A system of computer programs being developed at the NASA Langley Research Center to model these complex combustor flow fields is discussed. Each code solves a system of equations compatible with the type of flow being analyzed in any particular part of the combustor. For flows that remain supersonic throughout, a parabolic Navier-Stokes solver is being used successfully. An extension of this computer program, to partially introduce elliptic character into the analysis by accounting for a full 3-D pressure field, is being tested. This "partially elliptic" scheme accounts for the effects of streamwise pressure feedback present in the subsonic flow, thereby allowing the detection and calculation of embedded subsonic regions known to be present in the combustor. Although the partially elliptic procedure can handle mixed subsonic-supersonic flows, it still requires that a predominant flow direction exists; for recirculating flows, the fully elliptic Navier-Stokes equations are required. Since recirculating flow does exist in regions near points of fuel injection from struts in the engine, work is currently underway to begin development of a three-dimensional elliptic Navier-Stokes solver. Initial work has included development at Langley of a 2-D elliptic code for the analysis of slot fuel injectors. Each computer program is currently being applied to pertinent problem areas and is providing a good deal of insight about flow fields in the Langley scramjet engine.

## NOMENCLATURE

$A_i, B_i, C_i$	reaction rate parameters	$p_b$	reference pressure for combustion data = 2.173 MPa
$A_K, A_R$	constants in profile functions	$q$	heat flux vector
$\bar{c}_f$	mean skin friction coefficient	$R^0$	gas constant
$c_u$	mass fraction decay factor	$R$	mass flux profile parameter
$d$	fuel injector diameter	$S$	surface area of control volume
$d_j$	jet diameter	$S_\phi$	source function
$e$	stagnation internal energy per unit volume	$Sc$	Schmidt number
$e_s$	static internal energy per unit volume	$T$	Temperature
$f$	species mass fraction, streamwise stretching function or ratio of fuel to mainstream flow rate	$t$	time
$g$	transverse stretching function or mean square amplitude fluctuations in species concentrations	$\Delta t$	time increment
$h^0$	stagnation enthalpy	$U_\infty$	freestream velocity
$h$	duct height	$u, v, w$	streamwise, transverse and lateral velocity components
$K_{fi}$	reaction rate $i$ , forward direction	$\gamma$	velocity in TJI model
$K_{bi}$	reaction rate $i$ , reverse direction	$x, y, z$	streamwise, transverse and lateral physical coordinates
$k$	turbulence kinetic energy	$\bar{w}$	molecular weight
$l$	mixing length	$\dot{w}$	species rate of change
$L_x$	streamwise finite difference operator	$y_A$	upper boundary of physical domain
$L_y$	transverse finite difference operator	$y_B$	lower boundary of physical domain
$Le$	Lewis number	$\Delta X, \Delta Y, \Delta Z$	increments in computational finite difference grid
$M$	Mach number	$Z$	non-dimensional transverse coordi- nate in TJI model
$M_j$	mole fraction of species $j$	$\alpha$	numerical damping coefficient
$N_R$	number of reactions	$\alpha_B, \alpha_T, \alpha_F$	angles of bottom and top duct walls and jet (fig. 21)
$N_S$	number of species	$\beta_x, \beta_y$	stretching factors in coordi- nate transformation
$\dot{m}_0$	mainstream mass flow rate	$\Gamma$	diffusion coefficient
$n_i$	unit normal vector	$\gamma$	ratio of specific heats
$Pr$	Prandtl number	$\gamma'$	stoichiometric coefficient, forward rate
$P_{i,j}$	stress tensor	$\gamma''$	stoichiometric coefficient, backward rate
$p$	pressure	$\delta$	boundary layer thickness or local flow angle
$p_p$	pitot pressure	$\epsilon$	numerical damping coefficient or dissipation rate of turbulence
$P_{t,f}$	jet stagnation pressure		kinetic energy

## COMBUSTOR MODELLING FOR SCRAMJET ENGINES

J. Philip Drummond, R. Clayton Rogers, and John S. Evans  
Aerospace Engineers

NASA Langley Research Center  
Hampton, Virginia 23665  
U.S.A.

## SUMMARY

Combustor flow fields found in hydrogen fueled scramjets are quite complex and, therefore, difficult to analyze. Analyses that adequately model the combustor must not only consider highly turbulent and reacting flows with complex wave structure, but also must cope with the possibility of embedded subsonic regions and recirculation within a predominantly supersonic flow. Conventional analytic approaches to scramjet analysis and design have been global in nature or have been restricted to all-supersonic flow; they must therefore be extended to realistically describe actual combustor flow fields. A system of computer programs being developed at the NASA Langley Research Center to model these complex combustor flow fields is discussed. Each code solves a system of equations compatible with the type of flow being analyzed in any particular part of the combustor. For flows that remain supersonic throughout, a parabolic Navier-Stokes solver is being used successfully. An extension of this computer program, to partially introduce elliptic character into the analysis by accounting for a full 3-D pressure field, is being tested. This "partially elliptic" scheme accounts for the effects of streamwise pressure feedback present in the subsonic flow, thereby allowing the detection and calculation of embedded subsonic regions known to be present in the combustor. Although the partially elliptic procedure can handle mixed subsonic-supersonic flows, it still requires that a predominant flow direction exists; for recirculating flows, the fully elliptic Navier-Stokes equations are required. Since recirculating flow does exist in regions near points of fuel injection from struts in the engine, work is currently underway to begin development of a three-dimensional elliptic Navier-Stokes solver. Initial work has included development at Langley of a 2-D elliptic code for the analysis of slot fuel injectors. Each computer program is currently being applied to pertinent problem areas and is providing a good deal of insight about flow fields in the Langley scramjet engine.

## NOMENCLATURE

$A_i, B_i, C_i$	reaction rate parameters	$p_b$	reference pressure for combustion data = 2.173 MPa
$A_k, A_R$	constants in profile functions	$q$	heat flux vector
$\bar{c}_f$	mean skin friction coefficient	$R$	gas constant
$c_u$	mass fraction decay factor	$R$	mass flux profile parameter
$d$	fuel injector diameter	$S$	surface area of control volume
$d_j$	jet diameter	$S_\phi$	source function
$e$	stagnation internal energy per unit volume	$Sc$	Schmidt number
$e_s$	static internal energy per unit volume	$T$	Temperature
$f$	species mass fraction, streamwise stretching function or ratio of fuel to mainstream flow rate	$t$	time
$g$	transverse stretching function or mean square amplitude fluctuations in species concentrations	$\Delta t$	time increment
$H^0$	stagnation enthalpy	$U_\infty$	freestream velocity
$h$	duct height	$u, v, w$	streamwise, transverse and lateral velocity components
$K_{fi}$	reaction rate $i$ , forward direction	$V$	velocity in TJI model
$K_{bi}$	reaction rate $i$ , reverse direction	$x, y, z$	streamwise, transverse and lateral physical coordinates
$k$	turbulence kinetic energy	$W$	molecular weight
$l$	mixing length	$\dot{W}$	species rate of change
$L_x$	streamwise finite difference operator	$y_A$	upper boundary of physical domain
$L_y$	transverse finite difference operator	$y_B$	lower boundary of physical domain
$Le$	Lewis number	$\Delta X, \Delta Y, \Delta Z$	increments in computational finite difference grid
$M$	Mach number	$Z$	non-dimensional transverse coordinate in TJI model
$M_j$	mole fraction of species $j$	$\alpha$	numerical damping coefficient
$N_R$	number of reactions	$\alpha_B, \alpha_T, \alpha_F$	angles of bottom and top duct walls and jet (fig. 21)
$N_S$	number of species	$\beta_x, \beta_y$	stretching factors in coordinate transformation
$\dot{m}_0$	mainstream mass flow rate	$\Gamma$	diffusion coefficient
$n_i$	unit normal vector	$\gamma$	ratio of specific heats
$Pr$	Prandtl number	$\gamma'$	stoichiometric coefficient, forward rate
$P_{i,j}$	stress tensor	$\gamma''$	stoichiometric coefficient, backward rate
$p$	pressure	$\delta$	boundary layer thickness or local flow angle
$p_p$	pitot pressure	$\epsilon$	numerical damping coefficient or dissipation rate of turbulence kinetic energy
$p_{t,f}$	jet stagnation pressure		

$\eta_m$	mixing parameter	$\lambda$	laminar
$\kappa$	heat transfer coefficient or fuel mass fraction	$m$	mean value
$\mu$	viscosity	$n_{nx}, n_{ny}$	maximum grid points in x and y directions
$\rho$	density	$s$	property behind shock
$\sigma$	normal stress	$t$	turbulent or stagnation
$\tau$	shear stress	$u, v, w, H^0$	dependent variables
$\phi$	general dependent variable	$f, k, \epsilon, g$	
$\omega$	vorticity	$x, y, z$	in streamwise, normal or transverse direction
$\omega_c, \omega_p$	over-relaxation coefficient	$w$	wall conditions
<u>Subscripts</u>		$\delta$	edge of mixing region where $\kappa = 0$
$cl$	centerline	$\phi$	dependent variable
$e$	effective value or exit plane	$o$	mainstream
$f$	fuel jet	$2$	model plane of TJI model
$i, j, k$	x, y, and z grid indices or species and reaction indices	<u>Superscript</u>	
		$n$	time index

## 1.0 INTRODUCTION

The NASA Langley Research Center is conducting research on a hydrogen fueled supersonic combustion ramjet (scramjet) concept which will be capable of operating at hypersonic speeds in the atmosphere.<sup>1</sup> Scramjet performance becomes attractive at vehicle flight speeds of Mach 4 and above, and they offer the most viable propulsion option when operating at flight speeds in excess of Mach 6.<sup>2</sup> Hypersonic aircraft concepts are being developed in which the scramjet is integrated into the airframe of the vehicle (fig. 1) such that the vehicle itself performs part of the engine function by inlet air precompression and exhaust expansion while minimizing the drag associated with the engine. The engine is divided into several identical engine modules, one of which is shown in figure 2. (The side wall of the module has been removed to expose the engine's internal features.) The engine inlet has a varying rectangular cross-section with fixed geometry. Compression is initiated by the vehicle forebody ahead of the engine; the forebody compresses the flow vertically. Each module inlet compresses the flow horizontally with swept wedge shaped side walls. The wedges are designed such that their sweep causes spillage past the cowl of part of the inlet air not needed in the low and intermediate Mach number range of operation. Inlet compression is completed by three swept struts, that also provide locations for gaseous hydrogen fuel injection.

Fuel is introduced into the engine from the struts in both a parallel and transverse direction to the engine primary flow (fig. 2). This approach tailors the fuel injection to an optimum heat release schedule over the flight Mach number range of interest. Transverse fuel injection promotes more rapid fuel air mixing and is used wherever possible to promote reaction in the upstream portion of the combustor. At flight Mach numbers below 6, however, too much perpendicular injection results in thermal choking of the engine. Therefore the parallel injection mode predominates through the low Mach number range of the engine by slowing the mixing and, therefore, stretching out the reaction process. The flow, having undergone reaction in the combustor, begins to expand in a short nozzle section in the module. The aft portion of the vehicle behind the engine serves to complete the expansion process.

The flow field near transverse fuel injectors is particularly complex. Blockage and deflection of the supersonic mainstream by the perpendicular fuel jet results in an adverse pressure gradient which separates the turbulent boundary layer upstream of the injector. A mixed subsonic-supersonic region is produced and a strong bow shock which turns the mainstream over the fuel jet is formed. A region of subsonic separation and recirculation also forms downstream of the injector as a result of the rapid expansion of the mainstream flow behind the fuel jet. Weaker shocks also form at the upstream separation point as the supersonic flow turns over the thickened boundary layer and at the downstream reattachment point where the downstream separated flow reattaches.

The flow field near a parallel fuel injector can be regarded as a co-flowing shear flow with the mixing and reaction occurring within a turbulent shear layer between the hydrogen and air. The engine combustor begins near the transverse fuel injectors and extends downstream to the nozzle. Flow in the combustor is predominantly supersonic, but regions of embedded subsonic flow do occur as noted near the fuel injectors as a result of flow blockage and downstream of the injectors as a result of combustion. The flow field in the combustor is not only complex due to the embedded subsonic-supersonic flow that exists, but is also complicated by the highly turbulent mixing and reacting flow in this region.

As can be inferred from the discussion above, each region of an engine module (inlet, struts, combustor, and nozzle) can be characterized by a particular type or class of flow which can be described by particular forms of the Navier-Stokes equations. Flow in the module inlet is primarily inviscid with the exception of boundary layers near the wall. Therefore, inlet flow can be mathematically characterized and analyzed using the inviscid form of the governing equations (Euler equations) away from the walls and the boundary layer form of the equations near the walls. The flow field just ahead of and throughout the strut region of the engine is predominantly supersonic, but the regions of subsonic and recirculating flow are such that diffusion of mass, momentum, and energy occurs in all coordinate directions. Additionally, pressure disturbances occurring near the injector can affect the flow field upstream of the injector as well. Therefore, the governing equations describing the flow field near engine struts must be retained in their fully elliptic form. The flow field in the downstream portion of the combustor is again primarily supersonic with possible embedded subsonic flow, but no recirculation is present. Without streamwise diffusion, flow fields in the downstream combustor region can, therefore, be characterized reasonably using the parabolic form of the governing equations which are obtained by negating appropriate diffusion terms. Within subsonic regions a hybridized form of the parabolic equations termed the "partially elliptic" form is applied to account for possible upstream influences by the pressure field.

From an analysis standpoint, the flow field around the struts and in the combustor is complicated by

turbulence and chemical reaction. Solution of the Reynolds stress equations might provide the needed turbulence field, but such a solution is beyond the scope of current studies and available computer resources. Eddy viscosity models of turbulence have been developed primarily for boundary layer or shear layer type flows; only limited work has been done to adapt these models to complex flows such as those found in the combustor.<sup>3</sup> Turbulent kinetic energy models that describe the transport of turbulent kinetic energy and the dissipation of that energy were also developed for shear flows. However, these models have been shown to be adequate for significantly more complex flow fields.<sup>4</sup> Fortunately, a significant amount of work has been performed in the area of hydrogen-air chemistry.<sup>5</sup> Implementation of this work into an analysis tool for engine flow field predictions requires the solution of a large number of species equations in addition to the equations of motion. To completely describe the ignition-reaction phenomena that are important in the reaction of hydrogen with air, the consideration of at least 8 and perhaps as many as 25 ignition-reaction paths appears necessary.<sup>6</sup> However, simple chemistry models are also useful and have been employed extensively.

This paper discusses a system of computer programs developed to analyze and predict the flow field in the strut and combustor regions of a scramjet engine module. Although programs also are available to consider other regions of the engine, we will concentrate on our analysis capabilities for combustor modelling following the spirit and interest of the Specialist's Meeting. Each region of the combustor has a program tailored to its analysis that solves the governing equation system consistent with the type of flow field that is present in that region. The governing equations are solved numerically using one of two popular integration schemes. The turbulence is modelled using either an eddy viscosity model or a two equation turbulent kinetic energy transport model. Chemical reactions are modelled either with a simple equilibrium reaction model or a multi-reaction finite rate scheme containing up to 25 possible reaction paths.

We will report solutions with programs representative of each particular flow class present in the combustor. Additionally, we will also report solutions from a two-dimensional program used primarily for study and evaluation of turbulence and reaction models of current interest. Those results will in each case be compared with available experimental data so as to assess the accuracy of each code. Finally, we will give an overall assessment of our predictive capabilities in a supersonic combustor and indicate as a result of these conclusions the direction of our future research to develop an integrated combustor analysis tool.

## 2.0 TWO-DIMENSIONAL PARABOLIC FLOW PROGRAM

Although flow fields in the engine are always three dimensional in character, two-dimensional analyses have been used effectively to study limited regions of the combustor where the flow is nearly two dimensional. These analyses have also been used to test and develop turbulence and chemistry models for use in the analysis of combustor flow fields with other programs. A two-dimensional, parabolic program obtained from the Spalding group at Imperial College, London, has provided such a tool.<sup>7,8</sup> The original version of the program has been modified to meet the research needs of the hypersonic propulsion program. A description of the current version and of its application to several problems of interest is given here.

Solutions of parabolic partial differential equations governing the transport of momentum, energy, and mass are obtained using the finite difference technique of Patankar and Spalding.<sup>9</sup> The governing equations are

$$\frac{\partial F}{\partial x} + \frac{1}{\Gamma} \frac{\partial G}{\partial y} = S_\phi \quad (1)$$

where

$$F = \begin{pmatrix} \rho u \\ \rho u u \\ \rho u v \\ \rho u H^0 \\ \rho u f \\ \rho u k \\ \rho u \epsilon \\ \rho u g \end{pmatrix}$$

$$G = \begin{pmatrix} \rho v \\ \rho v u - \Gamma_u y^i \frac{\partial u}{\partial y} \\ \rho v v - \Gamma_v y^i \frac{\partial v}{\partial y} \\ \rho v H^0 - \Gamma_H y^i \frac{\partial H^0}{\partial y} \\ \rho v f - \Gamma_f y^i \frac{\partial f}{\partial y} \\ \rho v k - \Gamma_k y^i \frac{\partial k}{\partial y} \\ \rho v \epsilon - \Gamma_\epsilon y^i \frac{\partial \epsilon}{\partial y} \\ \rho v g - \Gamma_g y^i \frac{\partial g}{\partial y} \end{pmatrix}$$

Equation (1) defines, respectively, the differential equations for continuity, the momentum components, total enthalpy, species, turbulence energy, the dissipation rate of turbulence energy, and the mean square amplitude of fluctuations in species concentration. The first term of equation (1) represents convection in the principal flow direction; the second represents convection and diffusion in the transverse direction. The term  $\Gamma$  is a general diffusion coefficient that is made up of turbulent and laminar parts.

$$\Gamma = \frac{\mu_{eff}}{\Pr_{eff}} = \frac{\mu_t}{\Pr_t} + \frac{\mu_2}{\Pr_2} \quad (2)$$

All other terms are collected into  $S_\delta$ , the source term. Values of the diffusion coefficient and source term are given in Table I. Turbulence viscosity is computed from

$$\mu_t = \frac{C_\mu \rho k^2}{\epsilon} \cdot f_c \quad (3)$$

where  $f_c$  is a compressibility correction<sup>10</sup> whose magnitude varies between 0.25 and 1.0. The correction is an empirical expression derived from experimental observations and is calculated from

$$f_c = \begin{cases} 0.25 + 0.75/(1.0 + \exp(24.73(M_T - 2))), & M > 1.0 \\ 1., & M \leq 1.0 \end{cases} \quad (4)$$

where  $M_T = (k^{1/2}/u) M$ .

Details of the integration of the governing equations and of the application of the turbulence model have been well documented previously. Therefore, we will concentrate on recent modifications to the program, particularly multi-equation finite-rate chemistry modelling, and will present comparisons with experimental data. A short qualitative discussion of accuracy appears in reference 9.

In the original version of the program species concentrations based on chemical equilibrium were assumed. The program has been extended to include no reaction, complete reaction (i.e., the only species are  $O_2$ ,  $H_2$ ,  $H_2O$ , and  $N_2$ , with the condition that  $O_2$  and  $H_2$  cannot be simultaneously present), equilibrium chemistry, finite rate chemistry, and an eddy breakup model. The equilibrium and finite rate chemistry schemes have been developed in two versions. In the first version, the species  $H$ ,  $O$ ,  $H_2O$ ,  $OH$ ,  $O_2$ ,  $H_2$ , and  $N_2$  are related by eight elemental reactions and five additional differential equations must be solved. In the other version, the additional species  $N$ ,  $NO$ ,  $NO_2$ ,  $HNO_2$ , and  $HO_2$  are included. Twenty-five elemental reactions are used and ten additional differential equations (instead of five) must be solved.

Following Spiegler<sup>11</sup>, finite rate chemistry is described by a set of reactions of the form

$$\sum_{j=1}^{N_S} \gamma_{ij} M_j \xrightleftharpoons[k_{bi}]{k_{fi}} \sum_{j=1}^{N_S} \gamma_{ij}'' M_j \quad (5)$$

where  $i = 1, 2, \dots, N_R$  and  $j = 1, 2, \dots, N_S$ . The reaction rates  $k_{fi}$  and  $k_{bi}$  are given by expressions of the form

$$K_i = A_i T^{B_i} e^{-C_i/T} \quad (6)$$

The rate of change of species  $j$  by reaction  $i$  is

$$(\dot{M}_j)_i = (\gamma_{ij}'' - \gamma_{ij}') \left( K_{fi} \prod_{j=1}^{N_S} M_j^{\gamma_{ij}'} - K_{bi} \prod_{j=1}^{N_S} M_j^{\gamma_{ij}''} \right) \quad (7)$$

The total rate of change of species  $j$  is

$$\dot{w} = \dot{M}_j \times (\text{molecular weight}) \quad (8)$$

where  $\dot{M}_j = \sum_{i=1}^{N_R} (\dot{M}_j)_i$ .

The eight-reaction and the twenty-five reaction systems are described in Table II. The first seven species listed and the reactions marked with an asterisk constitute the eight reaction system; the remaining species and reactions are those added to test the importance of the extra reactions for obtaining accurate predictions.<sup>6</sup> Reaction rates are also listed in Table II.

When the eddy breakup model is used the chemical reaction rate is computed from

$$\dot{w} = -C_{EBU} \rho g^{1/2} (\epsilon/k) \quad (9)$$

The constant  $C_{EBU}$  is treated as an adjustable parameter to improve agreement between calculation and experiment; we have used the value  $C_{EBU} = 0.53$ . The factor  $g^2$  is the smaller of the root mean square fluctuations in  $H_2$  or  $O_2$  concentration. The two differential equations required for the eddy breakup model are transport equations for  $g_{H_2}$  and  $g_{O_2}$ . The ratio  $\epsilon/k$  provides a time scale representative of the rate at which large eddies break down into small eddies. For the eddy breakup model to represent well the rate of chemical reaction, it is necessary that the reaction rates be fast relative to the rate at which fuel and oxygen mix on a molecular scale; the mixing process is then the rate limiting process. When applicable, the eddy breakup model is particularly useful for modelling the reduced burning rate caused by "unmixedness" in turbulent flows. The unmixedness is used to describe the fact that, although fuel and air may be mixed on a scale comparable to turbulent eddy dimensions, they are still not mixed on a molecular

scale. For those cases in which reaction is kinetically controlled rather than mixing controlled, a finite rate chemistry scheme is needed. However, because of the very small step sizes required to solve these stiff chemical kinetic equations in a finite rate model, the cost may be large compared with the value of the results. In such cases one of the other options in the program for modelling chemistry may yield adequate results at lower cost.

The results of three calculations using the 2-D parabolic program are given to demonstrate some of its uses and to allow assessment of its accuracy by comparing calculated results with data. In the first case  $H_2$  was injected coaxially into a hot, supersonic, vitiated air stream. Vitiated air was obtained by burning hydrogen in air to obtain a hot gas mixture, and then oxygen was added to obtain a test gas with 21 percent oxygen by volume. The temperature was high enough so that auto-ignition occurred immediately. Geometry and initial conditions are given in figure 3; theory and experiment are compared in figures 4, 5, and 6. Agreement of the  $N_2$  curves with data indicates that mixing was correctly calculated. Prediction of the properties related to combustion are less satisfactory, although examination of figures 4, 5, and 6 shows that the calculated profiles develop with distance from the injection point in the same way as curves which could be drawn through the data points. Also, the peak heights of the calculated  $H_2O$  profiles are about the same as the peak heights of the data points. The principal difference appears to be that the calculated  $H_2O$  peaks lie farther from the axis than the data points indicate they should. Calculations made with the 25<sup>6</sup> reaction model did not produce any appreciable change in the calculated results. Since the reactions of the  $H_2$ - $O_2$  system are well known, the explanation probably lies in the effect of interaction between chemistry and turbulence.

The data used for the second case is from an experiment performed by Kent and Bilger,<sup>12</sup> in which a subsonic jet of  $H_2$  was injected into a coaxial stream of air. Both streams were cold and required an auxiliary ignition source. Figure 7 gives the details of geometry and initial conditions. The flow profiles shown in figure 8 demonstrate that reaction was essentially complete, since the complete reaction curves agree well with the data.

The eddy breakup model (eq. (9)) also was used to calculate the amount of reactions. The EBU results are compared with complete reaction results in figure 9. The eddy breakup results differ from complete reaction results only in the mixing region between the  $H_2$  and air layers. Where differences are present, agreement with data is better using the eddy breakup model. Calculations using the finite rate chemistry model also were attempted for this case, but were abandoned because of the high cost associated with solving the stiff chemical kinetic equations in subsonic flow.

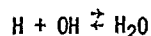
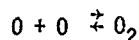
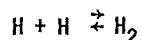
The last case was chosen to illustrate the program's capability for calculating transverse pressure profiles. No suitable data were available, but a test case was obtained by analyzing a ducted, supersonic air flow using an inviscid shock fitting program.<sup>13</sup> Air at room temperature and Mach 1.5 flows between two plates, as shown in figure 10. All property profiles are initially uniform. For values of  $x$  between .01 and .03, the distance  $y$  between the plates decreases linearly; elsewhere, the distance between the plates is constant. A shock wave begins where the channel starts to converge; the wave then moves across the flow and reflects from the opposite wall. A rarefaction moves into the flow from the point where the channel cross section expands and becomes constant again. The solid lines in figure 11 show the inviscid results, and the dashed lines show the results obtained using the parabolic marching program. Steep pressure gradients, such as those encountered across the shock wave, are smeared. However, the general shape and magnitude of the correct pressure profiles given by the inviscid results are obtained; and both the shock wave and the rarefaction are easily identified.

The two-dimensional parabolic program has proved to be a valuable basic research tool for the development and evaluation of turbulence and chemistry models. The experience gained from using the code is now finding direct application in a three-dimensional parabolic program currently being employed in combustion research and development. Details of the three-dimensional code are described in the next section.

### 3.0 THREE-DIMENSIONAL PARABOLIC PROGRAM

A three-dimensional analysis is required to model the flow field in a scramjet combustor. Well downstream of the fuel injection struts where flow recirculation does not exist and embedded regions of subsonic flow are small, the flow is essentially supersonic. Flow fields of this type can be modelled with solutions to the three-dimensional parabolic Navier-Stokes equations and one or more species equations. The principal program applied to this problem class is the SHIP computer code, described in its initial form in reference 14. Significant modifications to this program have been carried out to tailor the model to scramjet combustor flow fields.<sup>15,16</sup> Details of the program structure and significant modifications are described below.

The SHIP computer program was developed to calculate three-dimensional, turbulent, reacting, parabolic internal or external flows. The computational domain is limited to a rectangular parallelepiped with each boundary being either a wall, a symmetry plane, or a free-stream boundary. Walls may converge or diverge as smooth functions of the streamwise coordinate. Calculations are carried out in the physical plane (rather than a transformed computational plane), however, so that convergence or divergence angles are limited to about 16° to maintain acceptable accuracy. Thermodynamic properties are considered to be functions of temperature and species. Reaction is modelled with either an equilibrium or finite rate chemistry scheme. The equilibrium scheme considers four reactions:



The finite rate scheme is the same as that used in the two-dimensional parabolic program.

The governing equations for the program are in primitive variable form ( $\rho, u, v, w, p, H, f, k, \epsilon$ ) and are based on an Eulerian formulation in rectangular coordinates. For flows that are primarily supersonic, streamwise-diffusive effects are negligible, and the flow field is adequately described by the parabolic form of Navier-Stokes and species equations together with the equation of state for an ideal gas. These equations are:<sup>16</sup>

$$\frac{\partial U}{\partial z} + \frac{\partial F}{\partial x} + \frac{\partial G}{\partial y} = S_\phi \quad (10)$$

where

$$U = \begin{pmatrix} \rho w \\ \rho w u \\ \rho w v \\ \rho w w \\ \rho w H^0 \\ \rho w f \\ \rho w k \\ \rho w \epsilon \end{pmatrix}$$

$$F = \begin{pmatrix} \rho u \\ \rho u u - \Gamma_u \frac{\partial u}{\partial x} \\ \rho u v - \Gamma_v \frac{\partial v}{\partial x} \\ \rho u w - \Gamma_w \frac{\partial w}{\partial x} \\ \rho u H^0 - \Gamma_{H^0} \frac{\partial H^0}{\partial x} \\ \rho u f - \Gamma_f \frac{\partial f}{\partial x} \\ \rho u k - \Gamma_k \frac{\partial k}{\partial x} \\ \rho u \epsilon - \Gamma_\epsilon \frac{\partial \epsilon}{\partial x} \end{pmatrix}$$

$$G = \begin{pmatrix} \rho v \\ \rho v u - \Gamma_u \frac{\partial u}{\partial y} \\ \rho v v - \Gamma_v \frac{\partial v}{\partial y} \\ \rho v w - \Gamma_w \frac{\partial w}{\partial y} \\ \rho v H^0 - \Gamma_{H^0} \frac{\partial H^0}{\partial y} \\ \rho v f - \Gamma_f \frac{\partial f}{\partial y} \\ \rho v k - \Gamma_k \frac{\partial k}{\partial y} \\ \rho v \epsilon - \Gamma_\epsilon \frac{\partial \epsilon}{\partial y} \end{pmatrix}$$

Appropriate exchange coefficients  $\Gamma$  and source functions  $S_\phi$  are given in Table III. Where streamwise diffusion of mass, momentum, and energy is negligible, such that second order derivatives in that direction can be dropped, only first order derivatives of  $U$  remain. Therefore, only an initial condition on  $U$  needs to be satisfied, and the solution can be efficiently marched through elliptic flow cross stream planes from the initial to final downstream station. Thus, three-dimensional problems can be solved with a computer program requiring only two-dimensional storage.

Equation (10) is solved using a finite difference solution scheme.<sup>14</sup> As the solution marches from the initial station, each cross-stream plane is discretized with a nodal grid. All dependent variables with the exception of the cross-stream velocities are stored at these nodes; the cross-stream velocities are stored at midpoints between the nodes. This staggered storage of cross-stream velocities simplifies the calculation of convection terms. Also, staggering of the remaining variables relative to the cross-stream velocities simplifies the calculation of needed gradients for the calculation of those velocities.

Difference equations are formed at each node and staggered grid point by taking integrations over associated control volumes. Volume integration over  $U$  and  $S$  derivatives are carried out by assuming that dependent variables retain their value at the node point throughout the associated control volume. Volume integrals over  $F$  and  $G$  produce surface integrals of convective and diffusive fluxes across the control volume boundaries. The resulting derivatives are differenced by a combination of central and upwind differences. The system of simultaneous algebraic equations that results is solved by the SIMPLE (Semi-Implicit Method for Pressure Linked Equations) algorithm that is well documented in earlier literature.<sup>17</sup> In this solution technique, the velocity components are estimated initially for an assumed pressure. The pressure field is then corrected using a modified form of the continuity equation. Next, the velocity components are corrected and used with the pressure field to solve for the remaining dependent variables. Finally, temperature is calculated from the total enthalpy and velocity field, and density is calculated from the ideal gas law.

Boundary conditions are defined by specifying appropriate fluxes across the upper and lower boundaries



of the solution domain.<sup>16</sup> Along a wall, turbulent wall functions are used to define values of the dependent variables across the wall boundary layers. The calculation begins with values calculated at the upper limit of the boundary layer. At a symmetry boundary, flux values are forced to vanish. Initial conditions are specified at the inflow boundary before beginning a calculation. Typically the three velocity components, species, temperature, and pressure are specified. Then, the initial density and total enthalpy are calculated. Finally, the initial turbulent kinetic energy and dissipation are estimated from an eddy viscosity model of turbulence.

The current SHIP computer program has been evaluated by comparison with two sets of experimental data. The first experiment was conducted to study the three-dimensional turbulent mixing of helium in a ducted supersonic airstream downstream of parallel fuel injectors. This experiment was attractive for the first evaluation of the program since inert helium was substituted for hydrogen fuel, allowing assessment of the code without the additional complication of reaction. The second experiment considered the reaction of hydrogen injected parallel to a ducted supersonic air stream, thus allowing evaluation of the program with both turbulent mixing and chemical reaction.

The configuration for the first test case is presented in figure 12.<sup>18</sup> The duct had a cross section of 3.81 cm by 17.7 cm, and a length of 73.69 cm downstream of the injectors. The strut was centered in the shorter dimension and spanned the longer dimension of the duct cross section. Five equally spaced fuel injectors were located in the base of the strut. Flow to the duct was provided by a rectangular Mach 2.99 nozzle at a total temperature of 294K and a total pressure of 1.6 MPa. Helium was injected at a total temperature of 294K and a total pressure of 3.79 MPa. Further details regarding the experimental apparatus and instrumentation are given in reference 18.

Flow field surveys were made at two streamwise stations, the first just downstream of the injectors (4.21 cm) and the second at the end of the duct (73.69 cm). At the initial station, the flow field from jet to jet was nearly symmetric, i.e. planes of symmetry existed that were laterally equidistant between the jets. Additionally, since the strut was centered vertically in the duct, a plane of symmetry also existed through the injectors along the longer strut dimension. At the downstream station, the jet mixing regions were merged, but the symmetry that existed upstream between the jets and between the strut and each wall was still nearly preserved. Due to the overall symmetry of the flow field, the computational region for this case was chosen to be the flow downstream of the central injector bounded laterally by symmetry planes centered between the central injector and its two neighboring injectors and bounded vertically between the upper wall and the strut centerline. Initial conditions for the calculation were taken from data surveys at the 4.21 cm station, and downstream comparisons of experimental data and program calculations were made at the 73.69 cm station. Each cross-stream computational plane was spanned by an irregular grid with 11 lateral nodes and 30 vertical nodes.

Results for the first case are given in figure 13.<sup>15</sup> Comparisons of program results with experimental data at the downstream station generally show excellent agreement. Computed values of streamwise velocity and static temperature agree quite well with experimental measurements at all five lateral stations. The maximum differences between computational results and experimental data are about 6.3 percent for the velocity and 6 percent for the temperature. The maximum differences generally occur at measurement points near the duct wall where measured values may be perturbed by duct end effects, which may in turn be felt upstream through the duct boundary layer. Also, the determination of experimental velocities and temperatures from pitot and static pressure measurements assumed a constant total temperature and this assumption may have introduced small errors. Small computational errors may also be introduced near the wall by both the approximate boundary condition treatment (the application of wall functions) and relatively coarse grid discretizations near the wall. Even with these approximations, the comparisons of velocity and temperature are quite satisfactory.

The computed values of helium mass fraction also agree well with the experimental data except at the two outermost stations ( $\pm 1.27$  cm). There are several possibilities that could cause this disagreement. First, the helium mass flow calculated from the data at the downstream station is 11 percent higher than the values calculated upstream. The initial helium mass flow is computationally conserved, however, yielding an identical integrated value at the outflow station. Second, the lateral mixing of helium and air is computationally slower than the experimental mixing. This difference is most likely attributable to the turbulence model and the assumed isotropic nature of the flow. Third, the flow field associated with the central injector was assumed independent of the other injectors, whereas the flow of the center injector is likely affected to some extent. Finally, the downstream values of helium mass fraction are relatively quite small such that measurement accuracies may limit a detailed comparison of computation and experiment.

The second test case considered the reaction of hydrogen and air in a duct. The experimental apparatus is described in figure 14. Details of the experiment and data collection are discussed in references 19 and 20. Hydrogen was injected from a 0.4 cm stepped-wall injector at Mach 1.0 with a static pressure of 0.1 MPa and a static temperature of 254K. Vitiated air was supplied to the duct at Mach 2.44 with a static pressure of 0.1 MPa and a static temperature of 1270K. The duct cross section at the hydrogen injector was 5.1 cm wide and 9.38 cm high. The duct downstream of the injector was 35.6 cm long. Over that length, the duct height expanded linearly from 9.38 cm to 10.48 cm. Total temperature and composition measurements were made at both the initial station (the location of the hydrogen injector) and the duct exit station. Pitot pressure measurements were made only at the exit station.

Experimental data measured at the initial station were also used as initial data for the program. Profile data at the hydrogen injector and the duct immediately above were assumed to have a uniform transverse distribution. A constant wall temperature of 298K was assumed and heat transfer was allowed across the wall. Lateral flow field symmetry existed about the vertical centerline of the duct. Therefore, the calculation downstream of the injector was carried out in a domain defined vertically by the upper and lower duct walls and laterally by vertical planes at the duct wall and centerline. Initial turbulence kinetic energy and dissipation profiles were estimated using an algebraic eddy viscosity model of turbulence. The kinetic energy and dissipation equations were then applied using the following constants:

$$\begin{aligned}
 C_1 &= 1.44 \\
 C_2 &= 1.92 \\
 C_D &= 0.09 \\
 Pr_\ell &= 0.7 \\
 Pr_{t,\phi} &= 1.0 \text{ for } \phi = u, v, w, \text{ and } k \\
 Pr_{t,\epsilon} &= 1.3 \\
 Pr_{t,\phi} &= 0.5 \text{ for } \phi = H, f
 \end{aligned}$$

Reaction was modelled using equilibrium chemistry.

Comparisons of the computational results and experiment at the duct exit are given as a function of distance from the lower wall in figures 15 through 18.<sup>16</sup> Figure 15 shows a comparison between experiment and calculation of reactants and the water generated by reaction. Figure 16 compares outflow Mach number profiles. Figures 17 and 18 give a comparison, respectively, of the total temperature ratio and pitot pressure ratio. The calculation and experiment agree reasonably well in each case. Differences may well be caused by the chemistry and turbulence models.<sup>16</sup> The analysis used equilibrium chemistry to describe reaction, whereas the chemistry may be controlled by reaction rate rather than by the mixing of hydrogen and air. Such a situation would require finite rate modelling of the chemistry to adequately describe the reaction. The two-equation turbulence model was initially developed for shear-layer-like flows, and the model has been shown to provide a reasonable estimate of turbulence in such cases. This case does represent a shear-layer-like character, but is complicated with the additions of reaction and three-dimensional effects. Therefore, the present model may not adequately represent the turbulence field. Finally, the pressure increases downstream in the duct due to reaction. Effects of the pressure rise likely propagate upstream through the subsonic portion of the boundary layers and affect the flow field upstream. As noted earlier, such effects cannot be described by the parabolic set of governing equations used in the present program.

The parabolic flow computer programs have been used successfully to analyze flow fields typical of those found in scramjets. The programs are based on proven solution algorithms, and they have been improved to include more appropriate turbulence and chemistry modelling for scramjet flow fields. The codes have now progressed to where they appear adequate for modelling supersonic combustor flow fields in a scramjet.

Pressure effects that propagate upstream through embedded subsonic regions in the engine are present, however, due to the elliptic nature of the flow field in subsonic flow. Precise treatment of such flows requires solution of the elliptic form of the governing equations. A reasonable approximation of those equations can be made, however, when upstream propagation is important, but when flow recirculation is not present. The approximation is made by casting the governing equations into a "partially elliptic" form, as described in the following section.

#### 4.0 THREE-DIMENSIONAL PARTIALLY ELLIPTIC FLOW PROGRAM

The computer program for the calculation of partially elliptic flow (PELICAN) was developed from the SHIP code as described in reference 21. The basic concept of the code development is to account for the presence of local subsonic flow regions in an otherwise supersonic flow with a predominant flow direction. The approach was originated by Spalding.<sup>22</sup> Although this concept does not permit flow recirculation and separation zones, which would require solution of the fully elliptic governing equations, it does allow downstream disturbances to be felt upstream through pressure propagations in local subsonic flow regions. Thus, the flow field is approximately parabolic and only the pressure, which is governed by an elliptic equation, needs to be stored in a three-dimensional array. It is possible, therefore, to use a marching integration procedure like that in the SHIP code, with repetitive sweeps of the entire flow field until a converged solution is obtained. Each successive iteration uses an improved estimate of the pressure field obtained from the previous sweep.

Details of the development of the partially elliptic-flow computer code by application of the iterative concept to the original SHIP code are given in reference 21. The governing equations are essentially the same as those employed in the SHIP program, described in the previous section, and so the equations are not repeated here. Modifications to the equation that calculates the pressure field represent the only major change. In the SHIP program, the streamwise pressure gradient is decoupled from the cross-stream pressure gradients. Initially, the streamwise pressure gradient is assumed zero and cross-stream gradients are estimated from a Poisson equation. Therefore, the pressure field is treated as if it were independent of downstream quantities as are other dependent variables in a parabolic analysis.

In the partially elliptic formulation, an approximate initial three-dimensional pressure field is assumed. As the calculation proceeds through its first pass of the solution domain, the approximate pressure is corrected with a pressure correction governed by a three-dimensional elliptic equation derived from the continuity equation. Once the first pass is completed, the newly calculated pressure field is used for a second pass through the solution domain, again updating the pressure field. The procedure is repeated until no significant change is observed in the pressure field, i.e. the solution has converged. Details of the derivation of the equation governing the pressure correction terms and the computational procedure can be found in references 21 and 23.

The application of the partially elliptic program to a reacting ducted flow is described in figure 19.<sup>21</sup> Gaseous hydrogen is injected slightly subsonic ( $M = 0.98$ ) and parallel into a ducted supersonic air stream ( $M = 1.5$ ). The duct has a square cross section that converges downstream of the hydrogen injector. Chemical reaction is modelled using the equilibrium scheme described earlier and turbulence is again described with the two equation model.

The pressure rises downstream in the duct due to compression and reaction. Along the duct centerline (labeled O), there is a significant upstream shift of the static pressure rise computed by the partially elliptic program as compared to the parabolic program. Apparently, there is significant pressure feedback from the disturbance due to reaction that is accounted for by the partially elliptic program. Along the duct corner (labeled C), there is little difference between the two computational procedures. In embedded subsonic regions, these results emphasize the need to account for downstream influences that ultimately affect all results in a calculation.

At present the PELICAN code is being reviewed in an effort to improve the pressure iteration procedure and establish improved criteria for convergence. The application of the code to the analysis of supersonic combustor flow configurations for which data are available is anticipated in the near future.

For regions in the engine where there is no longer a predominant flow direction, i.e., near a transverse fuel injector where flow recirculation is present, a parabolic or partially elliptic analysis is no longer valid. Near a transverse injector, either the fully elliptic form of the governing equations must be solved, or the flow separation that is present must be modelled. The following section of the paper discusses two computer programs being used to study transverse fuel injectors in the engine, and presents several recent comparisons of the program with available data.

## 5.0 ELLIPTIC FLOW PROGRAMS

The flow field near transverse fuel injectors not only contains embedded regions of subsonic flow, but also contains separated recirculating regions as well. With such a flow, streamwise diffusive effects must be considered, and parabolic analyses described earlier cannot be used. The inclusion of streamwise diffusion results in an elliptic set of governing equations for the injector near field. These equations must either be solved directly or modelled to analyze the flow field. Both a flow-field model and a direct numerical solution are currently being employed to analyze the transverse injection flow field, and that work is described below.

### 5.1 Transverse Jet Interaction Model

The injection of hydrogen fuel from a wall injector directed transverse to the mainstream flow has been an essential feature of scramjet combustor designs since their inception. In order to obtain performance predictions of these combustor configurations, it is necessary to account for the effects of the transverse jet interaction (TJI) on the subsequent mixing and reaction. Analytical solutions of the complete details of the three-dimensional TJI flow field are difficult, because they must employ the elliptic form of the Navier-Stokes equations to account for the presence of certain aerodynamic features. These features, which are illustrated in figure 20, are caused by the transverse momentum and blockage of the injected fuel. In the TJI flow region the mainstream and jet contain separation and recirculation zones which initiate shock waves and may contain embedded regions of subsonic flow. At the present time, the numerical solution of such a three-dimensional, elliptic flow field is not practical because of the large storage and computational times required.

As an alternative to the numerical solution of the complete TJI flow field, a global model has been derived and applied to the prediction of some supersonic combustion data.<sup>24</sup> The concept of this global model approach is to transform the TJI region in a physically compatible way that can be computationally coupled with a more detailed solution of the downstream flow. Since the combustor flow well downstream of the fuel injection has a predominant flow direction and, generally, contains no separated flow regions or shocks, it can readily be computed using a parabolic numerical solution algorithm. The TJI model provides profiles of the flow variables at some point downstream of the jet by solving the integrated form of the conservation equations for the elliptic flow region caused by the jet disturbances. These profiles are then used to start the parabolic solution which provides details of the turbulent mixing and reaction through the remainder of the combustor. In this way, the TJI model provides a needed computational tool for the design and analysis of supersonic combustor flows with transverse injection of fuel.

The two-dimensional TJI model was derived by considering the observable physical and aerodynamic characteristics of the jet interaction, assuming nondimensional profiles of the flow variables, and evaluating the constants in the assumed profiles so as to satisfy the integrated form of the conservation equations. Before discussing the basic concept of the TJI model, however, it is of interest to briefly review the aerodynamic features of the jet interaction flow field. The features of the TJI flow, depicted schematically in figure 20, are typical of observations for both discrete orifice<sup>25</sup> and slot<sup>26</sup> injectors. Of particular interest to the development of a flow model are the flow separation and recirculation zones immediately upstream and downstream of the injector, the separation and bow shock waves caused by the jet blockage, and the so-called jet Mach disc shock internal to the jet flow. The upstream flow separation zone initiates a planar (in the two-dimensional case) oblique shock. The jet bow shock has been used to obtain the size of a solid body equivalent in blockage to the jet flow. Generally, as in the case of an unbounded mainstream flow, the bow shock produces no net turning of the flow, and approaches a Mach line at large distances from the jet. In the separated flow region immediately behind the injector, wall pressure data for a two-dimensional (slot) jet in nonreacting flow indicate that the flow expands rapidly from the raised pressure level caused by the combined effects of the upstream shock structure and at the downstream reattachment point, approaches the pressure of the undisturbed mainstream. The jet Mach disc shock occurs within the jet flow as the jet fluid expands supersonically from sonic conditions at the injector exit. The height of the jet Mach disc shock, which is generally considered to be characteristic of the transverse jet interaction disturbance<sup>25,28,29,30</sup> represents the penetration of the jet fluid into the supersonic mainstream. As such a scaling parameter, the jet Mach disc shock height has been correlated with injection pressure for both discrete orifice<sup>31</sup> and slot<sup>25,29</sup> injector configurations. Typically, the Mach disc marks the commencement of rapid mixing of the injected gas and mainstream.

Considering these pertinent characteristics of the TJI flow field, it is assumed that the flow in the vicinity of injection can be represented by the two-dimensional flow model presented in figure 21. The flow is considered to be confined within a two-dimensional duct with walls that diverge at small angles  $\alpha_p$  and  $\alpha_T$ . As can be seen from the figure, the flow model assumes a leading shock wave that is a linear combination

of the separation and bow shocks. This means that at large distances from the injector, the turning imparted to the flow by the combined shock is equal to that of the upstream separation region. The exit plane of the flow model is taken at the downstream location where the combined leading shock wave intersects the opposite wall of the duct. Reflection of the combined shock from the upper surface is not included in the flow model. The surfaces of the combined shock, the model exit plane, and the injection surface define the control volume shown by the broken lines in figure 21. The integration of the conservation equations over the control volume yields relations which must be satisfied by profiles of the flow variables at the exit plane. Such relations are then used to determine the characteristic parameters of these profiles.

Starting with the divergence form of the conservation equations and assuming that the flow is steady, body forces, conduction, and radiation are negligible, no chemical reactions occur, and the diffusion is small compared to convection, the equations reduce to

$$\text{mass} \quad \oint_S \rho v_i n_i dS = 0, \quad (11)$$

$$\text{momentum} \quad \oint_S (\rho v_i v_j - P_{ij}) n_i dS = 0, \quad (12)$$

$$\text{energy} \quad \oint_S (\rho e v_i - v_j P_{ij}) n_i dS = 0, \quad (13)$$

$$\text{species} \quad \oint_S \rho v_i \kappa_i n_i dS = 0. \quad (14)$$

In these equations,  $\rho$  is the density,  $v_i$  is the velocity vector,  $\kappa$  is fuel mass fraction, and  $e$  is the sum of internal and kinetic energies. The integrals are evaluated over the surface area  $S$  of the control volume; the  $n_i$  are unit normal vectors directed outward from each surface. Applying the equations to the flow model control volume, and assuming that the shear stress components of the stress tensor  $P_{ij}$  are negligible in comparison with the pressure terms except on the surfaces of the duct, the equations of motion (except the energy equation) per unit width of duct are:

$$\text{mass} \quad \int_0^h \rho_2 v_2 \cos \delta_2 dz' = (1+f)\dot{m}_0, \quad (15)$$

streamwise momentum

$$\int_0^h (\rho_2 v_2^2) \cos^2 \delta_2 dz' + \int_0^h p_2 dz' = \rho_0 v_0^2 h_0 + p_0 (h_0 + x_{LG} \tan \alpha_T) - S_F (\cos \alpha_B + \cos \alpha_T) + F_J \sin \alpha_F - F_W \tan \alpha_B, \quad (16)$$

transverse momentum

$$\int_0^h (\rho_2 v_2^2) \sin \delta_2 \cos \delta_2 dz' = F_J \cos \alpha_F + F_W - p_0 x_{LG} - S_F (\sin \alpha_T + \sin \alpha_B), \quad (17)$$

species

$$\int_0^h \rho_2 v_2 \kappa \cos \delta_2 dz' = f \dot{m}_0. \quad (18)$$

In this form  $h$  is the duct height,  $\delta$  is the local flow angle,  $f = \dot{m}_f / \dot{m}_0$  is the ratio of fuel and mainstream mass flow rates, and  $p$  is the static pressure. Subscripts 2 and 0 refer to properties in the model exit plane and the undisturbed mainstream, respectively. The skin friction force on each wall is defined as  $S_F = \frac{1}{2} \rho_0 v_0^2 \bar{c}_f x_{LG}$  where  $\bar{c}_f$  is the mean skin friction coefficient, and  $x_{LG} = x_L + x_s$  is the total length of the control volume. The integral of wall pressure on the injection wall is  $F_W$ . The total momentum of the jet gas is defined as  $F_J = (\rho_f v_f^2 + p_f) A_f$ .

The energy equation can be reduced to an algebraic relation between static temperature and velocity by assuming that convection dominates the energy transport. This assumption implies that the local stagnation enthalpy is directly related to the local composition through  $H_2^0 = \kappa H_f^0 + (1-\kappa) H_0^0$ , which gives the energy equation as

$$H_2(T) + V^2/2 = H_2^0 \quad (19)$$

These last five equations, along with the equation of state provide six equations in the six unknowns  $T$ ,  $V$ ,  $p$ ,  $\kappa$ ,  $\delta$ , and  $(\rho V)$ . It is convenient to write the equation of state in terms of the unknown parameters to obtain

$$V = (\rho V) R^0 T / p W \quad (20)$$

where  $W$  is the local molecular weight of the mixture.

$$W = [\kappa / W_f + (1-\kappa) / W_0]^{-1}$$

In order to solve these equations, it is necessary to know something about the profiles of the flow variables ( $p$ ,  $(\rho V)$ ,  $\kappa$ , and  $\delta$ ) that appear in the integral terms. The velocity and temperature can be obtained by simultaneously solving the energy and state equations once the pressure, mass flux, and composition are known. Since the goal of the TJI model is to obtain profiles of the flow properties, nondimensional profiles of these four flow variables were determined. Each assumed profile was represented by a mathematical function containing only one unknown parameter that was representative of the magnitude of the flow variable. For the fuel mass fraction and the mass flux, the profile functions were based on available data in an unconfined, nonreacting flow; for the static pressure and flow-angle profiles, simple functions were assumed subject to the constraints at the boundaries of the duct.

It was shown in reference 24 that the fuel mass fraction profile can be represented by the Gaussian type function

$$\kappa/\kappa_{\max} = \begin{cases} \exp(-A_k \hat{Z}^2), & z > z_k \\ (1 - \bar{\kappa}_w) \exp(-A_{ko} \hat{Z}^2) + \bar{\kappa}_w, & z \leq z_k \end{cases} \quad (21)$$

where the nondimensional coordinate  $\hat{Z}$  is defined as

$$\hat{Z} \equiv C_u (z/z_k - 1)$$

with  $C_u$  defined for  $z > z_k$  so as to make  $\hat{Z} = 1$  where  $\kappa = \kappa_{\max}/2$ ,

$$C_u = \left( \frac{z_k}{z_\delta - z_k} \right) \left[ - \frac{\ln(\kappa_\delta/\kappa_{\max})}{A_k} \right]^{1/2}$$

In these equations,  $z_k$  is the location of the peak concentration  $\kappa_{\max}$ , and  $z_\delta$  is the edge of the mixing region arbitrarily chosen as the point where the fuel mass fraction has decayed to  $\kappa_\delta = 0.0005 \kappa_{\max}$ .  $A_k = 0.6935$  is a constant and  $A_{ko} = \ln(\kappa_\delta/\kappa_{\max}(1 - \bar{\kappa}_w))$ . The value of the fuel mass fraction at the injection wall is arbitrarily taken as  $\bar{\kappa}_w = 0.5$ .

For the mass flux profiles, a reasonable fit to the data profiles between the injection wall and the edge of the mixing region was obtained with the modified Gaussian-type function.

$$R(Z) = (1 - C_R) \exp[-A_R(1 - Z/Z_\delta)^2] + C_R, \quad Z > Z_\delta, \quad (21a)$$

where  $Z \equiv z/h_2$ ,  $R \equiv (\rho V)/(\rho V)_\delta$ ,  $C_R = 0.15$  is the extrapolated value of  $(\rho V)/(\rho V)_\delta$  at  $Z = 0$ , and  $A_R = 10$  is chosen to make the exponential small enough so that  $R(0) \approx C_R$ . Between the edge of the mixing region and the opposite wall, the mass flux varies from  $R_\delta = (\rho V)_\delta$  at  $Z_\delta$  to the value  $R_L$  downstream of the combined shock at  $Z = 1$ . The profile function in the region was assumed to be a second order polynomial

$$R(Z) = 1 + \left( \frac{Z - Z_\delta}{1 - Z_\delta} \right)^2 \left( \frac{R_L}{R_\delta} - 1 \right), \quad Z > Z_\delta. \quad (22b)$$

The locations of the peak concentration  $z_k$  and the edge of the mixing region  $z_\delta$  in these functions were found from correlations presented in the literature.<sup>25,22,23</sup> The only unknowns in the profile functions are the peak concentration  $\kappa_{\max}$  and the mass flux at the edge of the mixing region  $(\rho V)_\delta$ , which are found from the species and mass equations, respectively.

Profile functions for the static pressure and flow angle in the model exit plane were assumed to be second order polynomials. Two of the three coefficients can be evaluated by the boundary conditions on the duct walls. At the injection wall, the pressure  $p_w$  is assumed to have returned to the undisturbed mainstream value, and the flow angle is the wall angle.<sup>w</sup> On the opposite wall values of  $p$  and  $\delta$  are known from the jump conditions across the shock. The third coefficient in the assumed functions was evaluated in terms of mean values of pressure  $p_m$  and flow angle  $\delta_m$  (or  $\tan \delta_m$ ). The resulting equations are

$$p_2 = p_w + Z(3Z - 4) p_w + Z(3Z - 2) p_L + 6Z(1 - Z) p_m, \quad (23)$$

with

$$p_m \equiv \int_0^1 p_2 dZ$$

and

$$\tan \delta_2 / \tan \delta_L = (1 - c) Z + cZ^2 + (1 - Z) \tan \alpha_B / \tan \delta_L, \quad (24)$$

with  $c$  evaluated to satisfy the mass averaged flow angle,

$$\tan \delta_m \int_0^1 (\rho V)_2 dZ = \int_0^1 \tan \delta_2 (\rho V)_2 dZ .$$

The unknown profile parameters  $p_m$  and  $\delta_m$  are found by iterative solution of the  $x$  and  $z$  momentum equations.

Through the preceding assumptions, each of the profiles of an unknown variable ( $\kappa$ ,  $(\rho V)$ ,  $p$ , and  $\delta$ ) in the model exit plane has been replaced by a mathematical function containing a single unknown parameter ( $\kappa_{\max}$ ,  $(\rho V)_\delta$ ,  $p_m$ , and  $\delta_m$ , respectively), that relates to the magnitude of the profile. Before the assumed profile functions can be used, however, the coordinates of the combined shock and the pressure distribution on the injection wall must be obtained to define the size of the control volume and provide the necessary boundary conditions for the assumed profiles.

The coordinates of the assumed combined shock used in the TJI model were obtained from a correlation that compared favorably with observed shock coordinates produced by hydrogen transverse jets in a Mach 2.72 airstream.<sup>25</sup> Relative to the jet diameter, the shock equation is

$$\frac{x}{d} = -\frac{x_s}{d} + \cot \theta_s \left\{ \left[ R_s^2 + \left( \frac{z}{d} \right)^2 \tan^2 \theta_s \right]^{1/2} - R_s \right\}, \quad (25)$$

where

$$\frac{x_s}{d} = \frac{R_B}{d} \left( 1 + \frac{D}{R_B} \right) \quad \text{and} \quad R_s = \frac{R_C}{R_B} \frac{R_B}{d},$$

with  $R_B$  equal to the radius of the jet equivalent body. For a spherically-nosed body, correlations of the shock stand-off distance  $D$  and the shock radius of curvature  $R_C$  are given as<sup>34</sup>

$$R_C/R_B = 1.143 \exp \left[ 0.54/(M_0 - 1)^{1.2} \right], \quad D/R_B = 0.143 \exp (3.24/M_0^2). \quad (26)$$

In the comparisons of reference 25, the radius of the equivalent body was taken as the location of the jet Mach disc shock above the injection surface. The Mach disc location has been related to the jet and mainstream properties and is given by<sup>24</sup>

$$\frac{R_B}{d} = \left[ \frac{3}{2} \left( \frac{p_0}{p_{t,0}} \right) \left( \frac{\gamma M_0^2}{\gamma_f M_{f,0}^2} \right)^{q_R} \right]^{1/2}. \quad (27)$$

The angle  $\theta_s$  in the shock coordinate equation is the asymptote that the shock approaches at large distances from the jet. The appropriate value was found by assuming 1) that  $\theta_s$  equals the angle of the separation shock caused by the recirculation zone upstream of the jet, and 2) that the pressure force on the wall upstream of the jet is the same for the separation and bow shocks in the real flow (fig. 20) and the combined shock in the model flow (fig. 21).

The wall pressure distribution downstream of the jet was modeled after data<sup>27</sup> for a 2-D slot injector in a Mach 2.61 freestream. Typically, these data indicate a rapid expansion of the flow behind the jet followed by a nearly linear recompression to the mainstream pressure at the downstream reattachment location. It also was observed that the distance to reattachment  $x_R$  is approximately equal to the upstream separation distance. Thus,

$$p_w = \begin{cases} p_{\exp} + (p_{w1} - p_{\exp}) x/x_R, & 0 < x < x_R \\ p_{w1}, & x > x_R \end{cases}$$

where

$$p_{\exp} = p_s(0)^{-1}, \quad p_{w1} = p_0, \quad \text{and} \quad x_R = x_{\text{sep}}.$$

This assumed wall pressure distribution is shown for a typical case in figure 22, along with some representative data from reference 27.

With the assumed profile functions and the coordinates of the combined shock, the conservation equations can be integrated and solved by iterating on  $p_m$  and  $\delta_m$ . First, initial values of  $p_m$  and  $\delta_m$  from a 1-D solution and profiles of the pressure and flow angle are computed. Then, nondimensional profiles of fuel mass fraction and mass flux are computed and the values of  $\kappa_{\max}$  and  $(\rho V)_\delta$  found from the species and mass equations, respectively. The temperature and velocity are obtained from the energy and state equations, and the imbalance of the streamwise and transverse momentum equations is computed. From this imbalance corrections to  $p_m$  and  $\delta_m$  are made using a Newton-Raphson procedure. Typical results of the TJI model are given in figure 23 in the form of profiles of density, pressure, velocity, and temperature. Each profile has been nondimensionalized by the value of the undisturbed mainstream flow.

The impetus for the development of the TJI model was to obtain a computational tool for the analysis

and design of supersonic combustor flows. An evaluation of this modelling approach was obtained by comparing some supersonic combustion data with computations using the profiles from the TJI model to initialize the previously described SHIP code. These data were acquired for transversely injected hydrogen in a supersonic stream confined within a two-dimensional duct. The test gas was supplied by a hydrogen-air burner with oxygen replenishment through a Mach 2.7 nozzle. Stagnation conditions of the test gas were nominally 2120 K and 2.173 MPa, which are representative of Mach 7 flight conditions. The hydrogen fuel was injected from a row of five circular orifices equally spaced across the top wall. The orifices operated choked with nominal stoichiometric fuel injection of 0.095 kg/s mass flow rate. Data measurements included static pressure along the centerline of the top (injection) and bottom (opposite) walls and surveys of the flow in a plane just downstream of the duct exit. In those surveys, pitot pressure and gas composition were acquired using a nine probe rake at six locations across the height of the duct.

Comparisons of one of the data cases with the SHIP predictions using the TJI model are presented in figures 24, 25, and 26. In all cases, the symbols indicate the data and the lines indicate results from SHIP with the solid line used for the equilibrium chemistry case, the broken line for complete reaction, and the dotted line for no reaction. Figure 24 presents distributions of the pressure along the injection and opposite walls. In general, the trend of the data and theory shows good agreement. The difference in the magnitude of the pressures for the data and theory, particularly on the injection wall near the injector, may be due to reaction of fuel in the separated flow zone upstream of the jet, which would raise the measured wall pressure well upstream of the jets. The TJI model used to start the SHIP calculation does not account for this effect since it is based on nonreacting, unconfined profile data, and assumes, therefore, that the pressure on the injection wall returns to the value in the undisturbed mainstream.

An interesting feature of the wall pressure comparisons is that oscillations in the SHIP results match in location those observed in the data. These oscillations in the data pressures are due to shock waves reflecting down the duct; in SHIP they result from the reversal of the transverse velocity component at the duct walls. The overall agreement in the trend of these comparisons is considered good, particularly with regard to the location of the peaks in the oscillations.

Figure 25 shows comparisons of the data and theory for the pitot pressure and fuel mass flux profiles. Note that for these profiles, the fuel is injected from the top ( $z/h_0 = 1.0$ ). For the pitot pressures, the general trend of both the data and the SHIP theory is lower values in the fuel rich region ( $z/h_0 > 0.5$ ) and higher values in the fuel lean region ( $z/h_0 < 0.5$ ). For the fuel mass fraction profiles, the agreement between data and theory is quite good except near the injection wall. This lack of quantitative agreement may be due to the 2-D solution algorithm in SHIP which tends to force the peak concentration to the boundary, or to 3-D effects present in the data that are suppressed in the 2-D calculation. In general, the overall agreement in the trends of the data and theory is considered good.

The final comparison is the distribution of the mixing parameter  $n_m$  shown in figure 26. The mixing parameter is the fraction of the injected fuel that has mixed to a reactable level. The symbol at the end of the distributions denotes the value obtained from the integration of the flow in the survey plane at the duct exit. An error band of  $\pm 5$  percent, based on the overall accuracy of the data integration is shown by the vertical bar. The agreement between the data and the theory is good.

The implication of this general agreement from the standpoint of applying the TJI model and SHIP code to the analysis or design of supersonic combustors, is that, even though fuel mass fraction profiles may not be accurately predicted, the prediction of the overall level of accomplished mixing can be good. With regard to the uncertainties inherent in the TJI model, the overall agreement between the data and theory results obtained is encouraging. The TJI model offers an attractive option for the analysis of the supersonic reacting flow field downstream of a transverse hydrogen jet.

## 5.2 Slot Injector Program

To directly describe the flow field about a transverse fuel injector without empirically modelling the jet requires that the elliptic form of the governing equations be solved. A computer program to analyze the injector near field has been developed.<sup>36</sup> The governing equations are solved numerically using a well-known predictor-corrector scheme, and turbulence is modelled with an algebraic eddy viscosity scheme. Only mixing of the hydrogen fuel and air is currently considered; reaction capability will be added at a later date. We noted earlier that the analysis of orifice injectors (where the flow field is three dimensional) is currently limited by the storage of existing computers. Therefore, this analysis is now restricted to two-dimensional slot fuel injectors. Details of this two-dimensional flow are useful for understanding flow field-phenomena near a transverse fuel injector, however, and experience gained in developing the two-dimensional code should provide the background for extension to three dimensions. The present program has been used to analyze two transverse fuel injector configurations. The results of these analyses are presented, and comparisons are made with available experimental data.

The flow near a transverse hydrogen fuel injector is governed by the full (elliptic) form of the Navier-Stokes, energy, and species equations. Written in conservation law form for two-dimensional rectangular coordinates, these equations in the absence of body forces can be expressed as:

$$\frac{\partial U}{\partial t} + \frac{\partial F}{\partial x} + \frac{\partial G}{\partial y} = 0 \quad (29)$$

where

$$U = \begin{pmatrix} \rho \\ \rho u \\ \rho v \\ e \\ \rho f \end{pmatrix}$$

$$F = \begin{pmatrix} \rho u \\ \rho u^2 + \sigma_x \\ \rho uv + \tau_{xy} \\ (e + \sigma_x) u + \tau_{yx} v + q_x \\ \rho u f - \Gamma \frac{\partial f}{\partial x} \end{pmatrix}$$

$$G = \begin{pmatrix} \rho v \\ \rho uv + \tau_{yx} \\ \rho v^2 + \sigma_y \\ (e + \sigma_y) v + \tau_{xy} u + q_y \\ \rho v f - \Gamma \frac{\partial f}{\partial y} \end{pmatrix}$$

and

$$\sigma_x = p - \lambda \left( \frac{\partial u}{\partial x} + \frac{\partial v}{\partial y} \right) - 2\mu \frac{\partial u}{\partial x}$$

$$\tau_{xy} = \tau_{yx} = -\mu \left( \frac{\partial u}{\partial y} + \frac{\partial v}{\partial x} \right)$$

$$\sigma_y = p - \lambda \left( \frac{\partial u}{\partial x} + \frac{\partial v}{\partial y} \right) - 2\mu \frac{\partial v}{\partial y}$$

$$\lambda = -\frac{2}{3} \mu$$

$$\kappa = \frac{\gamma \mu}{Pr}$$

$$q_x = -\kappa \frac{\partial e_s}{\partial x}$$

$$q_y = -\kappa \frac{\partial e_s}{\partial y}$$

$$\Gamma = \frac{\mu}{Sc} = \frac{\mu}{Pr} \quad (Le = 1)$$

$$e_s = cT$$

$$\mu = \mu_{\text{laminar}} + \mu_{\text{turbulent}}$$

The specific heat at constant volume  $c$  is a function of the local temperature and species concentrations. The pressure is calculated from the equation of state for an ideal gas

$$p = \rho R^o T / W$$

where the molecular weight  $W$  is a function of the local species concentrations. The laminar viscosity is calculated from Sutherland's law

$$\mu_{\text{laminar}} = \frac{1.458 \times 10^{-6} T^{3/2}}{(T + 110.33)} \text{ kg/m-s}$$

The turbulent viscosity is calculated from an algebraic eddy-viscosity turbulence model.<sup>3</sup>

For computational efficiency and accurate resolution of the flow field, the physical coordinate grid must be fine near the strut walls and the injector where flow-field gradients are large and viscous effects are important, and the grid must be coarse where flow-field gradients are small and viscous effects less important. Therefore, transformation of the independent variables with a nonuniform computational grid to a rectangular computational domain with a uniform grid is indicated. Equation (29) is transformed from the physical domain  $(x, y, t)$  to the computational domain  $(X, Y, t)$  using the independent variable transformation of Holst<sup>37</sup> as modified by Rudy.<sup>38</sup> Equation (29) becomes

$$\frac{\partial U}{\partial t} + \frac{dF}{dx} \frac{\partial F}{\partial X} + \frac{1}{y_A - y_B} \frac{dG}{dy_1} \frac{\partial G}{\partial Y} = 0 \quad (30)$$

All derivatives in the  $F$  and  $G$  vectors transform in similar fashion. Their final forms are:

$$\sigma_x = p - \lambda \left( \frac{dF}{dx} \frac{\partial u}{\partial X} + \frac{1}{y_A - y_B} \frac{dG}{dy_1} \frac{\partial v}{\partial Y} \right) - 2\mu \frac{dF}{dx} \frac{\partial u}{\partial X}$$



$$\tau_{xy} = \tau_{yx} = -\mu \left( \frac{1}{y_A - y_B} \frac{dg}{dy_1} \frac{\partial u}{\partial y} + \frac{df}{dx} \frac{\partial v}{\partial x} \right)$$

$$\sigma_y = p - \lambda \left( \frac{df}{dx} \frac{\partial u}{\partial x} + \frac{1}{y_A - y_B} \frac{dg}{dy_1} \frac{\partial v}{\partial y} \right) - \frac{2\mu}{y_A - y_B} \frac{dg}{dy_1} \frac{\partial v}{\partial y}$$

$$q_x = -\kappa \frac{\partial e_s}{\partial x} \frac{df}{dx}$$

$$q_y = -\kappa \frac{\partial e_s}{\partial y} \frac{dg}{dy_1}$$

The functions  $f$  and  $g$  compress the grid near walls and fuel injectors.

The time-split finite difference technique of MacCormack<sup>39</sup> is used to integrate the governing equations until a steady-state solution is reached. If a solution to equation (30) is known at some time  $t = n\Delta t$ , the solution at the next time step,  $t = (n+1)\Delta t$  can be calculated from:

$$U_{i,j}^{n+1} = L(\Delta t) U_{i,j}^n \quad (31)$$

for each node point  $(i,j)$  in a finite difference grid network within the boundaries of the computational domain. The finite difference operator  $L$  is split into two one-dimensional difference operators  $L_x(\Delta t)$  and  $L_y(\Delta t)$ . Each split operator consists of a predictor and corrector integration step;  $L_x$  is defined by:

$$U_{i,j}^{n+1} = L_x(\Delta t_x) U_{i,j}^n$$

where

$$\overline{U}_{i,j}^{n+1} = U_{i,j}^n - \frac{\Delta t_x}{\Delta x} \left( F_{i,j}^n - F_{i-1,j}^n \right) \frac{df}{dx} \quad (32)$$

$$U_{i,j}^{n+1} = \frac{1}{2} \left[ U_{i,j}^n + \overline{U}_{i,j}^{n+1} - \frac{\Delta t_x}{\Delta x} \left( \overline{F}_{i+1,j}^{n+1} - \overline{F}_{i,j}^{n+1} \right) \frac{df}{dx} \right] \quad (33)$$

$L_y$  is defined by

$$U_{i,j}^{n+1} = L_y(\Delta t_y) U_{i,j}^n$$

where

$$\overline{U}_{i,j}^{n+1} = U_{i,j}^n - \frac{\Delta t_y}{\Delta y} \left( G_{i,j}^n - G_{i,j-1}^n \right) \frac{1}{y_A - y_B} \frac{dg}{dy_1} \quad (34)$$

$$U_{i,j}^{n+1} = \frac{1}{2} \left[ U_{i,j}^n + \overline{U}_{i,j}^{n+1} - \frac{\Delta t_y}{\Delta y} \left( \overline{G}_{i,j+1}^{n+1} - \overline{G}_{i,j}^{n+1} \right) \frac{1}{y_A - y_B} \frac{dg}{dy_1} \right] \quad (35)$$

First derivatives in the  $F$  and  $G$  terms are differenced as follows. In the  $L_x$  operator all partial derivatives with respect to  $x$  contained in  $F$  are forward differenced in the predictor and backward differenced in the corrector. All derivatives with respect to  $y$  are central differenced in both the predictor and corrector. In the  $L_y$  operator, all partial derivatives with respect to  $y$  are forward differenced in the predictor and backward differenced in the corrector, and all derivatives with respect to  $x$  are central differenced. The one-dimensional operators are combined to form a two-dimensional operator through the symmetric operator sequence<sup>39</sup>

$$L(\Delta t) = L_y \left( \frac{\Delta t}{2} \right) L_x(\Delta t) L_y \left( \frac{\Delta t}{2} \right) \quad (36)$$

One pass through equation (36) advances the finite difference form of equation (30) through one time step,  $\Delta t$ .

Boundary conditions of the reflection type were used along walls or planes of symmetry.<sup>39</sup> For a wall along the lower boundary of the physical domain, no slip conditions ( $u = 0$ ,  $v = 0$ ) require

$$u_{i,1} = -u_{i,2} \quad (37)$$

$$v_{i,1} = -v_{i,2} \quad (38)$$

The wall is assumed adiabatic so that the normal derivative of temperature must vanish. This gives

$$T_{i,1} = T_{i,2} \quad (39)$$

The normal derivative of the hydrogen mass fraction is also required to vanish consistent with the no flux condition at a wall giving

$$f_{i,1} = f_{i,2} \quad (40)$$

The pressure and density along the boundary nodes are set equal to the values at adjacent nodes.

$$p_{i,1} = p_{i,2} \quad (41)$$

$$\rho_{i,1} = \rho_{i,2} \quad (42)$$

These boundary conditions are applied during both the predictor and corrector steps while integrating the continuity, momentum, energy, and species equations. For a wall along the upper physical boundary, equations (37) through (42) again specify (with an appropriate change of the  $j$  node index) the required boundary conditions. For a symmetry plane along the upper boundary, equations (37) and (38) become

$$u_{i,nnj} = u_{i,nnj-1} \quad (43)$$

$$v_{i,nnj} = -v_{i,nnj-1} \quad (44)$$

but equations (39) through (42) remain unchanged. Boundary conditions along the inflow plane are specified by holding all dependent variables fixed at their initial values. Along the outflow station all dependent variables are calculated by linear extrapolation from upstream values. At a hydrogen fuel injector, boundary conditions are specified by fixing all dependent variables at their initial values consistent with the required physical behavior of the jet. Initial conditions are normally specified before beginning a calculation by assuming that free-stream conditions exist at all nodes for each dependent variable.

Artificial viscosity must be added near the bow shock and reattachment shock to smooth pressure and temperature oscillations that develop in those regions. The fourth order numerical damping technique of MacCormack<sup>39</sup> is effective in smoothing these oscillations with moderate injector to free-stream pressure ratios. For high pressure ratios, the numerical diffusion cancellation method is employed. Details regarding the application of both techniques are given in reference 36.

Calculations have been performed for two test cases that consider sonic transverse injection of hydrogen into a supersonic air cross stream. The first case represents a two-dimensional equivalent of the flow between two scramjet engine struts with geometrically opposing hydrogen fuel injectors. Results from this analysis give insight into the nature of the flow field near fuel injectors and indicate likely locations for ignition of the fuel-air mixture that is present. The second case considers the sonic slot injection of hydrogen from a flat plate at zero angle of attack in a supersonic cross flow. Experimental wall data are available for the latter case, and comparisons of the data with the computer program are discussed in this section.

The configuration of the first case is shown in figure 27. Gaseous hydrogen is injected from two 0.127 cm slots at

$$M = 1.1$$

$$T = 242 \text{ K}$$

$$p = 0.526 \text{ MPa}$$

into a 6 cm high by 10 cm long duct having the following inlet air conditions

$$M = 2.7$$

$$T = 800 \text{ K}$$

$$p = 0.101 \text{ MPa}$$

The turbulent Prandtl Number was assumed to be 0.9. The physical domain was spanned by a finite difference grid with 39 nodes in the streamwise direction and 30 nodes in the transverse direction. Due to symmetry about the duct centerline, calculations were carried out only in the region between the lower wall and the duct centerline. The grid was compressed normally near the wall and in a streamwise direction about the injectors with transformation constants (ref. 37) specified as

$$\beta_x = 7.8$$

$$\beta_y = 1.1$$

$$X_0 = 5.0 \text{ cm}$$

The inflow station was placed approximately 1.5 cm upstream of the duct entrance. That placement was necessary to prohibit downstream events from propagating upstream through the subsonic region of the wall boundary layer to the inflow station where flow conditions were fixed. The outflow station was placed 5 cm downstream of the injectors where the flow was again predominantly supersonic to minimize the effect of the outflow boundary conditions on the flow field near the injectors.

Overall results from the first case are shown in figures 28 through 32. In each case the region being displayed lies between the lower duct wall and the duct centerline. The injector is located in the center

( $X = 5$  cm) of the computational domain. Figure 28 shows a plot of the velocity vector field in the lower half duct. Values of the uniformly spaced vectors are interpolated from nodal values on the nonuniform grid. The expected features of the flow field have been predicted by the analysis. The separated region upstream of the injector is apparent in the plot as indicated by a reversal of the velocity vectors that form a recirculation pattern. The separation shock that results from the thickened boundary layer upstream of the separation region can also be seen through a small upward deflection of the velocity vectors. The separation shock merges into a bow shock that turns the main-stream flow over the injector. The bow shock is quite strong and can be observed in figure 28 through a large upward deflection of the velocity vectors as the flow is processed by the shock. The downrunning bow shock from the upper injector (actually, in this case, a centerline reflection of the uprunning shock) is indicated by the velocity vectors as they turn downward from the centerline just beyond the point where the shock strikes the centerline. Inspection of the flow field in figure 28 near the injector shows that the hydrogen jet is turned in a nearly streamwise direction rather quickly by the air cross stream. Blockage of the cross flow by the jet results in another separated region behind the injector which can also be seen in the vector plot. The location of the reattachment shock following this separated region is not obvious in figure 28, but some indication of the shock is present in figure 29 where the velocity vectors turn from the wall and reorient in the mainstream direction. Figure 29 shows a magnified vector plot near the hydrogen injector. The region being considered is centered about the injector and has a range of

$$2.5 \text{ cm} \leq x \leq 7.5 \text{ cm}$$

$$0 \text{ cm} \leq y \leq 1.5 \text{ cm}$$

Velocity vectors are not plotted when their values become less than 5 percent of the maximum vector in the field. Examination of the recirculation region upstream of the injector reveals the presence of two counter-rotating eddies known to be present in the physical flow.

Figure 30 shows a contour map of the static pressure field in the duct. Each contour line represents a difference in pressure of 0.02 MPa. The presence of the separation shock, the bow shock, and its reflection can also be seen in this figure through pressure rises across the shocks. (Shocks are captured and smeared by the present analysis, and therefore, pressure rises across the shocks occur over some finite distance. This broadening of the shock structure results in a merging of the separation and bow shocks making visual resolution of the two shocks impossible.) The expansion of the hydrogen jet into the air cross stream can be seen along with the expansion of the hydrogen-air mixture over the injector. There is also some indication of a duct entry shock being captured, producing a small pressure rise across the shock.

Figure 31 displays a contour map of the static temperature field in the duct. Each contour line represents a change in temperature of 70 K. Note the temperature rise across the bow shock and the thermal boundary layer along the wall that thickens with movement towards the fuel injector. Significant cooling of the air by the expanding hydrogen jet can also be seen, particularly behind the injector. Some cooling is also experienced in the separated region upstream of the injector due to the limited presence of hydrogen.

Figure 32 provides a contour map for the hydrogen mass fraction distribution in the duct. Contour lines are plotted for hydrogen mass fractions of 0.75, 0.50, 0.25, and 0.01. With a static jet to static free-stream pressure ratio of 5, the penetration of the hydrogen jet into the air cross stream is significant. The one percent hydrogen contour line lies at 1/5 the duct height after proceeding only 2 cm downstream. The recirculating region upstream of the injector convects hydrogen forward of the jet, and the mixture goes from fuel lean to fuel rich as the slot is approached. The separated flow downstream of the slot captures hydrogen producing a very fuel rich region. These characteristics of the flow have been experimentally observed in scramjet tests; the upstream region provides a beneficial area for fuel ignition, and the downstream region (being fuel rich) imposes an ignition problem.

The first test case provides an examination of opposing slot fuel injectors using actual flow field conditions encountered in current scramjet engine concepts. The basic features of the flow described above compare well qualitatively with experimental observations near a fuel injector. Additionally, graphical representations of the final results, used to describe this case, provide a quick visualization of the overall flow field, as well as interesting details near the fuel injectors.

The second test case provides a comparison of the computer program with experimental data.<sup>41</sup> Gaseous hydrogen was injected from a choked 0.02 cm slot on a flat plate at zero angle of attack into a supersonic air cross stream. The slot was 5.08 cm long and located 25.6 cm from the leading edge of the plate. The flow field with this slot length was verified in reference 41 to be two dimensional within the region of interest. A turbulent boundary layer was produced by tripping the flow 2.54 cm from the plate leading edge. This experiment represented the only case known to the authors in which species measurements were made to determine hydrogen concentration away from the slot. The case was by no means ideal for verification of the present computer program, however. The jet to free-stream pressure ratio was significantly higher than ratios encountered in scramjet design (a static jet-to-freestream pressure ratio of 43 as compared to pressure ratios of 5 to 15 expected in a scramjet), and the slot width was quite narrow. These two conditions combined to produce extremely large gradients near the slot, complicating a numerical analysis of the problem. Large flow field gradients also complicate the accurate acquisition of data near a fuel injector. In addition, only conditions along the wall upstream of the slot were measured. No surveys were available away from the plate.

The conditions of the hydrogen at the slot exit were

$$M = 1.0$$

$$T = 243 \text{ K}$$

$$p = 7.28 \text{ MPa}$$

The conditions of the air just upstream of the leading edge of the flat plate were

$$M = 2.5$$

$$T = 130 \text{ K}$$

$$p = 0.169 \text{ MPa}$$

Two approaches were considered to define the computational domain for this case. In both approaches the domain was chosen to be 6 cm high and 10 cm long with the injector centered along the lower boundary. The overall plate length made it impracticable to begin the calculation at the leading edge. Therefore, for the first approach, initial conditions were specified by assuming the presence of a turbulent boundary layer on the plate beginning at the leading edge with the boundary layer thickness defined by<sup>42</sup>

$$\delta = 0.37 \times \left( \frac{\rho U_{\infty} x}{\mu_{\delta}} \right)^{-1/5}$$

The streamwise velocity in the boundary layer was defined using the one-seventh power law distribution<sup>42</sup>

$$\frac{u}{U_{\infty}} = \left( \frac{y}{\delta} \right)^{1/7}$$

For the second approach, the calculation was initialized assuming uniform free-stream conditions through the computational domain (as in the first case). There was little difference in the final steady-state results of the two approaches. The similarity was likely due to the fact that the subsonic portion of the boundary layer well upstream of the slot was quite thin when compared with the thickened boundary layer near the slot, and therefore, the conditions near the injector were relatively insensitive to conditions near the plate well upstream.

The turbulent Prandtl number in this case was assumed to be 0.7. The physical domain was spanned by a grid with 61 nodes in the streamwise direction and 30 nodes in the transverse direction. Free-stream conditions were assumed to exist along the upper boundary. The grid was again compressed transversely near the plate and in a streamwise direction about the injector with the following transformation constants (ref. 37):

$$\beta_x = 11.28$$

$$\beta_y = 1.002$$

$$X_{01} = 5.0 \text{ cm}$$

Comparisons of experimentally measured values of wall pressure and hydrogen mass fraction upstream of the slot with calculated values from the present analysis are made in figures 33 and 34, respectively. The calculated wall pressure (fig. 33) has the same basic shape as the experimental data but the calculated pressure rise begins at about 120 slot widths upstream of the injector as compared to the experimental pressure rise that begins at about 175 slot widths upstream of the injector. Calculated and experimental values of wall pressure are similar through the last 100 slot widths upstream of the injector, and there is reasonably good agreement for wall plateau pressures. Figure 34 presents a comparison of computed and measured values of hydrogen mass fraction along the plate upstream of the injector. The calculation underestimates the amount of hydrogen present initially. Closer to the slot (100 slot widths or less) the calculation of the hydrogen mass fraction agrees fairly well when compared with the experiment.

Differences between the calculation and experiment are attributable to two basic problems, the turbulence model and the numerics. Underprediction of the point of separation initiating a recirculation region upstream of a disturbance, with the resulting underprediction of initiation of the wall pressure rise, is typical of earlier observations by other researchers. In those cases, as well as in the present analysis, the point of separation is a strong function of the turbulence field in the flow. Other turbulence models have been applied to the present problem, and resulted in a significant variation in the separation point and the size of the recirculation region. The present turbulence model,<sup>3</sup> however, gives the most consistent overall results when compared with the experimental data. In such a complex turbulent mixing flow, a simple algebraic eddy viscosity turbulence model is obviously inadequate. Non-equilibrium effects are quite important in the separated region near the injector, and the turbulence field in this region is certain to be highly anisotropic. Neither effect has been accounted for in the models that have been used.

Oscillations present in the results of figures 33 and 34 between 30 and 80 slot widths upstream of the injector are likely to be numerical in origin. A very strong bow shock resulting from the highly underexpanded hydrogen injector was captured in this region. Pressure oscillations leading and trailing a significant static pressure increase when passing through a shock are typical occurrences with the present technique. Oscillations are also present very near the slot (0.1 cm), but the oscillations were small compared to the overall pressure rise (0.17 to 7.3 MPa). Severe gradients are experienced near the injector that require an extremely fine grid to adequately resolve. Even though the present grid is highly compressed near the bow shock and injector, truncation error is likely to be significant in this region.

To more accurately predict the complex flow regime near a fuel injector, the following changes to the program and its application are indicated. First, the turbulence model must be improved to account for the anisotropic nature of the turbulence field. Solution of the Reynolds stress equations seems premature at this point. However, application of the algebraic Reynolds stress model of Rodi<sup>43</sup> is promising since it would partially account for the anisotropy. Second, a finer discretization obtained by employing a larger number of nodes near fuel injectors would better resolve high gradients in this region. Computer core limitations restrict the number of nodes that can be considered, however. Finally, shock capturing, with attendant numerical smoothing, smears the separation and bow shock over a relatively large distance introducing error

downstream of the shocks. Fitting those shocks would produce a much better spatial resolution of the flow variables downstream of the discontinuities.

The two-dimensional elliptic program represents a first attempt to model a transverse injector with a purely numerical approach. Experience gained during the development of the program should be helpful when the work is extended to three dimensions. That extension is currently limited by computer resources and required processing time. The two-dimensional program does allow study of the basic flow field phenomena around a transverse fuel injector and this new capability should provide guidance in the ongoing scramjet design effort.

The transverse jet interaction model and the slot injector program provide two options for initializing a parabolic flow calculation downstream of the elliptic region surrounding fuel injectors. The TJI scheme models the fuel injector and is limited to inviscid flow. The program is computationally efficient, however, allowing parametric analyses to be carried out at modest cost. The slot injector program directly solves the governing equations describing viscous flow about transverse fuel injectors. Additionally, the program can consider other problems such as rearward facing steps upstream of the fuel injectors. Relaxing the governing equations to steady state is time consuming, however, making the procedure rather expensive for parametric studies. Therefore, extension of both the TJI model and the slot injector program to three dimensions is planned. Each program will be used to calculate initial conditions for the three-dimensional parabolic or partially elliptic program downstream of the fuel injectors. The coupling of these programs will provide an overall combustor analysis tool to aid in the design of the Langley scramjet engine.

## 6.0 CONCLUSIONS

A system of computer programs has been developed at the NASA Langley Research Center to model the combustor of a scramjet engine. The engine flow field can be divided into several physical flow domains, each of which can be described by appropriate forms of the Navier-Stokes and companion species equations. A program based on those governing equations has been developed for each region, and the programs are being combined to form an overall computational capability for scramjet combustor design. Some programs in the system have progressed to the design stage, and they are now being applied to actual combustor configurations. The remaining programs continue to be developed, but they already provide basic research tools for limited engine applications.

The parabolic flow computer programs are based on proven solution algorithms, and have been improved to include an appropriate turbulence model and multiequation finite rate chemistry models considered adequate for modelling supersonic combustor flow fields. Recent comparisons of the programs with experimental data have been quite encouraging. The partially elliptic computer program has proved effective for describing subsonic flow without separation in the combustor, but development is still continuing to provide a satisfactory convergence criteria for the computed pressure field. Results comparing parabolic and partially elliptic calculations in subsonic flow indicate differences sufficient enough to warrant continued work in this area. Elliptic programs, used to model the flow field near transverse fuel injectors are the most recent addition to the analysis system. Current two-dimensional analyses compare favorably with experimental data, but further work is needed, particularly to model the complex turbulence fields and chemical reactions. Extension of the elliptic flow program to three dimensions is limited by storage problems to all but the largest current or future vector computers until significant advancements occur in integration algorithms.

Further work is planned in turbulence and reaction modelling that will impact all of the combustor analysis programs. The highly anisotropic turbulence fields that must exist in some regions of the combustor must be considered in greater detail. Current interest exists for solution of the Reynolds stress equations to model the turbulence. Application of the algebraic Reynolds stress model of Rodi may offer a near term solution to that problem. Chemistry models will be extended to include the details of reaction and ignition in hydrogen-air reactions. Finally, the importance of coupling between chemical reaction and turbulence must also be considered in greater detail. The impact of that coupling on combustor modelling is not well understood at present. The current capabilities to model the scramjet combustor flow field do, however, represent an important step forward in engine design, and should provide guidance in the ongoing scramjet development effort at the NASA Langley Research Center.

## REFERENCES

1. Jones, R. A., and Huber, P. W., "Toward Scramjet Aircraft," *Astronautics and Aeronautics*, vol. 16, Feb. 1978, pp 38-48.
2. Hearth, D. P., and Preyss, A. E., "Hypersonic Technology - Approach to an Expanded Program," *Astronautics and Aeronautics*, vol. 14, Dec. 1976, pp 20-37.
3. Baldwin, B. S., and Lomax, H., "Thin Layer Approximation and Algebraic Model for Separated Turbulent Flows," *AIAA Paper No. 78-257*, Jan. 1978.
4. Launder, B. E., and Spalding, D. B., "The Numerical Computation of Turbulent Flows," *Computer Methods in Applied Mechanics and Engineering*, vol. 3, 1974, pp 269-289.
5. Bahn, G. S., "Calculations on the Autoignition of Mixtures of Hydrogen and Air," *NASA CR-112067*, Apr. 1972.
6. Evans, J. C., and Schexnayder, C. J., "Critical Influence of Finite Rate Chemistry and Unmixedness on Ignition and Combustion of Supersonic  $H_2$ -Air Streams," *AIAA Paper No. 79-0355*, Jan. 1979.
7. Spalding, D. B., Launder, B. E., Morse, A. P., and Maples, G., "Combustion of Hydrogen-Air Jets in Local Chemical Equilibrium (A Guide to the CHARNAL Computer Program)," *NASA CR-2407*, 1974.
8. Elghobashi, S., and Spalding, D. B., "Equilibrium Chemical Reaction of Supersonic Hydrogen-Air Jets (The ALMA Computer Program)," *NASA CR-2725*, 1977.

9. Patankar, S. V., and Spalding, D. B., "Heat and Mass Transfer in Boundary Layers," Int. Textbook Co., Ltd. (London), Second ed. Int., 1970.
10. Dash, S., Weilerstein, G., and Vaglio-Laurin, R., "Compressibility Effects in Free Turbulent Shear Flows," Air Force Office of Scientific Research, TR-75-1436, Aug. 1975.
11. Speigler, E., Wolfshtein, M., and Manheimer-Timnat, Y., "A Model of Unmixedness for Turbulent Reacting Flows," Acta Astronautica, vol. 3, 1976, pp 265-280.
12. Kent, J. H., and Bilger, R. W., "Measurements in Turbulent Jet Diffusion Flames," TN F-41, Dept. Mech. Eng., Univ. Sydney (Australia), Oct. 1972.
13. Salas, Manuel D., "Shock Fitting Method for Complicated Two-Dimensional Supersonic Flows," AIAA J., vol. 14, no. 5, May 1976, pp 583-588.
14. Markatos, N. C., Spalding, D. B., and Tatchell, D. G., "Combustion of Hydrogen Injected into a Supersonic Airstream (The SHIP Computer Program)," NASA CR-2802, 1977.
15. Pan, Y. S., Drummond, J. P., and McClinton, C. R., "Comparison of Two Computer Programs by Predicting Turbulent Mixing of Helium in a Ducted Supersonic Airstream," NASA TP-1166, 1978.
16. Pan, Y. S., "Evaluation of the Three-Dimensional Parabolic Flow Computer Program SHIP," NASA TM-74094, 1978.
17. Patankar, S. V., and Spalding, D. B., "A Calculation Procedure for Heat, Mass, and Momentum Transfer in Three-Dimensional Parabolic Flows," Int. J. Heat and Mass Transfer, vol. 15, 1972, pp 1787-1806.
18. McClinton, C. R., "Evaluation of Scramjet Combustor Performance Using Cold Nonreactive Mixing Tests," AIAA Paper No. 76-47, 1976.
19. Burrows, M. C., and Kurkov, A. P., "Supersonic Combustion of Hydrogen in a Vitiated Air Stream Using Stepped-Wall Injection," AIAA Paper No. 71-721, 1971.
20. Burrows, M. C., and Kurkov, A. P., "An Analytical and Experimental Study of Supersonic Combustion of Hydrogen in a Vitiated Airstream," AIAA Journal, vol. 11, 1973, pp 1217-1218.
21. Pan, Y. S., "The Development of a Three-Dimensional Partially Elliptic Flow Computer Program for Combustor Research," NASA CR-3057, 1978.
22. Pratap, V. S., and Spalding, D. B., "Numerical Computations of the Flow in Curved Ducts," The Aeronautical Quarterly, vol. 26, 1975, pp 219-228.
23. Hjertager, B. H., and Magnussen, B. F., "Computation of Some Three-Dimensional Laminar Incompressible Internal Flows," Proc. of 25th Heat Transfer and Fluid Mechanics Institute Meeting, Stanford University Press, 1976, pp 436-451.
24. Rogers, R. C., "A Model of Transverse Fuel Injection Applied to the Computation of Supersonic Combustor Flow," AIAA Paper No. 79-359, 1979.
25. Orth, R. C., Schetz, J. A., and Billig, F. S., "The Interaction and Penetration of Gaseous Jets in Supersonic Flow," NASA CR-1386, 1969.
26. Werle, M. J., Driftmyer, R. T., and Shaffer, D. G., "Two-Dimensional Jet Interaction with a Mach 4 Airstream," NOLTR-70-50, 1970.
27. Spaid, F. W., and Zukowski, E. E., "A Study of the Interaction of Gaseous Jets from Transverse Slots with Supersonic External Flow," AIAA J., vol. 6, no. 2, 1968, pp 205-212.
28. Zakkay, V., Calarese, W., and Sakell, L., "An Experimental Investigation Between Transverse Sonic Jets and a Hypersonic Stream," AIAA J., vol. 9, no. 4, 1971, pp 674-682.
29. Spaid, F. W., Zukowski, E. E., and Rosen, R., "A Study of Secondary Injection of Gases into Supersonic Flow," Jet Propulsion Lab. Tech. Rpt. 32-834, 1966.
30. Werle, M. J., "A Critical Review of Analytical Methods for Estimating Control Forces Produced by Secondary Injection," NOLTR 68-5, 1968.
31. Schetz, J. A., Hawkins, P. F., and Lehman, H., "Structure of Highly Underexpanded Transverse Jets in a Supersonic Stream," AIAA J., vol. 5, no. 5, pp 882-884.
32. Cohen, L. S., Coulter, L. J., and Egan, W. J., Jr., "Penetration and Mixing of Multiple Gas Jets Subjected to a Cross Flow," AIAA J., vol. 9, no. 4, 1971, pp 718-724.
33. Rogers, R. C., "Mixing of Hydrogen Injected from Multiple Injectors Normal to a Supersonic Airstream," NASA TN D-6476, 1971.
34. Billig, F. S., "Shock-Wave Shapes Around Spherical and Cylindrical Nosed Bodies," J. of Spacecraft, vol. 4, no. 6, 1967, pp 822-823.
35. Rogers, R. C., "Influence of Fuel Temperature on Supersonic Mixing and Combustion of Hydrogen," AIAA Paper No. 77-17, 1977.

36. Drummond, J. P., "Numerical Investigation of the Perpendicular Injector Flow Field in a Hydrogen Fueled Scramjet," AIAA Paper No. 79-1482, 1979.
37. Holst, T. L., "Numerical Solution of Axisymmetric Boattail Fields with Plume Simulators," AIAA Paper No. 77-224, Jan. 1977.
38. Rudy, D. H., Private Communication.
39. McCormack, R. W., and Baldwin, E. S., "A Numerical Method for Solving the Navier-Stokes Equations with Application to Shock-Boundary Layer Interactions," AIAA Paper No. 75-1, Jan. 1975.
40. Spradley, L. W., and Pearson, M. C., "Implementation of the GIM Computer Code on the CDC-STAR Computer for Analysis of Complicated Flow Fields," NASA CR-3157, 1979.
41. Thayer, W. J., "The Two-Dimensional Separated Flow Region Upstream of Inert and Chemically Reactive Transverse Jets," Ph.D. Thesis, Department of Mechanical Engineering, University of Washington, 1971.
42. Schlichting, H., Boundary Layer Theory, McGraw Hill, New York, 1968.
43. Rodi, W., "The Prediction of Free Turbulent Boundary Layers by Use of a Two Equation Model of Turbulence," Ph.D. Thesis, University of London, 1972.

## ACKNOWLEDGEMENT

The authors wish to acknowledge the contribution of Dr. Y. S. Pan to the development of the current versions of the three-dimensional parabolic and partially elliptic flow programs. His work was performed while he was a NRC-NASA Senior Research Associate at the NASA Langley Research Center and is documented in references 16 and 21.

TABLE I. EXCHANGE COEFFICIENTS AND SOURCE TERMS FOR THE 2-D PARABOLIC PROGRAM

$\phi$	$\Gamma_\phi$	$S_\phi$
1	0	0
u	$\mu_{eff}$	$- dp/dx$
$H^0$	$\mu_{eff}/Pr_{eff,H^0}$	$\frac{1}{y^i} \frac{\partial}{\partial y} \left\{ y^i \left[ (\Gamma_u - \Gamma_{H^0}) \frac{\partial}{\partial y} \left( \frac{u^2}{2} \right) + (\Gamma_k - \Gamma_{H^0}) \frac{\partial k}{\partial y} \right] \right\}$
f	$\mu_{eff}/Pr_{eff,f}$	$\dot{w}$
k	$\mu_{eff}/Pr_{eff,k}$	$\mu_t \left( \frac{\partial u}{\partial y} \right)^2 - \rho \epsilon$
$\epsilon$	$\mu_{eff}/Pr_{eff,\epsilon}$	$\left[ C_{\epsilon 1} \mu_t \left( \frac{\partial u}{\partial y} \right)^2 - C_{\epsilon 2} \rho \epsilon \right] (\epsilon/k)$
g	$\mu_{eff}/Pr_{eff,g}$	$\left[ C_{g1} \mu_t \left( \frac{\partial u}{\partial y} \right)^2 - C_{g2} \rho \epsilon \right] (1/k)$

TABLE II. SPECIES AND REACTIONS<sup>a</sup>

Species						
1	H	7	N <sub>2</sub>			
2	O	8	N			
3	H <sub>2</sub> O	9	NO			
4	OH	10	NO <sub>2</sub>			
5	O <sub>2</sub>	11	HO <sub>2</sub>			
6	H <sub>2</sub>	12	HNO <sub>2</sub>			
Reactions						
1	HNO <sub>2</sub> + M → NO + OH + M			14	OH + OH → H + HO <sub>2</sub>	
2	NO <sub>2</sub> + M → NO + O + M			15	H <sub>2</sub> O + O → H + HO <sub>2</sub>	
*3	H <sub>2</sub> + M → H + H + M			16	OH + O <sub>2</sub> → O + HO <sub>2</sub>	
*4	O <sub>2</sub> + M → O + O + M			17	H <sub>2</sub> O + O <sub>2</sub> → OH + HO <sub>2</sub>	
*5	H <sub>2</sub> O + M → OH + H + M			18	H <sub>2</sub> O + OH → H <sub>2</sub> + HO <sub>2</sub>	
*6	OH + M → O + H + M			19	O + N <sub>2</sub> → N + NO	
7	HO <sub>2</sub> + M → H + O <sub>2</sub> + M			20	H + NO → N + OH	
*8	H <sub>2</sub> O + O → OH + OH			21	O + NO → N + O <sub>2</sub>	
*9	H <sub>2</sub> O + H → OH + H <sub>2</sub>			22	NO + OH → H + NO <sub>2</sub>	
*10	O <sub>2</sub> + H → OH + O			23	NO + O <sub>2</sub> → O + NO <sub>2</sub>	
*11	H <sub>2</sub> + O → OH + H			24	NO <sub>2</sub> + H <sub>2</sub> → H + HNO <sub>2</sub>	
12	H <sub>2</sub> + O <sub>2</sub> → OH + OH			25	NO <sub>2</sub> + OH → NO + HO <sub>2</sub>	
13	H <sub>2</sub> + O <sub>2</sub> → H + HO <sub>2</sub>					
Reaction Rates						
Forward Rate Constant <sup>b</sup>			Reverse Rate Constant <sup>b</sup>			
A	B	C	A	B	C	
1	5.0 × 10 <sup>17</sup>	-1.0	25000	8.0 × 10 <sup>15</sup>	0	-1000
2	1.1 × 10 <sup>16</sup>	0	32712	1.1 × 10 <sup>15</sup>	0	-941
3	5.5 × 10 <sup>18</sup>	-1.0	51987	1.8 × 10 <sup>18</sup>	-1.0	0
4	7.2 × 10 <sup>18</sup>	-1.0	59340	4.0 × 10 <sup>17</sup>	-1.0	0
5	5.2 × 10 <sup>21</sup>	-1.5	59386	4.4 × 10 <sup>20</sup>	-1.5	0
6	8.5 × 10 <sup>18</sup>	-1.0	50830	7.1 × 10 <sup>18</sup>	-1.0	0
7	1.7 × 10 <sup>16</sup>	0	23100	1.1 × 10 <sup>16</sup>	0	-440
8	5.8 × 10 <sup>13</sup>	0	9059	5.3 × 10 <sup>12</sup>	0	503
9	8.4 × 10 <sup>13</sup>	0	10115	2.0 × 10 <sup>13</sup>	0	2600
10	2.2 × 10 <sup>14</sup>	0	8455	1.5 × 10 <sup>13</sup>	0	0
11	7.5 × 10 <sup>13</sup>	0	5586	3.0 × 10 <sup>13</sup>	0	4429
12	1.7 × 10 <sup>13</sup>	0	24232	5.7 × 10 <sup>11</sup>	0	14922
13	1.9 × 10 <sup>13</sup>	0	24100	1.3 × 10 <sup>13</sup>	0	0
14	1.7 × 10 <sup>11</sup>	0.5	21137	6.0 × 10 <sup>13</sup>	0	0
15	5.8 × 10 <sup>11</sup>	0.5	28686	3.0 × 10 <sup>13</sup>	0	0
16	3.7 × 10 <sup>11</sup>	0.64	27840	1.0 × 10 <sup>13</sup>	0	0
17	2.0 × 10 <sup>11</sup>	0.5	36296	1.2 × 10 <sup>13</sup>	0	0
18	1.2 × 10 <sup>12</sup>	0.21	39815	1.7 × 10 <sup>13</sup>	0	12582
19	5.0 × 10 <sup>13</sup>	0	37940	1.1 × 10 <sup>13</sup>	0	0
20	1.7 × 10 <sup>14</sup>	0	24500	4.5 × 10 <sup>13</sup>	0	0
21	2.4 × 10 <sup>11</sup>	0.5	19200	1.0 × 10 <sup>12</sup>	0.5	3120
22	2.0 × 10 <sup>11</sup>	0.5	15500	3.5 × 10 <sup>14</sup>	0	740
23	1.0 × 10 <sup>12</sup>	0	22800	1.0 × 10 <sup>13</sup>	0	302
24	2.4 × 10 <sup>13</sup>	0	14500	5.0 × 10 <sup>11</sup>	0.5	1500
25	1.0 × 10 <sup>11</sup>	0.5	6000	3.0 × 10 <sup>12</sup>	0.5	1200

<sup>a</sup>The first 7 species and the starred reactions constitute the 8-reaction system.<sup>b</sup>Form of rate constant is  $k = AT^B \exp(-C/T)$  with  $k$  in cm<sup>3</sup>/mole-sec or cm<sup>6</sup>/mole<sup>2</sup>-sec.



TABLE III. EXCHANGE COEFFICIENTS AND SOURCE TERMS FOR VARIABLE  $\phi$ 

$\phi$	$\Gamma_\phi$	$S_\phi$
1	0	0
u	$\mu_{\text{eff}}$	$-\frac{\partial p}{\partial x} + \frac{\partial}{\partial x} \left[ \frac{\mu_{\text{eff}}}{3} \left( \frac{\partial u}{\partial x} - 2 \frac{\partial v}{\partial y} \right) \right] + \frac{\partial}{\partial y} \left[ \mu_{\text{eff}} \frac{\partial v}{\partial x} \right]$
v	$\mu_{\text{eff}}$	$-\frac{\partial p}{\partial y} + \frac{\partial}{\partial y} \left[ \frac{\mu_{\text{eff}}}{3} \left( \frac{\partial v}{\partial y} - 2 \frac{\partial u}{\partial x} \right) \right] + \frac{\partial}{\partial x} \left[ \mu_{\text{eff}} \frac{\partial u}{\partial y} \right]$
w	$\mu_{\text{eff}}$	$-\frac{\partial p}{\partial z}$
$H^0$	$\frac{\mu_{\text{eff}}}{Pr_{\text{eff},H^0}}$	$\frac{\partial}{\partial x} \left[ \frac{\mu_{\text{eff}}}{Pr_{\text{eff},H^0}} (Pr_{\text{eff},H^0} - 1) \frac{\partial}{\partial x} \left( \frac{u^2 + v^2 + w^2}{2} \right) \right] +$ $\frac{\partial}{\partial y} \left[ \frac{\mu_{\text{eff}}}{Pr_{\text{eff},H^0}} (Pr_{\text{eff},H^0} - 1) \frac{\partial}{\partial y} \left( \frac{u^2 + v^2 + w^2}{2} \right) \right] +$ $\mu_{\text{eff}} \left[ \left( \frac{\partial u}{\partial x} \right)^2 + \left( \frac{\partial v}{\partial y} \right)^2 + 2 \frac{\partial u}{\partial y} \frac{\partial v}{\partial x} \right]$
f	$\frac{\mu_{\text{eff}}}{Pr_{\text{eff},f}}$	0
k	$\frac{\mu_{\text{eff}}}{Pr_{\text{eff},k}}$	$\mu_t \left\{ 2 \left[ \left( \frac{\partial u}{\partial x} \right)^2 + \left( \frac{\partial v}{\partial y} \right)^2 \right] + \left( \frac{\partial w}{\partial x} \right)^2 + \left( \frac{\partial w}{\partial y} \right)^2 + \right.$ $\left. \left( \frac{\partial u}{\partial y} + \frac{\partial v}{\partial x} \right)^2 \right\} - \rho \epsilon$
$\epsilon$	$\frac{\mu_{\text{eff}}}{Pr_{\text{eff},\epsilon}}$	$C_1 \frac{\epsilon}{k} \mu_t \left\{ 2 \left[ \left( \frac{\partial u}{\partial x} \right)^2 + \left( \frac{\partial v}{\partial y} \right)^2 \right] + \left( \frac{\partial w}{\partial x} \right)^2 + \right.$ $\left. \left( \frac{\partial w}{\partial y} \right)^2 + \left( \frac{\partial u}{\partial y} + \frac{\partial v}{\partial x} \right)^2 \right\} - C_2 \frac{\rho \epsilon^2}{k}$

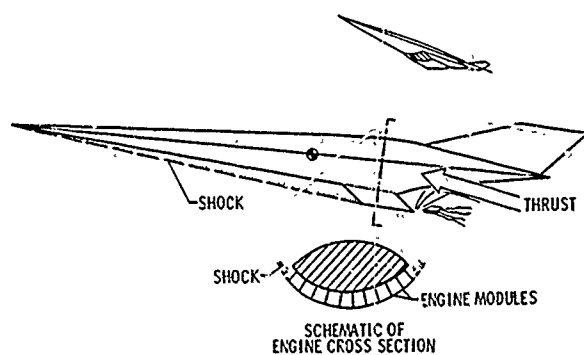


Fig. 1. Hypersonic vehicle with airframe-integrated scramjet.

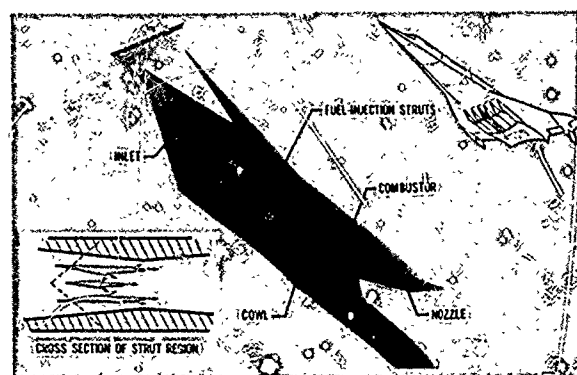
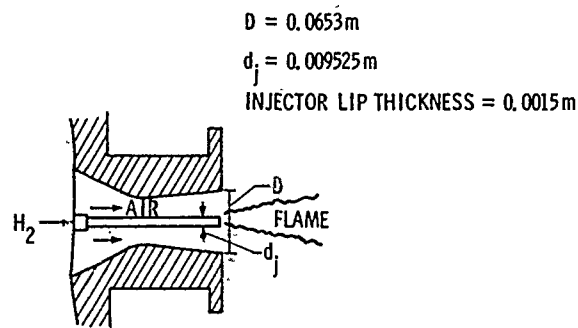


Fig. 2. Scramjet engine module.



	HYDROGEN JET	FREE STREAM
MACH NUMBER, M . . . .	2.00	1.90
TEMPERATURE, T, K . . . .	251	1495
VELOCITY, u, m/s . . . .	2432	1510
PRESSURE, p, MPa . . . .	0.1	0.1
MASS FRACTION:		
H <sub>2</sub> . . . . .	1.000	0
O <sub>2</sub> . . . . .	0	0.241
N <sub>2</sub> . . . . .	0	0.478
H <sub>2</sub> O . . . . .	0	0.281

Fig. 3. Beach experiment.

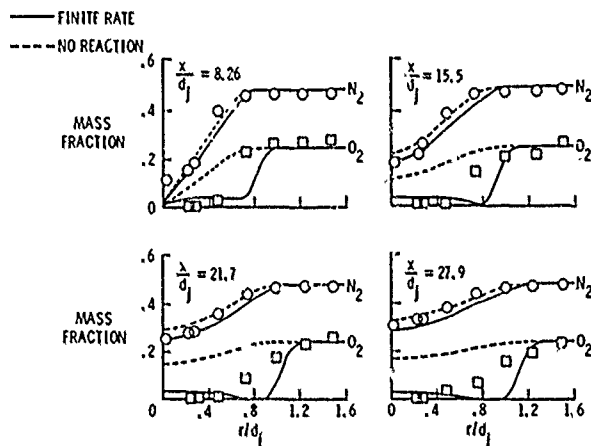
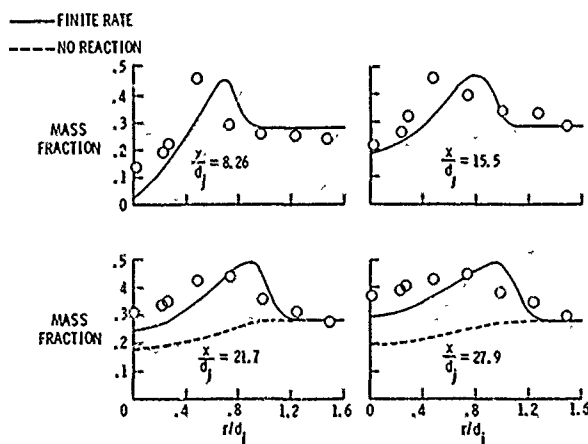
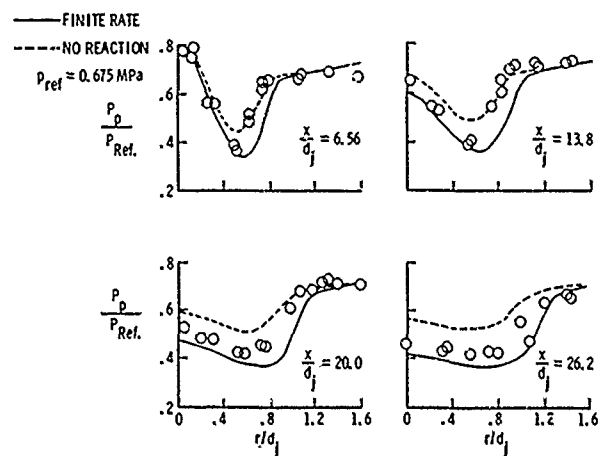
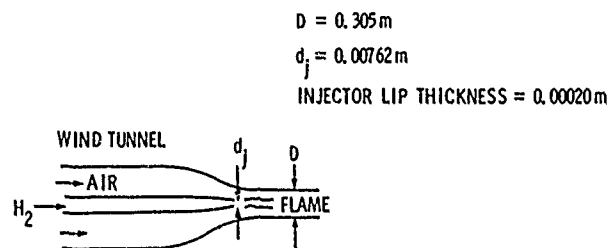
Fig. 4. Profiles of N<sub>2</sub> and O<sub>2</sub> mass fractions for Beach experiment.Fig. 5. Profiles of H<sub>2</sub>O mass fraction for Beach experiment.

Fig. 6. Pitot pressure profiles for Beach experiment.



	HYDROGEN JET	FREE STREAM
MACH NUMBER, M . . . .	0.135	0.043
TEMPERATURE, T, K . . . .	300	300
VELOCITY, u, m/s . . . .	178	15.1
PRESSURE, p, MPa . . . .	0.1	0.1
MASS FRACTION:		
H <sub>2</sub> . . . . .	1.0	0
O <sub>2</sub> . . . . .	0	0.232
N <sub>2</sub> . . . . .	0	0.768
H <sub>2</sub> O . . . . .	0	0

Fig. 7. Kent and Bilger experiment.

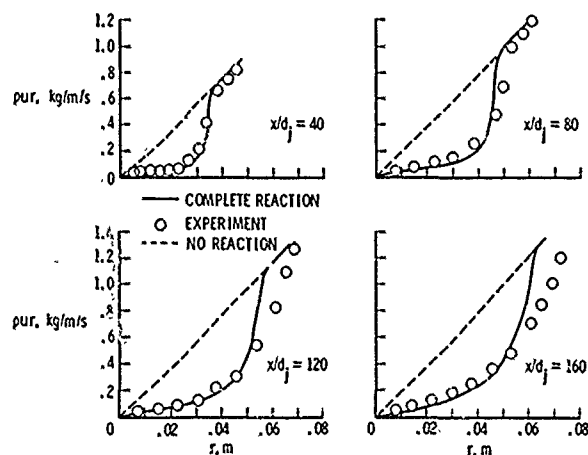


Fig. 8. Distribution of mass flow for Kent and Bilger experiment.

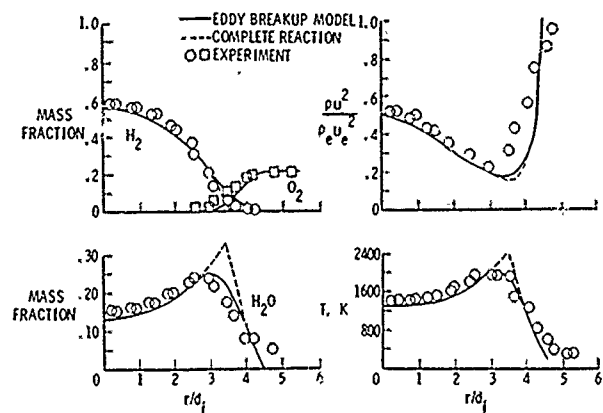


Fig. 9. Profiles of composition, dynamic pressure, and temperature for Kent and Bilger experiment ( $x/d_j = 40$ ).

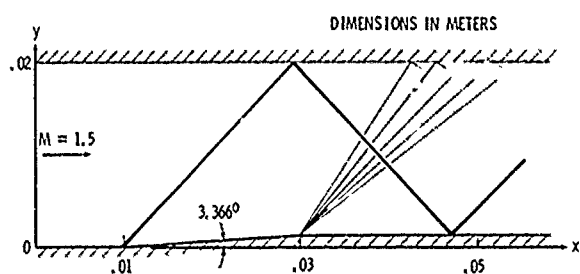


Fig. 10. Geometry and wave pattern of two-dimensional supersonic channel flow.

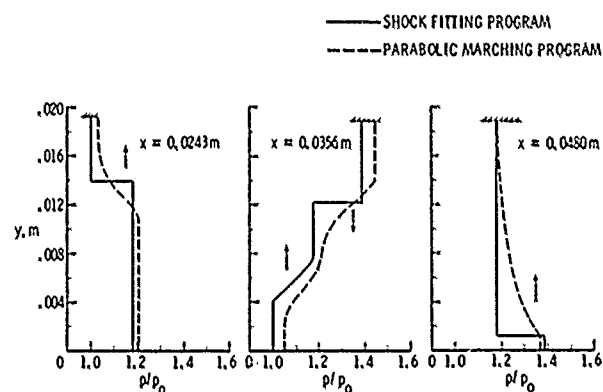


Fig. 11a. Pressure profile distributions for transverse shock waves in a duct.

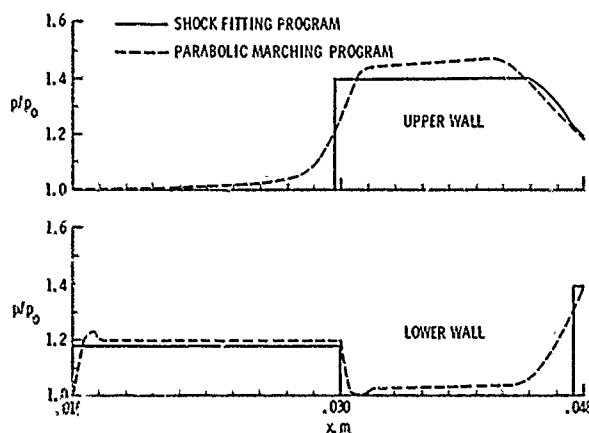


Fig. 11b. Wall pressure distributions for transverse shock waves in a duct.

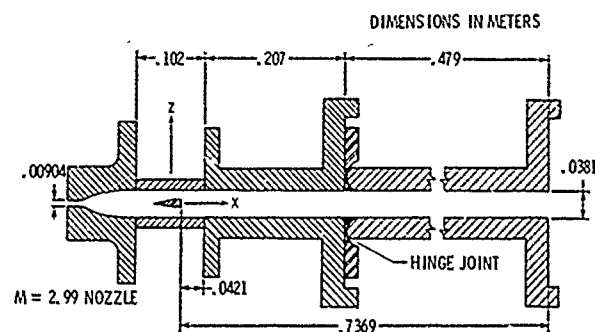


Fig. 12. Fuel injector strut and duct configuration.

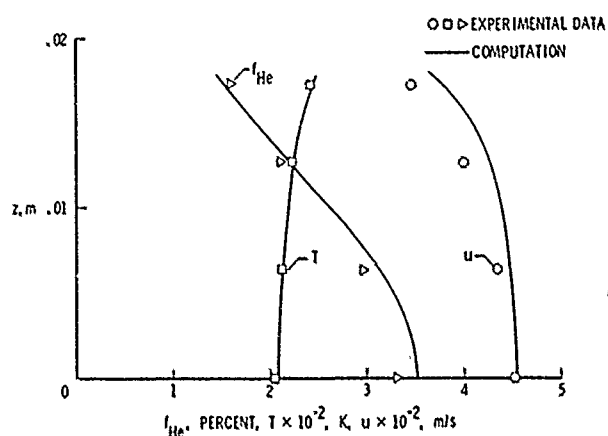


Fig. 13a. Comparison of computation and experimental results at downstream station ( $x = 0.7369$  m and  $y = 0.$ ).

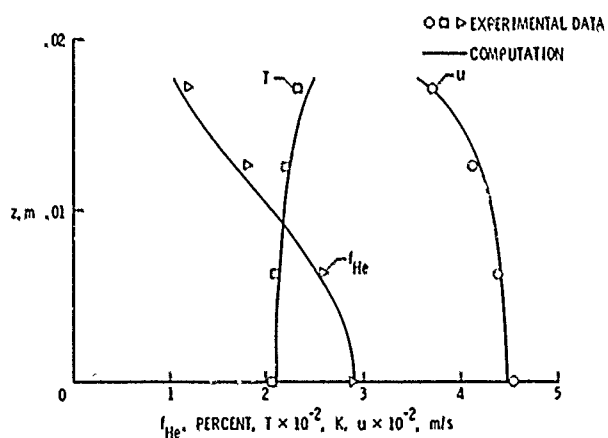


Fig. 13b.  $y = 0.0063$  m.

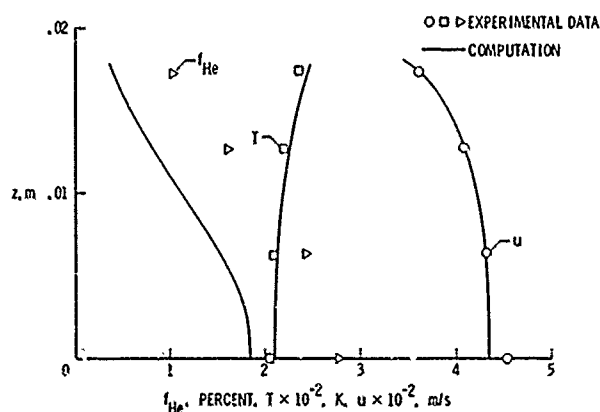


Fig. 13c.  $y = 0.0127$  m.

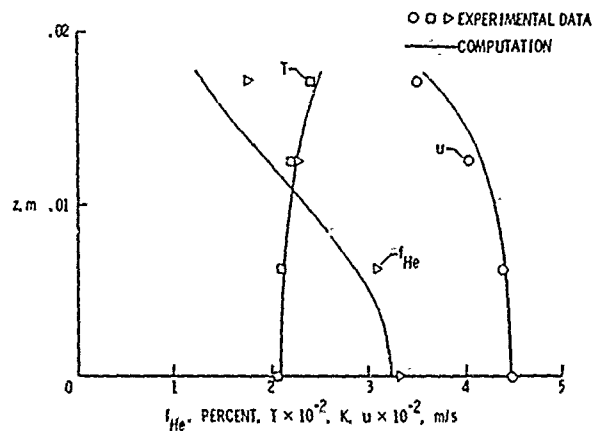


Fig. 13d.  $y = -0.0063$  m.

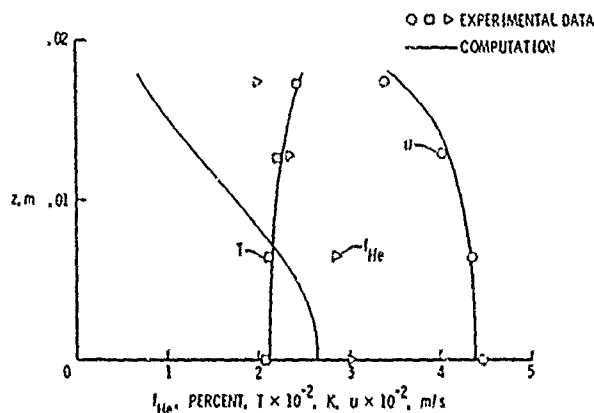


Fig. 13e.  $y = -0.0127$  m.

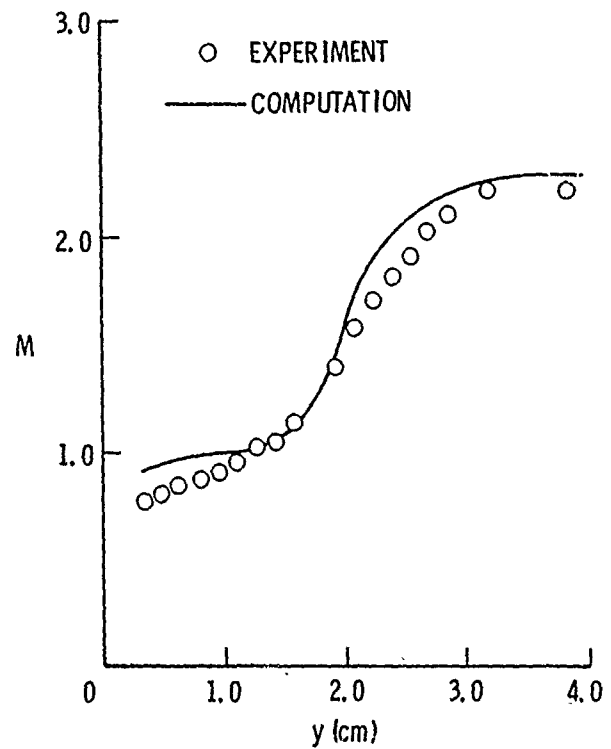


Fig. 16. Comparison of Mach number profiles for supersonic combustion of hydrogen and vitiated air ( $z = 35.6$  cm).

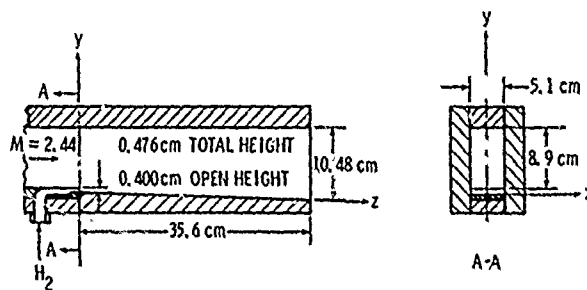


Fig. 14. Sketch of test section of combustor duct.

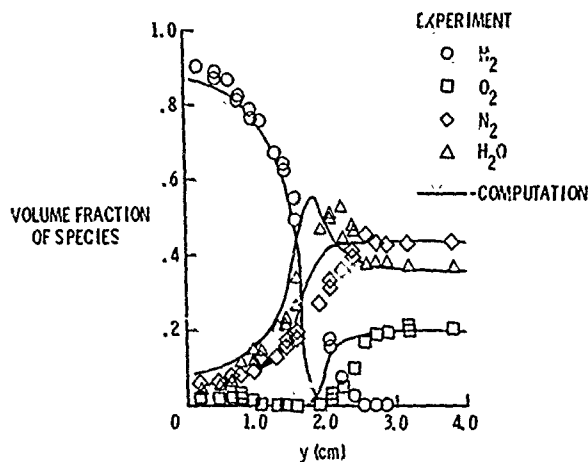


Fig. 15. Comparison of composition profiles for ducted supersonic combustion of hydrogen and vitiated air ( $z = 35.6$  cm).

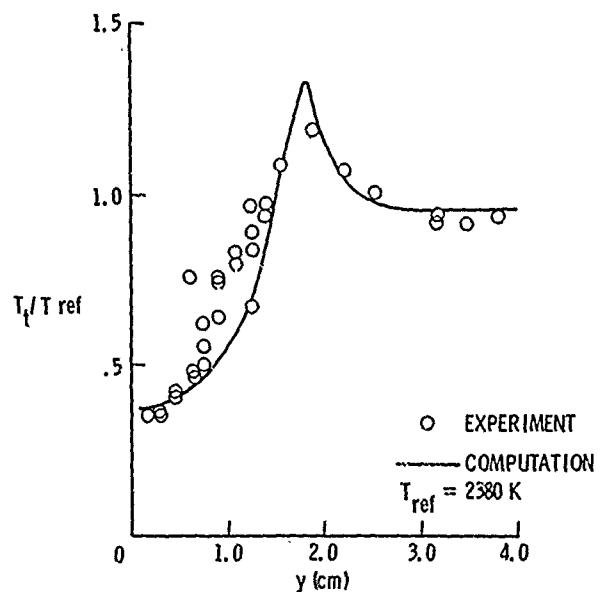


Fig. 17. Comparison of stagnation temperature profiles for ducted supersonic combustion of hydrogen and vitiated air ( $z = 35.6$  cm).

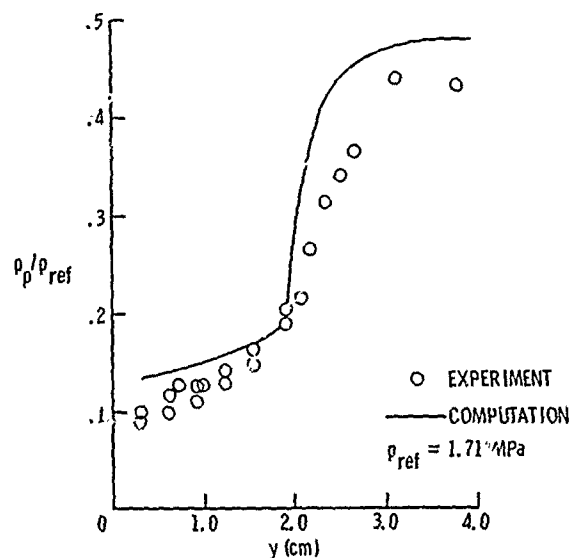


Fig. 18. Comparison of pitot pressure profiles for ducted supersonic combustion of hydrogen and vitiated air ( $z = 35.6 \text{ cm}$ ).

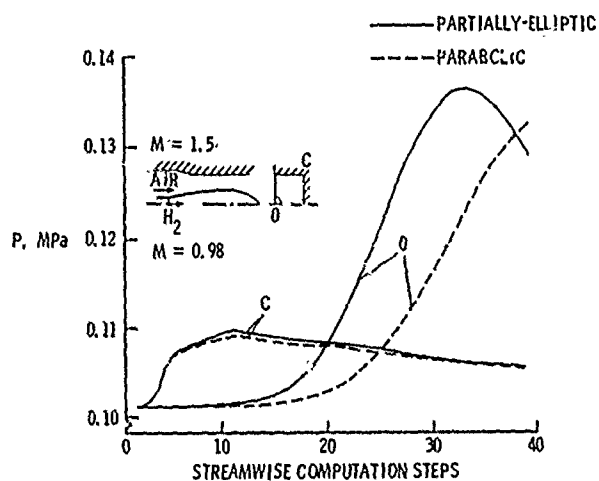


Fig. 19. Comparison of parabolic and partially elliptic flow programs for hydrogen-air reaction in a duct.

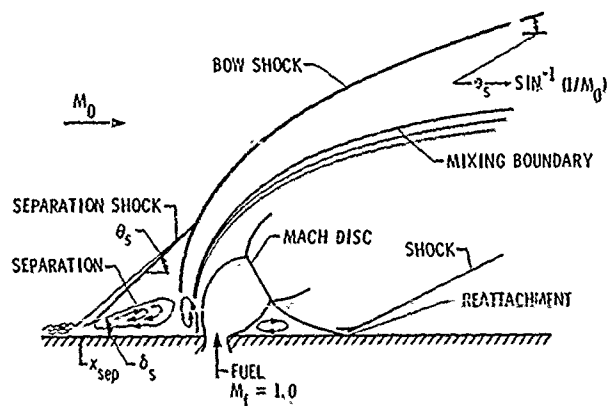


Fig. 20. Aerodynamic features of the transverse jet interaction.

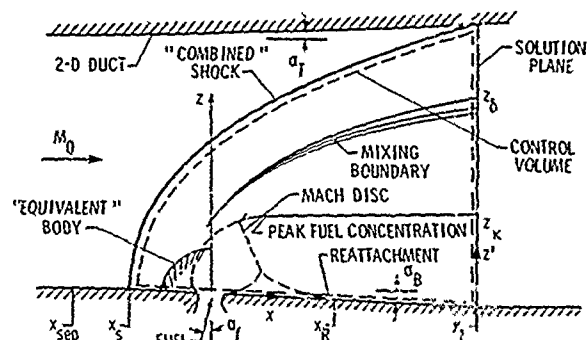


Fig. 21. Flow model of the transverse jet interaction.

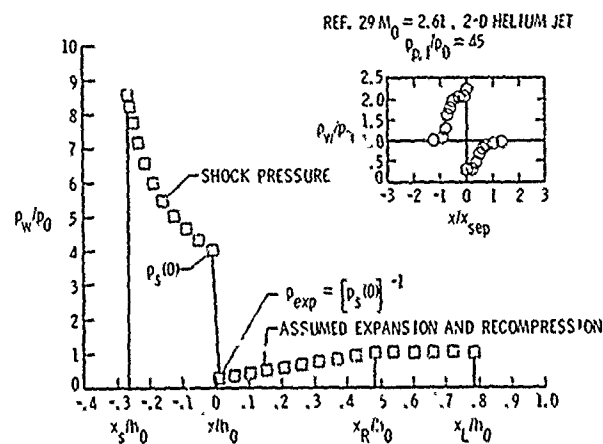


Fig. 22. Wall pressure distribution downstream of jet.

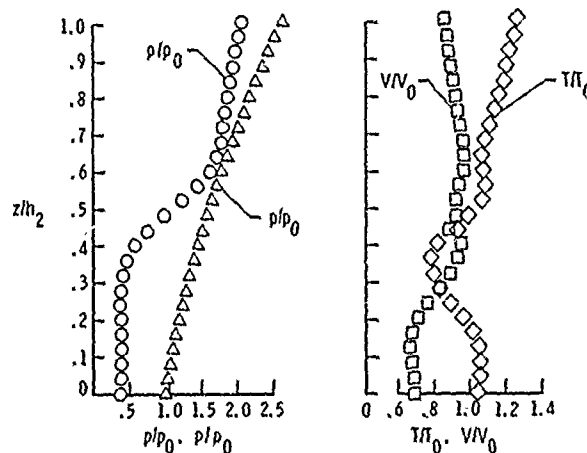


Fig. 23. Typical profiles of density, pressure, temperature, and velocity from TJI model.

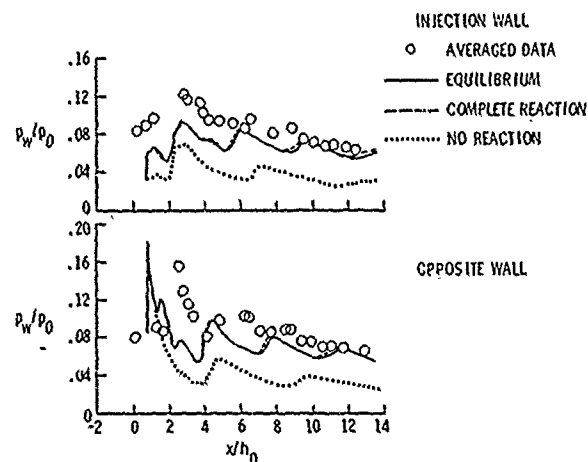


Fig. 24. Comparison of pressure distributions along injection and opposite walls.

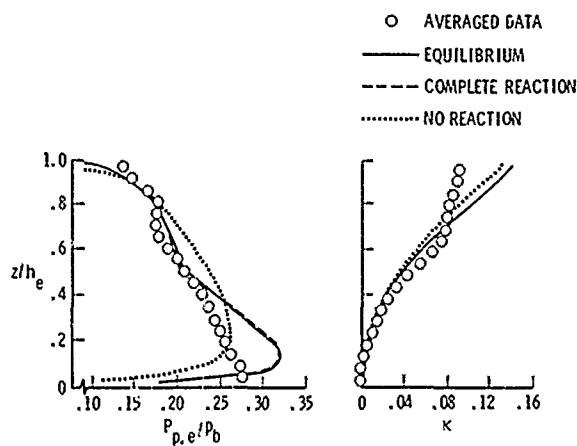


Fig. 25. Comparison of pitot pressure and fuel mass fraction profiles at the duct exit.

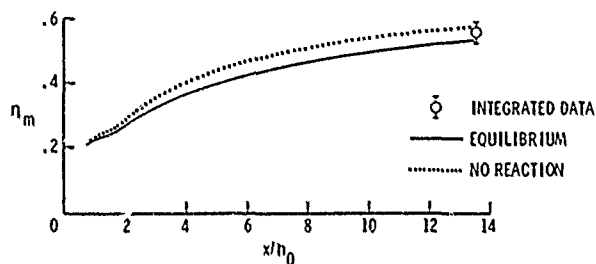


Fig. 26. Distribution of mixing parameter compared with integrated data at duct exit.

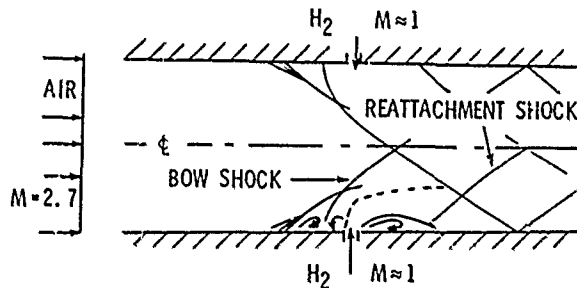


Fig. 27. Model problem for flow between two struts.

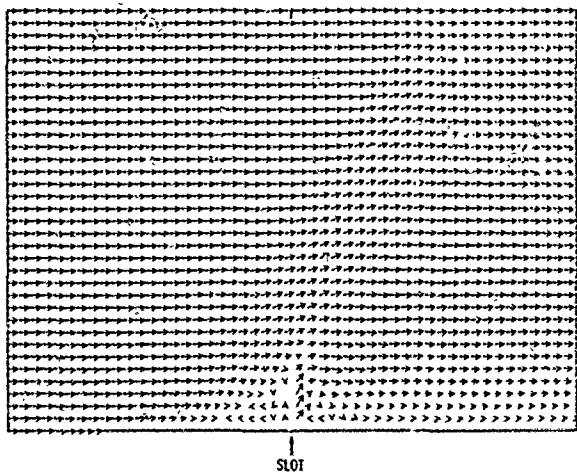


Fig. 28. Velocity vector field in lower half duct.

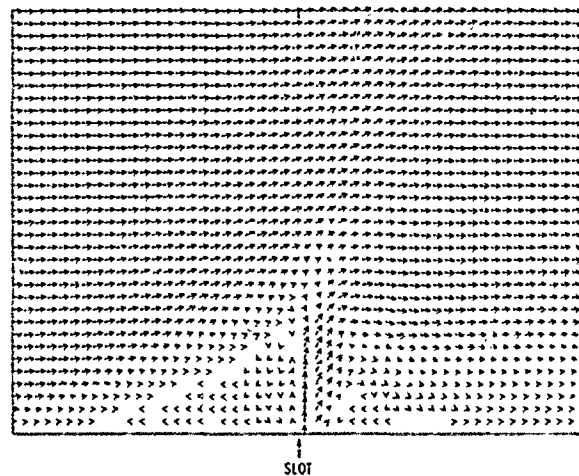


Fig. 29. Magnified velocity vector field about lower injector.

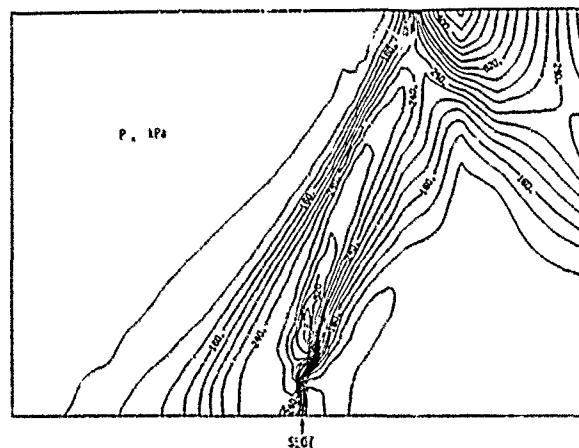


Fig. 30. Static pressure contours in lower half duct.

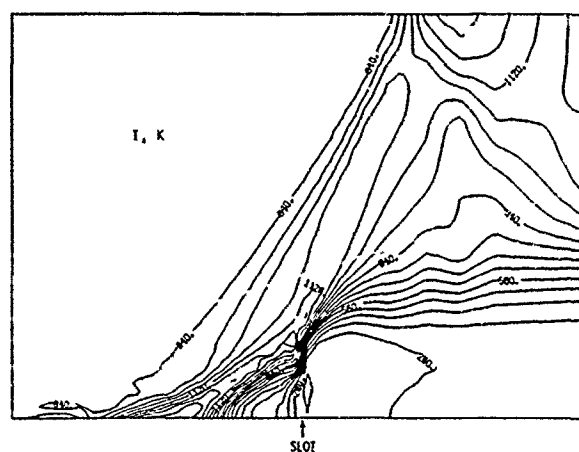


Fig. 31. Static temperature contours in lower half duct.

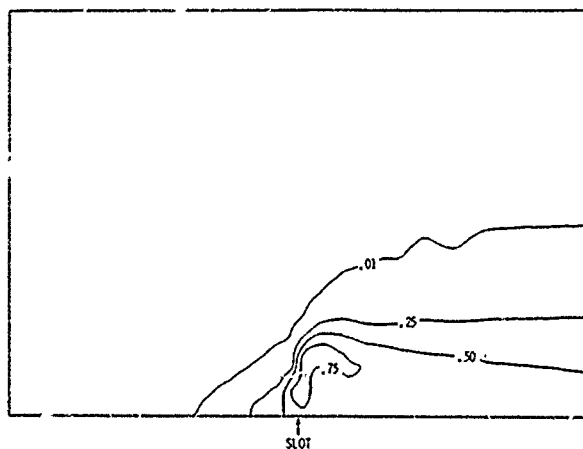


Fig. 32. Hydrogen mass fraction contours in lower half duct.

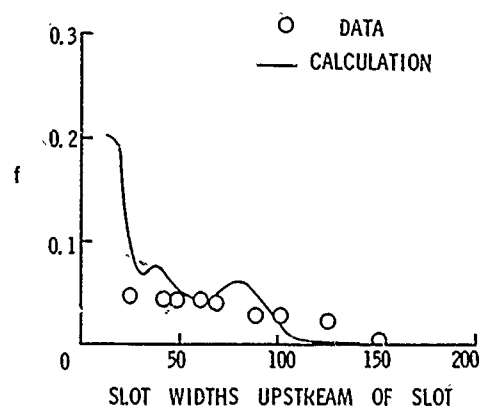


Fig. 34. Comparison of experimental and calculated hydrogen mass fractions along plate.

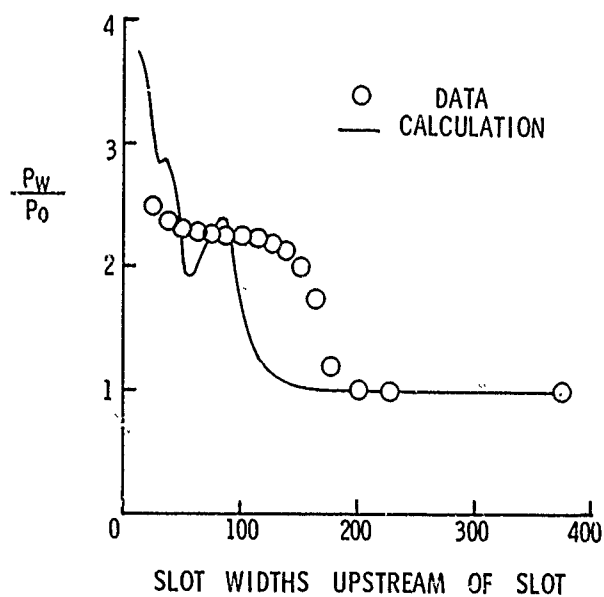


Fig. 33. Comparison of experimental and calculated static wall pressures.

## DISCUSSION

F.C.Lockwood, UK

The shock-induced separation zone is very dependent on the quality of the predictions for the impinging shock. How precisely do you manage to obtain the required good definition of the shock wave with a finite difference technique.

Author's Reply

Actually, the low shock preceding the upstream separation zone (Fig.28) does not impinge on the lower wall, the shock is initiated near the lower wall as a result of main stream flow blockage by the transverse jet (see page 10-9). All shock waves including the low shock are captured using the present technique. The capturing technique results in the shock being smeared over several node points; however, the jump conditions associated with each shock are satisfied although the conditions behind the shock are spatially displaced somewhat. We do plan at a later date to replace the present scheme with a shock fitting technique (see pages 10-18, 10-19). The fitting approach would more appropriately treat shocks as discontinuities.

J.H.Whitelaw, UK

In the first example you discussed the flow has  $Ma > 1$  in the stream and  $Ma = 0$  at the wall. You solved parabolic equations throughout. Did you have any difficulties in the near wall region. In the second example, you presented results and said that the "basic flow conditions have been predicted". What does this phrase mean in quantitative terms, bearing in mind the discrepancies mentioned earlier by Dr J.M.Cuirk in connection with isothermal, two-dimensional jets in mass flow.

Author's Reply

In the first example discussed during the oral presentation, we had no noticeable problem in the near wall region of the duct. No data were available very near the wall, and no data comparisons were attempted there (see Figures 15, 16, 17 and 18). To resolve steep gradients near the wall without using a large number of grid points, wall functions were used to define fluxes at near boundary grid points (see pages 10-6, 10-7). Therefore, the parabolic equations were not applied very near the wall where elliptic effects could be present.

The second example discussed during the oral presentations was intended to be qualitative as no data were available for comparisons (see page 10-17). The third example presented a quantitative comparison of elliptic code results with data. The basic flow conditions discussed in the talk and written paper referred to the separation, bow, and reattachment shocks, and the recirculating regions lying ahead of and behind the shock (see page 10-17). These phenomena were in qualitative agreement with experimental observations from a configuration similar to the strut flow model problem (Fig.27).

H.Wilhelmi, Ge

We published local concentration measurements for transverse fuel injection into supersonic flow (cf. H.Wilhelmi and G.Gross, Jr.: Turbulent Combustion, Progress of Aeronautics and Astronautics, L.Kennedy ed., New York 1978, pp.311/27). In this work, it was shown that also for supersonic flames the data in the mixing and reaction region can be correlated by a normalized error function with a high degree of accuracy. Surprisingly this even holds for regions of the flow field that are crossed by oblique shock waves. The experimental values yielded smooth curves for the values of constant concentration with a steadily increasing half width of the jet in downstream direction. These results did not show the inflection points and the maxima given in Figure 32 of this computational work. It is possible that these differences are due to the grid chosen for the computation, to the summing up of errors and to the turbulence model used.

Author's Reply

We believe the inflection point in the 1 percent contour line of Figure 32 is likely to be numerical in origin. The downrunning bow shock from the upper injector passes through the contour line at approximately this point. Mild oscillations of the dependent variables near a strong shock is typical with the present numerical techniques, and these oscillations would be most obvious with low hydrogen mass fractions. The velocity vector also turns downward as it passes through the downrunning shock, changing the streamwise component for hydrogen convection. This change may also affect the orientation of the contour line. We believe that the maxima present in the 25, 50 and 75 percent contour lines are a function of the strength of the hydrogen jet as compared to the strength of the air cross flow. The maxima were more pronounced with higher jet strengths, we have not considered any lower jet strengths than those presented in this paper.

It is of course possible that the present turbulence model introduces inaccuracies and the chosen grid may not accurately resolve the very high gradients close to the fuel injectors. The turbulence model is considered only an interim solution to the complex turbulence field that must be modelled. We are also considering other means for optimizing the discretization (floating grids, multi-grid schemes) and utilization of the STAR 100 vector computer at Langley Research Center to allow more modes to be used.



## DEVELOPMENT AND VERIFICATION OF RADIATION MODELS

H. BARTELDs  
International Flame Research Foundation  
IJmuiden  
The Netherlands

Present affiliation:  
TNO Organization for Applied Scientific Research  
Division of Technology for Society  
P.O. Box 342  
7300 AH Apeldoorn  
The Netherlands

## SUMMARY

The prediction of radiative heat transfer from a flame may be divided into three categories:

1. the evaluation of temperatures and radiating species concentrations,
2. the evaluation of the absorption-, emission- and scattering characteristics of the species at the prevailing temperatures,
3. the evaluation of the radiation exchange.

Models falling into category 2 and models falling into category 3 have been developed. The models have been verified by comparison with measured radiation intensities and measured radiative heat fluxes from relatively large gas flames.

As input to the models measured temperatures and species concentrations have been used. However, the models are well suited to be combined with each other and with prediction procedures for fluid flow and combustion.

## DEVELOPPEMENT ET VALIDATION DES MODELES DE RAYONNEMENT

## RESUME

La prédiction du transfert de chaleur rayonnante à partir d'une flamme peut se diviser en trois catégories:

1. évaluation des températures et des concentrations d'espèces rayonnantes,
2. évaluation des caractéristiques d'absorption, d'émission et de diffusion des espèces aux températures régnantes,
3. évaluation de l'échange radiatif.

On a mis au point des modèles appartenant aux 2ème et 3ème catégories. Pour valider ces modèles, des comparaisons ont été effectuées avec les résultats des mesures d'intensité de rayonnement et de flux de chaleur rayonnante émis par des flammes gazeuses de taille relativement importante.

Les mesures des températures et des concentrations d'espèces ont été incorporées aux modèles. Ces modèles peuvent être combinés ensemble et se prêtent bien aux procédures de prédiction d'écoulement fluide et de combustion.

## LIST OF SYMBOLS

a	weighting factor, black body factor in specified spectral region	-
a	subscript, referring to absorption	-
b	subscript, referring to black body radiation	-
b <sub>c</sub>	collision half width	m <sup>-1</sup>
b <sub>1n</sub>	constant in polynomial	-
b <sub>2n</sub>	constant in polynomial	K <sup>-1</sup>
b <sub>3n</sub>	constant in polynomial	K <sup>-2</sup>
b <sub>4n</sub>	constant in polynomial	K <sup>-3</sup>
c	velocity of light	m.s <sup>-1</sup>
c	concentration of soot	g.m <sup>-3</sup>
c	subscript, referring to carbon dioxide	-
co	subscripts, referring to carbon monoxide	-
f <sub>v</sub>	photon density	m <sup>-3</sup> .s <sup>-1</sup>
g <sub>v</sub>	subscript, referring to gas	-
h	Planck's constant	W.s <sup>2</sup>
I	intensity of radiation integrated over electromagnetic spectrum	W.m <sup>-2</sup>
I <sub>v</sub>	intensity of radiation at frequency v	W.m <sup>-2</sup> .s <sup>-1</sup>
I <sub>w</sub>	intensity of radiation at wavenumber w	W.m <sup>-1</sup> .s <sup>-1</sup>
K <sup>w</sup>	absorption/attenuation coefficient	m <sup>-1</sup>
k	gray gas/(averaged) specific spectral absorption coefficient	m <sup>-1</sup> .bar <sup>-1</sup>
k	gray gas/(averaged) specific spectral absorption coefficient	m <sup>2</sup> .g <sup>-1</sup>
m	number of gray gases/number of spectral regions	-

m	subscript, referring to methane	-
n	number, referring to gray gas or spectral region	-
$\hat{n}$	unit vector in the direction of pencil of radiation beams	-
P	total pressure	bar
p	partial pressure	bar
S	integrated spectral absorption coefficient	$m^{-2} \cdot bar^{-1}$
s	subscript, referring to scattering, source or soot	-
T	temperature	K
w	subscript, referring to water vapour	-
X	length of column of gas	m
x, y, z	Cartesian coordinates	m
z, r, $\theta$	cylindrical coordinates	m, m, -
$\alpha$	absorptivity	-
$\beta$	solid angle	-
$\gamma, \phi$	spherical coordinates	-
$\Delta$	indicates small increase/decrease	-
$\epsilon$	emissivity	-
$\lambda$	wavelength of radiation	m
$\nu$	frequency of radiation	$s^{-1}$
$\pi$	3.141592654	-
$\Sigma$	summation convention	-
$\sigma$	Stefan-Boltzmann constant, $.567 \times 10^{-7}$	$W \cdot m^{-2} \cdot K^{-4}$
$\omega$	wave number of radiation	$m^{-1}$
$\nabla$	differential vector operator	m

## 1. INTRODUCTION

Efficient use of energy, low pollutant emissions, low capital costs, while the process requirements are satisfied, are demands on combustion installations. Problems concerning flow, mixing, combustion, heat flux distributions and pollutant emission levels have to be solved for an optimum design of a burner/furnace combination. The ultimate universal solution to these problems can only be via the route of mathematical modelling techniques. Wide gaps exist in the computational development of these models and the physical and chemical information required. Furnace trials have been executed to obtain information on the physical and chemical processes occurring inside furnaces [1, 2]. The obtained information has to be generalized via mathematical models. In this paper mathematical modelling work concerning radiative heat transfer will be reported.

The prediction of radiative heat transfer from a flame may be divided into three categories:

1. the evaluation of temperatures and radiating species concentrations,
2. the evaluation of the absorption-, emission- and scattering characteristics of the species at the prevailing temperatures,
3. the evaluation of the radiation exchange.

In the present paper all three categories will receive attention both with respect to experiments and mathematical models. However, more detailed information will be presented concerning the development and verification of radiation models falling into categories 2 and 3.

## 2. TEMPERATURES AND RADIATING SPECIES CONCENTRATIONS

Before a radiation model can be applied it is necessary to evaluate the temperature distribution and the radiating species concentrations throughout the flame. The temperature field and the concentration fields can be obtained in different ways ranging from the practical experience of the combustion engineer to a more fundamental approach solving differential balance equations for mass, momentum, chemical species, enthalpy, etc. The latter approach has been investigated with varying success [3, 4, 5]. One can calculate furnace performance to a certain degree of accuracy for gas flames, however for heavy fuel oil- and coal flames complications occur. The determination of the concentration field of soot particles and the assessment of the radiation characteristics of soot particle clouds are very complex subjects, which are only mentioned briefly. The results to be presented refer to gas flames. The models, however, are not restricted to gas flames; coal- and oil flames may be treated by these models without too great difficulties.

For our purpose, the verification of radiation models, it is not possible to rely on temperatures and concentrations obtained in aforementioned w.s. The verification of radiation models is best done in isolation. Therefore as input to the models measured temperatures and species concentrations have been used.

## 3. RADIATION CHARACTERISTICS OF CHEMICAL SPECIES AND SURFACES

Radiation characteristics of the chemical species in a flame involve absorption-, emission- and scattering characteristics. Lowes and Heap [6] have shown that scattering for soot is negligible and scattering for large coal particles is forward directed. Consequently to a first approximation scattering can be ignored in luminous flames. Certainly scattering is not very important in gas flames. Therefore we will mainly concentrate on absorption and emission.

The basis of all methods for the solution of radiation problems is the equation of radiant energy transfer, which is derived by formulating a balance on the monochromatic

radiant energy taken along a pencil of rays enclosed within an elemental solid angle passing in a specified direction through a small volume element in an emitting-absorbing-scattering medium. This equation can be written in the form [7]:

$$(\hat{n} \cdot \vec{r}) I_{\omega} = -(k_{\omega a} p + k_{\omega s} p) I_{\omega} + k_{\omega a} p I_{b, \omega} + k_{\omega s} p \frac{1}{4\pi} \int_{4\pi} I_{\omega}(\beta) d\beta \quad (1)$$

(1)                      (2)                      (3)                      (4)

The physical situation underlying the development of Eq. (1) is illustrated in fig. 1 and fig. 2. Term (1) represents the gradient of intensity in the specified direction; term (2) represents the reduction in intensity due to absorption within the volume and the scattering into other directions of radiation which is in the specified direction upon arrival at the element; term (3) gives the increase in intensity due to emission from the volume; term (4) gives the increase in intensity due to scattering into the specified direction of radiation which is incident upon the volume from all other directions assuming isotropic scattering. Eq. (1) will be further clarified in subsequent paragraphs. Monochromatic radiant energy can be expressed as a function of wavenumber  $\omega$ , wavelength  $\lambda$  or frequency  $\nu$ . They are related as follows:  $\omega = 1/\lambda$ ,  $\nu = c/\lambda$ , while  $c$  is the velocity of light.

Although basically not necessary for convenience some simplifications will be introduced. As specified direction the x-direction will be taken, scattering will be neglected and  $k_{\omega s}$  is replaced by  $k_{\omega}$ ; then Eq. (1) can be written as

$$\frac{dI_{\omega}}{dx} = -k_{\omega} p I_{\omega} + k_{\omega} p I_{b, \omega} \quad (2)$$

The solution of this first order linear differential equation is

$$I_{\omega}(x) = I_{\omega}(x=0) e^{-k_{\omega} p x} + I_{b, \omega} (1 - e^{-k_{\omega} p x}) \quad (3)$$

It is assumed that  $k_{\omega, p}$  and  $I_{b, \omega}$  are constant or average values along the path  $x$ . Integration of Eq. (3) over the electromagnetic spectrum leads to

$$I(x) = \int_0^{\infty} I_{\omega}(x) d\omega = \int_0^{\infty} I_{\omega}(x=0) e^{-k_{\omega} p x} d\omega + \int_0^{\infty} I_{b, \omega} (1 - e^{-k_{\omega} p x}) d\omega \quad (4)$$

Eq. (4) forms the basis for the intensity calculations in following sections. Firstly information on physical backgrounds will be given.

The physics of absorption and emission will be discussed briefly. The absorption and emission of thermal radiation is associated with transitions between energy levels of the atoms or molecules that constitute the gas. Electronic, vibrational and rotational transitions of the molecules from excited energy levels to lower energy levels result in emission of radiation and radiation is absorbed when the transition occurs to higher energy levels. At the temperatures of interest in studies of radiant heat transfer in combustion systems, vibration-rotation transitions in the infrared frequencies make the most significant contribution to the observed radiant energy flux. The unit of energy released or absorbed when an energy level transition takes place is the photon. Each photon carries an energy of  $h\nu$  in which  $h$  is Planck's constant and  $\nu$  is the frequency of radiation. The molecular arrangements of gases is such that the number of vibrational degrees of freedom available is limited and in order to satisfy the fixed energy requirements for a change in excitation, transitions can only occur at discrete frequencies.

The fundamental quantity characterising radiation is the photon density  $f_{\nu}$ , which may be defined as the number of photons per unit volume, moving forward within the solid angle  $d\beta$ , and in the frequency interval between  $\nu$  and  $\nu + d\nu$ . The spectral intensity  $I_{\nu}$  being the amount of energy transported per unit time, unit area, unit solid angle and unit frequency interval is often used. The intensity of emission at a particular frequency due to an excitation level transition is proportional to the number of molecules occupying the vibrational-rotational level corresponding to the frequency and the probability that the transition will take place.

Because of the complexity of the evaluation of the intensity associated with each frequency experimental determination is necessary. The monochromatic intensity from a column of gas of partial pressure  $p$  and length  $x=X$  equals:

$$I_{\omega} = I_{b, \omega} (1 - e^{-k_{\omega} p X}) \quad (5)$$

where  $I_{b, \omega}$  is the black body intensity at the considered wave number and  $k_{\omega}$  the spectral (specific) attenuation (absorption) coefficient. The monochromatic intensity  $I_{\omega}$  is dependent upon the gas temperature (as  $I_{b, \omega}$  is a function of  $T$ ), partial pressure (concentration of radiating species) and path length, and the spectral absorption coefficient. The spectral absorption coefficient is dependent on gas temperature. The spectral absorption coefficient can be considered as one of the fundamental properties of a gas as far as radiation is concerned and it is the manner in which  $k_{\omega}$  varies over the spectrum which determines the total gas emissivity and absorptivity.

The discrete nature of the available energy transition frequencies leads to emission over very narrow frequency intervals and is known as line emission. No spectral line, however, is truly monochromatic but consists of a distribution of intensity within a small but finite frequency interval. If a number of emission lines are spaced closely together,

they may in some cases overlap; then they cannot be considered in isolation. Radiation from overlapping lines is known as band radiation. Although such bands are composed entirely of absorption-emission lines, the discrete band structure is commonly ignored by averaging over frequency intervals which include many lines.

The transition from one energy level to a lower level ideally occurs at a single frequency but in practice the emission line is broadened and spreads over a range of frequencies about the transition frequency. There is a natural line width that is the result of Heisenberg's Uncertainty Principle (natural line broadening), while broadening of lines can be caused further on by the perturbation of energy levels due to collision (collision broadening) and the thermal motion of the emitting and absorbing species relative to the observer giving a shift in the apparent frequency (Doppler broadening). Of these mechanisms collision broadening is the dominant broadening mechanism for most furnaces and combustion chambers but Doppler broadening becomes important at low pressures such as those encountered in rocket engine exhaust plumes at high altitude; see Hottel and Sarofim [8].

The distribution of absorption coefficient about the line wavenumber  $\omega$  is given for a collision broadened line by Penner [9], Tien [10] and Hottel and Sarofim [8].

$$k_{\omega} = \frac{S}{\pi} \frac{b_c}{(\omega - \omega_0)^2 + b_c^2} \quad (6)$$

where  $S$  is the area under the  $k_{\omega}$  -  $\omega$  curve for the broadened line and is called the integrated line intensity; and  $b_c$  is the collision half width for the line, fixing the position at which  $k_{\omega}$  falls to half its maximum value.

The intensity of radiation leaving a volume of gas due to emission from a single line can be found by integration of the spectral intensity over the entire spectrum.

$$I = \int_0^{\infty} I_{b,\omega} (1 - e^{-k_{\omega} pX}) d\omega \quad (7)$$

In most gases of practical interest the emission lines do not occur in isolation, but are spaced so closely together that the broadened lines overlap to a considerable extent. When a number of lines overlap the specific absorption coefficients are additive, and the contribution to the intensity of radiation from the entire band can be found by integration between the frequency limits of the band.

$$I = \int_{\omega_1}^{\omega_2} I_{b,\omega} (1 - e^{-k_{\omega} pX}) d\omega \quad (8)$$

The spectral absorption coefficient  $k_{\omega}$  represents the sum of the absorption coefficients from the considered lines at the wave number  $\omega$ .

The total gas emission can be found by integration over the entire spectrum. The total emissivity of a gas at temperature  $T_g$  is equal to the ratio of the emission by a gas layer of length  $X$  to the black body emission at temperature  $T_g$ .

$$\epsilon_g = \frac{\int_0^{\infty} I_{b,\omega}(T_g) [1 - e^{-k_{\omega}(T_g)pX}] d\omega}{\int_0^{\infty} I_{b,\omega}(T_g) d\omega} = f(T_g, pX) \quad (9)$$

In a similar way the total gas absorptivity can be evaluated, but in this case the distribution of energy in the spectrum is related to the temperature at which the intensity, absorbed in a certain gas layer, is emitted.

$$\alpha_g = \frac{\int_0^{\infty} I_{b,\omega}(T_s) [1 - e^{-k_{\omega}(T_g)pX}] d\omega}{\int_0^{\infty} I_{b,\omega}(T_s) d\omega} = f(T_g, T_s, pX) \quad (10)$$

where  $I_{b,\omega}(T_s)$  is emitted at a source temperature  $T_s$  and the spectral intensity is dependent on this source.

In Eq. (10)  $I_{b,\omega}$  is considered to be due to a black body emitter. However, the source does not have to be a black body (or gray body). The intensity can be due to e.g. a gas layer having a certain composition- and temperature distribution. The absorptivity then becomes:

$$\alpha_g = \frac{\int_0^{\infty} I_{\omega}(T_s) [1 - e^{-k_{\omega}(T_g)pX}] d\omega}{\int_0^{\infty} I_{\omega}(T_s) d\omega} = f(T_g, T_s, pX) \quad (11)$$

Now the source temperature does not have to be a constant but can be a temperature distribution. The distribution of the spectral intensity can be very complex in this case.

A number of models have been proposed to avoid the problem of formulating the attenuation coefficient as a complex function of wave number. The purpose has been to provide a model of the relative spacing and intensity of lines in a band. Such a model combined with a suitable description of the line broadening function leads to an analytical solution of the intensity of radiation from a band. Among the proposed models are the Elsasser, the Mayer-Goody or statistical model, and the box model developed by Penner [9]. More information about these models can be found in Johnson [11], Tien [10] and Hottel and Sarofim [8].

A fundamental approach of the emission/absorption problem must take account of the spectral

nature of gas radiation, but the problems involved in handling the spectral properties of the gas mixtures are enormous, so in many cases the problem is handled by using measured total radiation properties. Total water vapour emissivity and carbon dioxide emissivity charts in which information from several sources is used are presented in Hottel and Sarofim [8]. Johnson [11] discusses these charts and mentions more recent publications in which the regions, where the above-mentioned charts are less accurate, are indicated. However, at the moment the recognized standards for evaluating total emissivities of water vapour and carbon dioxide are these charts. Hadvig's charts [12] for total emissivities of water vapour/carbon dioxide mixtures are based on the charts in Hottel and Sarofim [8]. Lee and Happel [13] have measured emissivities for methane. Hottel and Sarofim [8] present a chart on the total emissivity of carbon monoxide based on the measurements of Ullrich [14].

In furnaces the gases normally are composed of two or more radiating components. For a mixture of two gases the total emissivity equals:

$$\begin{aligned}\epsilon_{1+2} &= \frac{\int_0^\infty I_{b,w} [1 - e^{-(k_{w,1}p_1 + k_{w,2}p_2)X}] d\omega}{\int_0^\infty I_{b,w} d\omega} \\ &= \frac{\int_0^\infty I_{b,w} [(1 - e^{-k_{w,1}p_1X}) + (1 - e^{-k_{w,2}p_2X}) - (1 - e^{-k_{w,1}p_1X})(1 - e^{-k_{w,2}p_2X})] d\omega}{\int_0^\infty I_{b,w} d\omega} \\ &= \epsilon_1 + \epsilon_2 - \Delta\epsilon_{1+2}\end{aligned}\quad (12)$$

The emissivity of a mixture of two gases is equal to the sum of the emissivities of the two gases minus a correction for spectral overlap. If there is no spectral overlap the correction factor equals zero.

Fig. 3, taken from Johnson [11], presents an idealized distribution of gas spectral absorption coefficients for  $H_2O$ ,  $CO_2$ ,  $CO$  and  $CH_4$ . It can be seen that overlap occurs in some parts of the spectrum so corrections are necessary. It should be realized that the absorption bands are composed of series of spectral lines close together and that these spectral lines are affected by temperature as can be seen in fig. 4, which is based on Lee and Happel [13]. The spectral absorptivity for the  $2.37 \mu m$  band for methane is shown in this figure. For the absorptivity  $\alpha_g$  (see Eq. 10) of a mixture of carbon dioxide and water vapour an approximate evaluation can be made by using the relations given by Hottel and Sarofim [8].

$$\alpha_c(T_g, T_s, pX) = \left(\frac{T_g}{T_s}\right)^{0.65} \epsilon_c(T_s, pX \frac{T_s}{T_g}) \quad (13)$$

$$\alpha_w(T_g, T_s, pX) = \left(\frac{T_g}{T_s}\right)^{0.45} \epsilon_w(T_s, pX \frac{T_s}{T_g}) \quad (14)$$

$$\alpha_{c+w} = \alpha_c + \alpha_w - \Delta\alpha_{c+w} \quad (15)$$

$\Delta\alpha_{c+w}$  is the correction factor for spectral overlap. These absorptivity formulations can be used if the radiation intensity is black body radiation from a surface at  $T_s$ . However, in a watercooled furnace with low wall temperatures the radiation from furnace walls is negligible and all the radiation within the enclosure is from gas radiation, which is not by any means black body radiation.

Combining Eqs. (4), (9) and (11) for  $X = x$  one arrives at

$$\begin{aligned}I(x) &= \int_0^\infty I_w(x=0) e^{-k_w p x} d\omega + \int_0^\infty I_{b,w} (1 - e^{-k_w p x}) d\omega \\ &= (1 - \alpha_g) \int_0^\infty I_w(x=0) d\omega + \epsilon_g \int_0^\infty I_{b,w} d\omega \\ &= (1 - \alpha_g) I(x=0) + \epsilon_g \frac{I_{b,w}}{\sigma T_g^4} \\ &= (1 - \alpha_g) I(x=0) + \epsilon_g \frac{I_g}{\pi}\end{aligned}\quad (16)$$

So the intensity  $I(x)$  in  $x$ -direction is composed of a transmitted fraction of  $I(x=0)$  through the layer  $x$  plus a part emitted in the layer  $x$ . In Eq. (16)  $I_b$  is the integrated black body intensity of the gas at temperature  $T_g$ , while  $\sigma$  is the Stefan-Boltzmann constant. When the intensity  $I(x=0)$  originates from a surface, as is often the case, one needs to know the radiative properties of the surface.

The radiant energy interchange within enclosures is affected by the radiative properties of the surrounding walls. To analyze the process within a furnace enclosure it is necessary to know the emission, reflection and absorption properties of the walls as the temperature level and -distribution in the gas volume is affected to some extent by these properties, while the heat transfer and heat transfer distribution to cooling loads are strongly influenced by these properties. Only radiation properties of black bodies are well established. The walls in furnaces normally do not behave like black bodies. The emissivity of furnace walls and tubes is a function of direction (angle of emergence), wave length and temperature; the importance of these parameters is influenced by the surface condition. Factors like roughness, oxide layers and physical and chemical contamination are used to describe the surface condition.

The electromagnetic theory can be used for a fundamental approach to the radiative properties of surfaces. However, the surface has to be very well defined for a theoretical treatment; it has to be optically smooth, physically, and chemically clean to allow a prediction of the monochromatic reflectance in the specular direction to be made. Furnace walls and tubes are normally not well enough defined for a theoretical treatment; deposits of combustion products on the walls change the characteristics of the walls during operation. Measured data have to be used to obtain the necessary knowledge about the surface behaviour. For metallic surfaces the emissivity falls down with wave length; the emissivity of iron and steel can vary from above .8 to below .05 between .2 and 10  $\mu\text{m}$ . Refractory materials can have a strong variation of emissivity with wave length; several minima and maxima can appear over the spectrum. The angular distributions of emissivity for metallic and refractory materials are not the same. For small angular inclinations relative to the normal on the surface the emissivity of metallic surfaces is quite constant; with increasing angles the emissivity increases quite sharp and the emissivity falls down to zero when the inclination angle approaches  $90^\circ$ . Refractory materials show a slight decrease in emissivity for inclination angles between  $0^\circ$  and  $60^\circ$ ; for higher angles the decrease is sharper with the emissivity approaching zero when the inclination angle equals  $90^\circ$ .

Although quite a lot of information on surface radiation is available in the literature e.g. in Perry [15], Sparrow and Cess [16], and Hottel and Sarofim [8], not very much is known concerning the radiative behaviour of furnace walls under combustion conditions. Normally one relies on total (integrated over the spectrum) hemispherical (integrated over all angles in an hemisphere) emissivities obtained from the literature. For iron and steel with different surface conditions values between .07 and .97 can be found. The emissivities of refractory materials, of which the grain structure is an important parameter, vary between .25 and .95. The effect of wall temperatures on the absorption coefficient for different furnace wall materials is shown in fig. 5; taken from van Kuijk and Spanjers [17].

Toor and Viskanta [18, 19] have studied the effect of radiative properties of surfaces on the radiant heat transfer between surfaces. They conclude that for an accurate prediction of local irradiation the directional characteristics must be considered while calculation of the irradiation on a non-gray basis does not yield improved results over a gray analysis. In furnaces these conclusions could loose their validity to some extent as between the walls gases radiate. The gas radiation is strongly dependent on wave length, so the absorptivity of the walls in the spectral regions, where gas emission is high, can be very important. In analyzing the radiative heat transfer within a furnace enclosure, the total emissivity of refractory surfaces is normally assumed to be about .5 while the total emissivity of steel tubes is assumed to be above .8.

As will be clear from this section for practical emission/absorption models one needs to simplify. This will be done in the next section.

#### 4. EMISSION/ABSORPTION MODELS

In this section a number of emission/absorption models for the prediction of radiation intensity will be developed.

##### A: Gray gas models

If the variation of the absorption coefficient  $K(=kp)$  with spectral position, partial pressure and temperature is neglected and a mean value for the absorption coefficient  $K$  is used, Eq. (16) can be written as

$$I(x) = I(x=0) e^{-Kx} + \frac{\sigma T_g^4}{\pi} (1 - e^{-Kx}) \quad (17)$$

In the gray gas model the emissivity equals the absorptivity

$$\epsilon_g = \alpha_g = 1 - e^{-Kx} = 1 - e^{-kp_x} \quad (18)$$

The gray gas model calculates measured emissivities correctly only at one value of pressure pathlength  $p_x$ . The choice of the absorption coefficient  $K$  has to be based on the combustion products (in our experiments from natural gas), the average pathlength (furnace dimensions) and gas temperatures. The chosen values are given in table I.

table I: constants of gray gas models for the products of methane combustion

K	0.1	0.2	0.3
---	-----	-----	-----

##### B: One clear/two gray gas model

A better way to represent the emissivity of a real gas is to take the sum of the weighted emissivities of one clear and two gray gases instead of using one gray gas.

$$\epsilon_g = \sum_{n=1}^3 \epsilon_{g,n} = \sum_{n=1}^3 a_{g,n} (T_g) (1 - e^{-k_n p_x}) \quad (19)$$

with, as chosen by Johnson [11]

$$a_{g,n} = b_{1n} + b_{2n} T_g \quad (20)$$

The weighting factor  $a_{g,n}$  can be considered as the quotient of the spectral black body intensity integrated over the wave number region where  $k_n = k_n (= \text{constant})$  and the spectral black body intensity integrated over the complete spectrum. Then

$$\sum_{n=1}^3 a_{g,n} = 1. \quad (21)$$

and Eq. (19) follows from Eq. (9) and Eq. (16) can be written as the sum of three intensities, each representing a part of the spectrum:

$$I(x) = \sum_{n=1}^3 I_n(x) = \sum_{n=1}^3 [I_n(x=0) e^{-k_n p x} + a_{g,n}(T_g)(1 - e^{-k_n p x}) \frac{\sigma T_g^4}{\pi}] \quad (22)$$

The factors of table II have been determined by Johnson [11] such that Eq. (19) closely fits to measured emissivity/pressure pathlength relationships for the combustion products of methane combustion. The emissivities based on measurements are given in Hadvig's charts [12]; 99 data points have been used.

table II: constants of one clear/two gray gas model for the products of methane combustion

n	$b_{1n}$	$b_{2n} \cdot 10^3$	$k_n$
1	+ .255	+ .260	0.00
2	+ .500	- .157	1.83
3	+ .245	- .103	32.30

The clear gas with  $k = 0.00$  corresponds to the weakly- and non-absorbing parts of the spectrum. The partial pressure  $p$  has to be taken as the sum of the partial pressures of the radiating gases (mainly carbon dioxide and water vapour).

With this model the maximum discrepancies between emissivities using Eq. (19) and measured emissivities amount about 10% for partial pressure pathlengths (px's) between .02 and 1.5 bar.m. Due to the clear gas the maximum emissivities at infinite pathlength for temperatures between 1000 and 2000 K are restricted to too low values. The maximum emissivities are on average lower than the measured emissivities at a pressure pathlength of 1.2 bar.m, while at this pressure pathlength Eq. (19) underpredicts emissivities by about 10%. This means that the model with the constants of table II becomes increasingly inaccurate if the mean pathlength is larger than 4 m for a natural gas flame with a partial pressure of carbon dioxide and water vapour of roughly 0.3 bar. For large furnaces the model seems to have deficiencies.

#### C: Four gray gas model

A more accurate calculation of emissivities can be obtained with the following formulations

$$\epsilon_g = \sum_{n=1}^4 a_{g,n}(T_g)(1 - e^{-k_n p x}) \quad (23)$$

$$a_{g,n} = b_{1n} + b_{2n} T_g + b_{3n} T_g^2 + b_{4n} T_g^3 \quad (24)$$

We have chosen a larger number of gray gases and a higher order of the polynomial than before to ascertain that the emissivity can be determined very accurate. The clear gas has been dropped to prevent the aforementioned problems at longer pathlengths. The constants of table III have been determined by fitting Eq. (23) against the same measured emissivity data as used for the previous model.

table III: constants of four gray gas model for the products of methane combustion

n	$b_{1n}$	$b_{2n} \cdot 10^3$	$b_{3n} \cdot 10^6$	$b_{4n} \cdot 10^9$	$k_n$
1	+ .218	+ .283	+ .065	- .026	0.106
2	+ .535	- .240	+ .009	+ .002	1.653
3	+ .131	+ .089	- .127	+ .032	21.212
4	+ .116	- .132	+ .053	- .008	146.308

The fit was made over the temperature range of 1000-2000 K and a partial pressure pathlength range of 0.003 - 1.2 bar.m. The emissivity calculation is very good as the average deviation from measured emissivities is less than 1% over the above ranges.

In table IV the weighting factors and the absorption coefficients are given for the four gray gases.

table IV: weighting factors and absorption coefficients of four gray gas model for the products of methane combustion

	1000 K	1200 K	1400 K	1600 K	1800 K	2000 K	1000 - 2000 K
$a_1$	.540900	.607500	.672000	.733100	.789600	.840200	$k_1$ .106165
$a_2$	.304100	.261200	.219300	.178300	.139300	.101300	$k_2$ 1.652860
$a_3$	.124900	.109900	.093870	.078390	.064960	.055120	$k_3$ 21.212000
$a_4$	.029980	.021390	.014810	.009851	.006139	.003296	$k_4$ 146.308000



Radiation intensities can be calculated using Eq. (22) with  $n$  from 1 to 4.

#### D: Spectral model

Representing a real gas by a series of gray gases for emission/absorption purposes misrepresents some physical realities. The wave length range in which emission occurs and the monochromatic emission/attenuation coefficients vary with gas temperature. Some radiation emitted at high temperature cannot be attenuated by gas at a lower temperature. The change in monochromatic emission/attenuation coefficients with temperature means a gray gas assumption over a temperature range is not valid. Total emissivity data are used to find  $a_n$  and  $k_n$ ;  $k_n$  is forced to be constant over the whole temperature range between 1000 and 2000 K. If the monochromatic absorption coefficients vary with temperature, the weighting factors  $a_n$  and specific absorption coefficients  $k_n$  do not have to be valid in exactly the same spectral regions for different temperatures. Or the division of the spectrum in four parts does not have to represent the same parts of the spectrum for the different temperatures. Figures given by Edwards and Balakrishnan [20] suggest that this could have considerable effect on the absorption of gas radiation coming from a source at a different temperature. To avoid these problems it is possible to divide the electromagnetic spectrum in discrete parts and to obtain averaged monochromatic absorption coefficients in these parts of the spectrum.

The division of the spectrum we decided to use is given in table V.

table V: Division of electromagnetic spectrum in water vapour and carbon dioxide bands of increasing strength

$n = 1$	0.0 - 2.6111 $\mu\text{m}$ , 2.7778 - 3.7778 $\mu\text{m}$ , 5.5556 - 5.7222 $\mu\text{m}$ , 6.9444 - 11.1111 $\mu\text{m}$ , 50.000 - $\infty$ $\mu\text{m}$
$n = 2$	2.6111 - 2.7778 $\mu\text{m}$ , 3.7778 - 3.9444 $\mu\text{m}$ , 4.7778 - 5.5556 $\mu\text{m}$ , 5.7222 - 6.9444 $\mu\text{m}$ , 11.1111 - 14.6667 $\mu\text{m}$ , 31.1111 - 50.0000 $\mu\text{m}$
$n = 3$	3.9444 - 4.2222 $\mu\text{m}$ , 4.3889 - 4.7778 $\mu\text{m}$ , 14.6667 - 31.1111 $\mu\text{m}$
$n = 4$	4.2222 - 4.3889 $\mu\text{m}$

The spectral region for  $n = 4$  contains the strongest absorbing part of the 4.3  $\mu\text{m}$   $\text{CO}_2$  band;  $n = 3$  contains weaker absorbing parts of the 4.3  $\mu\text{m}$   $\text{CO}_2$  band and the strongest absorbing parts of the 20  $\mu\text{m}$   $\text{H}_2\text{O}$  band with a part of the overlapped 15  $\mu\text{m}$   $\text{CO}_2$  band;  $n = 2$  contains the strongest part of the 2.7  $\mu\text{m}$   $\text{CO}_2$  and  $\text{H}_2\text{O}$  overlapped bands, weak absorbing parts of the 4.3  $\mu\text{m}$   $\text{CO}_2$  band, the strongest part of the 2.6  $\mu\text{m}$   $\text{H}_2\text{O}$  band, weaker parts of the 15  $\mu\text{m}$   $\text{CO}_2$  and 20  $\mu\text{m}$   $\text{H}_2\text{O}$  bands (partly overlapped); finally  $n = 1$  contains the wings of some of the above-mentioned bands plus some less important bands like the 1.1  $\mu\text{m}$ , 1.38  $\mu\text{m}$ , 1.87  $\mu\text{m}$   $\text{H}_2\text{O}$  bands and the 1.4  $\mu\text{m}$ , 1.6  $\mu\text{m}$ , 2.0  $\mu\text{m}$ , 7.5  $\mu\text{m}$ , 9.4  $\mu\text{m}$  and 10.4  $\mu\text{m}$   $\text{CO}_2$  bands. We replace the monochromatic absorption coefficients in each of the four regions by an average value at a fixed temperature. Eq. (9) can now be written as

$$\epsilon_g = \sum_{n=1}^4 [1 - e^{-k_n(T_g)px}] \frac{\int_0^\infty \frac{I_{b,\omega}(T_g)}{\int_0^\infty I_{b,\omega}(T_g) d\omega} d\omega}{\int_0^\infty I_{b,\omega}(T_g) d\omega} \quad (25)$$

Both integrals are only functions of temperature, so

$$a_{g,n}(T_g) = \frac{\int_0^\infty I_{b,\omega}(T_g) d\omega}{\int_0^\infty I_{b,\omega}(T_g) d\omega} \quad (26)$$

and

$$\epsilon_g = \sum_{n=1}^4 a_{g,n}(T_g) [1 - e^{-k_n(T_g)px}] \quad (27)$$

Eq. (27) looks similar to Eq. (23). However,  $k_n(T_g)$  is now a function of temperature and  $a_{g,n}(T_g)$  is found by specification of spectral regions. The integrals of Eq. (26) have been evaluated with tabulated black body fractions in Siegel and Howell [21] and the averaged monochromatic absorption coefficients have been calculated by a least squares method substituting total emissivity data in Eq. (27). The results are given in table VI.

table VI: Black body factors and absorption coefficients of spectral model for the products of methane combustion

	1000 K	1200 K	1400 K	1600 K	1800 K	2000 K
$a_1$	.547850	.627500	.696030	.752100	.797030	.832690
$a_2$	.289640	.239080	.196290	.161200	.132870	.110150
$a_3$	.135250	.109820	.088080	.070650	.056970	.046390
$a_4$	.027260	.023600	.019600	.016050	.013130	.010770
$k_1$	.117358	.129552	.127925	.118370	.108990	.101752
$k_2$	1.599540	1.674640	1.787490	1.803700	1.779150	1.584270
$k_3$	19.881100	20.554600	20.503700	20.851900	20.223200	23.533700
$k_4$	182.959000	130.647000	104.457990	71.579170	62.205950	25.195700



Although it is not known whether the division of the spectrum in the chosen 4 regions is the best possible subdivision, it is apparent from the above results that the averaged monochromatic absorption coefficients are increasing with increasing  $n$  like one would expect. Further on the averaged monochromatic absorption coefficients vary strongly with temperature. Exact polynomials are used to express the black body factors and the averaged monochromatic absorption coefficients as a function of temperature. These polynomials for  $a$  and  $k$  have been substituted in Eq. (27). The average deviation of the emissivities calculated with Eq. (27) from Hadvig's [12] 99 data points is less than 1%. Comparing table IV and table VI it appears that the order of magnitude of the weighting respectively black body factors and absorption coefficients agree. This indicates that the choice of the spectral regions for the spectral model is quite good.

Radiation intensities can be calculated in the same way as with the four gray gas model.

#### E: Spectral model for mixtures of gases and soot

The models developed in previous paragraphs are suited to be used for methane and natural gas flames. Similar models with different weighting factors or black body factors and absorption coefficients can be developed for oil flames. Johnson [11] and Beér and Claus [22] have shown some results indicating such an approach is possible. However, these models are limited in their application as they always refer to the combustion gases of one fuel.

A general model to calculate the emissivity of mixtures of gases and soot will be proposed. The model will be valid for mixtures containing methane (m), carbon monoxide (co), carbon dioxide (c), water vapour (w), etc. and soot (s). A similar approach will be followed as for the previous spectral model.

The emissivity can be written

$$\epsilon_g = \sum_{n=1}^m a_{g,n}(T_g) [1 - e^{-K_n(\text{composition}, P, T_g)x}] \quad (28)$$

with

$$K_n = k_{m,n}(p_m, P, T_g)p_m + k_{co,n}(p_{co}, P, T_g)p_{co} + k_{c,n}(p_c, P, T_g)p_c + k_{w,n}(p_w, P, T_g)p_w + k_{s,n}(\text{particle properties})c_s \quad (29)$$

The absorption coefficient  $K_n$  is found by adding the contribution of the components methane, carbon monoxide, carbon dioxide, water vapour and soot. The specific absorption coefficient  $k$  for a gas may be a function of composition (partial pressure  $p$ ), total pressure  $P$  and gas temperature  $T$ . The composition of the remainder of the gas has some effect on the absorption coefficient for one gas component as different species of colliding molecules affect the line half-width. However, normally the effect of the composition of the remainder of the gas is negligible. The pressure dependency of the averaged monochromatic specific absorption coefficients is included as the emissivity of a gas, at a fixed value of pressure path length  $px$  is dependent to some extent on partial and total pressure. However, these effects are quite small under normal furnace conditions. In Eq. (27) the specific absorption coefficient applies to a mixture of gases with a constant ratio between the partial pressures of these components. The pressure  $p$  equals the sum of the partial pressures of these components. In Eqs. (28) and (29) each component is treated independently.

The procedures to obtain the black body factors and the averaged monochromatic absorption coefficients are the same as for the previous spectral model. However, these procedures have to be executed for each radiating gas component and for soot, while the division of the electromagnetic spectrum has to take account of the radiative behaviour of all the components as a function of wavelength. Dependent on the required accuracy of the model the number of spectral regions can be extended.

For water vapour and carbon dioxide the spectral division of table V can be used. In table VII the spectral division for methane is given.

table VII: Division of electromagnetic spectrum in methane bands of increasing strength

$n = 1$	: 0.0 - 2.3419 $\mu\text{m}$ , 2.4096 - 3.1056 $\mu\text{m}$ , 3.6765 - 7.0423 $\mu\text{m}$ , 8.7336 - $\infty$ $\mu\text{m}$ .
$n = 2$	: 2.3419 - 2.4096 $\mu\text{m}$ , 3.1056 - 3.1646 $\mu\text{m}$ , 3.1646 - 3.6765 $\mu\text{m}$ , 7.0423 - 7.1429 $\mu\text{m}$ , 8.4459 - 8.7336 $\mu\text{m}$
$n = 3$	: 3.1646 - 3.5971 $\mu\text{m}$ , 3.5971 - 8.4459 $\mu\text{m}$

The strong absorbing parts of the 3.31  $\mu\text{m}$  and the 7.65  $\mu\text{m}$  band are in the spectral region  $n = 3$ . Weaker absorbing parts of the same bands and the strongest absorbing part of the 2.37  $\mu\text{m}$  band are in the spectral region  $n = 2$ , while the remainder of the spectrum is in the spectral region  $n = 1$ . Together with the 4 spectral regions of table V for carbon dioxide and water vapour emission the number of spectral regions for  $\text{CO}_2/\text{H}_2\text{O}/\text{CH}_4$  emission increases strongly. A limitation of the number of spectral regions can be found by taking into account the spectral division for  $\text{CO}_2/\text{H}_2\text{O}$  emission for the  $\text{CH}_4$  division of the spectrum as shown in table VIII.

table VIII: Rearranged division of electromagnetic spectrum in methane bands

$n = 1$	: 0.0 - 2.7778 $\mu\text{m}$ , 3.7778 - 6.9444 $\mu\text{m}$ , 11.1111 - $\infty$ $\mu\text{m}$
$n = 2$	: 2.7778 - 3.7778 $\mu\text{m}$ , 6.9444 - 11.1111 $\mu\text{m}$

The combination of the 4 spectral regions for  $\text{CO}_2/\text{H}_2\text{O}$  emission with the 2 spectral regions for  $\text{CH}_4$  emission results in 5 spectral regions for  $\text{CO}_2/\text{H}_2\text{O}/\text{CH}_4$  emission. The absorption coefficients for methane can be determined with the use of total emissivity data based on Lee and Happel [13] by a least squares procedure.

The division in spectral regions for carbon monoxide is given in table IX.

table IX: Division of electromagnetic spectrum in carbon monoxide bands of increasing strength

---

$n = 1 : 0 - 4.4944 \mu\text{m}, 4.8193 - \infty \mu\text{m}$   
 $n = 2 : 4.4944 - 4.8193 \mu\text{m}$

---

The strong absorbing part of the  $4.67 \mu\text{m}$  band is in the spectral region  $n = 2$ , while the weaker absorbing parts of the same band together with the  $2.3 \mu\text{m}$  band and the remainder of the spectrum are in the spectral region  $n = 1$ . A distribution for carbon monoxide which fits into the spectral regions chosen for  $\text{CO}_2/\text{H}_2\text{O}$  emission is given in table X.

table X: Rearranged division of electromagnetic spectrum in carbon monoxide bands

---

$n = 1 : 0 - 4.3889 \mu\text{m}, 4.7778 - \infty \mu\text{m}$   
 $n = 2 : 4.3889 - 4.7778 \mu\text{m}$

---

The absorption coefficients can be found again by a least squares procedure using a chart for the total emissivity of carbon monoxide presented by Hottel and Sarofim [8] based on the measurements of Ullrich [14].

The spectral regions for  $\text{H}_2\text{O}$  and  $\text{CO}_2$  emission together with the distribution for  $\text{CH}_4$  and  $\text{CO}$  emission that give the minimum number of spectral regions, results into the subdivision of the electromagnetic spectrum as given in table XI.

table XI: Division of electromagnetic spectrum in bands of different strength of methane, carbon monoxide, carbon dioxide and water vapour

---

$n = 1 : 0.0 - 2.6111 \mu\text{m}, 5.5556 - 5.7222 \mu\text{m}, 50.000 - \infty \mu\text{m}$   
 $n = 2 : 2.6111 - 2.7778 \mu\text{m}, 3.7778 - 3.9444 \mu\text{m}, 4.7778 - 5.5556 \mu\text{m},$   
 $5.7222 - 6.9444 \mu\text{m}, 11.1111 - 14.6667 \mu\text{m}, 31.1111 - 50.0000 \mu\text{m}$   
 $n = 3 : 2.7778 - 3.7778 \mu\text{m}, 6.9444 - 11.1111 \mu\text{m}$   
 $n = 4 : 3.9444 - 4.2222 \mu\text{m}, 14.6667 - 31.1111 \mu\text{m}$   
 $n = 5 : 4.2222 - 4.3899 \mu\text{m}$   
 $n = 6 : 4.3899 - 4.7778 \mu\text{m}$

---

The black body factors in the spectral regions of table XI can be found from tabulated black body functions and the averaged spectral absorption coefficients in each spectral region for each separate gas component can be determined by a least squares procedure using total emissivity data. For carbon dioxide and water vapour total emissivity data are presented in Hottel and Sarofim [8].

For soot radiation one needs to determine the soot concentration in the flame and the specific absorption coefficient for soot. For experimental conditions on laboratory scale it is difficult to obtain absorption coefficients to a good accuracy; the problems are much bigger if one wants to obtain absorption coefficients for fuel oil or pulverized coal flames in furnaces. As the particle properties are complexly related to fuel type and mixing history the variation of these properties throughout the flame is normally not known. However, soot radiation can be included in the presented model. The soot absorption coefficients have to be determined for the wave length regions of table XI. Soot absorption coefficients vary strongly with wave length. Johnson [11] discusses work from several authors on soot radiation. Kunitomo [23] reports that soot emission is mainly affected by the soot concentration and the soot particle size and the soot formation is influenced greatly by the excess air factor, the kind of burner and the fuel type for a range of liquid fuel flames.

Radiation intensities can be calculated using an equation similar to Eq. (22).

$$I(x) = \sum_{n=1}^6 I_n(x) = \sum_{n=1}^6 [I_n(x=0) \cdot e^{-K_n x} + a_{g,n}(T_g)(1 - e^{-K_n x}) \frac{\sigma T_g^4}{\pi}] \quad (30)$$

Emissivity data to test Eq. (28) is available both on gases with one radiating component and radiating gas mixtures of different composition [8, 12, 13, 14].

Experimental information to test Eq. (30) is available in Michelfelder and Lowes [1] for gas flames with methane, carbon monoxide, carbon dioxide and water vapour in the combustion gases and for luminous oil flames with mixtures of radiating gases and soot.

## 5. RADIATION HEAT EXCHANGE MODELS

The basis for radiation heat exchange is the equation of radiant energy transfer Eq.(1). This equation has to be integrated over the electromagnetic spectrum to find the energy transfer in one direction. For the heat exchange in a flame all directions at each point have to be considered. Therefore Eq. (1) must be integrated over all solid angles ( $4\pi$  ster-

radians) in addition to integration over all wavelengths. In this paper we will discuss a number of different techniques for the evaluation of radiation heat exchange. The mathematical details will not be presented as these are available in refs. [24 - 30]. The verifications we will present later on refer to axi-symmetrical systems. Therefore we mainly restrict ourselves to axi-symmetrical models.

#### AA: Zone method

The Zone method developed by Hottel and Cohen [31] is a method in which the furnace chamber and walls are divided in several zones. The exchange between each zone pair is calculated from the equation of radiant energy transfer. So-called exchange areas are available from tables [8]. The exchange areas refer to fixed zone sizes for a constant absorption coefficient. Therefore the Zone method cannot easily be combined with a spectral emission/absorption model in which absorption coefficients vary with temperature. If one wants to change the zone size one needs to change the exchange areas as well. Coarse zoning is a problem associated with the Zone method. In principle the Zone method is not limited to coarse zoning, however, the calculation of exchange between a large number of zones as would be necessary for direct coupling of the Zone method with a prediction procedure for fluid flow and combustion renders the Zone method computationally undesirable. The Zone method is considered a very accurate method when the zone sizes are small and the absorption coefficients are constant throughout the furnace. Johnson [11] developed a computer programme for the Zone method in which the furnace has been divided in 3 radial and 17 axial zones. The programme can be used with the emission/absorption models A, B and C of the previous section.

#### BB: Two-flux Schuster-Schwarzschild model

In a flux model the exact integro-differential equation (= Eq. (1) integrated over all wavelengths and all solid angles) of radiant energy transfer is replaced by approximate differential ones. Schuster [32] and Schwarzschild [33] developed a two-flux model in Cartesian coordinates. We developed a model in cylindrical coordinates [28]. It is assumed that the intensity  $I$  in fig. 2 is constant over the upper hemisphere ( $0 \leq \theta \leq \frac{\pi}{2}$ ) and constant over the lower hemisphere ( $\frac{\pi}{2} \leq \theta \leq \pi$ ). A discontinuity in the intensity distribution occurs at the interface between both hemispheres. Two partial differential equations are obtained by integrating separately over the upper and lower hemisphere. These differential equations are normally solved as ordinary ones by standard finite difference techniques. One obtains radiant heat fluxes in positive and negative radial direction at the chosen gridpoints in the furnace volume and at the furnace walls. The production of radiative heat per unit volume can be calculated as well at each grid point. These radiative heat production terms enter the differential energy balances, in which convective, diffusional and radiant heat fluxes are considered simultaneously, as source terms of energy. Therefore this model is well suited to be combined with prediction procedures for fluid flow and combustion. The same is true for the following models. All the emission/absorption models of the previous section can be used in combination with this and the following heat exchange models. The boundary conditions at walls are formulated as: leaving flux is equal to emissivity of wall times black body emissive power of wall plus reflectivity of wall times arriving flux. At the axis of an axi-symmetrical furnace system the net flux equals zero. These boundary conditions can be written for each gas or for each spectral region of the applied emission/absorption model.

#### CC: Two-flux Milne-Eddington model

The procedure to obtain the equations for the Milne-Eddington model [34, 35] differs from the procedure for the Schuster-Schwarzschild model. Gibson and Manahan [36] derived the two-flux equations in cylindrical coordinates. The equations for both two-flux models are very similar.

#### DD: Four-flux model

The reasons for our development of a four-flux model are:

1. the possibility to calculate radiant heat fluxes in the axial direction, which is important to account for the axial temperature gradients in a flame,
2. a better description of the intensity distribution around a point can be made, which will lead to a more accurate calculation of the heat fluxes.

The intensity around a point is assumed to be constant over  $\pi$  steradians in respectively (see fig. 2) positive radial direction, negative radial direction, positive axial direction and negative axial direction. Four partial differential equations are obtained by integrating the equation of transfer over  $\pi$  steradians separately for each coordinate direction. For the solution procedure use has been made of a central finite difference scheme. As the equations are coupled to some extent the solutions are obtained iteratively. Radiant heat fluxes in the four coordinate directions are obtained at the chosen grid points.

#### EE: Six-flux model

The two- and four-flux models have been developed for axi-symmetrical systems. For a Cartesian system a six-flux model is needed to calculate the heat fluxes in the six (positive and negative) coordinate directions. The intensity around a point is assumed to be constant over  $\frac{\pi}{3}$  steradians in each coordinate direction. Six partial differential equations are obtained by integrating the equation of transfer separately for each coordinate direction. In this model several improvements compared to the previous flux models have been included. In the two- and four-flux models the partial differential equations are solved as ordinary ones. When no proper account is taken of the direction of travel of individual radiation beams contributing to the heat flux in a certain

direction. In the six-flux model the heat flux in a point is a function of all the radiation beams through this point. Even if the major heat transfer is in an oblique direction relative to the main coordinate lines no special problems occur. The most favourable finite difference scheme can be chosen dependent on step sizes (distances between grid points) and absorption coefficients. Of course similar improvements could be incorporated in the two- and four- flux models, but we decided to develop the next model.

#### FF: CID-5 model

A limitation in the flux models is the assumption about the intensity distribution around a point. The solid angle of  $4\pi$  steradians is divided into a number of smaller solid angles in which the intensity is constant. Then discontinuities in the intensity distribution exist at the interfaces between the smaller solid angles. However, within a flame the discrete radiation beams form more or less a continuous pattern as a function of the spherical angles. For the CID-5 model we assume a continuous intensity distribution; 5 parameters are needed in an axi-symmetrical system. In ref. [28] it is proven that the chosen distribution can approach practical intensity distributions better than is possible with the four-flux distribution. The solid angle of  $4\pi$  steradians is integrated separately over  $\frac{2}{3}\pi$  steradians in each coordinate direction, namely positive and negative radial, axial and tangential direction. Six partial differential equations are obtained. Because of symmetry two of these are identical. In the CID-5 model many of the improvements mentioned for the six-flux model have been incorporated. As cylindrical systems are much complexer than Cartesian systems some of the directional effects have been omitted.

#### GG: CID-6 model

The same intensity distribution as for the CID-5 model can be used to build a radiation heat transfer model that is valid in a three-dimensional furnace where the coordinate system is Cartesian. In this model all the directional effects mentioned for the six-flux model can be incorporated.

### 6. EXPERIMENTS

Flames from simple burner geometries are produced with natural gas, propane and fuel oil in an approximately cylindrical furnace with an equivalent diameter of 2.22 m and a length of 6.29 m. These flames, of which a number combust throughout the length of the furnace, produce steep axial and radial temperature and concentration gradients, which should strongly test any radiation model. Two of the gas flames investigated will be used for the verification of the radiation models. In fig. 6 the flame shapes of both flames are shown. The first flame is a jet flame with a length of approximately 4.3 m. In this flame the gas temperatures vary between 350 K and 1600 K with several minima and maxima in axial and radial direction. As well steep concentration gradients are produced. The second flame is a short bulbous flame, almost completely burnt out within 0.5 m from the burner tip. For this flame the gas temperatures vary between 1000 K and 1800 K. The steepest gradients in gas temperature and concentrations occur close to the burner. The thermal input of both flames is about 3 MW.

Measurements of the heat flux to 17 cooling loops are taken for a large number of flames. In addition for each of the flames, measurements are made of hemispherical radiation flux to the walls, intensity of radiation, gas and wall temperature, concentration of chemical species and solids, flow field, etc. The incident radiation flux at the furnace wall is measured by a hemispherical radiometer, which is traversed at the furnace wall along the flame axis. The hemispherical radiometer accepts radiation from a hemisphere ( $2\pi$  steradians), while the narrow angle radiometer accepts radiation from only approximately  $0.000007\pi$  steradians. The latter instrument is traversed in steps across the flame through the flame axis. The measurements of radiation intensity start with the narrow angle radiometer looking from a short distance at a target of high emissivity. By withdrawing the radiometer from the target more flame gases are between the radiometer and the target. At several positions along the length of the flame traverses are made through the flame. The radiation intensities are caused by flame radiation when a cold target is used and by target radiation in addition to flame radiation when a hot target is used. Full details about the trials and the measurements are available in ref. [1]. In subsequent sections relevant experimental results will be presented.

### 7. VERIFICATION OF EMISSION/ABSORPTION MODELS

A first test on the emission/absorption models is predicting measured emissivities. In fig. 7 the results are shown. The gray gas models (A) are not accurate; the dependency of emissivity on gas temperature is not predicted. The one clear/two gray gas model (B) becomes increasingly inaccurate at pressure path lengths above 0.6 bar.m. Deviations above 10% exist at pressure path lengths higher than 1.2 bar.m. The four gray gas model (C) and the spectral model (D) predict measured emissivities very accurate.

A second test on the emission/absorption models is the agreement found comparing calculated and measured radiation intensities. The intensity calculations are started at the target, where the intensity equals the black body intensity of the target. A stepsize  $x$  of 0.1 m is taken and after each calculation  $x=0$  in Eqs. (17) and (22) is moved by the stepsize. So complete traverses of intensity are obtained from the target through the flame axis to the opposite wall. In fig. 8 distributions of temperature and partial pressures at a distance of 2.035 m from the burner wall are shown for flame I of fig. 6. In figs. 9 and 10 intensity predictions are compared with measurements. In fig. 11 distributions of temperature and partial pressures at a distance of 0.370 m from the burner wall are shown for flame II of

fig. 6. In fig. 12 intensity predictions are compared with measurements. Fig. 13 shows predicted and measured intensities for flame II at 4.25 m from the burner wall, where the distributions of temperature and concentrations are rather flat. Many more intensity predictions have been made using models A, B, C and D [28]. The gray gas models (A) are not very accurate; they do not predict the correct shape of the measured intensity distributions. The one clear/two gray gas model (B), the four gray gas model (C) and the spectral model (D) do not differ much in accuracy. Very severe tests on these models in regions with steep temperature and concentration gradients demonstrate that deviations up to 40% between the model predictions and the measurements can occur. The larger deviations develop when the predictions have progressed beyond the flame axis, which indicates that absorption of radiation emitted at high temperatures is not correctly predicted when the absorption occurs at low temperatures. With the models B, C and D accurate predictions are obtained, when the temperature and concentration distributions are rather uniform.

## 8. VERIFICATION OF RADIATION HEAT EXCHANGE MODELS

In figs. 14 and 15 predictions of incident radiative heat flux at the wall are compared with experimental results. The CID-5 model produces quite good results for flame I of fig. 6. In fact the same is true for the Zone method and the four-flux model. It is surprising that the inaccurate gray gas models and the more accurate one clear/two gray gas model produce similar results. However, gas volume elements contribute to the wall heat flux in different ways as is indicated by figs. 9 and 10. For flame II of fig. 6 the predictions of wall heat fluxes are shown in fig. 15 for the Zone method and the four-flux model. The larger deviations between measurements and predictions occur over the first part of the furnace near the burner end. However, in this part of the furnace the intensity predictions deviated as well from the measurements; so probably the deviations of fig. 15 are caused by the emission/absorption model applied.

As the comparisons between measurements and predictions are not conclusive about the accuracy of the heat exchange models theoretical investigations have been executed. A numerical solution and an exact Bessel function solution of the two-flux Schuster-Schwarzschild equations agree. The two-flux models, the four-flux model and the CID-5 model have been compared with the Zone method for theoretical test cases for which the Zone method produces accurate heat fluxes [28]. To summarize these investigations one can state:

- two-flux models do not predict accurate radial heat fluxes of flames with steep axial gradients
- the four-flux model is more accurate than the two-flux models
- the CID-5 model is more accurate than the four-flux model
- the two-flux, four-flux and CID-5 models can easily be combined with prediction procedures for fluid flow and combustion
- the CID-5 model accurately predicts local radiative heat production
- the CID-5 model and the Zone method are of comparable accuracy, however, the Zone method is problematic in combination with a prediction procedure for fluid flow and combustion, in combination with a spectral model for emission/absorption and in flames with high absorption coefficients.

## 9. CONCLUSIONS

Several emission/absorption models have been developed and verified. The one gray gas models are inaccurate, while the one clear/two gray gas model is inaccurate at higher pressure pathlengths. The four gray gas model and the spectral model predict measured emissivities very accurately. When no steep gradients in temperatures and concentrations exist, the one clear/two gray gas model, the four gray gas model and the spectral model predict measured radiation intensities from relatively large gas flames accurately. The deviations between measured and predicted intensities increase when the gradients become steeper, which is attributed to less accurate prediction of absorption in low temperature regions of radiation emitted in high temperature regions of the flame. We recommend our spectral model, as it is based more on fundamentals than the other models. A spectral model for mixtures of gases and soot is proposed, which can be used for flames with any composition of radiating components.

A number of radiation heat exchange models for cylindrical systems have been developed and verified while for Cartesian systems models have been developed. Two-flux models do not predict accurate radial heat fluxes for flames with steep axial gradients. The CID-5 model predicts heat fluxes quite accurately. The four-flux model is slightly less accurate. The CID-5 model and the Zone method are of comparable accuracy, however, the Zone method is problematic in combination with a prediction procedure for fluid flow and combustion, in combination with a spectral model for emission/absorption and in flames with high absorption coefficients. The flux- and CID-models can easily be combined with prediction procedures for fluid flow and combustion. The CID-5 model accurately predicts local radiative heat production. The deviations between measured and predicted heat fluxes can be partly ascribed to the emission/absorption model applied. For Cartesian systems a six-flux model and a CID-6 model are proposed, in which some definite improvements above the two- and four-flux models have been incorporated. Similar improvements have been introduced in the CID-5 model.

The information in this paper is not only relevant with respect to furnace flames, but as well for radiation heat exchange in flares, fires, buildings and the atmosphere.

## 10. REFERENCES

- [1] Michelfelder, S., and Lowes, T.M., Report on the M2-trials, Doc. nr. F36/a/4, I.F.R.F., IJmuiden, 1974.



- [2] Pai, B.R., Bartelds, H., and Michelfelder, S., Report on the M3-trials, Part A: cold heat sink. An experimental investigation on the influence of operational and design variables on heat transfer to the furnace hearth, Doc. nr. F36/a/6, I.F.R.F., IJmuiden, 1975.
- [3] Bartelds, H., Lowes, T.M., Michelfelder, S., and Pai, B.R., The prediction of heat flux distribution in furnaces and its experimental testing, Combustion Institute European Symposium (ed. F.J. Weinberg), 113, 680-685, Academic Press, London, 1973.
- [4] Michelfelder, S., Richter, W., Pai, B.R., and Bartelds, H., Uebersicht über Berechnungsmethoden zur Ermittlung des Wärmeübergangs in Brennkammern, VDI-Berichte 246, Düsseldorf, 1975.
- [5] Pai, B.R., Michelfelder, S., and Spalding, D.B., Prediction of furnace heat transfer with a three-dimensional mathematical model, Int. J. Heat Mass Transfer, 21, 571-580, 1978.
- [6] Lowes, T.M., and Heap, M.P., Emission/attenuation coefficients of luminous radiation, Second Members Conference, I.F.R.F., IJmuiden, 1974.
- [7] Viskanta, R., Radiative transfer and interaction of convection with radiation heat transfer, Advances in Heat Transfer (eds. Irvine, T.F. and Hartnett, J.P.), 3, 175-252, Academic Press, New York, 1966.
- [8] Hottel, H.C., and Sarofim, A.F., Radiative Transfer, McGraw-Hill, New York, 1967.
- [9] Penner, S.S., Quantitative Molecular Spectroscopy and Gasemissivities, Addison-Wesley, Reading, Mass., 1959.
- [10] Tien, C.L., Thermal radiation properties of gases, Advances in Heat Transfer (eds. Hartnett, J.P., and Irvine, T.F.), vol. 5, 253-324, Academic Press, New York, 1968.
- [11] Johnson, T.R., Application of the zone method of analysis to the calculation of heat transfer from flames, Ph.D. thesis, Sheffield University, 1971.
- [12] Hadvig, S., Gas emissivity and absorptivity: A thermodynamic study, J. Inst. Fuel, 43, 129-135, 1970.
- [13] Lee, R.H.C., and Happel, J., Thermal radiation of methane gas, Ind. and Eng. Chem. Fundamentals, vol. 3, no. 2, 167-176, 1964.
- [14] Ullrich, W., Sc. D. Thesis in Chemical Engineering, M.I.T., Cambridge, Mass., 1953.
- [15] Perry, J.H., Chemical Engineers' Handbook, McGraw-Hill, New York, 1963.
- [16] Sparrow, E.M., and Cess, R.D., Radiation Heat Transfer, Brooks/Cole, Belmont, USA, 1970.
- [17] van Kuijk, R.M., and Spanjers, Th.H., De overdracht van de in een vuurhaard van een stoomketel ontwikkelde warmte aan het door de verdamperpijpen stromende koelwater, Presentation to "Nederlandse Vereniging voor Vlamonderzoek", I.F.R.F., IJmuiden, 1973.
- [18] Toor, J.S., and Viskanta, R., Experiment and analysis of directional effects on radiant heat transfer, Journal of Heat Transfer, Trans. A.S.M.E., 459-466, november 1972.
- [19] Toor, J.S., and Viskanta, R., A critical examination of the validity of simplified models for radiant heat transfer analysis, Int. J. Heat Mass Transfer, 15, 1553-1567, 1972.
- [20] Edwards, D.K., and Balakrishnan, A., Volume interchange factors for non-homogeneous gases, Journal of Heat Transfer, Trans. of the A.S.M.E., 181-188, may 1972.
- [21] Siegel, R., and Howell, J.R., Thermal Radiation Heat Transfer, Vols. I, II and III, N.A.S.A., Washington, D.C., 1971.
- [22] Beér, J.M., and Claus, J., The "traversing" method of radiation measurement in luminous flames, J. Inst. Fuel, 35, 437-443, 1962.
- [23] Kunitomo, T., Luminous flame emission under pressure up to 20 atm., Heat Transfer in Flames (eds. Afgan, N.H., and Beér, J.M.), 18, 271-281, Scripta Book Company, Washington, D.C., 1974.
- [24] Michelfelder, S., Bartelds, H., Lowes, T.M., and Pai, B.R., Berechnung des Wärme-flusses und der Temperaturverteilung in Verbrennungskammern, Brennst.-Wärme-Kraft, 26, 1, 5-13, 1974.
- [25] Lowes, T.M., Bartelds, H., Heap, M.P., Michelfelder, S., and Pai, B.R., Prediction of radiant heat flux distribution, Heat Transfer in Flames (eds. Afgan, N.H., and Beér, J.M.), 10, 179-190, Scripta Book Company, Washington, D.C., 1974.
- [26] Bartelds, H., Zero and one-dimensional furnace models and their limitations, Course on performance prediction of furnaces and combustion chambers, jointly given by the International Flame Research Foundation, IJmuiden, and Imperial College, London, at Noordwijkerhout, 1976.
- [27] Bartelds, H., Lowes, T.M., Michelfelder, S., and Pai, B.R., A finite difference method for the prediction of radiation heat exchange, applicable to various furnace geometries, Proceedings of the Second European Symposium on Combustion, Orléans, 1975.
- [28] Bartelds, H., Radiative heat transfer in enclosures, Progress report no. 18 contract no. 68-02-0202, Development of combustion system design criteria for the control of nitrogen oxide emission from heavy oil and coal flames, Environmental Protection Agency, Durham, U.S.A., 1975.
- [29] Bartelds, H., Validity of radiation models, Course on performance prediction of furnaces and combustion chambers, jointly given by the International Flame Research Foundation, IJmuiden, and Imperial College, London, at Noordwijkerhout, 1976.
- [30] Lowes, T.M., Bartelds, H., Heap, M.P., Michelfelder, S., and Pai, B.R., Prediction of furnace heat transfer, presented at the 15th International Symposium of the Combustion Institute at Tokio, 1974.
- [31] Hottel, H.C., and Cohen, E.S., Radiant heat exchange in a gas-filled enclosure: allowance for non-uniformity of gastemperature, A.I.Ch.E. Journal, 4, 3-14, 1958.
- [32] Schuster, A., Astrophys. J., 21, 1-22, 1905.
- [33] Schwarzschild, K., Nachr. Akad. Wiss. Göttingen, Math. - Physik. Kl. 1, 41, 1906; Sitzber. Preuss. Akad. Wiss., Physik. - Math. Kl. 1183, 1914.
- [34] Milne, E.A., in Handbuch der Astrophysik, G. Eberhard et al., eds., 3, part 1, 65-255, Springer, Berlin, 1930.
- [35] Eddington, A.S., The internal Constitution of Stars, Dover Publ., New York, 1959.
- [36] Gibson, M.M., and Monahan, J.A., A simple model of radiation heat transfer from a cloud of burning particles in a confined gasstream, Int. J. Heat Mass Transfer, 14, 141-147, 1971.

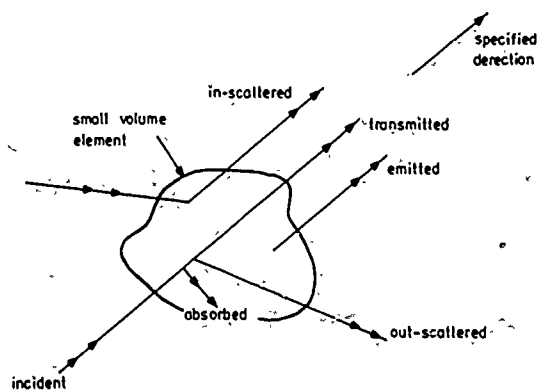


Fig.1: Radiant energy balance in a specified direction

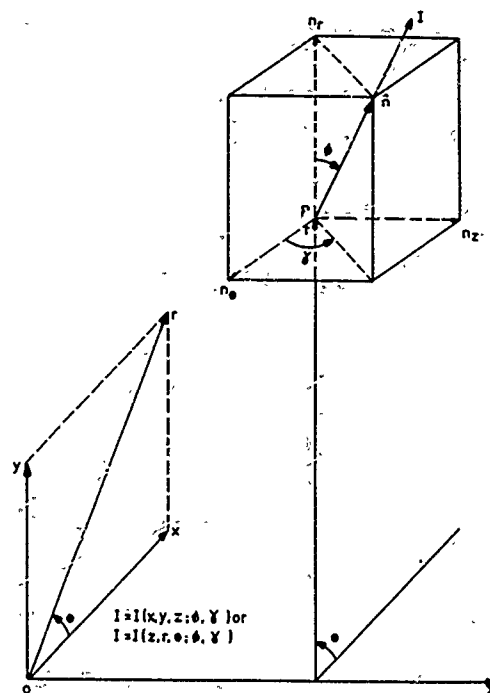


Fig.2: Coordinate systems defining position and direction of intensity

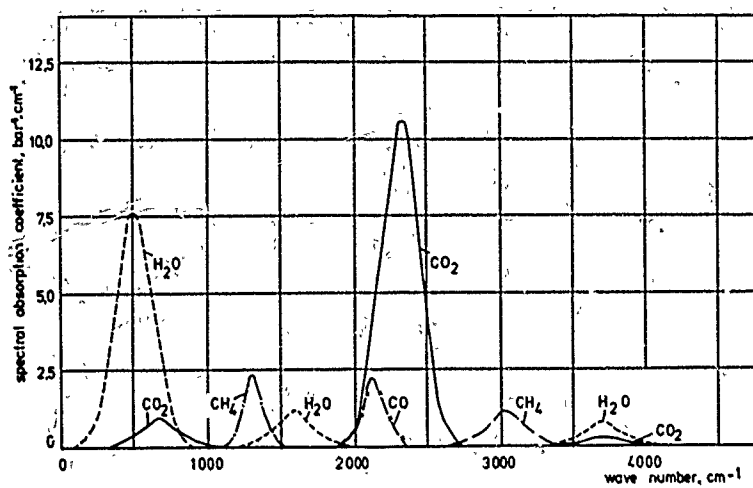


Fig.3: Idealized distribution of spectral absorption coefficients

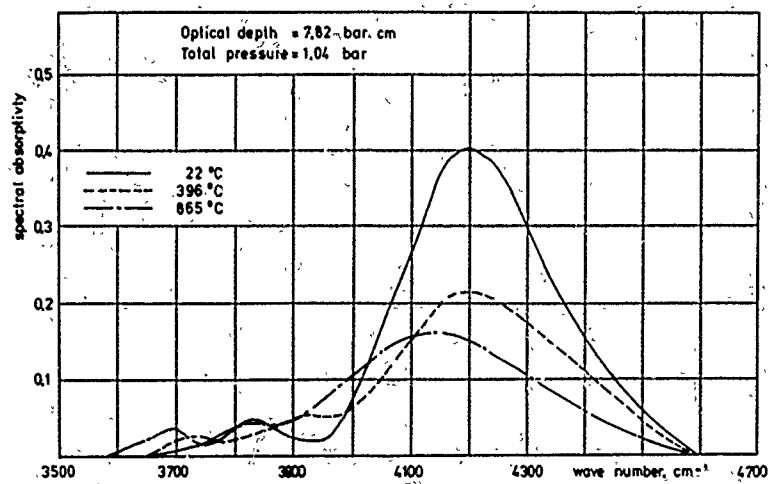


Fig.4: Effect of temperature on the 2.37-micron band of the methane spectrum.

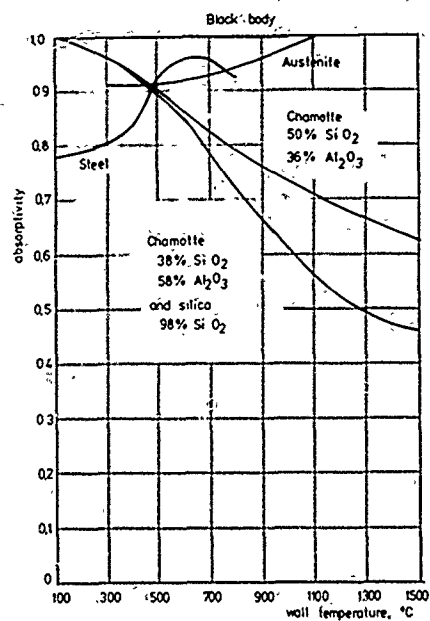


Fig. 5 Absorptivity as a function of wall temperature.

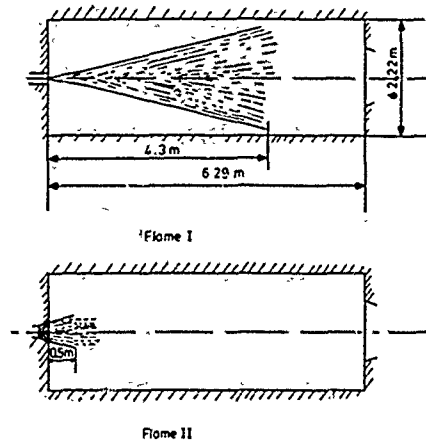


Fig. 6 Shapes of gas flames

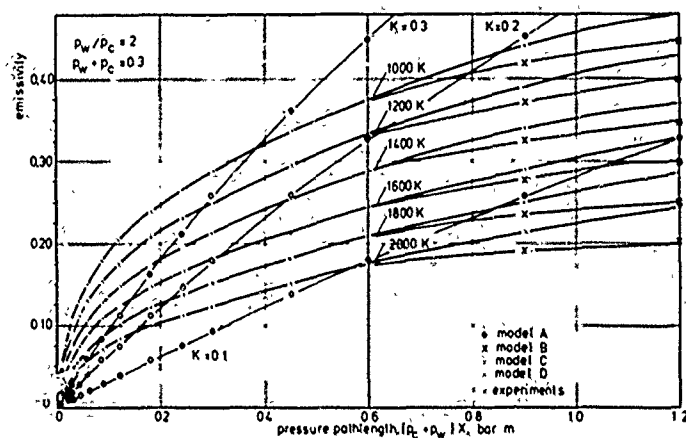


Fig. 7 Emissivity of the combustion products of methane

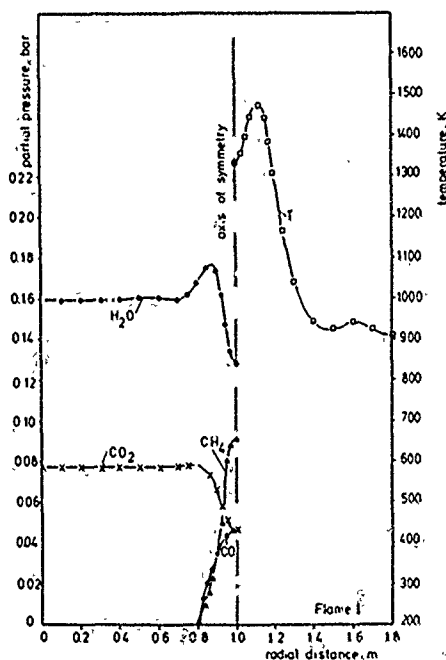


Fig. 8 Partial pressures and temperatures at an axial distance of 2.035 m



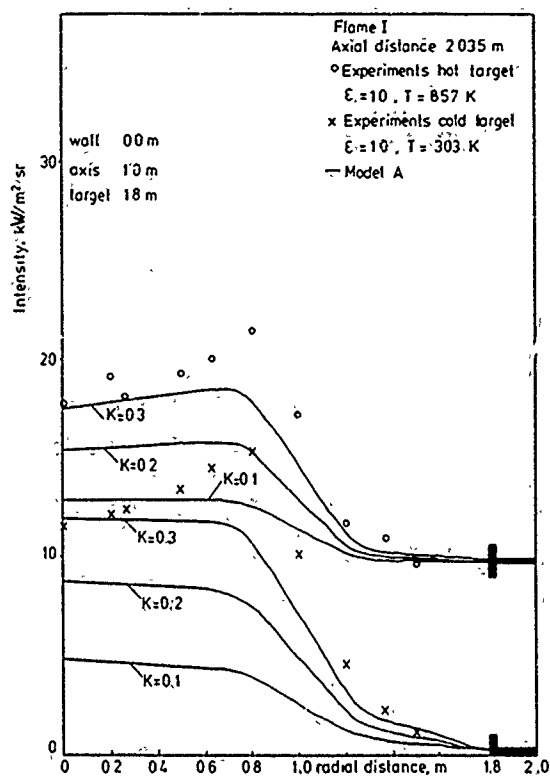


Fig.9: Prediction of narrow angle traverses using different gray gas attenuation coefficients.

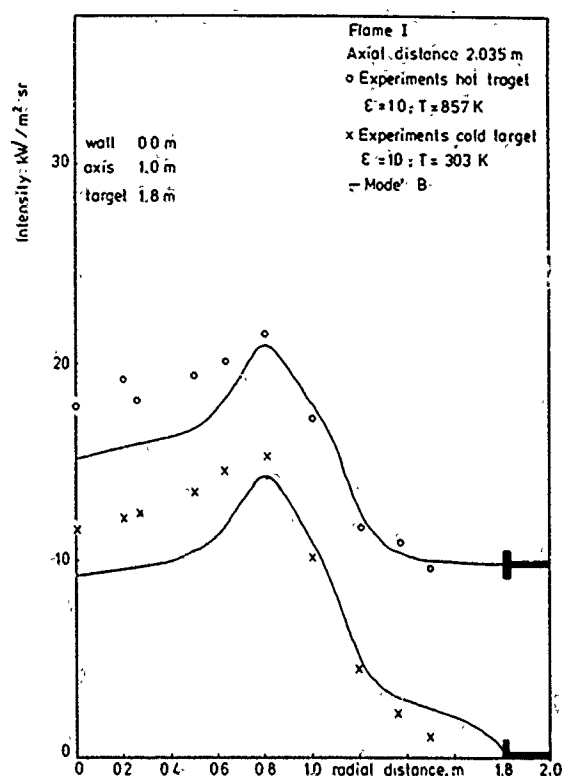


Fig.10: Prediction of narrow angle traverses using a 1 clear/2 gray gas attenuation formulation.

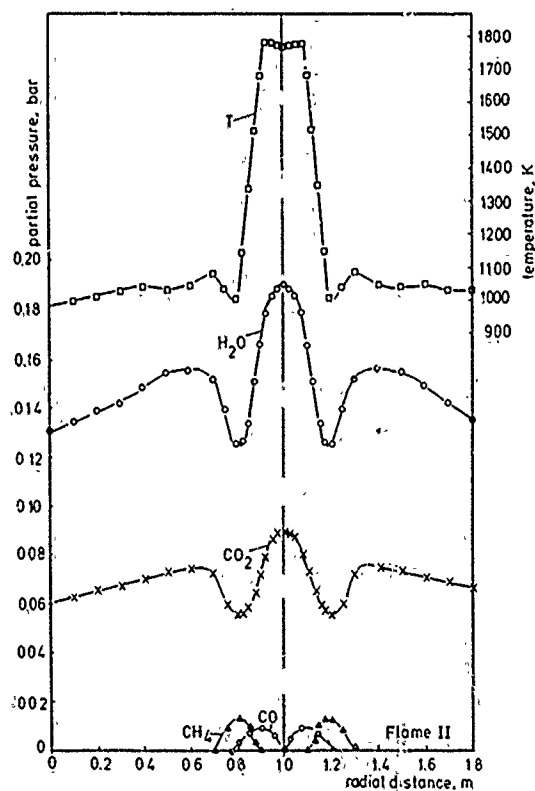


Fig.11: Partial pressures and temperatures at an axial distance of 0.370 m.

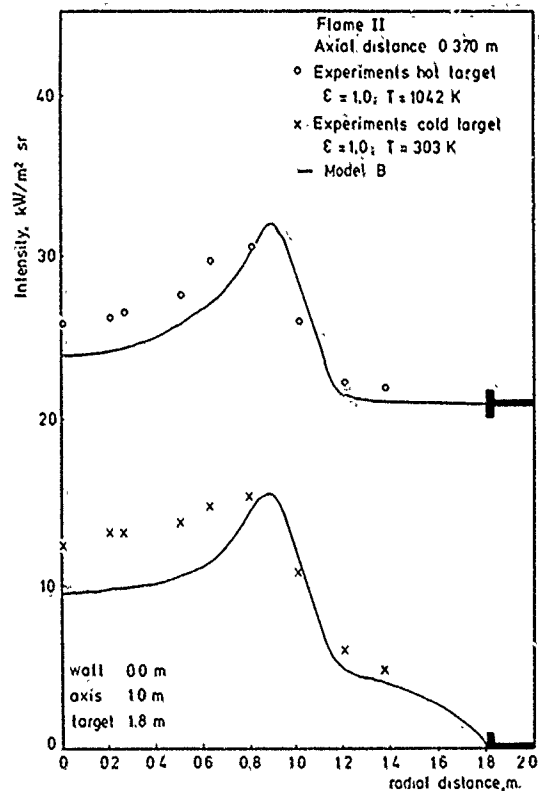


Fig.12: Prediction of narrow angle traverses using a 1 clear/2 gray gas attenuation formulation

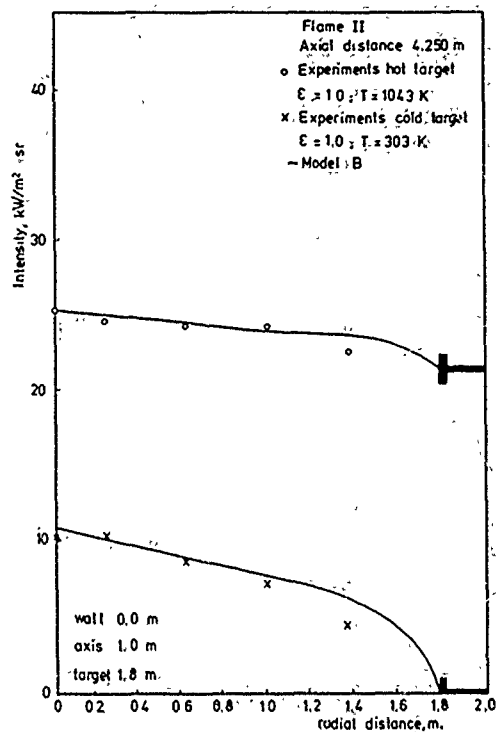


Fig.13: Prediction of narrow angle traverses using a 1-clear/2 gray gas attenuation formulation.

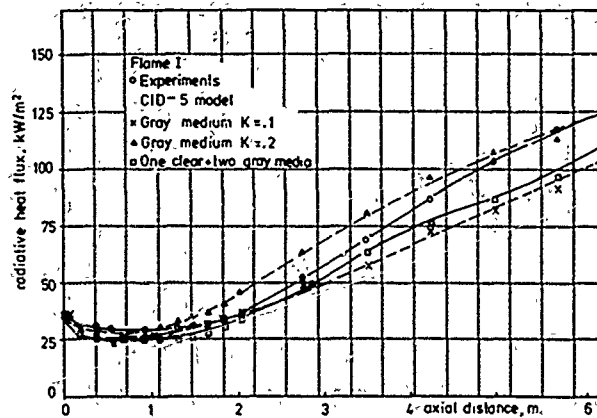


Fig.14: Comparison of predictions by the CID-5 model with experimental results.

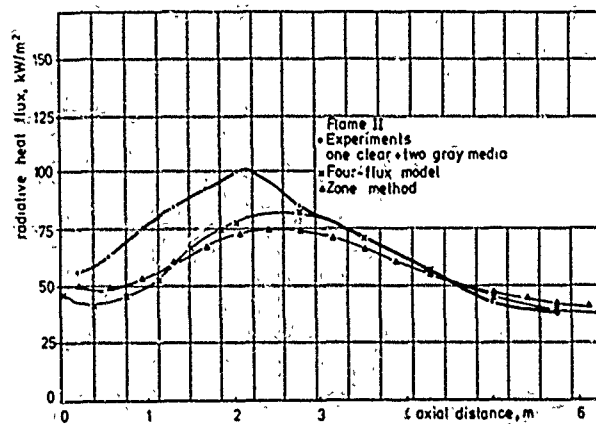


Fig.15: Comparison of predictions by zone method and four-flux model with experimental results.

## DISCUSSION

C.H. Priddin, UK

You mentioned briefly the Zone type method, but dismissed it because of the difficulty in combining it with a finite-difference code. There are conditions where radiation can be "decoupled" from the flow, and compatibility is then no problem. Would you recommend the use of Zone methods in this situation?

Author's Reply

The following problem areas can be mentioned with respect to the Zone method:

- coupling with finite difference procedure causes difficulties
- not well suited for complex furnace geometries
- for high absorption coefficients as occur in practical flames very small zone sizes are needed
- for flames with temperature gradients small isothermal zones are needed
- when a large number of small zones is used computer time and storage will be high
- not flexible when zone sizes are to be changed
- when absorption coefficients vary over furnace volume exchange areas cannot be determined accurately; this makes the Zone method less suited for flames with soot, for flames with concentration gradients and in combination with spectral emission/absorption model for flames with temperature gradients.

If the above mentioned problem areas do not exist the Zone method can be recommended. The Zone method produces accurate heat fluxes for certain well defined theoretical test cases. Then the Zone method can be used as a standard for the flux and CID models.

However, if the problem areas do exist I would recommend to consider radiation heat exchange models of the finite difference type. But then one has to take advantage of the full capacities of the latter models, which in practice is often neglected.

A.K. Varma, US

In turbulent flames there are significant interactions between the radiation emission and absorption and the turbulent fluctuations of temperatures and species.

Have you considered taking these effects into account?

Author's Reply

The differences between measurements and predictions of intensities have been investigated. One of the possible reasons for the differences are temperature and concentration fluctuation effects. Temperature and concentration both affect emission ( $\epsilon \sigma T^4$ ), but as the effect of temperature and concentration on emissivity  $\epsilon$  is small compared to the effect of temperature on  $T^4$ , temperature is the most important parameter for the emission. When temperature rises emissivity falls down which will reduce the effects of fluctuations on emission.

We assumed that the temperature at a point on a traverse varies between the minimum and maximum measured temperature on that traverse. A stepwise variation from a maximum value via the average value to a minimum value is used in such a way that the temperature is 25% of the time on the maximum value, 50% of the time on the average value and 25% of the time on the minimum value. The ratio between  $(T^4)$  average and  $(T_{\text{average}})^4$  has been calculated for all the traverses. One would expect the above strong temperature fluctuations only in the regions of steep temperature gradients in axial and radial direction. Only on a small part of the measured traverses the emission will increase significantly. The predicted intensities can be a few percent higher if temperature fluctuations are taken into account. Fluctuations do not explain the larger deviations between measurements and predictions of intensity. As well fluctuations do not explain the systematic behaviour of these deviations; measurements are below the predictions at the axis of the flame while at the wall the measurements are far above the predictions.

J.B. Michel, Ne

Can CID type model predict the spectral distribution of radiative intensity and if yes, do you envisage comparisons with measured spectral data?

Author's Reply

In principle the spectral emission/absorption model can predict spectral intensities. However the absorption coefficients have been determined using measured total (integrated over the spectrum) emissivity data. With good enough spectral information the spectral model can be tested and if necessary optimized.

However the CID models predict heat fluxes, which are intensities integrated with respect to solid angle. The CID models can be combined with spectral emission/absorption models. These combinations can be used to predict spectral radiative heat fluxes.

We envisage comparisons with measured spectral data only when enough (financial) interest exists.

F.C. Lockwood, UK

In our work with l'Air Liquide, France, on oxygen enriched flames we have found that the existing grey plus clear gas correlations for the absorption coefficient are not satisfactory at the very high temperatures we experience. Do you know of a correlation valid up to, say 2800 K?

**Author's Reply**

The weighting factors and the absorption coefficients for the one clear/two grey gas model and the four grey gas model have been determined using measured total emissivity data (as given in literature) for the temperature range from 1000 to 2000 K. For the spectral model the black body factors are based on black body functions. The absorption coefficients are based again on measured total emissivity data.

Some weighting factors of the one clear/two grey gas model and the four grey gas model go negative at 2800 K, which is physically unrealistic. Therefore the constants of Table II and III would need to be adjusted for higher temperature levels.

For the spectral model these problems do not exist. The black body factors are always positive. As a first approximation the information in Table VI could be used to calculate emissivities at 2800 K. A better solution is to extend Table VI to, say, 2200, 2400, 2600 and 2800 K.

The black body factors and absorption coefficients can then be expressed in polynomials in a similar way as in the paper.

# ASSESSMENT OF AN APPROACH TO THE CALCULATION OF THE FLOW PROPERTIES OF SPRAY-FLAMES

by  
Y. El Banhawy and J.H. Whitelaw  
Mechanical Engineering Department, Fluids Section,  
Imperial College of Science and Technology, LONDON, U.K.

## ABSTRACT

A method for the calculation of the local properties of spray flames is described briefly and its capabilities and limitations appraised by comparing calculated results with measurements. The method solves elliptic differential equations representing the conservation of mass, momentum, enthalpy and species concentrations in finite difference form. In addition, Lagrangian equations for the droplet motion and thermal balance are solved for finite ranges of droplet size. A two-equation turbulence model, a combustion model based on mean mass-fraction equations for fuel and oxidant and a four-flux radiation model are used. The droplet model assumes that the evaporating droplets act as distributed point sources of fuel vapour. The merits of the method are quantified by comparison with measurements obtained for three different spray flame geometries. The assumption of representing the spray by a finite number of size ranges has been also examined in the present work and the results indicate that the importance of this number is related to the spray type and the aerodynamic features of the flow close to the spray.

## NOMENCLATURE

$C_p$	specific heat under constant pressure ( $J/kg^{\circ}K$ )
$i$	stoichiometric oxygen requirements
$k$	turbulent kinetic energy ( $m^2/s^2$ )
$K_f$	thermal conductivity of gases ( $J/m^{\circ}K \cdot kg$ )
$L$	fuel latent heat of vaporization ( $J/kg$ )
$\bar{m}_{fu}$	fuel mass fraction
$\bar{m}_{ox}$	oxygen mass fraction
$\bar{m}_{min}$	the minimum value of $\bar{m}_{fu}$ and $\bar{m}_{ox}/i$
$m_p$	mass of droplet ( $kg$ )
$T$	temperature ( $^{\circ}K$ )
$T_{SAT}$	fuel saturation temperature ( $^{\circ}K$ )
$U_{p,i}$	droplet velocity in the $i$ -direction ( $m/s$ )
$\mu$	viscosity ( $kg/m \cdot sec.$ )
$\rho$	density ( $kg/m^3$ )
$\sigma$	Stefan-Boltzman constant
$\epsilon$	dissipation rate of the turbulent kinetic energy

### Subscripts

$f$	gas phase
$p$	droplet
$v$	vapour
$eff$	effective (including the effects of turbulence)

## 1. INTRODUCTION

In reference 1, the authors described a method for the calculation of the flow properties of a confined kerosene-spray flame. A preliminary assessment was obtained by comparison with the measurements of reference 2, obtained with a hollow-cone spray, and it was concluded that the number of size ranges was of little importance. In addition, discrepancies of more than  $400^{\circ}K$  were observed in temperature and were attributed to uncertainties in initial conditions and in the turbulence model. The present paper, reports calculated results obtained with an improved version of the method and makes comparisons with measurements obtained with both hollow-cone sprays and twin-fluid atomizers.

The calculations again made use of the two-equation turbulence model but, on this occasion, the combustion model has been changed from that of reference 1, which was appropriate only to diffusion flames, to that of reference 3 which can accommodate diffusion, premixed and arbitrary fuelled flames, albeit with the limitations imposed by source terms dependent upon mean mass fractions of fuel and oxidant. In addition, and although of secondary importance to gas turbine conditions, a coupled four-flux radiation model has been incorporated. The influence of the location of the grid nodes, necessary in the finite-difference procedure, has been investigated and suggests that the results presented here are not significantly affected by numerical features.

The purpose of the present work is to allow an appraisal of the calculation method over a wider range of fuel conditions and geometries than those of reference 1. The calculations are restricted to situations with comparatively small or zero preheat and the test is, as a result, more severe than required in practice.

The remainder of the paper is presented in three sections. The following section provides a brief statement of the equations solved and the boundary conditions used; the turbulence, combustion, droplet and radiation models are described briefly and assumptions indicated; the numerical scheme used to solve the equations is referenced and tests of the influence of grid locations described. The three test cases are described in the separate parts of section 3 and correspond to the measurements of references 4, 5 and 6; the results and corresponding discussion are presented in these three subsections. The paper ends with brief concluding remarks.

## 2. CALCULATION METHOD

As described in references 1 and 7, the equations representing conservation of mass, momentum, turbulence energy, dissipation rate, enthalpy and mean-species concentrations can all be written in the form:

$$\frac{\partial}{\partial x} (\rho U \phi) + \frac{1}{r} \frac{\partial}{\partial r} (r \rho V \phi) = \frac{\partial}{\partial x} (\Gamma \frac{\partial \phi}{\partial x}) + \frac{1}{r} \frac{\partial}{\partial r} (r \Gamma \frac{\partial \phi}{\partial r}) + S + S_d \quad (1)$$

This presumes that the mean flow is two-dimensional, axisymmetric and that turbulent diffusion can be represented by gradient assumptions and exchange coefficients,  $\Gamma$ . The source term,  $S$ , represents the generation or destruction of the dependent variable,  $\phi$ , by processes concerned only with the gas phase, and  $S_d$ , the generation or destruction due to the fuel droplets. The equation, with the boundary conditions and assumptions described in the following subsections, has been solved by the finite-difference procedure described in references 8 and 9.

### Boundary Conditions

The elliptic nature of the differential equations requires that each dependent variable, or its gradient, be specified on all sides of the solution domain. In the present case, wall and symmetry-line values were easily prescribed and zero-axial gradients were prescribed at downstream locations where this assumption did not influence the upstream calculated results.

Upstream flow boundary conditions are based on experimental information, where available, and on sensible guesses where not. The use of a sensible guess implies that its influence should be tested. In general, the flow boundary conditions for turbulence quantities are of secondary importance and are estimated on the basis of a mixing-length hypothesis. The values of the mean-velocity components are more important and specific comments will be made when the results are discussed. The initial droplet-size-distribution and injection velocity are also important and are also discussed in relation to the discussion of results.

### Turbulence model

The two-equation, effective-viscosity model used to represent the turbulence characteristics has been well documented and represents the simplest model appropriate to flows with recirculation. Higher-order models cannot be justified with the uncertainties introduced by the additional assumptions and particularly the combustion and droplet models. Equations for the turbulence energy and dissipation rate are solved in the form described, for example, in references 1 and 2, and the effective viscosity is assumed to have the form

$$\mu_t = C_D \cdot \rho k^2 / \epsilon$$

The "constant",  $C_D$ , and the other four "constants" required to represent aerodynamic features are identical to those of references 1 and 9. The exchange coefficient in the momentum equations has, therefore, the form

$$\Gamma = \mu_t / \rho$$

and in the enthalpy equation,

$$\Gamma = \mu_t / \sigma$$

where  $\sigma$  is an effective "Prandtl" number with a value of 0.9.

Consistent with the effective viscosity assumption and to minimize computer storage and run times, the dependent variables at the wall are linked to those at the first grid node from the wall by "wall functions" which presume the logarithmic law of the wall and are discussed in references 1 and 9.

### Combustion model

It is assumed that liquid-fuel droplets act as distributed sources of fuel which

evaporate to form a cloud of vapour and that, as a result, the combustion process can be regarded as gaseous. The transport and evaporation processes are represented by the droplet model and its influence on the S.-terms of the momentum, enthalpy and mean-species equations. The combustion process is represented by the model of reference 3 which presumes that the consumption of fuel is controlled by a turbulence-chemistry interaction i.e.

$$R_{fu} = 23.6 \left( \frac{v \cdot \epsilon}{k^2} \right)^{\frac{1}{2}} \cdot \frac{\epsilon}{k} \cdot \chi \cdot \bar{m}_{min} \cdot \rho \quad \text{kg/m}^3/\text{s}$$

where  $\chi$  is defined as the ratio between the local concentration of reacted fuel and the total fuel concentration, consequently

$$\chi = \frac{(1 - \bar{m}_{fu} - \bar{m}_{ox}) / (1 + i)}{(1 - \bar{m}_{fu} - \bar{m}_{ox}) / (1 + i) + \bar{m}_{fu}}$$

This combustion model can be used in arbitrary fuelled flames but is undoubtedly simplistic in its lack of direct consideration of the scalar fluctuations. It is, however, economic of computer storage and time and, in view of the additional uncertainties imposed by the droplet model, probably of acceptable precision.

The influence of density fluctuations, in combustions flows, is important and the present differential equations may be regarded as written in mass-weighted form, with the consequent assumption that the turbulence model is valid in the presence of these fluctuations. This implies that the calculated results should be compared with mass-weighted measurements and it is likely that the measured concentrations are close to mass-weighted.

#### Droplet model

The droplet-size distribution within the fuel spray is represented by a finite number of size ranges. The droplet-source terms,  $S_d$ , which provide the means for coupling the droplet and gas fields require, for their evaluation, the determination of the droplet location, size, temperature and velocity within the calculation domain. This is done by tracking the droplets representing different size ranges throughout their movement inside the calculation domain and consequently a Lagrangian framework is used to describe the droplet behaviour.

For each droplet size range, the momentum balance equation in the i-direction is written as

$$m_p \cdot \frac{dU_{p,i}}{dt} = \mu \cdot D_p \cdot U_{r,i} \cdot \frac{\pi}{6} \cdot C_D \cdot R_{e_i} \quad (2)$$

where  $R_{e_i}$  is the Reynolds number based on the droplet diameter,  $D_p$ , and the relative velocity,  $U_{r,i}$ .  $C_D$  is the drag coefficient and is calculated from the correlations given in reference 1. The mass transfer rate from the liquid to the gas phase, associated with evaporation, is given by

$$\dot{m}_p = 2\pi D_p \cdot \frac{k_f}{C_{p_f}} \cdot \ln(1+B) \cdot (1 + 0.28 R_{e_i}^{0.5})$$

where  $B = C_{p_v} (T_f - T_{sat}) / L$ . Also,

$$\dot{m}_p = -\frac{\pi}{6} \cdot \rho_p \cdot \frac{d(D_p^3)}{dt}$$

So that,

$$\frac{dD_p}{dt} = \frac{-2 k_f}{\rho_p \cdot C_{p_f}} \cdot (2 + 0.56 R_{e_i}^{0.5}) \cdot \ln(1+B) \cdot \frac{1}{D_p} \quad (3)$$

The droplet temperature during the preheating period is determined by solving the thermal balance equation for a droplet moving in a gas stream:

$$\frac{dT_p}{dt} = \frac{6}{D_p \cdot \rho_p \cdot C_{p_p}} \cdot \frac{k_f}{D_p} (2 + 0.56 R_{e_i}^{0.5}) \cdot (T_f - T_p) \quad (4)$$

The solution of the Lagrangian equations, 2, 3 and 4 provides the variation of droplet velocity, diameter and temperature in the time domain and a droplet tracking technique transfers this to the space domain. The droplet-source terms are obtained by calculating the loss or gain of the droplet mass, heat and momentum within each computational cell of the gas-field.

#### Radiation model

The present radiation model is based on the flux-model proposed by De Marco and Lockwood (10) where the directional dependence of the radiant intensity at a point, is approximated by a truncated Taylor series expression. The exact integro-differential radiation equation reduces to a set of approximate partial differential equations of the type described by equation 1. For axi-symmetric geometries and with the assumption

of an absorbing emitting non-scattering grey medium in local thermodynamic equilibrium, the equations can be written as

$$\frac{\partial}{\partial x} \left( \frac{1}{K} \cdot \frac{\partial R_x}{\partial x} \right) = \frac{4}{3} K (2R_x - R_r - \sigma T^4)$$

$$\frac{1}{r} \frac{\partial}{\partial r} \left( \frac{r}{K} \frac{\partial R_r}{\partial r} \right) = \frac{4}{3} K (2R_r - R_x - \sigma T^4)$$

where  $R_x$  and  $R_r$  are respectively the total axial and radial radiation fluxes and  $K$  is the absorption coefficient of the medium and has a calculated value of 0.3. The radiation energy contribution to the source term in the enthalpy equation is expressed as

$$S_H = (16/9) \cdot K \cdot (R_x + R_r - 2\sigma T^4)$$

### Numerical features

The droplet-gas coupling is incorporated in the numerical procedure as follows. An isothermal, droplet-free solution of the gas field is first obtained then droplet trajectories, size and temperature history are calculated, through the droplet-field equations, with known gas properties. The droplet source terms are then calculated and fed to the finite-difference form of equation 1 to obtain adjusted values for the dependent variables. These are used again in the solution of the droplet equations. This process of solving the gas-field equations followed by the droplet equations is repeated until all the equations are satisfied, see references 1-7.

The present numerical procedure is second-order accurate except when the Reynolds number of the computational cell is greater than 12. In such cases, an upwind-differencing scheme is used and is more likely to cause numerical errors if the streamlines do not orthogonally cross the finite-difference cells. These errors, which have the effect of introducing an additional "false-diffusion" into the equations, are dependent on the magnitude of the Reynolds number,  $U\Delta x/\nu$ , and therefore, can be minimized by reducing the characteristic dimension of the cell,  $\Delta x$ , at regions where the characteristic velocity  $U$ , is largely skewed to the orthogonal grid. For each of the sets of data described in the following section, calculations were performed to identify regions of high cell Reynolds number and the number of grid nodes and their locations were, accordingly, modified. Figure 1 shows a sample of the calculated results obtained with different arrangements of the grid nodes and corresponds to the isothermal mean-velocity measurements of reference 4, test case 1. The reported calculations of the present work were obtained with a grid composed of 25 x 25 nodes which provided the best compromise between computer storage, time and accuracy. The computing time for the reported calculations varied between 8 and 15 minutes of CDC 6600 time according to the number of size ranges considered and the flow features of each test case.

### 3. PRESENTATION AND DISCUSSION OF THE RESULTS

The present procedure has been applied for the prediction of the flow properties in the three flame geometries of references 4, 5 and 6. Details of the inlet conditions, experimental data and flame geometries corresponding to the three test cases are given in table 1 and figure 2. The calculated results for each test case were obtained with the upstream boundary conditions summarized in table 2.

#### Test Case 1

The experimental data of this test case, which were obtained with a rotating cup atomizer capable of producing a near-monosized spray, comprised measurements of the droplet size distribution within the spray and the droplet injection velocity. This allowed accurate representation of the droplet inlet conditions and reduced the uncertainties of the droplet model to those relating to the expression used to calculate the droplet evaporation rate. Supplementary experimental information regarding the upstream boundary conditions of the mean-velocity components and wall-temperature distributions were also available together with detailed measurements of air velocity within the combustor under isothermal conditions. Calculated results were obtained for the latter, as described previously, and were used to assess the accuracy of the present numerical procedure and the turbulence model. Therefore, the following comparison with the experimental data allows the present combustion model to be critically appraised.

Figure 3 shows the calculated and measured radial profiles of temperature, mass fractions of carbon dioxide ( $CO_2$ ) and oxygen ( $O_2$ ) at different axial distances along the combustion chamber. Also shown on the figure, for reference purposes, are the corresponding measured profiles of carbon monoxide (CO) concentration. The results of figure 3 show that the general features of the temperature and species concentrations are correctly predicted. However, discrepancies in the extent of chemical reaction and the corresponding temperature values are clearly indicated. At locations close to the combustion chamber wall, the  $O_2$  concentrations are under-predicted, by approximately 5%, with a consequent overprediction of the temperature values, where discrepancies of around 1000K can be observed. The accelerated consumption of oxygen, at this region, is attributed to deficiencies in the coupled turbulence/chemistry models and, to a lesser extent, to the boundary condition specifications. In the initial flame region,  $X/D < 0.3$ , and at radii corresponding to the maximum gradients in the measured temperature and species concentra-



tions, around  $R = 60$  mm the predicted profiles of  $O_2$  and  $CO_2$  are seen to be slightly shifted towards smaller radii which indicates an underestimation of the chemical reaction rates. With the presumed dependence of the reaction rate on the turbulent kinetic energy and its dissipation rate, this result is consistent with the underprediction of the central recirculation zone at this region which is evident in figure 1.

The large discrepancies in the temperature values, around  $400^\circ K$ , which can be seen in the radial profiles at  $X/D = 0.127$  and  $0.255$  and at  $R < 50$  mm are attributed to uncertainties in the present combustion model and in particular to the assumption of single step-chemical reaction and the neglect of intermediate species such as soot and carbon monoxide. It is clear that, although the  $O_2$  concentrations are, to some extent, correctly predicted in this region, the  $CO_2$  concentrations are overestimated by around 30% which can be explained by referring to the high  $CO$  values (10%) measured in this zone. In effect, and due to the comparatively high calorific value of  $CO$ , the calculated heat release rates are much higher than the actual values. At the far downstream regions of the flame, for example at  $X/D=4.5$ , the differences between the calculated and measured temperature values decreases to around  $100^\circ K$  and can be attributed, again, to deficiencies in the coupled turbulence/chemistry models.

#### Test Case 2

The calculations for this test case were performed, as indicated in table 2, for 5 and 10 droplet size ranges; the calculated and measured radial profiles of temperature and unburned hydrocarbon (UHC) concentrations are shown in figure 4. The calculated profiles in the upstream part of the flame,  $X/DISC < 0.437$  indicate a large overprediction of the temperature values, by around  $400^\circ K$ , and are qualitatively in error especially in the region surrounding the intense-combustion zone, which is indicated by the high temperature values at  $R/DUCT$  around 0.4. The present flow geometry, see figure 2, suggests that this region coincides with the shear layer separating the recirculation zone behind the disc and the surrounding air stream. It is likely that the large overprediction of the chemical reaction rate at this region, which is evidenced by the calculated radial profiles of UHC, is mainly due to inaccurate calculation of the mean flow and the turbulence characteristics within the shear layer. The predicted high temperature values in the initial flame region are also influenced by the uncertainties in the assumption of single step reaction (the measurements indicated comparatively high concentrations) and in the calculation of the evaporation and spreading of the fuel spray.

The predicted and measured temperature profiles, in the downstream part of the flame -  $X/DISC > 0.6$ , are shown to be qualitatively in agreement although the temperature values are generally underestimated by around  $100-200^\circ K$ . It can also be observed that the predicted UHC concentrations are well below the measured values. Apart from the related influence of the overprediction of the chemical reaction rate in the initial flame region, these discrepancies are due mainly to inaccuracies in representing the turbulent transport and spreading of the air stream surrounding the stabilizer disc which had a consequent dilution and cooling effects on the downstream part of the flame.

The calculated results of figure 4 which were obtained with 5 and 10 droplet size ranges indicate clearly that the increase in the number of size ranges has a relatively small influence on the predicted profiles. This small difference between the predicted results is probably related to both the spray type and the aerodynamic features of the present geometry. The hollow-cone type of the spray for this test case implies that most of the droplet trajectories are confined to a small spatial volume and it is likely that changes in the discretization level used in representing the spray would have insignificant influence on its overall characteristics, including both the evaporation and spreading rates. It is also likely that the high turbulent mixing rates in the near-spray region of the present flow geometry tend to diminish the influences of any small differences in the details of the spray evaporation and spreading processes associated with the change in the number of size ranges.

#### Test Case 3

The reported calculations for this test case were performed using 10 and 20 droplet size ranges as indicated in table 2. The calculated and measured centre line distributions of temperature, mass fractions of  $O_2$ ,  $CO$  (measured) and  $CO_2$  are shown in figure 5 and the corresponding radial profiles, at axial distances of 80 mm and 250 mm are shown in figure 6. It is evident from figure 5 that the calculated oxygen concentrations along the flame centreline and for the two cases with 10 and 20 size ranges are generally underestimated. For example, the calculated values at some points drop to below half the measured concentrations. Related discrepancies in the temperature and  $CO_2$  mass fraction can also be easily detected in figure 5. This overprediction of the chemical reaction rate is due, in part, to inaccuracies in representing the spray evaporation rate and to uncertainties in the present combustion model. The former is clearly demonstrated by the comparatively better agreement between the predicted and measured values obtained with the higher number of droplet size ranges. The latter may stem from the strong dependence of the reaction rate term on the turbulence characteristics of the flow which, in turn, are sensitive to the presumed upstream boundary conditions. It is also likely that, in the initial flame region, the combustion model may be deficient in its lack of direct consideration of the influence of the presence of high concentrations of fuel droplets on the calculation of the reaction rate.

It is clear from the radial profiles of figure 6 that the increase in the number of droplet size ranges (from 10 to 20) has led to a better representation of the flame

1230  
spreading rate and to a decrease in the discrepancies between the calculation and measurements. For example, the locations of the temperature maxima are shifted radially outward to coincide, approximately, with the measured locations. This is mainly due to the increased accuracy in calculating the evaporation and spreading rates of the fuel spray as a result of the reduced degree of discretization associated with the higher number of size ranges. The larger influence of the number of size ranges observed in this case is related to the spray type and the comparatively low turbulent mixing rates of the present flow geometry where an increase in the relative importance of the fuel spray characteristics in controlling the combustion process is anticipated.

The comparison between the experimental and predicted results for this case, and for the preceding two cases, is undoubtedly subject to the experimental uncertainties associated with each technique. Although assessment of these uncertainties is difficult, it is expected that the accuracy of temperature measurements will, in general, be better than 10% and that of the concentration measurements will, at the best, be in the range of  $\pm 15\%$ .

#### 4. CONCLUDING REMARKS

The present procedure has been applied for the calculation of the flow properties in three different spray flame geometries and the comparison with the corresponding experimental data indicated that the general features of the flow fields are correctly predicted. The magnitude of the discrepancies between the experimental and predicted results and the relative importance of the sources of uncertainties in the modelling assumptions was found to vary according to the flame geometry considered. For example, the results of test case 1 showed discrepancies in the temperature and oxygen concentrations of between 100 and 400°K and 1 and 5 O<sub>2</sub>% respectively which were mainly influenced by the deficiencies in the coupled turbulence/combustion models. The uncertainties in the droplet model, however, relating to the calculation of the spray evaporation and spreading rates were, however, found to contribute significantly to the observed discrepancies in the results of test case 3.

The second and third test cases of the previous section corresponded to significantly different spray and flow geometries and therefore, allowed the influence of the number of size ranges assumed within the droplet model to be examined over a wider range of spray flames than those of reference 1. In agreement with the conclusion of reference 1, the calculated results of test case 2 indicated a small influence of the number of size ranges on the predicted profiles. On the other hand, the results of test case 3 demonstrated clearly the importance of this number. Examination of both the spray characteristics and the aerodynamic flow features of the present two cases and those relating to the test case of reference 1 suggests that the influence will be small for sprays where the majority of droplets are confined to a small spatial volume (for example, hollow-cone sprays) and for flow conditions where a high degree of turbulent mixing exists in the near-spray region.

#### ACKNOWLEDGEMENTS

The authors gratefully acknowledge financial support from the Ministry of Defence (Procurement Executive) and helpful advice from colleagues in the Fluids Section of Imperial College and at the National Gas Turbine Establishment.

#### REFERENCES

1. Y. El Banhawy and J.H. Whitelaw. The calculation of the flow properties of a confined kerosine-spray flame. AIAA paper 79-7020, 1979.
2. K.H. Khalil, F.M. El Mahallawy and H.A. Moneib. Effect of combustion air swirl on the flow pattern in a cylindrical oil-fired furnace. 16th Symp. (Int.) on Combustion, The Combustion Institute, 135-143, 1977.
3. B.F. Magnussen, B.H. Hjertager, J.G. Olsen and D. Bhaduri. Effects of turbulent structure and local concentrations on soot formation and combustion in C<sub>2</sub>H<sub>2</sub> diffusion flames. 17th Symp. (Int.) on Combustion, 1978.
4. Y. El Banhawy. Unpublished work.
5. J.H. Tuttle, R.A. Shisler and A.M. Mellor. Investigation of liquid fuelled turbulent diffusion flames. Comb. Sci. and Tech. 14, 229, 1973.
6. A.C. Styles and N.A. Chigier. Combustion of air blast atomized spray flames. 16th Symp. (Int.) on Combustion, The Combustion Institute, 619-630, 1977.
7. Y. El Banhawy. The calculation of the flow properties of a confined kerosine-spray flame. Imperial College, Mech. Eng. Dept. Report FS/78/28.
8. A.D. Gosman and W.M. Pun. Lecture notes for a Course entitled "Calculation of recirculating flows" Imperial College, Mech. Eng. Dept., 1973.
9. A.D. Gosman, E.E. Khalil and J.H. Whitelaw. The calculation of two-dimensional turbulent recirculating flows. Turbulent shear flows, I., Ed. by F. Durst, B.E. Launder, F.W. Schmidt and J.H. Whitelaw, 237, 1979, Springer-Verlag.
10. A.G. De Marco and F.C. Lockwood. A new flux model for the calculation of radiation in furnaces. Italian Flame Days, La rivista dei Combustibili, 29, 184, 1975.

Table 1. Operating conditions for the three test cases

Test case number. (reference)	1 (4)	2 (5)	3 (6)
Flame geometry	figure 2,a	figure 2,b	figure 2,c
Fuel	kerosine	liquid propane	kerosine
Fuel atomizer	rotating cup -atomizer	simplex pressure atomizer	twin-fluid atomizer
Swirler angle	60°	-	-
Combustor pressure	1 atm	5 atm	unconfined 1 atm.
Preheat temperature	300°K	500°K	300°K
Combustion air flow rate	200 kg/hr	3600 kg/hr	-
Fuel flow rate	4.75 kg/hr	22.6 kg/hr	2.3 kg/hr
Experimental data	Radial profiles T, CO, CO <sub>2</sub> , O <sub>2</sub> droplet velocity - Isothermal axial velocity	Radial profiles T, CO, UHC, NO <sub>x</sub>	Radial and centreline profiles -T, CO, CO <sub>2</sub> , H <sub>2</sub> and CH <sub>4</sub> -droplet size, droplet velocity.

Table 2. Fuel spray upstream boundary conditions for the three test cases.

Test case no.	1	2	3
Droplet size distribution	near-monosized (measured) D <sub>mean</sub> = 47 μm (70% mass) D <sub>satellite</sub> = 24 μm (30% mass)	$\frac{dn^*}{n} = 4.21 \times 10^6 \left( \frac{D_p}{188} \right)^{3.5}$ $\exp. \left( -16.98 \left( \frac{D_p}{188} \right)^{0.4} \right)$ $\cdot \frac{dD_p}{188}$	$w^{**} = \exp. \left( -\frac{D_p}{110} \right) 0.68$
No. of size ranges	2	5-10	10-20
Droplets injection velocity (m/s)	(measured) Up 0.9-8 Vp 1.0-2.34 Wp 11.69-25.3	(calculated) Up 20.0 Vp 2 Wp 11.5	(measured) Up 20-25 Vp 0.03-2

\* dn and n are the number of droplets in the size range from D<sub>p</sub> to D<sub>p</sub> + dD<sub>p</sub> and the total number of droplets respectively.

\*\* w = mass fraction for droplets larger than D<sub>p</sub>

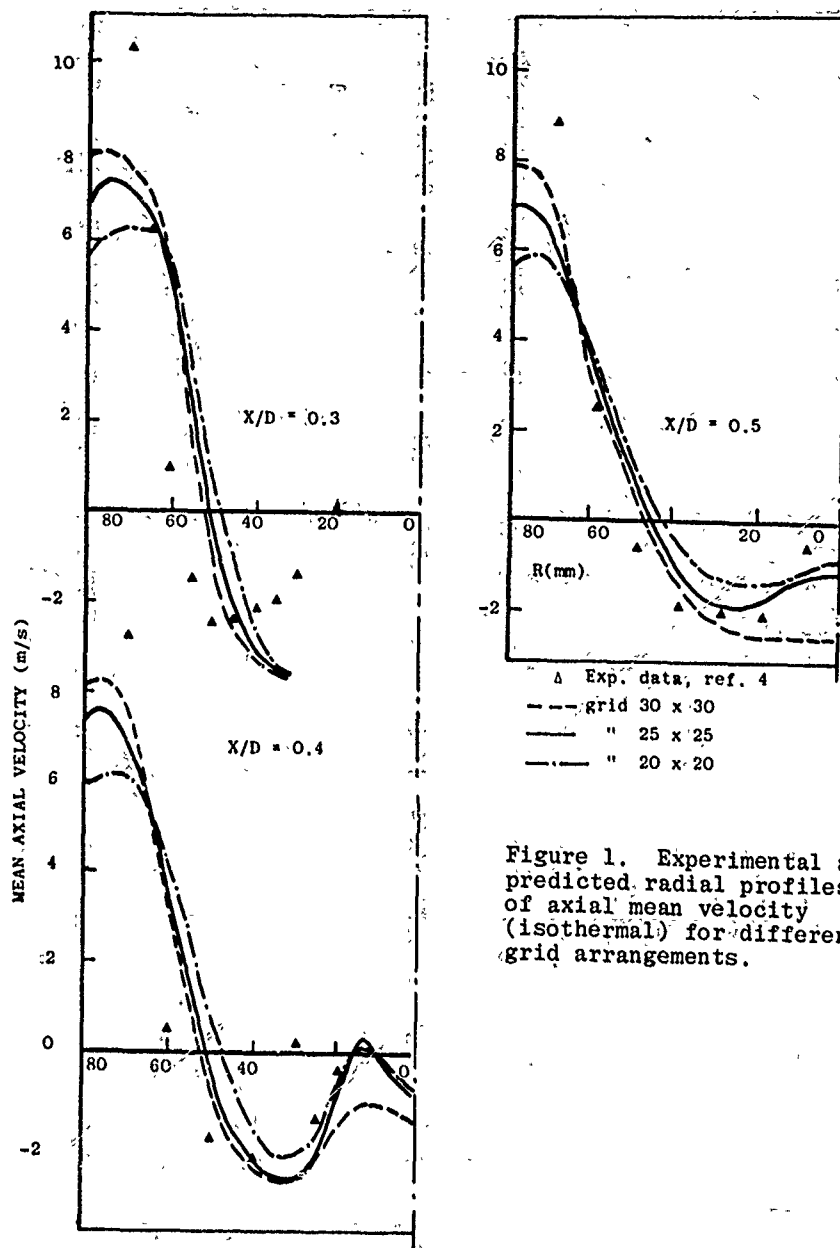


Figure 1. Experimental and predicted radial profiles of axial mean velocity (isothermal) for different grid arrangements.

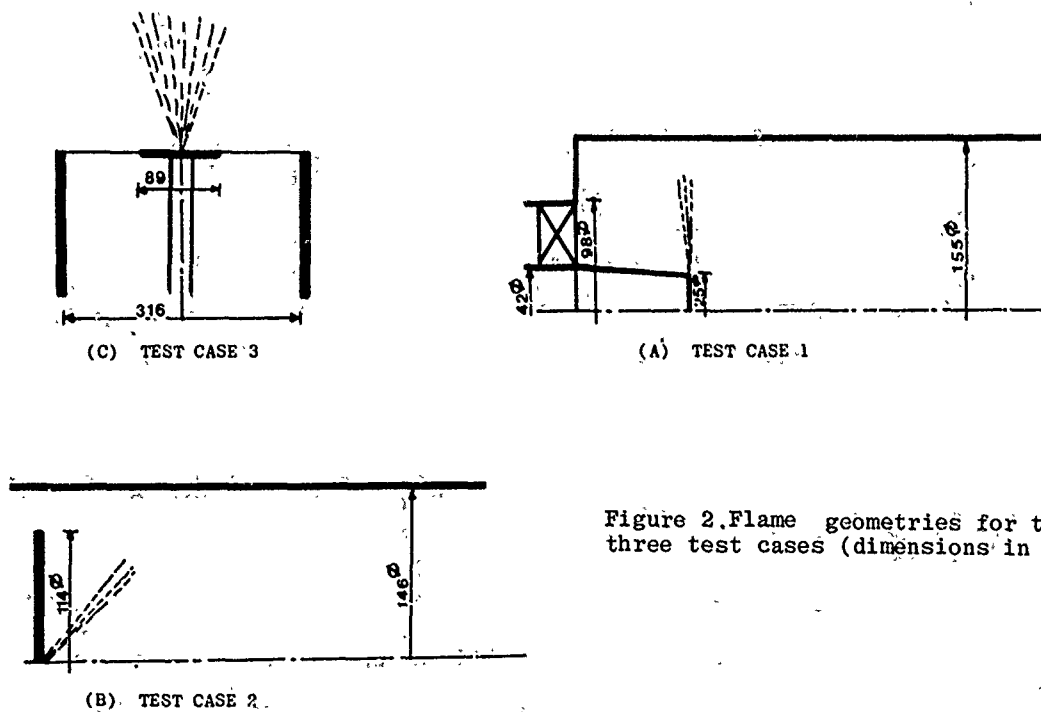


Figure 2. Flame geometries for the three test cases (dimensions in mm)

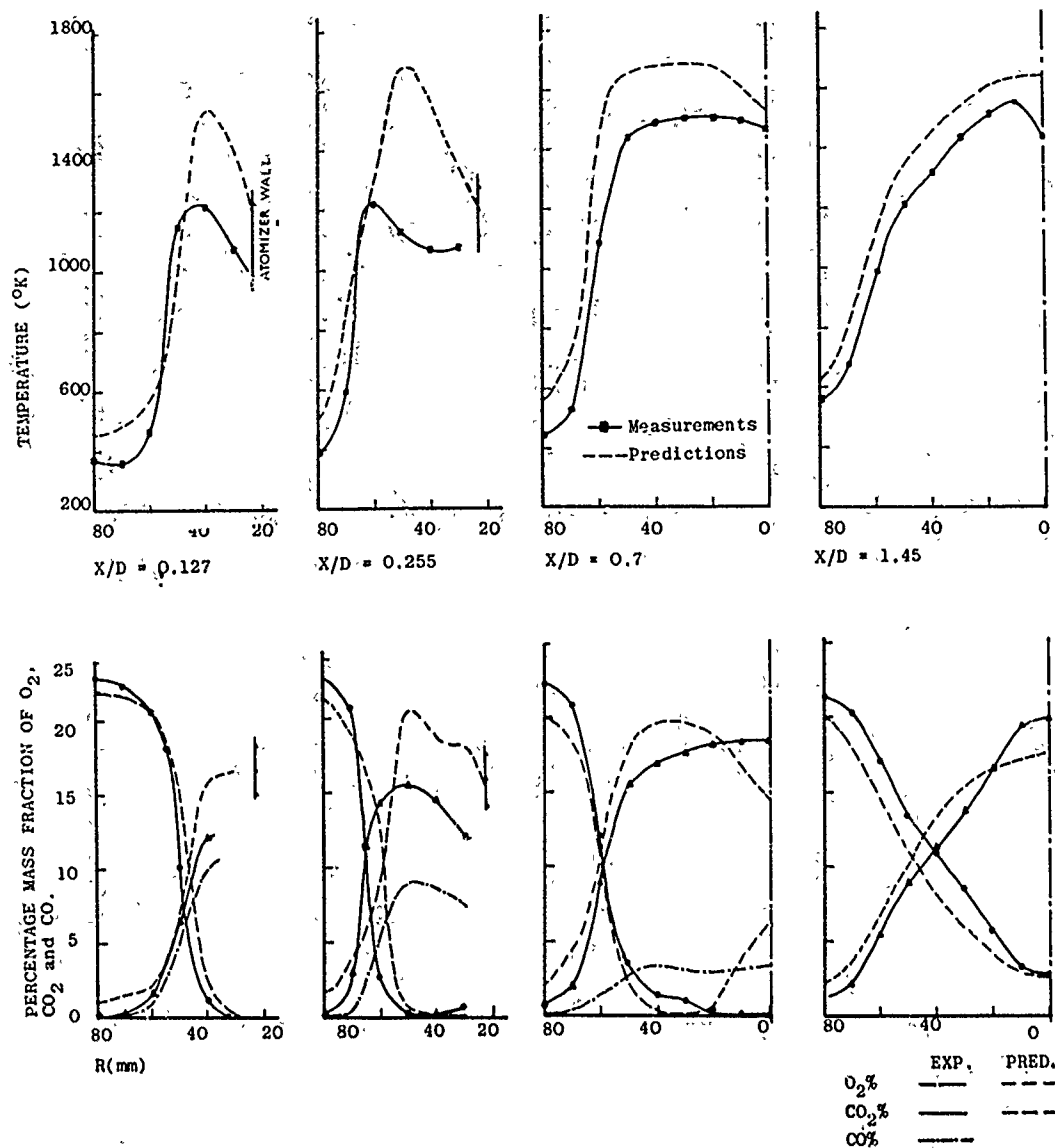


Figure 3. Experimental and predicted radial profiles of temperature and mass fractions of  $O_2$ ,  $CO_2$  and  $CO$  - Test case 1.

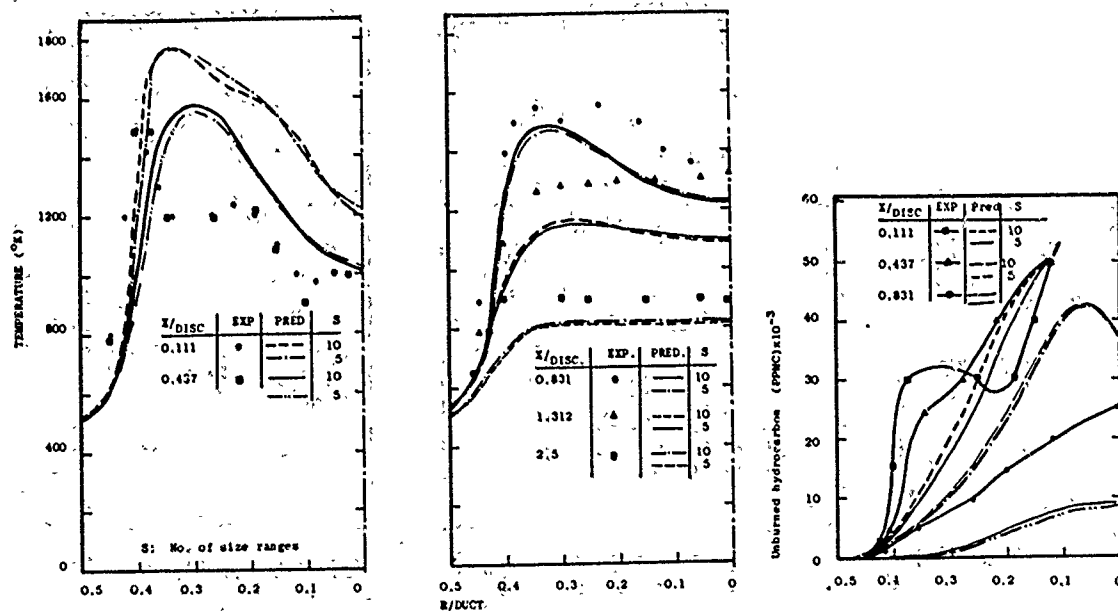


Figure 4. Experimental and predicted radial profiles of temperature and un-burned hydrocarbon concentrations. Test case 2.

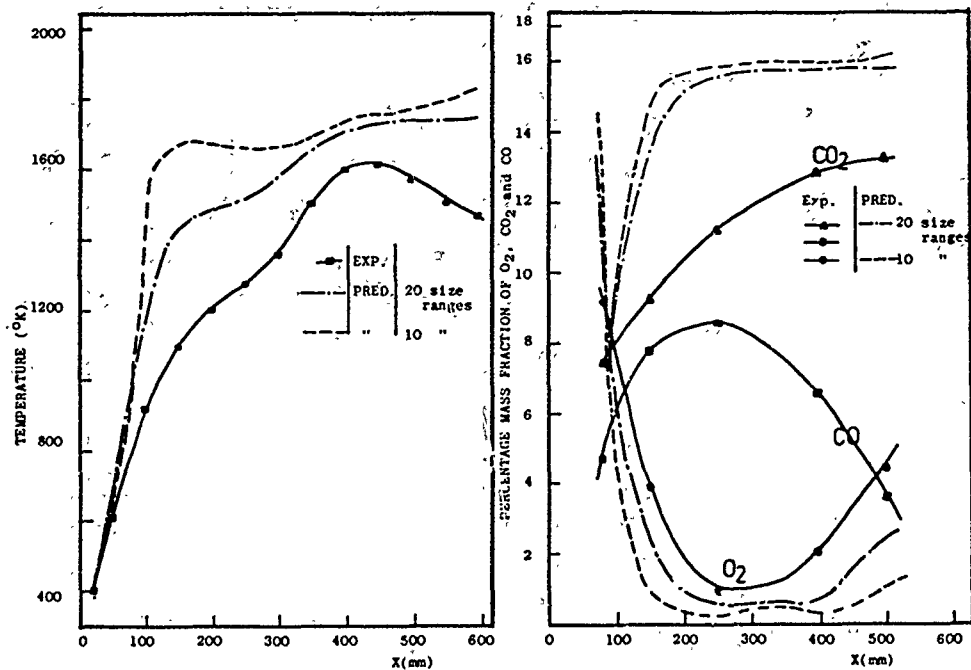


Figure 5. Experimental and Predicted centre-line distributions of of temperature and mass fractions of  $O_2$ ,  $CO_2$  and  $CO$  - Test Case 3.

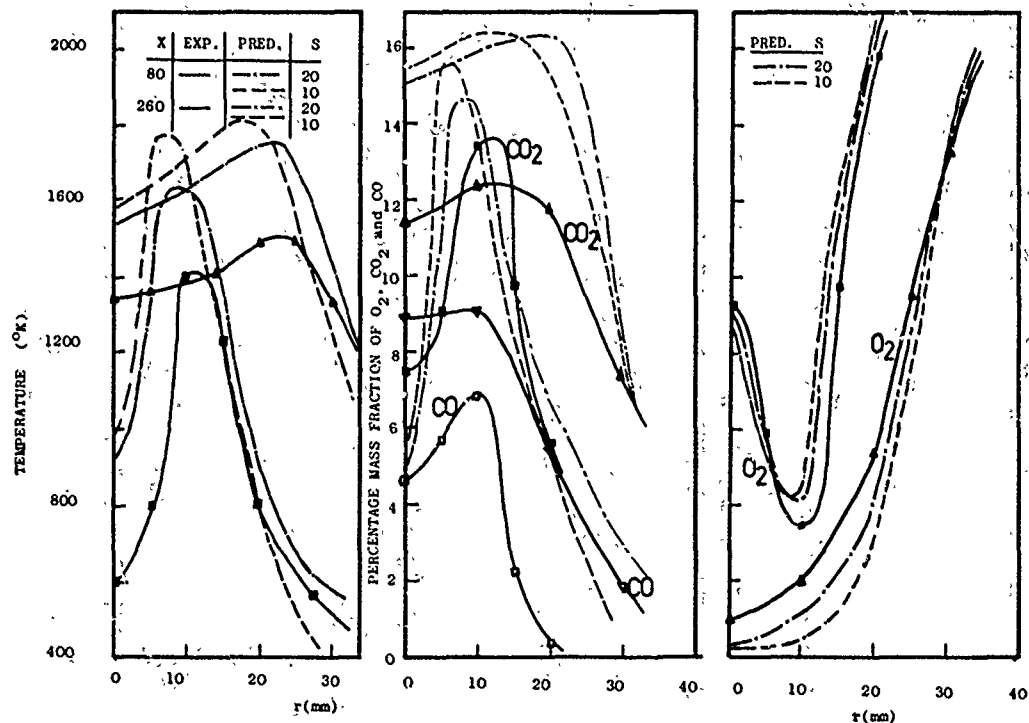


Figure 6. Experimental and predicted radial profiles of temperature and mass fractions of  $O_2$ ,  $CO_2$  and  $CO$  - Test Case 3.

**A.M. Mellor, US**

I believe that test case 2 shows little dependence on the number of size ranges used to model the spray for two reasons:

- (1) The liquid propane is thought to flash evaporate when injected into the combustor;
- (2) The flame you have modelled is thought to be controlled by the mixing of fuel vapor with air, that is, evaporation is rapid compared to this mixing (see Paper 24, this Symposium, Figures 10 and 11, and Reference 48 of Paper 24).

**Author's Reply**

The calculated results support Dr Mellor's interpretation and confirm that, of the three sets of data tested, only these from the twin fluid atomiser with its polydispersed solid spray, require a large number of size ranges. It is likely that, except at idle conditions, droplet considerations are of secondary importance for gas-turbine calculations.

**J. Swithenbank, UK**

- (1) Although it may be justifiable in some cases to use only a few droplet size ranges in evaporation computations, our studies<sup>1</sup> have shown that for a typical pressure jet atomizer we obtained virtually the same results with 20 and 40 increments and significant differences with the size ranges. We therefore feel that at least 10 size ranges are needed in such systems.
- (2) We should try to elevate the choice of grid size from the state of an 'art' to a 'science'. Perhaps the turbulence length scale can be used to iteratively optimize the grid.

I welcome your comments on these points.

1. Vincent, M.W. *Droplet Evaporation in Combustors*, Ph. D. Thesis, Sheffield University 1976.

**Author's Reply**

- (1) The results I presented have related to three sprays and show significant influence of the number of droplet-size ranges only for the solid spray. The more practical hollow-cone arrangements clearly did not require more than 5 size ranges. The previous comparisons, presented at the 4th Symposium on Air Breathing Engine Symposium support this view. This is not to say that sprays with different characteristics will allow different conclusions. However, it seems likely that the need to better represent the chemistry by, for example, a two-stage reaction will result in discrepancies which are more important than these introduced by the consideration of a small number of size ranges. The incorporation of this better chemistry, with appropriate influence of turbulence, may require considerable effort.
- (2) I agree with the view that the location of grid nodes requires skill and that a more systematic and automatic procedure is desirable. An important question is to identify good criteria for this choice. We have found, in some flows, that the consideration of the static pressure distribution, and the location of nodes with concentrations linked to the static-pressure gradients, gives good results. But the criteria may be preferable in different flows, and numerical experiments are necessary to identify them.

At the same time, we need research with the magnitude of numerical diffusion effects as a function of finite-difference scheme and flow. This is at least as important as automatic node selection, although the two may simply be coupled. In many practical flows, with realistic numbers of nodes, numerical diffusion is introduced to retain stability, with large but inadequately quantified effects. The effects need to be quantified and where necessary, avoided, either by a better distribution of grid nodes, by better numerical schemes or by a combination of both.

FUNDAMENTAL CHARACTERIZATION OF ALTERNATIVE  
FUEL EFFECTS IN CONTINUOUS COMBUSTION SYSTEMS

by

R. B. Edelman, A. Turan, P. T. Harsha, and E. Wong  
Science Applications, Inc.  
Combustion Dynamics and Propulsion Technology Division  
20335 Ventura Blvd/Suite 423  
Woodland Hills, California 91364

W. S. Blazowski  
Exxon Research and Engineering Company  
Government Research Laboratories  
P.O. Box 8  
Linden, New Jersey 07036

SUMMARY

Increased interest in alternative fuels use in gas turbines has prompted questions related to the impact of fuel property variability on the combustion process. Reduced hydrogen content is characteristic of syncrudes that have been identified as probable alternate fuel sources. An interrelated analytical and experimental program is being conducted in which chemical and aerodynamic interactions are being investigated in order to provide a technology base to aid in dealing with problems of burning alternative fuels. One element of this effort is devoted to characterizing the kinetics of the oxidation of alternative fuels. This paper is concerned principally with the problem of net soot generation which is aggravated by the reduced hydrogen content. The kinetics of the process is being modeled using the quasiglobal concept while experimental data is being developed primarily from a laboratory jet stirred combustor. Results are presented showing that soot emissions can be characterized in terms of major species and that soot oxidation must be included in the prediction of net soot generation. In addition, the techniques being employed for coupling the chemical and aerodynamic processes are outlined.

INTRODUCTION

Until recently the development of gas turbine combustors as well as the development of combustion chambers for most other applications has been based largely upon empirical methods. While reliable systems have been produced by this approach the cost is becoming prohibitive. Furthermore, time constraints for the development of new systems by this approach are not necessarily compatible with meeting near term requirements for cleaner burning and more efficient systems. Not only do the near term needs blunt purely empirical approaches but we are in a critical period where the development of new technology bases must be initiated and sustained to meet the long term requirements dictated by the increasingly changing fuel availability picture. Although economics and supply are primarily responsible for this recent interest in new fuel sources, projections of available worldwide petroleum resources also indicate the necessity for seeking non-petroleum based fuels.

Fuel variability has not been a factor commonly accounted for in empirically based design procedures. Because of the uncertainty in future fuels as well as the need to use less conventional petroleum based fuels, the requirement to develop fuel flexible systems is well established. The design of fuel flexible combustors that burn cleanly and efficiently requires a more precise understanding of the mechanisms that control flame structure than has been needed in the past.

The practical goal in understanding the combustion process is to relate the parameters in the control of the designer to the performance of the system. By performance we include in a general sense combustion efficiency and emissions characteristics.

In this paper emphasis is given to the effects of fuel properties on combustion but the relationship between the fuel and the aerodynamics of the gas turbine combustion process is also addressed.

FUEL EFFECTS ON GAS TURBINE COMBUSTION

Fuel characteristics which are most likely to affect the design of future gas turbines are fuel hydrogen content, viscosity, volatility, nitrogen content and thermal stability, Ref. 1.

The impacts of reduced fuel hydrogen content are associated with increased rates of carbon particle formation. Increased levels of carbon particle concentrations formed in fuel rich regions of the primary zone lead to higher liner temperatures and higher smoke emissions. Reduced volatility and increased viscosity affect droplet life times and atomization, respectively. Volatility affects the rate at which liquid fuel introduced into the combustor can vaporize. Since important heat release processes do not occur until gas phase reactions take place, a reduction of volatility reduces the time available for chemical reaction within the combustion system. In the aircraft engine this can result in difficulty in ground or altitude ignition capability, reduced combustor stability, increased emissions of carbon monoxide (CO) and hydrocarbons (HC), and the associated loss in combustion efficiency. Moreover, carbon particle formation is aided by the formation and maintenance of fuel-rich pockets in the hot combustion zone, Ref. 2. Low volatility allows rich pockets to



persist because of the reduced vaporization rate. Again, increased soot can cause additional radiative loading to combustor liners.

The desired formation of a finely dispersed spray of small fuel droplets is adversely affected by viscosity. Consequently, the shortened time for gas phase combustion reactions and prolonging of fuel-rich pockets experienced with low volatility can also occur with increased viscosity. Ignition, stability, emissions, and smoke problems also increase for higher viscosity fuels.

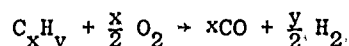
Increased fuel bound nitrogen levels can lead to increased NO<sub>x</sub> emissions. Indications are that bound nitrogen conversion to NO<sub>x</sub> can be minimized in fuel rich combustion, Ref. 3. Apparently, this will occur if sufficient time under fuel rich conditions is allowed for direct conversion of the bound nitrogen to N<sub>2</sub>. Problems of fuel stability are aggravated with increased bound nitrogen and undesirable levels of carbon deposit buildup in fuel management systems and on combustor components can occur.

While our investigations are addressing all of these fuel related problems it has become apparent that to characterize net soot generation requires a broader description of the kinetics of pyrolysis and partial oxidation.

While both carbon formation and carbon consumption processes occur in continuous combustion systems, the latter are very much slower. The optimum approach for preventing hardware distress and avoiding serious environmental consequences is to develop technology to avoid carbon formation while satisfying other system requirements (efficiency, gaseous emissions, hardware reliability, etc.).

#### NET SOOT GENERATION

The predominance of fundamental research activity has involved laminar premixed flames. Street and Thomas' work published in 1955 is extremely thorough in experimental detail and breadth of hydrocarbons examined; Ref. 4; it has become the classical paper in the field. Other publications are References 5-16. These investigations have universally confirmed that soot formation is a kinetically controlled process. Equilibrium calculations indicate that soot should not be present at fuel-air mixture conditions where the oxygen-to-carbon atomic ratio (O/C) is greater than one. That is, the general chemical equation



should define a soot formation threshold. All experimental results have shown soot formation at O/C substantially in excess of unity.

Another very important premixed flame experiment conducted at the British National Gas Turbine Establishment (NGTE) attempted to evaluate the effect of pressure on soot formation, Ref. 11. All previously mentioned work with premixed flames concerned atmospheric or sub-atmospheric conditions. The combustion system employed took special precautions to avoid flashing back to upstream locations, an additional difficulty associated with the high pressure operation. In addition to sooting limits, the amount of soot formed was determined and expressed as a "soot formation ratio" (the percent of fuel carbon evident as soot). The index of the soot quantity was found to increase with the cube of pressure. Very useful plots of pressure versus equivalence ratio for various values of soot formation ratio were presented. Examples are shown in Figure 1 for cyclohexane, cyclohexene, and benzene. Gas phase species were also determined during this testing and it was concluded that H<sub>2</sub>O and CO<sub>2</sub> (oxygenated compounds not predicted by equilibrium for the system  $C_xH_y + \frac{x}{2} O_2 \rightarrow xCO + \frac{y}{2} H_2$ ) are formed in substantial quantities and deplete the system of oxygen prior to consumption of all fuel.

Soot formation in laminar diffusion flames has also been studied, Refs. 17-20. The direct utility of this information for the gas turbine combustion application has been questioned, as the mixing rates and characteristic times for chemical reaction are very much different than those in the typical combustor. Shirmer, Ref. 21, has discussed the significant differences between such experiments and the actual combustion process. He is particularly critical of the use of the smoke point test as an index of fuel tendency to form carbon particulates. Turbulent diffusion flame results would appear to be more applicable, Ref. 22. Wright, Ref. 20, has examined soot formation in a diffusion flame burner and published results of soot measured when the fuel side of the flame is supplemented with oxygen at concentrations well below O/C = 1. Surprisingly, it was found that the addition of oxygen increases soot formation up to an optimal rate at which the influence abruptly reverses and soot suppression is accomplished at higher O<sub>2</sub> concentrations.

Wright's work involving soot formation in the jet stirred reactor, Refs. 23, 24, is perhaps of most interest to this discussion -- it is a combustion process similar to that at which soot forms in the primary zone of an actual continuous combustion system. As in the previously mentioned studies, it was determined that soot forms at O/C > 1 but the strong backmixing of the jet stirred reactor did afford some broadening of the soot-free O/C ratio. In addition to the establishment of sooting limits, as determined by the color of the flame (luminous yellow versus blue), Wright determined the concentrations of soot formed for some limited conditions of O/C below the soot limit. No analysis of this "yield" data to determine soot formation kinetics was undertaken but it is recognized that more such data might provide the basis for global carbon formation chemical model.

#### MODELS OF SOOT FORMATION

Many studies on soot formation have been carried out, but few lead to quantitative

predictions of soot production, and there is little agreement as to the details of the mechanism. Nevertheless, there seems to be general agreement that the overall soot formation reaction is triggered by hydrocarbon pyrolysis and involves subsequent soot nuclei formation, soot particle formation, and particle growth and coagulation. A model that treats these in some detail has been considered by Jensen, Ref. 25. Application of the model to a methane flame has led to qualitative agreement with experimental observations. Although this approach represents an attempt to deal with the problem at a mechanistic level the uncertainty of intermediate species, reactions and rates requires long term development to provide quantitative predictions. Tesner, et al., Ref. 26, have proposed a model in which soot formation is characterized by three rate equations. The feature of the model is that all the complex elementary steps associated with pyrolysis, nuclei formation and soot formation are grouped into three subglobal steps which are characterized by three separate equations. The model includes a first order (with respect to hydrocarbon concentration) pyrolysis rate, a chain branching and chain termination rate, and a soot formation rate:

$$\begin{array}{lll} \text{Pyrolysis:} & N_o = 10^{13} N_o e^{-170,000/RT} & 1 \\ \text{Nuclei Formation} & \frac{dn}{dt} = N_o + (f-g)n - g_o Nn & 2 \\ \text{Soot Formation} & \frac{dN}{dt} = (a - bN)n & 3 \end{array}$$

Values of the kinetic parameters (f, g,  $g_o$ , a, b) for acetylene and toluene are available, so that the model can be evaluated through comparison with experimental data. Comparisons with data developed in this investigation are presented later in this paper. Greeves, et al., Ref. 27, developed a model using diesel engine data obtained under high pressures. The model consists of a single global Arrhenius type equation:

$$\frac{dS}{dt} = 4.68 \times 10^{-5} P_{HC}^3 \phi_u^3 e^{-40,000/RT} \quad 4$$

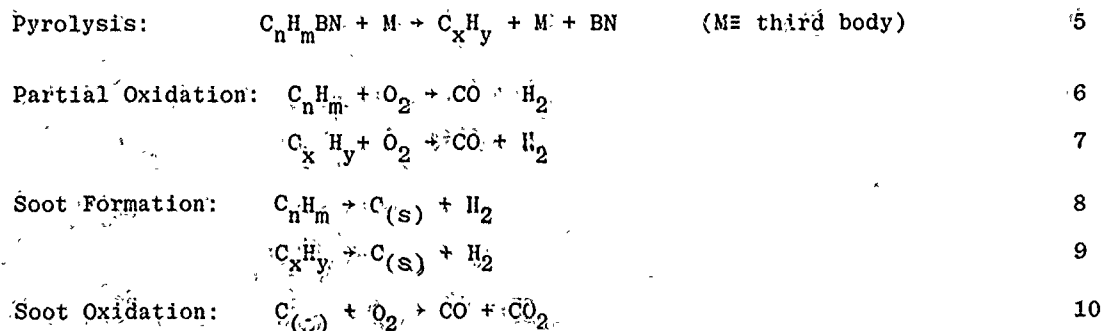
Where  $P_{HC}$  and  $\phi_u$  are the local partial pressure of the unburnt hydrocarbon and the local equivalence ratio, respectively. This type of one-step model lumps all intermediate reactions associated with nuclei formation and soot formation into one rate equation, and the application of the model requires knowledge of the local hydrocarbon concentration and the unburnt equivalence ratio.

Attempts to correlate data developed in this investigation with Greeve's model, Equation 4, are presented in this paper.

The Greeves and Tesner models represent the essential state-of-the-art of practical soot prediction methods. However, the process requires information on certain intermediates that must be assumed in order to implement these models in a strictly predictive mode. This information includes, for example, the local hydrocarbon and oxygen concentrations as well as the temperature. In addition, net soot generation requires not only consideration of soot formation but its oxidation as well. These factors are included in the current model development.

#### QUASIGLOBAL MODEL

The essential feature of the quasiglobal concept is the coupling of a set of subglobal steps to a set of detailed steps for those reaction chains for which sufficient information to accurately describe their kinetics and mechanisms exists. The basic quasiglobal model is described in Ref. 28. In addition to having demonstrated the ability of the quasiglobal model to predict experimental observations it has been shown to be ideally structured to account for the variation in fuel type, i.e. aliphatic vs. cyclic, etc. Of particular interest here is the current work on fuel rich systems for which this basic model is being extended. The new model includes the following additional subglobal finite rate reaction steps given below in skeleton form:



Where BN represents the bound nitrogen. Reactions 5 through 10 are coupled to detailed mechanisms describing the rate at which  $H$ ,  $CO$  and  $BN$  are converted to  $H_2O$ ,  $CO_2$  and  $NO_x$ . The rate constants for the subglobal steps are expressed in modified Arrhenius form and the rate of production (or consumption) is given by expression of the type:

$$\dot{C}_1 = A T^a C_1^b \exp(-E/RT) \quad 11$$

where the constants A, a, b, c and E are determined through controlled experiments. The

reactions and rates associated with the detailed steps are based upon available literature values.

The quasiglobal model has been used successfully for high energy fuels, such as shell-dyne-H and H-methylcyclopentadiene, as well as for conventional fuels such as propane and JP-types. The versatility of this approach has been demonstrated by comparisons with experimentally determined combustion characteristics including ignition delay times for both long chain and cyclic type hydrocarbons reacting in air. For example, Figure 2 shows some typical results of such a comparison between predictions and data obtained from a steady flow reactor. Figures 3, 4, 5, and 6 show comparisons of predictions with current data obtained in a reactor described later. Figures 3 and 4 compare data with predictions for  $O_2$  and CO concentrations. The agreement between the predictions and the data is very good. Of particular interest are the CO and hydrocarbon concentrations since they both relate to efficiency and emissions, while the hydrocarbon concentration relates to soot formation. Figure 5 shows the CO concentration comparison where data for three fuel types is given; a paraffin (isooctane), an aromatic (toluene), and an olefin (ethylene). While there are measurable differences amongst the fuel types the prediction for the CO concentration is reasonable, noting that the concentration levels are in percent. What is significant to note is the minimum in CO at equivalence ratios between .4 and .6 depending on the fuel. This minimum is reproduced by the prediction and is associated with the approach to blow-out at the low equivalence ratios where low temperatures (reduced reaction rates) enhance incomplete combustion, while at the higher equivalence ratios reaction rates increase since temperature is increasing, and although the system is out of equilibrium, the tendency toward equilibrium is consistent with the water gas shift reaction tending to increase CO (and  $H_2O$ ). The ability of the quasiglobal model to predict this type of detail is relevant to the determination of "optimum" operating conditions and to scaling to other operating conditions. Of equal importance to the CO concentration is the fuel conversion and Figure 6 shows the hydrocarbon concentration as measured and compared with predictions. The comparison is favorable considering the low concentration levels of fuel existing in the system under the particular operating conditions. The rapid rise in the hydrocarbon concentration corresponds to the approach to blow out and is consistent with the increase in CO previously cited.

The examples cited above were used to illustrate some of the features of the quasiglobal model. For the prediction of net soot generation additional information related to reactions 8, 9 and 10 is required. The soot model is constructed in terms of two steps reflecting the dependence of net soot generation on the simultaneous formation and oxidation of soot particles. The soot formation rate is assumed to be a function of the hydrocarbon concentration, the oxygen concentration and the temperature; viz.

$$\dot{R}_{c(s)}^+ = A T^a C_{HC}^b C_{O_2}^{-\alpha} e^{-E/RT} \quad 12$$

where A, b,  $\alpha$  and E are constants. The oxidation step is based upon data involving the consumption of soot (and carbon) particles in oxidizing environments, from, for example the work of Lee, Thring and Beer, Ref. 29, and the work of Nagle and Strickland-Constable Refs. 30 and 31. For the Lee, Thring and Beer model the rate of consumption per unit surface area is given by

$$\dot{R}_{c(s)}^- = 1.085 \times 10^4 \frac{P_{O_2}}{T^2} \exp \left( - \frac{39,300}{RT} \right), \quad 13$$

where  $P_{O_2}$  is the partial pressure of oxygen in the mixture. Reactions 12 and 13 are combined to yield the net rate of soot production as a function of hydrocarbon and oxygen concentrations and temperature. The constants A, a, b,  $\alpha$  and E have been determined from experimental data and it is interesting to note that net soot production is more strongly dependent upon the hydrocarbon concentrations than on the temperature. It is also important to note, as will be discussed later, that as much as 20-25 percent of the soot formed can be consumed by oxidation.

#### EXPERIMENTAL METHOD

The experimental program focused on a study of the soot formation process using the Jet-Stirred Combustor (JSC), shown schematically in Figure 7. This device is a modification of the Longwell-Weiss reactor, Ref. 32, with hemispherical geometry. The JSC has been used extensively in fluid mechanic and combustion modeling because combustion rates are limited by chemical kinetics as opposed to transport effects. A key advantage of the JSC for the work described here is that the strongly backmixed nature of this combustion process provides a simulation of the recirculating characteristics of the gas turbine primary zone. It is in this zone where mixture conditions are sufficiently rich to produce soot. Consequently, the JSC allows study of soot formation in an aerodynamic situation relevant to gas turbine systems. Another advantage of the stirred combustor is that the reactor is homogeneous in species concentration as well as temperature; each operating condition is characterized by a single set of temperature and concentration data rather than profiles of these parameters. This simplifies the tasks of obtaining and interpreting the data.

Details of the experimental apparatus and measurement techniques used have been reported by Blazowski, Ref. 38. The measurements include fuel and air mass flow rates and fuel/air mixture injection temperature, reactor gas samples and reactor internal and wall temperatures. Both gas-phase and particulate sampling systems are used, providing data on the incipient soot formation equivalence ratio and quantitative data on soot production (mg soot/liter).

## EXPERIMENTAL RESULTS

Detailed experiments were conducted using the Jet Stirred Combustor to determine the soot formation characteristics of ethylene, a hydrocarbon thought to produce combustion information representative of aliphatics, and toluene, a condensed-ring aromatic. Substantial differences in the behavior of these two hydrocarbons were noted and a number of other hydrocarbons were studied to determine whether they behaved as  $C_2H_4$  or as  $C_6H_5CH_3$ . Finally, the soot formation characteristics of two-component fuel blends and practical petroleum-derived fuels have been investigated.

### Characteristics of Ethylene and Toluene

Jet Stirred Combustor experiments with ethylene showed that CO was the major carbon-containing species and remained at a concentration of about twelve mole percent for all equivalence ratios tested. Total hydrocarbons increased significantly with equivalence ratio but  $CO_2$  decreased. Oxygen concentration was very low at an equivalence ratio of 1.77 but steadily increased at higher equivalence ratios--an indication of poor reactedness as the mixture was further enriched. Further, THC concentrations were found to be very significant at the even below the incipient soot formation limit.

For toluene, CO was again found to be the predominant species. However, a substantial difference between the data for toluene and that for ethylene was observed: whereas with toluene, incipient soot occurred as hydrocarbons begin to "break through" under rich operating conditions, the soot limit for ethylene occurred at conditions where hydrocarbon concentration is high - a factor of 36 times that for toluene.

Results for these two fuels, described in detail in Ref. 33, indicate significant differences between the soot formation process for ethylene and toluene:

1. Toluene soots at a much lower equivalence ratio (1.35) than ethylene (1.95), and the amount of soot formed with increasing equivalence ratio beyond the incipient limit is much larger.
2. In the case of ethylene, significant amounts of hydrocarbons (~3-8% as  $CH_4$ ) were present at equivalence ratios leaner than the soot limit, but with toluene the incipient soot limit corresponded approximately to the equivalence ratio for the initial presence of hydrocarbons in the combustion products.

### Sooting Characteristics of Other Hydrocarbon Types

The observations for ethylene and toluene indicate that there is a fundamental difference in the soot formation mechanisms for these two fuels under the strongly backmixed conditions of the Jet Stirred Combustor. These findings lend support to the possibility of developing useful simplified overall chemical kinetic models of the soot formation process (quasi-global models) based on hydrocarbon type. In order to further develop this concept a large number of other fuel types were screened to determine whether their sooting characteristics were similar to ethylene or toluene, or if they showed characteristics distinctly different from either of these fuels.

It was found that all hydrocarbons tested might be grouped into three categories as follows:

Like $C_2H_4$	Like $C_6H_5CH_3$	Unlike $C_2H_4$ or $C_6H_5CH_3$
Hexane	O-xylene	1-methyl-naphthalene
Cyclo-hexane	M-xylene	
N-octane	P-xylene	
Iso-Octane	Cumene	
1-octene	Tetralin	
Cyclo-octane	Dicyclopentadiene	
Decalin		

The first group produced large amounts of exhaust hydrocarbons without sooting as did ethylene and in no case was significant soot observed. The second group produced soot at the mixture ratio which corresponded to hydrocarbon breakthrough. In all cases the measured hydrocarbon composition was less than one percent at the incipient limit. Another commonality in the second group is that the amount of soot produced as equivalence ratio was increased beyond the incipient limit was similar for all the hydrocarbons. 1-methyl-naphthalene was significantly different in this respect producing much higher soot quantities than those in the second category.

### Sooting Characteristics of Fuel Blends

Blends of iso-octane and toluene were tested to determine the behavior of a two-component mixture with Group 1 (like- $C_2H_4$ ) and Group 2 (like- $C_6H_5CH_3$ ) hydrocarbons. These results are shown in Figure 8. Mixtures with 50 or more percent toluene produced soot while a 25% toluene blend did not. Clearly, for the mixtures which did soot, increases in the volume percent toluene result in increased soot production at all equivalence ratios. With less toluene in the blend, the concentration of hydrocarbons at the incipient limit tended to increase. These results indicate a combination of Group 1 and 2 behaviors; thus a combination of the analytical descriptions for toluene and iso-octane might be a reasonable approach for prediction of the sooting characteristics of fuel blends. An excellent correlation is obtained between soot concentration and hydrogen content, Fig. 9. This is in direct compliance

with actual gas turbine tests, Ref. 1. The similarity between sooting characteristics in the JSC and those in an actual combustor is evident.

### Mechanisms of Soot Formation

Many mechanistic models for soot formation have been proposed. Generally, it is recognized that condensed ring aromatic hydrocarbons can produce soot via a different mechanism than do aliphatic hydrocarbons. A simplified mechanism following Graham, et al., Refs. 34 and 35, is as shown schematically in Fig. 10:

Aromatic hydrocarbons can produce soot via two mechanisms: a) condensation of the aromatic rings into a graphite-like structure, or b) breakup to small hydrocarbon fragments which then polymerize to form larger, hydrogen deficient molecules which eventually nucleate and produce soot. Based on his shock tube studies of soot formation, Graham concludes that the condensation route is much faster than the fragmentation/polymerization route. Further, he has found that the mechanism by which an aromatic forms soot changes with temperature; below 1800 K the condensation path is favored while above this temperature the fragmentation/polymerization route is followed.

According to this simple model, aliphatics produce soot via the fragmentation/polymerization mechanism only. As a result, these hydrocarbons do not form the quantities of soot produced by the aromatics. Indeed, during the fuel rich combustion of a fuel blend composed of aromatics and aliphatics at a temperature less than 1800 K, the aromatic hydrocarbons would produce the major portion of soot. Combustion of the aliphatic portions of the fuel would influence temperature and hydrocarbon fragment concentration but soot formation via fragmentation/polymerization would be minimal. Above 1800 K, however, both the aliphatic and aromatic hydrocarbons would produce soot via the fragmentation/polymerization route.

The experimental results obtained in the present work are consistent with this model. It has been observed that soot formation with the condensed-ring aromatic fuels commences with the initial presence of hydrocarbons in the exhaust. If it is assumed that these breakthrough hydrocarbons maintain their aromatic character, this observation reflects the fast kinetics of the ring-building or condensation reactions. On the other hand, the aromatic molecule may be an effective source of  $C_2H_2$  and high concentrations of acetylene as fuel pyrolysis occurs may be responsible for extensive soot production. Further, the results for 1-methyl-naphthalene indicate that a double-ring aromatic provides the most rapid soot formation of the hydrocarbons studied. This observation is also consistent with either the ring building view (i.e., the first ring-joining has already occurred) or the polymerization mechanism (i.e., even higher amounts of  $C_2H_2$  are present in the pyrolysis zone).

These comparisons are not intended to establish the validity of any theory, but are noted to illustrate that the results obtained in this work complement existing simplified views of the soot formation process. Most importantly, the current results lend support to the utility of the approach of quasi global modeling of the soot formation process for various categories of hydrocarbons.

### COMPARISON OF DATA WITH PREDICTIONS

The majority of the soot data obtained to date has been on fuel rich combustion of toluene/air mixtures. Initially, predictions based upon the models of Tesner and Greeves were made and compared with the measured soot concentration data, Fig. 11. Although the Greeves model exhibits the sensitivity to inlet equivalence ratio shown by the data neither of the two models adequately represents the experimental observations. The disparity between the current data and Greeves and Tesner models has not been fully reconciled. However, an examination of their methods for obtaining rate constants suggests that they may have been influenced by aerodynamic effects.

The current model is based upon a broader base of data than the previous models had available and is structured to separately account for pyrolysis and partial oxidation of the fuel as well as oxidation of the soot. For the present purposes Eqs. 12 and 13 are combined into a model for net soot emission from a perfectly stirred reactor, viz.

$$s = \frac{A T^a [HC]^b [O_2]^{-\alpha} e^{-E/RT}}{\frac{\dot{m}}{\rho V} + \frac{6}{\rho_s d} \cdot \frac{1.085 \times 10^4 P_{O_2} e^{-39,300/RT}}{T^2}} \cdot \left( \frac{gm}{cm^3} \right) \quad 14$$

where  $[HC]$  and  $[O_2]$  are the molar concentrations of the hydrocarbon and molecular oxygen,  $\rho$  is the mixture density,  $\rho_s$  is the soot density,  $\dot{m}$  is input flow rate,  $V$  is the reactor volume and  $d$  is the soot particle diameter. Tentative values for the remaining rate parameters are:

$$\begin{aligned} A &= 5.0 \times 10^{13} & \alpha &= 0.5 \\ a &= -2 & E &= 32,000 \text{ cal./mole} \\ b &= 1.75 \end{aligned}$$

Figure 12 shows the comparison of the present model predictions with data, based upon a soot particle size of 250 $\mu$ . The air flow rate range covered by the data corresponds to a residence time range of from about 3 to 7 milliseconds. It should be noted that large scale unmixedness effects are the probable cause for the discrepancy observed at  $\phi=1.9$  for the air mass flow rate of 50 gm/min. This point corresponds to incipient blowout where unsteadiness is observed. However, the results in general are very encouraging and seem to support the concept of modeling soot emissions in terms of the major species

present in the flame. Furthermore, the effect of soot oxidation can be significant. The predicted reduction in soot emissions ranges from 20-25% at the high air flow rate (short residence time) down to 9-13% at the lowest air flow rate (longest residence time). These results represent the first known attempt to characterize net soot generation from a stirred combustor. Work in progress is designed to provide information for validation of the models over wider ranges of operating conditions including above atmospheric pressure levels and on mixtures of fuel types. Development of the overall quasiglobal model represents the major goal of this chemically related element of the program.

#### PHYSICAL PROCESSES

Combustor modeling provides a means to obtain a quantitative understanding of primary combustion phenomena, such as liquid fuel droplet vaporization and burning, solid particle burning, gas phase chemical reaction kinetics, radiation heat transfer from combustion products, and mixing of reactants and combustion products. These processes are defined by the interaction of a number of mechanisms which are conveniently described in terms of physically or chemically related processes. The *physical* processes are:

1. Liquid fuel injection and atomization
2. Spray penetration and spreading
3. Droplet breakup
4. Droplet evaporation
5. Heat transfer by radiation and convection
6. Aerodynamic flow patterns
7. Turbulent mixing

and the *chemical* processes include:

1. Pyrolysis
2. Bound nitrogen conversion
3. Dropwise combustion
4. Gas phase oxidation
5. Particulate formation
6. Particulate oxidation

In this paper we have emphasized the modeling of the chemical processes listed above, but although we have grouped these processes separately they are mutually coupled in the combustion process. It is the treatment of this coupling that is the task of combustor modeling.

The concept of modular modeling provides a rational framework for the development of engineering models of combustor flowfields, and it is this concept that is being used in the work outlined in this paper. Fundamentally, modular modeling involves delineating characteristic regions of a combustor flowfield, treating each region in detail using a technique appropriate to its characteristics, and coupling these treatments together through their boundary conditions (Refs., 36, 37, 38). The characteristic regions may be defined by their *scale*, for example, in the treatment of fuel injection phenomena for which an appropriate scale is related to the size of the injector orifice, or by their *fluid dynamics*, as in the representation of recirculation zones as opposed to regions in which there is a characteristic flow direction.

Gas turbine combustors involve fuel and dilution air injection regions, recirculation regions, and regions in which a single characteristic velocity field exists. In early modular model formulations, Refs., 39 and 40, these combustors were represented by a combination of plug-flow reactors, well-stirred reactors, or both, with the interconnection between model elements supplied by empirical information. The modular model used in this work differs in two major ways from these early formulations: detailed flowfield modeling replaces the one-dimensional plug flow reactors of the early models, and the coupling between model elements is computed rather than empirically specified. Thus far more detail can be obtained from the model results, providing a greater quantitative understanding of the primary combustion phenomena described at the beginning of this section.

In the modular formulation described in Refs. 36, 37, 38, the combustor flowfield characteristic regions are regions of recirculating flow and regions in which a characteristic flow direction can be assigned: directed flow regions. The recirculating flow is characterized as a well-stirred reactor, while the directed flow is described using a detailed solution of the boundary-layer form of the governing equation. This is not, however, the only way in which the model formulation can be carried out. For example, a detailed calculation of the overall combustor flowfield can be carried out, using simple overall reaction models to characterize the combustor heat release, and then coupled to a detailed chemical kinetics treatment in regions of the combustor in which the flowfield solution shows a detailed treatment is required. In this way, a modular formulation based on *reaction kinetics* is obtained. This type of modular model is described by Swithenbank, A. Turan, and P. G. Felton in paper No. 2 of this meeting; a similar approach is being used in the work outlined here to assist in the development of the modular formulation described in Refs. 36, 37, 38.



## CLOSURE

The information being generated in this program provides an improved understanding of the processes important to alternate fuels utilization. The "end item" is an analytical model which allows prediction of fuel effects in various types of continuous combustion devices, particularly gas turbines. Such a development will provide combustor designers with a tool to develop fuel flexible combustion systems which can utilize synfuels which are produced with minimum refining/upgrading and, hence, minimum cost and energy consumption during refining.

## REFERENCES

1. Jackson, T. A., and Blazowski, W. S., "Fuel Hydrogen Content as an Indicator of Radiative Heat Transfer in an Aircraft Gas Turbine Combustor," in Gas Turbine Combustion and Fuels Technology, ASME, United Engineering Center, 345 E. 47th St., New York, N.Y., November 1977, pp. 59-65.
2. Dodds, W. J., Peters, J. E., Coklet, M. B. and Mellor, A. M., "Preliminary Study of Smoke Formed in the Combustion of Various Jet Fuels," J. Energy 1, (2), March 1977.
3. Bartok, W., Engleman, V. S., Goldstein, R. and Del Valle, E. G., "Basic Kinetic Studies and Modeling of NO Formation in Combustion Processes," AIChE Symposium Series 68, (126), 1975, p. 30.
4. Street, J. C., and Thomas, A., "Soot Formation in Premixed Flames," Fuel, Vol. 34, 1955, pp. 4-36.
5. Daniels, P. H., "Carbon Formation in Premixed Flames," Combustion and Flame, Vol. 4, 1960, pp. 45-49.
6. Tesner, P. A., "Formation of Dispersed Carbon by Thermal Decomposition of Hydrocarbons," 7th Symposium on Combustion, 1959.
7. Chakraborty, B. B., and Long, R., "The Formation of Soot and Polycyclic Aromatic Hydrocarbons in Diffusion Flames III; Effect of Additions of Oxygen to Ethylene and Ethane Respectively as Fuels," Combustion and Flame, Vol. 12, 1968, pp. 469-476.
8. Homann, K. H., "Carbon Formation in Premixed Flames," Combustion and Flame, Vol. 11, 1967, pp. 265-287.
9. Gill, D. W., "Review No. 182 - Luminosity and Soot Formation in Hydrocarbon Flames," BCURA Monthly Bulletin, Vol. XXII, No. 12, November-December 1958, pp. 487-506.
10. Clarke, A. E., Hunter, T. G., and Garner, F. H., "The Tendency to Smoke of Organic Substances on Burning," J. Inst. Pet., Vol. 32, pp. 627-642.
11. MacFarlane, J. J., Holderness, F. H., and Whiteher, F. S. E., "Soot Formation Rates in Premixed C<sub>2</sub> and C<sub>6</sub> Hydrocarbon-Air Flames at Pressure Up to 20 Atmospheres," Combustion and Flame, Vol. 8, 1964, pp. 215-229.
12. Schalla, R. L., and Hibbard, R. R., "Smoke and Coke Formation in the Combustion of Hydrocarbon-Air Mixtures," Chapter IX in "Basic Considerations in the Combustion of Hydrocarbon Fuels with Air," NACA Report 1300, 1957, pp. 242-255.
13. Fennimore, C. P., Jones, G. W., and Moore, G. E., "Carbon Formation in Quenched Flat Flames at 1600°K," 6th Symposium (International) on Combustion, 1956, pp. 242-246.
14. Stehling, F. C., Frazee, J. E., and Anderson, R. C., "Carbon Formation from Acetylene," 6th Symposium (International) on Combustion, 1956, pp. 247-254.
15. D'Alessio, A., DiLorenzo, A., Sarofim, A. F., Beretta, F., Masi, J., and Venitozzi, C., "Soot Formation in CH<sub>4</sub>-O<sub>2</sub> Flames," 15th Symposium (International) on Combustion, 1974, pp. 1427-1438.
16. Palmer, H. B., and Cullis, C. F., "The Formation of Carbon from Gases," Chapter 5 in Chemistry and Physics of Carbon, edited by P. L. Walker, 1965.
17. Schalla, R. L., and McDonald, G. E., "Mechanism of Smoke Formation in Diffusion Flames," 5th Symposium (International) on Combustion, 1954, pp. 316-323.
18. Arthur, J. R., and Napier, D. H., "Formation of Carbon and Related Materials in Diffusion Flames," 5th Symposium (International) on Combustion, 1954, pp. 303-315.
19. Gaydon, A. G., and Fairbairn, A. R., "Carbon Formation in C<sub>2</sub>H<sub>2</sub> and CO in Discharge Tubes," 5th Symposium (International) on Combustion, 1954, pp. 324-328.
20. Wright, F. J., "Effect of Oxygen on the Carbon Forming Tendencies of Diffusion Flames," Fuel, Vol. 53, No. 4, October 1974, pp. 232-235.

21. Schirmer, R. M., "Effect of Fuel Composition on Particulate Emissions from Gas Turbine Engines," in Emissions from Continuous Combustion Systems edited by W. Cornelius and W. G. Agnew, Plenum Press, 1972, pp. 189-210.
22. Magnusson, B. F., "An Investigation into the Behavior of Soot in a Turbulent Free Jet  $C_2H_2$  Flame," 15th Symposium (International) on Combustion, 1974, pp. 1415-1425.
23. Wright, F. J., "The Formation of Carbon Under Well-Stirred Conditions," 12th Symposium (International) on Combustion, The Combustion Institute, Pittsburgh, Pa., 1968, pp. 867-875.
24. Wright, F. J., "Carbon Formation Under Well-Stirred Conditions, Part II," Combustion and Flame, Vol. 15, 1970, pp. 217-222.
25. Jenson, D. E., "Prediction of Soot Formation Rates: A New Approach," Proc. Roy. Soc. London, A. 338, 1974, p. 375.
26. Tesner, P. A., Snegiriova, T. D. and Knorne, V. G., "Kinetics of Dispersed Carbon Formation," Combustion and Flame, 17, 1971, pp. 253-260.
27. Khan, I. M., and Greeves, G., "A Method For Calculating The Formation and Combustion of Soot in Diesel Engines," Heat Transfer From Flames, N. H. Afgan and J. M. Beer, Editors, Scripts Book Co./Halstead Press, 1974, pp. 389-404.
28. Edelman, R. B. and Harsha, P. T., "Laminar and Turbulent Gas Dynamics in Combustors - Current Status," Progress in Energy and Combustion Science, Vol. 4, 1978, pp. 1-62.
29. Lee, K. B., Thring, M. W., and Beer, J. M., "On the Rate of Combustion of Soot in a Laminar Soot Flame," Combustion and Flame, Vol. 6, 1962, pp. 137-145.
30. Nagle, J., Strickland-Constable, R. F., "Oxidation of Carbon Between 1000 - 2000°C," Proc. Fifth Carbon Conf., 1., 1962, p. 154.
31. Park, C., Appleton, J. P., Shock Tube Measurements of Soot Oxidation Rates," Combustion and Flame, 20, 1973, p. 369.
32. Longwell, J. P. and Weiss, M. A., Ind. Eng. Chem., 47, 1955, p. 1634.
33. Blazowski, W. S., "Dependence of Soot Production on Fuel Blend Characteristics and Combustion Conditions," ASME Paper 79-GT-155, 24th International Gas Turbine Conference, March 1979; to be published in ASME Transactions.
34. Graham, S. C., Homer, J. B., and Rosenfeld, J. L. J., "The Formation and Coagulation of Soot Aerosols," Int. Shock Tube Symposium, 10th Proceedings, (1975).
35. Graham, S. C., Homer, J. B., and Rosenfeld, J. L. J., "The Formation and Coagulation of Soot Aerosols Generated by the Pyrolysis of Aromatic Hydrocarbons," Proc. Roy. Soc. London A., (1978) Vol. 344.
36. Edelman, R. B. and Harsha, P. T., AFOSR Interim Scientific Report, "Mixing and Combustion in High Speed Air Flows," AFOSR-TR-78-0878, (SAI-78-008-WH), Science Applications, Inc., April 1978 (AD-A054398).
37. Harsha, P. T., and Edelman, R. B., "Application of Modular Modeling to Ramjet Performance Prediction," AIAA Paper 78-944, July 1978.
38. Harsha, P. T. and Edelman, R. B., "AFOSR Interim Scientific Report: Mixing and Combustion in High Speed Air Flows," Report SAI-79-013-WH, Science Applications, Inc., Woodland Hills, California, May 1979.
39. Swithenbank, J., Poil, I., Vincent, M. W., and Wright, D. D., "Combustion Design Fundamentals," Fourteenth Symposium (International) on Combustion, The Combustion Institute, Pittsburgh, 1973, pp. 627-636.
40. Roberts, R. A., Aceto, L. L., Kollrack, R., Teixeira, D. P., and Bonnell, J. M., "An Analytical Model for Nitric Oxide Formation in a Gas Turbine Combustor," AIAA Journal, Vol. 10, No. 6, June 1972.

#### ACKNOWLEDGEMENT

This work was supported by the U.S. Department of Energy, Division of Fossil Fuel Utilization (Contract No. EC-77-C-03-1543). Dr. J. Birkeland of DOE is the responsible Program Manager and Dr. J. Fisher of Argonne National Laboratory is the Technical Program Monitor.



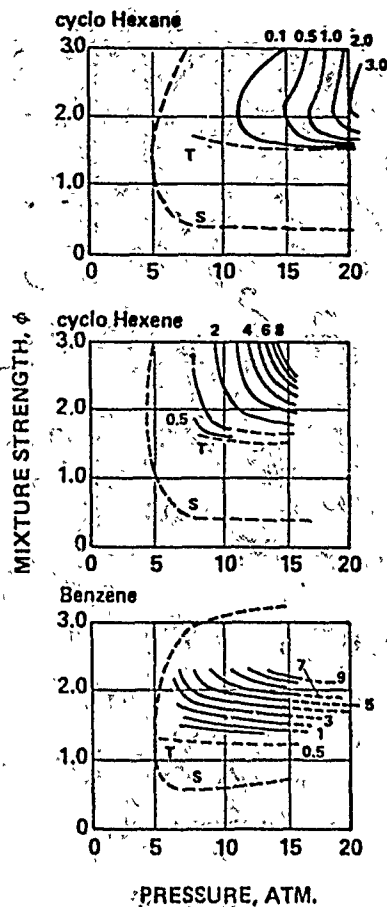


Figure 1. Effect of Pressure and Mixture Strength On Soot Formation

(S denotes flame stability limit, T the soot formation threshold, and numbers indicate conditions producing a constant "soot formation ratio") From Reference 37.

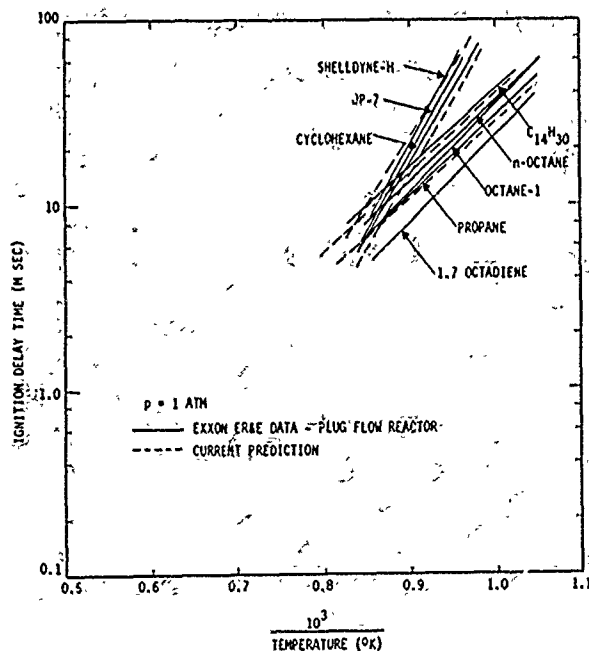


Figure 2. Experimental Ignition Delay Time Data - Comparison with Quasiglobal Kinetics Predictions for Aliphatic and Cyclic Type Hydrocarbons

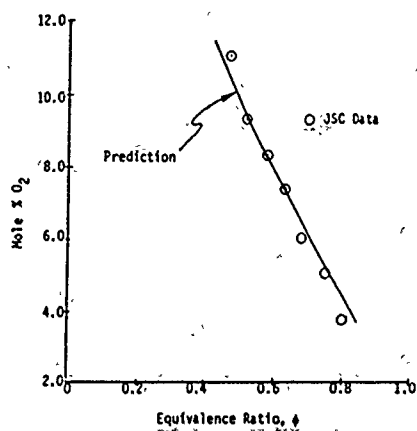


Figure 3. Comparison of Predicted and Measured  $O_2$  Concentration, Isooctane.

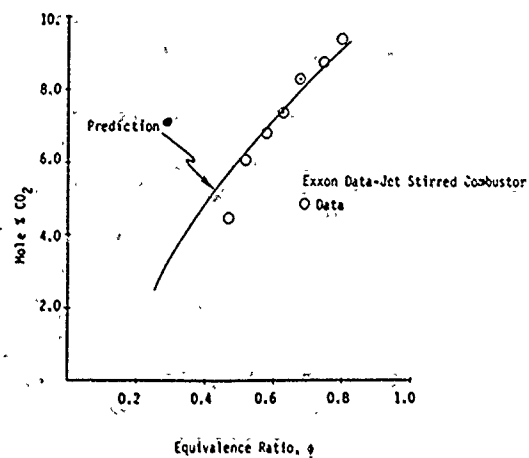


Figure 4. Comparison of Predicted and Measured  $CO_2$  Concentration, Isooctane.

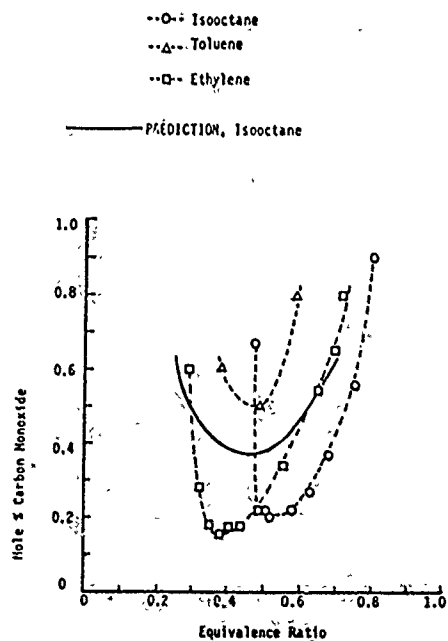


Figure 5. Comparison of Predicted with Measured  $CO$  Concentrations.

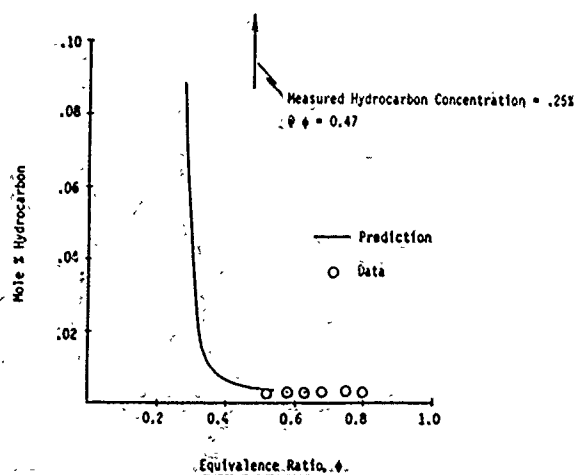


Figure 6. Comparison of Predicted and Measured Hydrocarbon Concentration, Isooctane.

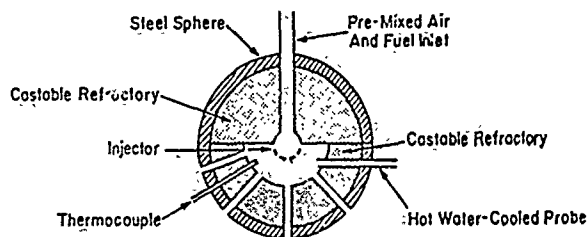


Figure 7. Schematic of Jet Stirred Combustor.

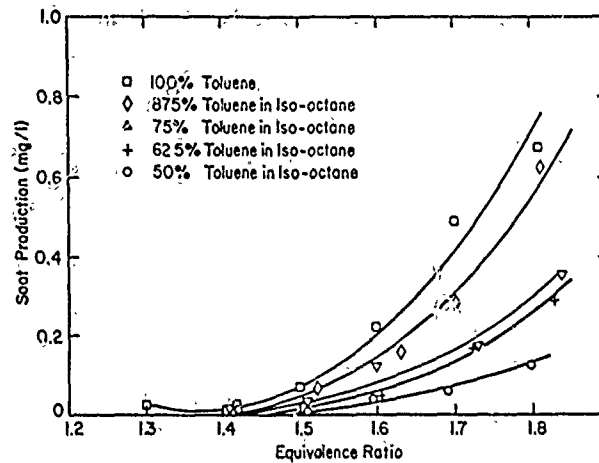


Figure 8. Soot Production vs. Equivalence Ratio for Toluene and Toluene/Iso-Octane Blends at 300 C Inlet Temperature and 112.5 gm/min Air Flow.

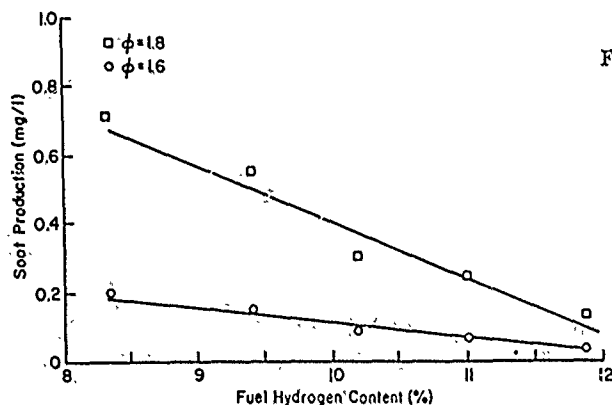


Figure 9. Dependence of Soot Production on Hydrogen Content of Toluene/Iso-Octane Blends.

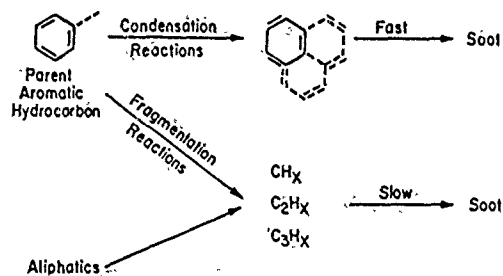


Figure 10. Simplified Soot Formation Mechanism.

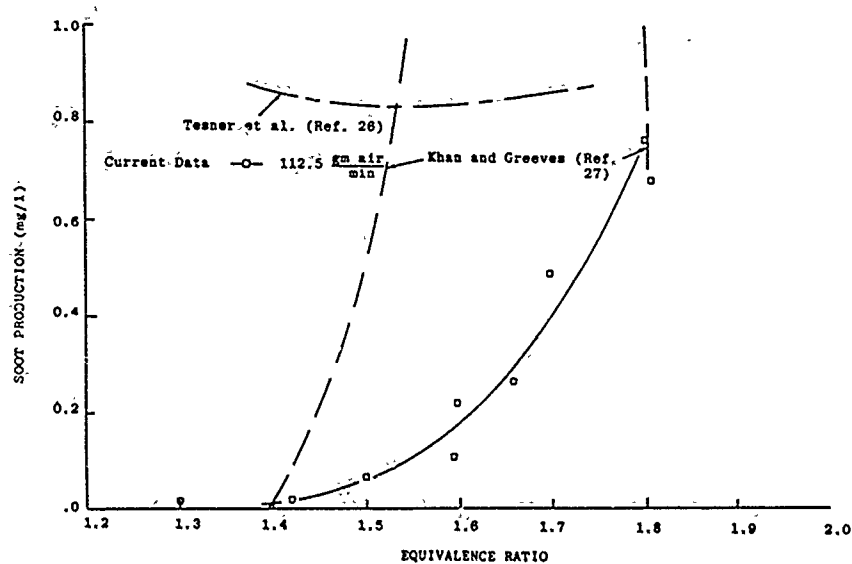


Figure 11. Comparison of Greeves and Tesner Model with Soot Production Data.

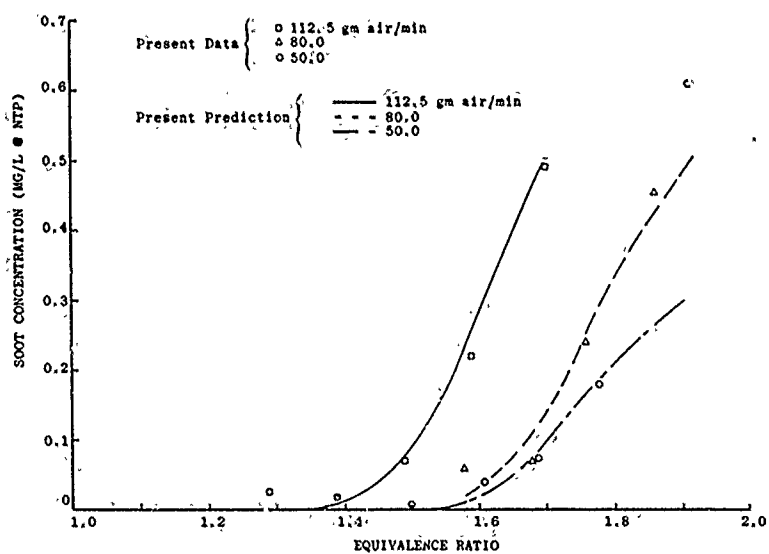


Figure 12. Comparison of Present Model Prediction with Soot Production Data For Toluene/Air Mixtures.

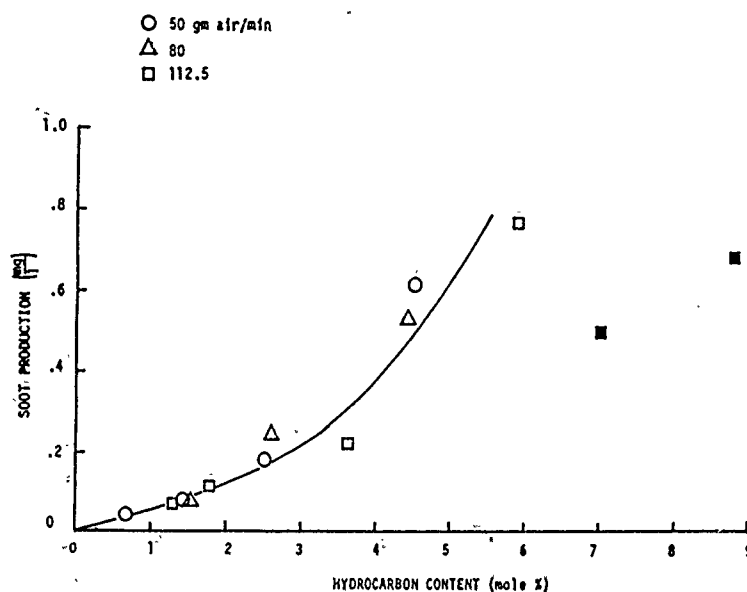


Fig.13 Correlation of soot production data with hydrocarbon concentration (Shaded data points indicates operation beyond rich blowout)

## DISCUSSION

A.M.Mellor, US

In your mechanism is  $C_nH_m$  a paraffin and  $C_xH_y$  an aromatic?

Author's Reply

The parent fuel ( $C_nH_m$ ) is an aromatic. The fuel manufactured by the pyrolysis of  $C_nH_m$  is anticipated to be a mixture of aliphatic and cyclic hydrocarbons. However it is worth noting that if the parent fuel is a mixture of an aromatic (toluene) and a paraffin (iso-octane) the sooting behaviour tends to follow the characteristics of the aromatics, i.e. soot is observed to occur at hydrocarbon break-through (see Figure 8). Measurements to be made in our program will define the manufactured fuel ( $C_xH_y$ ) and will serve to delineate the relationship between the parent fuel type and the hydrocarbon product.

J.Swithenbank, UK

Could you comment on:

- (1) The suggestion by C.Moses that soot formation is governed by the total Hydrogen content of the "fuel" including fuels emulsified with water, and the implied role of OH in the overall soot formation mechanism.
- (2) The effect of pressure on soot formation as predicted by your model.

Author's Reply

- (1) The results I have shown (see Figure 9 of the paper) tend to confirm what Moses inferred from his radiation measurements. However, Figure 9 shows a family of curves with equivalence ratio as the parameter while Figure 13 shows soot production to be a unique function of the hydrocarbon content in the reaction zone. Regarding the effect of OH, which will be influenced by added water, its presence will affect the intermediate species concentrations relevant to the formation of soot and consequently will affect the hydrocarbon content. In addition, it has been suggested that OH plays a direct role in the gasification of soot particles so that the net soot emissions appears to be a complex function of the OH radical as well as other intermediate hydrocarbon fragments.
- (2) Our soot production result is quite sensitive to pressure as seen in Equation 14. However, the actual dependence on pressure is a function of the concentration of the hydrocarbon and oxygen and of the temperature which are coupled in the quasiglobal model. This is a subject of our continuing program and it will include experiments over a range of pressure levels.

F.L. Dryer  
Mechanical and Aerospace Engineering  
Department  
Princeton University  
Princeton, New Jersey 08544, U.S.

C.K. Westbrook  
Lawrence Livermore Laboratory  
and  
Livermore, California 94550, U.S.

## SUMMARY

Chemical kinetic modelling of combustion in practical energy production systems is difficult for several reasons. First, very little information is available concerning the mechanistic details of fuel pyrolysis and oxidation for most typical hydrocarbon fuels. Secondly, in those few cases where many of the elementary reactions are known, rate data are generally unreliable or completely unknown. Finally, the large sets of chemical rate equations which arise are difficult and expensive to solve, even on the most powerful computers, when they are intimately coupled with fluid dynamics. As a result of these considerations, the conventional approach in many cases has been to use greatly simplified chemical kinetics models which avoid many of the above problems by confining attention only to the overall rates of fuel consumption and heat release. While extremely useful for interpretive calculations, this type of approach has been found to have certain significant limitations. The simplified models do not extrapolate well to conditions outside those for which the model itself was derived, quenching phenomena and pollutant formation are poorly described, and other results computed by such models can be misleading.

This paper describes the results of a systematic program designed to produce kinetic models for practical fuels. There are two principal goals to this work, both of which are immediately relevant to efficient combustor design. The first goal is the construction of detailed reaction mechanisms for the oxidation of typical hydrocarbon fuels, and the validation of these mechanisms through careful comparisons between computed and experimental data. These mechanisms are strongly hierarchical, with reactions for complex fuels containing subsets which describe the combustion of chemically simpler fuels. Progress to date includes relatively complete descriptions of carbon monoxide, hydrogen, methane, ethane, and methanol oxidation. In the development and verification of these reaction mechanisms we have attempted to use data from a variety of experimental sources, including flow reactor techniques, at intermediate temperatures (900 - 1300 K) and shock tube results for high temperatures (1300 - 2200K). In addition, ranges in fuel-air equivalence ratio between very lean ( $\phi < 0.1$ ) through stoichiometric to very rich ( $\phi > 5$ ) have been considered, all intended to make the models derived in this study as general as possible.

In addition to the direct utility of detailed kinetic models, such descriptions are very useful in the derivation and validation of appropriate simplified reaction schemes for practical fuels. Simplified models derived from detailed mechanisms are potentially more general than those derived entirely from experimental correlations. Furthermore, the additional kinetic insight gained by this approach can also provide additional insight into the operating characteristics of simplified mechanistic methods.

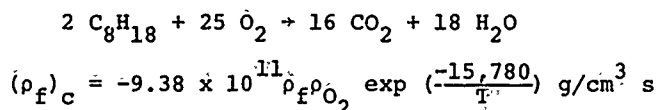
## INTRODUCTION

Numerical modeling is rapidly becoming an essential part of many combustion research programs. For a number of years numerical models have been used to assist in the interpretation of specific laboratory-scale experiments. In addition, computer analysis of idealized problems has provided useful insight into combustion problems which have been too complex to approach on an experimental basis. Yet, the eventual goal of more recent numerical work is the construction of representations which can assist directly in the design of practical combustors, i.e. which would be predictive as well as interpretive. Given the wide range of operating parameters experienced in most conventional combustion situations, it is clear that a suitable physical and numerical model for each of the many physical and chemical processes (atomization, vaporization, turbulence, heat transfer, chemical kinetics, etc.) must be embodied in this representation. These "sub models" must predict the independent phenomena as well as the correct coupling of various physical and chemical processes (e.g. turbulence and chemistry). Furthermore, calculations must be reliable even in parameter ranges where experimental data are not available to validate the predictions. Such numerical tools can be exceedingly valuable, reducing both the cost and the time required for the development of combustion systems. Here we wish to focus on some aspects of the construction of the submodel for combustion chemistry.

It should be recognized from the beginning that regardless of the apparent sophistication of some representations, all existing chemical kinetic models are in a real sense only approximations. Even the most detailed elementary chemical kinetic mechanisms which have been developed (e.g. those for  $H_2$ , CO,  $CH_4$  oxidation) are constructed on the basis of reproducing observable phenomena which are not all-encompassing. For more complex fuels, only limited kinetic information is available. Indeed in the case of aromatics, even the important species and elementary reactions remain in doubt. Furthermore, the evaluation of specific rate constants (or overall reaction) over ranges of temperature and pressure adequate for combustion modelling is an ever present

potential source of error.

In the following sections we shall discuss several techniques for describing the chemical kinetic behavior of combustion phenomena. At the simplest level have been the use of flame speed or single step heat release correlations. Such correlations may be cast as global or overall rate equations. For example, Butler et al. [1] have represented the combustion of n-octane as



where the subscript f refers to the fuel and the subscript c indicates the change in partial density due only to chemical reaction. Even simpler in kinetic terms is the specification of the rate of reaction as a function only of time. The functional dependence is derived from experimental data and used as input to the overall model. An example of this type of description is given by Blumberg [2] for combustion in stratified charge engines, where the fraction  $c$  of the mass which is burned, expressed as a function of crank angle  $\theta$ , is given by

$$c(\theta) = 1/2 \left( 1 - \cos \left( \frac{\theta - \theta_0}{\Delta\theta_c} \right) \right)$$

where  $\Delta\theta_c$  is the interval over which the combustion is assumed to take place. These approaches have been frequently employed in combustion modeling and have often been found to be adequate for interpretive calculations of overall system performance.

However, description of hydrocarbon combustion chemistry in substantial detail is required when considering a number of other practical combustion problems of current interest. These include:

- Transition to fast chemical reaction
  - a) spark ignition
  - b) compression ignition
  - c) engine detonation
  - d) transition from deflagration to detonation
  - e) explosion
- Flame quenching and hydrocarbon emission
  - a) by walls
  - b) by charge stratification
  - c) by rapid expansion
- Flame inhibition and extinction
- Fuel nitrogen conversion
- Thermal  $\text{NO}_x$  production within flame structures
- $\text{SO}_2/\text{SO}_3$  conversion in post-flame gases
- Soot formation, particularly for aromatics
- Soot oxidation
- Catalytic processes

In these areas, the chemistry and other submodels are generally coupled closely, and fluctuations in local enthalpy and species concentrations become important. Indeed, one probably cannot suitably model turbulent combustion without a detailed treatment of the combustion chemistry. However, we shall for this presentation exclude consideration of kinetic/turbulence coupling. The importance of this problem is clearly recognized. It has more recently been common to attempt validation of turbulent combustion models in which the chemistry submodel is known to be unrealistic. We believe the problem cannot be defined adequately without first assembling turbulence and chemistry models which correctly predict uncoupled phenomena.

In addition to difficulties in constructing a detailed chemical model its use is limited by several severe problems associated with the computer solution of the coupled chemistry/fluid mechanics equations. These problems are all related to the fact that even the best current scientific computers have size and speed limitations which cannot be neglected. In the most direct method of formulation, the concentration of each chemical species in the reaction mechanisms is represented by a single differential equation; common techniques then replace this differential equation with a finite difference equation. If the problem is one in which only chemical kinetics need be considered, neglecting spatial variations of physical quantities, then the number of equations to be solved is equal to the number of species, together with an equation for energy or enthalpy. Such sets of coupled difference equations (coupled through nonlinear reaction rate terms) are already often difficult to solve in an efficient and accurate manner.

When spatial variations of all quantities are included in the model, then difference equations for all species and the energy must be solved at each point in the physical domain, usually represented by a finite difference spatial mesh. The total number of equations to be solved, the amount of computer time required, and the computer storage requirements increase very rapidly. All of these limits are severely tested even for applications in which the spatial variations are limited to one dimension. For problems with two- and three-dimensional spatial variations, reaction mechanisms with many chemical species (>10) are probably too slow and expensive in terms of computer requirements. This is particularly true if one needs to perform any type of parametric numerical study. Thus, some kind of mechanism simplification must be considered for these cases.

These simplified mechanisms often lie between the two extremes of model complexity discussed above, and in addition to identifying some of the key properties and limitations of detailed and global reaction models we shall discuss at some length one of the more popular simplification approaches which have been proposed. The discussions below depend heavily on our earlier work [3,4,5,6,7,8,9] to illustrate these characteristics. Let us begin by first addressing the most complex approach, that of detailed mechanistic modelling.

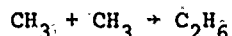
#### DETAILED KINETIC MECHANISMS

Table I gives an example of a comprehensive detailed chemistry model. This reaction mechanism for methanol oxidation which we have recently derived [3], accurately reproduces observed experimental chemical kinetic behavior for various experiments over the temperature range 1000-2180 K, the pressure range 1-5 atm, and the equivalence ratio range 0.05-3.0.

Examination of Table I provides some insight into the structure of detailed mechanisms for hydrocarbon oxidation. The methanol oxidation mechanism consists of 84 elementary reactions (each of which includes a finite rate in both the forward and reverse directions) involving 26 chemical species. If  $\text{NO}_x$  chemistry were to be considered, another 4 species ( $\text{N}$ ,  $\text{NO}$ ,  $\text{NO}_2$ ,  $\text{N}_2\text{O}$ ) and 10-15 reactions would be required. Consideration of fuel-bound nitrogen in the form of  $\text{NH}_3$  or  $\text{HCN}$  would require a further enlargement of the mechanism.

Reactions 40-56 provide a reasonably complete description of  $\text{H}_2$ - $\text{O}_2$  mixtures, and together with reactions 36-39 are adequate to describe carbon monoxide oxidation in the presence of water vapor. Experiments carried out in the Princeton University turbulent flow reactor for CO oxidation [10] at atmospheric pressure and ~1000 K have been accurately described with this reaction mechanism [7]. Figure 1 compares experimental and calculated results for the temperature, CO mole fraction, and  $\text{CO}_2$  mole fraction, all plotted as functions of distance (time) from the plug flow reactor inlet. The agreement between computed and experimental data for this one-dimensional reaction zone is excellent (Fig. 1b). It is interesting to note that when reactions involving  $\text{HO}_2$  and  $\text{H}_2\text{O}_2$  (Reactions 44 and 46-53) are omitted from the reaction mechanism, the model predictions do not agree well with experiment (Fig. 1a). The importance of  $\text{HO}_2$  and  $\text{H}_2\text{O}_2$  in CO systems has not been commonly appreciated [6], but it is clear from Fig. 1 that even the relatively simple case of CO oxidation is substantially modified by these reactions. It has often been suggested that these reactions are unimportant in combustion systems at temperatures above 1000 K. However, recent work [6] has shown that these species remain important for temperatures up to 1800 K at elevated pressure ( $P > 10$  atm). We have also recently noted a key role these species play in determining the pressure dependence of laminar flame velocity [9].

Reactions 11-35 and 57-84, together with the  $\text{CO}$ - $\text{H}_2$ - $\text{O}_2$  mechanism, comprise a methane oxidation mechanism which has been used to describe turbulent flow reactor results [7]. Typical results are shown in Fig. 2. In this study it was found that even for very lean ( $\phi = 0.05$ ) methane oxidation, it is important to include methyl radical recombination



and ethane oxidation reactions. The methane oxidation mechanism has been further applied to studies of the shock tube ignition of mixtures of methane and ethane [8,11] in order to assess the possible dangers of detonability in mixtures of liquified natural gas (LNG) and air. Some of these results are shown in Fig. 3, in which the ignition delay time  $\tau$  of a shocked gas sample is plotted as a function of reciprocal temperature. The upper solid line represents experimental data for stoichiometric methane-air and the lower solid line for stoichiometric ethane-air. Computed ignition delay times for stoichiometric mixtures of methane-ethane-air are shown as dashed lines. This study again confirms that ethane formation and oxidation is an essential part of the methane oxidation mechanism.

There are several general observations to be made with respect to the detailed reaction mechanism for methane. First, it should be noted that as a result of the difficulty with which methyl radicals are oxidized, there are complexities in the oxidation of even this simple fuel molecule. When these effects are included it is possible to reproduce experimental data for a wide variety of conditions, ie for both flow reactor and shock tube environments. Unfortunately, the strong dependence of the radical pool on the methyl radical oxidation reactions is uncharacteristic of larger alkyl hydrocarbon oxidation processes. Thus the resulting long induction period and oxidation character of methane do not closely simulate the combustion properties of conventional liquid fuel components.



Computed results for methane oxidation indicate several distinct phases or steps during which different reaction groups control the overall rate of oxidation. After the induction phase there is a period during which fuel is rapidly converted primarily to CO, followed by a phase dominated by the oxidation of CO to CO<sub>2</sub> (Fig. 2). The maximum CO mole fraction occurs at a distance of approximately 50 cm from the inlet end of the cylindrical duct. Other major intermediate species reach their maximum values at different locations. Some of these are CH<sub>2</sub>O (20 cm), C<sub>2</sub>H<sub>6</sub> (30 cm), C<sub>2</sub>H<sub>4</sub> (40 cm) and H<sub>2</sub> (45 cm). Using the rate expressions in Table I, at flow reactor temperatures,  $k(\text{CH}_2\text{O} + \text{OH}) > k(\text{C}_2\text{H}_6 + \text{OH}) > k(\text{H}_2 + \text{OH}) > k(\text{CO} + \text{OH})$ , and similar trends appear for reactions with O and H atoms. This ordering in reaction rates is responsible for relative locations where the species maximum concentrations occur. In fact, the hydrogen abstraction reaction rate of any alkyl hydrocarbon and a hydroxyl radical is more than 100 times larger than the CO + OH reaction rate at these temperatures. Since nearly all CO oxidation takes place by reaction with OH, it is clear that CO will react very slowly in the presence of hydrocarbons. The exothermicity of the carbon monoxide conversion provides a large fraction of the total heat of combustion for fuel-air mixtures. Thus, much of the energy release appears only after the fuel and major intermediate hydrocarbon species have been consumed. The interactive character of the carbon monoxide and methane oxidations is characteristic of that noted for larger alkyl hydrocarbon oxidation.

Reactions 1-10 in Table I were added to the earlier methane-ethane mechanism and used to describe methanol oxidation [3]. The mechanism was shown to describe shock tube and turbulent flow reactor data over wide ranges of fuel-oxygen equivalence ratio, temperature and pressure. Additional work showed that the reaction mechanism was able to predict laminar flame speeds for methanol-air mixtures over similarly wide ranges of operating conditions [9]. In order to have the capacity for making such predictions, the mechanism had to be thoroughly validated in a variety of experimental environments and over wide ranges of conditions. With this testing completed, the model predictions can be treated with greater confidence than if the mechanism had been able to reproduce only the shock tube or only the flow reactor experiments.

Flame speeds predicted by the model are shown in Figs. 4-6. In Fig. 4 the variation in laminar flame speed  $S_u$  with unburned gas temperature  $T_u$  is shown. Fig. 5 shows the variation of  $S_u$  with pressure  $P$ , and Fig. 6 describes the dependence of  $S_u$  on equivalence ratio,  $\phi$ . These predictions all agree well with the available experimental data, and a great deal of additional information is available from the computed flame results. For example, the nonlinear dependence of  $\log S_u$  on  $\log P$  in Fig. 5 has been observed for many years in flames of air with methane and other fuels, but no specific process had been shown to be responsible. With the detailed calculations, it was observed [9] that the contributions of  $\text{H} + \text{O}_2 + \text{M} \rightarrow \text{HO}_2 + \text{M}$ , become increasingly important with increase in pressure, leading to the observed flame speed dependence on pressure. This same reaction character must be of similar importance in any other hydrocarbon-air flame.

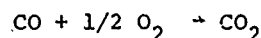
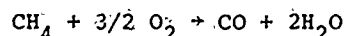
While we have demonstrated some of the favorable properties of detailed kinetic modelling, comprehensive mechanisms have been formulated and tested for only a few relatively simple fuels. Work is continuing on enlarging the number and types of fuels, the important elementary reactions, but the solution of large networks of differential equations can be both difficult and expensive to solve numerically. For practical purposes, when large detailed reaction mechanisms are used it is essential to simplify or idealize the geometrical domain to a single spatial coordinate. Problems with two or three spatial coordinates require prohibitive computer expenses. However, many practical problems which at first appear to be hopelessly two- and three-dimensional can be approached by considering a related but simplified one dimensional problem. Such simplified studies of stratified charge engine environments [12,13], flame quenching in expanding combustion chambers [14], and wall quenching in thermal boundary layers [15] have been able to provide a great deal of useful information through the use of detailed mechanisms.

#### GLOBAL REACTION MECHANISMS

Simpler reaction mechanisms than those described above can be needed for several reasons. These might include limited computer facilities, the necessity of using a fuel for which a detailed kinetics mechanism is unavailable, or a geometry for which two- or three-dimensional effects cannot be ignored or avoided. For such applications a greatly simplified reaction mechanism is needed which will provide sufficient accuracy for the given problem. In this section we will describe briefly some of the approaches which have been taken in defining and using global reaction mechanisms.

In many applications a single reaction step can be used. As we mentioned earlier, often the heat release from chemical reactions is used as an input quantity to the model, using this to determine other output quantities. In order to use this type of description it is necessary to have previously carried out enough experiments to be able to prescribe the heat release function accurately. Since a large part of the NO<sub>x</sub> formation in many combustion systems is a function of temperature in the burned gases, the amount of reacted gas, and the residence time in the combustion volume, this simple type of reaction model can give a surprisingly good estimate of NO<sub>x</sub> production. In order to obtain further kinetic detail it is necessary to make certain assumptions, such as the validity of chemical equilibrium in the burned gas, or partial equilibrium among the radical pool, etc.

The most commonly used simple mechanisms are the global types, with one or two overall reactions. The n-octane reaction discussed earlier is an example of a single step global reaction. An example of a frequently used two-step global mechanism is that for methane, developed by Dryer and Glassman [10] for post-induction phase lean oxidation of methane in the flow reactor, at atmospheric pressure,



The rates for these two reactions are given by

$$-\frac{d}{dt} [\text{CH}_4] = 10^{13.2} \exp(-48400/RT) [\text{CH}_4]^{0.7} [\text{O}_2]^{0.8} \text{ mole/cm}^3\text{-sec}$$

$$\frac{d}{dt} [\text{CO}_2] = 10^{14.75} \exp(-43000/RT) [\text{CO}]^{1.0} [\text{H}_2\text{O}]^{0.5} [\text{O}_2]^{0.25} \text{ mole/cm}^3\text{-sec.}$$

When these expressions are used to model the flow reactor experiments discussed earlier and summarized in Fig. 2, the agreement between the computer results using the simplified mechanism and the detailed mechanism is very good, as shown in Fig. 7.

These two-step global expressions have been used to model a variety of combustion systems. For example, the model yields a reasonable value of about 40 cm/sec for the laminar flame speed in stoichiometric methane-air at atmospheric pressure. However, as the pressure is increased, the simplified mechanism does not predict the  $P^{-0.5}$  dependence of flame speed on pressure. As a result, at 25 atm and above, the same mechanism gives a flame speed which is too large by a factor of more than five. In a study of charge stratification in internal combustion engines [12], it was necessary to reduce the rate of the first global reaction (consuming  $\text{CH}_4$ ) by about a factor of ten in order to achieve the same average flame speed as a detailed kinetic calculation. The original mechanism has also been used to study the propagation of reactive shock waves through methane/air clouds [16]. However, the shock-heated gas mixture in a detonation wave must undergo an induction phase before it can be oxidized, but the Dryer and Glassman mechanism was derived from post-induction phase methane oxidation. The use of shock tube correlations for the post induction oxidation of methane [17]

$$-\frac{d}{dt} [\text{CH}_4] = 7.9 \times 10^{11} \exp \left( \frac{-41600}{RT} \right) [\text{CH}_4]^{0.7} [\text{O}_2]^{0.8} \text{ moles/cm}^3\text{-sec}$$

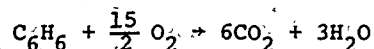
is equally invalid. This is true because under these conditions the total oxidation time for a shock heated mixture of fuel and air is about the same order as the chemical ignition delay time.

Potentially serious deficiencies in one-and two-step global mechanisms have been pointed out for the case of flame propagation through engine chambers [12]. First, global reaction schemes typically assume that the reaction goes to completion in the forward direction and that there is no reverse reaction. With the exception of low temperature combustion cases, this results in an overestimate of the total heat release, since in practice equilibrium exists in the burned gases. Neglecting this effect can lead to an overprediction of the final temperature and pressure (for fixed volume combustion) of 10-15%. A simple solution for this error is to artificially reduce the heat of combustion to give the correct final temperature. Alternatively the limit to which CO is oxidized to  $\text{CO}_2$  could be defined from equilibrium calculations.

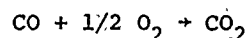
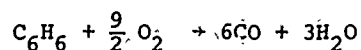
Another qualitative error associated with global reaction mechanisms is the implied assumption that energy is released instantaneously upon the consumption of reactants. A large fraction of the heat of reaction results from the oxidation of CO to  $\text{CO}_2$ , so in this respect the two-step mechanism is superior to the single-step scheme. The assumption of instantaneous heat release was shown [12] to lead to an interesting positive feedback phenomenon. The rates of the global reaction steps increase with increasing temperature and density, and when a sound wave compresses and heats a sample of reactants, the reaction rate increases. Since the increased reaction rate results in an immediate release of energy, the temperature again rises, further increasing the reaction (heating) rate. The detailed reaction mechanism produces a time delay following the fuel consumption, before the heat of combustion is available to heat the gases. In fact, many of the early steps in the reaction mechanism are endothermic, so for some brief time there is very little heat release. Also, the detailed mechanism correctly predicts that CO cannot react to form  $\text{CO}_2$  until all of the fuel has been consumed, further delaying the heat release process. This type of problem can be avoided by artificially reducing the rate of the CO oxidation step until the fuel is gone, reproducing qualitatively the behavior of the real system. A second approach is to place the heat of reaction in an artificial "reservoir" internally in the computer program; one then must prescribe the rate at which this energy is released to heat the product gases. Both solution methods are attempts to reconstruct the time-energy history of the reactants, a history which the detailed mechanism reproduces correctly.

Perhaps the most important advantage which global reaction mechanisms possess is the ability to "describe" arbitrary fuels. Thus it is possible to immediately write

down a global reaction for benzene, for example,



or



This says nothing about the details of how such reactions really occur, but in the absence of a better solution, such a scheme provides a way to attack the problem.

The following key points must be re-emphasized about global simplifications for oxidation of real fuels. First, the steps involved do not necessarily bear any direct relationship to the actual kinetic reaction sequence, even for CO oxidation. The rates of those global steps are derived from experimental data and are valid only under the same conditions as those experiments. The nature of the application must also be examined to be sure the global model is appropriate to that environment. Oxidation conditions and induction conditions, for example, are not the same and one should not expect the global reaction rates to be the same in the two environments. Global rate expressions are notoriously unreliable when extrapolated to conditions beyond those for which they were derived. This includes pressure ranges, equivalence ratios, and temperature ranges. Rates expressed for environments with N<sub>2</sub> diluent (as in real air) may not be valid when Argon diluent is used. Effects of mixtures of reactants, such as when two distinct fuels are mixed together with air, cannot be predicted properly. Still, if the global expressions to be used have been correlated with specific experimental results, and if those expressions are used carefully within their limits of validity, they can be very useful and provide a means of analysis for complex systems.

There is one further type of global rate expression which may be quite promising but which awaits development. For those fuels for which detailed reaction mechanisms have been developed (currently CO, H<sub>2</sub>, CH<sub>4</sub>, CH<sub>3</sub>OH, C<sub>2</sub>H<sub>6</sub>, and perhaps C<sub>2</sub>H<sub>4</sub> and C<sub>2</sub>H<sub>2</sub>), it is possible to use the detailed mechanism to predict global reaction rates as functions of operating parameters. This would then include the effects of equivalence ratio, temperature, pressure, and any other parameters in an explicit manner. This type of global rate expression would automatically be applicable to all of the conditions for which the detailed mechanism had been used. Production of this type of global rate expression directly from the detailed model is a readily available goal and would be very useful in many applications, however, the available detailed reaction mechanisms have not yet been used to generate this information.

#### SIMPLIFIED REACTION MECHANISMS

A type of mechanism simplification which has received considerable attention is the so-called quasi-global approach first developed by Edelman and Fortune [18]. This consists of representing the reaction of fuel and oxygen to form CO and H<sub>2</sub> by a single global step, followed by a detailed treatment of CO and H<sub>2</sub> oxidation. Edelman has reported [19,20] considerable success with this type of model for both plug flow and well stirred conditions. However, application of the same modeling techniques to turbulent flow reaction experiments [6] indicate some deficiencies in the approach.

In principle the concept of the quasi-global mechanism is very attractive. It combines the ability to describe arbitrary complex fuels with some estimate of radical species levels. For those fuels where a detailed reaction mechanism is available, the quasi-global mechanism is probably not very useful. This is due to the fact that the CO-H<sub>2</sub>-O<sub>2</sub>-NO mechanism used in the quasi-global model contains a large number of chemical species, approximately 13-15, depending on whether or not HO<sub>2</sub> and H<sub>2</sub>O<sub>2</sub> are included. The solution of 15 equations per time step per spatial cell represents an appreciable amount of computational effort. Thus the extension to the complete detailed mechanism does not represent an additional order of magnitude increase in the amount of computer labor required. Therefore, the benefits of the quasi-global approach are to be found primarily in its flexibility to accommodate any fuel, particularly those for which detailed mechanisms are not available.

In order to illustrate some of the properties and problems of the quasi-global model, two sets of calculations are reported here. The first set consists of a comparison between computed and measured species and temperature profiles for lean propane oxidation in the turbulent flow reactor [21]. The experimental data are summarized in Fig. 8, showing a steady consumption of the propane fuel which finally disappears at a distance of about 90 cm from the injection point. The concentrations of many species gradually increase as fuel is consumed, however CO<sub>2</sub> and temperature begin to increase rapidly. The peak in the CO concentration profile also occurs at about the same location, i.e. 90 cm.

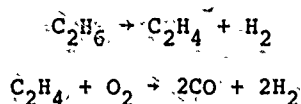
Calculated results using the most recent quasi-global reaction mechanism and the conditions of Fig. 8 are shown in Fig. 9, indicating that for this case the fuel disappearance rate computed using the quoted rate parameters is considerably too small. In addition, the computer CO mole fraction never exceeds  $5 \times 10^{-4}$ , a concentration much lower than the observed peak of about  $4 \times 10^{-3}$ . The computed CO<sub>2</sub> and temperature profiles also rise

steadily even though fuel remains unburned. The general conclusion one reaches is that in this case the quasi-global model underestimates the fuel consumption and overestimates the CO oxidation rate.

Some relatively minor modifications were made to the quasi-global mechanism in order to attempt correction of these problems. The pre-exponential term in the rate expression of the global reaction of  $C_3H_8$  to CO and  $H_2$  was increased from  $6 \times 10^4$  to  $1.5 \times 10^5$  in order to reproduce the propane disappearance rate. In order to inhibit the heat release until after the fuel was consumed, the rate of  $CO + OH \rightarrow CO_2 + H$  was artificially reduced until the fuel concentration was less than 1% of its initial value. As seen in Fig. 10, the computed results achieved with these modifications are qualitatively much closer to the experimental data.

A similar sequence of numerical model predictions were carried out and compared for flow reactor oxidation of 2-methylpentane (Fig. 11). With the considerably more complex fuel molecule, there are a variety of intermediate species which are present in significant amounts. The original quasi-global mechanism results are shown in Fig. 12. The fuel consumption is seen to be predicted accurately when the global reaction rate has a pre-exponential value of about  $2 \times 10^4$ . However, the predicted temperature rise is far too rapid, and the computed CO and  $CO_2$  profiles are seriously incorrect, even when the CO oxidation is inhibited (Fig. 13).

This disagreement is not entirely unexpected in that other intermediates containing large amounts of carbon are produced during the initial fuel consumption. To account for this effect, an additional global expression which models intermediate production and consumption must be proposed. This approach has been suggested by Cohen [22] for ethane oxidation:



but the rates of the global steps are different in the fuel-rich and fuel-lean regimes. The procedure of dividing the global step into several smaller but still global reaction steps is clearly promising but still not reliable for making predictive calculations.

#### SUMMARY

This paper has described a systematic study of kinetic oxidation models for practical fuels. The construction of detailed reaction mechanisms for the oxidation of typical hydrocarbon fuels, and the validation of these mechanisms through careful comparisons between computer and experimental data have been discussed. These mechanisms are strongly hierarchical, with reactions for complex fuels containing subsets which describe the combustion of chemically simpler fuels. Progress to date includes relatively complete descriptions of carbon monoxide, hydrogen, methane, and methanol oxidation. In the development and verification of these reaction mechanisms data from a variety of experimental sources, including flow reactor techniques at intermediate temperatures (900-1300 K) and shock tube results at high temperatures (1300-2200 K) have been used. In addition, ranges in fuel-air equivalence ratio between very lean ( $\phi < 0.1$ ) through stoichiometric to very rich ( $\phi > 5$ ) have also been considered.

Detailed models derived in this manner are themselves often very useful in the analysis of very specific combustion problems, in which simplified geometrical configurations or other approximations can be employed. Such analyses, using these detailed models, have been applied to the problems of bulk quenching of flames by rapid expansion of flame propagation through stratified charge conditions of generation of unburned hydrocarbon pollutants in thermal boundary layers in engines, and of detonation hazards in liquified natural gas.

In addition to the direct utility of detailed kinetic models, such approaches can be extremely useful in the derivation and validation of appropriate simplified reaction schemes for practical fuels. Simplified models which are derived from detailed mechanisms are potentially more general than those derived from experimental correlations.

However, detailed kinetic modeling of practical fuel oxidation is currently not possible. First, very little information is available concerning the mechanistic details of fuel pyrolysis and oxidation for most typical hydrocarbon fuels. Secondly, in those few cases where many of the elementary reactions are known, rate data are generally unreliable or completely unknown. Finally, the large sets of chemical rate equations which arise are difficult and expensive to solve, even on the most powerful computers, when they are intimately coupled with fluid dynamics. As a result of these considerations, the conventional approach in many cases has been to use greatly simplified chemical kinetic models developed from only limited experimental data. Interest has often been confined only to the overall rates of fuel consumption and heat release. While extremely useful in interpretive calculations, this approach has been shown to have several limitations which cause uncertainty in its use for predictive modelling. Such global models do not extrapolate well to conditions existing outside those for which the model was derived, or the analysis of quenching phenomena and/or pollutant formation. More general simplified schemes based on quasi-global modelling techniques show promise for improving modelling capabilities for conventional hydrocarbon fuels, but such models

probably remain too complicated for application in fully two and three dimensional time dependent computations.

#### REFERENCES

1. Butler, T.D., Cloutman, L.D., Dukowicz, J.K., Ramshaw, J.D., and Krieger, R.B., Toward a Comprehensive Model for Combustion in a Direct Injection Stratified Charge Engine, Proceedings of the General Motors Research Laboratories International Symposium on Combustion Modeling in Reciprocating Engines, Warren, Michigan, November, 1978. Available as University of California Los Alamos Scientific Laboratory Report LA-UR-78-3223.
2. Blumberg, P.N., Nitric Oxide Emissions from Stratified Charge Engines: Prediction and Control, Combustion Science and Technology 8, 5 (1973).
3. Westbrook, C.K. and Dryer, F.L., A Comprehensive Mechanism for Methanol Oxidation, Combustion Science and Technology 20, 125 (1979).
4. Dryer, F.L. and Glassman, I., Combustion Chemistry of Chain Hydrocarbons, Proceedings of Project SQUID Workshop on Alternative Hydrocarbon Fuels: Combustion and Chemical Kinetics, Columbia, Maryland, September 1977. Available in Volume 62 of Progress in Astronautics and Aeronautics, C.T. Bowman and J. Birkeland, eds.
5. Chang, J.S. and Westbrook, C.K., Recent Developments in Computer Modeling of Chemical Combustion Systems, Departments of Energy and Commerce Workshop on High Temperature Chemical Kinetics: Applications to Combustion Research, National Bureau of Standards, Gaithersburg, Maryland, December 1977.
6. Dryer, F.L. and Westbrook, C.K., Detailed Models of Hydrocarbon Combustion, Proceedings of the Department of Energy Workshop on Modeling of Combustion in Practical Systems, Los Angeles, California, January 1978. Available as University of California Lawrence Livermore Laboratory Report UCRL-80896, March 1978.
7. Westbrook, C.K., Creighton, J., Lund, C. and Dryer, F.L., A Numerical Model of Chemical Kinetics of Combustion in a Turbulent Flow Reactor, J. Phys. Chem. 81, 2542 (1977).
8. Westbrook, C.K., An Analytical Study of the Shock Tube Ignition of Mixtures of Methane and Ethane, Combustion Science and Technology 20, 5 (1979).
9. Westbrook, C.K. and Dryer, F.L., Prediction of Laminar Flame Properties of Methanol-Air Mixtures, to appear in Combustion and Flame.
10. Dryer, F.L. and Glassman, I., High Temperature Oxidation of CO and CH<sub>4</sub>, Fourteenth Symposium (International) on Combustion, The Combustion Institute, Pittsburgh, 1973.
11. Westbrook, C.K. and Haselman, L.C., Chemical Kinetics in LNG Detonations, Proceedings of the Seventh International Colloquium on Gasdynamics of Explosions and Reactive Systems, Gottingen, West Germany, August 1979. Available as University of California Lawrence Livermore Laboratory Report UCRL-82293, March 1979.
12. Westbrook, C.K., Propagation of a Flame Through a Stratified Charge Combustion Chamber, Acta Astronautica 5, 1185 (1978).
13. Westbrook, C.K., Fuel Motion and Pollutant Formation in Stratified Charge Combustion, Society of Automotive Engineers Paper SAE-790248, March 1979.
14. Smith, O.I., Westbrook, C.K. and Sawyer, R.F., Lean Limit Combustion in an Expanding Chamber, Seventeenth Symposium (International) on Combustion, The Combustion Institute, Pittsburgh, 1979.
15. Westbrook, C.K., Adamczyk, A.A., And Lavoie, G.L., A Numerical Study of Laminar Flame Wall Quenching, to be published.
16. Boni, A.A., Wilson, C.W., Chapman, M. and Cook, J.L., A Study of Detonation in Methane/Air Clouds, Acta Astronautica 5, 1153 (1978).
17. Penner, S.S., Heffington, W.M., Parks, G.E. and Sulzmann, K.G.P., Oxidation Rates in the Post-Induction Period for Methane Over a Wide Range of Equivalence Ratios, Paper 76-47 presented at the Fall 1976 Western States Section Meeting of the Combustion Institute, La Jolla, California.
18. Edelman, R.B. and Fortune, O.F., A Quasi-Global Chemical Kinetic Model for the Finite Rate Combustion of Hydrocarbon Fuels with Application to Turbulent Burning and Mixing in Hypersonic Engines and Nozzles, AIAA Paper 69-86, 1969.
19. Edelman, R.B., The Relevance of Quasi-Global Kinetics Modeling as an Aid in Understanding the I.C. Engine Process, Proceedings of the NSF (RANN) Workshop on the Numerical Simulation of Combustion for Application to Spark and Compression Ignition Engines, SAI, La Jolla, California, April 1975.

20. Edelman, R.B. and Harsha, P., Current Status of Laminar and Turbulent Gas Dynamics in Combustors, Spring Meeting of the Central States Section of The Combustion Institute, Lew Research Center, Cleveland, Ohio, March 1977.
21. Cohen, R.S., The High Temperature Oxidation and Pyrolysis of Ethane, Ph.D. Thesis, Princeton University, July 1977.
22. Cohen, R.S., Dryer, F.L. and Glassman, I., The Combustion of Hydrocarbons in an Adiabatic Flow Reactor, Joint Fall Meeting of the Central and Western States Sections of The Combustion Institute, San Antonio, Texas, April 1975.

#### LIST OF TABLE

1. Detailed reaction mechanism for methanol oxidation. See reference [3] for further details on reaction rates.

#### LIST OF ILLUSTRATIONS

1. Comparison between experimental data (open circles) and computed results (solid curves) for flow reactor oxidation of carbon monoxide. Top row gives results for calculations without  $\text{HO}_2$  and  $\text{H}_2\text{O}_2$  reactions, bottom row includes those reactions.
2. Comparison between experimental data (open circles) and computed results (solid curves) for flow reactor oxidation of methane.
3. Post-shock induction times for stoichiometric mixtures of methane and ethane. Top solid line represents experimental data for methane, lowest solid line for ethane. Dashed lines show computed results, with the legend indicating the fuel percentages of methane and ethane, respectively.
4. Flame speed ( $S_u$ ) in stoichiometric methanol-air mixtures as a function of unburned gas temperature ( $T_u$ ).
5. Flame speed in stoichiometric methanol-air mixtures as a function of pressure for unburned gas temperatures of 300 K and 600 K. Also shown are high and low pressure limiting expressions for flame speed.
6. Flame speed ( $S_u$ ) as a function of equivalence ratio at different pressures, with  $T_u = 300$  K.
7. Comparison between experimental data (solid curves) and computed results (dashed curves) for methane oxidation in the turbulent flow reactor. Computed results determined by the two-step global mechanism.
8. Experimental flow reactor data for propane oxidation.
9. Computed results for propane oxidation in the flow reactor, using the basic quasi-global mechanism.
10. Computed results for propane oxidation in the flow reactor, using the basic quasi-global mechanism (solid curves) and the modified quasi-global mechanism (marked with an X). Note the much higher CO level with the modified mechanism.
11. Experimental flow reactor data for oxidation of 2-Methylpentane.
12. Computer results for oxidation of 2-Methylpentane in the flow reactor, using the basic quasi-global mechanism.
13. Computed results for oxidation of 2-Methylpentane in the flow reactor, using the basic quasi-global mechanism (solid curves) and the modified quasi-global mechanism (marked with an X). Note the much higher CO level with the modified mechanism.

#### ACKNOWLEDGMENTS

This work was performed in part under the auspices of the U.S. Department of Energy by the Lawrence Livermore Laboratory under contract number W-7405-ENG-48 and in part by EC-77-S-02-4272. The authors also wish to thank Dr. A.K. Varma of Aeronautical Research Associates of Princeton for presenting this paper to the 54th (B) meeting of the Propulsion and Energetics Panel of AGARD.

Due to circumstances beyond their control, neither author was able to attend this conference.

#### NOTICE

This report was prepared as an account of work sponsored by the United States Government. Neither the United States nor the United States Department of Energy, nor any of their employees, makes any warranty, express or implied, or assumes any legal liability or responsibility for the accuracy, completeness or usefulness of any information, apparatus, product or process disclosed, or represents that its use would not infringe privately-owned rights.

Reference to a company or product name does not imply approval or recommendation of the product by the University of California or the U.S. Department of Energy to the exclusion of others that may be suitable.

Table I

Methanol oxidation mechanism. Reaction rates in  $\text{cm}^3 \cdot \text{mole}^{-1} \cdot \text{sec}^{-1}$  units,  $k = A T^n \exp(-E_a/RT)$

Reaction		Rate		
		log A	n	$E_a$
1	$\text{CH}_3\text{OH} + \text{M} \rightarrow \text{CH}_3 + \text{OH} + \text{M}$	18.5	0	80.0
2	$\text{CH}_3\text{OH} + \text{O}_2 \rightarrow \text{CH}_3\text{OH} + \text{HO}_2$	13.6	0	50.9
3	$\text{CH}_3\text{OH} + \text{OH} \rightarrow \text{CH}_3\text{OH} + \text{H}_2\text{O}$	12.6	0	2.0
4	$\text{CH}_3\text{OH} + \text{O} \rightarrow \text{CH}_3\text{OH} + \text{OH}$	12.2	0	2.3
5	$\text{CH}_3\text{OH} + \text{H} \rightarrow \text{CH}_3\text{OH} + \text{H}_2$	13.5	0	7.0
6	$\text{CH}_3\text{OH} + \text{H} \rightarrow \text{CH}_3 + \text{H}_2\text{O}$	12.7	0	5.3
7	$\text{CH}_3\text{OH} + \text{CH}_3 \rightarrow \text{CH}_3\text{OH} + \text{CH}_4$	11.3	0	9.8
8	$\text{CH}_3\text{OH} + \text{HO}_2 \rightarrow \text{CH}_3\text{OH} + \text{H}_2\text{O}_2$	12.8	0	19.4
9	$\text{CH}_3\text{OH} + \text{M} \rightarrow \text{CH}_3\text{O} + \text{H} + \text{M}$	13.4	0	29.0
10	$\text{CH}_3\text{OH} + \text{O}_2 \rightarrow \text{CH}_3\text{O} + \text{HO}_2$	12.0	0	6.0
11	$\text{CH}_3 + \text{M} \rightarrow \text{CH}_3 + \text{H} + \text{M}$	17.1	0	88.4
12	$\text{CH}_3 + \text{H} \rightarrow \text{CH}_3 + \text{H}_2$	14.1	0	11.9
13	$\text{CH}_3 + \text{OH} \rightarrow \text{CH}_3 + \text{H}_2\text{O}$	3.5	3.08	2.0
14	$\text{CH}_3 + \text{O} \rightarrow \text{CH}_3 + \text{OH}$	13.2	0	9.2
15	$\text{CH}_3 + \text{HO}_2 \rightarrow \text{CH}_3 + \text{H}_2\text{O}_2$	13.3	0	18.0
16	$\text{CH}_3 + \text{HO}_2 \rightarrow \text{CH}_3\text{O} + \text{OH}$	13.2	0	0.0
17	$\text{CH}_3 + \text{OH} \rightarrow \text{CH}_3\text{O} + \text{H}_2$	12.8	0	0.0
18	$\text{CH}_3 + \text{O} \rightarrow \text{CH}_3\text{O} + \text{H}$	14.1	0	2.0
19	$\text{CH}_3 + \text{O}_2 \rightarrow \text{CH}_3\text{O} + \text{O}$	13.4	0	29.0
20	$\text{CH}_3\text{O} + \text{CH}_3 \rightarrow \text{CH}_4 + \text{HCO}$	10.0	0.5	8.0
21	$\text{CH}_3 + \text{HCO} \rightarrow \text{CH}_4 + \text{CO}$	11.5	0.5	0.0
22	$\text{CH}_3 + \text{HO}_2 \rightarrow \text{CH}_4 + \text{O}_2$	12.0	0	0.4
23	$\text{CH}_3\text{O} + \text{M} \rightarrow \text{CH}_3\text{O} + \text{H} + \text{M}$	13.7	0	21.0
24	$\text{CH}_3\text{O} + \text{O}_2 \rightarrow \text{CH}_3\text{O} + \text{HO}_2$	12.0	0	6.0
25	$\text{CH}_3\text{O} + \text{M} \rightarrow \text{HCO} + \text{H} + \text{M}$	16.7	0	72.0
26	$\text{CH}_3\text{O} + \text{OH} \rightarrow \text{HCO} + \text{H}_2\text{O}$	14.7	0	6.3
27	$\text{CH}_3\text{O} + \text{H} \rightarrow \text{HCO} + \text{H}_2$	12.6	0	3.8
28	$\text{CH}_3\text{O} + \text{O} \rightarrow \text{HCO} + \text{OH}$	13.7	0	4.6
29	$\text{CH}_3\text{O} + \text{HO}_2 \rightarrow \text{HCO} + \text{H}_2\text{O}_2$	12.0	0	8.0
30	$\text{HCO} + \text{OH} \rightarrow \text{CO} + \text{H}_2\text{O}$	14.0	0	0.0
31	$\text{HCO} + \text{M} \rightarrow \text{H} + \text{CO} + \text{M}$	14.2	0	19.0
32	$\text{HCO} + \text{H} \rightarrow \text{CO} + \text{H}_2$	14.3	0	0.0
33	$\text{HCO} + \text{O} \rightarrow \text{CO} + \text{OH}$	14.0	0	0.0
34	$\text{HCO} + \text{HO}_2 \rightarrow \text{CH}_3\text{O} + \text{O}_2$	14.0	0	3.0
35	$\text{HCO} + \text{O}_2 \rightarrow \text{CO} + \text{HO}_2$	12.5	0	7.0
36	$\text{CO} + \text{OH} \rightarrow \text{CO}_2 + \text{H}$	7.1	1.3	-0.8
37	$\text{CO} + \text{HO}_2 \rightarrow \text{CO}_2 + \text{OH}$	14.0	0	23.0
38	$\text{CO} + \text{O} + \text{M} \rightarrow \text{CO}_2 + \text{M}$	15.8	0	4.1
39	$\text{CO}_2 + \text{O} \rightarrow \text{CO} + \text{O}_2$	12.4	0	43.8
40	$\text{H} + \text{O}_2 \rightarrow \text{O} + \text{OH}$	14.3	0	16.8
41	$\text{H}_2 + \text{O} \rightarrow \text{H} + \text{OH}$	10.3	1	8.9
42	$\text{H}_2\text{O} + \text{O} \rightarrow \text{OH} + \text{OH}$	13.5	0	18.4
43	$\text{H}_2\text{O} + \text{H} \rightarrow \text{H}_2 + \text{OH}$	14.0	0	20.3
44	$\text{H}_2\text{O}_2 + \text{OH} \rightarrow \text{H}_2\text{O} + \text{HO}_2$	13.0	0	1.8
45	$\text{H}_2\text{O} + \text{M} \rightarrow \text{H} + \text{OH} + \text{M}$	16.3	0	105.1
46	$\text{H} + \text{O}_2 + \text{M} \rightarrow \text{HO}_2 + \text{M}$	15.2	0	-1.0
47	$\text{HO}_2 + \text{O} \rightarrow \text{OH} + \text{O}_2$	13.7	0	1.0
48	$\text{HO}_2 + \text{H} \rightarrow \text{OH} + \text{OH}$	14.4	0	1.9
49	$\text{HO}_2 + \text{H} \rightarrow \text{H}_2 + \text{O}_2$	13.4	0	0.7
50	$\text{HO}_2 + \text{OH} \rightarrow \text{H}_2\text{O} + \text{O}_2$	13.7	0	1.0
51	$\text{H}_2\text{O}_2 + \text{O}_2 \rightarrow \text{HO}_2 + \text{HO}_2$	13.6	0	42.6
52	$\text{H}_2\text{O}_2 + \text{M} \rightarrow \text{OH} + \text{OH} + \text{M}$	17.1	0	45.5
53	$\text{H}_2\text{O}_2 + \text{H} \rightarrow \text{HO}_2 + \text{H}_2$	12.2	0	3.8
54	$\text{O} + \text{H} + \text{M} \rightarrow \text{OH} + \text{M}$	16.0	0	0.0
55	$\text{O}_2 + \text{M} \rightarrow \text{O} + \text{O} + \text{M}$	15.7	0	115.0
56	$\text{H}_2 + \text{M} \rightarrow \text{H} + \text{H} + \text{M}$	14.3	0	96.0
57	$\text{C}_2\text{H}_6 \rightarrow \text{CH}_3 + \text{CH}_3$	19.4	-1	88.3
58	$\text{C}_2\text{H}_6 + \text{CH}_3 \rightarrow \text{C}_2\text{H}_5 + \text{CH}_4$	-0.3	4	8.3
59	$\text{C}_2\text{H}_6 + \text{H} \rightarrow \text{C}_2\text{H}_5 + \text{H}_2$	2.7	3.5	5.2
60	$\text{C}_2\text{H}_6 + \text{OH} \rightarrow \text{C}_2\text{H}_5 + \text{H}_2\text{O}$	13.8	0	2.4
61	$\text{C}_2\text{H}_6 + \text{O} \rightarrow \text{C}_2\text{H}_5 + \text{OH}$	13.4	0	8.4
62	$\text{C}_2\text{H}_6 \rightarrow \text{C}_2\text{H}_5 + \text{H}$	13.6	0	38.0
63	$\text{C}_2\text{H}_6 + \text{O}_2 \rightarrow \text{C}_2\text{H}_5 + \text{HO}_2$	12.0	0	5.0
64	$\text{C}_2\text{H}_6 + \text{C}_2\text{H}_5 \rightarrow \text{C}_2\text{H}_5 + \text{C}_2\text{H}_6$	17.5	0	35.8
65	$\text{C}_2\text{H}_6 + \text{O} \rightarrow \text{CH}_3 + \text{HCO}$	13.0	0	1.1
66	$\text{C}_2\text{H}_6 + \text{M} \rightarrow \text{C}_2\text{H}_5 + \text{H} + \text{M}$	17.6	0	98.2
67	$\text{C}_2\text{H}_6 + \text{H} \rightarrow \text{C}_2\text{H}_5 + \text{H}_2$	13.8	0	8.0
68	$\text{C}_2\text{H}_6 + \text{OH} \rightarrow \text{C}_2\text{H}_5 + \text{H}_2\text{O}$	14.0	0	3.5
69	$\text{C}_2\text{H}_6 + \text{O} \rightarrow \text{CH}_3\text{O} + \text{CH}_3$	13.4	0	5.0
70	$\text{C}_2\text{H}_6 + \text{M} \rightarrow \text{C}_2\text{H}_5 + \text{H} + \text{M}$	16.5	0	40.5
71	$\text{C}_2\text{H}_6 + \text{M} \rightarrow \text{C}_2\text{H}_5 + \text{H} + \text{M}$	14.0	0	114.0
72	$\text{C}_2\text{H}_6 + \text{O}_2 \rightarrow \text{HCO} + \text{HCO}$	12.6	0	28.0
73	$\text{C}_2\text{H}_6 + \text{H} \rightarrow \text{C}_2\text{H}_5 + \text{H}_2$	14.3	0	19.0
74	$\text{C}_2\text{H}_6 + \text{OH} \rightarrow \text{C}_2\text{H}_5 + \text{H}_2\text{O}$	12.8	0	7.0
75	$\text{C}_2\text{H}_6 + \text{O} \rightarrow \text{C}_2\text{H}_5 + \text{OH}$	15.5	-0.8	17.0
76	$\text{C}_2\text{H}_6 + \text{O} \rightarrow \text{CH}_3 + \text{CO}$	13.8	0	4.0
77	$\text{C}_2\text{H}_6 + \text{O}_2 \rightarrow \text{HCO} + \text{CO}$	13.0	0	7.0
78	$\text{C}_2\text{H}_6 + \text{O} \rightarrow \text{CO} + \text{CH}_3$	13.7	0	0.0
79	$\text{CH}_2 + \text{O}_2 \rightarrow \text{HCO} + \text{OH}$	14.0	0	3.7
80	$\text{CH}_2 + \text{O} \rightarrow \text{CH} + \text{OH}$	11.3	0.68	25.0
81	$\text{CH}_2 + \text{H} \rightarrow \text{CH} + \text{H}_2$	11.4	0.67	25.7
82	$\text{CH}_2 + \text{OH} \rightarrow \text{CH} + \text{H}_2\text{O}$	11.4	0.67	25.7
83	$\text{CH} + \text{O}_2 \rightarrow \text{CO} + \text{OH}$	11.1	0.67	25.7
84	$\text{CH} + \text{O}_2 \rightarrow \text{HCO} + \text{O}$	13.0	0	0.0



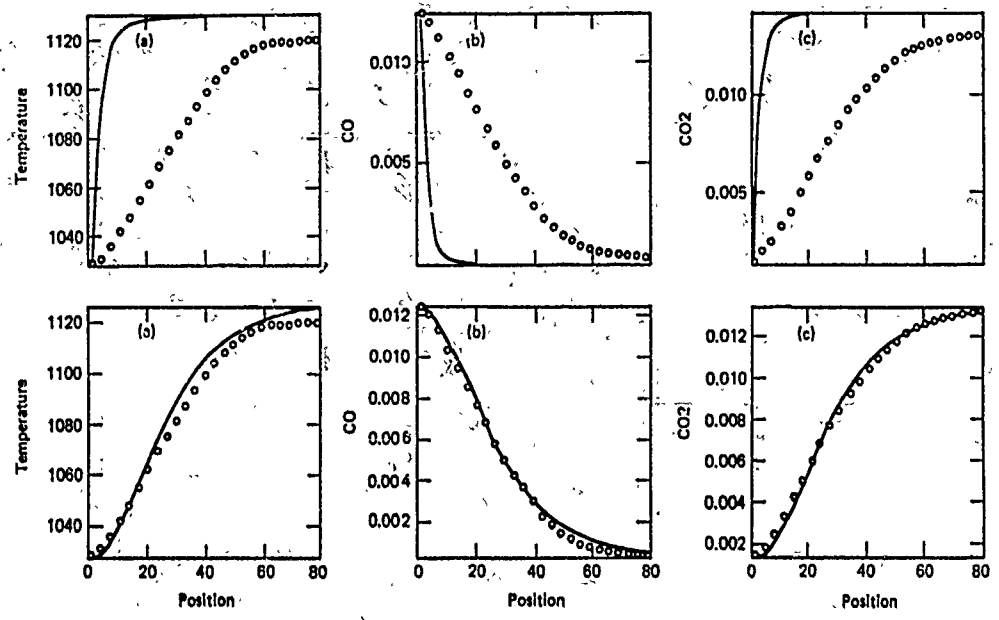


Figure 1

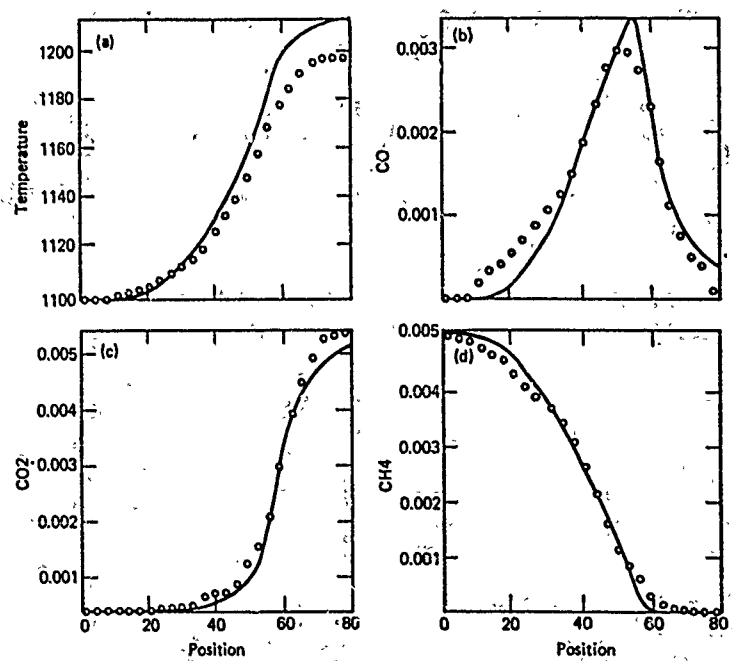


Figure 2



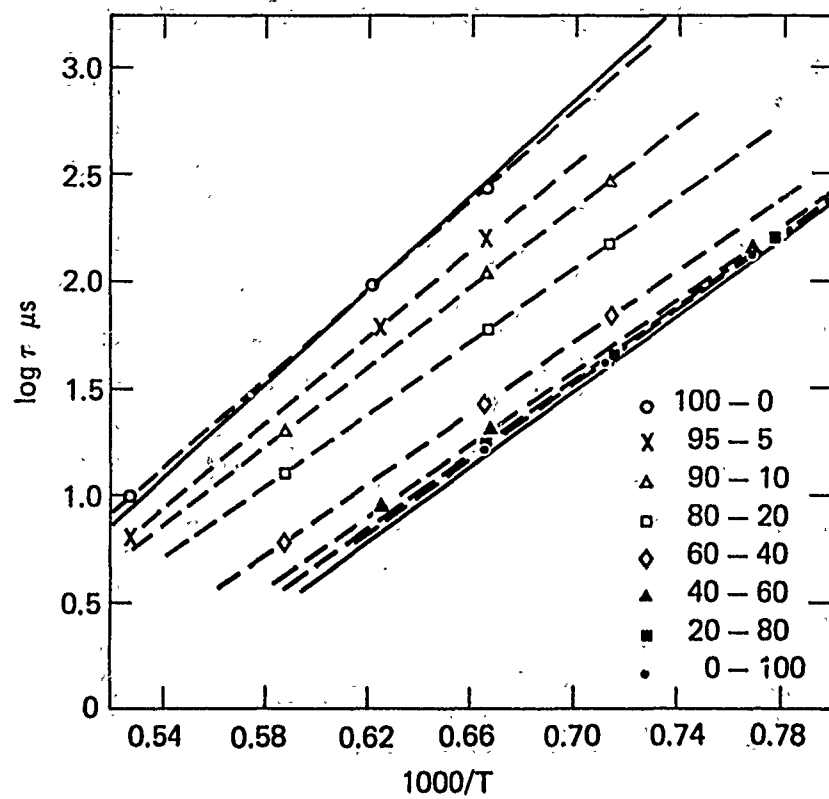


Figure 3

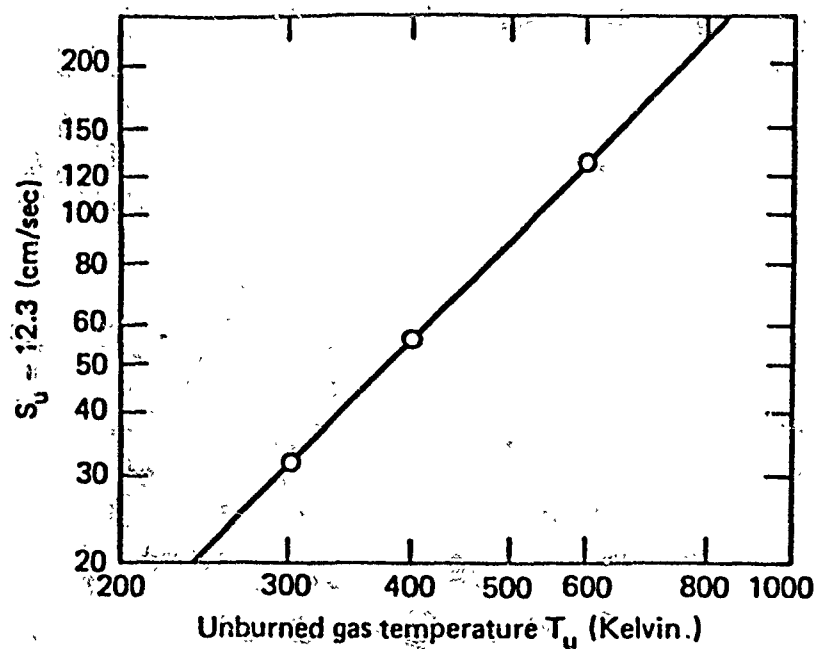


Figure 4

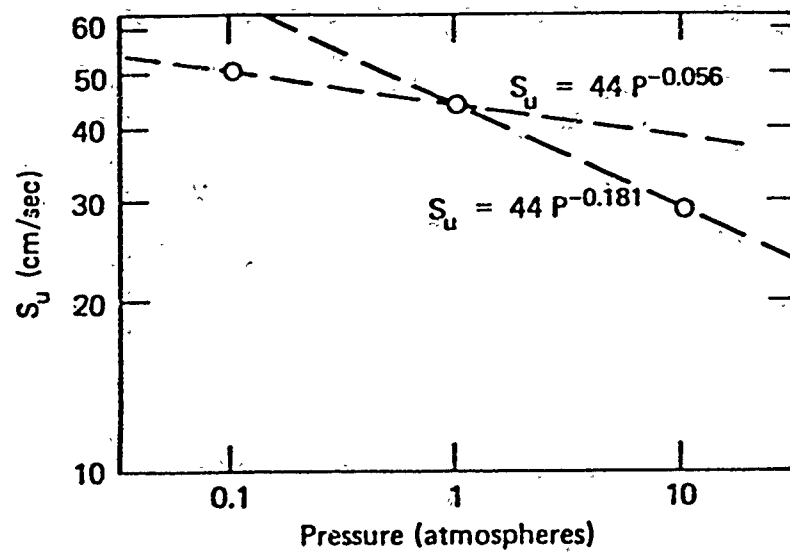


Figure 5

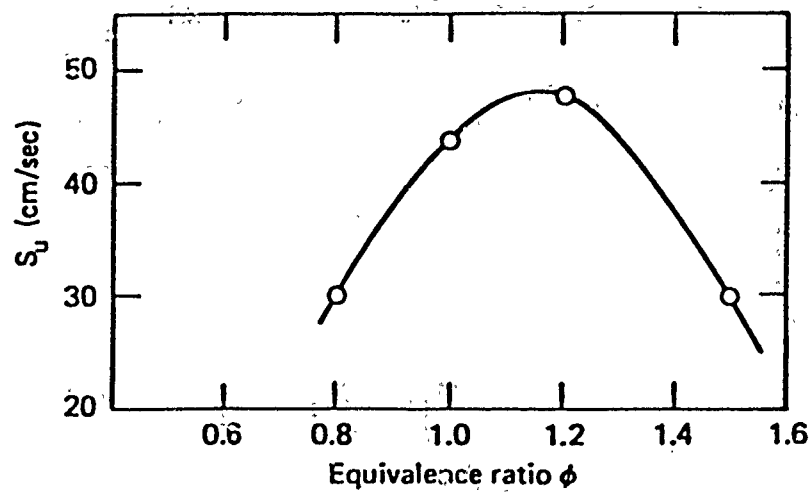


Figure 6

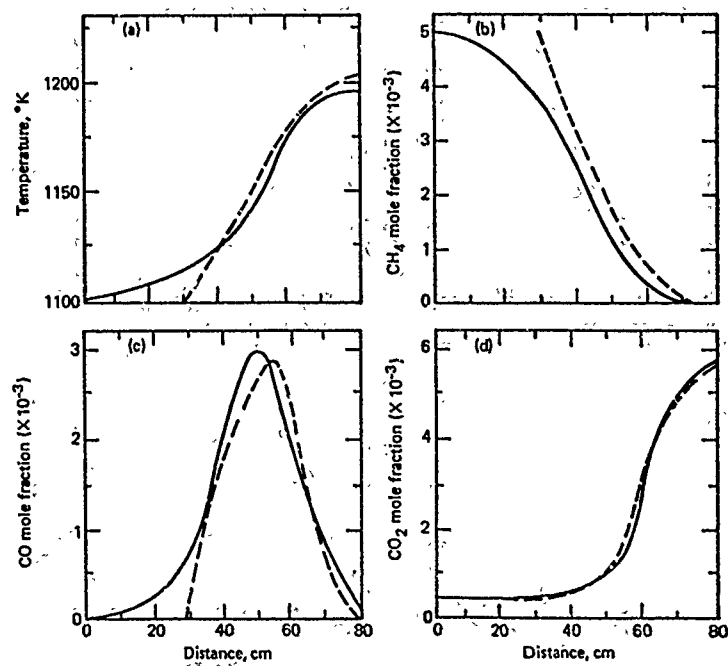


Figure 7

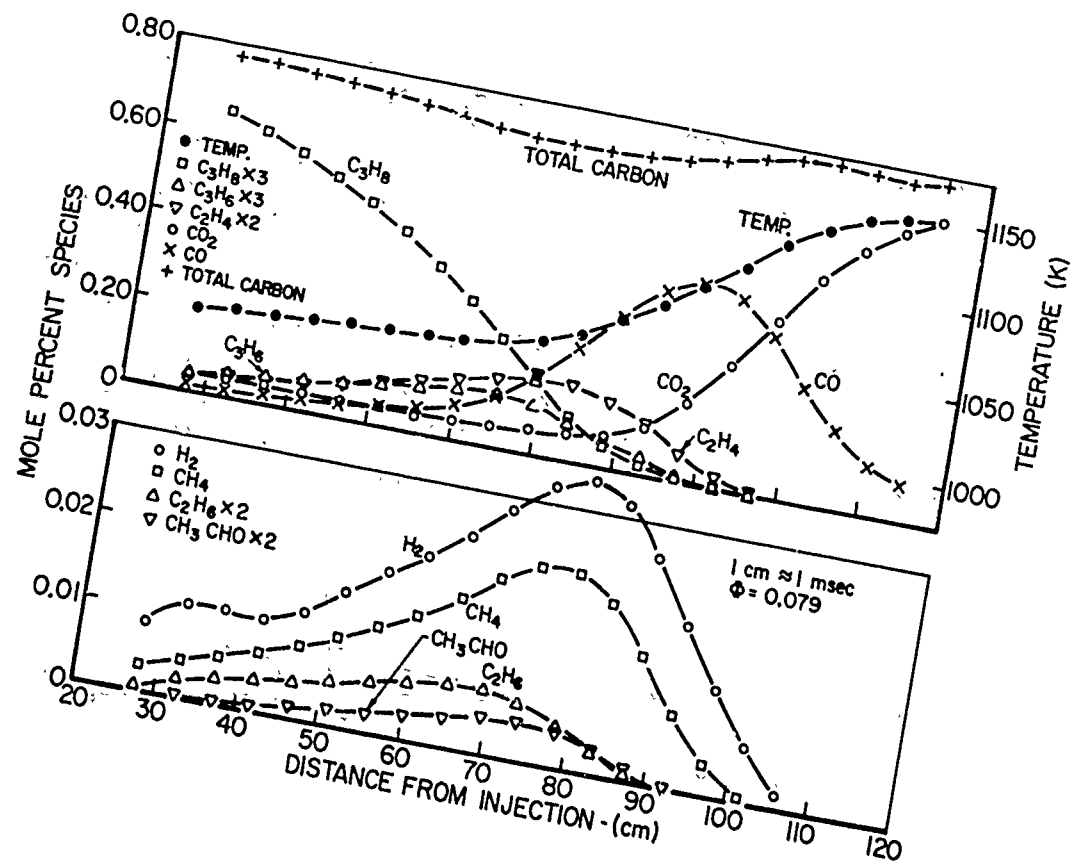


Figure 8

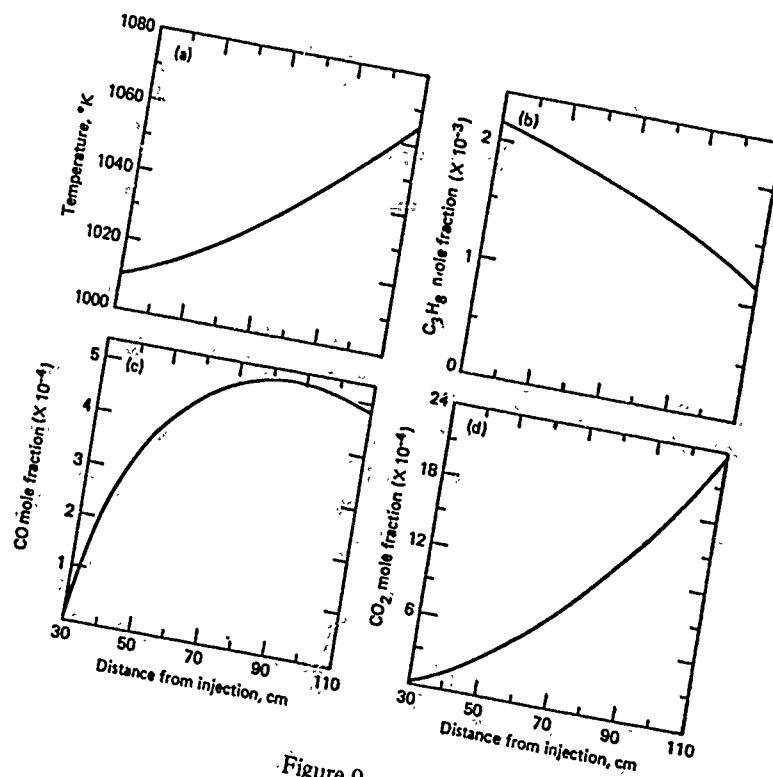


Figure 9

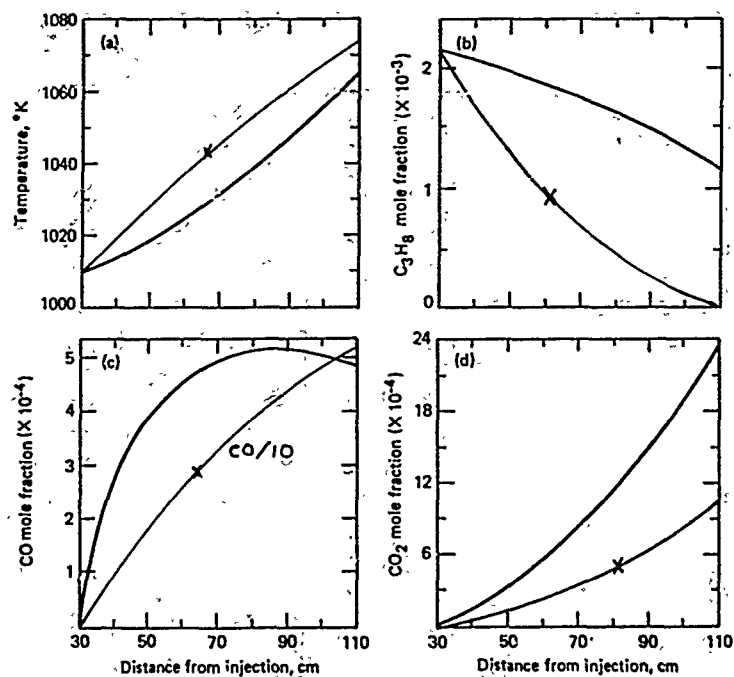


Figure 10

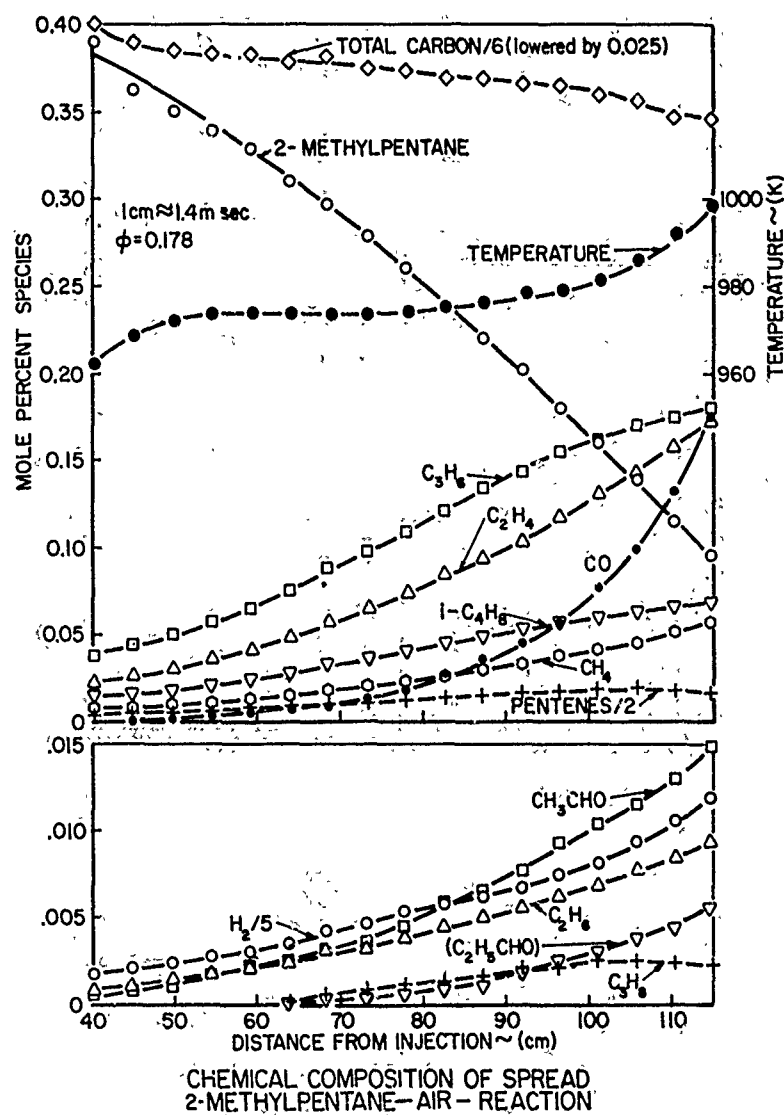


Figure 11

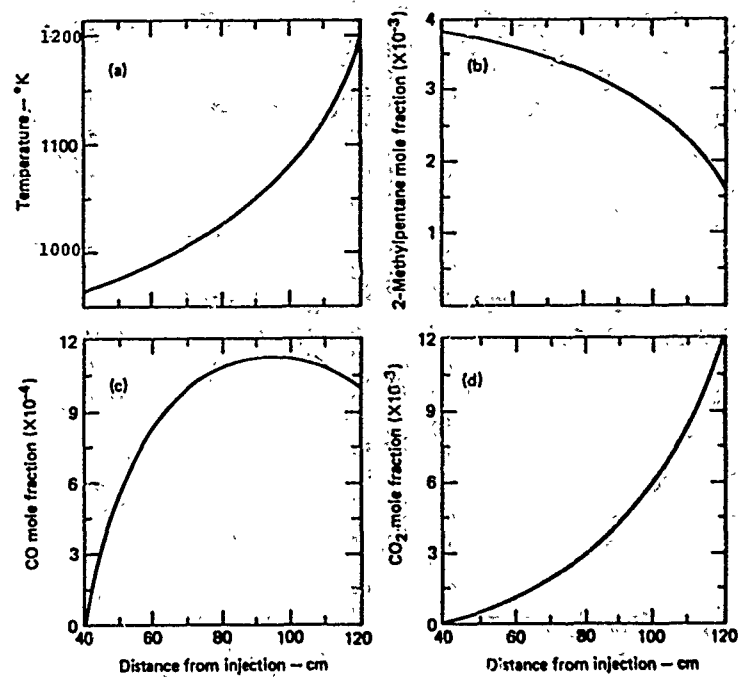


Figure 12

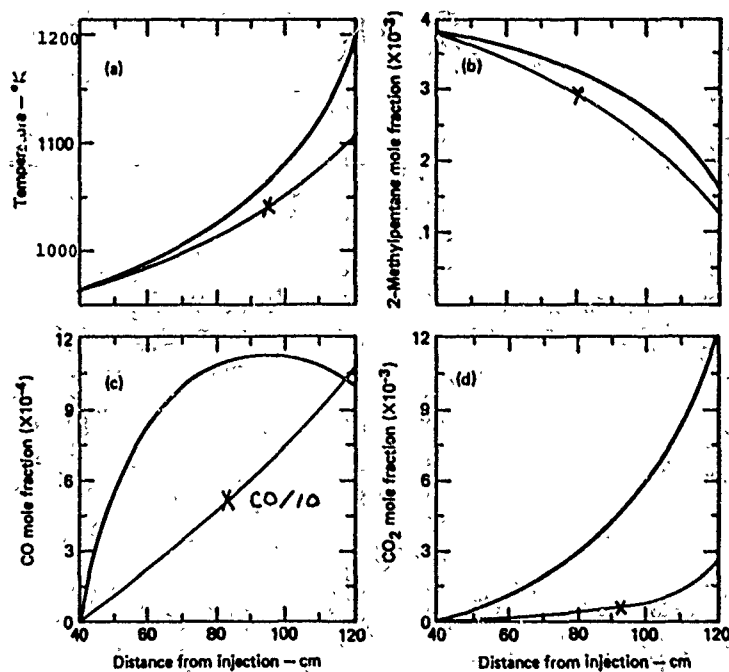


Figure 13

## DISCUSSION

## Comment by N.Peters, Ge

You pointed out that global models such as the one of Dryer and Glassman can not describe processes where the initial kinetic steps are important. However, there are very old proposals, of two step models, for instance, that of Zeldovich ( $A + B \rightarrow 2B$ ,  $2B \rightarrow C$ ), that concentrate on the initial kinetics. In this model the intermediate species may be interpreted as a radical that catalyses the fuel consumption. In his recent thesis, W.Hocks<sup>1</sup> calculated the fuel consumption during wall quenching by elementary methanol kinetics and by Zeldovich's two step kinetics. The global model did a good job in this case.

1. Hocks, W.

PhD Thesis — Institut für Allgemeine Mechanik, RWTH Aachen, Germany.

## Coalescence/Dispersion Modelling of Gas Turbine Combustors

David T. Pratt, Professor and Chairman  
Department of Mechanical Engineering and Applied Mechanics  
The University of Michigan  
Ann Arbor, Michigan 48109  
USA

Mellor has shown that  $\tau_{s1}$ , the turbulent mixing time, is the most dominant single characteristic time over the entire range of present or advanced concept combustors, and over the full load range from idle to full power<sup>(1)</sup>. Unfortunately, classical reactor-theoretic or "modular" models, as well as finite-difference approximate solutions to the governing differential equations, have heretofore regarded  $\tau_{s1}$  as either zero or infinite. Stochastic or Monte Carlo methods have shown promise for including effects of  $\tau_{s1} > 0$ , but only for simple chemistry. Preliminary experience with a newly-developed algorithm for integration of batch-reaction chemical rate equations shows great promise in making tractable the combined modelling of both finite-rate micromixing and complex, finite-rate chemistry, which is necessary for modelling of pollutant formation and combustor stability.

### 1. CHARACTERIZATION OF COMBUSTOR PROCESSES

A. M. Mellor has usefully characterized the complex interaction of serial and competing processes of chemistry, heat, mass and momentum transfer within a gas turbine combustor in terms of "characteristic times" (or reciprocal frequencies) of the dominant processes.<sup>(1)</sup> These are summarized in Table I. (All tables and figures appear at the end of the paper.)

In designing new combustors, or analysing or modifying existing combustors for improved efficiency, wider turndown ratio or stability limits, reduced pollutant production, or improved pattern factor, it is conceivable that any of the processes represented in Table I could become the dominant or controlling step. For example, high-altitude flameout or extinction is thought to be due to  $\tau_{fc}$  controlling at low pressures.<sup>(2)</sup>

In conventional combustors,  $\tau_{eb}$  can usually be removed from controlling status by improved vaporization, typically by reducing the mean fuel nozzle drop diameter. With airblast atomizers,  $\tau_{fz}$  may become important in controlling pollutant emissions, but it is negligible for pressure atomization.<sup>(1)</sup>

Mellor has shown that  $\tau_{s1}$ , the turbulent mixing time, is the most dominant single characteristic time over the entire range of present or advanced concept combustors, and over the full load range from idle to full power. In other words, at the conditions typical of gas turbine operation, chemical and heat release are always strongly influenced by, and frequently controlled by, the rate of turbulent mixing of

- a) vaporized fuel with air,
- b) recirculated burned gases with reactants in the primary zone, or
- c) dilution air with products in the secondary zone.<sup>(1,3)</sup>

### 2. MODELLING

Historically, gas turbine combustor development has been principally a trial-and-error process. After thirty years of cumulative experience, only cautious, incremental improvements in combustor design<sup>(4)</sup> are possible. Unlike compressors and turbines, in which aerodynamic and structural vibrations are to some extent predictable, combustors have largely defied quantitative characterization. However, in recent years, the need to modify or redesign combustors for reduced smoke and gaseous pollutant formation - always while maintaining or improving combustion efficiency, turndown ratio and pattern factor - has created a need for better understanding of the subtle interaction of these coupled non-linear processes.

The concurrent advent of the digital computer has raised the hope that more sophisticated analytical modelling might lead to reduced expenditures of time and manpower in achieving improved designs. While this promise has by no means been fully realized, there are some encouraging signs. For example, the present development of prevaporized, premixed combustors for low pollutant formation originated from numerical parametric studies which showed that there should exist a narrow window of fuel-air ratio, temperature and residence time within which stable, efficient combustion could be achieved, with low  $\text{NO}_x$ , CO and UHC as well.<sup>(5)</sup>

Generally speaking, modelling efforts to date stem from one of two fundamentally distinct approaches:

- a) Those based on chemical reactor-theoretic or "population balance" models - sometimes called the 'modular' approach - in which the fluid mechanics are simplified to the extent that convective flow and turbulent mixing is represented by interconnected well- or perfectly-stirred reactors (PSR's) and plug flow reactors (PFR's).<sup>(6)</sup>
- b) The second approach is to solve the finite-difference approximated differential equations for conservation of mass, species, momentum and energy, usually simplifying the chemistry to the point where pollutant formation processes cannot be adequately represented.<sup>(7)</sup>

What both of these approaches have lacked to date is the ability to model the effects of  $\tau_{s1}$ , the most universally important characteristic time within the combustor. In the modular approach,  $\tau_{s1}$  is, by definition, equal to zero in PSR's, and is zero for cross-stream mixing and infinite for age mixing (axial diffusion) in PFR's. In view of these inherent restrictions on PSR's and PFR's, Swithenbank's attempt to account for finite  $\tau_{s1}$  (6) is simply equivalent to increasing the value of  $\tau_{hc}$ , which still remains a homogeneous reaction time. Predictions resulting from this simplification may be useful for trend analysis, but cannot be valid for quantitative prediction of pollutant formation and destruction, as the effects of inhomogeneity or segregation (3) are still not represented.

In finite-difference modelling, it has been necessary heretofore to treat turbulent exchange processes as quasi-laminar; that is, to assume that, within a computational cell, local molecular homogeneity exists, or  $\tau_{s1} = 0$ . Some attempts have been made to include moment equations for the probability density function (PDF) of a passive scalar mixture fraction (7), which accounts for the effects of finite  $\tau_{s1}$ , but only with the "flame-sheet" assumption that  $\tau_{hc} = 0$ . Thus both approaches to date fail as quantitatively correct models for pollutant production, because both  $\tau_{hc}$  and  $\tau_{s1}$  are known to play essential roles.

In an actual combustor, recirculating flow is necessary for flame stabilization, while plug or stream flow is required to move the working fluid from compressor to combustor, to allow combustion reactions to progress towards completion within the combustor, and to move the working fluid from the combustor to the turbine inlet. A PSR is an idealization of a region with strong convective recirculation, whereas a PFR is an idealization of a simple stream tube flow. Due to recent advances in computation of stochastic or "Monte Carlo" methods (3,8), together with improved algorithms for calculating equilibrium and non-equilibrium chemistry (9,11), it is now possible to introduce finite-rate micromixing into both the PSR (age mixing) and PFR (cross-stream mixing only) models. In the PSR, this improvement allows assessment of the effects of primary-zone inhomogeneities due to fuel-air ratio, temperature, and "age", or degree of reactiveness within fluid elements. In the PFR regions, finite-rate mixing of secondary air admission into the post-primary stream may be described, leading eventually to prediction of mixing inhomogeneities on pattern factors.

### 3. THE COALESCENCE/DISPERSION (C/D) MODEL

A simple Bragg combustor model is assumed for present purposes: An imperfectly-stirred reactor represents the primary zone, followed by a plug-flow region.

The primary zone contents are discretized into computational cells or "turbules", which may be regarded conceptually (but not literally) as primitive representations of single-scale turbulent eddies. The mass flow rate through the primary zone is then represented by a number flow rate of turbules given by

$$\dot{N} = \dot{m}N / \langle \rho \rangle V = N / \tau ; \quad \tau \equiv \langle \rho \rangle V / \dot{m} \quad (1)$$

where  $\langle \rho \rangle$  is the ensemble mass density in the primary zone,  $V$  is the volume,  $\dot{m}$  the mass flow rate,  $N$  is the number of turbules and  $\tau$  is the mean residence time in the primary zone.

Micromixing, or mixing between turbulent eddies at the micro-scale level, is simulated by consideration of Corrsin's time constant for decay of a concentration fluctuation in an isotropic turbulent field,  $\beta$  (3). Defining  $I_m$  as the ratio of mixing frequency  $\beta$  ( $\tau_{s1}^{-1}$ ) to feed frequency ( $\tau^{-1}$ ), pairs of turbules within the reactor are allowed to simply average their properties, with one such "coalescence and dispersion" pair interaction allowed per time interval ( $\tau / I_m N$ ). Pairs are chosen by random selection so that there is no bias with respect to turbule age, thus representing a well-stirred reactor with non-zero segregation (3). During the time interval between C/D events, all turbules undergo adiabatic batch reaction, using either an infinite rate (equilibrium) assumption or a chemical kinetic mechanism and rate data, as desired. Whenever a feed time interval ( $\tau / N$ ) has elapsed, one turbule is selected at random to be removed from the assembly, and is replaced by a fresh feed turbule.

The assembly of turbules is initialized by assuming a homogeneous PSR distribution of mole numbers and corresponding temperatures. The C/D simulation is allowed to run for three to five equivalent residence times, until the ensemble statistics (mean and variance of properties) are observed to stabilize. Each turbule is then allowed to undergo further batch reaction for the secondary zone residence time; no further mixing is considered to occur in the model in the present state of development. Finally, ensemble averages are obtained to represent the mean properties at combustor exit. Mean and standard deviation (rms) values are obtained from the ensemble of  $N$  turbules using the elementary moment equations of descriptive statistics. For example, for temperature,

$$\langle T \rangle = \frac{1}{N} \sum_{i=1}^N T_i \quad (2)$$

and

$$T_{rms} \equiv \left[ \frac{1}{N} \sum_{i=1}^N (T_i - \langle T \rangle)^2 \right]^{1/2} \quad (3)$$

### 4. SUMMARY OF COMPUTATIONAL METHODS

For finite-rate gaseous chemistry, either premixed or non-premixed, it was found necessary to develop a new algorithm for integration of the coupled, non-linear, first-order ordinary differential equations describing the variation in composition and temperature with elapsed time within a constant-pressure, adiabatic batch reactor (turbule). The required characteristics for this algorithm were:

- (a) Speed. The large number of species (15-30) and turbules (presently 20, eventually up to 500) requires the fastest possible speed of execution.



- (b) Stability. The infinity of initial conditions, equivalence ratio and chemical time scales resulting from random selection procedures requires an extremely robust algorithm, preferably with automatic stepsize variation.
- (c) Accuracy. This is relatively unimportant, consistent with the crude assumptions on which the entire scheme is predicated. Further, accumulated roundoff errors leading to violation of atom conservation tend to be "flushed away" by the replacement of outflowing turbules with the steady inflow of reactants of prescribed stoichiometry.

An algorithm was developed which meets all of the above criteria, and is described in detail in Reference (11).

Briefly, consider the set of species conservation equations for transient batch reaction,

$$\frac{d\sigma_i}{dt} = -r_i, \quad i = 1, NS$$

where  $\{\sigma_i\}$  represents  $(i=1, NS)$  gas phase mole numbers, where  $r_i$  is the mass-specific rate of disappearance of  $i$ th species as given by

$$r_i = \frac{1}{\rho} \sum_{j=1}^{JJ} (\alpha'_{ij} - \alpha''_{ij}) (R_j - R_{-j}), \quad i=1, NS \quad (5)$$

where  $\rho$  is the mixture gas density  $\rho = P/RT\sigma_m$ ,  $\sigma_m$  is the sum of all mole numbers and where  $R_j$  and  $R_{-j}$ , the forward and reverse rates of the  $j$ -th reaction ( $j = 1, JJ$ ), are given by a modified Arrhenius expression

$$R_j = 10^{B_j} T^{N_j} \exp(-T_j/T) (\rho\sigma_m)^{\bar{\alpha}_j} \prod_{k=1}^{NS} (\rho\sigma_k)^{\alpha'_{kj}} \quad (6)$$

and

$$R_{-j} = 10^{-B_j} T^{-N_j} \exp(-T_j/T) (\rho\sigma_m)^{\bar{\alpha}_j} \prod_{k=1}^{NS} (\rho\sigma_k)^{\alpha''_{kj}} \quad (7)$$

Following Liniger and Willoughby (12), the solution to Eq. (4) over the short time interval  $h$  is first approximated by a "tunable trapezoid",

$$\sigma_i = \sigma_i^* - h[(1-W_i)r_i + W_i r_i^*], \quad i = 1, NS \quad (8)$$

where the "tuning" or integrating factor  $W_i$  is to be determined by "exponential-fitting" of  $r_i$  over the interval  $h$ , as follows:

If  $r_i$  should vary exponentially with time over  $h$ , so also would  $\sigma_i$ , as it is the integral of  $r_i$ ; therefore

$$\frac{d\sigma_i}{dt} = -r_i = c_i \sigma_i \quad (9)$$

Brandon (13) defines a diagonal transition matrix  $Z_i$  for the eigenvalue  $c_i$  over the integration interval  $h$  so that Eq. (9) is given by

$$-\frac{d\sigma_i}{dt} \equiv r_i = \left(\frac{Z_i}{h}\right) \sigma_i \quad (10)$$

With the substitution of Eq. (10) into Eq. (8), algebraic manipulation leads to the identity

$$W_i = \frac{1}{Z_i} - \frac{1}{(e^{Z_i} - 1)} \quad (11)$$

If  $r_i$  should actually vary exponentially over  $h$ , then  $Z_i$  is given precisely by Eq. (7). However, for arbitrary, non-exponential variation of  $r_i$ , Brandon (13) suggests an approximation to  $Z_i$  over the interval  $h$ , as follows:

$$Z_i = \frac{h}{2} \sum_{k=1}^{NS} \left[ \left( \frac{\partial r_i}{\partial \sigma_k} \frac{r_k}{r_i} \right)^{(o)} + \left( \frac{\partial r_i}{\partial \sigma_k} \frac{r_k}{r_i} \right)^{(s)} \right], \quad (12)$$

where the superscripts (o) and (s) refer to values evaluated at the zero-th and current (or last) iteration during convergence of Eqs. (8).

In the present application, a Newton-Raphson functional was defined for convergence of Eqs. (8),

$$f_i = \frac{\sigma_i - \sigma_i^*}{(1-W_i)h} + \frac{W_i}{(1-W_i)} r_i^* + r_i, \quad i = 1, NS \quad (13)$$

Following Gordon and McBride (14), a wise choice of correction variables for solving Eq. (13) are the natural logarithms of the NS mole numbers ( $\sigma_i, i=1, NS$ ); of the sum of the mole numbers,

$$\sigma_m \equiv \sum_{k=1}^{NS} \sigma_k \quad ; \quad (14)$$

and of the temperature T.

The Newton-Raphson correction equation for Eq. (13) may now be written as

$$\begin{aligned} \sum_{k=1}^N \frac{\partial f_i}{\partial \log \sigma_k} \Delta \log \sigma_k + \frac{\partial f_i}{\partial \log \sigma_m} \Delta \log \sigma_m \\ + \frac{\partial f_i}{\partial \log T} \Delta \log T = -f_i, \quad i = 1, NS. \end{aligned} \quad (15)$$

Noting that the integrating factors  $W_i$  are considered constant during each iteration, partial derivatives of the species -i functional  $f_i$  of Eq. (13) are

$$\frac{\partial f_i}{\partial \log \sigma_k} = \frac{\delta_{ik}}{(1-W_i)h} + \frac{1}{\rho} \sum_{j=1}^{JJ} (\alpha'_{ij} - \alpha'_{ij}) (R_j \alpha'_{kj} - R_{-j} \alpha'_{kj}), \quad i = 1, NS \quad (16)$$

$$\frac{\partial f_i}{\partial \log \sigma_m} = \frac{1}{\rho} \sum_{j=1}^{JJ} (\alpha'_{ij} - \alpha'_{ij}) (R_{-j} n'_j - R_j n'_j) + r_i \quad (17)$$

and

$$\begin{aligned} \frac{\partial f_i}{\partial \log T} = \frac{1}{\rho} \sum_{j=1}^{JJ} (\alpha'_{ij} - \alpha'_{ij}) \left[ R_j \left\{ N_j + \frac{T_{-j}}{T} - \bar{\alpha}_j - n'_j \right\} \right. \\ \left. - R_{-j} \left\{ N_{-j} + \frac{T_{-j}}{T} - \bar{\alpha}_j - n'_j \right\} \right] + r_i \end{aligned} \quad (18)$$

The functional for reciprocal mixture mole number,  $\sigma_m$ , is simply

$$f_m \equiv \sum_{k=1}^{NS} \sigma_k - \sigma_m \quad (19)$$

and the corresponding correction equation is

$$\sum_{k=1}^{NS} \sigma_k \Delta \log \sigma_k - \sigma_m \Delta \log \sigma_m = \sigma_m - \sum_{k=1}^{NS} \sigma_k \quad (20)$$

The functional for temperature is the equation for conservation of thermal energy for adiabatic batch reaction,

$$f_T \equiv \frac{H^*}{RT} - \sum_{i=1}^{NS} \frac{\sigma_i h_i}{RT} \quad (21)$$

and the corresponding correction equation

$$\begin{aligned} \sum_{k=1}^{NS} \frac{h_k \sigma_k}{RT} \Delta \log \sigma_k + \sum_{i=1}^{NS} \frac{C_{p,i}}{R} \sigma_i \Delta \log T \\ = \sum_{i=1}^{NS} \frac{\sigma_i h_i}{RT} - \sum_{i=1}^{NS} \frac{h_i^* \sigma_i}{RT} \end{aligned} \quad (22)$$

The partial derivatives required in Eq. (12) for the approximated diagonal transition matrix elements  $Z_i$  are given by

$$\frac{\partial r_i}{\partial \sigma_k} = \frac{1}{\sigma_k} \frac{\partial r_i}{\partial \log \sigma_k} = \frac{1}{(\rho \sigma_k)} \sum_{j=1}^{JJ} (\alpha'_{ij} - \alpha'_{ij}) (R_j \alpha'_{kj} - R_j \alpha'_{kj}) \quad (23)$$

which may be seen to be related to the second term on the RHS of Eq. (16).

In order to preserve the absolute A - stability of the implicit formulation (15) and to avoid numerical singularities, the integrating factors of Eq. (11) are actually calculated in the code as

$$W_i = \begin{cases} 0.5 & , Z_i \leq 0.015 \\ \frac{1}{Z_i} - \frac{1}{Z_i(e^{Z_i} - 1)} & , Z_i > 0.015 \end{cases} \quad (24)$$

The evaluation of the Jacobian for Eqs. (13) is done analytically, following the efficient coding techniques of CREK (9). As the Jacobian elements also contain the expressions required for evaluation of the integrating factors  $W_i$  (which are regarded as constants during each iteration) both accuracy and efficient computation are achieved.

Limited experience to date with the new algorithm has shown it to be remarkably stable and accurate. For all practical purposes, the limiting factor in its use appears to be resolution, rather than stability or accuracy. Of course, execution time is directly proportional to the desired resolution, independent of other considerations.

Stability is insured simply by using a modified version of the same "self-adjusting" underrelaxation parameter used in CREK (9, 10). This technique, originally due to Gordon and McBride (14), calculates underrelaxation parameters designed to assure that, for any iteration,

- i) Major species (mole fraction  $> 10^{-8}$ ) may not increase by more than a factor  $\exp(2)$ .
- ii) Minor species (mole fraction  $\leq 10^{-8}$ ) may not increase so as to exceed  $10^{-4}$  mole fraction.

In the present application, underrelaxation parameters so determined are applied not to the mole number and temperature Newton-Raphson corrections at a fixed step size, but rather to the time step size  $h$  itself.

In practice, the above criteria insure stability, but do not insure adequate resolution. Therefore, an additional constraint was added:

- iii) The temperature may not change by more than  $20^\circ\text{C}$ .

With this additional constraint, automatic stepsize control was easily achieved, and resulted in between 2 and 5 iterations per time step on the test problems considered thus far.

## 5. APPLICATIONS - I: COMBUSTION OF PREMIXED HYDROGEN AND AIR IN A JET-STIRRED REACTOR

A Longwell jet-stirred reactor, such as that described in Reference (16), and shown in Figure 1, may be thought of as an idealization of a highly loaded gas turbine premixed, prevaporized combustor primary zone. For this reactor, the mixing parameter may be estimated to be about  $I_m = 10$ , with  $I_m = 50$  being a practical upper bound. (17)

The effects of temperature and mole number segregation due to degree of reactedness are demonstrated in this first attempt to include finite-rate chemical kinetics with complex chemistry, using the simplified mechanism for  $\text{H}_2/\text{air}$  combustion given in Table II.

The simulation was run for five mean residence times, a sufficient time for the ensemble statistics to stabilize. The effect of segregation on ensemble-mean reaction rates can be characterized by a "contact index" (3)  $X_j$  for an individual reaction, defined as the ratio of ensemble-mean reaction rate to the apparent rate based on ensemble-mean properties:

$$X_j \equiv \frac{\{r_j(\{T_i, T\})\}}{r_j(\langle T \rangle)} \quad , \quad i = 1, NS \quad (25)$$

The calculated values of contact index for each forward and reverse reaction are given in Table II. Also shown are the ensemble mean and rms values of temperature,  $\langle T \rangle$  and  $T_{rms}$ , as calculated by Eqs. (2) and (3). As would be expected, the reactions with highest activation temperatures  $T_j$  (and therefore those most sensitive to temperature) show the greatest deviation of  $X_j$  from unity.

## 6. APPLICATIONS - II: PREMIXED, PREVAPORIZED COMBUSTION IN A SWIRL-CAN COMBUSTOR

The purpose of this investigation was to assess the applicability of C/D modelling in predicting pollutant formation in gas turbine combustion. This combustor was selected for C/D modelling since measured emission index data are available (18), and the additional complications of fuel spray evaporation are not present in premixed, prevaporized combustors.

A simplified model of an array of swirl-can modules (Figure 2) was developed (19), with the following assumptions:

- (1) Upon entry to the combustor primary zone, the fuel is completely vaporized and thoroughly mixed with the primary air.
- (2) The combustor may be represented as a modified Bragg combustor (2) as shown in Figure 3.
- (3) A 17-step mechanism for CO and H<sub>2</sub> oxidation and NO<sub>x</sub> formation due to Waldman (20), together with a global pyrolysis step,  $C_{12}H_{23} + O_2 \rightarrow CO + H_2$ , of Edelman (21) is used, as shown in Table IV.

The combustion chamber was represented by a zone-type model, shown schematically in Figure 3. The sizing and location of PSR (perfectly-stirred reactor) and PFR (plug-flow reactor) elements was done by inspection from Figure 2.

The primary zone was modeled in two different ways, first as a homogeneous (fully micromixed) PSR with zero segregation ( $\tau_{sl} = 0$ ), using the complex kinetics code CREK (9, 10), and secondly as a partially segregated WSR (well-stirred reactor), with effects of segregation modeled by the C/D model with  $I_m = 2.0$  assumed. The secondary zone was treated identically in both cases as simple PFR batch reaction of the effluent gases from the primary zone without further mixing ( $\tau_{sl} \rightarrow \infty$ ;  $I_m = 0$ ). Test conditions for the calculations are given in Table V.

In Figures 4 and 5, comparative results of measured and predicted values of emission index values for NO<sub>x</sub> and for CO, respectively, are presented.

In Figure 4, it may be seen first that the premixed, prevaporized concept results in considerable reduction of NO<sub>x</sub> below the equilibrium values. The predicted values for assumed homogeneous ( $\tau_{sl} = 0$ ) PSR primary zone shows the correct order of magnitude but a "peaky" trend that differs considerably from measured values. A single computation using the C/D model with  $I_m = 2$ , and the same conditions, at (F/A) = 0.03, shows far better agreement with the data than does the homogeneous ( $I_m \rightarrow \infty$ ;  $\tau_{sl} = 0$ ) PSR prediction.

In Figure 5, the CO emission index values predicted by the homogeneous PSR model are seen to approximate very closely the equilibrium values as (F/A) approaches stoichiometric; at fuel-lean conditions, the effect of  $\tau_{sl}$  is seen in the upward trend of COEI. The single point represents the COEI predicted by the C/D model with  $I_m = 2$ , at (F/A) = 0.03. As with the NOEI in Fig. 4, the "smearing" effect of segregation or inhomogeneity is seen to give better agreement with the data.

## 7. DISCUSSION AND CONCLUSIONS

Needless to say, a single point comparison of computation with the C/D model with the NASA data is insufficient grounds for drawing strong conclusions. However, compared with a conventional modular, homogeneous ( $I_m \rightarrow \infty$ ) PSR-PFR Bragg model, the (C/D) Bragg model with  $I_m = 2$  is seen to improve the comparison with data at very fuel-lean conditions, for both CO and NO<sub>x</sub> emission indexes. These results are at least encouraging. Of more significance is the fact that the computation is feasible at all.

The preliminary results reported are therefore encouraging for the use of coalescence/dispersion modelling for prediction of pollutant formation and eventually flame stabilization in high-intensity continuous combustors. Extensions of the concept to flows lacking the strong convective recirculation characteristic of the present system are possible (3), and such work is presently in progress.

An additional benefit of C/D modelling that has not been explored here is the potential ability to predict realistic combustor stability or blowout maps, as well as transient behavior. However, the variation of  $I_m$  with combustion temperature during transient would have to be calculated. (22)

## 9. REFERENCES

1. Mellor, A.M., Gas Turbine Engine Pollution, in Progress in Energy and Combustion Science, Vol. 1, N.A. Chigier, Ed., Pergamon Press, 1976.
2. Bragg, S.L. and Holliday, J.B.: The Influence of Altitude Operating Conditions on Combustion Chamber Design, in Selected Combustion Problems, II, M.W. Thring, Ed., Butterworths Scientific Publications, 1956.
3. Pratt, D.T., Mixing and Chemical Reaction in Continuous Combustion, Progress in Energy and Combustion Science, Vol. 1, N.A. Chigier, Ed., Pergamon Press, 1976.
4. Hazard, H. R., Combustor Design, in Sawyer's Gas Turbine Engineering Handbook, Vol. I, J. W. Sawyer, Ed., Gas Turbine Publications, Inc., 1972.
5. Wade, W.R., Shea, P.I., Owens, C.W. and McLean, A.F., Low Emissions Combustion for the Regenerative Gas Turbine, Part 1: Theoretical and Design Considerations, ASME Paper No. 73-GT-11, 1973.
6. Swithenbank, J., Turan, A. and Felton, P.G., Fundamental Modelling of Mixing, Evaporation and Kinetics in Gas Turbine Combustors, Paper 15-2, this volume.
7. Elghobashi, S., Studies in the Prediction of Turbulent Diffusion Flames, Studies in Convection - Vol. 2, B.E. Launder, Ed., Academic Press, 1977.
8. Flagan, R.C. and Appleton, J.P., Combustion Flame 23, p. 249, 1974.
9. Pratt, D.T. and Wormeck, J.J.: CREK A Computer Program for Calculation of Combustion Reaction Equilibrium and Kinetics in Laminar or Turbulent Flows, Report WSU-TEL-76-1, Washington State University, 1976.

10. Pratt, D.T.: Calculation of Chemically Reacting Flows with Complex Chemistry, in Studies in Convection-Vol.II, Academic Press, 1976.
11. Pratt, D.T., New Computational Algorithms for Chemical Equilibrium and Kinetics, 10th Macerian Research Symposium, National Bureau of Standards, 1979.
12. Liniger, W. and Willoughby, R.A.: Efficient Numerical Integration of Stiff Systems of Ordinary Differential Equations, IBM Research Report RL-1970 (1967).
13. Brandon, D.M. Jr.: A New Single-step Implicit Integration Algorithm with A-Stability and Improved Accuracy, Simulation, 17-29, July 1974.
14. Gordon, S. and McBride, B.: Computer Program for Calculation of Complex Chemical Equilibrium Compositions, NASA SP-273 (1971).
15. Lapidus, L. and Seinfeld, J.H.: Numerical Solution of Ordinary Differential Equations, Academic Press (1971).
16. Malte, P.C. and Pratt, D.T., Combustion Science Technology 9, p. 221, 1974.
17. Evangelista, J.J., Shinnar, R. and Katz, S., Twelfth Symposium (International) on Combustion, p. 401, The Combustion Institute, 1969.
18. Niedzwiecki, R.W. and Jones, R.E.: Pollution Measurements of a Swirl-Can Combustor, NASA TM S-63160, 1972.
19. Brewster, M.Q. and Pratt, D.T., Modelling of Pollutant Production in a NASA Swirl-Can Combustor, Western States Section/The Combustion Institute Paper No. WSS/CI 78-38, 1978.
20. Waldman, C.H., Wilson, R.O., Jr., and Maloney, K.L.: Kinetic Mechanisms of Methane-Air Combustion with Pollutant Formation, Environmental Protection Technology Series EPA-560/2-74-045, 1974.
21. Edelman, R.B., Fortune, O. and Weilerstein, G.: Some Observations on Flows Described by Coupled Mixing and Kinetics, Emissions from Continuous Combustion Systems, Plenum Press, 1972.
22. Riley, J.J. and Pratt, D.T., A Proposed Hybrid Technique for the Simulation of Mixing with Chemical Reaction, Technical Memorandum No. 146, Flow Research Company, Kent, Washington, november (1977).

#### 8. ACKNOWLEDGEMENTS

This work was supported in part by the National Science Foundation, Grant No. ENG-7684533, by the Kistler Glass Research Fund of the University of Utah and by the AVCO-Lycorning Corporation, Stratford, Connecticut, and has been reported previously at the Project SQUID Workshop on Gas Turbine Combustion, Purdue University, May 31-June 1, 1970.

Patti L. Case provided valuable technical assistance during the development of the computational algorithm.

#### 9. TABLES AND FIGURES

Table I

Mellor's "Characteristic Times" for Combustion and Pollutant Formation in Two-phase Turbulent Combustion (Ref.1)

Time	Symbol	Physical or Chemical Process
Fuel droplet lifetime	$\tau_{eb}$	Droplet evaporation and/or combustion
Eddy dissipation time for injected fuel	$\tau_{fi}$	Small-scale turbulent mixing near the fuel injector in the recirculation zone
Eddy dissipation time in the shear layer	$\tau_{sl}$	Large-scale turbulent mixing between fresh air and the recirculating burned gas-fuel mixture
Fuel ignition delay and burning time	$\tau_{hc}$	Homogeneous combustion of the fuel to $CO_2$
NO formation time	$\tau_{no}$	Homogeneous kinetics for NO formation

TABLE II

Conditions for C/D Simulation of Mixing Limited Combustion of Premixed Hydrogen and Air in a Jet-stirred Reactor

Fuel:	Gaseous $H_2$ at 300 K
Oxidizer:	Air at 300 K
Fuel-air Ratio:	Overall fuel-air equivalence ratio = 0.5 (fuel lean)
Reactor Pressure:	100 kPa (1 bar)
Reactor Loading:	$500 \text{ kg m}^{-3} \text{ bar}^{-2} \text{ s}^{-1}$
Residence Time:	Ca. 5 ms.

TABLE III. Mechanism, Activation Temperatures and Calculated Contact Indexes for Mixing Limited Combustion of Premixed Hydrogen and Air in a Jet-Stirred Reactor.  $P = 1 \text{ bar}$ ,  $I_m = 10$ ,  $\phi = 0.5$ , inlet  $T = 300\text{K}$ ;  $\langle T \rangle = 1112\text{K}$ ,  $T_{\text{RMS}} = 252^\circ\text{C}$ ;  $T_{\text{EQ}} = 1643\text{K}$ ,  $T_{\text{PSR}} = 1233\text{K}$ .

Reaction	$T_f/T_b$	$X_f/X_b$
1. $H_2 + O_2 \rightleftharpoons O + OH$	16.5 0.5	1.3 0.9
2. $H_2 + O \rightleftharpoons H + OH$	9.4 7.3	0.5 1.1
3. $H_2O + O \rightleftharpoons OH + OH$	18.1 1.0	2.1 1.1
4. $H + H_2O \rightleftharpoons H_2 + OH$	19.9 4.8	2.0 0.5
5. $N + O_2 \rightleftharpoons NO + O$	6.3 41.4	1.0 7.1
6. $N_2 + O \rightleftharpoons N + NO$	75.5 0.3	64.6 1.1
7. $NO + M \rightleftharpoons N + O + M$	149.0 -6.1	13,840.0 0.9
8. $H + H + M \rightleftharpoons H_2 + M$	0.0 101.3	1.1 8.6
9. $O + O + M \rightleftharpoons O_2 + M$	0.3 115.5	1.0 894.1
10. $H + OH + M \rightleftharpoons H_2O + M$	0.0 111.2	0.8 1,059.0
11. $H_2 + O_2 \rightleftharpoons OH + OH$	43.0 25.0	1.6 3.4

TABLE IV

Mechanism and Rate Data for Global Pyrolysis  
and Oxidation of Fuel and Air

$$k_j = 10^{B_j} T^{N_j} \exp(-T_j/T), \text{ SI units}$$

				$B_j$	$N_j$	$T_j$
$C_{12}H_{23}$	+ 6 $O_2$	= 12 CO + 11.5 $H_2$		11.5	0.0	12200.*
CO	+ OH	= CO <sub>2</sub> + H		6.602	0.5	0.0
CO <sub>2</sub>	+ M	= CO + O + M		12.0	0.0	50353.
H	+ OH	= H <sub>2</sub> + O		6.903	1.0	3525.
H <sub>2</sub> O	+ M	= OH + H + M		12.477	0.0	52870.
H	+ HO <sub>2</sub>	= OH + OH		11.398	0.0	957.
OH	+ H <sub>2</sub>	= H + H <sub>2</sub> O		10.398	0.0	0.0
H	+ O + M	= OH + M		9.903	0.0	0.0
OH	+ O	= H + O <sub>2</sub>		10.398	0.0	0.0
H	+ O <sub>2</sub> + M	= HO <sub>2</sub> + M		9.176	0.0	503.5
OH	+ OH	= H <sub>2</sub> O + O		9.778	0.0	503.5
OH	+ N	= H + NO		8.778	0.5	4028.
H	+ N <sub>2</sub> O	= OH + N <sub>2</sub>		10.903	0.0	7533.
N	+ NO	= N <sub>2</sub> + O		10.176	0.0	0.0
N	+ O <sub>2</sub>	= NO + O		6.778	1.0	3172.
N <sub>2</sub> O	+ O	= NO + NO		11.0	0.0	15000.
N <sub>2</sub> O	+ M	= N <sub>2</sub> + O + M		11.0	0.0	25176.

$$* r_j = 10^{B_j} \left(\frac{P}{P_0}\right)^{-0.815} \exp(-T_j/T) \left[\frac{9T}{10^4} - \frac{1}{2}\right] (C_{12}H_{23})^{1/2} (O_2), \text{ from Ref. (21).}$$

TABLE V

Conditions for Homogeneous PSR and C/D Modelling of  
Premixed, Prevaporized Combustion in a NASA Swirl Can Combustor

Fuel:  $C_{12}H_{23}$  (representing liquid fuel ASTM-A1  
with hydrogen/carbon mass ratio of 0.161)

Lower Heating Value of Fuel: 43.3 J/kg  
(18,600 BTU/lb)

Fuel-Air Ratio: 0.02 - 0.09 kg fuel/kg air

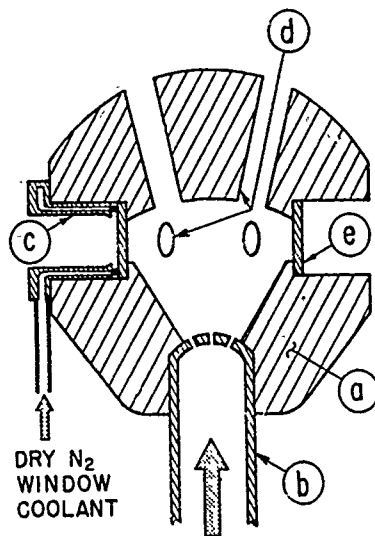
Stoichiometric F/A Ratio: 0.0685 kg fuel/kg air

Equivalence Ratio: 0.29 - 1.31

Pressure: 5-6 bar

Inlet Temperature: 613 K

Mass Flow Rate of Air: 38-45 kg/s (85-100 lb/s)



PREMIXED  
FUEL/AIR  
Figure 1

Jet-stirred reactor with optical access. Details: (a) zirconia reactor wall; (b) reactant feed tube with feed jets; (c) spring-loaded window holder; (d) exhaust ports; and (e) sapphire window.

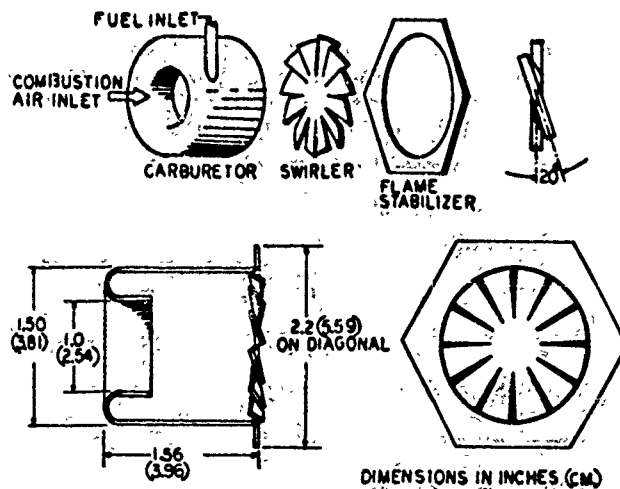
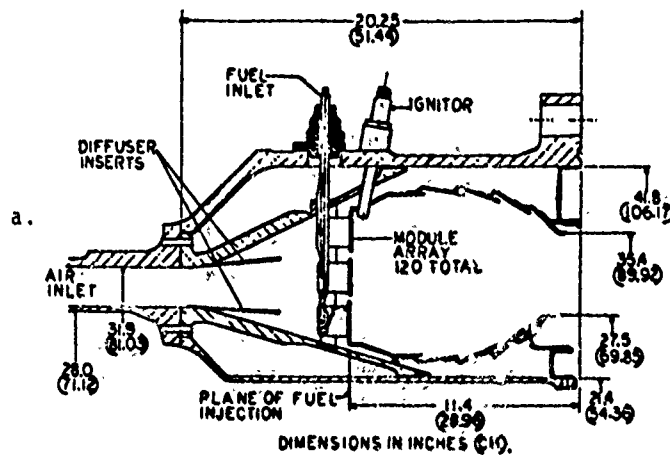


FIGURE 2

- a. NASA Swirl-can Modular Combustor Array (Ref.18)
- b. NASA Swirl-can Modular Details (Ref. 18)



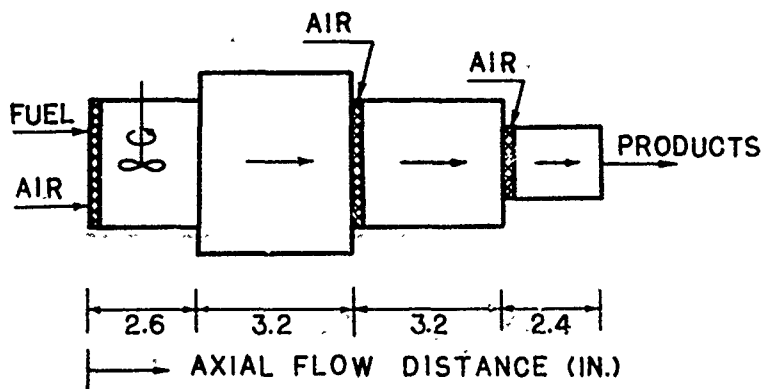


Figure 3. Swirl-can combustor zone model

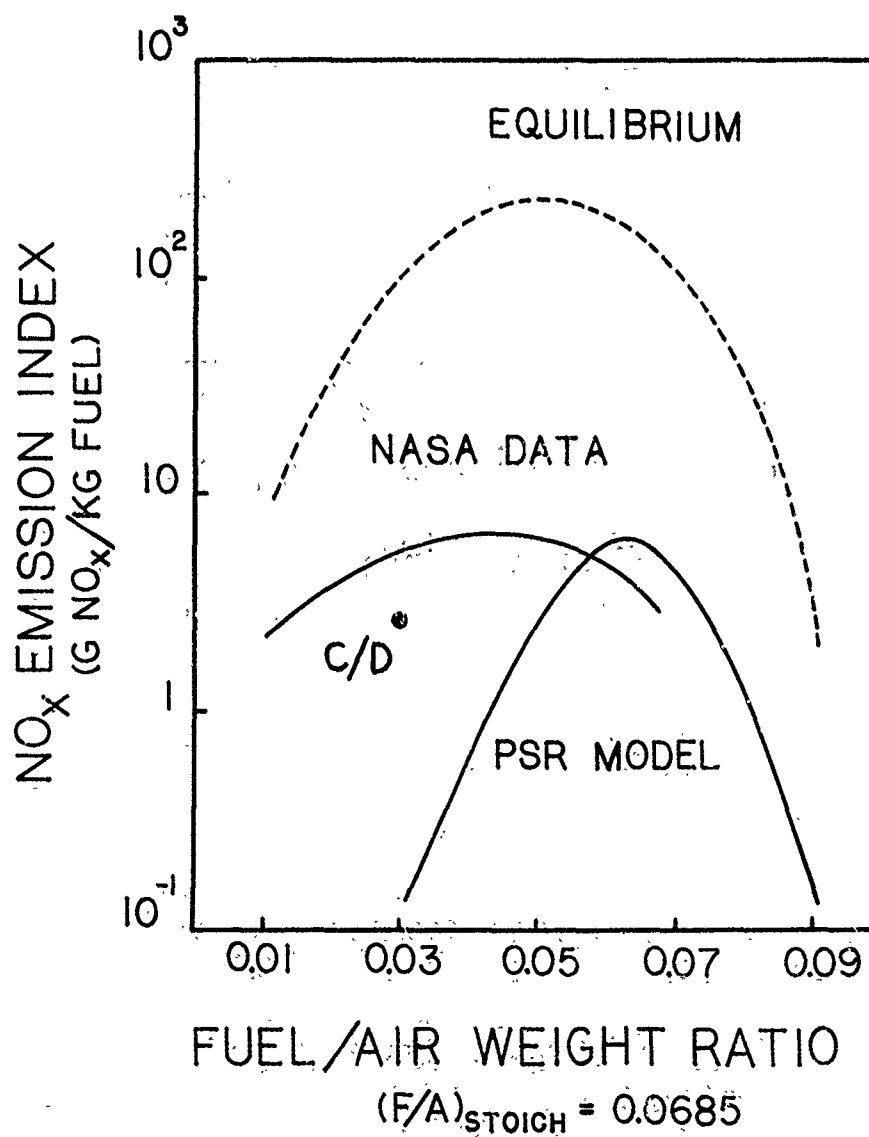


Figure 4.  $\text{NO}_x$  Emission Index for 6 atm operation

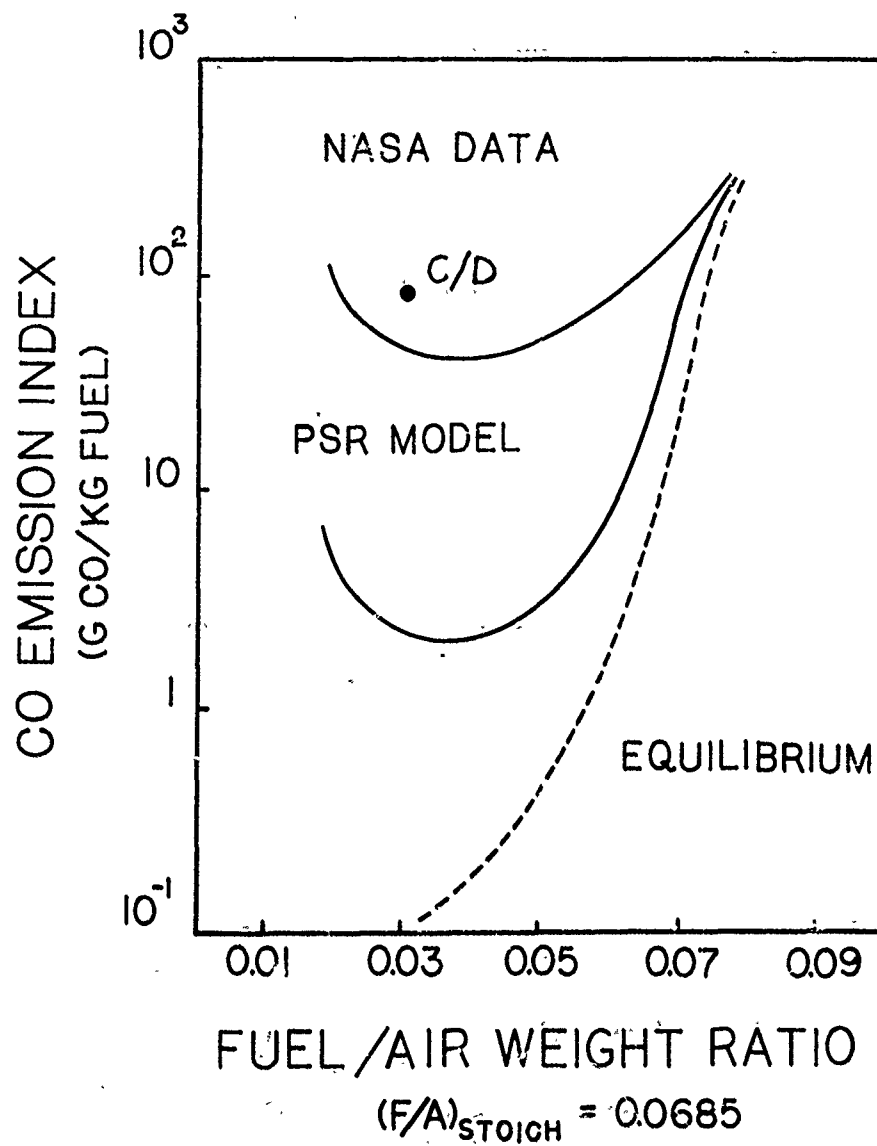


Figure 5, CO Emission Index for 8 atm operation

## DISCUSSION

**W.P.Jones, UK**

You showed a graph with some measurements from the NASA combustor and one prediction with your coalescence/dispersion model. In a log-scale, I have difficulties to assess the level of agreement. Could you tell us what the actual numbers were?

**Author's Reply**

Yes, it was a log-scale, and the right numbers are on the scale (see Figure 4). Comparing the data we found one order of magnitude difference (a factor of 2 or 3). I don't think it's terribly important. The conclusion stated in the paper is that it was going in the good direction.

# MODELISATION DE ZONES DE COMBUSTION EN REGIME INSTATIONNAIRE

par Francis HIRSINGER et Hélène TICHITSKY  
Office National d'Etudes et de Recherches Aérospatiales (ONERA)  
92320 Châtillon (France)

Les différents types de zones de combustion susceptibles d'être étudiées et modélisées présentent un certain nombre de caractères communs : elles sont le siège d'écoulements assez complexes, en général tridimensionnels, comportant souvent des zones de recirculation et des zones d'injection localisées. Par ailleurs, les phénomènes de combustion présentent un aspect instationnaire qu'il est important de mettre en évidence et de représenter. La simulation numérique devrait en outre compléter les études expérimentales difficiles à mener, plus particulièrement dans les régimes transitoires.

Une modélisation des écoulements les plus simples, présentant cependant simultanément ces divers caractères, a été entreprise afin de dégager des comportements caractéristiques plutôt que de tenter de représenter l'ensemble des phénomènes intervenant dans des zones de combustion réelles, géométriquement compliquées. La technique de modélisation consiste à écrire les équations de bilans instationnaires de l'aérothermochimie, tenant compte de la dynamique des gaz de la diffusion laminaire turbulente et de la cinétique chimique, pour un ensemble de cellules représentant le domaine à étudier. Ces équations de bilan sont traitées de façon intégrale dans l'espace et différentielle dans le temps. Cette méthode permet de suivre exactement les phénomènes instationnaires réels ou d'accéder plus rapidement aux régimes établis, par des évolutions instationnaires virtuelles.

Les applications présentées correspondent à un écoulement bidimensionnel dans un canal partiellement obstrué par une plaque tenant lieu d'accroche-flamme, et à un écoulement tridimensionnel dans un domaine pouvant représenter une portion de tube à flamme alimenté par des orifices latéraux. Cette méthode a permis de simuler l'établissement de l'écoulement froid à partir du repos, puis un allumage à partir d'une petite zone à température élevée et les oscillations qui en résultent ainsi que l'établissement d'une flamme stabilisée.

## COMBUSTION ZONE MODELING IN UNSTEADY REGIME

The various types of combustion zones likely to be studied and modeled present a number of common features : they are the seat of rather complex, usually three-dimensional flows, often including recirculation pockets and zones of localized injection. Moreover, combustion phenomena present an unsteady character that it is important to bring to light and to describe. A numerical simulation of such phenomena should complement experimental studies, rather difficult to carry out, especially in transient regimes.

A modelling of the flows as simple as possible, but still presenting these simultaneous features, has been undertaken with a view to reveal characteristic behaviours rather than to represent the whole set of phenomena taking place in actual, geometrically complicated combustion zones. The modelling technique consists in writing the equations of unsteady aerothermochemical budgets, account being taken of the gas dynamics of the laminar or turbulent diffusion and of the chemical kinetics, for a series of cells representing the domain under study. These budget equations are treated in an integral manner in space and a differential manner in time. This method makes it possible to exactly follow the actual unsteady phenomena or to have a faster access to steady regimes through virtual unsteady evolutions.

The applications presented in the paper correspond to a two-dimensional flow in a duct partially choked by a plate representing a flame-holder, and to a three-dimensional flow in a domain representing a section of flame tube fed by lateral orifices. This method permitted the simulation of the establishment of the cold flow from rest, then an ignition initiated in a small zone at high temperature and the resulting oscillations, as well as the onset of a permanent flame.

## 1) INTRODUCTION

Le problème de la modélisation des zones de combustion est abordé depuis longtemps par de nombreuses équipes [1 à 6], tant sur le plan de l'étude fondamentale des mécanismes physico-chimiques complexes dont elles sont le siège, que sur le plan du calcul de chambres de combustion.

A l'heure actuelle, les performances recherchées par les constructeurs, en particulier de turbomachines, que ce soit pour l'amélioration des consommations ou pour le contrôle de l'émission des polluants, placent ces chambres dans des domaines de fonctionnement où il n'est plus possible d'ignorer les phénomènes instationnaires, ceci étant également vrai pour les machines complètes.

Ces phénomènes concernent principalement : l'allumage, l'extinction, le réallumage en altitude, les instabilités de combustion à basse (rumble) et à haute fréquence (screech), la distorsion aérodynamique, thermique et chimique provoquée par une alimentation perturbée du moteur, les interactions des chambres et des autres éléments du moteur (par exemple celle concernant la chambre principale lors de l'allumage de la réchauffe), les effets de la régulation, etc....

Les phénomènes instationnaires correspondants doivent être étudiés finement pour permettre, soit d'en limiter les effets, soit de les exploiter en recherchant les régimes transitoires les plus avantageux.

Ces différentes raisons ont amené l'ONERA, outre des études en régime stationnaire [7 à 10], à développer une approche instationnaire de la modélisation des zones de combustion. Cette approche vise dans un premier temps à analyser et modéliser les différents phénomènes dans un environnement type chambre de combustion, en particulier en présence de zones de recirculation ; dans ce but, les configurations géométriques utilisées, tant sur le plan numérique qu'expérimental, ne correspondent pas rigoureusement à des chambres de combustion réelles ; ce sont des configurations stylisées, assurant la présence de phénomènes analogues à ceux rencontrés dans les chambres réelles, mais conçues de manière à faciliter les modifications géométriques, tant sur le plan numérique qu'expérimental, ainsi que l'implantation des mesures. Cette approche doit donc permettre l'exploration d'un vaste domaine de fonctionnement et donner la possibilité, dans une étape ultérieure, de transposer les différents modèles développés dans des calculs de chambres réelles.

L'étude présentée ici fait le point des premières tentatives effectuées sur le plan numérique.

## 2) PRINCIPES DE L'APPROCHE NUMERIQUE

Les principes de l'approche numérique ont été déjà longuement décrits, références [11 à 14] et seront ici simplement rappelés.

Les phénomènes considérés sont complexes ; les écoulements sont en général turbulents, sièges de réactions chimiques où la cinétique ne peut être négligée, souvent polyphasiques ; des zones sub-, trans- et supersoniques peuvent exister simultanément. Différentes études menées à l'ONERA, tant dans le domaine du calcul de champs continus que dans celui de la modélisation de systèmes complets, ont permis de dégager une technique systématique de simulation numérique pour ce type de problèmes. Le champ ou le système étudié est constitué à partir d'un assemblage modulaire de cellules pour lesquelles sont écrites les équations de bilan instationnaires classiques, sous forme intégrale par rapport à l'espace et différentielle par rapport au temps.

La figure 1 présente le cas le plus général d'une cellule déformable de volume  $V$ , dont la frontière mobile  $A$  peut être constituée de différentes portions  $A_i$  représentant soit des frontières fluides, soit des parois, soit des orifices d'injection, etc.... La vitesse d'une phase quelconque est représentée par le vecteur  $V$ , la vitesse de déplacement d'un point de la frontière étant caractérisé par le vecteur  $V_p$ . Si  $\rho$  est la masse volumique d'une phase, et  $g$  une grandeur massique correspondant à cette même phase, l'équation de bilan correspondante peut être écrite sous la forme générale :

$$\frac{\partial}{\partial t} \int_V \rho g dV + \int_A (\rho g (V - V_p) \cdot n) dA = \int_V \rho \dot{w}_g dV$$

où  $n$  est le vecteur normal extérieur à la surface, et  $\dot{w}_g$  la production massique de la grandeur  $g$ . Suivant la définition de  $g$ , cette équation correspond à un bilan de :

- masse :  $g = 1$
- quantité de mouvement :  $g = V$
- énergie :  $g = \frac{V^2}{2}$
- espèce chimique :  $g = Y_i$  (fraction massique)
- etc....

Le premier terme représente l'accumulation, le deuxième les flux de convection et de diffusion, et le troisième les productions. Ces équations traduisent le principe de l'état local, chaque cellule ne dépendant que d'elle-même et de son environnement immédiat. Elles sont rigoureuses quelque soit la taille des cellules (maillage ou système), mais ne sont pas exploitables numériquement sous cette forme. C'est le problème de la discrétisation qui suppose que l'ensemble du champ soit caractérisé par un nombre fini de paramètres et que des hypothèses supplémentaires soient prises en compte concernant la structure de l'évolution des paramètres. Les hypothèses choisies ici sont inspirées de celles utilisées dans la technique des réacteurs homogènes [15-16]. Chaque paramètre (voir figure 2) est supposé avoir une valeur constante à l'intérieur de chaque cellule, et une valeur constante sur chaque portion de frontière cette valeur pouvant être différente des valeurs dans les cellules adjacentes. L'explicitation des intégrales dans les équations de bilan est alors évidente :

$$\frac{\partial (\rho g V)}{\partial t} = - \sum_i \rho_i g_i (V_i - V_{p_i}) n_i A_i + \rho \dot{w}_g V$$

les variables non indicées étant les variables internes, l'indice  $i$  caractérisant les portions de frontière.

Les inconnues principales choisies sont les valeurs internes ; pour que le problème soit entièrement défini, il faut compléter le jeu d'hypothèses en développant des estimations des valeurs des paramètres d'interface en fonction des inconnues de base ou de paramètres connus comme les conditions aux limites. Le choix de ces hypothèses est libre et peut être différent suivant la portion de frontière considérée. La technique de base est l'interpolation simple entre les valeurs dans les cellules adjacentes. Lorsque cette technique est insuffisante du fait de la sévérité du problème traité, elle peut être remplacée par une estimation locale plus sophistiquée qui peut par exemple découler d'une quasi-résolution locale des équations du problème.

La formulation obtenue est particulièrement simple, et la méthode s'apparente à la technique des "volumes finis". La formulation intégrale est conservative, les paramètres intervenant aux frontières par leur propre valeur et non celle de leur dérivée ce qui donne à la méthode un caractère très physique.

Les conditions aux limites sont soit naturelles (parois, plans de symétrie, cols soniques, etc...) soit imposées (entrée, sortie). Les conditions aux limites contrôlées sont les mêmes que dans un dispositif expérimental. La simulation numérique est obtenue en initialisant le champ par un régime réaliste connu (régime stationnaire comme le repos ou régime transitoire réel), puis en intégrant temporellement le système d'équations par une méthode Runge-Kutta explicite du 4ème ordre à stabilité conditionnelle.

### 3) MODELISATION D'UNE RECHAUFFE SCHEMATISEE

L'étude est abordée dans l'hypothèse d'écoulement bidimensionnel. Le domaine (voir figure 3) est constitué d'un champ rectangulaire dans lequel est placé un obstacle mince perpendiculaire à la direction générale de l'écoulement. Il est alimenté par un écoulement prémélangé constitué d'air et de combustible gazeux. La combustion est supposée régie par un modèle de combustion proposé par Spalding et baptisé "Eddy-Break-up" [17] ; il s'agit d'un modèle classique de combustion turbulente où celle-ci est contrôlée par le mélange. Le fluide est visqueux et les caractéristiques thermodynamiques des gaz brûlés sont supposées identiques à celles des gaz frais, ceci pour alléger la résolution numérique. Les équations de bilan de chaque cellule prennent alors la forme :

$$\frac{\partial}{\partial t} \int_V \rho \, dV + \int_A \rho \underline{v} \cdot \underline{n} \, dA = 0 \quad (\text{masse})$$

$$\frac{\partial}{\partial t} \int_V \rho Y_K \, dV + \int_A \rho Y_K \underline{v} \cdot \underline{n} \, dA = \int_A (\nabla \cdot \underline{g}_{K0} Y_K) \underline{n} \, dA + \int_A \rho \dot{w}_K \, dV$$

(masse du combustible)

avec  $\dot{w}_K = -C \frac{Y_K}{Y_{K,0}} (Y_{K,0} - Y_K)$

$$\frac{\partial}{\partial t} \int_V \rho \underline{v} \, dV + \int_A \rho \underline{v} (\underline{v} \cdot \underline{n}) \, dA = - \int_A p \underline{n} \, dA + \int_A \underline{T} \underline{n} \, dA$$

(quantité de mouvement)

$$\begin{aligned} \frac{\partial}{\partial t} \int_V \rho \left( u + \frac{v^2}{2} \right) \, dV + \int_A \rho \left( H + \frac{v^2}{2} \right) \underline{v} \cdot \underline{n} \, dA = & \int_A (\underline{T} \underline{n}) \cdot \underline{v} \, dA \\ & + \int_A \underline{p} \underline{n} \, dA + \Delta Q \int_A (\nabla \cdot \underline{g}_{K0} Y_K) \underline{n} \, dA \end{aligned}$$

(énergie)

avec :  $u = C_v T + Y_K \Delta Q$

et :  $H = u + \frac{p}{\rho}$

$Y_K$  est la fraction massique de combustible,  $Y_{K,0}$  celle correspondant au prémélange,  $D$  le coefficient de diffusion,  $\dot{w}_K$  la production de combustible par unité de masse,  $C$  une constante du modèle de combustion,  $\tau$  le tenseur des forces de viscosité qui dépend du modèle choisi,  $U$  l'énergie interne physico-chimique,  $H$  l'enthalpie physico-chimique,  $\Phi$  le flux thermique et  $\Delta Q$  la chaleur de combustion. Les réactions chimiques sont schématisées de façon simple par une réaction globale unique entre le combustible  $K$  et le comburant  $O$ , donnant des produits de combustion entièrement brûlés :



Le domaine est décomposé en cellules rectangulaires identiques. Le passage aux équations discrétisées exploitables numériquement, effectué conformément à la technique décrite au § 2, est évident et ne sera pas détaillé ici. Les traitements d'interface choisis diffèrent suivant qu'il s'agisse d'interfaces ordinaires ou limites. Au niveau d'interfaces ordinaires, les valeurs des paramètres sont les moyennes arithmétiques des valeurs correspondantes dans les cellules adjacentes. Au niveau des parois, la vitesse est nulle, les dérivées spatiales des composantes de la vitesse, intervenant dans les termes d'effort sur les frontières dans les équations de quantité de mouvement, sont modélisées de manière à restituer le frottement local, les pressions et températures sont égales à leur valeur dans la cellule (gradients locaux nuls). Aux interfaces d'entrée, la pression d'arrêt, la température d'arrêt et la composition sont imposées fonction du temps, la vitesse étant déduite par extrapolation des vitesses à l'intérieur du domaine. Aux interfaces de sortie, seule la pression statique est imposée, tous les autres paramètres étant extrapolés.

La simulation numérique est réalisée en deux étapes : mise en mouvement à partir du repos, de l'écoulement sans combustion, jusqu'à obtention d'un régime stabilisé, puis initiation de la combustion en aval de l'obstacle.

La mise en mouvement du fluide est obtenue en augmentant progressivement (5ms) la pression d'arrêt (de 50.000 à 52.000 pascals) et la température d'arrêt à l'entrée, simulant la compression isentropique d'un réservoir situé à l'amont, et en maintenant constante la pression de sortie (50.000 pascals). La figure 4 présente des cartographies de vitesse aux temps  $t = 3 - 8$  et 13 ms, montrant un écoulement tout d'abord collé aux parois, puis le déclenchement progressif de la zone de recirculation à la pointe de l'obstacle et son développement. La figure 5 présente la configuration d'écoulement obtenue en régime asymptotique mettant en évidence une zone de recirculation longue (8 fois la hauteur de l'obstacle). Ce résultat correspond à un modèle de viscosité turbulente homogène importante,  $\mu_t = 0.1$ . La figure 6 présente l'évolution temporelle de la vitesse d'entrée et de la vitesse de sortie au milieu de la portion libre du canal. Les oscillations mettent en évidence les temps caractéristiques (10 ms) de propagation des ondes dans le canal ; le temps global de mise en vitesse ( $\approx 60$  ms) caractérise l'inertie de la colonne gazeuse ; le décalage progressif des deux vitesses caractérise le développement de la zone de recirculation et des pertes dues aux effets visqueux.

L'initiation de la combustion est obtenue en supposant que le combustible contenu dans la cellule située au centre de la recirculation brûle instantanément. La constante  $C$  du modèle de combustion est prise ici égale à 500. La figure 7 présente des cartographies de températures obtenues à des instants successifs en maintenant constantes les conditions aux limites. Au début de la séquence, les processus de diffusion thermique prennent le pas sur la combustion et la zone d'initiation se refroidit au profit des cellules environnantes. Par la suite, la combustion devenant plus intense, le niveau général de température augmente. Le processus étant très rapide, la masse contenue dans les cellules où se produit la combustion varie peu, et la pression augmente considérablement devenant largement supérieure aux pressions imposées aux deux extrémités du champ ce qui provoque un refoulement à l'entrée et à la sortie, phénomène réaliste, mais ne permettant pas d'atteindre un régime stabilisé.

Pour éviter ce phénomène, un pilotage des conditions aux limites d'entrée a été mis au point réalisant la simulation d'une alimentation par col sonique désamorçé, l'onde de choc se plaçant à proximité de la section d'entrée et réagissant instantanément à l'évolution des conditions dans cette section. Ce sont toujours les pression et température d'arrêt amont qui sont imposées : la pression d'arrêt, au lieu d'être maintenue constante est continuellement réajustée de manière à induire un débit d'entrée constant, la température d'arrêt est maintenue constante.

La figure 8 présente les résultats obtenus dans ces conditions. Pendant les premiers instants, le processus est identique à celui du cas précédent mais dès que la pression dans la zone de combustion augmente notablement, la pression d'entrée réagit et augmente entraînant une convection de la zone de combustion vers l'aval. La fraction de gaz chauds restant derrière l'obstacle provoque l'inflammation des gaz frais dépassant l'obstacle et une deuxième poche de combustion est formée. Le processus se poursuit jusqu'à obtention vers  $t = 75$  ms d'un régime entièrement stabilisé où la zone de combustion se développe latéralement à partir de la zone de recirculation avec laquelle elle se trouve en équilibre dynamique et énergétique. La zone de recirculation est alors considérablement plus courte.

La figure 9 présente l'évolution temporelle de la pression statique dans la cellule où la combustion a été provoquée et de la pression d'arrêt à l'entrée. Les oscillations sont le résultat du couplage entre les conditions d'entrée et la combustion. Le déphasage peu important entre les deux profils est dû à la faible distance entre l'entrée du domaine et le point d'initiation.

Les résultats suivants concernent la comparaison entre les régimes stabilisés sans et avec combustion. La figure 10 présente les profils longitudinaux de vitesse pour deux lignes situées dans la partie libre et dans la partie obstruée du canal. Elle met en évidence l'accélération de l'écoulement due à la combustion. La figure 11 présente sur ces mêmes lignes les profils de température. La figure 12 reproduit des profils transversaux de température et de vitesse, légèrement en aval de l'obstacle, dans la zone de recirculation. La figure 13 présente des profils longitudinaux de pression statique dans la partie libre du canal ; leur forme est classique de ce type d'écoulements. La figure 14 présente pour différentes positions transversales, des profils longitudinaux de fraction massique de combustible mettant en évidence le degré d'avancement le plus élevé de la combustion dans la zone de recirculation bien que limité par le niveau des échanges de cette zone avec le fluide sain. La validité des résultats obtenus du point de vue de la combustion ne sera pas discutée ici car elle est essentiellement liée aux modèles choisis.

La modélisation des effets visqueux reste un problème délicat. Des modèles de turbulence ont été essayés qui permettent de retrouver des résultats voisins de ceux obtenus ici, cependant ces résultats sont extrêmement sensibles aux valeurs des constantes introduites dans les modèles. Cependant, cette étude met en évidence la capacité de la méthode à aborder l'étude des régimes transitoires lors de l'allumage d'une réchauffe où le débit d'entrée est également fixé, et la possibilité d'accéder aux niveaux de perturbation, problème important pour les motoristes.

#### 4) APPROCHE DE LA MODELISATION D'UNE ZONE PRIMAIRE SCHEMATISEE

Une étude de modélisation de zone primaire a été engagée, en collaboration sur le plan expérimental avec l'équipe MAGRE-HEBRARD [18], dans l'optique développée au § 1. La chambre de combustion réalisée pour l'étude expérimentale (voir figure 15) est composée de deux volumes parallélépipédiques mis en communication l'un avec l'autre par des orifices de caractéristiques ajustables tenant lieu d'orifices primaires. Le fluide traverse complètement le boîtier d'alimentation (volume inférieur), une partie du flux pénétrant dans la chambre (volume supérieur). Les deux débits sont réglés par des cols soniques placés dans le même plan à la sortie de la maquette. L'injection du carburant peut être réalisée par différents systèmes : cannes de prévaporisation, injecteurs tourbillonnaires, etc... Un programme de calcul tridimensionnel a été réalisé sur le même principe que le programme bidimensionnel déjà présenté. Le domaine de calcul (voir figure 15) correspond strictement à la géométrie d'une cellule élémentaire de la chambre expérimentale. Les résultats présentés ici correspondent aux premières tentatives de calcul sans combustion.

La technique de simulation de la présence des cols des deux chambres ayant présenté des difficultés de mise au point, la technique de contrôle des conditions aux limites utilisées en bidimensionnel a été reprise ici. La pression d'arrêt à l'entrée du boîtier d'alimentation a été montée en 5 ms de 100.000 à 108.000 pascals, la pression statique de sortie du même boîtier a été montée dans le même temps de 100.000 à 105.000 pascals, la pression statique de sortie de la chambre a été maintenue constante. La figure 16 présente les évolutions temporelles des débits d'entrée dans le boîtier d'alimentation (E), de sortie de ce boîtier (A), dans l'orifice primaire (T) et de sortie de la chambre (C). Elle met en évidence les déphasages entre les différents points du domaine et le temps caractéristique inertiel ( $\approx 30 \mu s$ ). Le débit primaire en régime stabilisé correspond à 15 % du débit total.

La figure 18 présente des cartographies de vitesse (échelle logarithmique) pour le régime stabilisé. La configuration de l'écoulement, complexe, fait apparaître des zones de recirculation en fond de chambre et latérales par rapport au jet. La valeur relativement peu élevée du débit primaire et la forte viscosité ( $\mu = 0,4$ ) expliquent l'inclinaison modérée du jet et la faiblesse de l'impact sur la paroi opposée. L'allure du profil de vitesse en sortie de chambre est dû aux différences de pertes de pression d'arrêt entre les différents filets de courant. Les résultats expérimentaux correspondant ne sont pas encore disponibles. Des calculs sont en cours pour des niveaux de viscosité plus faible et un domaine allongé. Là encore, le modèle de viscosité a une grande influence sur les résultats.

#### 5) CONCLUSION

Le principe de l'approche adoptée par l'ONERA, pour les études en régime instationnaire des zones de combustion avec recirculation, fondé sur une simulation numérique dans des configurations de chambre schématisées, permet d'aborder l'étude des régimes transitoires qui intéressent actuellement les motoristes. Elle se situe à la jonction de l'analyse des mécanismes fondamentaux de la combustion turbulente et de la prévision de leurs effets dans l'environnement d'une chambre de combustion. Les résultats obtenus actuellement sont partiels mais retrouvent déjà l'importance des fluctuations de pression lors des phases d'allumage ; le programme de calcul tridimensionnel, qui, avec un nombre de mailles raisonnable (2400 cellules de 1 cm de côté), aboutit à des descriptions d'écoulements déjà complexes, sera un instrument efficace, et la confrontation des résultats obtenus avec les résultats expérimentaux correspondant, tant en régime transitoire qu'en régime stationnaire, doit permettre l'élaboration et la validation de modèles de turbulence et de combustion réalistes et transposables à des chambres industrielles.



## REFERENCES

1. M. BARRERE - R. PRUDHOMME "Eléments d'Aérothermochimie", Editions Masson.
2. M. BARRERE "Aérodynamique des chambres de combustion de turboréacteurs. Aspects fondamentaux" Revue Française de Mécanique, n° 55-56 (3è et 4è trimestre 1975).
3. R. BORGHI "Etude théorique de l'optimisation de la combustion dans les foyers de turbomachines." Acta Astronautica, vol. 1, p. 667 (1974).
4. R. ROBERT, L.D. ACETO, R. KOLLBACK "An analytical model for nitric oxide formation in a gas turbine combustion chamber" AIAA paper 71.715.
5. D.B. SPALDING "Computer modelling techniques of laminar and turbulent combustion" Central States section meeting - Comb. Institute - March 28-30 (1977) Cleveland, Ohio.
6. F.C. LOCKWOOD, A.S. NAGUIB "The predictions of the fluctuations in the properties of free, round jet, turbulent; diffusion flames" Combustion and flame, vol. 24, n° 1 (feb.75)
7. R. BORGHI "Réactions chimiques en milieu turbulent" Pub. ONERA 1977/4.
8. V.P. SINGH, R. BORGHI, P. MOREAU "Réactions chimiques dans les flammes turbulentes" 2è Symp. Int. sur la dynamique des réactions chimiques - Padoue 1975.
9. P. MOREAU "Turbulent flame development in a high velocity premixed flow" AIAA paper 77-49.
10. P. MOREAU, C. BONNIOT "Production des oxydes d'azote dans une flamme turbulente" Entropie n° 69 (1976).
11. F. HIRSINGER "Modélisation en aérothermodynamique instationnaire" La Recherche Aérospatiale 79-5.
12. R. BORGHI, F. HIRSINGER, H. TICHITSKY "Méthodes disponibles à l'ONERA pour le calcul des chambres de combustion" Entropie n° 81 (mai-juin 1978)
13. F. HIRSINGER, H. TICHITSKY "Modélisation numérique de l'établissement d'une zone de combustion avec recirculation" GAMNI Congrès international sur les méthodes numériques dans les sciences de l'ingénieur - Paris 27 novembre - 1 décembre 1978.
14. D.DUTOYA "Flux de chaleur transféré par un écoulement en combustion turbulente" 6th Int. Meeting on Heat transfert. Toronto, Aug.1978.
15. J. DUTERQUE, R. BORGHI "Combustion du propane dans un foyer homogène" La Recherche Aérospatiale n° 1975-6p. 347-357.
16. O. LEVENSPIEL "Chemical reaction engineering" Wiley International Edition (1962).
17. D.B. SPALDING 13 th International Symposium of Combustion - p. 649 (1971).
18. P. HERRARD, P. MAGRE "Etude de l'aérodynamique d'une chambre de combustion en vue d'une modélisation semi-empirique" Meeting AGARD on combustion modelling PEP 54th (B) Linder Höhe Porz-Wahn-Heide - Köln 3-5 octobre 1979.

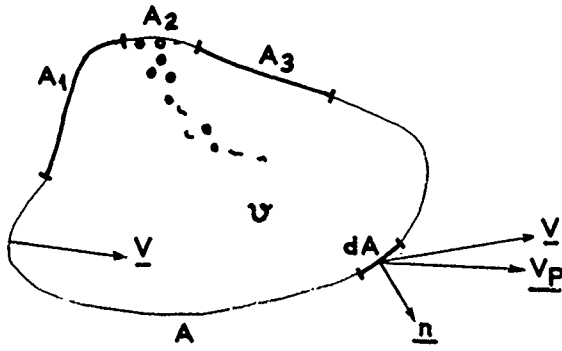


Fig. 1 - Cellule déformable quelconque.

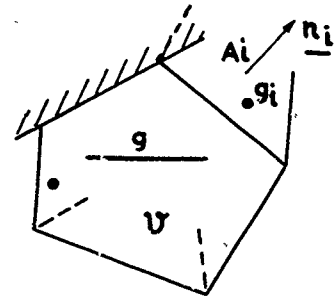


Fig. 2 - Principe de la discrétisation.

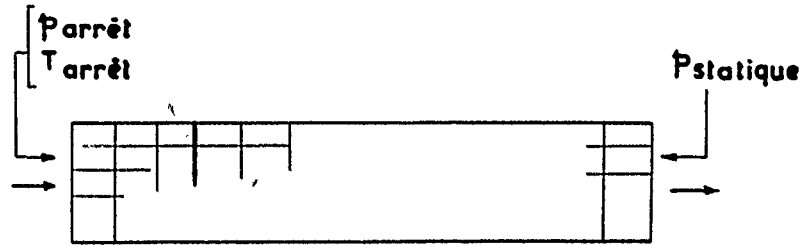


Fig. 3 - Domaine de la simulation.

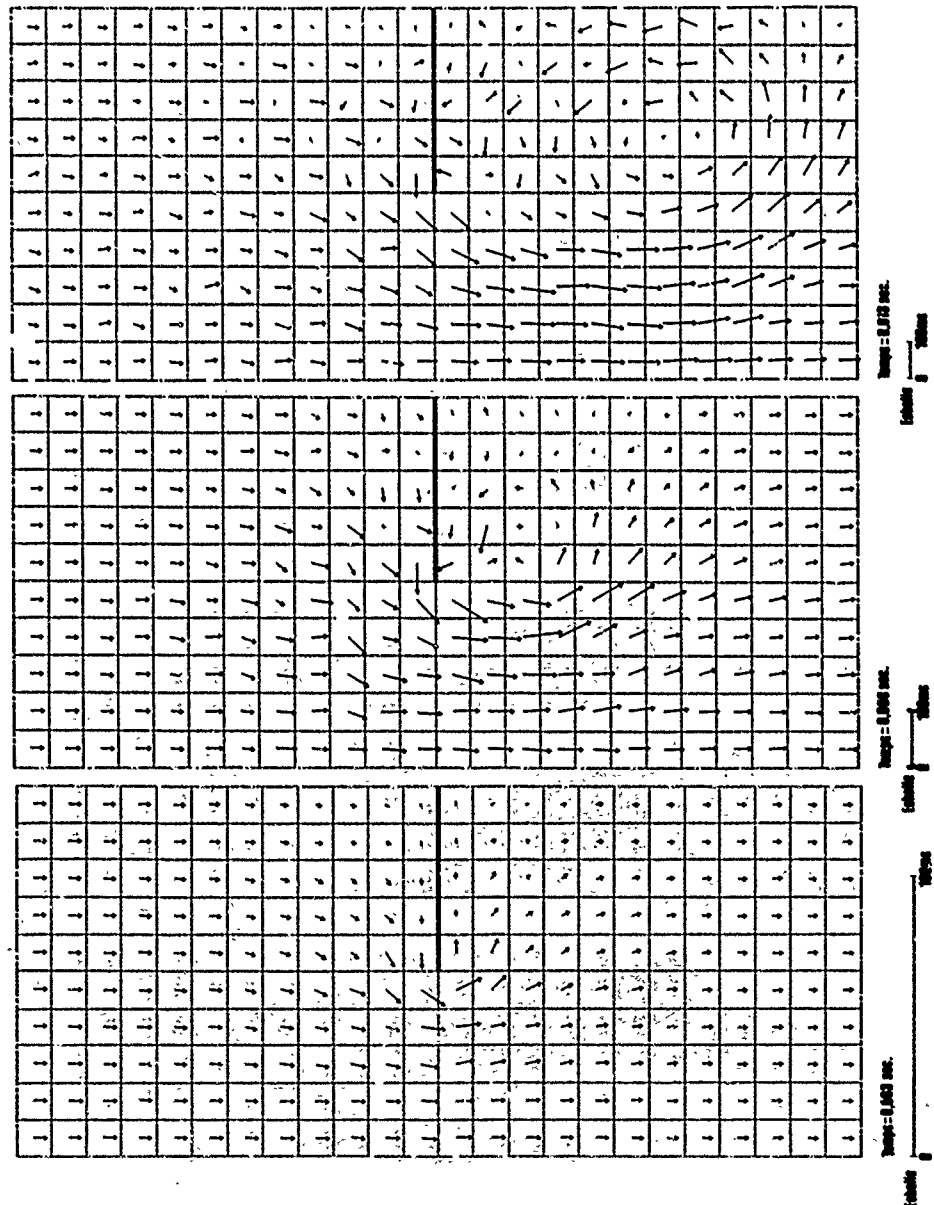


Fig. 4 - Cartes de vecteurs vitesses à divers temps de calcul (viscosité nulle).

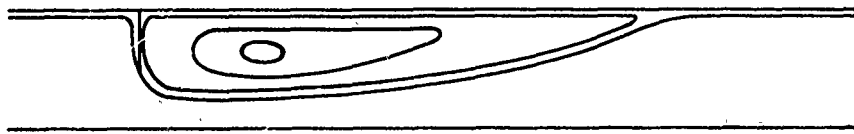


Fig. 5 - Ecoulement en régime asymptotique.

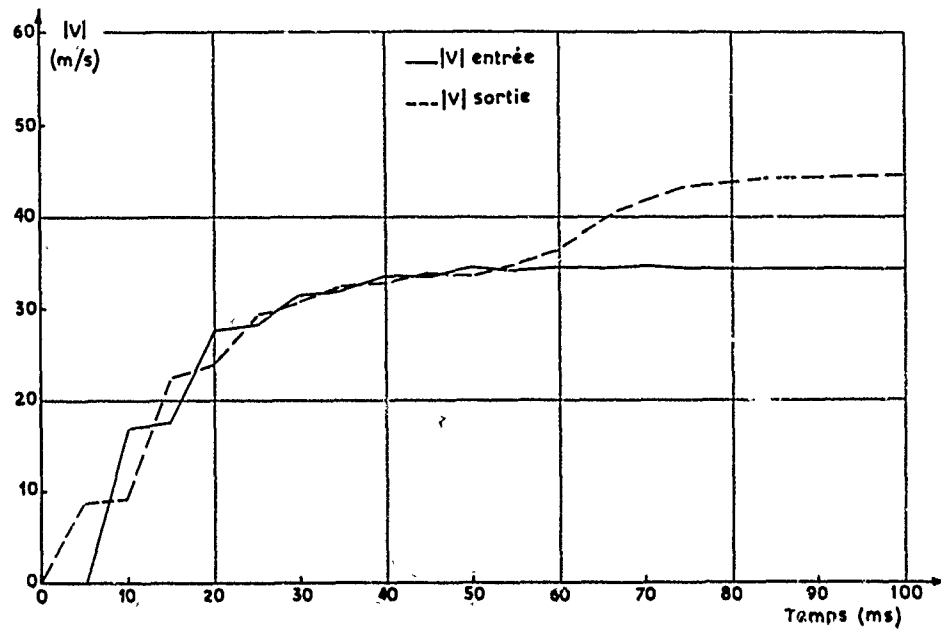


Fig. 6 - Evolution temporelle des vitesses d'entrée et de sortie.

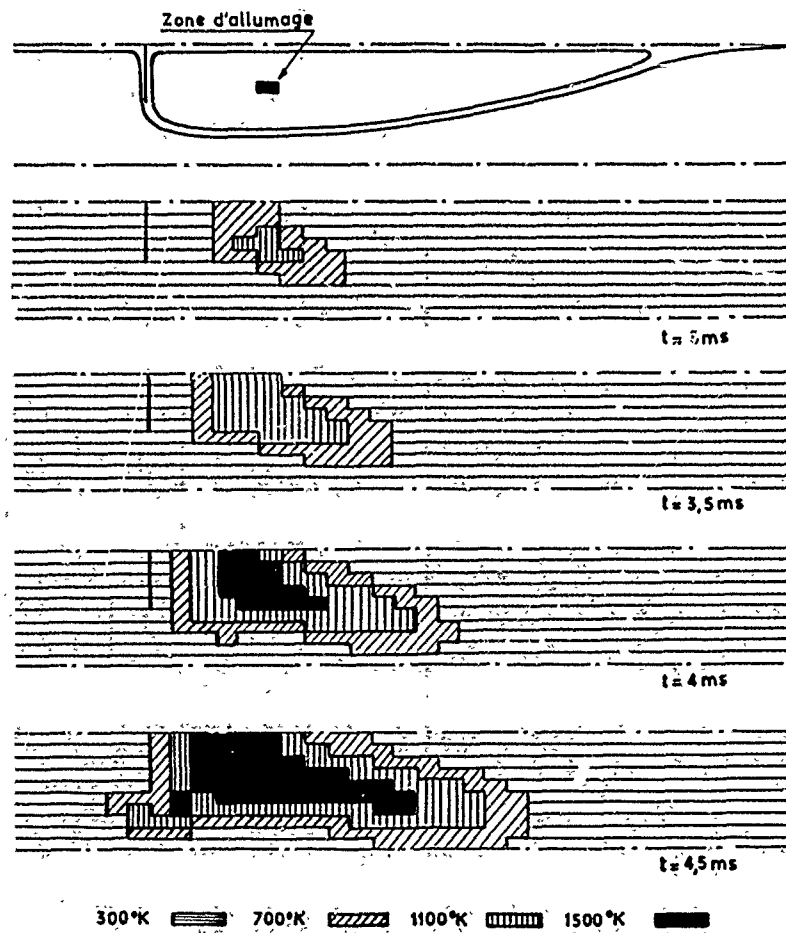


Fig. 7 - Propagation de l'inflammation. Conditions d'entrée constantes.

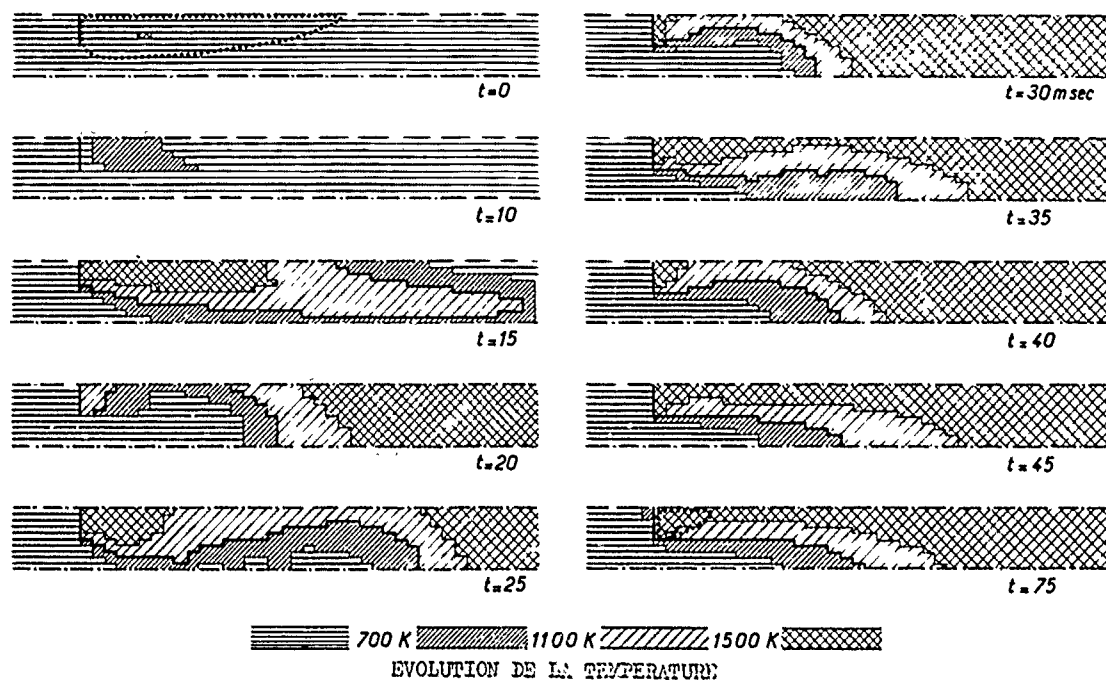


Fig. 8 — Allumage et stabilisation de la combustion.

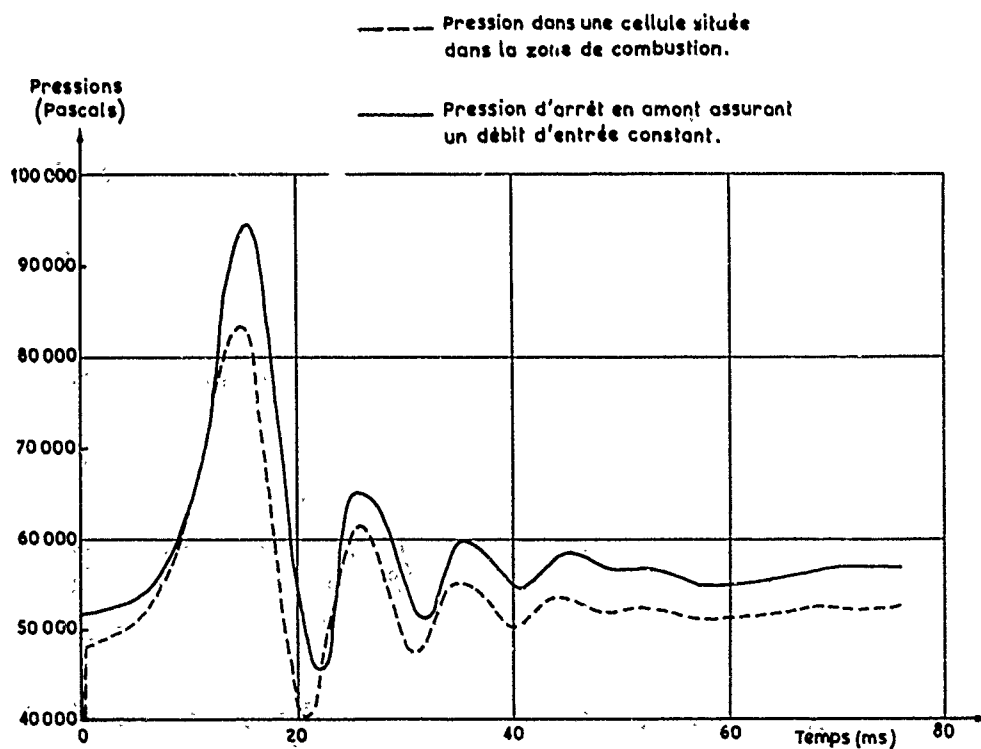


Fig. 9 — Evolution temporelle de la pression d'arrêt d'entrée et de la pression statique au centre de la recirculation.

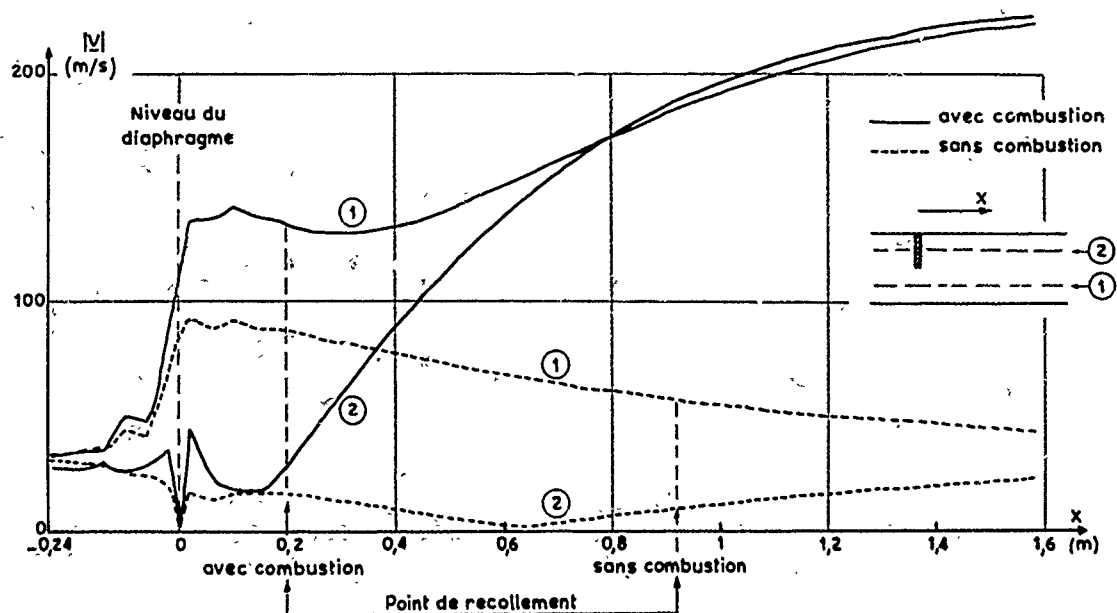


Fig. 10 - Profils longitudinaux de vitesse - Combustion stabilisée ( $t = 75$  ms).

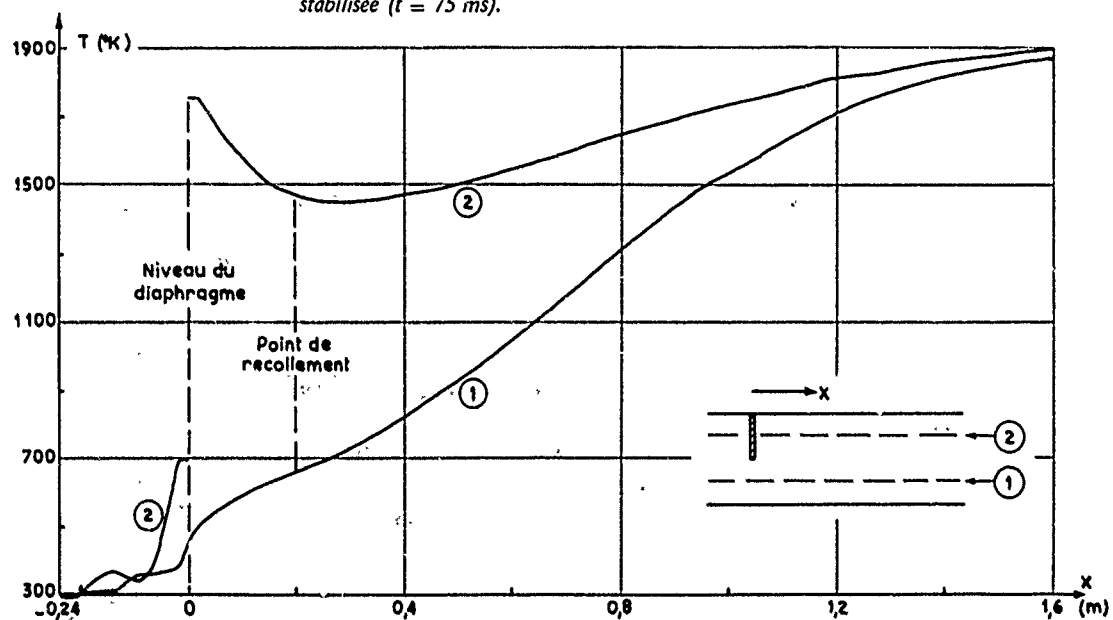


Fig. 11 - Profils longitudinaux de température - Combustion stabilisée ( $t = 75$  ms).

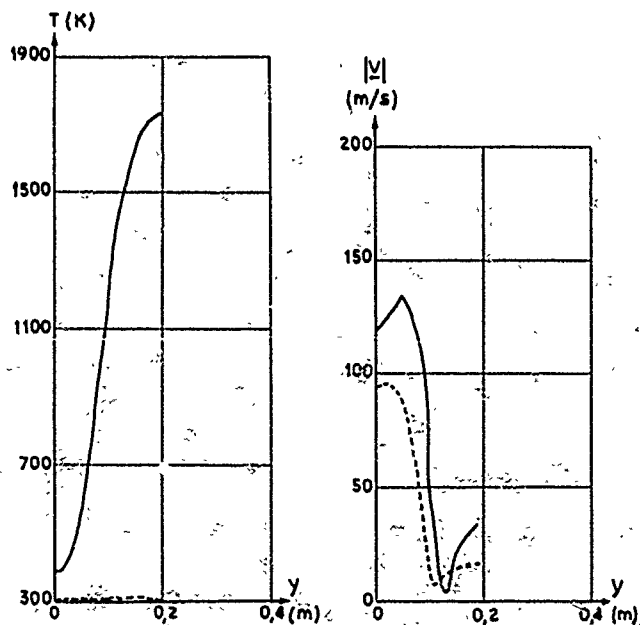


Fig. 12 - Profils transversaux de température et vitesse - Combustion stabilisée ( $t = 75$  ms).

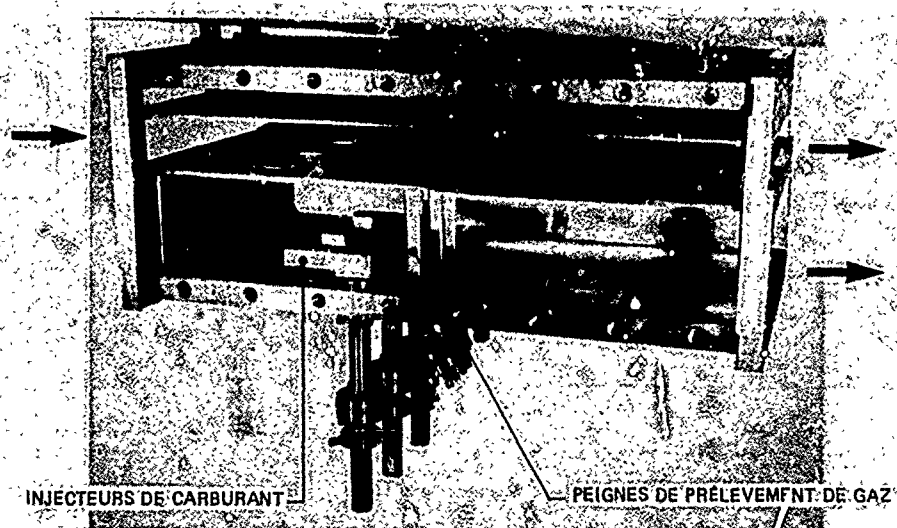
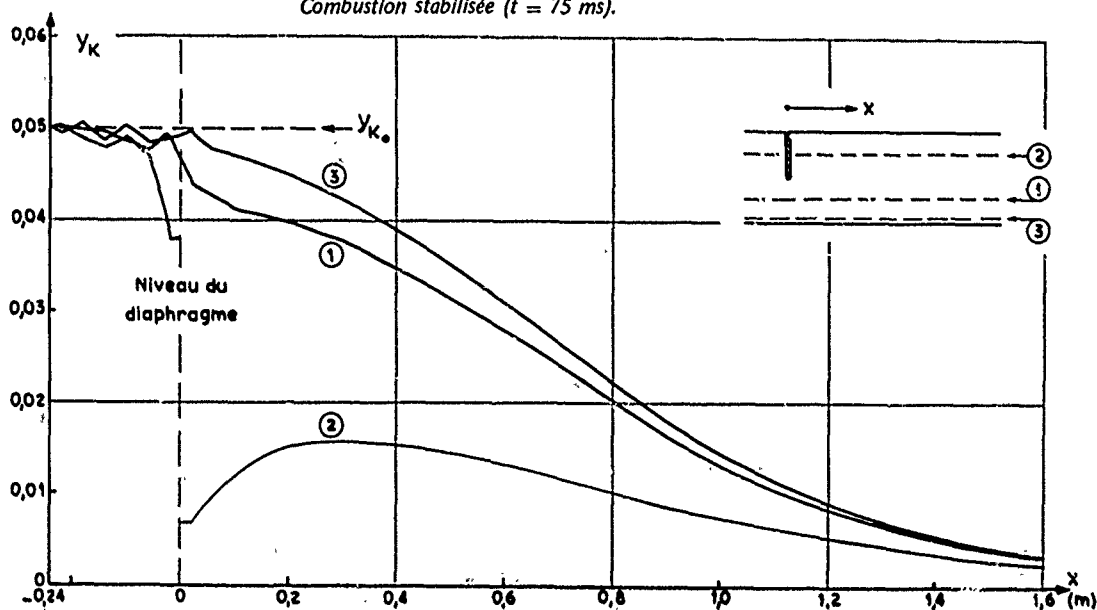
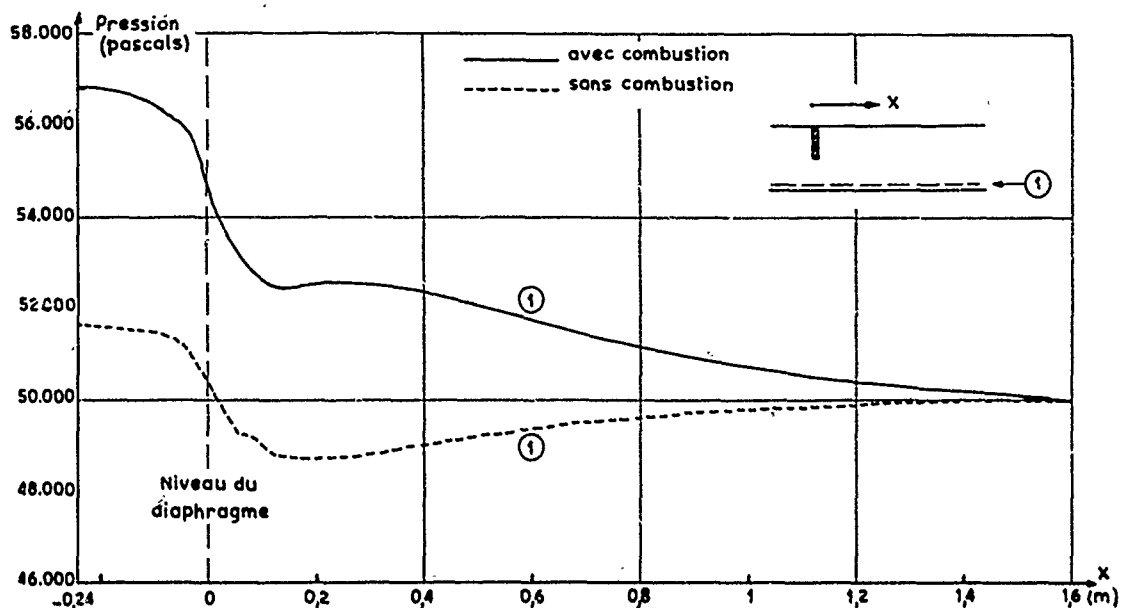


Fig. 15 - Maquette de zone primaire schématisée.

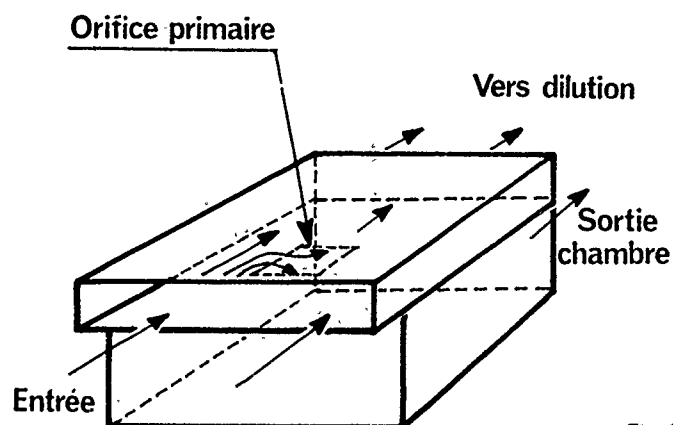


Fig. 16 – Domaine de calcul de la zone schématisée.

Fig. 17 – Evolution temporelle des débits. Entrée admission E ; sortie admission A ; orifice primaire T ; sortie chambre C.

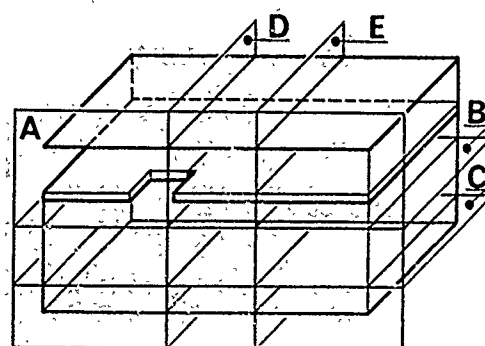
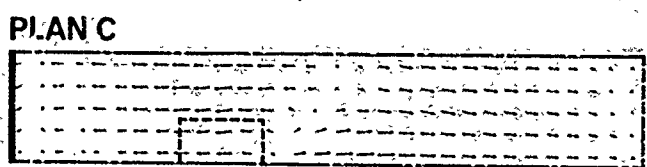
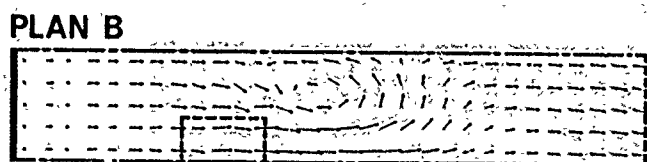
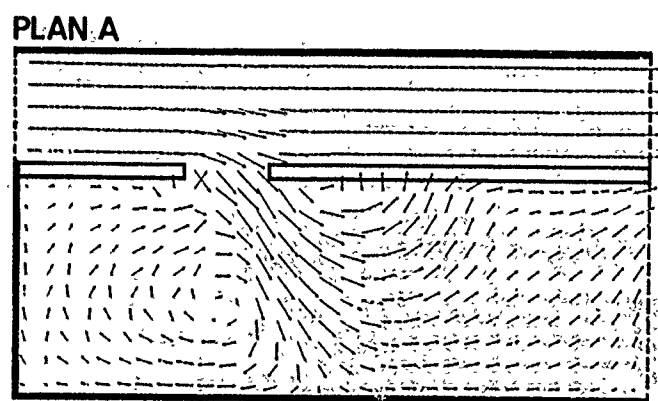
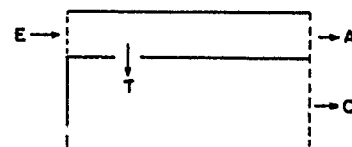
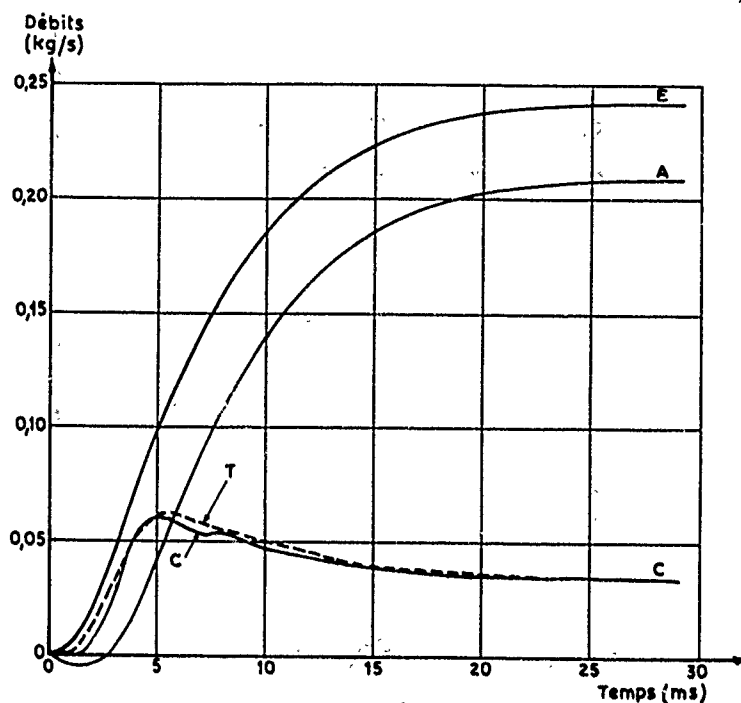


Fig. 18 – Configuration théorique d'écoulement dans le cas d'une injection par un orifice rectangulaire.

# ANALYSIS OF LOW-FREQUENCY DISTURBANCES IN AFTERBURNERS

FRANK E. MARBLE, PROFESSOR OF ENGINEERING  
California Institute of Technology  
205-45  
Pasadena, CA 91125

MALLADI V. SUBBAIAH  
SEBASTIEN M. CANDEL

## SUMMARY

The transient response of large burners depends primarily upon fluid mechanical adjustment rather than upon a time delay associated with chemical response. Examples of this behavior are the non-steady behavior of burners in utility boilers, and the low-frequency response of afterburners in aircraft gas turbines. Previous investigations have shown that the distorted flame interface during non-steady operation causes an active response to acoustic input at selected frequencies. This result depends upon fluid dynamic behavior of the gas of very different densities upstream and downstream of the flame front.

In the present work, the behavior of these stabilized flame zones are examined when they are situated in an afterburner. The turbine discharge and the nozzle inlet planes are represented by appropriate admittance functions for low frequencies. The distances which separate turbine discharge, flame holders, and nozzle throat, as well as the number of flame holders, are parameters in the problem.

The results show that small disturbances which originate in combustion roughness, may be amplified to serious amplitudes and the amplitude level is a strong function of the geometric parameters of the flame-afterburner arrangement. In some instances instability may result.

## 1. INTRODUCTION

Combustion noise and combustion instability in propulsion systems frequently is associated with the response of the combustion process to local pressure and velocity disturbances and to the acoustic characteristics of the complete system (1, 2). The frequency spectrum that is important depends upon the acoustic modes of the system; in gas turbines and rocket motors, the frequencies often lie in the range of several hundred to several thousand cycles per second. When the frequencies are of the order of a kilohertz, the rates of the chemical reactions contribute to the time delay in an essential way (3). Using this fact it has been possible to scale the results of experiments on combustion systems utilizing various fuel types (4) and different geometric configurations. For frequencies of, say, 100 Hertz or less, the chemical times are less important and other features of the combustion system determine the detailed response of the burner. Recently two of us (5) considered a flame stabilized at the center of a two-dimensional channel of infinite length, by a central body of finite size. Under steady operation the flame spreads from the center body to the duct walls; when the combustion process between the burned and unburned gas can be characterized, the flame shape and the flow field may be calculated. This steady configuration was then perturbed by an acoustic wave, the bodies of high-density gas,  $p_1$ , and low-density gas,  $p_2$ , were disturbed and the flame interface distorted to accommodate these disturbances. The process of recovery to the steady-state flame shape constitutes the "response" of the combustion process; the magnitude of the response and its time delay are thus features of the combined transient motion of the gas and the flame front. The results of calculations based on this model showed acoustic transmission and reflection coefficients indicating signal amplification at certain characteristic frequencies. It appeared, therefore, that with certain reflection conditions ahead of and behind the burner, large pressure oscillation levels could be maintained and, perhaps instability.

The present investigation applies the results of our previous investigation to a rudimentary afterburner configuration. The work constitutes the first step in constructing a rational model for low-frequency disturbances in afterburners.

## 2. ANALYTICAL DESCRIPTION OF A NON-STEADY STABILIZED FLAME

Consider a flame in a duct of half-width  $l$ , fixed at a point near the centerline by a flame holder, Fig. 1. The flame is described as a sheet, thin in comparison with other significant lengths of the problem, and characterized by a local flame speed  $w_1$  which denotes the component of gas velocity, normal to the flame on the upstream side, measured relative to the flame sheet. The position of the flame sheet is described by its distance  $\eta(x, t)$  from the center line of the duct, the  $x$ -axis. Neglecting gravitational effects, the flow fields ahead of the flame, region 1, and downstream of the flame, region 2, are described by equations of continuity and motion

$$\frac{\partial \rho}{\partial t} + \frac{\partial}{\partial x}(\rho u) + \frac{\partial}{\partial y}(\rho v) = 0 \quad (1)$$

$$\frac{D u}{D t} + \frac{1}{\rho} \frac{\partial p}{\partial x} = 0 \quad (2)$$



$$\frac{Dv}{Dt} + \frac{1}{\rho} \frac{\partial p}{\partial t} = 0 \quad (3)$$

together with the thermodynamic relation

$$\frac{1}{\rho} \frac{Dp}{Dt} - \frac{1}{\rho} \frac{D\epsilon}{Dt} = \frac{1}{c_p} \frac{D\epsilon}{Dt} = 0 \quad (4)$$

which states that there are no entropy-producing mechanisms apart from the flame itself. The variables describing the upstream and downstream fields are indicated by subscripts 1 and 2. The state of the gas far ahead of the flame is uniform, irrotational and of uniform entropy.

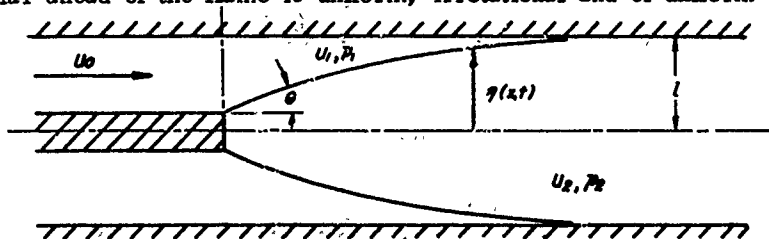


Figure 1. Notation and Geometry for Flame Stabilized in Duct.

The two flow fields are matched across the flame sheet by mass and momentum conservation relations and by the kinematic conditions that the flame sheet and the flow fields deform in a consistent manner. These kinematic conditions resemble that at the liquid surface in conventional wave theory but here there are fixed propagation speeds of the surface with respect to the upstream and downstream fields. These relations are

$$\frac{\partial y}{\partial t} + u_1(x, y, t) \frac{\partial y}{\partial x} = v_1(x, y, t) + w_1 \sec \phi \quad (5)$$

$$\frac{\partial y}{\partial t} + u_2(x, y, t) \frac{\partial y}{\partial x} = v_2(x, y, t) + w_2 \sec \phi \quad (6)$$

where  $\phi$  is the local angle between the flame sheet and the x-direction,  $w_1$  is the normal flame velocity, defined on the upstream side of the flame, and  $w_2$  is the corresponding quantity downstream of the flame.

Conservation laws across the flame sheet are applied in reference frame of the flame itself and involve values of the field variables at the flame. Mass conservation takes the form

$$\rho_1 w_1 = \rho_2 w_2 \quad (7)$$

which defines the value of  $w_2$  in equation 6. The momentum balance normal to the flame surface is

$$\rho_1 w_1^2 + p_1 = \rho_2 w_2^2 + p_2 \quad (8)$$

and because the pressure is continuous along the flame, the momentum component parallel to the flame surface is conserved and reduces to the condition that the tangential velocity component is conserved.

$$u_1 \cos \phi + v_1 \sin \phi = u_2 \cos \phi + v_2 \sin \phi \quad (9)$$

The combustion process within the flame produces an increase  $\Delta H$  in stagnation enthalpy which, because it is large in comparison with the change in kinetic energy, permits writing

$$(p_2/\rho_2)(\rho_1/\rho_2) \approx 1 + \Delta H/c_p T_1 \quad (10)$$

Moreover, according to equation 8, the pressure ratio across the flame is of order of the square of the Mach number based upon the flame propagation speed. It is quite satisfactory to neglect this pressure change as it affects the temperature ratio across the flame, but it is essential in the momentum balance and in determining the shape of the flame sheet. Then with very good accuracy

$$\rho_1/\rho_2 \approx 1 + \Delta H/c_p T_1 \quad (11)$$

and hence from equation 7,

$$w_2/w_1 \approx \gamma = 1 + \Delta H/c_p T_1 \quad (12)$$

## 3. THE INTEGRAL RELATIONS

The description of a stabilized flame that is disturbed by plane acoustic waves consists of three zones: (1) that far ahead of the flame, in which an acoustic signal originates, (2) the region near the flame which responds to the pressure field imposed by the wave impinging from upstream, and (3) the region far downstream into which an acoustic signal is transmitted as a result of the reaction of the flame zone to the imposed signal. There will, of course, be an acoustic wave "reflected" into the region from which the signal originated. Treatment of the gas as incompressible in the flame zone simply implies that the large density change which takes place across the flame sheet dominates any small density changes that arise from the acoustic disturbance or from the relatively small gas velocities near the flame.

The flow fields near the flame zone are described by an integral technique in which the equations of continuity and motion are integrated with respect to  $y$  between the flame and the duct wall. On the upstream side of the flame the region of integration is from  $y = \eta(x, t)$  to  $y = b$  and the continuity equation in region 1 becomes

$$\frac{\partial}{\partial t}(1-\gamma) + \frac{\partial}{\partial x}\{(1-\gamma)\bar{u}_1\} + u_1 \sec \vartheta = 0 \quad (13)$$

where we define  $\bar{u}_1 = \frac{1}{b-\eta} \int_{\eta}^b u_1 dy$  as the mean velocity across the region upstream of the flame sheet. Applying the same technique to the equation of motion in the  $x$ -direction leads to

$$\frac{\partial}{\partial t}\{(1-\gamma)\bar{u}_1\} + \frac{\partial}{\partial x}\{(1-\gamma)\bar{u}_1^2\} + \frac{(1-\gamma)}{\rho_1} \frac{\partial \bar{p}}{\partial x} + u_1(x, \eta, t) u_1 \sec \vartheta = 0 \quad (14)$$

and the second equation of motion, equation 3 assures that the variation of pressure in the  $y$ -direction is small so that the mean pressure  $\bar{p}_1(x, t)$  is nearly independent of  $y$ . The similar set of equations downstream of the flame sheet are

$$\frac{\partial \gamma}{\partial t} + \frac{\partial}{\partial x}(\gamma \bar{u}_2) - u_2 \sec \vartheta = 0 \quad (15)$$

$$\frac{\partial}{\partial t}(\gamma \bar{u}_2) + \frac{\partial}{\partial x}(\gamma \bar{u}_2^2) + \frac{\gamma}{\rho_2} \frac{\partial \bar{p}}{\partial x} - u_2(x, \eta, t) u_2 \sec \vartheta = 0 \quad (16)$$

The relevant matching conditions, given by equations 5 - 12, may be combined to eliminate the vertical velocity component that no longer appears in the integrated equations. By subtracting equation 5 from equation 6 and employing the conservation of momentum component parallel to the flame sheet, we find that

$$\begin{aligned} u_2(x, \eta, t) - u_1(x, \eta, t) &= (\gamma-1) u_1 \sin \vartheta \\ v_2(x, \eta, t) - v_1(x, \eta, t) &= (\gamma-1) u_1 \cos \vartheta \end{aligned} \quad (17)$$

where equation 12 and the fact that  $\frac{\partial \eta}{\partial x} = \tan \vartheta$  have been utilized in the reduction. Similarly equation 8 becomes

$$p_1(x, \eta, t) - p_2(x, \eta, t) = (\gamma-1) \rho_1 u_1^2 \quad (18)$$

and hence the pressure drop across the flame sheet is independent of location. Therefore the pressures at any value of  $x$  differ only by a constant value, depending upon whether the point is ahead of or behind the flame.

No difficulty arises in neglecting the pressure variations with  $y$  in each region so that, approximating  $p(x, y, t)$  by  $\bar{p}(x, t)$ , equation 18 holds also for the difference  $\bar{p}_1(x, t) - \bar{p}_2(x, t)$ . The values  $u_1(x, \eta, t)$ ,  $u_2(x, \eta, t)$  that occur on the right-hand sides of equations 13 and 17 cannot, however, be replaced by the corresponding average values  $\bar{u}_1(x, t)$ ,  $\bar{u}_2(x, t)$  without violating the conservation of momentum in the duct. Rather, the matching conditions across the flame must be utilized to approximate local values for these quantities. Calculations of the detailed flow field ahead of the flame suggest that the horizontal velocity component at the upstream face of the flame surface is well described by

$$u_1(x, \eta, t) \approx \left\{ \bar{u}_1(x, t) - \frac{\partial \eta}{\partial x} \sin \vartheta \right\} \cos \vartheta \quad (19)$$

We utilize this approximation and the matching conditions, equations 5, 6, 9, to determine the remaining three velocity components in terms of the flame shape.

## 4. STEADY STATE AND PERTURBATION PROBLEMS

Calculations based upon these four equations, 13 - 16, divide naturally into two parts: the steady state solution which gives the shape of the flame sheet and the distributions of velocity upstream and downstream, and time dependent perturbations from this caused by acoustic disturbances that impinge upon the region. The dependent variables may be decomposed appropriately as, for example,

$$\bar{u}_1(x, t) = \bar{u}_1^{(0)}(x) + \bar{u}_1^{(1)}(x, t) \quad (20)$$

where  $u_1''(x, t)$  is of small magnitude determined by the impressed acoustic disturbance. Then the steady flame sheet is described by the zeroth order set of equations, ref. 5, in which  $u_1^{(0)}$ ,  $p_1^{(0)}$  are prescribed at some point ahead of the flame and the condition

$$p_1^{(0)}(x) - p_2^{(0)}(x) = (\gamma - 1) \rho_1 u_1^2 \quad (21)$$

relates the two pressure fields. We assume that a small flame holder exists on the axis of the channel so that the flame sheet begins a small distance off the x-axis and the upstream flow is appropriately deformed in the vicinity of the flame holder. Immediately downstream of the flame holder the initial value of the gas velocity vanishes,  $u_2^{(0)}(0) = 0$ , corresponding to conditions behind a bluff-body flame stabilizer. The shape and velocity distribution for a steady, stabilized flame is then determined by integration of these four non-linear differential equations.

Under steady operating conditions the ratio of normal flame velocity  $u_0$  is the dominant parameter which fixes the shape of the steady flame envelope. Although the similarity is not exact, the horizontal coordinate  $(x/L)(w/u_0)$  gives a representation that is independent of  $w/u_0$  in the range of interest. This general representation is shown in Figure 2. The dependence upon the density ratio  $\rho_1/\rho_2$  and the approach Mach number is rather weak, at least for values of  $u_0/c_1 \equiv M_0 \leq 0.3$ .

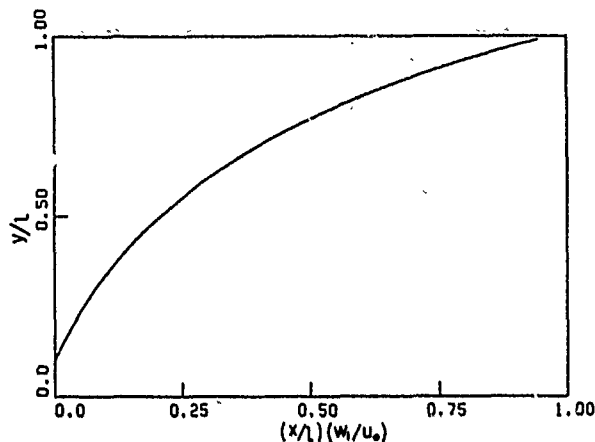


Figure 2. Steady State Flame Shape.

There is considerable empirical evidence indicating that  $w_1 \sim u_0$  for turbulent flame zones and therefore the shape of the flame envelope is rather insensitive to changes in the approach velocity. These results may be compared with those obtained by Tsien (6) in his model for the steady ducted flame and by Fabri (7) in his more detailed calculations for the same problem. The steady solutions shown in Figure 2 form the basis of the non-steady perturbation analysis.

Now for the non-steady solution we retain the first-order perturbation terms from equations 13 - 16, with the result that we obtain a set of four linear first order partial differential equations (5) whose coefficients are functions of  $x$  determined from the steady flame calculation. The matching conditions across the flame sheet again supply the additional relations required to determine the complete set of dependent variables. Equation 8 shows the perturbation pressure to be continuous across the flame,

$$p_1'''(x, t) = p_2'''(x, t) \quad (22)$$

so that, in reality there is only a single pressure perturbation variable. In addition, because the flame sheet is held at the flame holder,

$$\eta'''(0, t) = 0 \quad (23)$$

and the axial velocity perturbation

$$u_1'''(0, t) = 0 \quad (24)$$

is specified by the flame holder. For periodic solutions  $\sim e^{-i\omega t}$ , which is our interest here, these become a set of linear ordinary differential equations with variable, complex coefficients. Pressure and velocity disturbances outside the flame zone are described by waves of dimensionless strength  $P^+$  and  $P^-$  in the positive and negative  $x$ -directions.

To examine the non-steady behavior we consider two cases. First, let a periodic pressure wave of strength  $P_1^+$  and radian frequency  $\omega$  impinge from upstream. A pressure wave of strength  $P_1^-$  is reflected from the flame zone and a wave of strength  $P_2^+$  is transmitted to the right, downstream of the flame zone. Because there is no acoustic wave that radiates into the flame zone from downstream,  $P_2^- = 0$ . The corresponding acoustic matching conditions with the solutions to the differential equations in the flame zone determines the complete solutions for this particular radiation problem (5):

The pressure transmission and reflection coefficients are of primary importance because it is

these quantities that couple the non-steady combustion process with the behavior of an engine or furnace in which it is situated. For Case 1, in which the acoustic input  $P_1^+$  approaches from upstream, the transmission coefficient is  $T = P_2^+/P_1^+$  while the reflection coefficient is  $R = P_1^-/P_1^+$  both of which are complex. The magnitudes  $|T|$ ,  $|R|$  and phase  $\phi$  and  $\psi$  for the transmission and reflection coefficients are shown in Figure 3 for an acoustic disturbance ahead of the flame. The Mach number of the approach flow is  $M_0 = 0.2$ , the flame velocity  $w_1/u_0 = 0.1$  and the density ratio  $\rho = 4.5$ . The magnitudes of the transmission and reflection coefficients

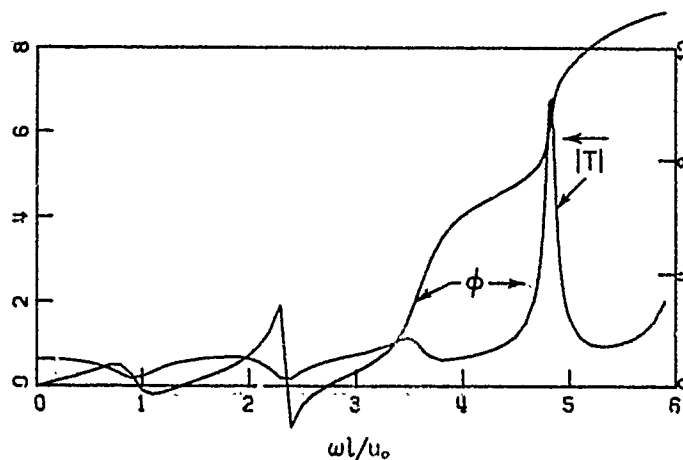


Figure 3a. Acoustic Response; Wave From Upstream.  $M_0 = 0.2$ ,  $w_1/u_0 = 0.1$ ,  $\rho_1/\rho_2 = 4.5$ .  
a) Transmission - Coefficient Magnitude,  $|T|$  and Phase,  $\phi$ .

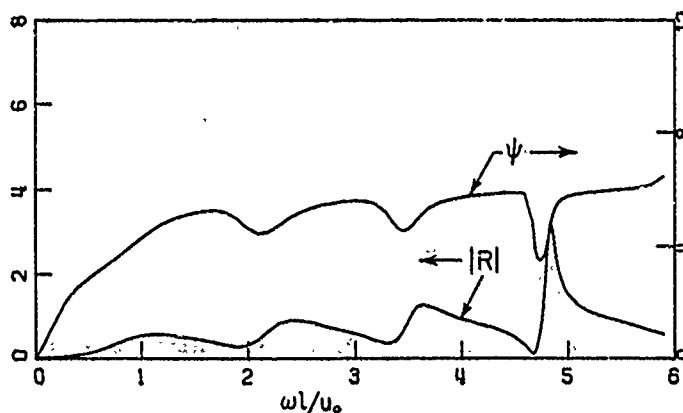


Figure 3b. Acoustic Response; Wave From Upstream,  $M_0 = 0.2$ ,  $w_1/u_0 = 0.1$ ,  $\rho_1/\rho_2 = 4.5$ .  
b) Reflection Coefficient Magnitude,  $|R|$  and Phase,  $\psi$ .

show well-defined peaks at certain values of the reduced frequency  $\omega l/u_0$ . The maximum values of these coefficients are of remarkable strength and it is well to remember that because the combustion process is active and may feed acoustic energy into the system, the classical implications of "reflection" and "transmission" are inappropriate. The corresponding results for different values of  $w_1/u_0$  show similarly strong reflection coefficients but with peaks that occur at a different selection of reduced frequencies.

Second, let a pressure wave of strength  $P_2^-$  impinge upon the flame zone from the region downstream of the flame. A consideration similar to that above gives the relationship between the field variables on the downstream edge.

Because the acoustic disturbance  $P_2^-$  originates downstream of the flame zone, the transmission coefficient is  $T = P_1^+/P_2^-$  while the reflection coefficient is  $R = P_2^+/P_2^-$ . The magnitudes and phases of these quantities are shown in Figure 4 for the same set of flame conditions as those for Case 1 shown in Figure 3. When the disturbance originates downstream, a similar set of pressure peaks is observed as in Case 1. The physical interpretation of this response is discussed in reference 5.

##### 5. LOW FREQUENCY RESPONSE OF AFTERBURNER

Consider a rudimentary afterburner configuration of constant cross sectional area; the plane of the flame holder is located at  $x = 0$  and there are four flame holder pairs across the diameter (two rings). Thus if the diameter of the burner is  $D$ , the value of  $l$  in our flame calculation is  $D/8$ . Suppose the turbine discharge is located a distance  $L_1$  ahead of the flame holder plane, the flame zone has a length  $L$ , and the nozzle throat is located a distance  $L_2$  downstream from the end of the flame zone. Thus the nozzle throat is located at  $x = L + L_2$ .

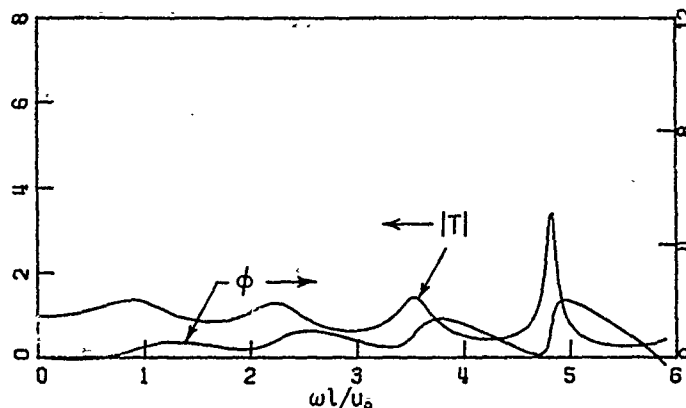


Figure 4. Acoustic Response; Wave From Downstream.  $M_0 = 0.2$ ,  $w_1/u_0 = 0.1$ ,  $\rho_1/\rho_2 = 4.5$ .

a) Transmission - Coefficient Magnitude,  $|T|$  and Phase,  $\phi$ .

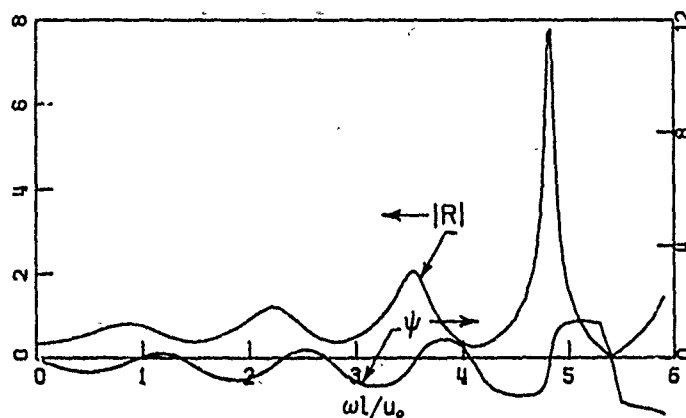


Figure 4. Acoustic Response; Wave From Downstream.  $M_0 = 0.2$ ,  $w_1/u_0 = 0.1$ ,  $\rho_1/\rho_2 = 4.5$ .

b) Reflection Coefficient Magnitude,  $|R|$  and Phase,  $\psi$ .

In the regions outside flame zone the pressure and velocity fluctuations of a plane wave acoustic field may be written

$$\frac{p}{\gamma p_0} = P^+ e^{-i\omega(t - \frac{x}{u+c})} + P^- e^{-i\omega(t - \frac{x}{u-c})} \quad (25)$$

$$\frac{u}{c} = P^+ e^{-i\omega(t - \frac{x}{u+c})} - P^- e^{-i\omega(t - \frac{x}{u-c})} \quad (26)$$

where  $u$  and  $c$  are the local gas and sonic velocities respectively;  $P^+$  and  $P^-$  are the complex amplitudes of the forward and backward running waves. Then if we define the admittance function  $\xi(x)$  to be

$$\xi(x) = \frac{u(x,t)}{p(x,t)} \left( \frac{\gamma p_0}{c} \right) \quad (27)$$

then substituting from above, we may represent the ratio of  $P^-$  to  $P^+$  at any point  $x$  as

$$P^-/P^+ = \frac{1-\xi}{1+\xi} e^{i(\frac{2\omega x}{c})} \left( \frac{1}{1-M^2} \right) \quad (28)$$

where  $M \equiv u/c$  is the local Mach number.

It is then a straightforward problem in one-dimensional acoustics to match wave fields in  $-L_1 \leq x \leq 0$  with the turbine admittance at  $x = -L_1$  and the flame reflection coefficient at  $x = 0$ . Likewise a wave field in the region  $L \leq x \leq L + L_2$  may be devised that matches with the end of the flame zone,  $x = L$ , and satisfies the nozzle admittance at  $x = L + L_2$ .

With this formulation, calculations were made of the response of the burner to a unit input of prescribed frequency located at  $x = 0$ , the flame holder plane. Figure 5 shows pressure response spectra for a set of calculations made for  $M_0 = 0.2$ ,  $L_1/l = 5.2$ ,  $L/l = 10$  and  $L_2/l = 26$ . The values of the acoustic admittance at the turbine and the nozzle were  $\xi(-L_1) = -0.25$ ,  $\xi(L + L_2) = 0.11$  respectively, the second of these corresponding to a nearly choked nozzle. The pressure responses,  $p'/p_1$ , made dimensionless by the imposed pressure amplitude  $p_1$ , are shown in Figures 5a, 5b, 5c,

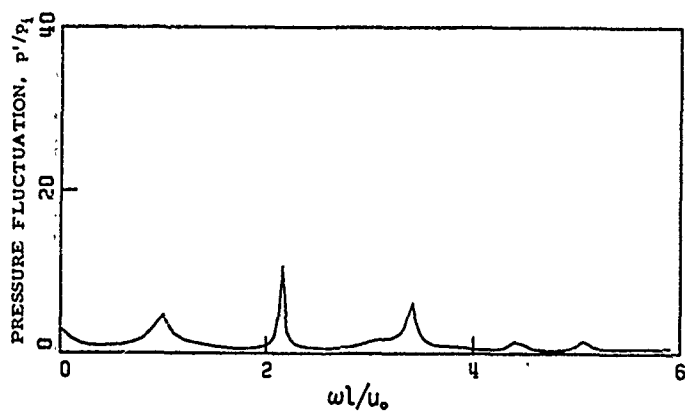


Figure 5. Pressure Fluctuation Spectrum,  $L_1/l = 5.2$   
a) Turbine Discharge

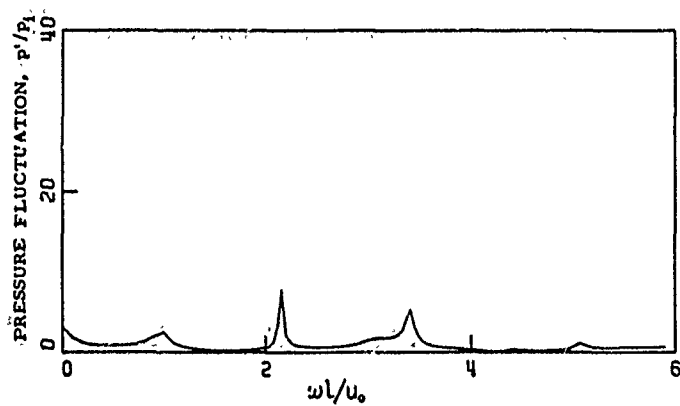


Figure 5. Pressure Fluctuation Spectrum,  $L_1/l = 5.2$   
b) Flame Holder

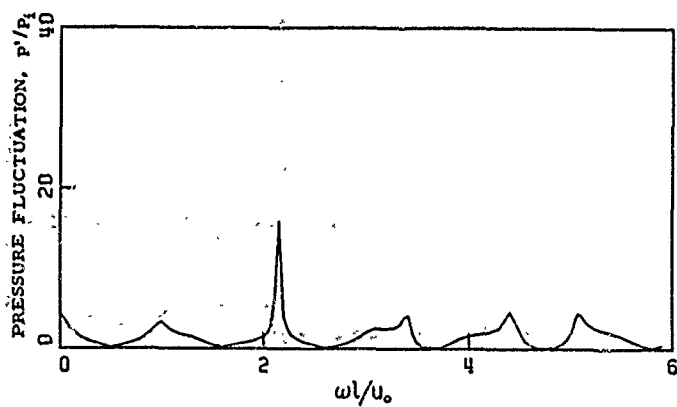


Figure 5. Pressure Fluctuation Spectrum,  $L_1/l = 5.2$   
c) End of Flame Zone

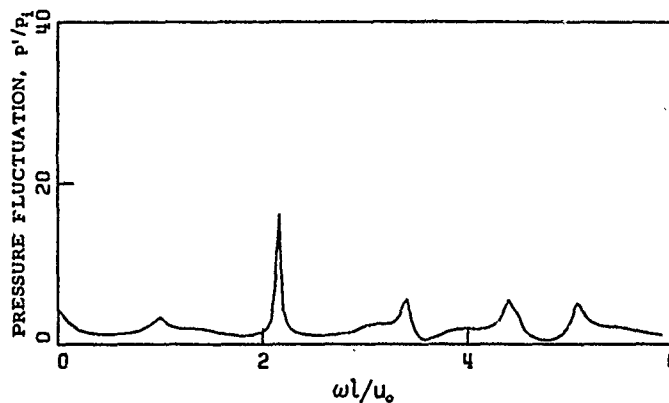


Figure 5. Pressure Fluctuation Spectrum,  $L_1/l = 5.2$   
d) Nozzle Inlet

5d for stations located at the turbine discharge, the plane of the flame holder, the end of the flame zone, and the nozzle entrance. The images of the flame zone amplification bands are clearly shown and the peak of most interest is that which occurs at a reduced frequency of  $\omega l/u_0 \sim 2.2$ . The pressure response reaches a value of  $\sim 15$  near the end of flame zone and at the plane of the nozzle.

The magnitude of these pressure peaks, and indeed, which of the burner "modes" is amplified depend rather sensitively upon the entire afterburner geometry as well as upon the admittance of the turbine and nozzle element. Because our interest here is primarily in the structure of the model, rather than in the performance of a particular afterburner, we shall examine only two of these parameters, the distance from the turbine to flame holder and the acoustic admittance at the turbine discharge.

Figure 6 shows the pressure response at the four stations examined previously, when the distance from turbine to flame holder is reduced to  $L_1/l = 5.55$ . Note particularly that the maximum response had moved to a higher "burner mode" and a higher frequency. The pressure fluctuation ratio at the turbine discharge plane has increased to a value of nearly 40 from a value of about 5 when  $L_1/l = 5.2$ . Pressure fluctuation levels at the other three stations are correspondingly large.

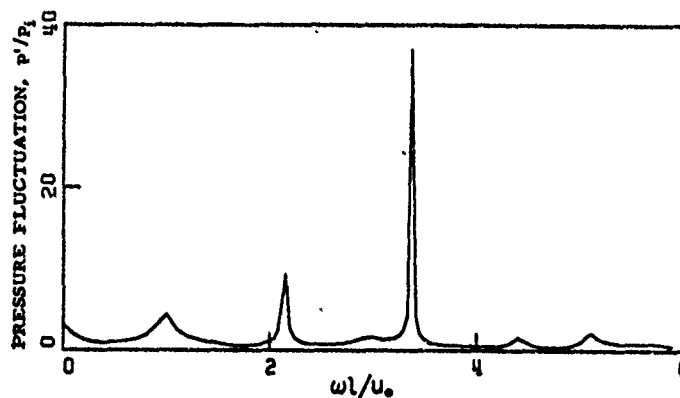


Figure 6. Pressure Fluctuation Spectrum,  $L_1/l = 5.55$   
a) Turbine Discharge

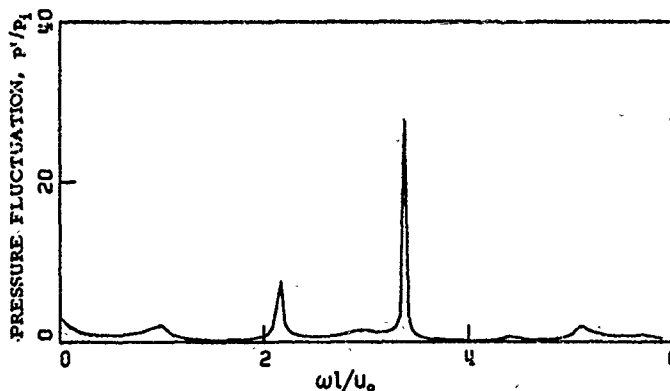


Figure 6 Pressure Fluctuation Spectrum,  $L_1/l = 5.55$   
b) Flame Holder

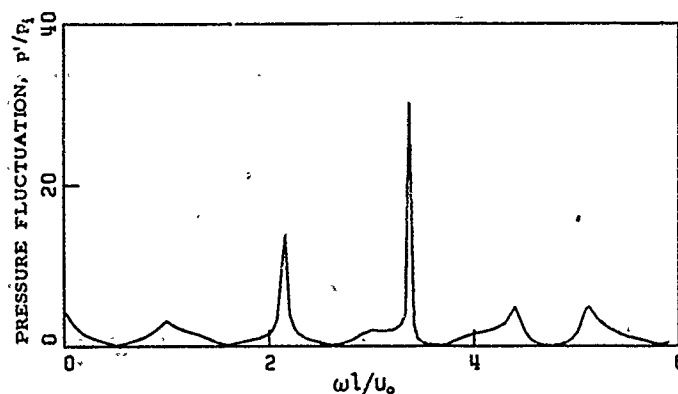


Figure 6. Pressure Fluctuation Spectrum,  $L_1/l = 5.55$   
c) End of Flame Zone

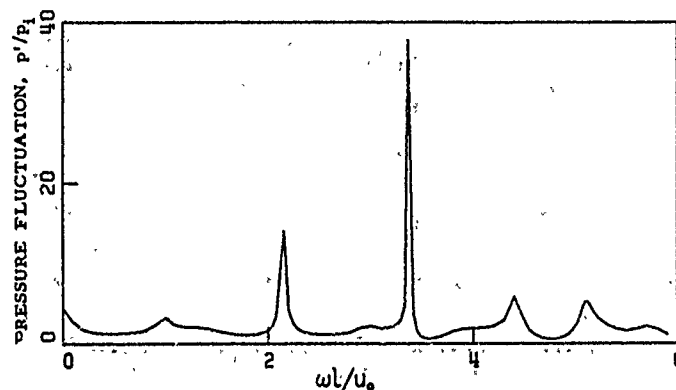


Figure 6. Pressure Fluctuation Spectrum,  $L_1/l = 5.55$   
d) Nozzle Inlet

To demonstrate the sensitivity of this response we show, in Figure 7, the pressure fluctuation at the turbine discharge as distance between the flame holder and the turbine is changed. The specific

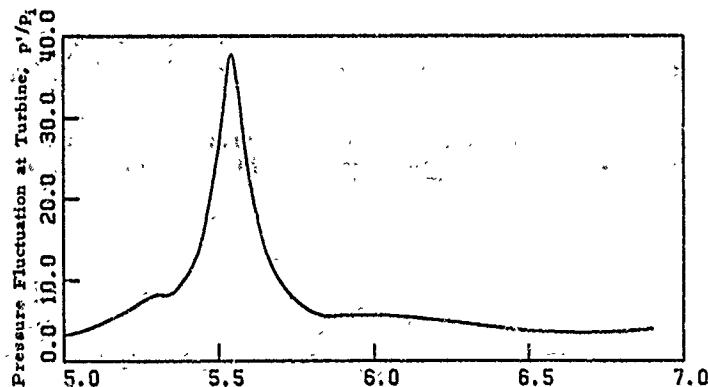


Figure 7. Pressure Fluctuation as a Function of Distance From Turbine to Flame Holder.

results are for the mode at  $\omega l/u_0 \sim 3.37$ , that are discussed in connection with Figure 6. It is remarkable that the response may be increased by a factor of 8 with a change in distance of less than 10%. This result also suggests the importance of considering the details of the geometry more accurately. It seems clear that situating the flame holder rings at different locations will influence the results of Figure 7 considerably. Similarly, details of the turbine discharge should be correspondingly important. It is clear, however, that the basic non-steady flame model may be adapted to more complex configurations.

Finally, in Figure 8, we show the effect of turbine acoustic admittance upon the pressure fluctuation, using the flame holder location of  $L_1/l = 5.54$  which was found to give the maximum response for a turbine reflection coefficient of 0.6. Note that this reflection coefficient  $\alpha$  is related to the turbine  $\xi$  through  $\alpha = (1 - \xi)/(1 + \xi)$ . As the reflection coefficient is decreased slightly, the pressure fluctuation at the turbine discharge increases sharply and the burner becomes unstable at a turbine reflection coefficient of about 0.57.



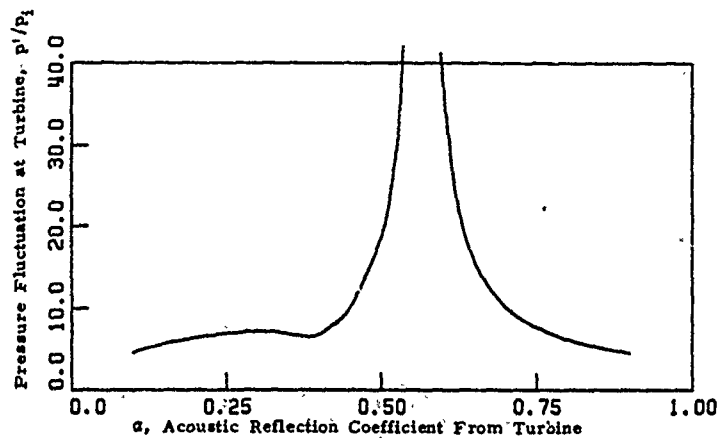


Figure 8. Pressure Fluctuation as a Function of Acoustic Reflection Coefficient at Turbine Discharge.  $L_1/l = 5.54$ , Corresponding to Maximum Amplitude From Figure 7.

#### REFERENCES

1. L. Crocco, Aspects of Combustion Stability in Liquid Propellant Rocket Motors, J. Amer. Rocket Soc. 21, 163-178 (1951); 22, 7-16 (1952).
2. H.S. Tsien, Servo-Stabilization of Combustion in Rocket Motors, J. Amer. Rocket Soc. 22,... (1952).
3. D.E. Rogers and F.E. Marble, "A Mechanism for High Frequency Oscillations in Ramjet Combustors and Afterburners", (1955 Heat Transfer and Fluid Mechanics Institute, pp. VIII-1-31 (June 1955).
4. C.L. Barker, "Experiment: Concerning the Occurrence and Mechanism of High-Frequency Combustion Instability", Ph. D. Thesis, California Institute of Technology, Pasadena, Calif. (1958).
5. F.E. Marble, and S.M. Candel, "An Analytical Study of the Non-Steady Behavior of Large Combustors", Proceedings, Seventeenth International Symposium on Combustion, Leeds, England, August 1978.
6. H.S. Tsien, "Influence of Flame Front on the Flow Field", Journal of Applied Mechanics, p. 188, June 1955.
7. J. Fabri, R. Siestrunk, and C. Fouré, "On the Aerodynamic Field of Stabilized Flames", Fourth Symposium (International) on Combustion, p. 443, September 1952.

## DISCUSSION

O.K.L.Lee, UK

- (1) Does the flame-zone considered in your present modelling need to be compact relative to the low oscillatory frequency?
- (2) IF YES  
Would the solution break down completely if your modelling is applied to smaller scale laboratory burners which, under forced conditions, may have the parameter  $(l/u_0)$  close to your limitation of  $1/4$  wavelength compactness.

Author's Reply

The model rests on the assumption that the waves propagating in the duct are plane. This is so if the wavelength is large compared to the duct width, the flame zone need not be compact relative to the wavelength. An additional comment is worth giving. Consider the greatest reduced frequency used in the calculations:  $w/u_0 = 6$ .

The associated wavelength in the cold stream is then  $\lambda \approx l/M_0$ . For  $M_0 = 0.1$  the wavelength is about ten times the duct half width ( $\lambda \approx 10l$ ). If we also assume that the ratio of normal flame speed to free stream velocity is  $w_1/u_0 = 0.1$  then the corresponding flame length is about ten times the duct half width ( $L \approx 10l$ ). Thus at the greatest reduced frequency considered in the paper the wavelength is of the order of the flame length and the flame zone is nearly compact.

A.Sotheran, UK

You are saying that the maximum response is when the flame holders are situated at  $5D$  downstream of the turbine. It would be a fairly closed system. In practice when the flame holders are near the turbine it's very difficult to make an after burner. Engines like the TF30, which are close coupled to the turbine have a by-pass stop.

If you imagine a plane wave travelling through the flame front it may cause a transverse pressure gradient, that explodes the flame. Is there any possibility of expanding your analysis to include this cross stream effect?

Author's Reply

I think it's possible. We would assume 2 pressure perturbations in the 2 streams. The difficulty in integral technique is that we have to relate those 2 perturbations, maybe by the momentum equation. We don't use the momentum equation in the  $Y$  direction: pressures are the same above and below the flame. This equation is able to accommodate a pressure gradient in the  $Y$  direction.

Comment by A.Sotheran, UK

Incidentally, in after burners we see a recovery of the flame, after its collapse, remarkably similar to the film presented in the previous lecture (Paper 16 by F.Hirsinger and H.Tichtinsky).

D.K.Hennecke, Ge

Do you want to keep your model 1-D?

Author's Reply

The calculations are indeed performed in the case of a constant area duct. However an extension to the variable area duct seems possible. The basic integral relations used in the model would have to be slightly modified. As an example Equation (13) describing mass conservation in region 1 should be written

$$\frac{\partial}{\partial t} \rho_1 (l - \eta) + \frac{\partial}{\partial x} \rho_1 (l - \eta) \bar{u}_1 + w_1 \sec \theta = 0$$

where  $l = l(x)$ .  $\rho_1$  should be allowed to vary with  $x$  and similarly  $\rho_2$  would also become a function of  $x$ . Two additional equations would then be required and might be obtained by considering the balance of energy in regions 1 and 2.

As implied by Dr Hennecke's question this extension seems worthwhile.

## SURVEY C. PREDICTION PROCEDURES FOR THE CALCULATION OF FURNACE PERFORMANCE

by

J.B. MICHEL, S. MICHELFELDER<sup>\*)</sup> and R. PAYNE  
 International Flame Research Foundation  
 c/o Hoogovens IJmuiden BV  
 Building 3G.19  
 Postbox 10 000  
 1970 CA IJmuiden/The Netherlands

## SUMMARY

The design of a furnace, or more specifically the prediction of the performance of a chosen design, can be carried out at several levels of sophistication. Dividing the performance of a furnace into separate processes, one can distinguish between fluid flow, mixing, combustion, radiative and convective heat transfer, conduction, noise generation, generation of pollutants, etc. Although it is desirable to understand all these processes for an optimum design or operation of a furnace/burner combination, in practice it is usually not possible to attain the desired objective due to limitations in time, money and knowledge.

Due to this restriction prediction procedures have been developed for separate processes and in this paper it is attempted to classify the numerous published mathematical models for the prediction of furnace heat transfer into three categories. The degree of subdivision chosen for the heat transfer calculations (dimensionality) has been used as main criterion. It is shown that the flow pattern and the desired accuracy determine the required degree of subdivision, which can be zero dimensional (model type I), one dimensional (model type II) or multi dimensional (model type III). The survey on models and some applications show also that all model types have their justification and their specific range of application.

Models of the type I and II are generally considered to be especially suitable for practical furnace calculations and parameter studies. In principle these calculations can also be performed with models of the type III although their applicability is as yet confined to special cases which can be handled computationally and where the greater effort and expense is justified. The latter is fulfilled in cases where data on flow pattern are required to decide if models of the type I and II are applicable, or when the flow data are needed as inputs and cannot be provided by simple isothermal modelling techniques. Type III models could also be of great value for parametric studies of such quantities whose effect on heat transfer and/or other furnace performance data cannot be predicted with sufficient accuracy by the simpler models.

For typical 3D geometries and if pollution emission data are to be predicted, which depend heavily on local properties, the use of type III models is indispensable. However, the use of type III models is unfortunately to date limited in their application to practical situations as some of the conditions met in industrial practice can only be approximated or cannot even be handled computationally, i.e. strongly swirling flows, geometry of industrial burners, soot formation and radiation etc.

## NOMENCLATURE

A	Area, m <sup>2</sup>
C <sub>p</sub>	specific heat at constant pressure, kJ/kg <sup>o</sup> K
E <sub>b</sub>	black body emission, kW/m <sup>2</sup>
$\overline{GG}$	total exchange area between two gasvolumes, m <sup>2</sup>
$\overline{GS}$	total exchange area between a gasvolume and a surface element, m <sup>2</sup>
$\overline{SS}$	total exchange area between two surfaces, m <sup>2</sup>
H	lower calorific value of fuel, kJ/kg
h	enthalpy, kJ/kg
J <sub>j</sub> , J <sub>h</sub>	molecular diffusion flux vector of m <sub>j</sub> respectively h, kg <sub>j</sub> /m <sup>2</sup> s and kW/m <sup>2</sup>
K	attenuation coefficient, in m <sup>-1</sup>
k	heat transfer coefficient at the wall kW/m <sup>2</sup> OK
L	flame length, m
$\dot{m}$	massflow, kg/h
m <sub>j</sub>	massconcentration of chemical species j, kg <sub>j</sub> /kg
p	pressure, N/m <sup>2</sup>
Q	heat flow, kW
q	heat flow density, kW/m <sup>2</sup>
q <sub>str</sub>	absorbed radiative energy per unit volume and time, kW/m <sup>3</sup>
R <sub>j</sub>	production rate of m <sub>j</sub> per unit volume and time, kg <sub>j</sub> /m <sup>3</sup> .s
T, t	temperature OK and OC
T <sub>v</sub>	shear stress tensor, N/m <sup>2</sup>
V	gasvolume
x, y, z	cartesian co-ordinates
r, z, $\theta$	cylindrical co-ordinates
$\alpha$	convective heat transfer coefficient kW/m <sup>2</sup> OK
$\Delta$	difference between two values

<sup>\*)</sup> Formerly director of the Research Station at IJmuiden; presently employed by Steinmüller GmbH, Gummersbach/Germany

$\epsilon$	emissivity
$\eta$	furnace efficiency
$\rho$	density, kg/m <sup>3</sup>
$\psi$	dimensionless stream function
$\vec{u}$	velocity vector, m/s

The quantities of equation (8 - 11), which are marked with  $\bar{\phantom{x}}$ , represent averaged respectively fluctuating quantities. The sign  $\otimes$  stands for a tensor multiplication.

## INDICES

a	air
f	fuel
G	gas
jet	forward gas flow
i, j, k, l	characterization of gas and furnace elements, running number
in	entering gas flow
net	net exchange
out	leaving gas flow
r	recirculating flow
U	ambient
W	wall, heat sink

## 1. INTRODUCTION

The vast amount of money involved in the combustion of fossil fuels in industrial furnaces has for many years stimulated efforts to optimize furnace performance. As the achievement of this goal via large scale experiments on individual furnaces is expensive and therefore undesirable, attempts have been made to develop mathematical prediction procedures for furnace heat transfer for almost half a century. The inability to accurately describe the complex interactions of the physical transport phenomena and the chemical reactions within industrial combustion chambers prevents however an exact mathematical solution of furnace heat transfer. This resulted in the development and publication of a great number of mathematical models with different restrictions and limitations as the selection of the necessary assumptions and approximations is generally based on specific conditions. The large number of models and their individual range of applicability often makes it difficult to decide which model is best suited to a particular purpose. To some extent these difficulties can be overcome when the models are classified into various groups, characterized by well defined specific limitations and application ranges. To give such a classification is the objective of this paper.

The testing and further development of procedures to predict furnace heat transfer has been one of the major research lines at the Research Station of the IFRF in recent years (1971-1977) and the close contact with many different approaches lead to a classification of the models into three basically different types. These model types differ both in their degree of complexity and the information which can be obtained from their application:

- Type I : zero dimensional models  
Models for the prediction of an averaged furnace heat transfer, the furnace efficiency, and other averaged properties
- Type II : one dimensional models  
Models which allow the prediction of an one dimensional heat flow distribution and other properties. Mostly as representative dimension the furnace (flame) axis is chosen.
- Type III : multi dimensional (2D, 3D) models  
Models which allow the determination of the spatial distribution of heat flow and other properties. Cylindrical furnaces can be dealt with by comparatively simple two dimensional (2D) procedures, whereas most industrial furnaces require a three dimensional approach.

In spite of the substantial differences between many of the mathematical furnace models described in the literature, most can be classified under one of the three groups (model types) mentioned above. In chapter 2 the main features of the various model types and the approaches used at the Research Station are discussed.

## 2. MATHEMATICAL MODELS FOR THE PREDICTION OF FURNACE HEAT TRANSFER

All three model types can serve the same basic goal, the prediction of furnace performance from known input and boundary conditions. Final objectives may however be very different, firstly by nature e.g. for fundamental research or industrial application, and secondly for their major field of interest e.g. aerodynamics, heat transfer, flame mechanisms.

As far as fundamental research is concerned, modelling techniques can generally be simplified either from theoretical hypothesis or from the particular design of a test rig. In this case the various combustion processes can be separated and the selection of a model becomes therefore a rather easy task. However, in the field of industrial

application a model is expected to yield comprehensive information with less time and at less cost than large scale experiments as a means to improve furnace, burners or process design. The following will mainly be concerned with industrial furnace models where emphasis is given to heat transfer performance. Information required as input and obtainable as output for the three model types is given on fig. 1.

General information to be specified before calculation	Additional specific information required, depending on model type	Information to be obtained, depending on model type
<b>A. Input conditions</b> Mass flows, enthalpy flow fuel and air composition	<b>TYPE I - UNIFORM FLOW FIELD</b> Average convective heat transfer coefficient	Average values of gas temperature ( $T_G$ ), wall- and charge temperature ( $T_W$ ), heat flow to wall and charge ( $Q_W$ ) and furnace efficiency
<b>B. Boundary conditions</b> Geometry, conductivity and emissivity of furnace wall and charge	<b>TYPE II - UNIDIRECTIONAL FLOW FIELD</b> Macro flow pattern (forward and recirculating gas flow), axial decay of chemical energy, local convective heat transfer coefficient	Same as type I, but additionally one dimensional distribution of gas ( $T_G$ ) and wall temperature ( $T_W$ ) and heat flow density
<b>C. Radiative constants</b> Gas emission and absorption data depending on radiative submodel	<b>TYPE III - MULTIDIRECTIONAL FLOW FIELD</b> Complete flow pattern and spacial gas concentrations, turbulent exchange coefficient for heat, local convective heat transfer coefficient	Same as type I, but additionally complete spacial distribution of gas ( $T_G$ ) and wall temperature ( $T_W$ ) and heat flow density

Fig. 1 : The information required for and obtained from the calculation of furnace heat transfer with the model types I to III; the various specific information can be provided from measurements or mathematical submodels.

The detail in the input and output information can be seen to increase from model type I to type III, and is accompanied by an increase in the degree of subdivision of the furnace under consideration into more and more elements as shown in fig. 2.

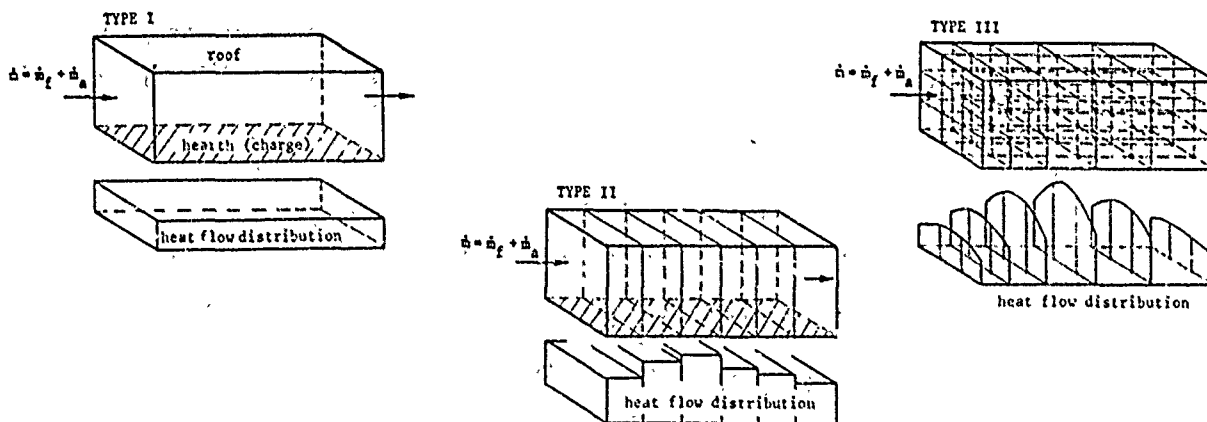


Fig. 2 : The degree of subdivision required for a rectangular furnace - and the heat flow distribution obtained - in dependency of the model type to be applied.

The representative model types I, II and III used at the IFRF are all based on the well-known Zone Method developed by Hottel et al. [1] for the calculation of radiative heat transfer in enclosures.

### 2.1. Model type I (zero dimensional model, fig. 2, type I)

The determination of the distribution of the heat flow density over the surface of the stock is desirable and sometimes necessary, although a proper orienting first step which often suffices is the determination of the total heat transfer as a function of fuel and air inputs. Even if this is the sole objective, knowledge of the detailed interaction of radiation and convection with mass transfer and combustion is in principle necessary. However, integral formulations are tolerant of casual treatment of detail, especially in the presence of the levelling effect of radiation, and a surprisingly accurate overall performance is predictable from a relatively simple model.

A zero dimensional model does not take account of length- and time dimensions within the furnace. In such a model gradients of quantities like velocities, temperatures,

heat flux densities etc. are neglected in all three co-ordinate directions, which implies that all these properties are considered to be uniform. The model is thus based upon the assumption that the processes inside the combustion chamber can be described with a reasonable accuracy by one representative average value for

- combustion pattern;
- gas temperature;
- temperatures of the heat sinks;
- gas concentrations;
- soot particle concentrations;
- radiation characteristics;
- convective heat transfer to the sinks;

similar to the processes in an ideal well stirred reactor.

For many years such models have been used for the design of radiant cells of boilers, furnaces of the petrochemical and other industries. Well documented examples of zero dimensional models have been published by Hottel and Sarofim [1], Jeschar and Schupe [2] and Hotte [3]. Major differences between the numerous models to be found in literature are the treatment of:

- the radiative exchange between gas-, walls- and heat sinks (stock) within the furnace (e.g. gray or non-gray gas radiation) and
- the furnace walls, either adiabatic or with wall losses.

Although a truly zero dimensional situation cannot exist in practice and the accuracy of the predicted results depends on the degree of deviation from zero dimensionality of the furnace/burner system under consideration, these models can predict the right trends for the effect of operational variables on the overall furnace performance in most cases, i.e. the effect of:

- adiabatic flame temperature (fuel type);
- heat sink temperature;
- firing rate;
- heat loss through walls;
- excess air;
- air preheat;
- oxygen enrichment, etc.

Large deviations from the assumed well stirred conditions upon which the model is based, can cause substantial discrepancies between the real and the calculated overall efficiency. For long furnaces with a small cross-section (no gas recirculation) and cold walls, fired by a short flame, the overall efficiency can be underpredicted by more than 20% (flame D.2.2, ref [38]). Overpredictions of the same order of magnitude have to be envisaged when the model is applied to long narrow flames in a comparatively wide combustion chamber (flame 29, ref. [34]).

The Research Station's model type I, used also for the predictions discussed in chapter 3.1, is a modified version of the model described explicitly in [3]. Major changes adopted are the inclusion of wall losses and a non-gray gas radiation model. For each of the heat sinks  $i$  (fig. 2, furnace hearth, sidewall, roof) and for the gas volume, energy balances are drawn up:

heat sinks  $i$

$$\overline{GS}_i E_G + \sum_j \overline{S}_j S_i E_j - A_i \varepsilon_i E_i + A_i \bar{\alpha}_i (T_G - T_{W,i}) = A_i k_i (T_{W,i} - T_U) \quad (1)$$

arriving radiative heat flux      off radiative heat flux      net convective heat flow      net heat flow

$$\overline{GG} E_G + \sum_j \overline{S}_j S_i E_j - 4KV_G E_G - A_j \bar{\alpha}_j (T_G - T_{W,j}) + \dot{m}_F H + C_p \dot{m} (T_{in} - T_G) = 0 \quad (2)$$

arriving radiative heat flux      off radiative heat flux      net convective heat flow      latent enthalpy flow

A detailed description of the derivation of the total exchange areas  $\overline{GG}$ ,  $\overline{GS}$  and  $\overline{SS}$  can be found in [1,4,5]. The solution of these non-linear algebraic equations yields the average temperatures of the heat sinks ( $T_{W,i}$ ) and the gas volume ( $T_G$ ) as well as the heat flows to all heat sinks  $i$  considered within the furnace.

## 2.2 Model type II (one dimensional model, fig. 2, type II)

When the combustion system under consideration deviates strongly from the well stirred assumption, the heat flow distribution will lose its uniformity. Although adjustments can be made in order to calibrate the zero dimensional models to enable the determination of an overall efficiency in such cases, they can never give information on the distribution of the heat flux density over the stock, respectively the heat sink. This latter information is however required under circumstances where the heat flow densities have to be kept in between certain limits, i.e. because of the danger of overheating of the charge or of hazard to the plant. To obtain more detailed information is possible only by the introduction of "dimensions" like time and length.

In many furnaces the heat flow density varies dominantly in one direction, which is generally the main flow direction. In this case, it is often sufficient to introduce only a length dimension to allow the determination of the most important heat flow and temperature distribution. The prediction procedure then becomes a one dimensional model, an illustrated example of which is shown on the centre of fig. 2.

In one dimensional furnace models generally only one length dimension is taken into account. Gradients of the different quantities in the two other co-ordinate directions are neglected. This implies that the velocities, temperatures etc. are assumed to be uniform in finite cross-sections along the main co-ordinate direction. Furnaces for which this assumption is reasonable are usually long in comparison to their width as in such furnaces the gradients perpendicular to the length dimension are often of minor importance. As shown in chapter 3.2 the application range of one-dimensional models can be extended also to reverberatory type furnaces (length to diameter ratio small) when the latter assumption is modified, i.e. when the recirculating gas flows are taken into account. Of course the information on the flow pattern required as input to the model calculations increases with increasing complexity of the adopted flow model.

The subdivision of the furnace into a sequence of individual sections does not cause a fundamental change in the calculation procedure, only the number of equations increases as for all individual elements in a section balance equations have to be drawn up. Each section can be treated in a way similar to the procedure described in chapter 2.1.

The main differences encountered in published work on one-dimensional furnace models are in the treatment of radiative heat exchange and the assumptions of the idealized flow pattern adopted in the models.

The most well-known type II model is the so-called long furnace model after Hottel and Sarofim [1]. Some of the major assumptions made are: no recirculation of gases in the furnace, combustion completed at the burner exit, no net radiative exchange in main gas flow direction.

Selçuk et al. [6] assume also a plug flow pattern (i.e. uniform "forward" velocity, temperature and species concentration at any cross-section), whilst taking account of radiative interchange between different locations in the main flow direction and allowing for a gradual "stepwise" chemical heat release along the flame axis.

In situations where the real flow pattern is not approximated by the plug flow concept, e.g. with the appearance of substantial recirculation zones in the combustion chamber, the plug flow assumption leads to an overprediction of heat flow density, especially at locations where considerable heat release occurs. Some type II models allow account to be taken of gas recirculation zones, when these are confined to the burner near region, by using a well stirred plug flow concept for the description of the flow pattern. Here the burner near section is treated as well stirred, the successive sections as plug flow. The length of the well-stirred section is usually chosen to cover the area from the burner inlet to the point of impingement at the wall, i.e. the part where recirculation occurs. Models of this type have been suggested by Michelfelder and Lowes [5], Lucas and Lockett [7] and Clement [8].

The application of this idealized flow pattern description is obviously not suitable for furnaces in which the recirculation zone stretches over the entire furnace length or covers the major part of the furnace (heaters in chemical industry, reverberatory furnaces etc.). To determine a heat flow distribution in such furnaces requires a more realistic description of the flow pattern, i.e. a mass interchange in forward and backward direction between adjacent sections has to be considered. At the IFRF a model has been developed [10] which allows account to be taken of gas recirculation by using the flow pattern model shown on fig. 3.

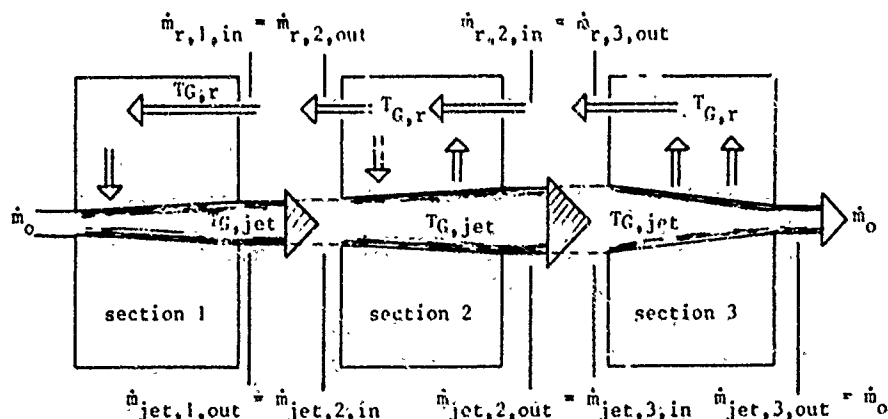


Fig. 3 : Flow pattern model suggested for the determination of an one-dimensional heat flow distribution in reverberatory furnaces after [10].

As indicated on this figure the flow is separated into a forward and a recirculation region with different temperatures. Although the radiation exchange is calculated with a mean section gas temperature (one-dimensional model) a pseudo two-dimensional treatment of the flow is introduced by relating the mean radiation temperature to the recirculation- ( $T_r$ ) and jet-temperature ( $T_{jet}$ ).

With the radiation exchange calculation based again on the Zone Method [1] the balance equations for each section can be written as:

gas volume 1

$$\begin{aligned} \sum_j \overline{G_j G_1} E_j + \sum_k \overline{S_k G_1} E_k - 4K\overline{V}_{G,1} E_{G,1} - \sum_k A_k \alpha_k (T_{G,r,1} - T_{W,k}) + H \dot{m}_{F,1} + (C_p \dot{m} T_G)_{jet,1,in} - \\ (C_p \dot{m} T_G)_{jet,1,out} + (C_p \dot{m} T_G)_{r,1,in} - (C_p \dot{m} T_G)_{r,1,out} = 0 \end{aligned} \quad (3)$$

heat sink element i (furnace walls, charge)

$$\sum_j \overline{G_j S_i} E_j + \sum_k \overline{S_k S_i} E_k - A_i \epsilon_i E_i + A_i \alpha_i (T_{G,r,1} - T_i) = A_i k_i (T_{W,i} - T_a) \quad (4)$$

Apart from the general input conditions for all prediction procedures the solution of the equations requires specific data on the global forward and recirculating gas flows, the chemical heat release and the convection coefficients for each section. These data can be obtained via two routes:

- for simple configurations, from separate calculation procedures as f.i.: Thring-Newby [11] or Craya-Curtet [12];
- from measurements in an isothermal model and/or in the furnace.

The various temperatures appearing in equations (3) and (4) have to be related by empirical functions. For the correlation between mean radiation temperature and the recirculation or jet temperature an area weighting factor concept has been suggested in [10]. The weighting factors depend on the flow pattern, i.e. characterized by the ratio of recirculation and forward flow area.

The calculations discussed in chapter 3 have been performed with following relations:

mean radiation temperature

$$T_{G,1} = \frac{(8T_{G,r,1,out})^4 + (T_{G,jet,1,out})^4}{9} \quad (5)$$

recirculation temperature

$$T_{G,r,1} = \frac{T_{G,jet,1,out} + T_{G,r,1,in} + T_{W,i}}{3} \quad (6)$$

For the heat release pattern an empirical correlation has been applied which correlates the flame length with the burn-out:

$$\dot{Q}_{chem} = H \cdot \dot{m}_F (1 - e^{-4.605 (\frac{x}{L})}) \quad (7)$$

The range of applicability of one-dimensional models has been widened considerably by the introduction of the forward/recirculation flow treatment developed in [10], now to some extent also two-dimensional flows can be handled with this model. If the transport of heat and mass is important in all three dimensions of real combustion systems, then the only model which can be applied with confidence is a three-dimensional model as shown on fig. 2, model type III.

### 2.3 Model type III (three-dimensional models, fig. 2, type III)

Apart from typical three-dimensional situations there are a few more conditions which require the use of three-dimensional models. The prediction of the following quantities can, under three-dimensional condition, be obtained with some only with two- or three-dimensional procedures:

- spacial distribution of temperatures and heat flux densities (fig. 2, type III);
- flow pattern and species concentrations;
- pollutant emission ( $SO_x$ ,  $NO_x$  etc.), because the formation of pollutants is strongly influenced by local properties within the combustion chamber.

The application of three-dimensional models requires the subdivision of the furnace into many individual sections. Usually this subdivision is along the directions of the chosen co-ordinate system, regardless of the main flow direction (fig. 2, type III). The geometry of the combustion chamber and the position of the flame(s) within the gas volume dictate the number of dimensions which have to be taken into account. An example of a three-dimensional system which can accurately be described by two co-ordinates only is a vertical axi-symmetric furnace with a central flame. For this specific case the subdivision in annular section is most suitable (2-D), whereas for an asymmetric heat sink in a rectangular enclosure parallelepipeds have to be chosen (fig. 2, type III). Depending on the calculated quantities the published work on multi-dimensional prediction procedures can be divided into two groups:

- models (type IIIa) which are based on the Zone Method [1], which require detailed special input information prior to the calculation of the spatial heat flux and temperature distribution (fig. 1, model type III);



- models (type IIIb) which are based on the numerical solution of the convective transport equations, the solution of which yields information on the spatial distribution of all properties. Similarly to the model type I only the general inputs described on fig. 1 are required for the application of this model.

### 2.3.1 Three-dimensional models based on the Zone Method of analysis (type IIIa)

For this model type energy balances are formulated for all the elements of the subsections similar to the model type II. The only basic difference between model types II and IIIa is that for the latter the energy and mass transport between gas volumes is no more confined to one direction. As for the model type I and type II total exchange areas have to be determined from so-called direct exchange areas which are available for two different geometries in [1], in graphical form for cubes and tabulated for annular sections (axi-symmetric systems).

Richter and Bauersfeld [13] reported a computer programme which is capable of calculating direct exchange areas for annular sections of rectangular cross-section, with different attenuation coefficients in the various sections.

Models based on the Zone Method have been applied successfully to the calculation of the spatial heat flow distribution in different types of combustion chambers [14-16]. Of special interest to IFRF members are the applications of the Zone Method approach to the Nr. 1 furnace of the Research Station [4, 18]. A major shortcoming of the model type IIIa is the large amount of detailed input data required on flow, mixing and chemical heat release before the solution procedure for the determination of the heat transfer can be started (fig. 1). Global assumptions similar to those made for the model type II are not suitable for model type IIIa, as the accuracy of the prediction depends heavily on the quality of the input data. The specific inputs can be obtained in enough detail only from isothermal models or predictions from models of type IIIb. Furthermore it is virtually impossible to correctly incorporate the simultaneous dependency of the attenuation coefficient on the local gas temperature and the temperature of the radiation source within the conventional Zone Method. This can however be overcome by the application of the Monte Carlo Method for the calculation of direct or total exchange areas. Published examples of this method can be found in [13, 19, 20].

### 2.3.2 Models which are based on the numerical solution of the convective transport equations (type IIIb)

With the model type IIIa energy balance equations are solved to predict spatial heat flux and temperature distributions. Before the model can be used detailed information on the flow and concentration field is required as input. If the determination of these properties should be included in the prediction procedure, then equations describing the transport of species and momentum are to be included. Models of the type IIIb are capable of doing so as they are derived from the basic differential equations which describe the exchange of all time averaged properties. For a quasi stationary flow and with some simplifications these equations can be written in vector form as:

$$\text{Continuity equation} : \operatorname{div}(\bar{\rho} \bar{w}) = 0 \quad (8)$$

$$\text{Transport of momentum} : \operatorname{div}(\bar{\rho} \bar{w} \otimes \bar{w}) + \operatorname{div}(\bar{\rho} \bar{v} \otimes \bar{w}) = - \operatorname{grad} \bar{p} + \operatorname{div} \bar{T}_v \quad (9)$$

$$\text{Transport of species} : \operatorname{div}(\bar{\rho} \bar{m}_j \bar{w}) + \operatorname{div}(\bar{\rho} \bar{m}_j \bar{v}) = \bar{R}_j \quad (10)$$

$$\text{Transport of energy} : \operatorname{div}(\bar{\rho} \bar{h} \bar{w}) + \operatorname{div}(\bar{\rho} \bar{h} \bar{v}) = \bar{q}_{\text{str}} \quad (11)$$

The numerical procedure for the solution of equations (8 - 11) involves the setting-up of an orthogonal computational grid to cover the flow field and the specification of boundary conditions along the flow field boundaries. The grid nodes represent centres of small volume elements over which the differential equations are numerically integrated. Solution procedures have been published by Spalding [21] for axi-symmetric (2-D) systems and by Zuber [22] for three-dimensional systems. Models of the type IIIb have been used with some success by Michelfelder et al. [4], Gibson and Morjan [23], Lowes et al. [24] and Richter et al. [25-27].

In trying to apply models of the type IIIb to combustion systems one has to face several principle problems:

- The physical relevance of the solution of the flow equation depends strongly on the correlation terms for the turbulent properties  $\bar{\rho} \bar{w} \otimes \bar{w}$ ,  $\bar{\rho} \bar{m}_j \bar{w}$  and  $\bar{\rho} \bar{h} \bar{w}$ , which describe the increase of momentum-, species- and enthalpy transport due to turbulent exchange. A number of turbulence models have been suggested [28]. It is however still necessary to "calibrate" the empirical constants of these relations to the flow problem under consideration. Recent investigations at the Research Station [29] indicated, that the so-called kW model [30] can be used with good confidence for enclosed non-swirling double concentric jets.
- The importance of radiative exchange in furnaces and the difference in nature between the transport of the other quantities - mass, momentum, species and enthalpy - which can accurately be described by differential equations and radiation which, due to its integral nature, can only be approximated by differential equations, introduces another principle problem for type IIIb models.

Due to its importance an exact solution of radiative exchange is desirable. With the large number of elementary volumes required for a reasonable accuracy of the flow calculation this would however lead to a tremendous demand in computer time and storage. A simultaneous solution of both flow- and concentration-fields and heat flow distribution is possible only when simplified radiation models are used. Such models have been suggested by Richter and Bauersfeld [13], Bartelds et al. [31] for two-dimensional systems and by De-Marco and Lockwood [32] for three-dimensional systems.

- The subdivision of three-dimensional systems (number of volume elements) has to be restricted due to the excessive computer time and storage of the solution. For this reason, to date only qualitative information has been obtained with applications of type IIIB models [22, 33].

The above mentioned problem areas and shortcomings of the type IIIB models (against type IIIA models) are balanced by the tremendous advantage of the minimum of input data required.

Presently the best solution for three-dimensional models appears to be a combination of the advantages of both model types by combining them to one prediction procedure. A first step in this direction has been undertaken at the IFRF [4, 39, 40].

### 3. COMPARISON OF CALCULATED AND MEASURED DATA

To provide data which allow the testing and further development of mathematical models a series of furnace trials have been carried out at the IFRF over the past years. The measured data referred to below have been obtained from the M2 [34] and M3-A trial [35].

A major difference between both trials was the arrangement of the water-cooled heat sink within the furnace. Whereas a symmetrical heat sink was chosen for the M2 trials, to enable an approximation of the furnace/flame configuration by a two-dimensional system, the M3 trial heat sink was restricted to the furnace hearth in order to produce a typical three-dimensional configuration with respect to heat transfer. Detailed information on the experimental set-up, burners and fuels used have been given elsewhere [4, 34, 35].

The calculated data presented below have been determined with the prediction procedures described in chapter 2. Depending on the model type used and the flame/furnace configuration under consideration the input and boundary conditions required have been provided according to fig. 1.

#### 3.1 Model type I

The zero-dimensional model has been used to calculate the furnace efficiency, the overall heat transfer to furnace walls and to the water-cooled heat sink and the mean temperatures of the walls and the gas volume for a series of gas flames fired in the M3-A trial [35] furnace configuration. The following assumptions have been made:

- non-gray gas radiation (1 clear/2 gray gas approximation, see [1]);
- specific heat  $C_p = f(\text{temperature, concentration})$ ;
- to take account of wall losses an overall heat transfer coefficient has been introduced;
- total exchange areas ( $\overline{SS}$ ,  $\overline{SG}$ ,  $\overline{GG}$ ) have been evaluated according to [1, 3].

Below some of the predicted data are compared with the corresponding measurements. The effect of furnace loading has been investigated with four natural gas (NG) flames (0.75, 1.5, 3 and 4 MW thermal input), the effect of the fuel LCV has been studied with three 3 MW gas flames, i.e. a blast furnace-gas (BFG), a NG/BFG- and a NG-flame. All flames were fired with the same burner. Fig. 4 shows a comparison of the measured and predicted effect of these two variables (load, LCV) on the furnace efficiency.

Although the furnace efficiency is underpredicted in all cases by between 3 and 5%, the overall effect of the variables is predicted very well. The discrepancy between the absolute values has to be attributed to the deviation between the assumed (well-stirred) and the real flow pattern. The fact that the model predicts the correct tendency indicates however that an improvement of the accuracy of the predicted individual efficiencies is possible when the model is adjusted to, or calibrated for the furnace under consideration. For this purpose Hottel et al. [1, 3] recommend the introduction of a temperature difference between the furnace gas volume and the flue gas.

The difference between assumed and real flow pattern has a less pronounced effect on the accuracy of the calculated mean roof temperatures; they are compared with representative averaged measured roof temperatures on fig. 5.

Further parameters whose effect on the furnace efficiency was investigated in the M3-A trials were various burner and flame types. The effect of these parameters cannot be taken account of by type I models. At a furnace loading of 3 MW the maximum and minimum efficiency recorded was  $\eta_{\max} = 56\%$  and  $\eta_{\min} = 46\%$ . This difference gives an indication of the range of uncertainty which one can be faced with when using type I models without adjustment for different furnace configurations. However, this type of model is rather easy to handle and its high degree of flexibility makes it applicable to a great number of situations.

Possible applications can be:

- preliminary design of a furnace and estimation of dimensions;
- parameter study;
- provision of starting values for more complex models (II, III);
- optimization of the overall energy consumption of a furnace in relation to process variables (capacity, product temperature etc.).

This latter application was considered during the IFRF G1 trials [36, 37] concerning the use of blast furnace gas as a fuel for high temperature furnaces of the steel industry, such as slab reheating furnaces.

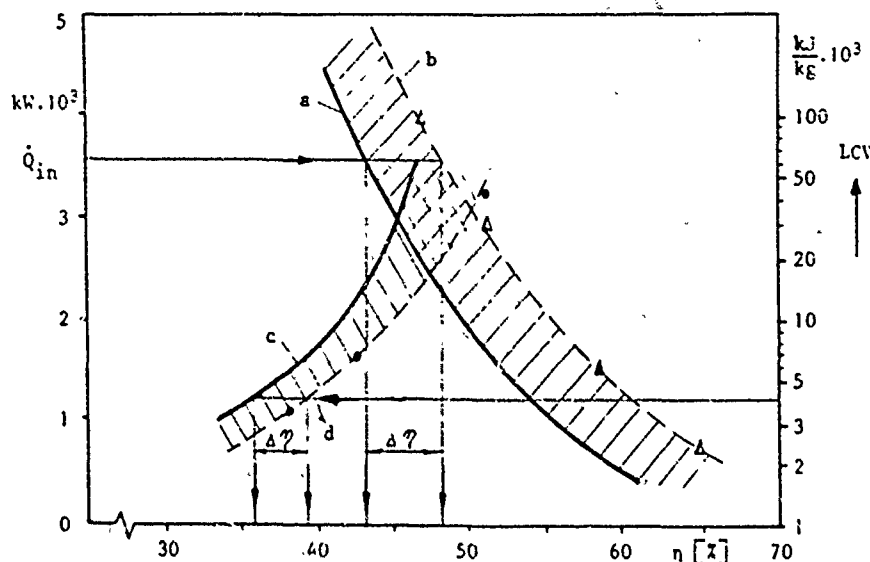


Fig. 4 : Measured and calculated furnace efficiencies for flames 1, 2, 3, 4 (variable furnace loading) and 3, 9, 11 (variable lower calorific value LCV) from the M3-A trials [35]

Effect of furnace loading :

a calculated

b measured

Effect of LCV :

c calculated

d measured

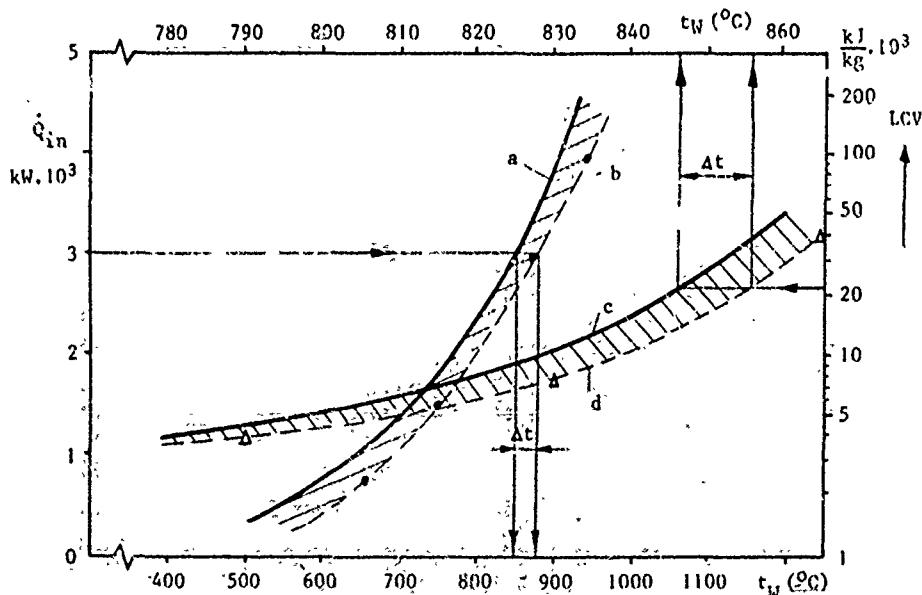


Fig. 5 : Measured and calculated mean roof temperatures for flames 1, 2, 3, 4 (variable furnace loading) and 3, 9, 11 (variable lower calorific value LCV) from the M3-A trials [35]

Effect of furnace loading :

a calculated

b measured

Effect of LCV :

c calculated

d measured

## 3.2 Model type II

The type II model described by the equations (3-7) has the widest range of applicability of all type II models mentioned in chapter 2.2. If however flow pattern can be approximated by simple assumptions, other type II models like the long furnace model [1] or the well-stirred plug-flow approach can yield excellent results. The importance of the flow pattern/model combination is shown at the example of two (natural gas) flame/furnace configurations, i.e.:

- flame D.2.2 fired in the Delft vertical water-cooled furnace (0.9 m diameter, 5 m length; see [38], and
- flame 29 (M2 trials, [34]) fired in the IFRF furnace Nr. 1 (2 x 2 m cross-section, 6.25 m length).

Flame D.2.2 was a strongly swirling wide flame fired in a rather narrow furnace ( $L/D \sim 5.5$ ). The external recirculation was due to the confined situation limited to the burner near region. This configuration is almost ideal for the well-stirred plug flow approach.

Flame 29, however, was a narrow non-swirling jet flame fired in a rather wide furnace ( $L/D \sim 3$ ) with an external recirculation over the entire furnace length.

The heat flux distribution for both flames has been calculated with the well-stirred plug flow model of the IFRF [5, 9]. For flame 29 a second calculation was performed with the model described by the equations (3-7) [10].

As shown on fig. 6 the predictions obtained from the well-stirred plug flow model are excellent for flame D.2.2. The calculation was carried out with assumptions similar to those made for model type I and following special input data:

- burn-out completed within first section;
- first two sections well-stirred, all following sections plug flow;
- convective heat transfer coefficients as measured in the furnace [38].

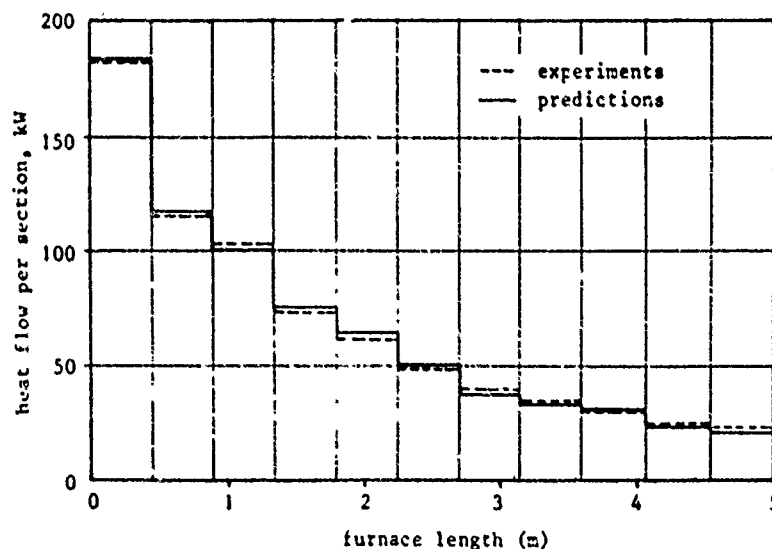


Fig. 6 : Measured and predicted heat flow distributions to the water-cooled furnace walls of the Delft furnace (flame D.2.2, [38])

Using the same approach for the calculation of the heat flow distribution from flame 29 resulted in a complete misprediction. In comparison to the measurements the local heat flow predictions were up to 100% too high and at the rear of the furnace 50% too low (fig.7). The misprediction has mainly to be attributed to the wrong assumption of the flow pattern. For furnace configurations which result in similar flow pattern as flame 29 (most reverberatory furnaces) the recirculation has to be taken account of. With the "recirculation" model [10] a second calculation has been performed using following inputs:

- chemical heat release as determined by equation (7) from the visible flame length;
- information on flow pattern (fig.3) obtained from an isothermal physical model;
- convective heat transfer coefficients obtained from isothermal model.

As can be seen from fig. 7, curve b, the prediction with the "recirculation" model is reasonable. This proves that with only a rough incorporation (pseudo 2D description) of the real flow pattern the applicability of one-dimensional models can be extended to situations with two-dimensional flow fields. This type of model is thus well-suited to long furnaces and strongly unidirectional processes e.g. rotary kilns, glass smelters, refinery process heaters and steel reheating furnaces.

Absolute predictions are generally accurate enough to help in the design or modification of an industrial furnace (heat sink geometry, position and distribution of heat

along the process length). The exercise of selecting adequate submodels viz. for flame radiation of heat release, requires however a good knowledge and experience of the application of interest.

Moreover, in most test rigs for liquid or solid fuel characterization, which are often designed to be mono-dimensional, such a heat transfer model can be linked with a similar kinetic model and become an efficient tool for research.

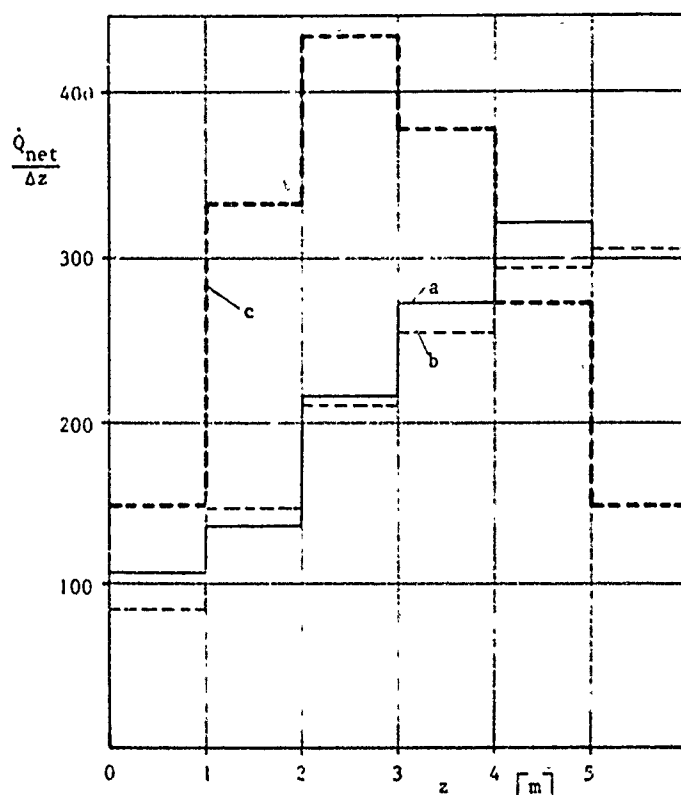


Fig. 7 : Measured and predicted heat flow distribution from flame 29 [34].

- a - measured
- b - predicted with "recirculation" model [10]
- c - predicted with well-stirred plug flow model [9]

### 3.3 Model type III

In respect to the calculation of flow and gas concentration fields multi-dimensional models (type IIIb) are still in the development stage. For this reason their application is usually limited as yet to symmetrical (2-D) systems. In [4] a first application of a combination of the type IIIa and type IIIb models has been reported upon. Because of its well-defined flow pattern flame 29 [34] had been chosen for this test too.

Discrepancies found between the measured and predicted flow pattern had been attributed to the oversimplifying ad hoc turbulence model used. This turbulence model has now been replaced by the better suited kW model [29, 30]. The former calculations have now been repeated with the following assumptions:

- the rectangular furnace Nr. 1 has been approximated by an equivalent cylinder;
- chemical heat release is determined by  $\text{mixcd} = \text{burnt}$ ;
- gray gas radiation with  $K = 0.15 \text{ m}^{-1}$ ;
- two flux radiation model [13];
- convective heat transfer coefficient as measured in isothermal model (same as chapter 3.2).

On fig. 8 the calculated flow pattern is plotted against the measured stream lines.

A comparison with the earlier results [4] shows a considerable improvement of the predictions, and the excellent agreement in the area of forward flow is especially impressive. Also the predicted isotherms plotted together with the measured values on fig. 9 show reasonable agreement. Discrepancies near the jet boundaries can be a result of the unmixedness which has not been taken into account in the calculation procedure.

Similar to [4] the heat flow distributions have been calculated with the Zone Method (model type IIIa); the calculated flow- and heat release pattern (output model type IIIb) have been used as input information (fig.1) required for model type IIIa. In spite of the differences between measured and predicted local heat flow in the rear part of the furnace the heat flow distribution obtained is satisfactory, especially

if one considers that these results have been obtained from general input data only (fig. 10).

As expected, due to the unchanged boundary conditions, there is an obvious similarity between the heat flux distributions at nominal thermal input (flame 29) and at half load (flame 35).

Validation of type IIIb models is thus achieved in simple furnace-burner systems. Nevertheless many problems remain unsolved for their general application to large and complex industrial furnaces. The modelling of the detailed interaction of some physical phenomena which is the key to many of these problems is still in the development stage, where practical experiments on a pilot scale are required [41, 42].

Full scale experiments and comparisons are also shown to be realistic [43, 44] and would justify the expense of further developments of these models. Possible future applications of such procedures would finally be most suitable for general industrial needs, in view of material and space saving for furnace construction, adaptation of the burners to the process, antipollution control techniques etc.

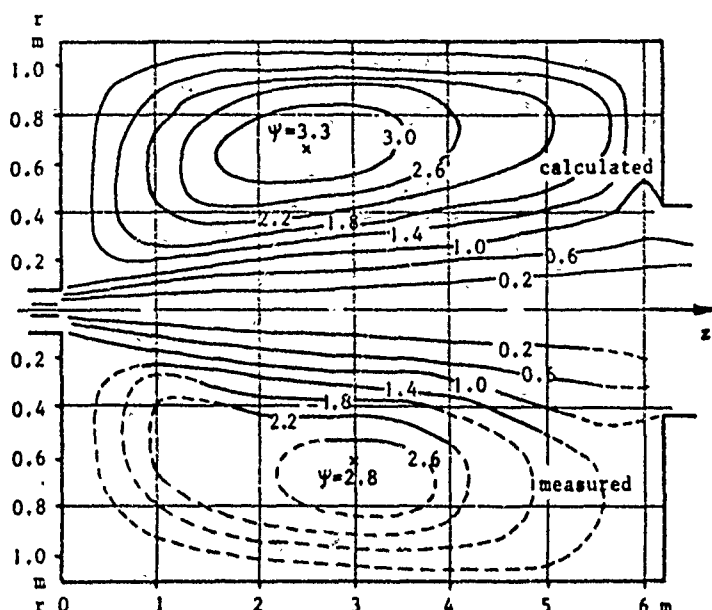


Fig. 8 : Comparison between predicted and measured flow pattern (flame 29, M2 trials [34]). The dotted lines are extrapolated from measurements. ( $\phi = f(r, z)$ )

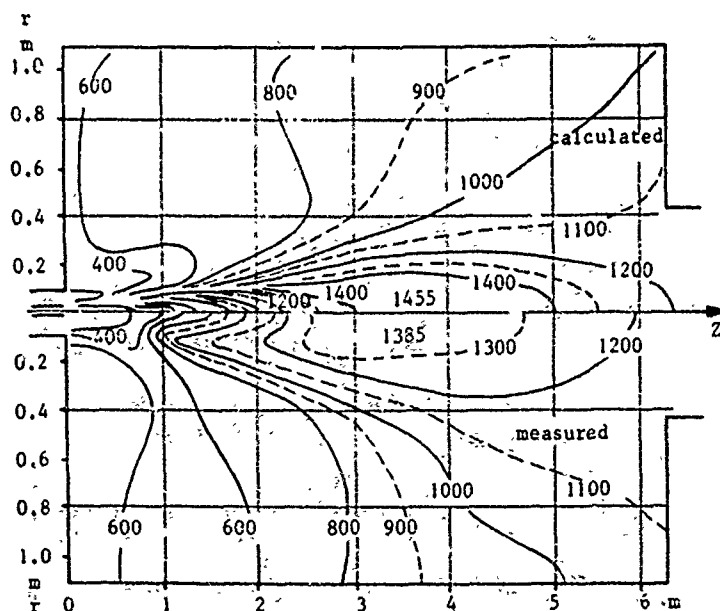


Fig. 9 : Comparison between predicted and measured isotherms (flame 29, M2 trials [34]). ( $t = f(r, z)$  in  $^{\circ}\text{C}$ )

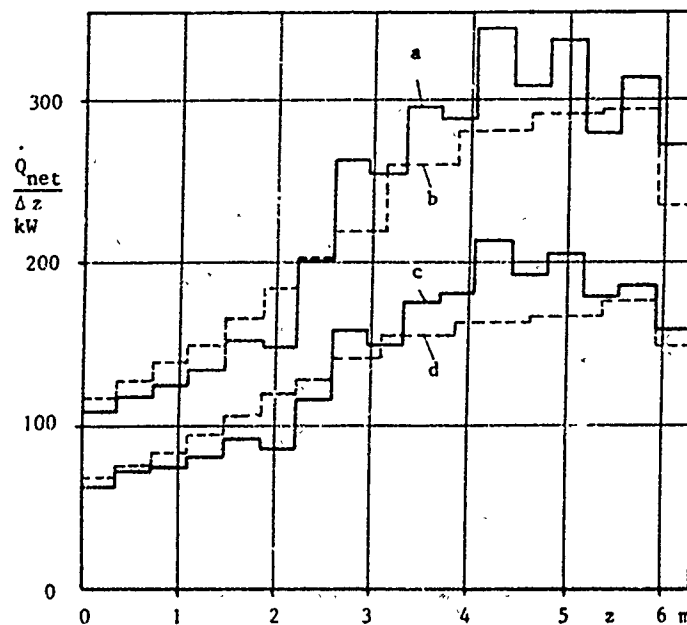


Fig. 10 : Comparison between predicted and measured axial heat flux distribution (model type IIIa with inputs from model type IIb)

flame 29 [34]

flame 35 [34]

a measured

c measured

b predicted

d predicted

#### 4. CONCLUSIONS

As a synthesis of the present review fig. 11 shows a general classification in terms of objectives, dimensionality for the various mathematical models of furnace performance. A differentiation of important input variables between those specific to the furnace (and process), the fuel/air characteristics and the burners, is also given. This permits the possible application range of these models, together with their limitations, to be identified.

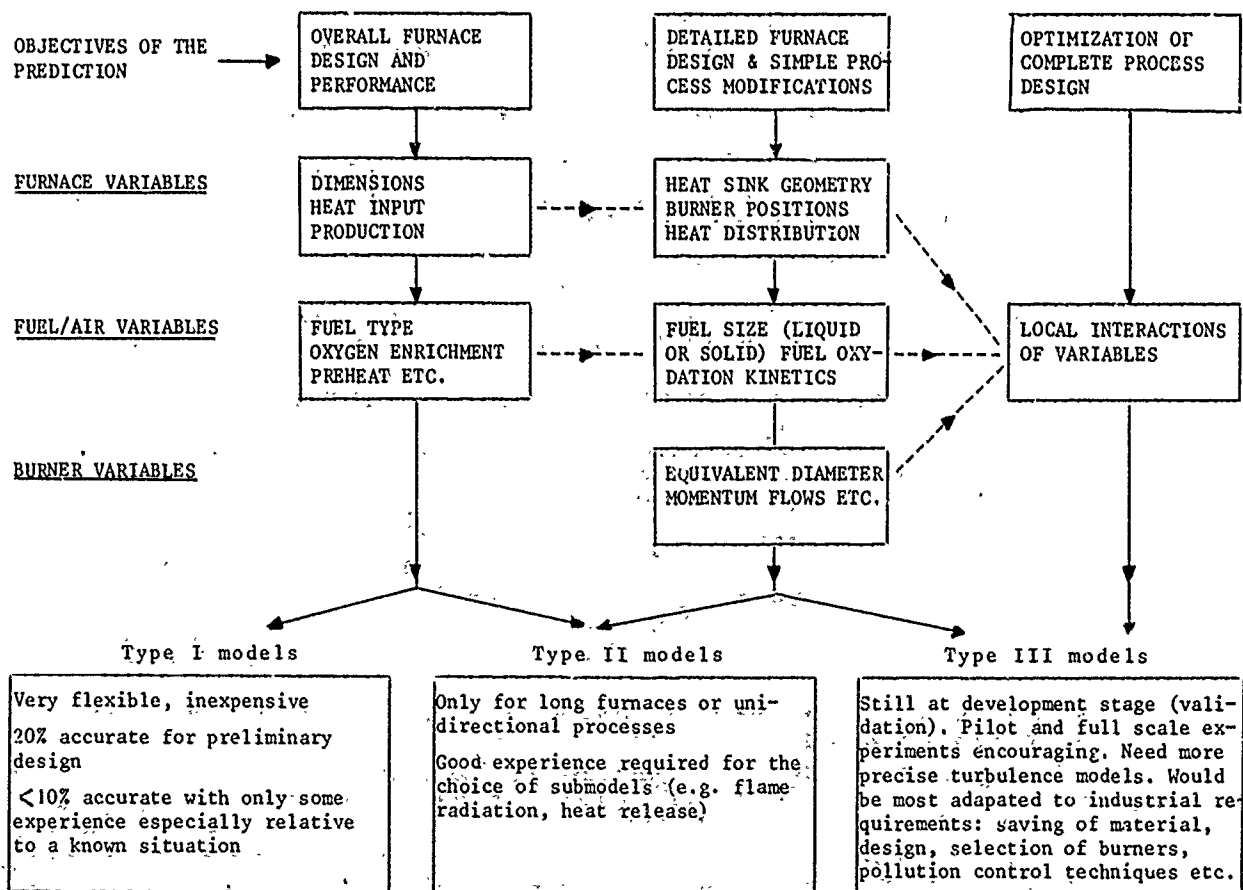


Fig. 11 : Overall classification of mathematical models of furnace performance

## 5. REFERENCES

- [1] H.C. HOTTEL and A.F. SAROFIM : Radiative transfer. New York, McCraw-Hill (1967)
- [2] R. JESCHAR and W. SCHUPE : Simplified mathematical models for convective and radiative heat transfer with special reference to heat recovery. IFRF, 3rd Members Conference, Chapter III (1974)
- [3] H.C. HOTTEL : First estimates of industrial furnace performance - The one-gas model re-examined. International Seminar on Heat Transfer from Flames, Trogir, Yugoslavia (1973). Published in Heat Transfer in Flames, eds. N.H. Afgan and J.M. Beér, Scripta Book Company, Washington DC USA
- [4] S. MICHELFELDER, H. BARTELD, T.M. LOWES and B.R. PAI : Berechnung des Wärme-flusses und der Temperaturverteilung in Verbrennungskammern. VDI Berichte Nr.211 (1974) p. 23 ff.
- [5] S. MICHELFELDER and T.M. LOWES : Strahlungsaustausch in Glasschemlzföfen. Glas-technische Berichte 46 (1973) Nr. 5, pp. 99-108
- [6] N. SELÇUK, R.G. SIDDALL and J.M. BEÉR : A comparison of mathematical models of the radiative behaviour of an industrial heater. IFRF Doc.nr. F 19/a/12
- [7] D.M. LUCAS and A.A. LOCKETT : Mathematical modelling of heat flux and tempera-ture distribution in Shell boilers. 4th Symposium on Flames and Industry. Inst. Fuel and BFRC (1972)
- [8] Ph. CLEMENT : Methode de calcul de la distribution des flux de chaleur sur les parois d'un générateur de vapeur. IFRF, 2nd Members Conference, Chapter XIII (1971)
- [9] T.M. LOWES and S. MICHELFELDER : A simple model for heat flux prediction. IFRF Doc.nr. F 36/a/5
- [10] A. FABER and S. MICHELFELDER : A one-dimensional mathematical model for the cal-culation of heat flux distributions in furnaces with substantial external recir-culation. IFRF Doc.nr. G 04/a/8 (1976)
- [11] M.W. THRING and M.P. NEWBY : Combustion length of enclosed turbulent jet flames. 4th Symposium on Combustion, Baltimore (1953)
- [12] A. CRAYA and R. CURTET : Sur l'évaluation d'un jet en espace confiné. C.R. Acad. Sci. 241 (1955) pp. 621-622
- [13] W. RICHTER and G. BAUERSFELD : Radiation models for use in complete mathematical furnace models. IFRF, 3rd Members Conference, Chapter II (1974)
- [14] F. FITZGERALD and A.T. SHERIDAN : Prediction of temperature and heat transfer distribution in gas fired pusher reheating furnaces. 4th Symposium on Flames and Industry. Inst. Fuel and BFRC (1972)
- [15] R. LATSCH : Mathematisches Modell für eine turbulente Diffusionsflamme und deren zylindrischen Brennraum. Universität Karlsruhe, Thesis (1972)
- [16] K. BAMMERT and H. REHWINKEL : Berechnung der örtlichen Wärmeübertragung und des Rauchgastemperaturfeldes in zylindrischen Brennkammern von Strahlungskesseln. VDI Berichte Nr. 211 (1974)
- [17] F.R. STEWARD and H.K. GÜRÜZ : Mathematical simulation of an industrial boiler by the zone method of analysis. International Seminar on Heat Transfer from Flames, Belgrade, Int. Centre Heat and Mass Transfer (1973)
- [18] T.R. JOHNSON : Application of the zone method of analysis to the calculation of heat transfer from flames. Sheffield University, Thesis (1971)
- [19] F.R. STEWARD and P. CANNON : The calculation of radiative heat flux in a cylin-drical furnace using the Monte Carlo Method. Int. J. Mass Transfer 14 (1971), pp. 245-262
- [20] J.A. ARSCOTT, J. GIBB and R. JENNER : The application of N-E diffusion theory and Monte Carlo Methods to predict the heat transfer performance of a 500 MW power station boiler from isothermal flow data. Combustion Inst., European Sym-posium (1973), Acad. Press London and New York
- [21] A.D. GOSMAN, W.M. PUN, A.K. RÜNCHAL, D.B. SPALDING and M. WOLFSHTEIN : Heat and mass transfer in recirculating flows. New York, Acad. Press, (1969)
- [22] I. ZUBER : Ein mathematisches Modell des Brennraums. Monographs and Memoranda Nr. 12. Staatliches Forschungsinstitut Bechovice/CSSR
- [23] M.M. GIBSON and B.A. MORGAN : Mathematical model of combustion of solid parti-cles in a turbulent stream with recirculation. J. Inst. Fuel 43, pp. 517-523 (1970)
- [24] T.M. LOWES et al. : Prediction of furnace heat transfer. 15th International Symposium on Combustion, Tokyo (1974)
- [25] W. RICHTER and R. QUACK : A mathematical model of a low volatile pulverized fuel flame. International Seminar on Heat Transfer from Flames, Belgrade, Int. Centre Heat and Mass Transfer (1973)
- [26] W. RICHTER : Prediction of heat and mass transfer in a pulverized fuel furnace. Letters in Heat and Mass Transfer Vol. 1, pp. 83-94 (1974)



- [27] W. RICHTER and G. FLEISCHHANS : Theoretical study of the effect of fuel, burner and furnace parameters on the behaviour of enclosed non-swirling anthracite p.f. flames. IFRF Doc.nr. F 24/ga/12 (1976)
- [28] B.E. LAUNDER and D.B. SPALDING : Mathematical models of turbulence. London, New York, Acad. Press (1972)
- [29] B.R. PAI, W. RICHTER and T.M. LOWES : Flow and mixing in confined axial flows. IFRF Doc.nr. G 02/a/24
- [30] D.B. SPALDING : A two-equation model of turbulence. VDI Forschungsheft 549, pp. 5-15 (1972)
- [31] H. BARTELDs, T.M. LOWES, S. MICHELFELDER and B.R. PAI : A finite difference method for the prediction of radiant heat exchange, applicable to various furnace geometries. 2nd European Symposium on Combustion, Orléans (1975)
- [32] A.G. DE MARCO and F.C. LOCKWOOD : A new flux model for the calculation of radiant furnaces. 2nd Italian Flame Days, San Remo (1975)
- [33] S.V. PATANKAR and D.B. SPALDING : Simultaneous predictions of flow pattern and radiation for three dimensional flames. International Seminar on Heat Transfer from Flames, Belgrade, Int. Centre Heat and Mass Transfer (1973)
- [34] S. MICHELFELDER and T.M. LOWES : Report on the M2 trials. IFRF Doc.nr. F 36/a/4
- [35] B.R. PAI, H. BARTELDs and S. MICHELFELDER : Report on the M3-A trials. IFRF Doc. nr. F 36/a/5
- [36] J.B. MICHEL and R. PAYNE : Report on the G1 trials. IFRF Doc.nr. F 01/a/100
- [37] J.B. MICHEL, R. PAYNE and P.A. ROBERTS : An optimization procedure for the use of fuel gases based on a well-stirred mathematical model. To be presented at ICHMT 1979 Summer Seminar, Dubrovnik
- [38] H.L. WU and N. FRICKER : An investigation of the behaviour of swirling jet flames in a narrow cylindrical furnace. IFRF, 2nd Members Conference, Chapter IX (1971)
- [39] S. MICHELFELDER : Beitrag zur Berechnung des Abbrandes und der Wärme-übertragung von nichtleuchtenden Gasflammen. Thesis (IFRF Doc.nr. G 04/a/7)
- [40] B.R. PAI, S. MICHELFELDER and D.B. SPALDING : Prediction of furnace heat transfer with a three-dimensional mathematical model. Int. J. Heat and Mass Transfer, vol. 21 (1978) pp. 571-580
- [41] D.B. SPALDING : Numerical computation of practical combustion chamber flows. AGARD Conference Proceedings Nr. 164 (1975), pp. 1-24
- [42] F.C. LOCKWOOD : Furnace and combustion chamber prediction: a short statement of the problems and the present position. IFRF, 2nd joint meeting of Pulverized Fuel and Heat Transfer Panel, IFRF Doc.nr. F 21/ca/22 (1977)
- [43] E.E. KHALIL and J.S. TRUELOVE : Calculation of radiative heat transfer in a large gas fired furnace. Letters in Heat and Mass Transfer (1977) vol. 4, pp.353-365
- [44] T.R. JOHNSON and L.A. JUNIPER : Modelling of heat transfer, combustion and ignition phenomena in pulverized coal fired furnaces. Conference on Coal Combustion Technology and Emission Control, California (Febr 1979)

## 6. ACKNOWLEDGEMENTS

This survey is based on the work of most of the scientific staff employed at the Research Station of the IFRF over recent years. The authors would therefore like to express their thanks to their many present and former colleagues for their contributions to this paper.

The work reported relates however not only to the IFRF but is drawn from many sources. In particular a great benefit has been drawn from the expertise of Dr. W. Richter of the University of Stuttgart who provided the data on the predictions with the type III models. This valuable contribution is gratefully acknowledged.

## DISCUSSION

H.Bartelds, Ne

If you try to cover such a broad field as Mr Michel and co-authors have tried, you are bound to make one or two omissions. I would like to mention work on three dimensional radiation models in addition to the work of De Mareo and Lockwood. It concerns work of an unknown author and you can find it in Reference 28 of Paper 11 of this meeting.

Author's Reply

I agree completely with you and I do apologize for this omission.

# NUMERICAL ANALYSIS AND EXPERIMENTAL DATA IN A CONTINUOUS FLOW COMBUSTION CHAMBER: A COMPARISON.

F. GAMMA, C. CASCI, A. COGHE, and U. GHEZZI

Politecnico di Milano, Italy

## 1) INTRODUCTION.

In recent years a large increase in numerical modelling of real combustion phenomena has been observed.

These techniques, if reliable and correctly developed, should be able to avoid a large part of the experimental work necessary to develop a new combustor giving informations otherwise obtainable only by means of troublesome experiments.

In fact it is necessary to observe that by means of the classical methods very reliable and high efficiency combustors have been obtained, and what it is to be expected from numerical modelling is not a quality jump in combustor performances, but rather an easier and less expensive design.

Non linear partial differential equations must be solved in numerical modelling; this leads to numerical problems f.e. of convergence and stability, to difficulties connected with computer storage capacity etc..

All this problems can be overcome also if there is large room to improvement.

Other kind of difficulties are connected with physical structure of the phenomenon, and they can be of more troublesome solution.

We refer to the necessity of introducing physical models to represents some aspects of the problem, with particular regard to turbulence and chemical kinetics.

Not always such phenomena are physically well understood and then the model must cover some ignorance.

Concerning turbulence, the existing models are in general well experienced, and can be used with confidence in many cases.

Chemical kinetics can be introduced in the model by means of suitable hypothesis, as f.e. instantaneous reaction between fuel and oxidant or a global reaction rate mechanism. Of course also more complicated schemes can be used; in many cases, however, simple hypothesis are suitable at least from an engineering point of view.

Also radiating heat transfer (flame radiation), very important in large combustors, must be modelled, and rather good results have been obtained in this field.

A lot of progress has been done in recent years, and now tridimensional problems, combustion of spray and pulverized coal can be analyzed by means of numerical modeling. At this point, however, if numerical techniques must be improved, a large amount of comparison with experimental results must be performed.

Reliable experimental results are not always easy to be obtained in real furnaces but they represent a fundamental stage in prediction techniques improvement.

In the present paper numerical results obtained by finite difference solution of the equations controlling combustion in an experimental furnace using methane as fuel have been compared with experimental results.

Velocity and temperature have been measured inside the combustor.

## 2) EXPERIMENTAL SET UP AND MEASUREMENTS.

The experimental combustor is essentially a cylinder of inner diameter of 200 mm and having a test length of 1.000 mm.

A scheme of the experimental set up is shown in fig. 1 ; the fuel nozzle is placed axially in the injection head, while the oxidizer is feeded by means of two different lines.

The primary air is flowing through a tube surrounding the fuel nozzle, while the dilution air is entering at the periphery of the injection head.

Swirl vanes at  $\approx 60^\circ$  are located in correspondence of primary and dilution air ports.

Details of injection head are shown in fig. 2 .

Fuel and oxidizer flow are controlled by means of flowmeters and valves (fig. 1 ).

Optical windows are placed along the combustion chamber length to allow optical measurements (L. D. V., line reversal, etc.); thermocouple probes can also be inserted through the holes shown in fig. 3 .

Combustion chamber is instainless steel.

The experimental conditions are reported in table I.

TABLE I

TEST	METHANE FLOW RATE (kg/s)	PRIMARY AIR FLOW RATE (kg/s)	DILUTION AIR FLOW RATE (kg/s)
I	$0.3 \times 10^{-3}$	$8.13 \times 10^{-3}$	$4.25 \times 10^{-3}$
II	$0.3 \times 10^{-3}$	$9.38 \times 10^{-3}$	$4.25 \times 10^{-3}$
III	$0.24 \times 10^{-3}$	$8.13 \times 10^{-3}$	$7.50 \times 10^{-3}$

#### EXPERIMENTAL CONDITIONS

Velocity and temperature measurements have been performed in the points shown in fig. 4 ; L. D. V. was used for velocity measurements and thermocouples for temperature field analysis.

Some details concerning velocity and temperature measurements are given in what follows.

##### - L. D. V. measurements.

The laser Doppler Velocimetry (L.D.V.) was chosen to measure the velocity profiles because the usual intrusive measuring techniques are of little help in a high temperature reactive medium with large thermal gradients.

Despite the complexity of a theoretical model of the L.D.V. system, the output from this instrument (Doppler frequency) is linearly related to the velocity of tracer particles seeded in the gas flow and no problem is concerned with calibration.

The major advantage of the L.D.V. is the high spatial and temporal resolution associated with its directional sensitivity.

The most important theoretical and experimental problems related to L.D.V. have been reported in Refs. (9)(10)(11).

It is now well established that the differential L.D.V. mode of operation, in conjunction with a burst counter processor, is the best suited for measurements in gases because of its higher signal to noise characteristics at moderate concentrations of tracer particles. The main advantage of the differential L.D.V. is that it is quite simple to align and is not sensitive to small vibrations.

Also, the Doppler frequency is independent of the detection angle and forward or back-scatter systems can be employed.

The optical set-up is illustrated in fig. 5 : the two laser beams, coming from the same source and a beam-splitter unit, are focused in the cross-volume.

The scattered waves produced by tracer particles are heterodyned on the photomultiplier surface and give rise to a photocurrent modulated at the Doppler frequency:

$$f_D = 2V \sin(\beta/2) / \lambda$$

where  $V$  is the particle velocity component perpendicular to the bisector of the incident cross-beams,  $\beta$  is the cross angle and  $\lambda$  is the wavelength of the laser beam.

The transmitting optics was based on a DISA Optics (mod. 55 X) including the frequency shift option that allows to resolve the directional ambiguity of the velocity vector. Forward and back scatter geometries can be selected.

An Argon-Ion laser (Spectra Physics mod. 166 ) was used at a nominal power of about 200 mw, and  $\lambda = 488$  nm and an interferential optical filter, centered at the same wavelength, was introduced in the receiving optics in order to reduce the background flame radiation.

The photomultiplier signal was processed by a burst counter processor (DISA mod. 55 L90)

that allows working with moderate particle concentrations and does not have dropout problems.

The experimental conditions are summarized in tab. II.

Since the LDV requires the presence of microscopic particles in the air flow, this complicates the use of the techniques considerably.

In fact, the particles seeded in the flow should be small in size in order to follow the gas flow accurately.

Such capability can be roughly estimated from the Bassett's general equation (Refs. (9) (10)).

In unsteady flows the LDV instruments must be treated as a transducer for which the transfer function is determined by the dynamics of tracer particles.

LDV experiments were performed by using alumina particles in the micron range carried by a secondary air flow.

Some check of particle mean size was made experimentally by using the visibility parameter (Refs. (9) (14)) and theoretical evaluations shown that particle were small enough to give correct mean velocity informations.

#### -Temperature measurements.

The measure of the gas temperature was performed by using small thermocouples inserted in the combustion chamber at same fixed axial positions.

Wires of Pt-Pt/Ro 10% were preferred for this application with a spherical hot junction 5 mm in diameter, that was small enough because we were only interested in mean values of the gas temperature.

Some corrections for radiation and conduction heat losses were applied in the hottest regions of the flame.

Such corrections were determined by comparison with results obtained by optical methods (sodium D-line reversal) in a laboratory methane-air flame.

### 3) THEORETICAL ANALYSIS.

From the geometrical configuration of the combustion chamber it appears that a bidimensional analysis must be performed; cylindrical polar coordinates are the most suitable in this case (fig. 6).

Bidimensionality depends on the fact that dilution air is injected along all the periphery of the injection head and no circumferential dissimetry is introduced. In this case the governing equations can be expressed in terms of velocity components (U and V) and pressure (P) or in terms of stream function ( $\psi$ ) and vorticity ( $\omega$ ). This second formulation is here employed also because in this way it is possible to cancel the pressure from the equations.

Both procedures are rather classical; anyway the equations in terms of velocities and pressure and in terms of  $\psi$  and  $\omega$  are reported in the appendix; also if the problem is bidimensional, an equation for the swirl velocity W is introduced. In this equation the product  $r.W$  is used as an unknown, being r the distance from the combustor axis.

#### - Turbulence.

The equations are time averaged and then a turbulence model must be introduced.

A k-E model has been employed (k = kinetic energy of turbulence, E = dissipation rate of k), and the turbulent viscosity  $\mu_t$  is given by:

$$\mu_t = \rho C_\mu k^2 / E$$

being  $\rho$  the fluid density and  $C_\mu$  a suitable coefficient (see appendix).

The effective viscosity  $\mu_{eff}$  is given by:

$$\mu_{eff} = \mu_t + \mu$$

where  $\mu$  is the fluid viscosity.

#### -Combustion.

Fuel and oxidizer are separately injected in the combustor and then a diffusion flame is obtained.

Two different combustion models have been adopted:

a) instantaneous reaction rate with combustion controlled by diffusion

b) global reaction rate assumed.

a) Instantaneous reaction rate.

Fuel and oxidizer can not exist together at the same point (and at the same time).

A concentration variable is introduced, defined as:

$$f = m_{fu} - m_a / \alpha_{st}$$

where  $m_{fu}$  is the mass fraction of the fuel,  $m_a$  the mass fraction of the oxidizer and  $\alpha_{st}$  the stoichiometric oxidizer-fuel ratio (in mass).

Turbulent fluctuations are taken into account by means of the time mean square of the concentration fluctuations  $q = \overline{f^2}$ .

A distribution function can be defined starting from  $q$ , and  $m_{fu}$  and  $m_a$  to be effectively adopted, calculated.

The shape of the distribution function to be adopted is rather arbitrary; here a Gaussian clipped distribution function has been used (see appendix).

b) Global kinetics.

In this case an effective volumetric reaction rate  $R_{fu}$  (for the fuel) given by:

$$R_{fu} = -A m_{fu} \phi \quad \phi < 1$$

$$R_{fu} = -A m_{fu} \quad \phi > 1$$

where  $\phi$  is the equivalence ratio and A a constant ( $A \approx 1$ ) has been used.

This is a simplified version of the reaction rate equation proposed in (8).

It is also assumed that

$$R_a = \alpha_{st} R_{fu}$$

- Temperature determination.

Temperature (T) is deduced from the total enthalpy given by:

$$h_t = m_{fu} \Delta H + \bar{C}_p T + K$$

where  $\Delta H$  is the caloric value of the fuel,  $\bar{C}_p$  is the specific heat of the fluid and K its mean kinetic energy.

- Heat exchange.

Due to the size of the combustor and to the type of fuel radiation has been neglected.

Heat exchange at the walls has been calculated by means of Reynolds analogy.

- Walls.

Wall functions have been adopted in order to avoid the numerical analysis of the logarithmic layer.

The following expression of general use have been employed (fig. 7):

$$u^+ = \frac{1}{\chi} \ln(E y^+)$$

$$\frac{\partial k}{\partial y} = 0$$

$$\epsilon y = \frac{1}{\chi} C_\mu^{3/4} k^{3/2}$$

where

$$u^+ = u C_\mu^{1/4} k^{1/2} \rho / \tau$$

$$y^+ = y (C_\mu^{1/2} k)^{1/2} / \nu$$

with  $\chi$  and E constants ( $\chi = .4$ ,  $E = 9$ ) and  $\tau$  the shear stress at the wall.

Table II: parameters of the L D V system

Laser power	200 mW
Laser wavelength	488 nm
Beam cross angle	5°
Fringe spacing	5.6 $\mu$ m
Probe volume dimension	X=0.143 mm
	Y=3.28 mm
	Z=0.143 mm
Fringe number	N=25

4) RESULTS.

Measurements have been carried out in correspondence of sec. 1, 2, 3, 4 of fig. 4; three conditions I, II, III have been tested during experiments.

Mean values of temperature, axial velocity and swirl velocity were measured.

- Temperature.

Measured and computed temperature distribution are reported in figg. 8-22.

In correspondence of sec. 2, 3, 4 the accord between measured and calculated results can be considered enough good.

Near the injection head (sec. 1) experimental and computed results are rather different, also if, in some cases, a sort of common trend can be recognized at least for model b in tests I and II, and for model a in test III.

As a general behaviour computed temperature are higher than the calculated ones.

It can be considered that in the injection region (near sec. 1) model b works a little better than model a.

This seems to mean that instantaneous reaction rate hypothesis is not particularly suitable to be employed in this zone probably because of the rather high mixing rate, leading to a competition between chemical kinetics and fluidodynamics.

On the other hand also the global kinetics here used does not seem to be satisfactory in this zone.

It could be deduced that in this region the "real" kinetics plays an important role also from the point of view of mean values calculations.

Probably near the injection head a global kinetics can hardly be fitted to represent the real kinetics.

Down stream the injection zone the introduced models appear to be substantially more reliable.

- Axial velocity (fig. 23-29).

As in the case of temperature, the largest discrepancies between measured and calculated results are in correspondence of injection region.

In particular the width of the recirculation zone is under estimate in both models.

Down stream the injection they seem to work rather well with respect to axial velocity.

In tests I and II the global kinetics model appears to offer a better performance near sec. 1; at the same section both model can be considered practically equivalent in test III.

- Swirl velocity (fig. 30-33).

The trend is the same as in the case of axial velocity; the injection region is the most critical in the comparison.

On the whole, the accord between experiments and theoretical values can be considered as satisfactory enough.

5) CONCLUSIONS.

What precedes shows that in general the agreement between theory and experiments can be considered as acceptable, also if near the injection region the discrepancies are not negligible.

If however from an engineering point of view the results could be satisfactory, they do not appear to be adequate, if a more sophisticated analysis of the phenomenon must be performed.

In particular near sec. 1 (injection region) the differences between measured and computed temperatures are large enough to influence considerably the reaction rate, if it is made dependent on temperature.

Then if elementary reactions must be introduced, rather large errors can arise; f. e. a pollutants generation analysis can hardly be carried out.

The performances of both models are rather similar, especially down stream the injection region.

Also if the global kinetics model seems to lead to better results near the injection head, it is not able to improve substantially the results with respect to the instantaneous

reaction rate hypothesis.

Probably the rather strong mixing, also increased by the peripheral swirl, is responsible for this kind of behaviour.

It seems that in this zone the introduction of a more sophisticated and realistic kinetic model is a fundamental stage to improve the agreement between theory and experiments.

Concerning turbulence models, a  $k-\epsilon$  formulation has been here employed; this model is at the same time rather well experienced and not particularly troublesome to be used.

It has not been analyzed here if other and more complex models could be more suitable, also if the peripheral centrifugal field (due to dilution air swirl) can increase the complexity of the turbulent field and require a more sophisticated analysis.

Thermal exchange has been treated in a rather simple way; on the other hand the rate of the heat exchange through the walls is less than 10% of the rate of heat generation in the furnace and then not able to introduce substantial changes in the results.

Classical time averaging has been adopted here, and other types of averaging (f. e. Favre averaging) have not been tested, also if they are able to give good results in many cases.

From a numerical point of view, the greatest difficulties have been encountered with the equations having rather complicated source terms ( $k, \epsilon, q$  equations).

They have been overcome by means of under relaxation and of a some kind of linearization.

The computer time for the calculation was about 5 minutes with an Univac 1100/80 computer with a non uniform  $21 \times 21$  grid.

#### 6) REFERENCES

- (1) Gosman A.D. et al. "Heat and mass transfer in recirculating flows", Academic Press, 1969
- (2) Tennekes M. and Lumley J.L., "A first course in turbulence", M.I.T. Press, 1972.
- (3) Launder B.E. and Spalding D.B., "Mathematical models of turbulence", Academic Press, 1972.
- (4) Launder B.E. and Spalding D.B., in: "Computer methods in Applied Mechanics and Engineering", vol. 3, pp. 269-289, 1974.
- (5) Hinze J.O., "Turbulence", Mc Graw Hill Book Co., New York, 1975.
- (6) Lockwood F.C. and Naguib A.S., "Combustion and Flame", 24, p. 109, 1975.
- (7) Bracco F.V. ed.: "Special issue on turbulent reactive flows", Combustion Science and Technology, vol. 13, n. 1-6, 1976.
- (8) Magnussen B.F. and Hjertager B.H., 16th Symposium (International) on Combustion, p. 719 (1976).
- (9) Durst F., Melling A. and Whitelaw J.H., "Principles and Practice of laser Doppler anemometry", Academic Press, 1976.
- (10) Cignoli F., Coghe A., Ghezzi U. and Pasini S., "Flow field in the wake of a blunt body by laser Doppler Anemometry", AGARD Conference Meeting on: "Applications of non-intrusive instrumentation in fluid flow research", Saint-Louis, France, 1976.
- (11) Durrani T.S. and Greated C.A., "Laser Systems in Flow Measurement", Plenum Press, 1977.
- (12) Coghe A. and Ghezzi U., "Turbulence characteristics in the recirculation region behind a disc: isothermal and non isothermal flow." 19th Israel Annual Conference on Aviation and Astronautics, Haifa, 1977.
- (13) Gibson M.M., Jones W.P., Mc Guirk J.J. and Whitelaw J.H., "Fundamentals of turbulence and their application in calculation methods", Imperial College, London, 1978.
- (14) Coghe A. and Ghezzi U., "LDA Signal Analysis", Dynamic Flow Conference 1978, Marseille (France), 1978.

#### -OBSERVATION

In many cases the results of test II are very similar to results of test I, and are not reported here.



## APPENDIX

## STANDARD EQUATIONS

- Standard equation in the model using velocities and pressure ( $\varphi$  = unknown):

$$\frac{1}{\tau} \frac{\partial}{\partial \tau} (\rho \tau v \varphi) + \frac{1}{\tau} \frac{\partial}{\partial x} (\rho \tau u \varphi) = \frac{1}{\tau} \frac{\partial}{\partial \tau} (\tau \Gamma_{\varphi} \frac{\partial \varphi}{\partial \tau}) + \frac{1}{\tau} \frac{\partial}{\partial x} (\tau \Gamma_{\varphi} \frac{\partial \varphi}{\partial x}) + S_{\varphi}$$

where:

$u$  = velocity along  $x$  axis

$v$  = velocity along  $r$  (radial velocity)

$w$  = swirl velocity

$S_{\varphi}$  = source term

$\Gamma_{\varphi}$  = exchange coefficient for  $\varphi$ .

In the instantaneous reaction rate model (model a) the unknown variables ( $\varphi$ ) are:

1 (continuity equation),  $u, v, w$  (swirl equation),  $h_t, k, \epsilon, f, g$ .

In the model assuming a global kinetics (model b) the unknown variables ( $\varphi$ ) are:

1,  $u, v, w, m_{fu}, m_a, h_t, k, \epsilon$ .

In table A are reported the expressions of  $\Gamma_{\varphi}, S_{\varphi}$  employed and the values of the constant introduced.

- Standard equation in the model using vorticity ( $\omega$ ) and stream function ( $\psi$ ).

$$a_{\varphi} \left[ \frac{\partial}{\partial x} \left( \rho \frac{\partial \psi}{\partial \tau} \right) - \frac{\partial}{\partial \tau} \left( \rho \frac{\partial \psi}{\partial x} \right) \right] - \frac{1}{\tau} \frac{\partial}{\partial x} \left[ b_{\varphi} \tau \frac{\partial (c_{\varphi} \varphi)}{\partial x} \right] - \frac{1}{\tau} \frac{\partial}{\partial \tau} \left[ b_{\varphi} \tau \frac{\partial (c_{\varphi} \varphi)}{\partial \tau} \right] = S_{\varphi}$$

In the model a (instantaneous reaction rate) the unknown are:  $\omega/r, \psi, rw, h_t, f, g, k$ .

In the model b (global kinetics) the unknown are:  $\omega/r, \psi, rw, h_t, m_{fu}, m_a, k$ .

The values of  $a, b, c$  and  $S$  are specified in table B.

TABLE A

$\varphi$	$\Gamma_{\varphi}$	$S_{\varphi}$
1	0	0
$u$	$\mu_{eff}$	$-\frac{\partial p}{\partial x} + \frac{1}{\tau} \frac{\partial}{\partial \tau} (\tau \mu_{eff} \frac{\partial v}{\partial x}) + \frac{\partial}{\partial x} (\mu_{eff} \frac{\partial u}{\partial x})$
$v$	$\mu_{eff}$	$\frac{\rho w^2}{\tau} - \frac{\partial p}{\partial \tau} + \frac{1}{\tau} \frac{\partial}{\partial \tau} (\tau \mu_{eff} \frac{\partial v}{\partial \tau})$
$\tau w$	$\mu_{eff}$	0
$h_t$	$\mu_{eff}/\sigma_h$	0
$f$	$\mu_{eff}/\sigma_f$	0
$g$	$\mu_{eff}/\sigma_g$	$P_g - C_{g2} \rho \epsilon / k g$
$m_{fu}$	$\mu_{eff}/\sigma_{fu}$	$P_{fu}$
$m_a$	$\mu_{eff}/\sigma_a$	$R_a$
$k$	$\mu_{eff}/\sigma_k$	$P_k - \rho \epsilon$
$\epsilon$	$\mu_{eff}/\sigma_{\epsilon}$	$C_1 \epsilon / k P_k - C_2 \rho \epsilon^2 / k$

TABLE B

$\varphi$	$a_\varphi$	$b_\varphi$	$C_\varphi$	$S_\varphi$
$\omega/\tau$	$\tau$	$\tau^2$	$\mu_{eff}$	$\frac{\partial}{\partial x}(\rho w^2) - \tau \left[ \frac{\partial}{\partial x} \left( \frac{\mu^2 + v^2}{2} \right) \frac{\partial \rho}{\partial \tau} - \frac{\partial}{\partial \tau} \left( \frac{\mu^2 + v^2}{2} \right) \frac{\partial \rho}{\partial x} \right]$
$\gamma$	0	$1/\rho \tau^2$	1	$-\omega/\tau$
$\tau w$	$1/\tau$	$\mu_{eff} \tau^2$	$1/\tau^2$	0
$\rho_{ht}$	$1/\tau$	$\mu_{eff}/\sigma_{\rho_t}$	1	0
$f$	$1/\tau$	$\mu_{eff}/\sigma_f$	1	0
$g$	$1/\tau$	$\mu_{eff}/\sigma_g$	1	$P_g - C_{g2} \rho E/k g$
$m_{fu}$	$1/\tau$	$\mu_{eff}/\sigma_{fu}$	1	$R_{fu}$
$m_a$	$1/\tau$	$\mu_{eff}/\sigma_a$	1	$R_a$
$k$	$1/\tau$	$\mu_{eff}/\sigma_k$	1	$P_k - \rho E$
$E$	$1/\tau$	$\mu_{eff}/\sigma_E$	1	$C_1 E/k P_k - C_2 \rho E^2/k$

$$P_k = 2 \mu_t \left[ \left( \frac{\partial \mu}{\partial x} \right)^2 + \left( \frac{\partial v}{\partial \tau} \right)^2 + \left( \frac{v}{\tau} \right)^2 + \frac{1}{2} \left( \frac{\partial \mu}{\partial \tau} + \frac{\partial v}{\partial x} \right)^2 + \frac{1}{2} \left( \frac{\partial w}{\partial x} \right)^2 + \frac{1}{2} \left( \frac{\partial w}{\partial \tau} - \frac{w}{\tau} \right)^2 \right]$$

$$P_g = C_{g1} \mu_t \left[ \left( \frac{\partial f}{\partial x} \right)^2 + \left( \frac{\partial f}{\partial \tau} \right)^2 \right]$$

$$\sigma_\varphi = \frac{\mu_{eff}}{\Gamma_\varphi}$$

$$\sigma_k = 0.8$$

$$\sigma_f = 0.8$$

$$\sigma_{fu} = 0.8$$

$$\sigma_a = 0.8$$

$$\sigma_g = 0.8$$

$$\sigma_k = 1$$

$$\sigma_E = 1.2$$

$$C_1 = 1.44$$

$$C_2 = 1.92$$

$$C_\mu = 0.09$$

$$C_{g1} = 2.8$$

$$C_{g2} = 2$$

- Gaussian clipped distribution function.

The Gaussian clipped p.d.f. has the shape shown in FIG.a; it can be quantitatively defined f.e. by means of the method reported in (6) starting from the calculated values of f and g.

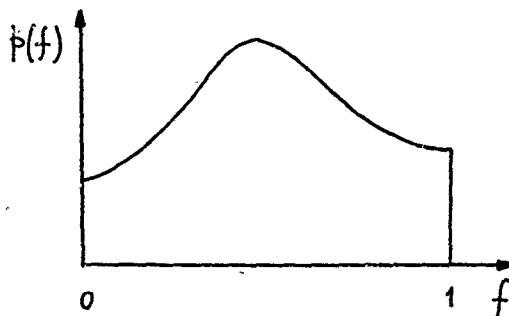


FIG. a

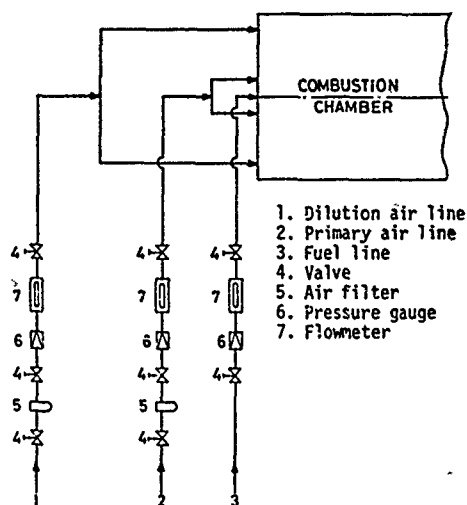


FIG. 1

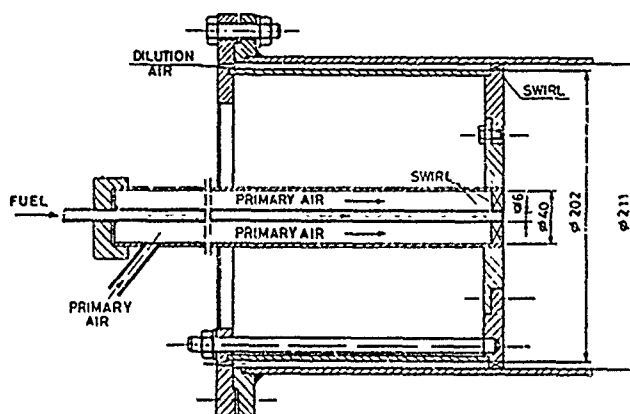


FIG. 2

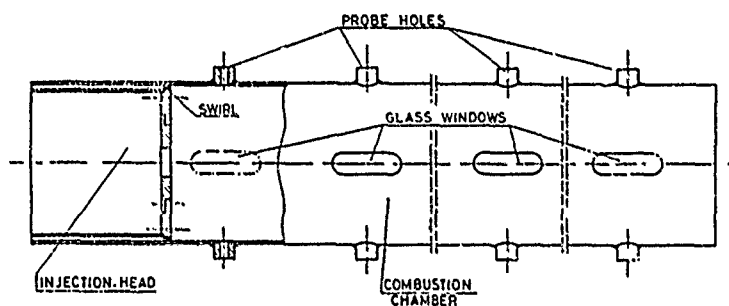


FIG. 3

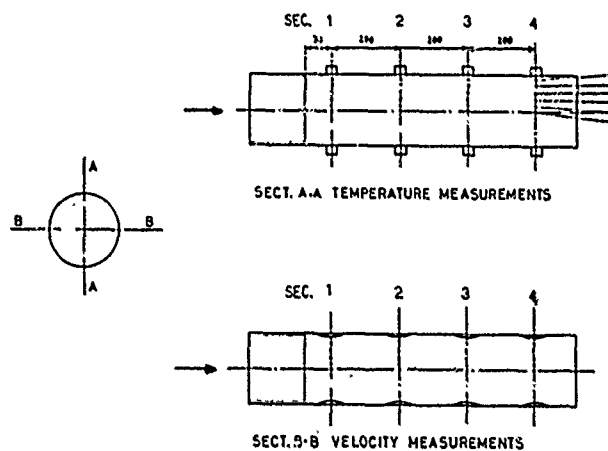


FIG. 4

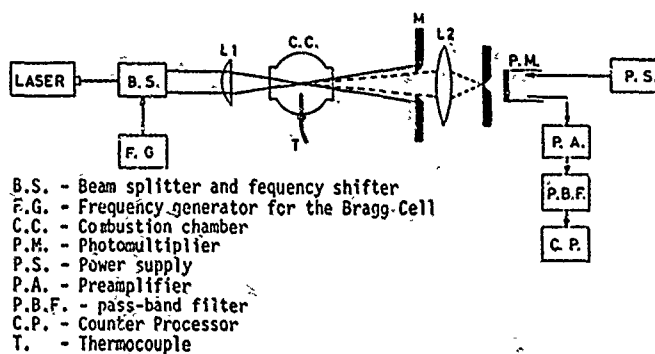


FIG. 5

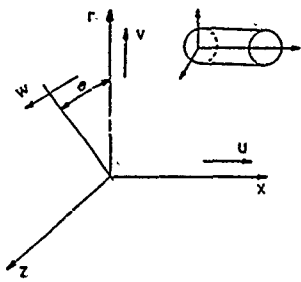


FIG. 6

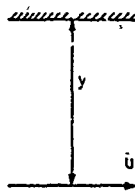


FIG. 7

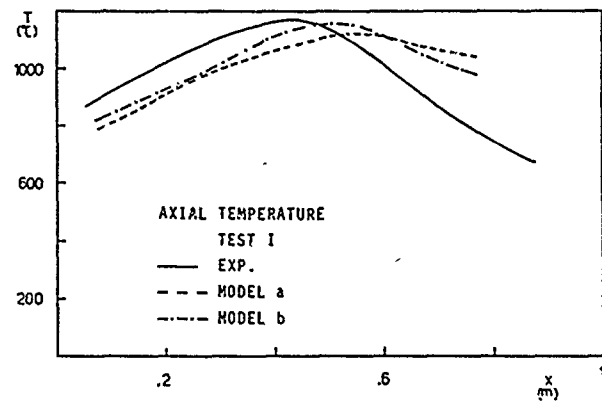


FIG. 8

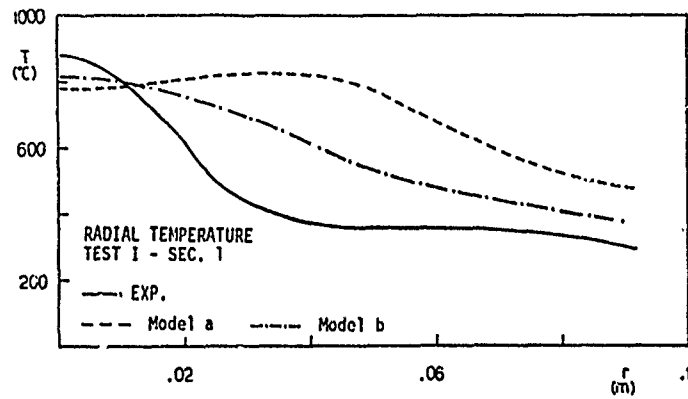


FIG. 9

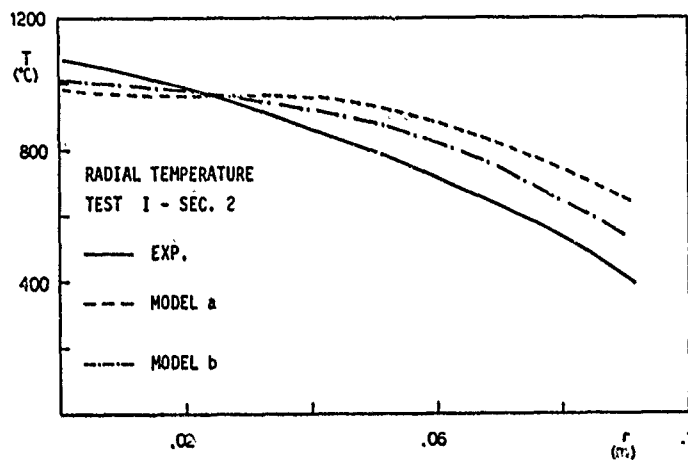


FIG. 10

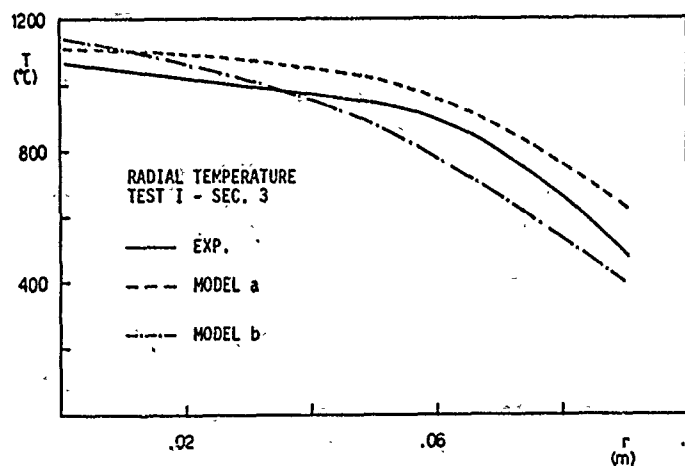
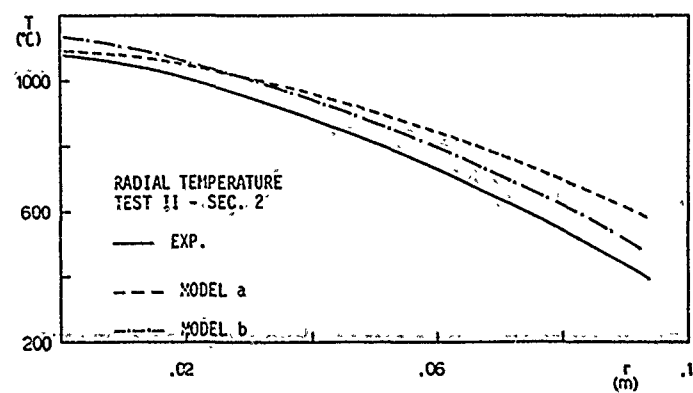
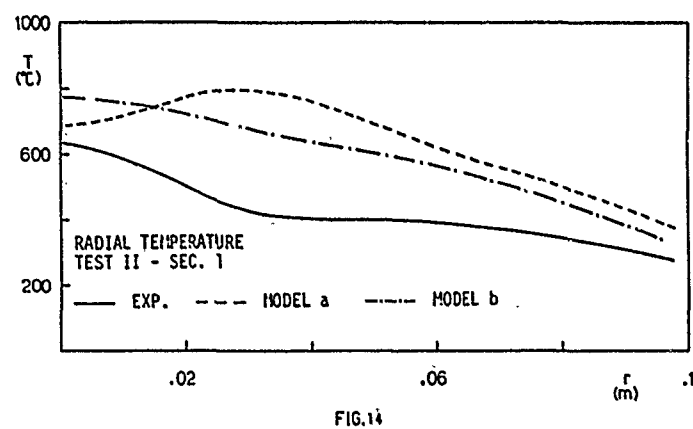
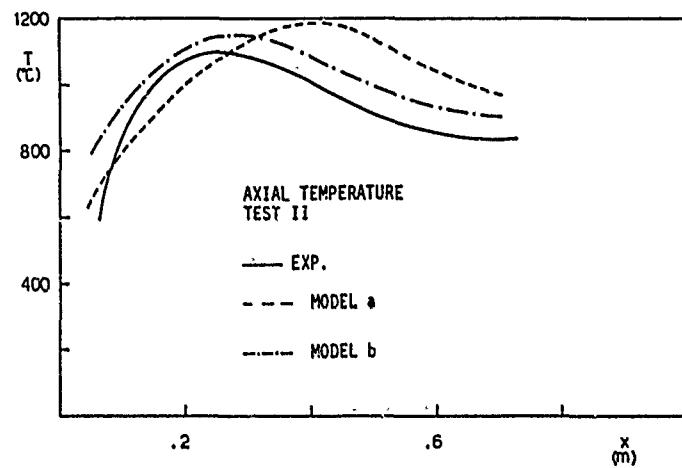
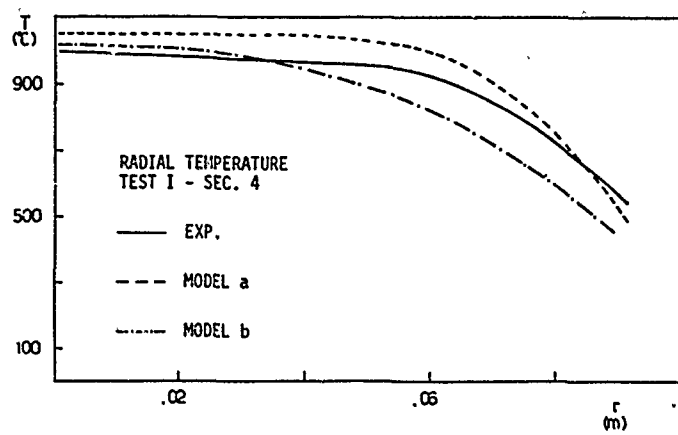


FIG. 11



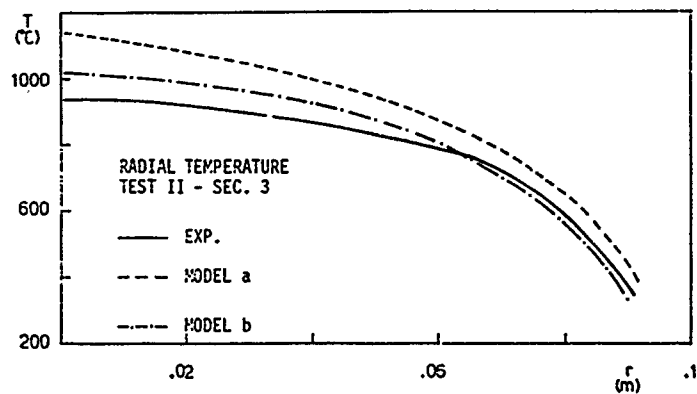


FIG. 16

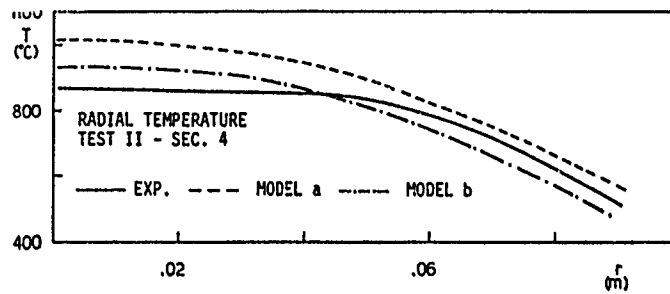


FIG. 17

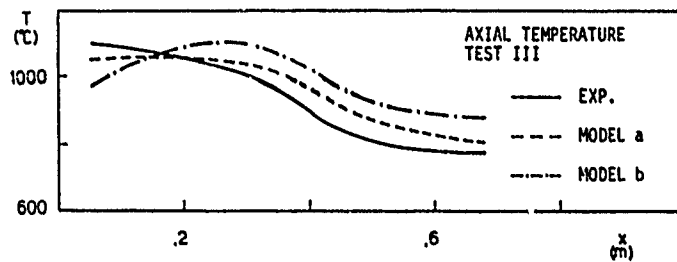


FIG. 18

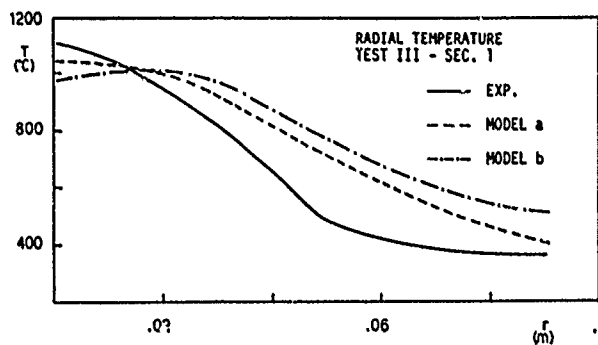


FIG. 19

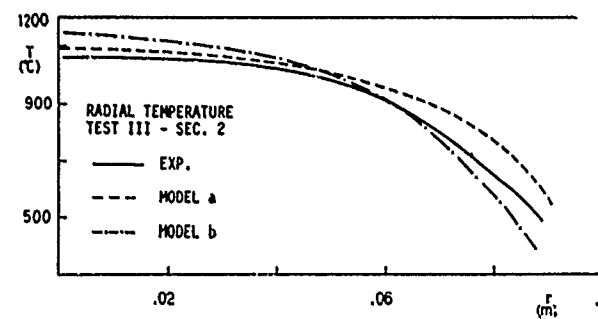


FIG. 20

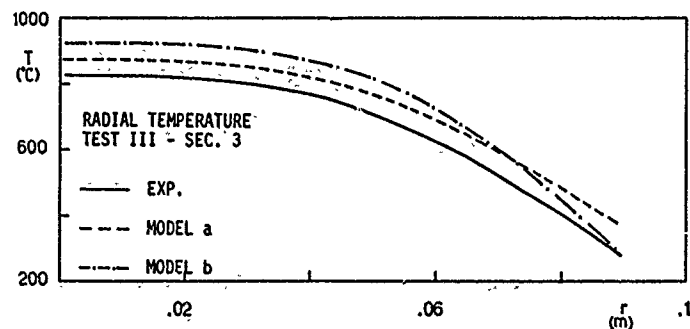


FIG. 21

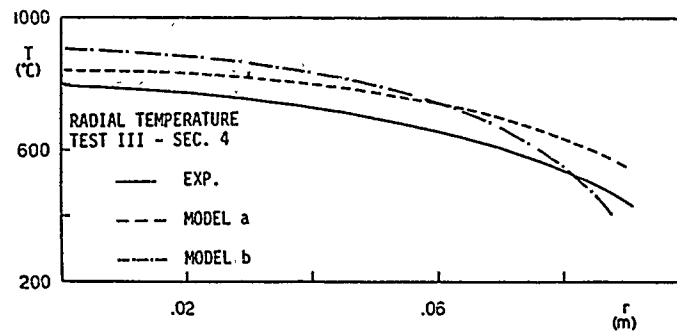


FIG. 22

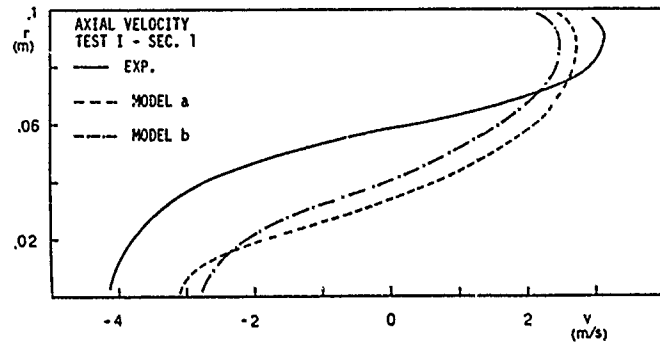


FIG. 21

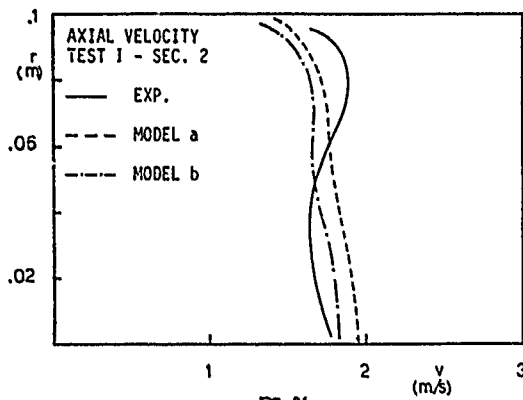


FIG. 24

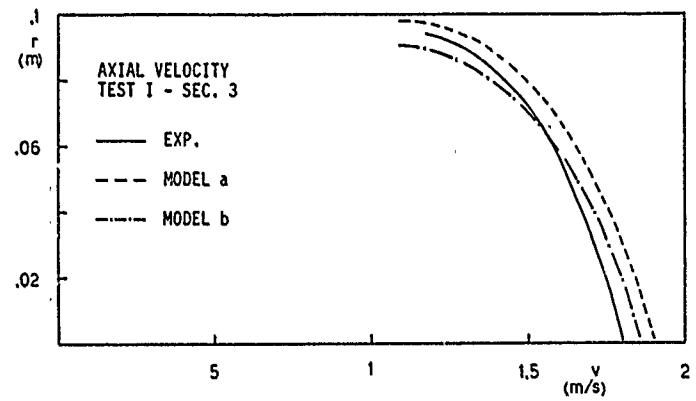


FIG. 25

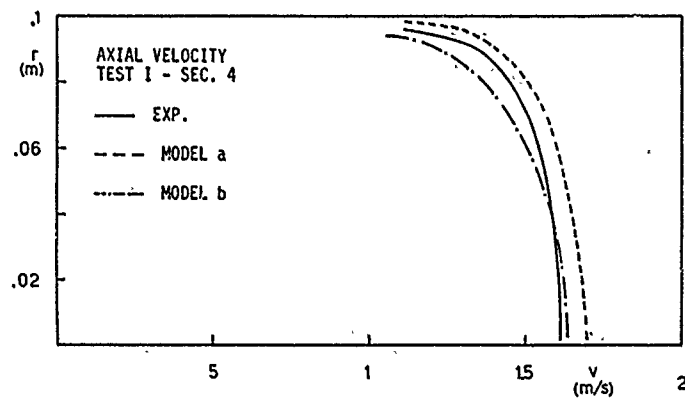


FIG. 26

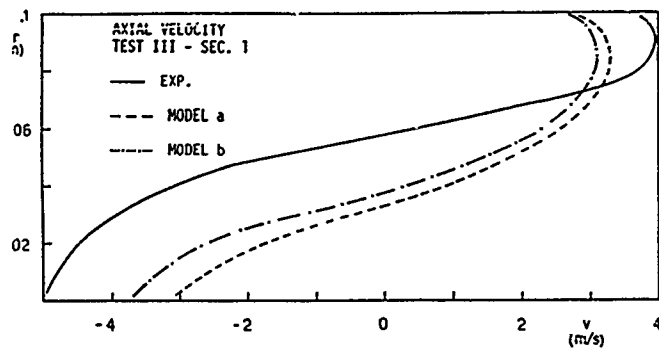


FIG. 27

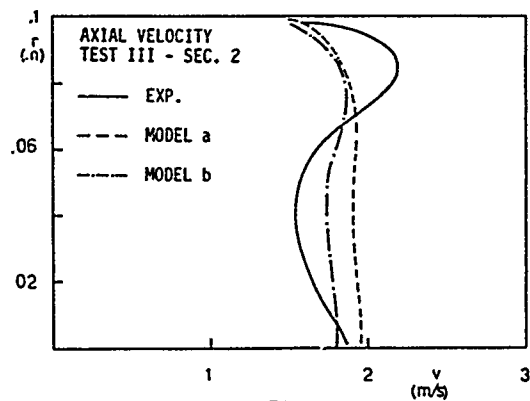


FIG. 28

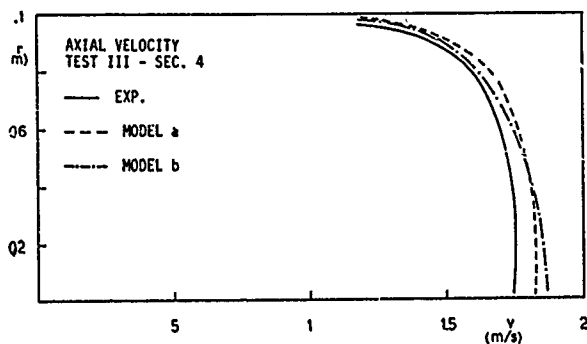


FIG. 29

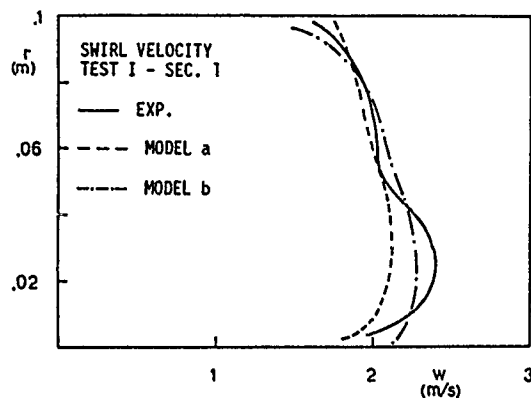


FIG. 30

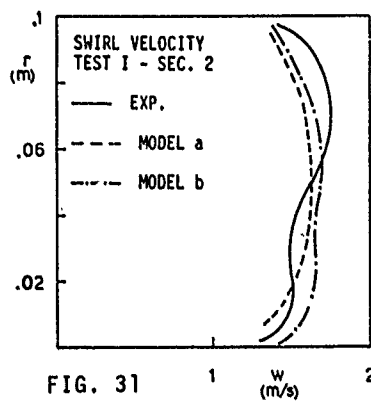


FIG. 31

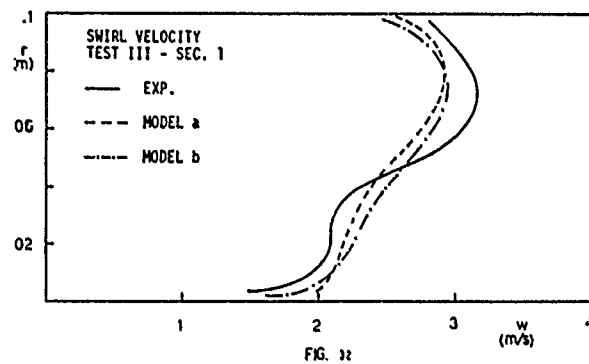


FIG. 32

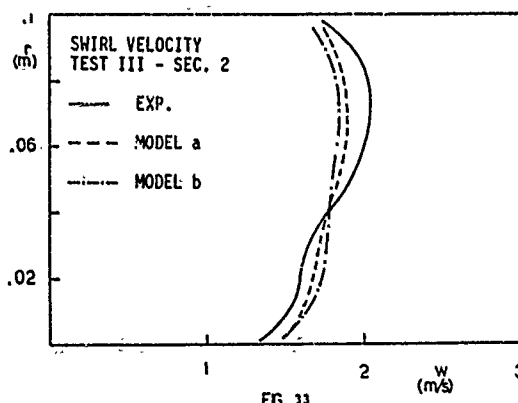


FIG. 33



## DISCUSSION

**C.H.Priddin, UK**

Do you have any plans to measure turbulence quantities in your experiments? It would be especially interesting to have Reynolds Stress measurements as this would enable to separate influences of the turbulence model and numerical method.

**Author's Reply**

We have plans to measure turbulence but these measurements were not performed here in an organized form.

I agree that Reynolds stresses could be able to give more information concerning source of errors.

**J.H.Whitelaw, UK**

- (1) Can you explain these low values of the maximum temperature and also comment on the accuracy of the temperature measurements.
- (2) The discrepancies between calculated and measured results are, as expected, greatest at station 1. Would you please comment on the uncertainty in the assigned wall boundary condition for temperature along the end plate and on its influence. Also, numerical errors are likely to be greatest in this upstream region and I would appreciate your estimate of their possible magnitude.

**Author's Reply**

- (1) In our opinion low values of temperature are due to the peripheral swirl leading to a strong mixing of dilution  $\gamma$  in the reaction region with a high air-fuel ratio. Errors with thermocouples are not more than 40 or 60°C following our calibration and not able to explain the low temperature level.
- (2) Concerning wall boundary conditions for temperature, I agree they can influence rather strongly the results in sec. 1. A constant temperature was assigned along the end plate and walls and refining this condition, can improve the solution.

Concerning numerical errors in the upstream region, stability was observed to be more troublesome here. At the end of calculations the relative errors here are of the same order of magnitude as the errors in downstream region.

Probably numerical errors upstream are larger than in other regions but it is rather difficult to estimate them precisely.

# MODELISATION DES FOURS ALIMENTES A L'AIR ENRICHI EN OXYGENE

R. GUENOT, A. IVERNEL  
L'AIR LIQUIDE C.R.C.D.  
JOUY-EN-JOSAS, France

F.C. LOCKWOOD, A.P. SALOOJA  
IMPERIAL COLLEGE OF SCIENCE AND TECHNOLOGY  
LONDON SW7, England

La modélisation numérique des chambres de combustion utilisant des brûleurs alimentés à l'air fortement enrichi en oxygène, présente des difficultés particulières liées d'une part aux dissociations thermiques se produisant à haute température, et d'autre part au rôle accru des échanges par rayonnement.

Le présent article montre comment on peut adapter les programmes de calculs existant, afin de tenir compte de ces phénomènes.

Le modèle utilisé est en cours de vérification au moyen de mesures effectuées sur un four expérimental de 300 kW, conçu pour fonctionner avec des brûleurs à haute intensité alimentés par du gaz naturel et de l'air fortement suroxygéné, ou même de l'oxygène pur.

Les premiers résultats expérimentaux sont en bon accord avec les prévisions du modèle.

## I. INTRODUCTION

### I.1. OBJET DE L'ETUDE

Pour certaines applications, l'Industrie utilise de plus en plus fréquemment des brûleurs alimentés en air suroxygéné ou même en oxygène pur, impliquant une dissociation appréciable des produits de combustion.

Les programmes de simulation des chambres de combustion qui ont été employés avec succès (1)(2) pour les brûleurs classiques, ne donnent pas satisfaction pour les brûleurs à air fortement enrichi en oxygène.

Le présent article expose les premiers résultats d'une étude destinée à étendre ces programmes au cas d'un comburant, dont la richesse en oxygène peut atteindre 100 %.

Dans les flammes à haute température résultant de la suroxygénation du comburant, les dissociations thermiques des produits de combustion jouent un rôle capital. Elles absorbent en effet une partie importante de la chaleur normalement dégagée par la combustion, et diminuent ainsi la température des flammes.

Cette chaleur, stockée sous forme chimique, est d'ailleurs récupérable par recombinaison au niveau des surfaces de pièces ou des parois de fours, de sorte que c'est finalement l'enthalpie, et non la température, qui intervient dans les équations de transfert thermique par convection et diffusion.

Par contre, si l'on veut incorporer dans le modèle les échanges par rayonnement, il est nécessaire, en cours de calcul, de tenir compte de la température et - à un degré moindre - des fractions massiques des espèces existant à l'équilibre.

Dans la présente communication seront exposés successivement : les modèles mathématiques récents, utilisés à l'Imperial College, pour la simulation des chambres de combustion, les modifications apportées pour tenir compte des dissociations, les méthodes expérimentales mises en oeuvre et les premiers essais de confrontation entre les résultats de calculs et les résultats expérimentaux.

### I.2. POSITION DU PROBLEME

La preuve est maintenant faite (voir par exemple (1) et (2) que le fonctionnement des chambres de combustion alimentées au gaz et à l'air peut être prévu avec un degré d'exactitude largement acceptable du point de vue des applications, du moins pour les brûleurs n'utilisant pas ou peu l'effet de "swirl". Quoi qu'il en soit, le problème traité dans le présent article a été jusqu'ici peu étudié. Il concerne la prévision des chambres de combustion alimentées au gaz et à l'air enrichi en oxygène, ou même à l'oxygène pur. Ces recherches impliquent des problèmes complémentaires de modélisation plutôt d'ordre chimique qu'hydrodynamique.

Etant donné qu'on peut supposer avec réalisme que, pour la plupart des fours, le taux de réaction globale est gouverné par le taux de dissipation de la turbulence et non par la cinétique chimique, on peut conclure que la seule forme de chimie nécessaire dans le cas des flammes à haute température résultant d'un enrichissement à l'oxygène est la chimie d'équilibre. L'objectif essentiel de l'étude présentée dans cet article est d'incorporer un traitement de l'équilibre chimique raisonnablement économique dans un procédé général de prévision décrit en (1). La valeur des prévisions du procédé résultant font l'objet d'un programme de vérification expérimentale en cours d'achèvement, utilisant des flammes enrichies à l'oxygène, et réalisé au Centre de Recherche CLAUDE-DELMORE de L'AIR LIQUIDE.

Le problème du "swirl" n'est pas abordé ici. Il convient de remarquer au passage que le manque de validation pour les exemples de brûleurs à grand nombre de swirl provient d'autres limitations, à savoir, que les écoulements avec swirl sont imparfaitement évalués par le modèle de turbulence "standard" à deux équations, car l'hypothèse inhérente d'une viscosité turbulente isotrope n'est pas satisfaisante.

Un modèle turbulent de tensions de Reynolds serait préférable, mais la surcharge due aux estimations des paramètres nécessaires, ajoutée aux calculs déjà coûteux nécessaires à la prévision des chambres de combustion, le rend pratiquement inabordable. Pour contourner cette difficulté, il suffit d'employer un modèle algébrique économique pour les tensions de Reynolds de la forme décrite en (3), mais il reste encore à étudier son application aux chambres de combustion. Le brûleur utilisé par L'AIR LIQUIDE ne comportant pas de swirl permet de faire des études de validation à l'aide de solides connaissances de base obtenues dans la modélisation des flammes sans swirl et non enrichies à l'oxygène. En fait, l'enrichissement à l'oxygène permet la stabilisation de la flamme, en l'absence d'une zone de recirculation intense à la sortie du brûleur.

## II. LA MODELISATION PHYSIQUE

### II.1. LE MODELE DE TURBULENCE

On emploie le modèle usuel de turbulence à deux équations dans lequel on résout les équations relatives à l'énergie cinétique de la turbulence,  $k$ , et à son taux de dissipation,  $\epsilon$ ; une viscosité isotrope effective étant définie à partir de ces deux valeurs (3). Malgré des recherches poussées sur des modèles plus compliqués, dans lesquels on résout des équations pour les tensions de Reynolds elles-mêmes, (voir par exemple (4)), rien n'a encore permis de déplacer le modèle  $k-\epsilon$  de la position prééminente qu'il occupe dans les calculs d'application parce qu'il représente une combinaison pratique d'économie et d'exactitude.

En ce qui concerne les écoulements sans "swirl" dont on parle ici, les imperfections éventuelles de ce modèle peuvent être en grande partie attribuées non pas à l'usage du concept de viscosité effective, mais aux défauts de modélisation des équations pour  $k-\epsilon$  qui ne sont en aucun cas faciles à rectifier.

### II.2. LA MODELISATION DU RAYONNEMENT

Dans le genre de four considéré les pertes de chaleur aux parois réfractaires ne sont pas très importantes. Il n'est donc pas nécessaire d'avoir recours à un modèle très précis de transfert par rayonnement. Nous avons utilisé pour le rayonnement le modèle de flux décrit en détail en (5), qui assure une exactitude acceptable pour des dépenses très limitées. Ce type de méthode est brièvement résumée dans le paragraphe suivant :

La répartition angulaire de l'intensité est représentée par une série tronquée de Taylor, substituée dans l'équation du transfert de chaleur par rayonnement. Cette équation est ensuite intégrée sur des angles solides bien choisis, le nombre d'angles correspondant au nombre de termes dans le développement. On obtient ainsi un système fermé de six équations aux dérivées partielles du premier ordre ayant pour inconnues les coefficients du développement de Taylor. Pour le problème à deux dimensions traité ici, nous ne retiendrons que quatre termes de la série. Afin de rendre possible leur solution à l'aide de l'algorithme numérique à matrice tri-diagonale employé pour les calculs d'écoulement, les quatre équations du premier ordre pour les coefficients sont combinées de façon à donner la paire des équations du second ordre ci-dessous :

$$\frac{\partial}{\partial r} \left( \frac{1}{k} \frac{\partial R_r}{\partial r} \right) = k \left( \frac{8R_r}{3} - \frac{4}{3} R_z \right) - \frac{4}{3} kE$$

$$\frac{\partial}{\partial z} \left( \frac{1}{k} \frac{\partial R_z}{\partial z} \right) = k \left( \frac{4}{3} R_r - \frac{8}{3} R_z \right) - \frac{4}{3} kE$$

où  $r$  et  $z$  sont les coordonnées radiale et axiale,  $k$  est le coefficient d'absorption,  $E = \sigma T^4$  est la puissance émissive du corps noir, et  $R_r$  et  $R_z$  sont reliés aux coefficients de la série de Taylor. Ces équations ne sont pas appliquées directement au gaz de combustion mais à un système classique de 4 gaz gris équivalents.

### II.3. MODELISATION DES PROCESSUS THERMIQUES

La prévision correcte des processus thermique est très importante pour le déroulement des calculs. Le modèle utilisé est décrit en détail dans (6).

En ce qui concerne les transports de chaleur et de masse accompagnant la combustion, on fait l'hypothèse classique que tous les coefficients de diffusion turbulente sont égaux. Le mélange des constituants est alors régi par une équation portant sur le rapport de mélange  $f$  quantité indépendante de l'évolution des réactions et égale à la fraction massique de combustible dans l'état imbrûlé.

Similairement le transport de chaleur est caractérisé par une seule équation enthalpique où la température et la composition chimique n'interviennent pas explicitement.

En ce qui concerne le processus de combustion, on suppose en premier lieu une réaction chimique globale simplifiée entre le combustible gazeux et le comburant aboutissant à la production de  $CO_2$  et  $H_2O$ . En second lieu, on surajoute à ce schéma de base les calculs d'équilibre chimique exposé dans la section suivante, pour tenir compte de la dissociation des produits de combustion.

Dans le schéma de base l'état thermodynamique du mélange réagissant est fonction de deux variables seulement ; la fraction de mélange,  $f$ , et le degré d'avancement,  $r$ , défini par  $r = (m_j - m_{j,u}) / (m_{j,b} - m_{j,u})$  (reactedness), où  $m_j$  est la fraction massique de toute espèce chimique réagissante, et où  $b$  et  $u$  désignent le fluide brûlé et non-brûlé. Pour une flamme de diffusion,  $r = 1$ , et la turbulence entraîne des fluctuations de  $f$  uniquement, tandis que pour une flamme parfaitement prémélangée,  $f$  est constante et  $r$  varie.

On suppose pour les fluctuations des deux variables, que les fonctions densité de probabilité (d.p.) ont des formes a priori. Pour le cas de  $f$ , on utilise une distribution Gaussienne "sectionnée", complètement spécifiée par la connaissance de la fraction de mélange moyenne dans le temps,  $\bar{f}$ , et sa variance,  $g_f = (\bar{f} - f)^2$ . L'hypothèse d'une cinétique chimique rapide comparée au taux de mélange turbulent paraît bien fondée dans la plupart des calculs d'applications; elle est compatible avec une loi de probabilité (d.p.) simple de  $r$  constituée de deux fonctions delta (au sens de DIRAC), ces fonctions de delta étant centrées sur les valeurs limites  $r = 0$  et  $r = 1$ . La grandeur des fonctions delta est en liaison directe avec le degré d'avancement moyen dans le temps,  $r$ , qui peut être obtenue à partir de la solution d'une équation de bilan portant sur la fraction molaire moyenne (dans le temps) de l'une des espèces réagissante, le combustible par exemple.

Une formule est nécessaire pour le taux de réaction moyen de l'espèce choisie, qui représente un terme de source dans l'équation de bilan considérée. Dans l'hypothèse où la réaction globale est contrôlée par le taux de mélange de turbulence, le taux de réaction est égal au taux de dissipation des fluctuations de  $r$ . On a proposé plusieurs expressions reliant le taux de dissipation de la turbulence à des variables connues. Ils ont une base physique commune, bien que voisine. Heureusement, les calculs sont insensibles à la forme exacte de l'expression. Celle que nous avons utilisée est :

$$\bar{R}_j = C \bar{p} (\bar{m}_{j,b} - \bar{m}_{j,u}) [\bar{r} (1 - \bar{r})]^{1/2} \epsilon/k$$

où  $\bar{R}_j$  est le taux de réaction moyen dans le temps de l'espèce réagissante choisie. Dans cette formule s'incrit l'hypothèse simple, que le taux de dissipation des fluctuations du degré d'avancement est proportionnel d'une part à leur écart-type, qui, pour la loi de probabilité simple constituée de deux fonctions de deltas,

s'écrit :  $[\bar{r} (1 - \bar{r})]^{1/2}$ ; et d'autre part à l'échelle de temps de grands tourbillons,  $\epsilon/k$ . La constante empirique,  $C$ , a été trouvée égale à 0.35 environ.

On s'intéresse dans la plupart des cas aux quantités moyennes dans le temps et cette moyenne dans le temps s'exprime pour toute propriété thermodynamique,  $\phi$ , par :

$$\bar{\phi} = \int_0^1 \int_0^1 \phi(\bar{f}, r) p(\bar{f}, r) d\bar{f} dr$$

où  $p(\bar{f}, r)$  est la fonction jointe de probabilité de densité pour  $\bar{f}$  et  $r$ . Il y a peu de chances que les variations de  $\bar{f}$  et  $r$  soient fortement corrélées; on peut donc, de manière justifiable, décomposer  $p(\bar{f}, r)$  en séparant les variables et écrire :

$$\bar{\phi} = \int_0^1 \int_0^1 \phi(\bar{f}, r) p(\bar{f}) p(r) d\bar{f} dr$$

où  $p(\bar{f})$  et  $p(r)$  sont respectivement les d.p. Gaussienne sectionnée, et delta couplée, mentionnées ci-dessus. Pour plus de détails on se référera à (7).

### III. / PRINCIPE DE LA METHODE NUMERIQUE DE RESOLUTION /

#### III.1. EQUATIONS A RESOUDRE

On doit résoudre des équations pour les composantes axiale,  $u$  et radiale,  $v$ , l'énergie cinétique de la turbulence,  $k$ , et son taux de dissipation,  $\epsilon$ , la fraction de mélange,  $f$ , et sa variance,  $g$ , la fraction massique du combustible,  $m_{fu}$ , l'enthalpie spécifique,  $h$ , et enfin les paramètres de rayonnement  $R_r$  et  $R_z$ . Pour la géométrie cylindrique polaire traitée ici, ces équations sont toutes de la forme :

$$\frac{\partial}{\partial x} (r \rho u \phi) + \frac{\partial}{\partial r} (r \rho v \phi) - \frac{\partial}{\partial x} (r \Gamma_\phi \frac{\partial \phi}{\partial x}) - \frac{\partial}{\partial r} (r \Gamma_\phi \frac{\partial \phi}{\partial r}) - r S_\phi = 0$$

où  $\phi$  représente toute variable dépendante énoncée ci-dessus, et  $S_\phi$  est un terme de source (par exemple  $P_{fu}$  dans le cas de l'équation relative à  $m_{fu}$ , fraction massique résiduelle de combustible).

#### III.2. METHODE DE RESOLUTION

Les équations sont résolues à l'aide du processus standard de différence finie décrit en (8) et (9), et rattaché au code d'ordinateur TEACH-T. Les grilles d'ordinateur utilisées comprennent 400 nœuds qui, lorsqu'ils sont disposés convenablement, donnent des résultats indépendants de la grille.

Les conditions aux limites utilisées correspondent à celle du brûleur expérimental. Certaines données manquantes sont remplacées par des estimations raisonnables (émissivité de la paroi par exemple). Les caractéristiques d'absorption et d'émission du gaz sont celles du modèle classique à 4 gaz gris. A chaque itération les variables correspondant aux équations ci-dessus sont en principe réévaluées, ainsi que les grandeurs qui en dépendent.

Toutefois le réajustement des valeurs moyennes liées au modèle stochastique de combustion n'intervient que tous les 5 à 10 itérations.

### IV. / PRISE EN COMPTE DES ASSOCIATIONS INTERVENANT A HAUTE TEMPERATURE /

#### IV.1. PRINCIPE DU REAJUSTEMENT AU MOYEN DES CALCULS D'EQUILIBRE

Nous considérons qu'en chaque point, l'état thermodynamique du mélange est atteint en 2 étapes à cinétique très rapide.

La première est une combustion fictive dans laquelle le mélange de départ COMBUSTIBLE + OXYGENE (+ INERTE) donne  $\text{CO}_2 + \text{H}_2\text{O} + \text{EXCES} (+ \text{INERTE})$ .

Par EXCES on entend soit l'excès d'oxygène, soit l'excès du combustible subsistant après combustion stochiométrique. Le mélange de départ est par définition le mélange local qu'on obtiendrait en l'absence de combustion.

Dans le cas général où il peut exister plusieurs arrivées de comburant (oxygène pur et air plus ou moins enrichi par exemple), et où le combustible peut contenir des inertes, la composition de départ est définie par les fractions massiques  $f$  et  $i$  de combustible et d'inerte respectivement. Elle s'obtient par 2 équations de transport ne comportant pas de terme de source. Dans le cas limite d'un prémélange complet  $f$  et  $i$  sont constants. En l'absence d'échange par rayonnement l'enthalpie du mélange réel  $h_{\text{AD}}$  est fonction linéaire de  $f$  et  $i$  et ne nécessite pas d'équation particulière.

Par contre, si le rayonnement est pris en compte, l'équation de transport de l'enthalpie comporte un terme de source, et doit être résolu séparément. Il conduit à une valeur locale de  $h$  différente de  $h_{\text{AD}}$  et l'écart traduit l'influence des pertes par rayonnement. On peut le caractériser par un rapport d'adiabaticité sans dimension  $\varphi$  défini par :

$$\varphi = \frac{h - h_R}{h_{\text{AD}} - h_R} \quad \text{où } h_R \text{ est une enthalpie de référence prise égale à celle}$$

du mélange brûlé idéal (non dissocié) ramené à la température ambiante.

La seconde étape est un retour adiabatique aux conditions d'équilibre chimiques, que l'on peut obtenir par un sous-programme d'équilibre chimique, dans lequel les variables d'entrées sont l'enthalpie locale  $h$  et la composition élémentaire déduite de  $f$  et  $i$ .

En fait, il est plus commode d'utiliser au lieu de  $h$  le rapport d'adiabaticité  $\varphi$  défini plus haut.

L'utilisation systématique d'un sous-programme d'équilibre pour calculer en chaque point et à chaque itération la température, la densité et la composition en fonction de  $f$ ,  $i$  et  $\varphi$  est exclue du point de vue économique.

La difficulté a été tournée en calculant au préalable des valeurs d'équilibre pour un nombre limité de valeurs de  $\varphi$ ,  $f$  et  $i$ , et en interpolant au moyen de formules d'ajustement.

Dans une première étude limitée au cas extrême d'un brûleur à l'oxygène pur, un tableau à 2 entrées  $\varphi$ ,  $f$  comportant environ 100 résultats d'équilibres a été établi à partir de sous-programmes d'équilibres dérivés de ceux de HARKER et SMITH (10).

Comme première approche, ces résultats ont été condensés en une formule d'ajustement du type :

$$T_{\text{EQ}} = A_0 + A_1 \varphi + A_2 \varphi^2 + A_3 \varphi^3$$

avec les  $A_i$  sont fonctions de  $\varphi$ , et une formule similaire pour la densité.

Si on négligeait à ce stade les fluctuations de la fraction de mélange, on pourrait utiliser directement cette formule pour chaque point, en utilisant pour  $\varphi$  la valeur donnée par l'équation de transport correspondante :

$$T_{\text{EQ}} = A_0 + A_1 \varphi + A_2 (\varphi)^2 + A_3 (\varphi)^3$$

En réalité la formule d'ajustement fournit une valeur instantanée à partir de laquelle la valeur moyenne correcte s'exprime par :

$$\bar{T}_{\text{CORR}} = A_0 + A_1 \bar{\varphi} + A_2 (\bar{\varphi}^2) + A_3 (\bar{\varphi}^3) \text{ soit encore}$$

$$\bar{T}_{\text{CORR}} = T_{\text{EQ}} + A_2 g + A_3 (M_3 - (\bar{\varphi})^3)$$

$g$  désignant comme précédemment la variance de fluctuation de  $\varphi$  et  $M_3$  un moment non-centré du 3<sup>e</sup> ordre

$$M_3 = \int \varphi^3 p(\varphi) d\varphi$$

$M_3$  se calcule facilement à partir des paramètres de la densité de probabilité considérée précédemment.

La méthode conduit à des corrections  $T_{\text{COR}} - T_{\text{EQ}}$  généralement faibles sauf au voisinage du nez du brûleur où la validité du calcul peut être mise en doute.

En effet, on ne dispose pas de formules d'ajustement unique valable entre 0 et 1, et l'utilisation d'une telle formule est en principe erronée dans les zones où les fluctuations de  $\varphi$  sont importantes.

Une autre méthode, en cours de réalisation, revient à utiliser un ajustement par tronçons et calculer directement l'intégrale :

$$\bar{T}_{\text{CORR}} = \int T_{\text{EQ}}(\varphi) p(\varphi) d\varphi$$

par intégration numérique.

#### IV.2. METHODE ITERATIVE DE CORRECTION DU RAYONNEMENT

La méthode de réajustement exposée ci-dessus suppose connue l'enthalpie du mélange en tout point. En réalité l'équation enthalpique contient un terme de source qui ne peut être calculé correctement par le modèle de rayonnement décrit précédemment, que si la température et la concentration des espèces absorbantes sont eux même connus. Il convient donc d'effectuer les réajustements nécessaires au cours d'itérations successives. Au stade actuel nous nous sommes bornés à des réajustements de température et de densité.

#### V. / DISPOSITIF EXPERIMENTAL /

L'installation comprend essentiellement une chambre de combustion et des moyens de mesures des températures, et de vitesses. de prélèvement de gaz et de rayonnement :

##### V.1. LA CHAMBRE

Cette chambre est un four expérimental (figure 1) revêtu intérieurement de réfractaires en corindon (94% d'alumine), et permettant d'atteindre des températures de 2000 K.

Sa capacité de chauffage nominale est de l'ordre de 250 kW mais peut varier pratiquement entre 150 et 400 kW en fonction du taux d'oxygénation du comburant et des températures intérieures du four auxquelles on veut faire les essais. Il est équipé pour fonctionner avec des combustibles liquides et gazeux, et comme comburant de l'air suroxygéné et de l'oxygène pur.

Ce four est muni d'un certain nombre d'ouvertures latérales qui permettent l'introduction des sondes de mesure (températures, vitesses) des prises de gaz, et des radiomètres.

Des thermocouples incorporés dans la paroi interne permettent de suivre les températures intérieures en 3 points du four sur une même génératrice.

##### V.2. LES BRULEURS

Les brûleurs utilisés sont du type industriel "face mélange", pour éviter tout risque de rentrée de flamme (figure 2).

Ils comprennent :

- une arrivée de gaz combustible (méthane) par une canne axiale, débouchant par 6 trous faisant un angle de divergence de 20° avec l'axe; ce dispositif assure un meilleur mélange du gaz avec l'oxygène périphérique.

- une arrivée périphérique d'oxygène, dont la section est adaptée au débit mis en jeu, de façon à conserver tout au long des essais une vitesse de sortie d'oxygène relativement constante.

- une 2ème arrivée périphérique d'air dont la section est également ajustée au débit de ce comburant.

##### V.3. MESURES DES TEMPERATURES DANS LA FLAMME

Les températures atteintes dans les flammes suroxygénées étant souvent supérieures à 2000 K, il était nécessaire de disposer d'un pyromètre ayant des performances supérieures à celles d'un pyromètre à aspiration classique.

L'appareil utilisé a été du type à "double col sonique" avec lequel on détermine la température par variation de masse volumique après détente sonique. L'étude de cet appareil a été réalisée par l'O.N.E.R.A. (11).

- Principe du double col (figure 3)

A partir de l'équation de BARRE de ST VENANT à la traversée d'un col sonique et la relation de HUGONIOT, on déduit le débit à travers un orifice sonique en fonction de la pression et de la température d'arrêt. Aux faibles vitesses auxquelles on travaille, ces valeurs peuvent être confondues avec les valeurs statiques. La figure (3) indique la méthode de calcul et précise les notations utilisées.

La mesure porte sur les inconnues du second membre ( $P_1$ ,  $P_2$ ,  $T_2$ ). On notera que  $\gamma_1$  et  $M_1$  sont des fonctions de la température cherchée  $T_1$ , ce qui nécessite un calcul par itération.

Le rapport des sections des cols  $\frac{A_2}{A_1}$  a été déterminé par étalonnage avec un pyromètre à aspiration muni d'un thermocouple en platine dans une zone de température allant jusqu'à 2000 K.

##### V.4. MESURE DES VITESSES

La mesure des vitesses est faite de façon classique avec une "Sonde de Prandtl" refroidie par eau.

Les deux prises de pression sont reliées à un capteur différentiel ACB très sensible dont le signal électrique est enregistré sur un Servotrace.

##### V.5. ANALYSE DES GAZ

Pour chaque flamme et à chaque fenêtre des prélèvements de gaz ont été effectués au moyen d'une canne d'aspiration énergétiquement refroidie. Les gaz supposés "trempés" sont analysés au chromatographe,

qui fournit les concentrations molaires en  $\text{CO}_2$ ,  $\text{CO}$ ,  $\text{H}_2$ ,  $\text{N}_2$ ,  $\text{O}_2$ .

Etant données les dissociations importantes rencontrées dans les flammes à haute température, et la rapidité de recombinaison des espèces dissociées, il a été nécessaire de disposer d'une sonde de prélèvement à figeage particulièrement efficace. La SNECMA a mis au point une "Sonde à détente supersonique" dont le tube d'aspiration est tel que dès l'entrée de la sonde l'écoulement devient supersonique, permettant ainsi un refroidissement très rapide et plus efficace que le seul refroidissement par circulation d'eau (figure 4). (12)

#### V.6. MESURES DE RAYONNEMENT

Les mesures de rayonnement sont effectuées avec 2 types de pyromètres à rayonnement total :

- un pyromètre à "faible angle d'ouverture" permettant la visée d'une tranche de flamme à travers le four, et la mesure de sa température équivalente "corps noir"; une telle mesure complète les données fournies par l'application de la méthode de SCHMIDT en monochromatique ( $\epsilon_\lambda$  et température réelle) et permet la détermination du facteur d'émissivité total.

- un pyromètre à "grand angle d'ouverture" ( $2\pi$  stéradians), qui permet de mesurer le rayonnement reçu par un point de la paroi du four, et provenant de l'ensemble four-flamme vu par ce point.

#### VI. CONFRONTATION ENTRE LES CALCULS ET LES RESULTATS EXPERIMENTAUX

Les résultats de calcul actuellement disponibles doivent être considérés comme provisoires, car ils ne tiennent pas compte des derniers perfectionnements évoqués plus haut (intégration directe à partir de la loi de probabilité).

Le tableau I donne les champs de température obtenus avec et sans prise en compte des dissociations, il démontre clairement la nécessité d'introduire les dissociations pour obtenir des résultats valables.

La figure (5) représente dans ces 2 hypothèses les profils de température calculés sur l'axe de la chambre et les résultats de mesure correspondants.

La première campagne d'essais ayant dû être interrompue à la suite d'une détérioration du four nécessitant d'importantes réparations, nous n'avons pu obtenir que très peu de résultats expérimentaux.

Une nouvelle campagne d'essais est actuellement en cours.

#### VII. CONCLUSION

Sous réserve de confirmation des premiers résultats disponibles, la méthode proposée paraît en mesure de prédire de façon satisfaisante les chambres de combustion compte tenu des échanges par rayonnement, des fluctuations et des dissociations chimiques apparaissant à haute température.

#### VIII. REMERCIEMENTS

Les auteurs remercient vivement Messieurs B. ARGUEYROLLES et L. MOUFFLET (C.R.C.D.) de leur précieuse collaboration pour la mise au point du programme de calcul et la réalisation des essais de validation.

- 1/ GOSMAN, A.D., LOCKWOOD, F.C. et SALOOJA A.P.  
"The prediction of cylindrical furnaces gaseous fueled with premixed and diffusion burners" 17th Symposium (International) on Combustion, The Combustion Institute, 1979.
- 2/ ABOU ELLAIL, M.M.M; GOSMAN, A.D., LOCKWOOD, F.C. et MEGARED, I.E.A.  
"Description and validation of a three-dimensional procedure for combustion chamber flows" J. Energy, AIAA, April 1978. Also Progress in Astronautics and Aeronautics, Turbulent Combustion, vol. 58, Editor : Lawrence A. Kennedy, Published by AIAA, 1978.
- 3/ LAUNDER, B.E. et SPALDING, D.B. "Mathematical models of turbulence". Academic Press, 1972.
- 4/ BRADSHAW, P. (ed) "Topics in Applied Physics-Turbulence" 12, Springer Verlag, 1976.
- 5/ LOCKWOOD, F.C. et SHAH, N.G. "An improved flux model for the calculation of radiation heat transfer in combustion chambers"  
Proceedings of 16th National Heat Transfer Conference, Aug. 1976, ASME paper no. 76-HT-55.
- 6/ LOCKWOOD, F.C. "The modelling of premixed and diffusion turbulent combustion" Combustion and Flame, Vol 29, No. 2, p. 111, 1977.
- 7/ WU, H.L. et FRICKER, N. "Second Members Conference of the IFRF", IX-1, 1971.
- 8/ CARETTO, L.S., GOSMAN, A.D., PANTANKAR, S.B. et SPALDING, D.B.  
"Proc. 3rd Int'l Conf. on Numerical Methods in Fluid Mechanics", Springer Verlag, 1972.
- 9/ GOSMAN, A.D., LOCKWOOD, F.C. et WHITELAW, J.H.  
"Outline lecture notes on the prediction of the performance of combustion chambers and furnaces", Imperial College, Mech. Eng. Dept., Fluids Section report FS/78/29, 1978.
- 10/ HARKER, J.H. "The calculation of equilibrium flame gas compositions". Journal Inst. of Fuel, May 1967 p 206 - Also SMITH, M.Y. Journal Inst. Fuel. June 1969 p 248.
- 11/ MESTRE, A et BENOIT, A.  
14eme Symposium International sur la combustion. 1972 pp 719 - 725
- 12/ S.N.E.C.M.A. Note Interne (Villaroche), 24 juillet 1975.



## AVEC DISSOCIATION

$$I = I_0 \left( 1 - \frac{1}{2} \frac{v}{c} \right)$$

TEMPERATURE

**J= 2 A J= 16=**

[illegible]

## SANS DISSOCIATION

$$I = 1 \text{ A} \quad I = 16 \text{ T} \quad V = 1 \text{ V}$$

TEMPERATURE

J= 2 A J=: 16-M-M-M-M-M-M-M-M-M-M-M-M-M-M-M-M

[illegible]

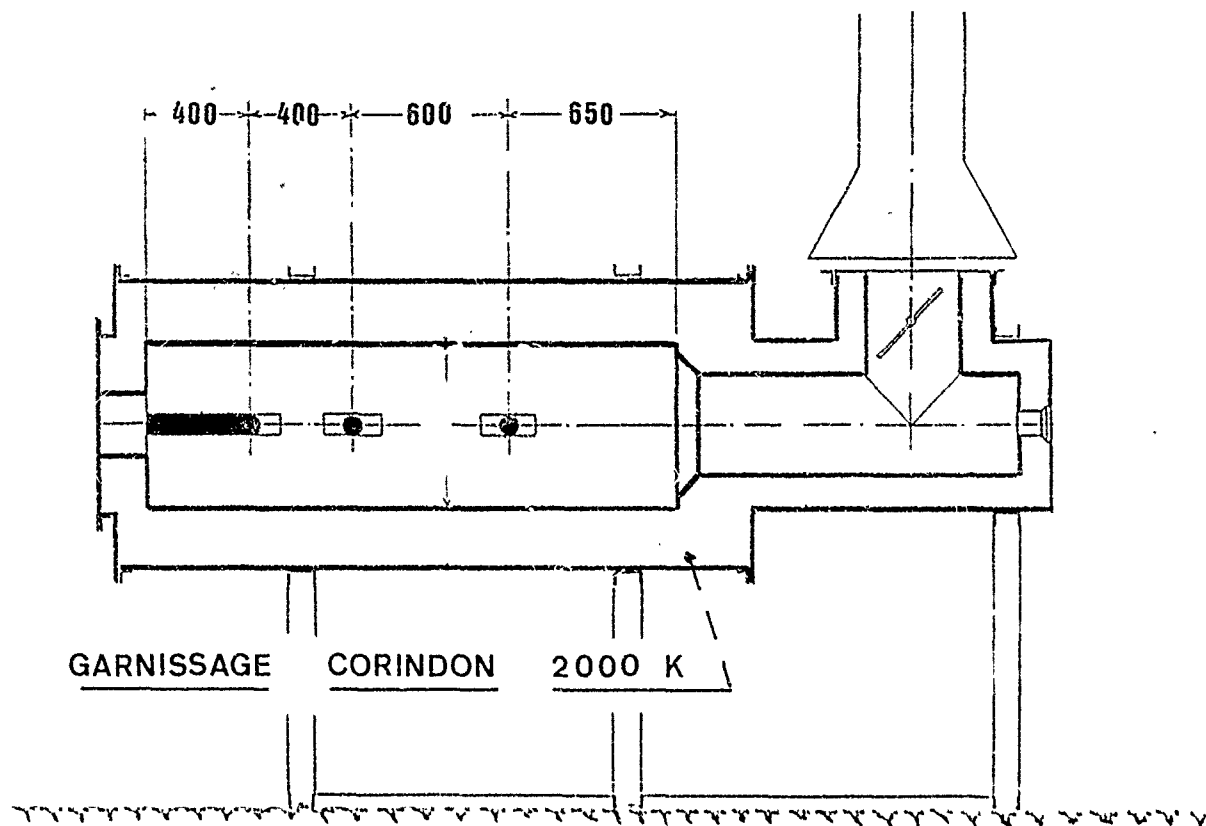


Fig.1 Four 300 KW

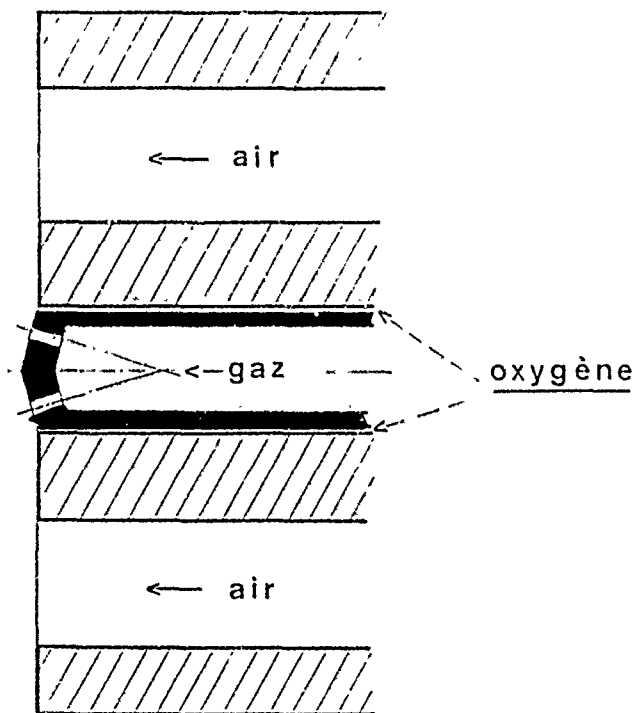
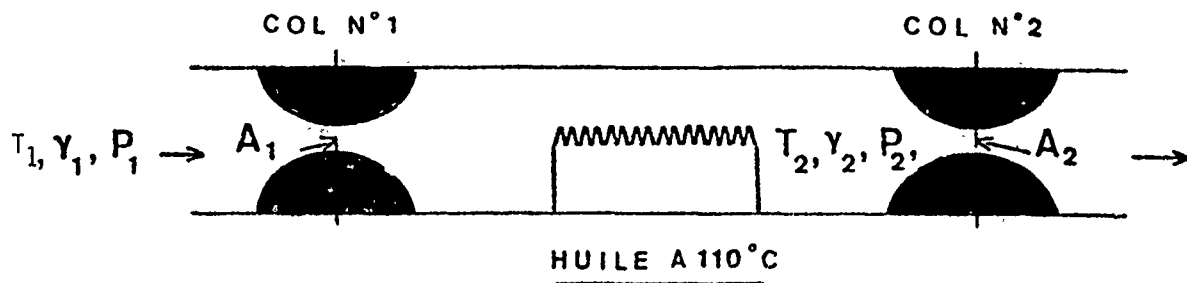


Fig.2 Schéma du brûleur



### EQUATION DE CONTINUITE :

$$P_1 A_1 \sqrt{\gamma_1 \left( \frac{2}{\gamma_1 + 1} \right)^{\frac{\gamma_1 + 1}{\gamma_1 - 1}} \frac{M_1}{R T_1}} = P_2 A_2 \sqrt{\gamma_2 \left( \frac{2}{\gamma_2 + 1} \right)^{\frac{\gamma_2 + 1}{\gamma_2 - 1}} \frac{M_2}{R T_2}}$$

d'où

$$f_1 \left( \gamma_1, \frac{M_1}{R T_1} \right) = f_2 \left( \gamma_2, \frac{M_2}{R T_2} \right) \frac{P_2 A_2}{P_1 A_1}$$

— le rapport  $\frac{A_2}{A_1}$  est étalonné expérimentalement.

— les pressions  $P_1$  et  $P_2$  mesurées.

—  $f_2$ , calculé ( $M_2$  et  $T_2$  connus).

—  $T_1$  obtenu à partir de  $f_1$

Fig.3 Principe du double col

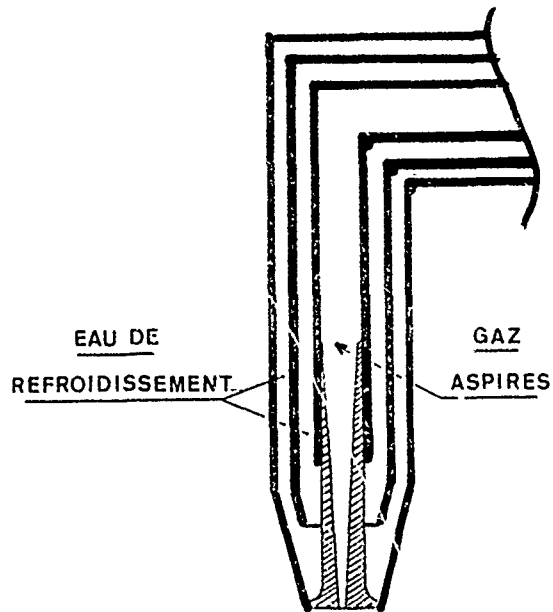


Fig.4 Sonde de prelevement sonique

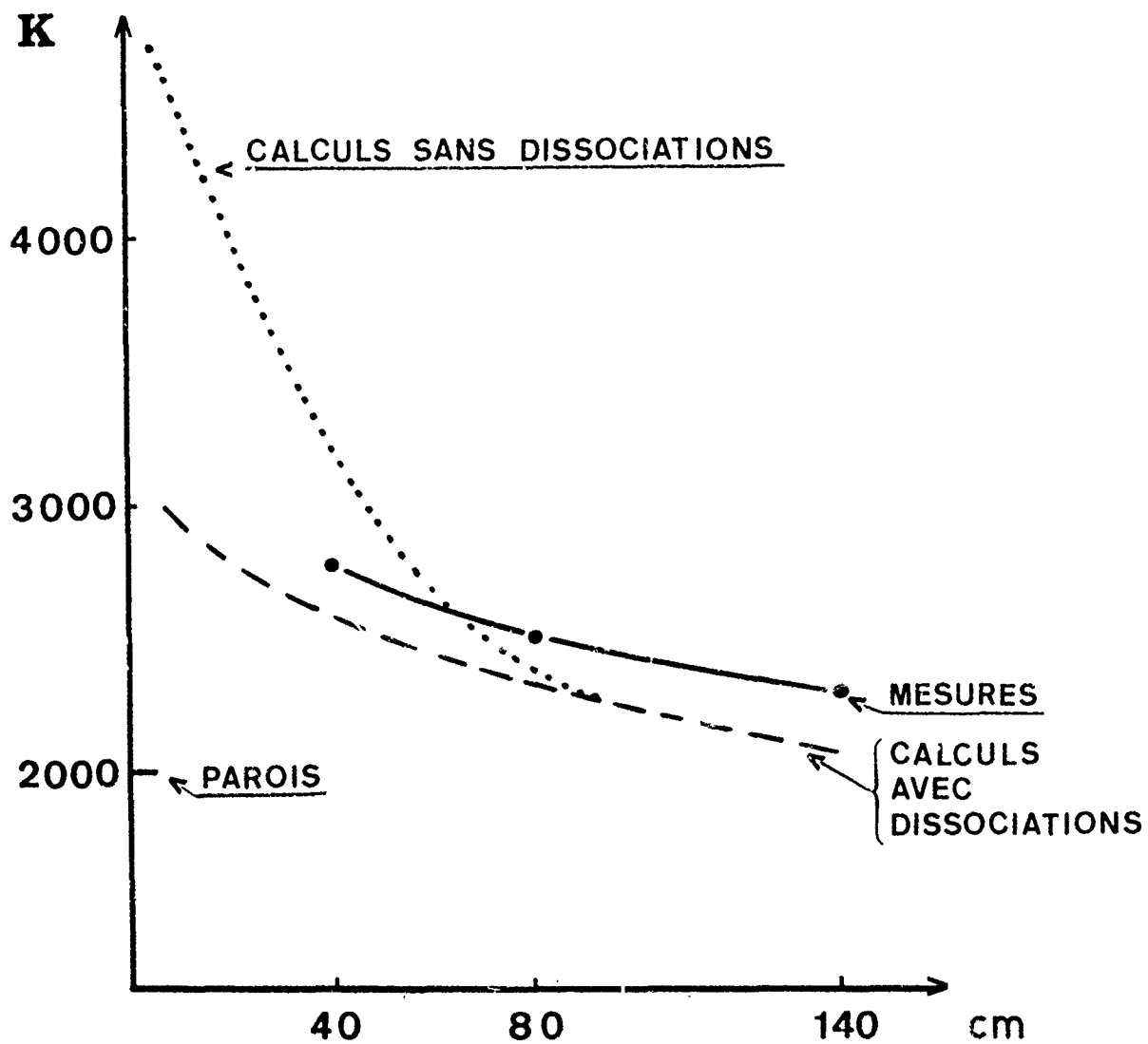


Figure 5

## DISCUSSION

**E.Perthuis, Fr**

Les calculs et expériences menés par les auteurs ont-ils permis de mettre en évidence l'intérêt d'un faible facteur émissif de la flamme et des gaz dans ce four dont les parois sont très chaudes?

**Réponse d'Auteur**

Il aurait fallu décrire dans le détail les variations des propriétés émissives des gaz en fonction de la température et des concentrations. Le modèle de Salooja et Lockwood est basé sur une méthode perfectionnée de flux avec 4 gaz gris comme principe de simulation. Un des conférenciers précédents a indiqué que cette méthode donnait des résultats presque aussi bons que des méthodes plus sophistiquées basées sur la répartition spectrale. Cependant, il ne faut pas dire que les pertes par rayonnement sont négligeables; elles sont importantes et influent sur le profil de température en raison des niveaux de température beaucoup plus élevés qu'à l'habitude.

**J.B.Michel, Ne**

Pour commenter la question précédente sur l'effet de l'émissivité moyenne des gaz de combustion sur le calcul du rayonnement avec température élevée de la charge, il faut dire que cet effet n'est pas très important avec des flammes où le comburant est de l'air ( $\epsilon = 0,15$  à  $0,20$ ) mais il est assez important pour des flammes à l'oxygène pur et l'on ne peut pas négliger la variation de l'émissivité avec la température.

**Réponse d'Auteur**

A titre de commentaire, il faut préciser que la méthode n'utilise pas la valeur  $(\bar{T})^4$  mais  $\bar{T}^4$  calculé à partir du modèle probabiliste de Salooja et Lockwood.

**N.Peters, Ge**

Nous avons fait des expériences sur des flammes enrichies à l'Oxygène et mesuré les  $\text{NO}_x$ . On a trouvé des niveaux inférieurs à ceux attendus si on utilise des formules simples pour calculer ces niveaux des  $\text{NO}_x$ .

Pour des flammes alimentées en air préchauffé, on constate le même phénomène. Nous pensons que cela est dû au rayonnement très important, dans ce type de flamme. Pouvez vous évaluer le pourcentage d'énergie rayonnée par la flamme?

**Réponse d'Auteur**

Ces pertes, très variables suivant la position dans le four, sont en moyenne de 20%.

Th.T.A. Paauw, A.J. Stroo, C.W.J. van Koppen  
Laboratory for Thermal Power Engineering  
Delft University of Technology  
Rotterdamseweg 139A  
Delft, The Netherlands

# ABSTRACT

The conservation equations governing the flow field and the combustion process in isothermal and in diffusion controlled combustions confined flows are solved using a numerical finite difference technique; the results are compared with measurements.

The combustion process of the hydrocarbon fuel has been modelled by using instant reaction with fluctuations in the mixture fraction, and with three different assumptions for the chemical conditions: frozen chemistry, equilibrium chemistry and partial equilibrium chemistry.

Attention is paid to the formation of nitrogen oxides, and it is shown that in hydrocarbon diffusion flames a substantial amount of the NO formed is due to 'prompt NO' formation. For this process an effective model is presented.

## 1. INTRODUCTION

During the last decade considerable effort has been devoted to the modelling of furnace phenomena. In general two distinct lines of approaching the problem can be observed. Some authors have tried to model the furnace by dividing it into several separate sections, each representing a simple system, s.a. well stirred or a plug flow reactor [1]. Although such methods are useful for the prediction of the trends in furnace behaviour or pollutants formation, additional model assumptions and empirical data are often required for particular calculations. On the other hand methods have been developed that simulate the furnace performance in more detail, generally by solving the conservation equations in finite difference form [2-4]. These methods lead to a fair prediction of the influence of furnace geometry and configuration dependent phenomena s.a. furnace heat transfer and flame furnace wall interaction. However, these more sophisticated models also require some assumptions, normally regarding the turbulence model, the radiation model and the combustion model.

In the present work such a detailed method is used for the prediction of the completely diffusion controlled combustion of gaseous hydrocarbons in an axisymmetrical combustion chamber. Several combustion models are investigated, all based on instant reaction combined with scalar fluctuations. The main scalar being in this case the so-called mixture fraction, and particularly, attention is paid to the accurate prediction of the fluctuations of this scalar.

In this framework the mixing process of a scalar and the production of scalar fluctuations in an isothermal combustor geometry is firstly investigated by comparing the results of numerical calculations with extensive measurements by BECKER [5-6].

Furthermore, the assumptions concerning the combustion process are investigated in a detailed comparison between experimental and numerical data for natural gas flames.

Finally, the developed models are tested by comparison of calculations with measurements obtained in the Delft furnace for a low NO<sub>x</sub> burner geometry.

## 2. MATHEMATICAL AND PHYSICAL ANALYSIS

### 2.1. Basic equations.

The calculation procedure consists of solving the partial differential equations representing the conservation of the time averaged flow properties in an axisymmetrical flow geometry. The general, elliptic form of these equations can be expressed as:

$$\frac{\partial}{\partial x} (\rho_\phi u_\phi) + \frac{1}{r} \frac{\partial}{\partial r} (\rho_\phi v r_\phi) = \frac{\partial}{\partial x} (\mu_\phi \frac{\partial \phi}{\partial x}) + \frac{1}{r} \frac{\partial}{\partial r} (\mu_\phi r \frac{\partial \phi}{\partial r}) + S_\phi \quad (1)$$

in which  $u$  and  $v$  represent axial and radial velocity, and  $\phi$  a flow property, with  $\mu_\phi$  as its viscosity and  $S_\phi$  as its source term.

In the case of furnace calculations  $\phi$  represent subsequently  $(u, v)$  axial and radial velocity,  $(k, \epsilon)$  the turbulent kinetic energy and its dissipation,  $h$ , the stagnation enthalpy,  $(R_x^k, R_r^k)$  the radiant heat flux in the  $x$  and  $r$  direction for radiant gas  $k$ ,  $(\bar{Y}_f, \bar{Y}_f^{1/2})$  the mixture fraction and its root mean square value and finally  $Y_{NO}$ , the mass fraction of thermal NO.

The values of  $\rho_\phi$ ,  $\mu_\phi$  and  $S_\phi$  are given in table I. Constants necessary to solve these equations are given in table II.

When no recirculation takes place, as in the case of free diffusion flames, the second form on the right-hand side of (1) can be omitted, transforming the partial differential equation to a parabolic form, which is easier to solve numerically.

For the solution of equation (1) it is necessary to define boundary conditions; at the axis of symmetry ( $r = 0$ ) these are:  $v = 0$  and  $\partial \phi / \partial r = 0$  for all other quantities, at the solid boundary empirical wall functions can be used to relate  $(\partial \phi / \partial r)$  to the local values of  $\phi$ , for  $u, v, k, \epsilon$  and  $h$  [2, 7],

and for  $R_x^k, R_r^k$  [8]; the other values of  $\phi$  are set to zero. At the exit of the duct and furnace calculations  $(\partial \phi / \partial r)$  was assumed to be zero, and at the entrance all variables  $\phi$  were specified.

## 2.2. Turbulence model.

The two-equation turbulence model used in the present work is based on the solution of the equations for the turbulent kinetic energy  $k$  and its dissipation rate  $\epsilon$ ; in this model the logic assumption for the turbulent viscosity is:  $\mu_e = C_\mu \rho k^2 / \epsilon$ . This viscosity has to be added to the laminar viscosity.

The chosen model had been shown to give good predictions in boundary layer type flows [9], and also in more strongly elliptic flows of the same geometry as has been used here [2, 10]. Because of the uncertainties in the combustion model more refined turbulence models are judged to be over-sophisticated at this stage of the development.

## 2.3. Radiation model.

The four-flux radiation model adapted here is based on the formulation of GOSMAN e.a. [8], which reduces the original four equations for the radiation fluxes in four directions,  $I_{x+}^k$  and  $I_{x-}^k$  for radiant gas  $k$ , to two equations governing the distribution of the sum parameters  $R_x^k = (I_{x+}^k + I_{x-}^k)/2$ , and  $E_x^k = (I_{x+}^k - I_{x-}^k)/2$ . Although this formulation is efficient a deficiency can be the uncoupling of the fluxes in radial and axial direction. Nevertheless summations of radial and axial fluxes, representing fluxes in directions under  $45^\circ$  with the symmetry axis, are evidently coupled. Also the dependency of  $\mu_R^k$  on  $r$  correctly represents the

consequences in radial direction of an anisotropic flux distribution.

Moreover the physical constant to be applied to the scattering and absorption of the calculus are uncertain, not at least because of the occurrence of luminous radiation.

Therefore scattering has to be assumed negligible, and two models for the absorption and emission coefficients have been tested. In a first model the absorption and emission constant have simply been chosen constant ( $\alpha_1 = \epsilon_1 = 4$ ), representing a one gray radiating gas. In a second model the constants have been assumed to be temperature and mixture dependent ( $\alpha_k(Y_{CO_2}, Y_{H_2O}, \rho, T)$  and

$\epsilon_k(Y_{CO_2}, Y_{H_2O}, \rho, T)$  for gas  $k$ ) in a one clear, three gray gas formulation for natural gas developed and used by the IFRF [11] for natural (Groningen) gas in similar calculations.

## 2.4. Combustion models.

In the literature concerning combustion models two categories of models have been proposed. The first category consists of models in which the governing parameter is the fuel mass fraction. The conservation equation for the fuel mass fraction is solved using an effective source term, being either an Arrhenius type reaction rate or a flow pattern dependent reaction rate, s.a. the eddy break-up rate proposed by SPALDING [2] or in a different way by BRAY [12]. These models seem to be particularly suited for modelling premixed flames because there the effective reaction rate is the controlling factor.

In diffusion flames, however, the mixing process is much slower than the chemical reaction. Consequently the combustion process is controlled by mixing, the reaction rate can be assumed as infinitely fast, and a parameter like the mixture fraction, defining the mixing process, controls the reaction. The relation between the reaction process and the mixture fraction in this case can be found via the quantity:

$$f = r \cdot Y_{fu} - Y_{ox} \quad (2)$$

where  $Y_{fu}$  and  $Y_{ox}$  denote fuel and oxidant mass fractions and  $r$  is the stoichiometric mass ratio between fuel and oxidant.

The conservation equation governing the distribution of  $f$  has a source term equal to zero. Furthermore the following identity can be deduced:

$$Y_f = \frac{f - f_{ox}}{f_{fu} - f_{ox}} \quad (3)$$

where  $Y_f$  in the fuel phase is equal to one, and in the oxidant phase equal to zero.

At the stoichiometric conditions:  $f_{st} = 0$ , and  $Y_{f, st} = 1/(r+1)$ . For the Groningen natural gas used in our experiments  $r = 13.07$  and  $Y_{f, st} = .071$ .

So far we have made no proposals for the reaction process, beside the fact that it is slower than the mixing process. In the paper three models will be discussed: the well known frozen composition model [2], the equilibrium composition model and a so-called partial equilibrium composition model.

### 2.4.1. Frozen composition model (model 1).

In this model it is assumed that the infinitely fast reaction is restricted to an infinitely small reaction zone, situated at the surface where  $Y_f = Y_{f, st}$ . Outside this reaction zone the reaction is

considered to be completely quenched, and the composition is in effect frozen.

Under these assumptions it is a simple matter to define mass fractions and temperatures, for example:

$$Y_{fu} = 0 \quad \text{for} \quad Y_f < Y_{f, st}$$

and

$$Y_{Ox} = 0 \quad \text{for } Y_f > Y_{f, st} \quad (4)$$

The respective  $Y_{Ox}$  and  $Y_{fu}$  can be found by means of equations (2) and (3). The temperature is calculated with help of the calculated enthalpy and an average value of the specific heat. The density follows from the equation for a perfect gas. Curves for the temperature and the oxygen concentration under adiabatic conditions are depicted in figure 1.

#### 2.4.2. Equilibrium composition model (model 2).

In this model it is assumed that the infinitely fast reaction is not restricted to only a reaction surface, but does occur in the whole field, both for forward and backward reactions. This results in a local equilibrium composition, governed by the local equivalence ratio related to the mixture fraction and the local enthalpy. In this case it is not possible to obtain a straight forward relation between the relevant properties (e.g. the temperature) and the mixture fraction and enthalpy. To avoid this difficulty the following procedure has been adopted [14]. A two-dimensional mapping has been made of all relevant thermodynamic and chemical properties: temperature  $T$ , density  $\rho$ , viscosity  $\mu$ , and mass fractions  $Y_{O_2}$ ,  $Y_{CH_4}$ ,  $Y_{CO_2}$ ,  $Y_{CO}$ ,  $Y_{H_2O}$ ,  $Y_{H_2}$ ,  $Y_{N_2}$ , and  $Y_O$ .

Using a least square method, this mapping has been fitted in Chebyshev double polynomials:

$$Y_i(h, Y_f) = \sum_{i=1}^I \sum_{j=1}^J a_{ij} T_i(h^*) T_j(Y_f^*) \quad (5)$$

in which  $h^*$  and  $Y_f^*$  denote normalised values of  $h$  and  $Y_f$ , whereas  $T_i$  denotes a Chebyshev polynomial of degree  $i$  and  $I$  and  $J$  have values up to eight.

Equation (5) represents an efficient instrument for the calculation of the equilibrium conditions, when the recurrence relations for Chebyshev polynomials are used. However, in the iterative procedure to solve the finite difference form of the partial differential equations, mentioned before, a much more economical procedure is employed by making use of the mentioned two-dimensional mapping employing bilinear interpolation. Also in this case calculated curves of  $T$  and  $Y_{O_2}$  are given in figure 1 for adiabatic conditions.

It should be noted that the temperature sharply decreases at the rich side of the stoichiometric point; the decrease coincides with an increase in  $Y_{H_2}$  and  $Y_{CO}$ .

#### 2.4.3. Partial equilibrium composition model (model 3).

In figure 1 experimental data obtained from mass fraction profiles, measured in attached turbulent natural gas diffusion flames [14] are also reported. From these results it appears that the equilibrium composition assumption gives temperatures that are too low, while the frozen composition temperatures are much too high. More surprising, however, are the molecular oxygen curves. Theoretically the  $O_2$  mass fraction at fuel rich condition ( $Y_f > 0.071$ ) should be essentially zero both in the frozen and the equilibrium condition and even taking into account the unmixedness the highest value for  $Y_{O_2}$  to be expected below near stoichiometric conditions ( $Y_f = .11$ ) is 1.5%, whereas values beyond 5% are measured.

Obviously nearly all fuel (mainly  $CH_4$ ) is consumed, but due to the short residence time in the flame front only part of the  $O_2$  has reacted, resulting in high  $CO$  and  $H_2$  mass fractions.

Behind the flame front the further reaction of  $O_2$  is apparently suppressed and a frozen composition is found but with a finite  $O_2$  mass fraction.

The reason for the quenching lies in the fact that in hydrocarbon flames  $O_2$  mainly reacts with  $H$  radicals, and as shown by BULAU a.o. [18] the  $OH$ ,  $H$  and  $O$  radicals effectively almost fully recombine for  $\phi > 1.65$  ( $Y_f > .088$ ).

To take these effects into account a partial equilibrium hypothesis is introduced, stating that oxygen in the fuel rich region does not react and so gives a constraint. The other species concentrations and the temperature have been calculated based on an equilibrium assumption with the constraint  $O_2$  concentration. In figure 1b this hypothesis is illustrated by a straight line through the measured data points and gives a value at  $Y_f = Y_{f, st}$  of  $Y_{O_2} = 4\%$ .

The calculated equilibrium temperature curve following from the quenched equilibrium hypothesis, using this  $Y_{O_2}$  constraint, is drawn in figure 1a and is seen to compare favourable with the measured data.

On behalf of further flame calculations the most relevant species and thermodynamic properties were calculated for quenched equilibrium conditions as function of the enthalpy and the mixture fraction, and also transformed in Chebyshev polynomials in the way, explained in section 2.4.2.

#### 2.5. Nitrogenoxide formation model.

In diffusion flames it is often assumed that most of the nitrogenoxide is found by high temperature reaction between oxygen and nitrogen molecules and atoms. This so-called thermal NO formation is usually based on the Zeldovich mechanism, with reaction rate:

$$\dot{w}_{NO}(Y_f) = 2k_z \rho \frac{Y_{N_2}(Y_f)}{M_N} \cdot \frac{Y_O(Y_f)}{M_O} \exp(-E_z/T(Y_f)) \quad (6)$$

with  $k_z = 10^{11.15}$  and  $E_z = 37.5 \cdot 10^3$ ,  $M_{N_2}$  and  $M_O$  denote the molecular weights.



The atomic oxygen mass fraction may be calculated either by the assumption of chemical equilibrium between molecular and atomic oxygen for the frozen chemistry models or by using equations like (5) for the equilibrium chemistry models.

In calculations for natural gas diffusor flames we found that especially for the equilibrium models the calculated thermal NO mass fraction was much smaller than the measured NO mass fraction. This may indicate that 'super equilibrium' oxygen concentration (see 2.4.3) play a role. Another possible explanation is 'prompt NO', often neglected in diffusion flames studies. As 'prompt NO' is formed only inside the reaction zone a frozen flow composition description for calculating the additional formation of thermal NO can be used. To test this last assumption measured NO mass fractions in attached natural gas diffusion flames are plotted against the mixture fraction in figure 2. This has been done for several values of both the Froude number ( $Fr = u^2/gD$ , with burner velocity  $u$  and burner diameter  $D$ , representing the influence of buoyancy forces on the flame and the Damköhler number ( $Da = (D/u)/\tau_c$ , with  $\tau_c$  as a critical combustion time, chosen here to be  $5 \cdot 10^{-5}$  s, the characteristic blow-out time of a homogeneous reactor), representing the influence of shear on the reaction process. From figure 2 it is clear that a correlation between  $Y_{NO}$  and  $Y_f$  does exist. The "too low" experimental NO values on the fuel richside can be explained by the fact that 'prompt NO' is partly preceeded by HCN [25], not measured here. The higher values of NO for fuellean mixture can be explained by the influence of additional thermal NO. The nitrogenoxide mass fraction at the stoichiometric  $Y_f$  value ( $x_{NO} = 38$  ppm) compares well with the 'prompt NO' concentrations measured in premixed stoichiometric hydrocarbon flames [19]. The thin line in figure 2 drawn through the full circles represents a slightly lifted flame ( $x_{ign}/D = 3.5$ ). It is clear that in this case the constrained, unreacted oxygen did not produce NO and the correlation mentioned above and drawn in figure 2 has to be changed, using the  $Y_f$  value of the ignition-point. In the following calculations both the thermal NO formation and the frozen flow 'prompt NO' contribution have been determined and added to give a total NO mass fraction.

## 2.6. Probability formulation of the mixing process.

The usefulness of a probability description of flames is illustrated by figure 1a where small fluctuations in  $Y_f$  around the stoichiometric value result in large fluctuations in temperature, especially in the case of the equilibrium models. By reverse it is evident that momentary temperatures can be much higher than the average temperatures, resulting e.g. in instantaneous reaction rates that are orders of magnitude higher than those based on the average temperature. Time average flow properties, the spatial distributions of which prescribed by equation (1), can be reaveraged as moments of the probability density function (PDF) governing the time dependent behaviour of the observed property. When a gaussian PDF is assumed the first and second moment of the PDF (representing the mean value and the root mean square value) completely determine the PDF. In our calculations such an assumption has been made for the PDF of the mixture fraction; the fact that  $Y_f$  can not be lower than the oxidant value or higher than the fuel value being taken into account by the use of a clipped gaussian shape, following LOCKWOOD e.a. [20]. From the PDF for the mixture fraction,  $P(Y_f)$ , the PDF for the temperature:  $P(T)$  can simply be derived by putting:

$$P(T) |dT| = P(Y_f) |dY_f| \quad (7)$$

The contributions to  $P(T)$  above and below the stoichiometric value of  $Y_f$  have to be added. In figure 3 measurements of  $P(T)$  in natural gas diffusion flames [15], around the stoichiometric reaction zone are shown and compared with the results of calculations. Each calculated curve is based on 16 points, (smoothed histograms, being composed of 16 bars) obtained by using calculated  $Y_f$  and  $\overline{Y_f'^2}$  ( $= Y_f'$ ) values and assuming a clipped gaussian PDF. Also here it is clear that the partial equilibrium flow, gives the better results by imposing a certain upper temperature limit ( $T \sim 1900$  K) much lower than the adiabatic value ( $T = 2210$  K). Using equation (5) representing the combustion models and a Schwab-Zeldovich coupling function between  $h$  and  $Y_f$  [21]:  $h = \beta(Y_f)$  and assuming that the Lewis number unity, the mean concentrations for the chemical properties can be defined by:

$$\overline{Y_i} = \int_0^1 Y_i(\beta(Y_f), Y_f) P(Y_f) dY_f \quad (8)$$

with  $i = O_2, N_2, CH_4, H_2O, H_2, CO, CO_2$  and  $O$ . The same procedure is followed for the physical properties  $T$ ,  $\rho$  and  $\mu$  and for the 'prompt NO', where the linear relation drawn in figure 2 (thick line) has been applied to determine  $Y_{NO}(Y_f)$ .

The formation of thermal NO is governed by the averaged source term (6):

$$\overline{\dot{w}_{NO}} = \int_0^1 \dot{w}_{NO}(Y_f) P(Y_f) dY_f \quad (9)$$

source terms for the four flux models are formulated as:

$$\overline{\epsilon_k T^4} = \int_0^1 \epsilon_k(Y_f) T^4(Y_f) P(Y_f) dY_f \quad \text{and}$$

$$\bar{\alpha}_k = \int_0^1 \alpha_k(y_f) P(y_f) dy_f \quad (10)$$

In (9) and (10) it is anticipated that the temperature, density and concentration dependencies can be expressed in a mixture fraction dependency.

## 2.7. Solution procedure.

To solve differential equations represented by equation (1) and table I, these equations are expressed in finite difference form and solved by the algorithms for the elliptic case and the parabolic case as given in respectively [22] and [23]. The calculations for the elliptic case were performed with a 20 x 20 nodes grid geometry. The number of iterations required to reach the convergence criterion defined in [22] was 300 in the case of isothermal confined flow. For the free jet diffusion flame with a simple model for the absorption and emission coefficients it reached 600 and for the case of more elaborate radiation constants, up to 1000. This same number of iterations was required for confined combustion calculations. The use of a combustion model led to an increase of necessary computing time per iteration with a factor of two compared with isothermal flow calculations. The elaborate radiation model led to an increase with a factor of three. The parabolic scheme for the free jet diffusion flames calculation was two orders of magnitude faster than the elliptic scheme however.

## 3. RESULTS AND COMPARISON WITH EXPERIMENTS

From the previous paragraphs concerning the combustion models and the introduction of the PDF it is clear that the mixture fraction and its fluctuations play an important role in the calculation procedure.

Mostly the stoichiometric value of the mixture fraction is small (natural gas:  $y_{f,st} = 0.071$ ) which means that small variations in the gradient slope of the axial  $y_f$  profiles result in large variations in the predicted temperature curves. Confinement and recirculation strongly influence the accuracy of the prediction of the mixture fraction field and therefore the elliptic program was first tested for isothermal confined jets. Subsequently unconfined diffusion flames have been calculated with both the parabolic and the elliptic program in order to test the accuracy of the latter program and the influence of the grid arrangement, and for the comparison of the combustion models with experiments. At last comparison is made between furnace calculations and measurements.

### 3.1. Confined isothermal jet calculations.

To verify the equations that govern the mixture fraction and its fluctuations in a confined flow we decided first to compare calculations in isothermal flow with measurements. The only available experimental results in confined jet flow providing information about the mixture fraction and its fluctuations are those of BECKER [5], [6], [16].

The results also concern detailed measurements of the mean flow pattern and the static wall pressure. The data have been obtained in a cylindrical duct (.197 m diameter, 1.25 m length, smooth wall), in the center of which an air jet initial velocity  $u_{c,o}$ , (uniform profile, 6.35 mm diameter) was situated, surrounded by a secondary, uniform ground stream (velocity  $u_{w,o}$ ).

The calculations have been carried out for different combinations of primary and secondary velocities, yielding Craya-Curtet numbers of 1.22, .673, .345 and .212. These numbers correspond to flow patterns with increasing recirculation. The Ct number is defined as:

$$Ct = \bar{u}_f / u_{f,o}^*, \text{ with } u_{f,o}^{*2} = \bar{u}_f^2 - (u_{w,o}^2 + \bar{u}_f^2)/2,$$

where  $\bar{u}$  and  $\bar{u}^2$  are the area-averaged velocities [5], and  $u_{f,o}^{*2}$  can be regarded as a measure of the non-uniformity of the momentum flux distribution at the inlet.

The ducted flow can be regarded as being divided into three regions: a region of jet growth, a recirculation zone, and post-jet mixing zone. This becomes particularly clear from the axial profiles of  $u_o/(u-u_w)$  and  $y_{fo}/(y_f-y_{f,w})$  given in figure 4 and 6, where  $u_w$  and  $y_{f,w}$  refer to the ground stream.

The relation between the reciprocals of mixture fraction and velocity and the axial distance is linear in the jet growth region, whereas the curves bend steeply upwards in the final region. Here the ground stream velocity tends to the velocity at the axis. Especially for lower Ct numbers there is a good agreement between calculated and measured data. The changes in mixing regime are also well represented in the static pressure profile (figure 5) where the position of the sudden increase in pressure corresponds with the eye of the recirculation zone. However, the absolute values of the pressure rise are conspicuously high in comparison to the measured results, indicating that overprediction of wall friction or internal friction in the recirculation zone does possibly occur. It should be noted that the pressure rise does sensitively depend on the profile of the nozzle flow, here assumed to be essential uniform. Similar overpredictions of the pressure are also reported by KANG e.a. [10] using the same method in confined flows with comparable Ct numbers.

The post-jet mixing behaviour is mainly characterised by the mixture fraction fluctuations; some results are depicted in figure 7. Beyond the recirculation zone, i.e. when the jet has reached the wall, the production of fluctuations diminishes and dissipation results in their decrease. This is reproduced in the calculations for the lower Ct numbers, although the maximum predicted fluctuation intensity at low axial distances are higher than those measured by BECKER [30]. Measurements in free jets by Haberdad show a better agreement. For the lower Ct numbers investigated the maximum influence of the mixture fraction fluctuations on the temperature field can be expected to occur in the reaction zone around  $y_{f,st}$  considering the combustion model that was applied. For natural gas,  $y_{f,st} = .071$ , corresponds with  $x/D_f > 15$ ; in this region the predictions are fairly correct.

For the highest Ct number the axial profile of mixture fraction fluctuations is not influenced by the confinement and resembles the calculated profiles in free jets using the same set of partial differential equations as in table I but in a parabolic form [17], [24]. In the last case the value of  $Y_f'/\bar{Y}_f$  on the axis is only slightly smaller than the value of .227 obtained here.

### 3.2. Free jet diffusion flames.

In order to validate the combustion models described before, we decided to compare calculations for the relatively simple turbulent diffusion flame with detailed measurements concerning the temperature, mass fractions, velocity and radiation field in such flames. For the comparison a vertical natural gas flame with  $D = 10^{-2}$  m,  $\bar{u}_0 = 20$  m/s,  $Re = 14500$ ,  $Fr = 3900$  and  $Da = 21$  was selected; because of both the considerable shear stress and buoyancy in this flame no local laminarisation of the flame front is to be expected.

#### 3.2.1. Influence of the numerical method.

The numerical predictions for the flame have been obtained in two ways: using a parabolic flow program and using a elliptical program, with respectively a  $20 \times 25$  and a  $21 \times 30$  grid arrangement. The axial and radial grid locations have been chosen finely distributed around the burner, both with a node density for grid II two times higher than for grid I.

Presumably in this region the grid II is smaller than the turbulent macrolength scale whereas it is slightly larger in grid I. The results indicate that an underprediction of the production of turbulence follows from the larger grid spacing. The outer radial grid point (the wall) is situated at a distance of .5 m from the burner. Here a secondary flow with a velocity of .2 m/s is assumed in combination with zero wall gradients. Varying these assumptions within reasonable limits did not influence the flame structure.

The mean axial temperatures calculated with combustion model 2 and the different numerical schemes are presented in figure 8. The coarse grid I obviously leads to a slower mixing process than the finer grid II, resulting in a stoichiometric mixture and a maximum temperature further downstream. Using grid II leads to an upstream shift of this point both for the elliptic and the parabolic scheme. By combining the parabolic and the elliptic scheme in an additional calculation it was shown that the influence of the grid spacing was mainly restricted to the region between the burner mouth and  $x/D = 5$ . Using the results of the fine grid parabolic scheme in this point as initial values for coarse grid elliptic scheme calculations further downstream brought the position of the maximum temperature within 10% from the position obtained with a completely fine grid calculation. The proceeding results show that for turbulent, diffusion flame-like combustion processes (free jet flow or confined flow with a large Ct number) a careful choice has to be made for the grid location in high intensity mixing zones. Grid spacings as given for grid II have been used for all the following combustion calculations.

#### 3.2.2. Influence of the combustion model.

With the fine grid spacing the diffusion flame defined before has been recalculated with the frozen composition and the partial equilibrium combustion model. The predicted temperature profiles, velocity and mixture profiles both using the parabolic and elliptic computation scheme are presented in figure 9 and figure 10 and are compared with experimental data obtained with respectively micro-thermocouples (diameter 20  $\mu$ m), a laser-doppler anemometer and a detailed gaschromatographic analysis [15]. Experimental probability density functions for the temperature, compared with calculated values for the equilibrium and the partial equilibrium model were shown earlier in figure 3. For the temperatures the agreement between calculation and experiment is very good for both the equilibrium and the partial equilibrium; however the last model is to be preferred because of the better agreement in PDF values. The difference in temperature predicted by subsequently the elliptic and the parabolic computational scheme as shown in figure 9 for the equilibrium composition model is small and is also typical for calculations using the other combustion models. The main conclusion to be drawn from figure 9 is that the frequently applied frozen composition model leads to an unrealistic short flame length and too high a maximum temperature. Considering also figure 3 (and figure 16) the partial equilibrium model appears to be more realistic than the equilibrium model. From figure 9 further a small shift in the position of the predicted flame front given by the maximum temperature is observed in comparison with the experimental data. This is possibly caused by imperfections in the turbulence model. However, optimisation of the chosen turbulence constants is omitted.

The axial profiles for velocity and mixture fraction presented in figure 10 show the mutual deviations between the distinct numerical procedures and combustion models to be rather small for these quantities. The difference between measurements and predictions is much larger, however, particularly near the burner. The cause being that the flame was lifted to a height of  $x/D = 9$  above the burner mouth. The agreement further down stream stems from the enhanced mixing by buoyancy forces, these causing high axial velocities around the maximum temperature region. Predictions with a somewhat more elaborate combustion model, designed a.o. to predict ignition, are depicted in figure 10 by the curves c. The agreement is very good for both the velocity and mass fraction; the temperature curves as presented in figure 9, do not change in the new model. More details on the improved combustion model will shortly be published, after completion of its development.

#### 3.2.3. Radiation prediction.

Although the radiant heat transfer in the diffusion flame investigated is relatively small it provides an opportunity to test the various radiation models.

Experimental data obtained with the Shell radiation pyrometer [15] are given in figure 11 together with predictions using the equilibrium and partial equilibrium combustion models and various radiation models. For the simple one gray gas model ( $\alpha_k = 0.4$ ) gave a higher (radial) radiative heat transfer than the partial equilibrium model reflecting the fact that the maximum temperatures are higher for

the equilibrium model (see figure 3). The maximum value of the measured radiative heat flux lies between the two predicted values. The predictions based on the IFRF correlation ([11], 3 gray/1 clear gas, verified for natural gas only) show good agreement with the measurements. However, the computing time using this correlation was much higher, while the improvement of the prediction was smaller than the influence of the combustion model. Therefore the simple radiation model was preferred for subsequent furnace calculations.

### 3.2.4. Pollutants prediction.

The calculation of NO formation is divided in 'prompt NO' formation and 'thermal NO' formation in the manner discussed before. The 'prompt NO' values are given separately in figure 12 and appear to be fairly independent of the combustion model used. However, as shown in figure 2, lifting of the flame (equivalent to pre-mixing!) influences the NO concentration. So, using the improved combustion model (section 3.22), to estimate the lift of the flame, calculations of prompt NO concentrations have been made both for the lifted and the attached flame. The results show that in the attached flame the maximum prompt NO concentration is found well inside the fuel rich part of the flame; in both flames  $Y_{f,st}$  is reached at  $x/D = 80$ . For the lifted flame, however, the maximum prompt NO concentration

occurs near the stoichiometric point, as does the maximum NO concentration.

The thermal NO profiles calculated for the different combustion models are also shown in figure 12. They reflect the important influence of the temperature on the NO formation. The thermal NO formation in the frozen composition and the equilibrium model is substantial, because in these models the adiabatic combustion temperatures can be reached. However, the measured results from figure 3 indicate that the low thermal NO profiles obtained with the partial equilibrium model must be considered as being the most reliable. Addition of the preferred 'thermal NO' and 'prompt NO' profiles leads to a total NO profile comparing fairly well with the profile measured with the chemoluminescent method [15]. The shift to the richer part of the calculated profile compared with the measurements might be due to the fact that part of the 'prompt NO' is decomposed to HCN, not measured here. However, it is more likely that the flame is simply some 10 D shorter than the predicted one. A similar shift is also reflected in the temperature profile in figure 9 (curves a and b).

The identified importance of 'prompt NO' is largely in accordance with the results obtained by TAKAGI e.a. [28], in propane diffusion flames. In most other investigations the role of the 'prompt NO' is wrongly overlooked.

### 3.3. Cylindersymmetrical furnace calculations.

To test the models for furnace applications we used the extensive experimental data obtained in the Delft furnaces equipped with a newly designed central air burner (CAB) [29]. The CAB was designed to combine a stable combustion process, with easy dual fuel burning and low NO formation. The basic idea is that introduction of the gas through an annulus around a cylindrical airjet leads to a small effective hydraulic diameter of the gasflow and consequently to flames with a short reaction zone, a low residence time in the reaction zone and a low total NO formation. Calculations were made to test this hypothesis. Moreover several additional calculations have been made using central gas burners (CGB) in order to investigate the influence of scaling up of the furnace on NO formation.

#### 3.3.1. CAB calculation and measurement.

The CAB calculations concerned a CAB, burning Groningen natural gas with a capacity of .75 MW, at an overall equivalence ratio of .98, and producing a flame essentially attached to the burners. The main dimensions of the system are: primary air stream, diameter 95 mm, width of annular gas slot 6 mm, furnace diameter 0.6 m, length of (horizontal) furnace 5 m. The walls of the furnace are cooled to about 350 K by means of water.

Gravity effects have been neglected because no influence of buoyancy was detected in the experiments. The initial velocity profiles are not known, but aerodynamic resistances (wire mesh in the gas flow, perforated plate in the air flow) are applied to make them uniform. The furnace walls (estimated emissivity = .8) are water cooled and have been assumed to be smooth; the short chimney at the end of the furnace is replaced by sudden enlargement, for reasons of simplicity.

Following GÜNTHER [32] we define the radiative heat transfer in the furnace with the dimensionless

THRING number:  $Th = \frac{\dot{m} h_c}{S \dot{q}_{rc}}$ , where  $\dot{m}$  is the mass flow,  $h_c$  the specific enthalpy for a stoichiometric

natural gas-air mixture, ( $h_c = 2.8$  MJ/kg),  $S$  is the furnace wall surface and  $\dot{q}_{rc}$  the radiative heat flux calculated with the adiabatic flame temperature of natural gas with a emissivity  $a = .4$  ( $\dot{q}_{rc} = .53$  MW/m<sup>2</sup>). The THRING number is often referred to as the reduced firing density; in our case its value amounts to .3.

For the convective heat transfer and for similarity in the gas flow the CRAVA-CURTET number, defined before, and the burner Reynolds number have been applied as similarity parameters, following KANG e.a. [29]. The numerical values are  $Ct = .18$  and  $Re_p = 2.10^5$  ( $Re_p$  refers to the air flow).

The axial temperature and NO mass fraction profiles together with experimental data are presented in figure 13. The substantial difference between the predicted and measured temperature profiles thereby suggesting an unrealistic forward position of the flame. The two combustion models as such lead to limited differences in the predicted temperatures.

It has often be observed that the pyrometer tends to stabilize the flames, presumably due to the 2.5 cm diameter suction pyrometer used for the temperature measurements.

As for the calculated NO mass fraction profiles agreement results between the results of the partial equilibrium model and the measured  $Y_{NO}$  profile is striking, apart from the axial shift mentioned

earlier. The calculated thermal NO contribution is very small ( $> 1$  ppm for the partial equilibrium, and  $< 3$  ppm for the equilibrium model; consequently nearly all NO predicted is due to 'prompt NO'). The differences in the temperature profiles are reflected in the predicted heat flux profiles at the furnace wall (see figure 14), most notably downstream of  $x/D_f = 3$ . However, for both combustion

models the total local heat flux corresponds fairly well with the measured values (determined with an accuracy of  $\pm 3\%$  from the heat balance of the water, cooling the distinct wall segments).

The results of separate measurements of the radiative heat flux, using an ellipsoidal pyrometer and the predicted radiation are depicted in the lower curves of figure 14. The discrepancy between measured and calculated radiative heat fluxes is not clear and is possibly due to an incorrect angle dependent sensitivity of the used pyrometer.

The large contribution of the convective heat transfer to the total heat transfer particularly near the maximum, should be noted.

The double peaked value of the total heat flux found with the partial equilibrium model is due to two peaks in the convective heat transfer curve. From these and other calculated data it appears that the dip in the heat transfer curve as  $x/D_f = 3$  occurs at some distance beyond the end of the recirculation zone. This position corresponds well with the end of the recirculation zones that was calculated to be situated between  $x/D_f = 2 - 3$  for isothermal flow and  $Ct = .212 - .675$  (figure 5).

The first peak can be traced back near the point of reattachment to a high value of the turbulent kinetic energy. This higher turbulent level leads to heat transport to the wall. The second peak is due to the maximum in the temperature of the gas near the wall, occurring some distance beyond the reattachment point in this case.

Further support of the reliability of our predictions of the excessive heat transfer around the recirculation zone was obtained from experimental data of KRALL e.a. [30]. Calculations for a geometry similar to his experimental setup and at  $Ct$  number within the experimental range (.25 - .66) resulted in the same sharp increase in heat transfer in the recirculation zone as observed [31]. The quantitative agreement between Krall's measurements and our predictions was satisfactory, indicating that the calculation method is well founded.

### 3.3.2. Influence of furnace size on NO formation and flame length.

Because the prediction method of NO and the wall heat transfer has been shown to give realistic results for smaller furnaces, some scouting calculations were made to test its applicability for larger furnaces dimensions and furnace loads. The calculations were restricted to the vertical cylinder symmetrical open ended furnace.

The similarity parameters were kept constant at  $Ct = .18$  and  $Th = 3$ ; these values being chosen because of their frequent occurrence in real furnaces.

As for the burners the primary gas flow diameters were taken at .03, .09 and .27 m, and the burner loads at 1.9, 17.1 and 155 MW. The overall equivalence ratio was taken equal to .96 and the gas velocity equal to 75 m/s in all three cases. The corresponding burner  $Re$  numbers are  $2.10^5$ ,  $18.10^5$  and  $160.10^5$ . The velocity in the annular streams of air surrounding the cylindrical gas stream was set at 25 m/s.

The predicted mean 'thermal NO', 'prompt NO' and 'total NO', concentrations at the furnace outlet are given in figure 15. The furnace size is characterized by the parameter  $D_h/\bar{u}_b$  ( $D_h$  = hydraulic diameter of gas flow,  $\bar{u}_b$  = mean flow velocity at the burner); for the geometrically similar furnaces considered this parameter is proportional to the residence times of the gas in the flame zone and in the furnace as a whole. Relating the parameter to the chemical reaction rate yields the earlier defined Damköhler number.

From the results it can be concluded that for the burner and furnace dimensions investigated, most of the NO formed is 'prompt NO'. However,  $D_h/\bar{u}_b > 1.5 \cdot 10^{-2}$ , which corresponds to  $Da > 200$ , the 'thermal NO' formation becomes dominant.

The calculated flame length, being defined as the distance between the burner mouth and the point where the maximum temperature is reached and nearly all fuel has been burned, is shown in figure 16 and compared with several data obtained from the scarce literature.

The flame length for large vertical enclosed diffusion flames might become a more important parameter in the future due to the tendency to build more furnaces using bottom fired large diffusion flames. With an ensemble of these slender well defined flames it is easier to exploit the available furnace volume optimally, than with strongly swirling flames [34].

It is clear from figure 16 that the calculations show the same trend as the measurements quoted by GÜNTHER [32] and NIEPENBURG [34]. Yet the predicted flame lengths are considerably larger; this may be due to the fact that weak swirl is often applied in the measured practical flames. The calculated data points can be matched with the correlation:

$$L = .21(\dot{Q})^{0.5}, \text{ where } L \text{ stands for the flame lengths (in m) and } \dot{Q} \text{ is the burner load (in MW).}$$

### CONCLUSIONS

From the presented comparisons between measurements and calculations, a number of pertinent conclusions can be drawn.

1. Out of the presented combustion models for natural gas diffusion flames, the so-called partial equilibrium composition model gives the best general agreement between theoretical and experimental results.
2. The equilibrium composition model might be satisfying for the prediction of the mean flow and temperature field, but it predicts too large temperature fluctuations and too high instantaneous temperatures; consequently it is less suitable for estimating the temperature dependent NO formation.
3. The frequently used frozen composition model clearly leads to erroneous results.
4. It can be expected that the partial equilibrium conditions depend on the turbulent stretch in the flow, but measurements in natural gas flames with different stretch levels [15], characterized by  $Da = 2-200$ , reveal that in practical diffusion flames the influence of stretch is very small. Because of the high hydrocarbon content of Groningen natural gas, it can be anticipated that these conclusions are generally valid for hydrocarbon flames.
5. Further it is found that the thermal NO formation in non-preheated hydrocarbon flames is relatively small, particularly for the small and medium size hydrocarbon flames used in experimental studies. On the contrary the contribution of prompt NO is particularly relevant; its formation is satisfactory modelled in our study.

6. When interpreting NO data in diffusion flames one has to be careful when dealing with lifted flames. In that case the NO mass fraction profiles in the fuel rich region derived from prompt NO formation can be changed completely, due to premixing with air.
7. Taking into account mixture fraction fluctuations, calculations using the k- $\epsilon$ -turbulence model have been made for isothermal furnace flows; the results were found to be in general agreement with experimental data [5, 6]. Subsequent furnace calculations show a very good agreement between measurements and calculations for the NO mass fraction and the total wall heat transfer.
8. Further the calculations lead to the conclusion that in the slender cylindrical furnaces investigated, characterised by  $Th = .3$ ,  $Ct = .18$  and  $Re_b = 210^5$ , the contribution of convective heat transfer dominates in the total wall heat flux particularly in the recirculation zone.
9. The parameter study finally shows that the applied numerical technique is well suited for the prediction of the influence of furnace size and proportions on such quantities as NO formation, flame length and heat transfer. However, further validation of the method is required in this field.

#### ACKNOWLEDGEMENTS

The authors like to acknowledge the cooperative support provided by prof. D.B. Spalding and dr. A.S.C. Ma of Imperial College, London in arranging the basic computer program used in the present calculations and developed by Combustion, Heat and Mass Transfer Ltd.

#### REFERENCES

- 1 OSGERBY, I.T.,  
Literature Review of Turbine Combustor modeling and emissions.  
AIAA journal, 6 (1974), p. 743.
- 2 KHALIL, E.E., SPALDING, D.B. and WHITELAW, J.H.  
The calculation of local flow properties in two-dimensional furnaces.  
Int. J. Heat Mass Transfer, 18 (1975), p. 775.
- 3 HUTCHINSON, D., KHALIL, E.E. and WHITELAW, J.H.  
The calculation of wall heat transfer rate and pollutant formation  
in symmetric furnaces.  
4th Members conf. IFRF, paper I3, Noordwijkerhout, (1976).
- 4 MICHELFELDER, S., BARTELD, H. LOWES, T.M. and PAI, B.R.  
Berechnung der Wärmeflusses und der Temperaturverteilung in  
Verbrennungskammern.  
VDI Berichte 211 (1974), p. 23.
- 5 BECKER, H.A., HOTTEL, H.C. and WILLIAMS, G.C.  
Mixing and flow in ducted turbulent jets.  
9th Int. Symp. on Combustion (1963), p. 7.
- 6 BECKER, H.A., HOTTEL, H.C. and WILLIAMS, G.C.  
Concentration fluctuations in ducted turbulent jets.  
11th Int. Symp. on Combustion (1967), p. 791.
- 7 LAUNDER, B.E. and SPALDING, D.B.  
Mathematical models of turbulence.  
Academic Press (1972) London.
- 8 GOSMAN, A.D. and LOCKWOOD, F.C.  
Incorporation of a flux model for radiation into a finite-difference  
procedure for furnace calculations.  
14th Int. Symp. on Combustion (1972), p. 661.
- 9 LAUNDER, B.E., MORSE, A. RODI, W. and SPALDING, D.B.  
The prediction of free shear flows - a comparison of six turbulence  
models.  
NASA Conf. on Free Shear Flows, Langley (1972).
- 10 KANG, Y.M. and SUZUKI, K.  
Numerical study of confined jets, a prediction of flow pattern and  
turbulence quantities.  
Mem. of the faculty of Engng, Kyoto University, Vol. AL (1978), p. 41.
- 11 LOWES, T.M., BARTELD, H. HEAP, M.P., MICHELFELDER, S. and PAI, B.R.  
The prediction of radiant heat transfer in axi-symmetrical systems.  
IFRF report G02/a/25 (1973), IJmuiden.
- 12 EDWARDS, D.K. and BALAKRISHNAN, A.  
Thermal radiation by combustion gases.  
Int. J. Heat Mass Transfer, 16 (1973), p. 25.
- 13 BRAY, K.N.C. and MOSS, J.B.  
A unified statistical model of the premixed turbulent flame.  
Acta Astronautica 4 (1977), p. 291.

- 14 VAN DUYNENVOORDEN, C.  
Benadering van fysische en chemische grootheden uit rookgassen van Groningen aardgas/lucht mengsels door Chebyshev dubbel polynomen (in Dutch).  
Laboratorium voor Energievoorziening, Rep. VS7703 (1977), Delft.
- 15 PAAUW, Th. T.A.  
Nitrogenoxide formation in turbulent natural gas flames.  
Dissertation, Technical University Delft (to be published in early 1980).
- 16 BECKER, H.A.  
Concentration fluctuations in ducted jet mixing.  
Ph. D. Thesis (1961), Mass. Inst. Techn.
- 17 HABERDA, F.  
Die berechnung turbulenter diffusionsflammen unter berücksichtigung von Konzentrationsschwankungen.  
Ph. D. Thesis (1977), Karlsruhe.
- 18 BULAU, J.R.  
Radical overshoots and dissociation in methane/air flames.  
Journal of Chem. Phys. 62 (1975) 3605.
- 19 EBERIUS, K.H. and JUST, Th.  
NO formation in fuel rich flames, a study of the influence of the hydrocarbon structure.  
Agard Conf. Proc. no. 125 (1973), pp. 16-1.
- 20 LOCKWOOD, F.C. and NAGUIB, A.S.  
The prediction of the fluctuations in the properties of free round jet turbulent diffusion flames.  
Comb. and Flame 24 (1975), p. 109.
- 21 WILLIAMS, F.A.  
Combustion Theory.  
Addison Wesley Publ. (1965), Reading Mass.
- 22 PUN, W.M. and SPALDING, D.B.  
A general computer program for two-dimensional elliptic flows.  
Imperial College, M.E. Dept. Rept. HTS/76/2, (1976).
- 23 PATANKAR, S.V. and SPALDING, D.B.  
Heat and Mass transfer in boundary layers.  
Intertext Books (1970), London.
- 24 SPALDING, D.B.  
Concentration fluctuations in a round turbulent free jet.  
Chem. Engng. Sc. 26 (1971), p. 95.
- 25 TAKAGI, T, OGASAWA, M, FUJII, K. and DAIZO, M.  
A study on nitric oxide formation in turbulent diffusion flames.  
15th Int. Symp. on Combustion (1975), p. 1051.
- 26 VAN WEES, F.G.H.  
Metingen aan de centrale luchtbrander.  
Laboratorium voor Energievoorziening, Rep. VS7403, (1974), Delft.
- 27 VAN STAA, H.  
Private communication.
- 28 THRING, M.W.  
Application of Similarity principles to thermal transport systems.  
Nature 159 (1947), p. 203.
- 29 KANG, Y, SUZUKI, K. and SATO, T.  
Convective heat transfer in an axi-symmetrical confined jet.  
(1979) to be published.
- 30 KRALL, K.M. and SPARROW, E.M.  
Turbulent heat transfer in the separated reattached and redevelopment regions of a circular tube.  
J. Heat Transfer 88 (1966), p. 131.
- 31 SUZUKI, K.  
A numerical study on fluid mechanics and heat transfer in recirculating flows.  
Laboratorium voor Energievoorziening, Rep. EV1011 (1977), Delft.
- 32 GÜNTHER, R.  
Verbrennung und Feuerungen.  
Springer Verlag (1974), Berlin, pp. 284, 414.

- 33 QUAN, V, KIEGEL, J.R., DE VOLO, N.B. and TEIXEIRA, D.P.  
Analytic scaling of flow field and nitric oxide in combustors.  
Comb. Sc. and Techn. 9 (1974), p. 209.
- 34 NIEPENBERG, H.P.  
Entwicklungstendenzen im grossbrennerbau, in Industrieöfen und-  
Feuerungen.  
Ed. K. Giesen, Haus der Technik (1972), p. 28.

#### NOMENCLATURE

$C_{\epsilon_{1,2}}, C_{\epsilon_{1,2}}, C_D$	constants in turbulence model
D	diameter
E	wall function parameter
$E_z$	action energy
f	variable
g	gravitation constant
h	stagnation enthalpy
$h_c$	mixture averaged heat of reaction
K	wall function constant
$k_z$	pre-exponential factor
k	turbulent kinetic energy
L	flame length
M	molecular weight
$\dot{m}$	mass flow
p	pressure
$\dot{Q}$	thermal load
$\dot{q}_r$	radiation wall heat flux
$R_r^k, R_x^k$	radiation heat flux in r and x direction
r	radial distance
r	stoichiometric fuel-oxygen mass ratio
S	furnace wall area
T	temperature
$T_i$	chebyshev polynomial of order i
u	velocity
$v_o^*$	characteristic velocity in Ct
$\bar{v}_f, \bar{v}_o$	averaged velocity over furnace, burner area
$\bar{v}_f^2$	averaged square velocity over furnace area
v	radial velocity
$\dot{w}$	reaction rate
x	axial distance
X	mole fraction
Y	mass fraction
$Y_f$	mixture fraction
$Y_f^2$	square of mixture fraction functions
$\alpha_k$	absorption coefficient
$\epsilon_k$	emission coefficient
$\epsilon$	turbulent kinetic energy dissipation
$\phi$	equivalence ratio
$\mu$	viscosity
$\rho$	density
$\sigma$	Stefan-Boltzmann constant
$\tau_c$	characteristic reaction time

#### SUBSCRIPTS

b	burner
e	effective
f	furnace or duct
fu	fuel
ox	oxidant
i	chemical species
k	gray gas
o	inlet condition
st	stoichiometric
w	wall

#### DIMENSIONLESS NUMBERS

Ct	Craya-Curtet number
Da	Danköehler number
Fr	Froude number
Re	Reynolds number
Th	Thring number
$\sigma$	Prandtl number



TABLE I PHYSICAL QUANTITIES TO BE SUBSTITUTED IN CONSERVATION EQUATION (1)

Quantity	$\phi$	$\rho_\phi$	$\mu_\phi$	$S_\phi$
Mass	1	$\rho$	0	0
Axial momentum	u	$\rho$	$\mu_e$	$\frac{\partial}{\partial x} (\mu_e \frac{\partial u}{\partial x}) + \frac{1}{r} \frac{\partial}{\partial r} (\mu_e r \frac{\partial v}{\partial x}) - \frac{\partial p}{\partial x} + \rho g_x$
Radial momentum	v	$\rho$	$\mu_e$	$\frac{\partial}{\partial x} (\mu_e \frac{\partial u}{\partial r}) + \frac{1}{r} \frac{\partial}{\partial r} (\mu_e r \frac{\partial v}{\partial r}) - 2 \mu_e \frac{v}{r^2} - \frac{\partial p}{\partial r}$
Turbulent kinetic energy	k	$\rho$	$\frac{\mu_e}{\sigma_k}$	$G_{k1} - \rho \epsilon$
Dissipation rate	$\epsilon$	$\rho$	$\frac{\mu_e}{\sigma_\epsilon}$	$\frac{\epsilon}{k} (C_{\epsilon 1} G_{k1} - C_{\epsilon 2} \rho \epsilon)$
Stagnation enthalpy	h	$\rho$	$\frac{\mu_e}{\sigma_h}$	$\sum_k (2 \bar{\alpha}_k (R_x^k + R_y^k) - 4 \sigma_{\epsilon k} T^4)$
Mixture fraction	$Y_f$	$\rho$	$\frac{\mu_e}{\sigma_f}$	0
Mixture fraction fluctuations	$Y_f'$	$\rho$	$\frac{\mu_e}{\sigma_f}$	$C_{f1} G_{f1} - C_{f2} \rho \epsilon_k Y_f'$
NO mass fraction	$Y_{NO}$	$\rho$	$\frac{\mu_e}{\sigma_f}$	$\bar{\rho}_{NO}$
Radial radiant total heat flux gas k	$R_r^k$	0	$\frac{1}{\bar{\alpha}_k + 1/r}$	$-\bar{\alpha}_k R_r^k + \sigma_{\epsilon k} T^4$
Axial radiant sun heat flux gas k	$R_x^k$	0	$\frac{1}{\bar{\alpha}_k}$	$-\bar{\alpha}_k R_x^k + \sigma_{\epsilon k} T^4$

$$G_{k1} = \mu_e (2 ((\frac{\partial u}{\partial x})^2 + (\frac{\partial v}{\partial r})^2 + (\frac{v}{r})^2) + (\frac{\partial u}{\partial r} + \frac{\partial v}{\partial x})^2)$$

$$G_{f1} = \mu_e ((\frac{\partial Y_f}{\partial x})^2 + (\frac{\partial Y_f}{\partial r})^2)$$

TABLE II COMPILATION OF MODEL CONSTANTS

## Fuel constants:

Slochteren natural gas (vol. %) CH<sub>4</sub> - 81.3, N<sub>2</sub> - 14.4, C<sub>2</sub>H<sub>6</sub> - 2.9 + higher hydr.

$$r = 13.07$$

## Turbulence constants:

$$C_{\epsilon 1} = 1.40, C_{\epsilon 2} = 1.92, C_D = .09, C_{f1} = 2.8, C_{f2} = 2.0, K = .40, E = 9.0$$

## Prandtl numbers:

$$\sigma_k = 1.0, \sigma_\epsilon = 1.3, \sigma_\phi = .7$$

TABLE III

Grid location in the case of grid I and II from figure 8.

## Radial grid locations grid I:

r/D = 0.0, 0.25, .50, .75, 1., 1.5, 2.5, 4.0, 5.5, 7.0, 9.0, 11., 13., 17., 21., 25., 29., 33., 37., 41., 44., 47., 49., 50.

## Radial grid locations grid II:

r/D = 0.0, .125, .25, .50, .75, 1.0, 1.25, 1.8, 2.2, 2.7, 3.3, 4.0, 4.8, 5.5, 7.0, 8.4, 10.1, 12.0, 14.4, 17.2, 20.6, 24.7, 29.7, 35.6, 40.6, 45.6, 48.5, 49.5, 50.

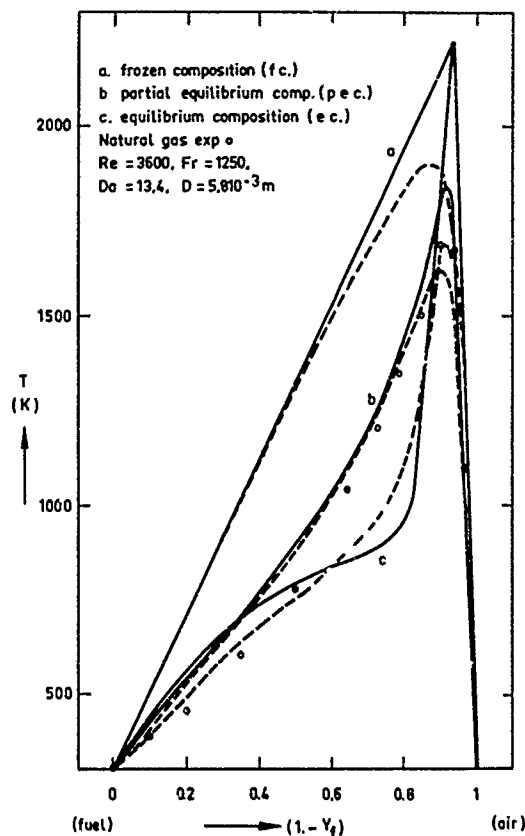


fig. 1a. Theoretical temperature as a function of the mixture fraction for different combustion models and experimental data obtained in a attached diffusion flame (dashed lines give the estimated influence of unmixedness).

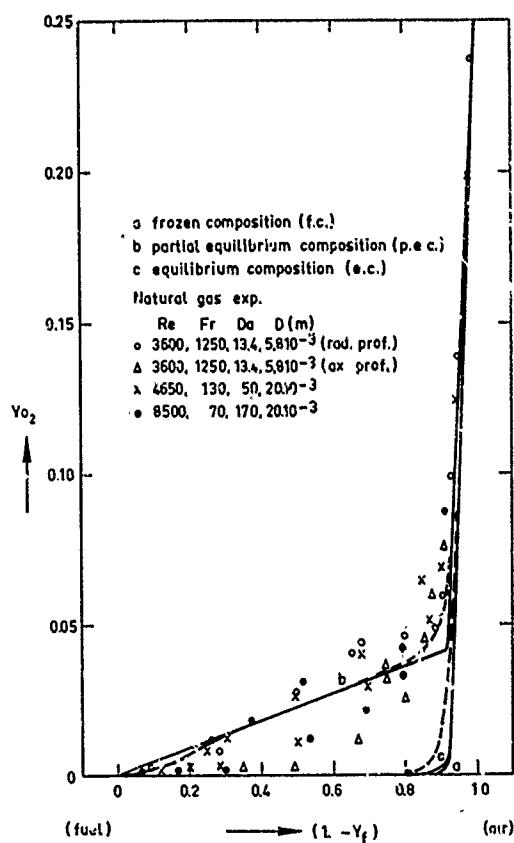


fig. 1b. Theoretical oxygen mass fraction as a function of the mixture fraction for different combustion models and experimental data obtained in attached diffusion flames (dashed lines give the estimated influence of unmixedness).

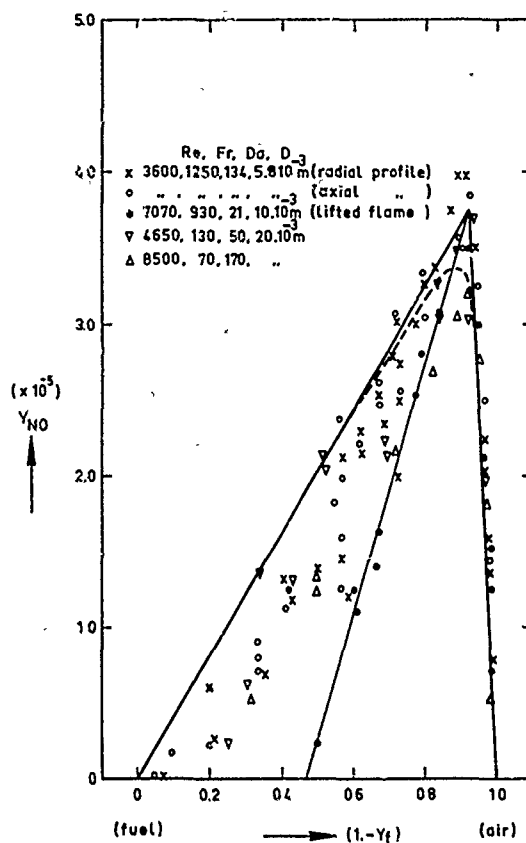


fig. 2. Theoretical prompt NO mass fraction as a function of the mixture fraction for a frozen composition prompt NO chemistry (maximum prompt NO level = 38 ppm) compared with experimental data obtained in diffusion flames. Dashed curve gives the estimated influence of unmixedness.

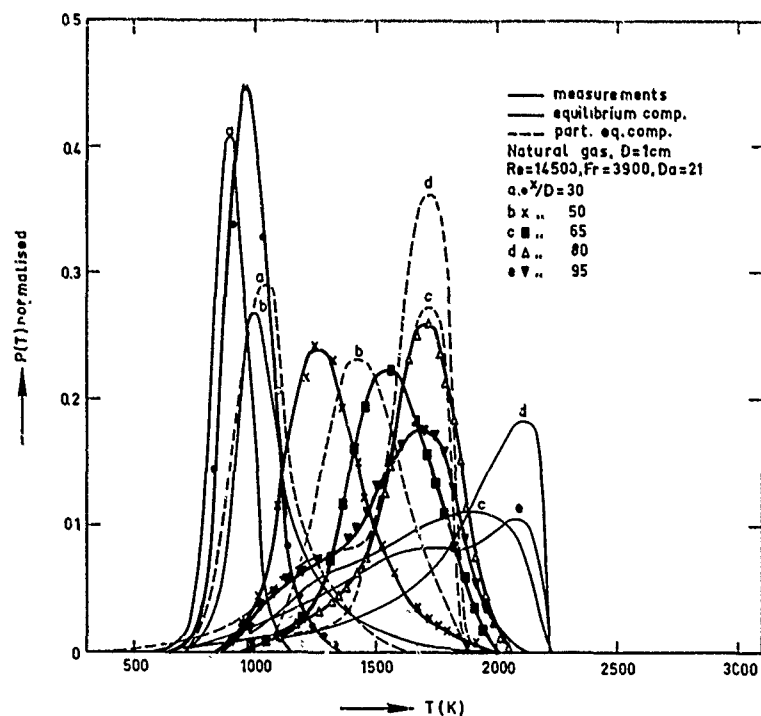


fig. 3. Measured normalised probability density functions for the temperature on the axis of a diffusion flame, compared with calculated P.D.F.'s obtained with different combustion models.

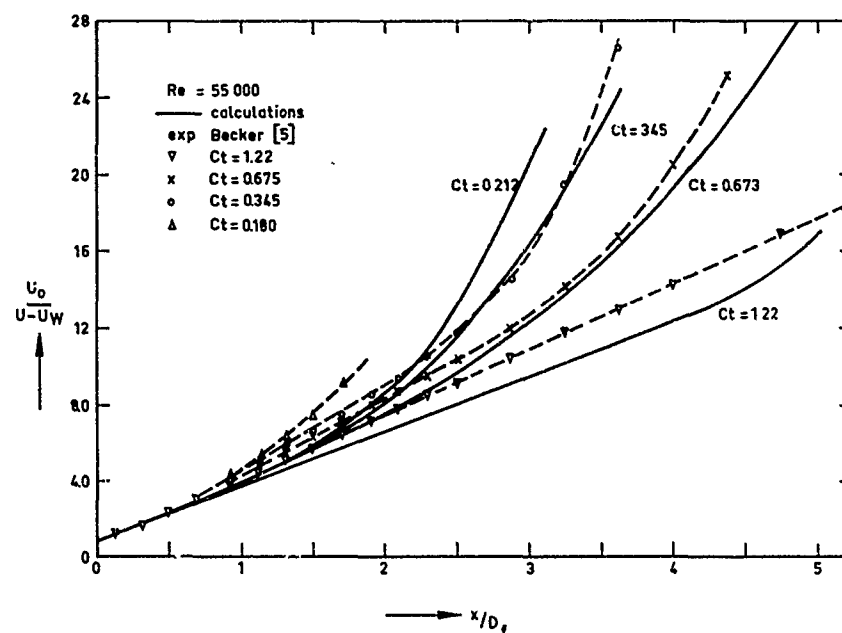


fig. 4. Calculated axial velocity decay in ducted isothermal jet flow compared with measurements.

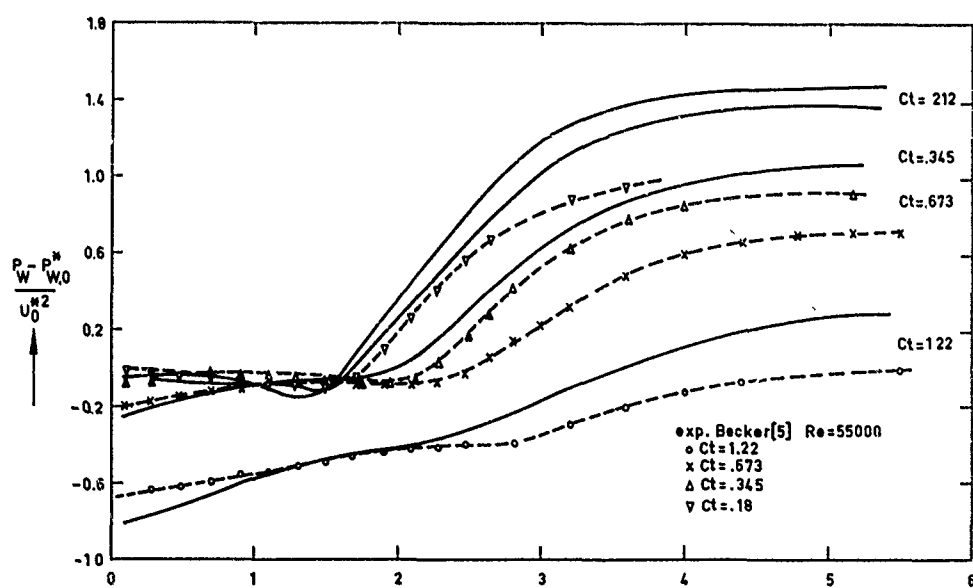


fig. 5. Calculated axial static pressure profiles at the duct wall compared with experiments for isothermal ducted jet flow ( $P_{w,0}^* = P_{w,0} + v_o^{*2}/2$ ).

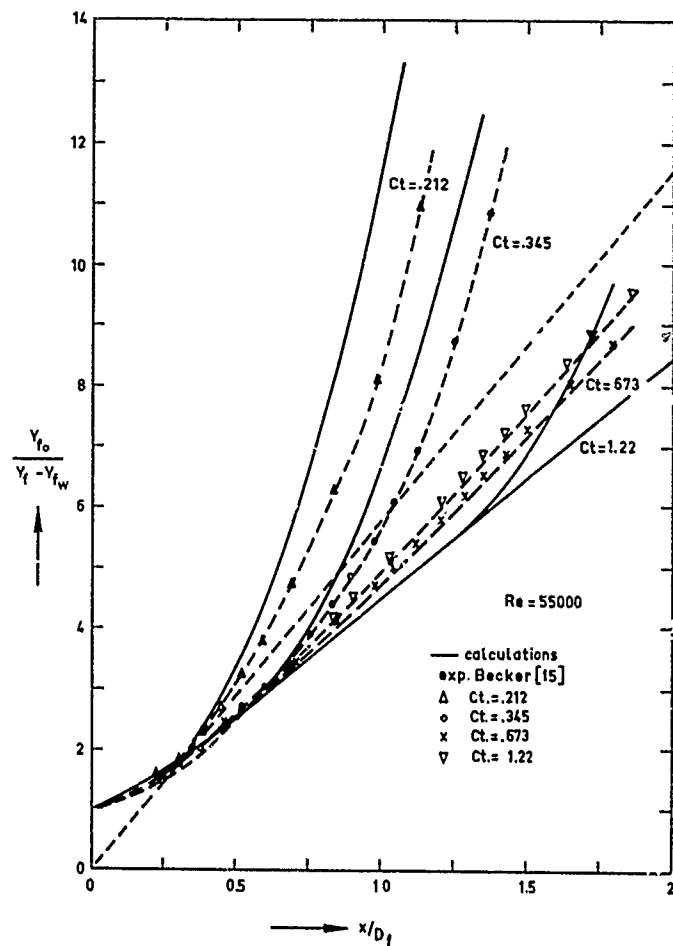


fig. 6. Calculated axial decay of the mixture fraction in ducted isothermal jets compared with measurements.

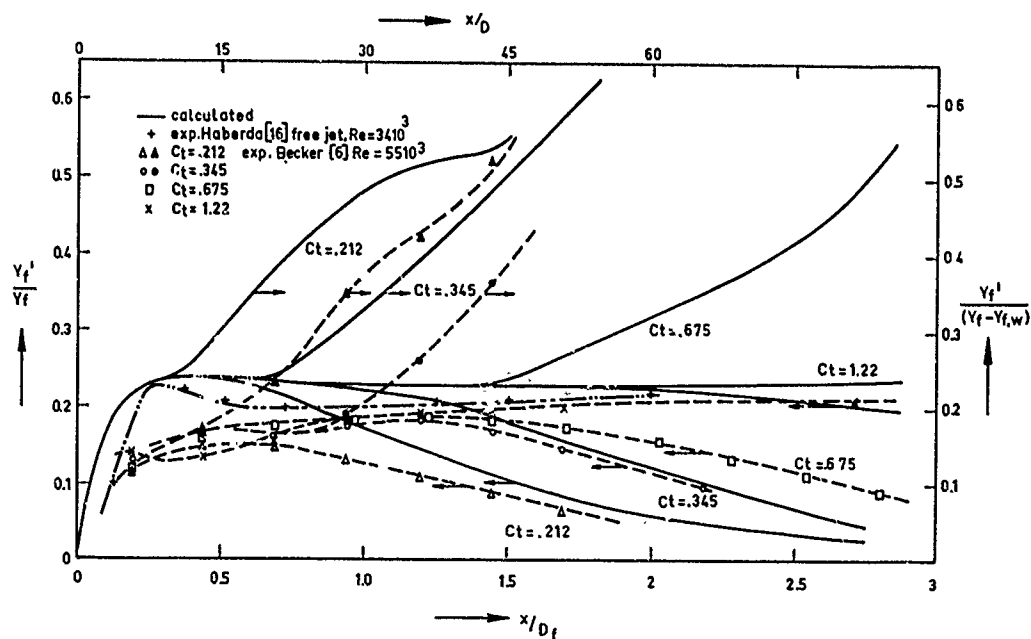


fig. 7. Calculated axial decay of the mixture fraction fluctuations in ducted isothermal jets ( $x/D_f$ ) and in free jets ( $x/D$ ), compared with measurements.

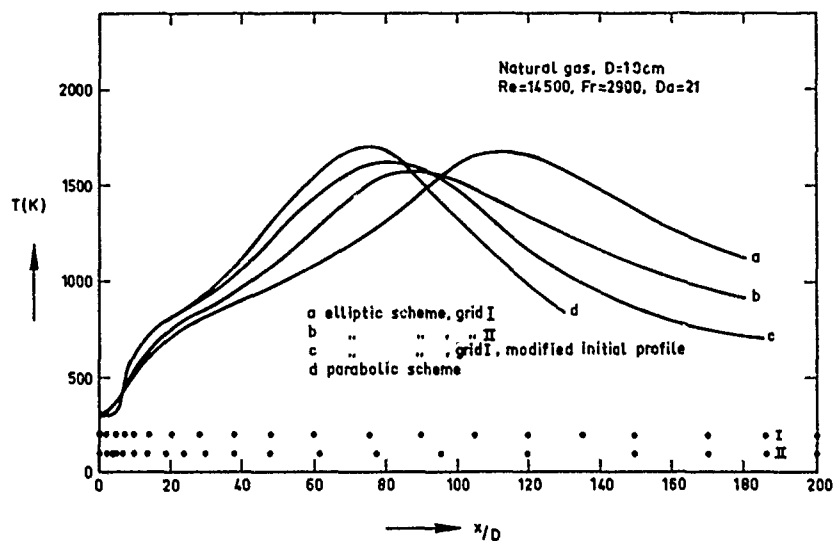


fig. 8. Calculated axial temperature profiles for a free turbulent diffusion flame using both a parabolic flow and an elliptic flow finite difference scheme. Also the influence of modifications in initial profile and grid arrangement are given (axial grid locations represented by dots and radial grid locations as given in table III).

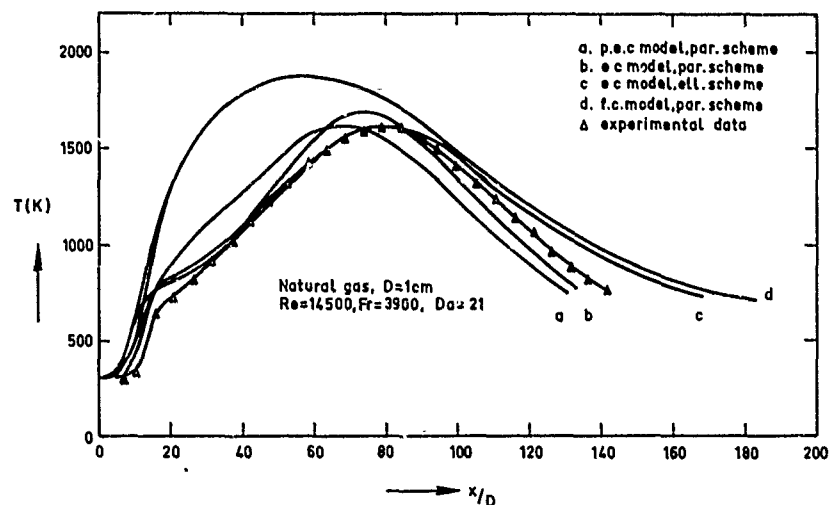


fig. 9. Calculated axial temperature profiles for a free jet diffusion flame using a frozen composition, equilibrium or partial equilibrium composition combustion model, compared with measurements.

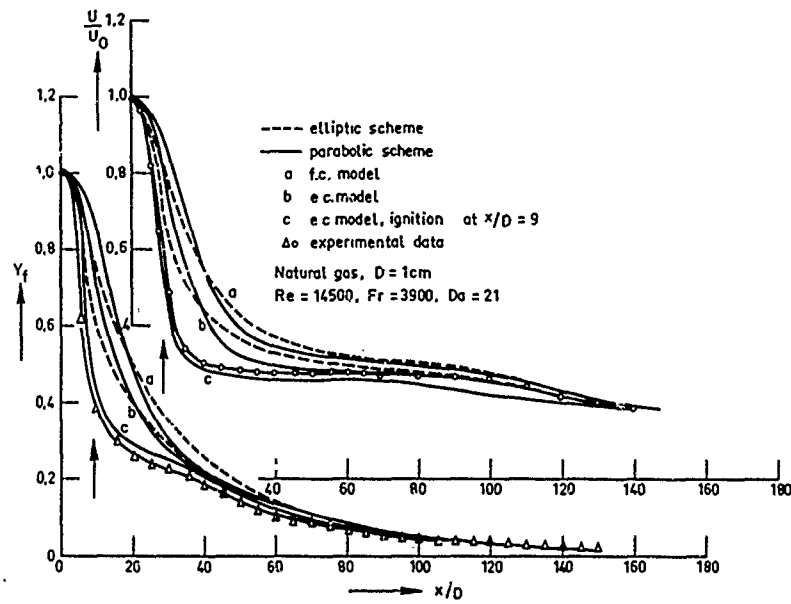


fig. 10. Calculated axial velocity and mixture fraction profiles for a free jet diffusion flame. (The arrow indicates the calculated and measured ignition point).

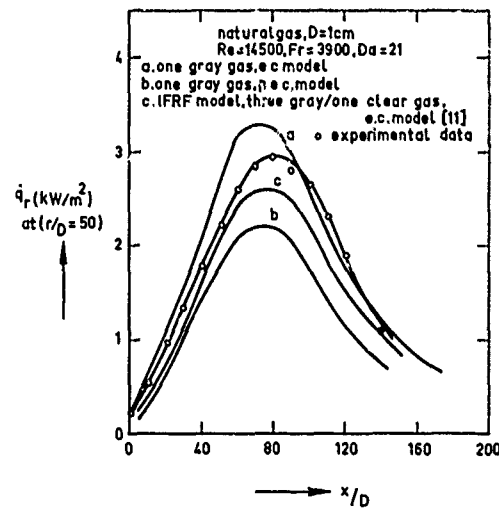


fig. 11. Calculated radial radiation fluxes at  $r/D = 50$ , for turbulent diffusion flames and various combustion and radiation models, compared with experimental data.

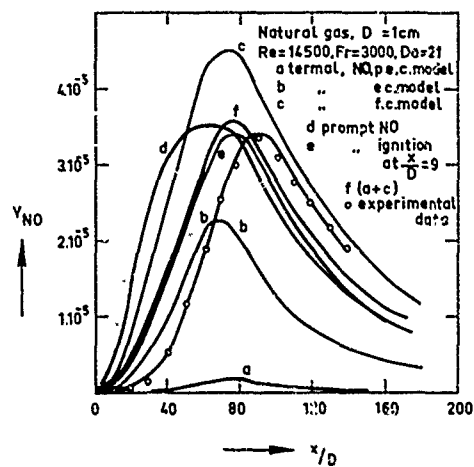
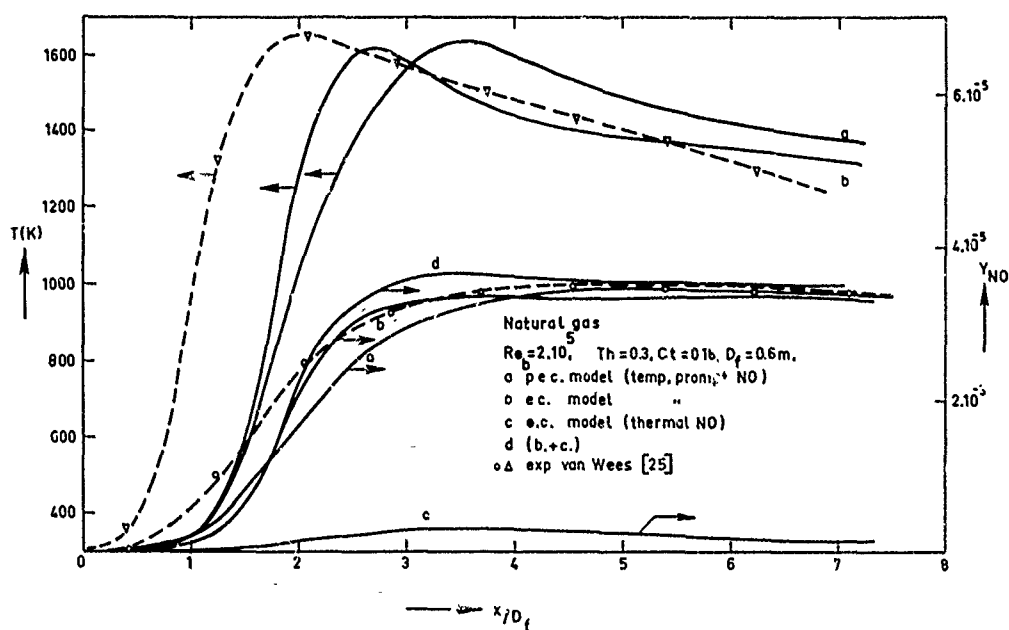


fig. 12. Calculated and measured axial nitrogenoxide profiles of the turbulent diffusion flame in case of thermal and prompt NO formation.



i.g. 13. Measured and calculated axial nitrogenoxide and temperature profiles in an axisymmetrical natural gas fired furnace, equipped with a central-air burner.



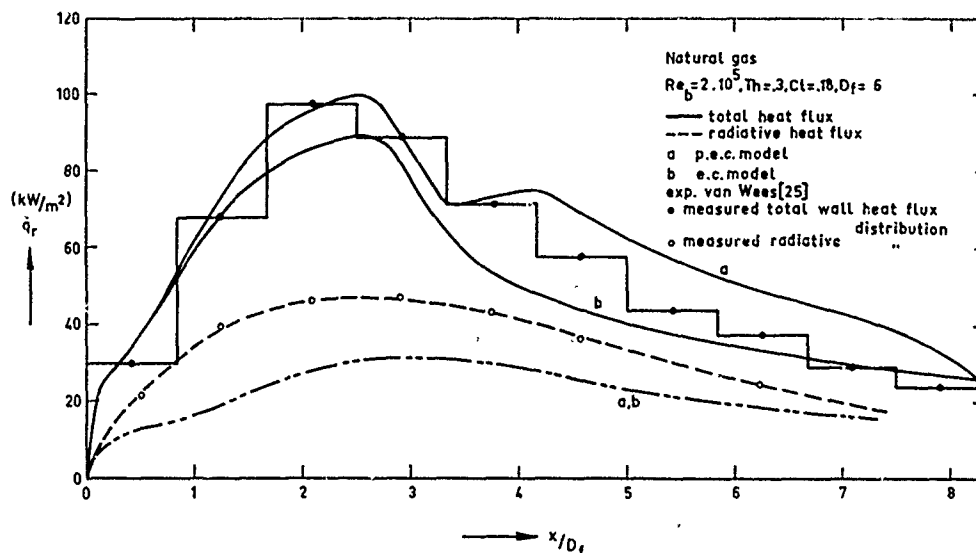


fig. 14. Measured and calculated radiative and total wall heat flux distribution at the furnace wall of an axisymmetrical natural gas fired furnace (central-air burner).

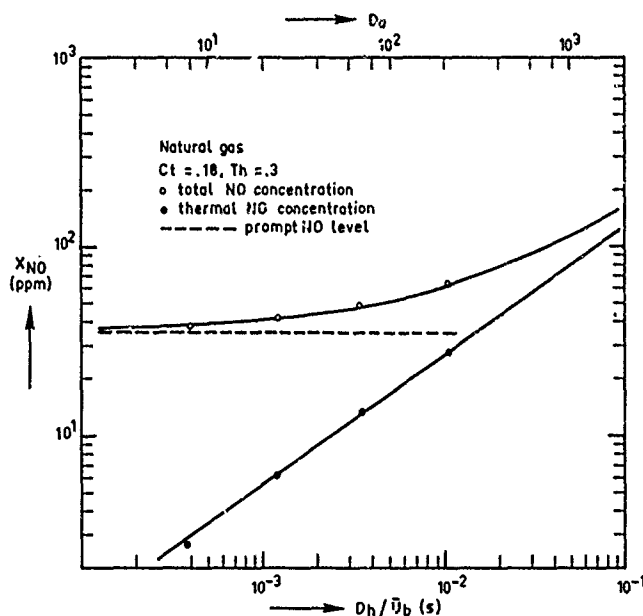


fig. 15. Calculated influence of (cylindrical) furnace size on prompt NO, thermal NO and total NO concentration. Furnace dimensions proportional to burner diameter. Furnace size characterised by time parameter  $D_h/\bar{u}_b$  ( $D_h$  = hydraulic diameter of entering gas flow). The point with lowest thermal NO concentration represents the central-air burner calculation.

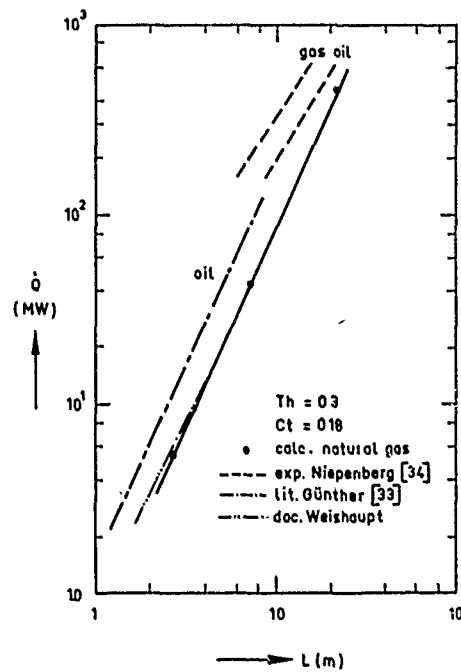


fig. 16. Correlation between burner load and flame length for vertical, cylindrical, natural gas fired furnaces, and some experimental data.

## DISCUSSION

H.Eickhoff, Ge

Did you measure and predict CO-concentrations also? If so, how well do they agree and especially what is your highest predicted CO-concentration?

Author's Reply

The maximum CO mass-fraction predicted with the partial equilibrium composition model is about 3%, a value that compares well with the measured maximum CO mass-fractions. CO mass-fractions calculated with the frozen composition model are very low, while CO mass-fractions calculated with the equilibrium model can reach much too high values, up to 10%.

N.Peters, Ge

Let me first congratulate you for this well documented piece of work. Also I would like to comment on the relatively large oxygen values that you find on the fuel rich side of the flame. I would think that this is rather due to turbulence effects than to quenching. In a comment to Janicko's and Kollmann's paper it was noted that the fuel rich shift of NO-production could be attributed to turbulence. I believe that a similar reasoning could be applied to the oxygen shift.

Author's Reply

In the first instance we have also tried to explain the too high oxygen mass-fractions on the fuel rich side with turbulence smearing out, or better unmixedness. When we take into account turbulent intensities of the mixture fraction at the fuel rich side, reaching a value of about 45% as calculated with the finite difference technique, we also obtain much too low values of the oxygen mass-fraction, as depicted in Figure 1b by the dashed line above c. Also we found high CO and H<sub>2</sub> mass-fractions up to respectively 3% and .3% mainly in the fuel rich side, which indicates that there, incomplete reaction has to take place. The chosen partial equilibrium model predicts well also these mass-fractions.

M.Nina, Po

Could you give some details on how the calculation scheme accommodates for the height of the lifted flame base.

Author's Reply

As noted in the paper the height of the lifted flame base chosen in Figure 10 is deduced from experiments. However a procedure has been worked out and presented before<sup>1</sup> to calculate this height in the calculation scheme. With this procedure we were able to reproduce the measured values accurately.

1. Paauw, Th.T.A.      *Use of the Well Stirred Reactor Concept for the Prediction of Flame Stabilization,*  
     Bakker, R.      4th Members Conference, IFRR, Paper 15, Noordwykerhout (1976).

MODELISATION MATHÉMATIQUE DU FONCTIONNEMENT  
DES CHAUDIÈRES DE CHAUFFAGE

E. PERTHUIS, Ingénieur Principal "Techniques d'Applications Energétiques"  
INSTITUT FRANCAIS DU PETROLE, 1 et 4 avenue de Bois Préau, 92506 RUEIL MALMAISON, France

Résumé

Le modèle mathématique présenté ici a pour but de décrire les phénomènes régissant le fonctionnement d'une chaudière, et d'étudier leur évolution en fonction des paramètres pratiques d'exploitation.

On peut simuler le fonctionnement d'un appareil donné opérant en régime continu ou discontinu.

Le calcul permet d'estimer l'influence qu'auront, sur les performances de la chaudière, des paramètres tels que : qualité du calorifugeage, fraction de charge, réglages du brûleur, réglage du différentiel de l'aquastat.... On peut également prévoir l'ordre de grandeur de la consommation d'entretien, caractéristique particulièrement difficile à déterminer sur plate-forme d'essais.

# SYMBOLES GENERAUX

A	aire
a	épaisseur d'une paroi
CW	chaleur spécifique du fluide caloporteur
EXC (ou e)	excès d'air
H	coefficient de transfert
h	coefficient de convection
k	coefficient de conductivité thermique
P <sub>i</sub>	puissance calorifique au brûleur
P <sub>u</sub>	puissance utile de la chaudière
P <sub>f</sub>	pertes par les fumées
P <sub>p</sub>	pertes par les parois
p <sub>p</sub>	pression
Q (ou DQ)	débit calorifique
T (ou t)	température absolue (ou Celcius)
T <sub>ad</sub>	température adiabatique de flamme
V	volume
WE, WF	masses en eau échangeur, foyer
ΔH	variation d'enthalpie
ε	facteur émissif
η	rendement
σ	constante de Stephan-Boltzmann

## Indices

c	régime continu
d	régime discontinu (cyclique)
F	foyer
f	fumées évacuées

## INTRODUCTION

En France, la consommation des produits pétroliers destinés au chauffage domestique et à la production de l'eau chaude sanitaire est de l'ordre de 21 MTEP. C'est un secteur où de substantielles économies d'énergie peuvent être obtenues tant par l'agencement des bâtiments que par le choix judicieux et l'exploitation optimale des générateurs de chaleur.

La très grande majorité des installations fonctionnent en régime intermittent dit "tout ou rien". La puissance nominale de la chaudière étant calculée pour répondre aux besoins des périodes les plus froides, il en résulte que sur une saison de chauffe (correspondant en moyenne à 220 jours/an), l'appareil peut n'avoir fonctionné qu'entre 20 et 30 % du temps. Or, pendant les périodes d'arrêt, l'eau de chauffage est maintenue en température, ce qui provoque des pertes paroiétales relativement plus importantes dans les périodes de mi-saison que dans les périodes de fort chauffage. Il en résulte que le rendement annuel d'exploitation du générateur sera d'autant meilleur que l'écart entre sa puissance nominale et les besoins thermiques réels sera faible, et que les pertes par les parois seront réduites.

Ceci revêt une importance particulière dans le cas des maisons individuelles : des études entreprises par les sociétés pétrolières avant la crise de 1973 avaient déjà montré que les chaudières en service étaient en général très nettement surpuissantes par rapport aux besoins, et que cette surpuissance provoquait une dégradation des rendements d'exploitation.

Parmi les formes d'action envisagées depuis lors, pour promouvoir l'amélioration des installations de petite puissance alimentées au Fuel-Oil Domestique, la profession décida entre autres choses d'étudier le fonctionnement des unités de chauffage non plus en régime permanent bien stabilisé comme il est procédé au cours des essais normalisés, mais dans des conditions aussi voisines que possible de celles effectivement rencontrées chez les usagers.

Dans le cadre de l'Institut Français du Pétrole, une étude coopérative coordonnée par l'Union des Chambres Syndicales de l'Industrie du Pétrole et regroupant les principales Sociétés Pétrolières, fut entreprise en 1973-74 avec les objectifs suivants :

- 1/ Etudier sur un certain nombre de pavillons les besoins réels en chauffage et les consommations.
- 2/ Procéder à des essais sur plateformes de chaudières de petite puissance, représentatives du parc existant.
- 3/ Dégager les techniques permettant de réduire les sur-consommations engendrées par le fonctionnement à charge partielle.
- 4/ Etablir un modèle mathématique calé à partir des essais effectués en laboratoire, et simulant le fonctionnement des chaudières. Ce modèle devait être un instrument de travail mis à la disposition des constructeurs pour leur permettre une mise au point rapide de leurs fabrications, en éliminant un certain nombre d'essais longs, fastidieux et onéreux.

Les résultats de cette Etude coopérative ont été publiés par ailleurs [1], [2].

L'objet de la présente communication est d'exposer les principes du modèle mis au point à I.F.P., et d'illustrer son emploi par quelques exemples caractéristiques.

Rappelons que si de nombreuses études concernant la modélisation des générateurs de chaleur ont été effectuées dans le domaine du chauffage industriel, très peu ont été consacrées au domaine du chauffage domestique. Les quelques travaux disponibles dans la gamme des puissances s'échelonnant entre 15 et quelques centaines de kW, concernent essentiellement l'étude expérimentale et la simulation mathématique des transferts de chaleur dans des chambres de combustion à parois froides pour des fonctionnements continus stabilisés [3], [4].

## I - PRÉSENTATION DU MODÈLE

I.1. Objet du modèle et structure d'ensemble

Le modèle a pour but de décrire les phénomènes régissant le fonctionnement d'une chaudière, et d'étudier leur évolution en fonction de différents paramètres physiques intéressant la conception et l'exploitation du générateur tels que : réglage du brûleur, état d'isolation des parois externes, réglage de l'aquastat...

Dans la version présentée ici, ce modèle est destiné aux chaudières de chauffage à eau chaude de petite puissance alimentées au fuel-oil domestique ou au gaz naturel.

Il comprend deux parties essentielles, permettant de simuler respectivement le fonctionnement d'un appareil donné en régime continu et en régime discontinu. Dans son principe, le modèle est préalablement "calé" sur un point de fonctionnement expérimental obtenu au banc d'essais ou sur site en régime continu. A partir de ce calage initial, on peut alors estimer par le calcul l'influence qu'auront -sur les performances de la chaudière- la qualité du calorifugeage, la charge, l'excès d'air, le réglage de l'aquastat....

Ecrit en FORTRAN IV, la simulation comporte trois programmes distincts nommés CALAGE, CONTIN et SIMULCH. Les deux premiers se rapportent au fonctionnement continu, le dernier au fonctionnement discontinu d'une chaudière.

I.2. Simulation du fonctionnement continuI.2.1. Hypothèses de base

La chaudière est schématisée sur la figure 1. Elle est assimilée à deux éléments distincts : le foyer et l'échangeur.

L'eau rentre par le foyer à TE et sort par l'échangeur à TS, sous le débit massique QW.

Dans chacun de ces deux éléments, les gaz de combustion ont des propriétés homogènes et une température uniforme caractérisée par TGF dans le foyer et TGE dans l'échangeur. Néanmoins, les températures de "transfert" Tech (sortie foyer) et Tf (sortie chaudière) peuvent être différentes des températures "effectives" TGF et TGE.

Dans le foyer, les transferts entre gaz et parois s'opèrent par rayonnement et convection. S'il y a un briquetage, celui-ci est traité comme un mur adiabatique retransmettant le rayonnement incident par diffusion-réémission.

Dans l'échangeur, les transferts thermiques s'opèrent uniquement par convection. On considère que cet élément se comporte comme un échangeur "méthodique" gaz-eau.

Les parois de la chaudière se partagent entre surfaces humides et surfaces sèches. Suivant la nature des fluides présents de part et d'autre d'un élément de paroi, et suivant l'emplacement de ce dernier, on distingue les 6 cas ci-après :

Parois humides	{	1 - paroi type gaz-eau échangeur (GEE)
		2 -   gaz-eau foyer (GEF)
		3 -   eau-air échangeur (EAE)
		4 -   eau-air foyer (EAF)
Parois sèches	{	5 - paroi type gaz-air échangeur (GAE)
		6 -   gaz-air foyer (GAF)

Les parois externes en contact avec l'air ambiant peuvent être ou non munies d'un calorifugeage.

Les flux de chaleur  $\dot{Q}$  et les coefficients d'échange  $H$  correspondant à ces situations sont symbolisés sur la figure 2.

### 1.2.2. Transferts thermiques dans le foyer.

Le foyer est traité suivant la méthode dite du "foyer isotherme", dont la théorie est due à HOTTEL [5].

#### a/ Bilan énergétique du foyer

La puissance calorifique  $\dot{Q}_F$  transmise à la surface de captation  $A_1$  s'exprime sous deux formes traduisant respectivement :

- le bilan calorifique des gaz de combustion,

$$\dot{Q}_F = P_1 - [\Delta H_g]_{T_0}^{T_{ech}} \quad (1)$$

- le bilan des transferts par rayonnement et convection

$$\dot{Q}_F = \overline{GS}_1 \cdot \sigma \cdot (T_{GF}^4 - T_1^4) + A_1 h_1 (T_{GF} - T_1) \quad (2)$$

Le terme  $\overline{GS}_1$  caractérise une "aire équivalente" d'échanges par rayonnement, dont la valeur est calculée à partir de données géométriques propres au foyer (surface de captation  $A_1$ , surface réfractaire  $A_r$ , facteur d'angle  $F_{r1}$  entre  $A_r$  et  $A_1$ ), des facteurs émissifs des gaz  $\epsilon_g$  et de la surface de captation  $\epsilon_1$ .

On a, pour un foyer à 2 zones de surfaces  $A_1$  et  $A_r$  :

$$\frac{1}{\overline{GS}_1} = \frac{1}{(\overline{GS}_1)_N} + \frac{1 - \epsilon_1}{A_1 \epsilon_1} \quad (3)$$

$$\text{avec : } (\overline{GS}_1)_N = \epsilon_g \cdot A_1 \left[ 1 + \frac{A_r/A_1}{1 + \frac{\epsilon_g}{(1 - \epsilon_g) F_{r1}}} \right]$$

Pour décrire numériquement le facteur émissif  $\epsilon_g$ , on se base sur les travaux de JOHNSON et BEÉR [6] effectués à la Fondation de Recherches Internationales sur les flammes (FRIF).

La formulation repose sur la fait qu'on représente le facteur émissif  $\epsilon_g$  du milieu gazeux "réel" comme étant la somme pondérée des facteurs émissifs  $\epsilon_{g,n}$  de  $n$  composants gazeux fictifs "gris" rayonnant sous l'épaisseur caractéristique  $L$ . Avec les auteurs, on adopte ici  $n = 3$ , et on pose :

$$\epsilon_g = \sum_{n=1}^3 a_{g,n} [1 - \exp. (-K_n L)] \quad (4)$$

Le facteur de pondération  $a_{g,n}$  dépend de la température effective des gaz foyer TGF par une relation de la forme :

$$a_{g,n} = b_{1,n} + b_{2,n} \cdot TGF$$

Le coefficient d'extinction  $K_n$  est la somme des coefficients relatifs à la suie et aux "gaz clairs"  $CO_2$  et  $H_2O$ . La valeur est calculable à partir de la pression partielle du mélange ( $CO_2 + H_2O$ ) connue par l'excès d'air, et de la concentration moyenne en particules de suie des gaz foyer, qu'il faut estimer d'après l'expérience acquise sur les flammes de diffusion.

Toutes les constantes numériques permettant d'entrer dans (4) sont tirées de la référence [6], suivant la nature du combustible (produit pétrolier liquide ou gaz naturel riche en méthane).

Quant à l'épaisseur caractéristique de rayonnement  $L$ , elle est définie d'après la relation de HOTTEL

$$L = 3,5 \cdot \frac{V_F}{A_F}$$

Le coefficient de convection  $h_1$  à introduire dans (2) ne peut s'obtenir pratiquement que par l'expérience. En nous basant sur des travaux effectués antérieurement à l'I.F.P. sur des foyers expérimentaux [7], on a pu établir la relation empirique :

$$h_1 (W/m^2 \cdot K) = 25,6 \left[ 1 - \exp. (-QS/1000) \right] \quad (5)$$

$QS$  étant une vitesse massique spécifique ( $kg/h \cdot m^2$ ) des gaz dans le foyer.

Pour tenir compte de l'évolution du coefficient de convection  $h_1$  avec la température, on a utilisé les travaux de GANAPATHY [8], et introduit dans (5) un terme correctif tel que l'expression finale de  $h_1$

devienne :

$$h_1 = 26,4 \left[ 1 - \exp. (-QS/1000) \right] \left[ 1 - \exp. (-2,6 \cdot \frac{TGF}{1000}) \right] \quad (6)$$

La résolution simultanée des équations (1), (2)... (6) permet d'obtenir :

- la puissance calorifique transmise dans le foyer  $\dot{Q}_F$ , donc le rendement de ce dernier  $\eta_F = \dot{Q}_F / P_1$  ;
- les parts respectives du rayonnement et de la convection ;
- la température effective des gaz foyer TGF, mais à condition que soit connue la température  $T_{ech}$  des gaz quittant le foyer.

C'est cette dernière valeur expérimentale qu'il faut nécessairement fournir pour "caler" préalablement le modèle mathématique sur l'expérience. Si la température  $T_{ech}$  n'a pu être mesurée, on pourra néanmoins poser à titre d'approximation :

$$T_{ech} = TGF - \Delta,$$

$\Delta$  étant généralement comprise entre 150 et 200°C.

#### b/ Evolution du rendement de foyer

En dehors des conditions d'exploitation de la chaudière qui ont servi au calage du modèle, il est nécessaire de savoir estimer les nouvelles performances du foyer.

A cet effet, le calcul du rendement des transferts gaz-parois  $\eta_F$  en fonction des paramètres de réglage du brûleur s'effectue au moyen de la relation de corrélation de type universel proposée par HOTTEL [5] :

$$\eta'_F D' + \tau^4 = (1 - \eta'_F + \Delta')^4 \quad (7)$$

avec  $\eta'_F = \eta_F \cdot \frac{T_{ad} - T_o}{T_{ad}}$  (rendement réduit)

$$D' = \frac{P_1}{\mathcal{A} T_{ad}^3 (T_{ad} - T_o)} \quad (\text{densité de feu réduite})$$

$$\tau = \frac{T_1}{T_{ad}} \quad (\text{température de paroi réduite})$$

$$\Delta' = \frac{\Delta}{T_{ad}} \quad (\text{écart réduit des températures des gaz foyer, avec la même valeur de } \Delta \text{ que celle du calage}).$$

La température adiabatique de combustion  $T_{ad}$  se calcule simplement à partir de l'excès d'air, du pouvoir calorifique du combustible et de tables enthalpiques sans tenir compte des dissociations, ce qui est ici plausible du fait des excès d'air pratiqués dans les chaudières de chauffage domestique (supérieurs à 15-20 %).  $\mathcal{A}$  est une "aire équivalente d'échange", calculable à partir des grandeurs  $\overline{GS}_1$ ,  $h_1$  et TGF définies précédemment :

$$\mathcal{A} = \overline{GS}_1 + A_1 \cdot \frac{h_1}{4 \sigma \left( \frac{T_1 + TGF}{2} \right)^3}$$

En fait, en dehors des conditions de calage du modèle (CAL), l'aire équivalente  $\mathcal{A}$  n'est pas calculée directement, et la densité de feu  $D'$  nécessaire pour entrer dans (7) est estimée d'après la relation de proportionnalité

$$D' = [D]_{CAL} \cdot \left[ \frac{Q_{FUEL}}{Q_{CAL}} \right] \cdot \left[ \frac{T_{ad}^{CAL}}{T_{ad}} \right]^3 \cdot \left[ \frac{T_{ad}^{CAL} - T_o}{T_{ad} - T_o} \right] \quad (8)$$

La température  $T_1$  de paroi est présumée demeurer constante d'une condition à l'autre (de l'ordre de 400°K dans une chaudière à eau chaude).

L'emploi combiné des relations (7) et (8) permet alors d'estimer le rendement réduit  $\eta'_F$  pour toute condition de réglage du brûleur autre que la condition de référence ayant servi à "caler" le modèle, d'où l'on tire les nouvelles valeurs :

- du rendement des transferts gaz-paroi

$$\eta_F = \eta'_F \cdot \frac{T_{ad}}{T_{ad} - T_o}$$

- de la puissance calorifique transmise aux parois

$$\dot{Q}_F = P_1 \cdot \eta_F$$

- de la température des gaz en sortie de foyer  $T_{ech}$  telle que

$$\dot{Q}_F = \left[ \Delta H_g \right]_{T_o}^{T_{ech}}$$

- de la température effective de foyer

$$TGF = T_{ech} + \Delta_{CAL}$$

#### c/ Bilans thermiques relatifs à l'eau et aux parois du foyer

Connaissant  $\dot{Q}_F$  et  $T_{GF}$ , on se propose de calculer :

- la puissance utile transmise à l'eau du foyer PUF,
- les pertes par les parois humides DQEF et celles par les parois sèches DQAF,
- la température de l'eau quittant le foyer TEF.



Cette séquence du modèle utilise en particulier la méthode de calcul préconisée par la Norme Belge NBN 234 [9] pour l'estimation du flux de chaleur perdu par une paroi externe de la chaudière connaissant sa température superficielle  $T_p$  et la température ambiante  $T_o$ .

Les parois sont assimilées à des résistances thermiques pures. Pour un élément de paroi comportant  $n$  couches de matériaux superposées (dont 1 étant le métal constitutif), la résistance est égale à

$$\sum_n \frac{a_n}{k_n}, \quad a_n \text{ étant l'épaisseur et } k_n \text{ le coefficient de conductivité de la couche de rang } n.$$

Les équations de base rendent compte :

- de la quantité de chaleur transmise à l'eau :

$$\begin{aligned} \text{avec} \quad DQGEF &= PUF + DQEAF \quad \text{avec} \\ PUF &= CW \cdot QW(TEF - TE) \end{aligned} \quad (9)$$

- de la quantité de chaleur totale transmise dans le foyer :

$$\dot{Q}_F = DQGEF + DQGAF \quad (10)$$

A ces équations sont associées des relations faisant intervenir les coefficients de transfert :

- entre gaz et paroi interne HGF
- entre paroi et eau HEAU (de l'ordre de 580 W/m<sup>2</sup>.K)
- entre paroi externe et ambiance HA.

On écrit ainsi :

$$DQGEF = A_1 \cdot HGEF \cdot (TGF - \frac{TE + TEF}{2}) \quad (11)$$

avec  $1/HGEF = 1/HGF + 1/HEAU + \frac{a}{k}$  (1 épaisseur de métal côté foyer)

$$DQEAF = A_1 \cdot ECHA \cdot (\frac{TE + TEF}{2} - T_o) \quad (12)$$

avec  $1/ECHA = 1/HA + 1/HEAU + \sum a/k$  (1 épaisseur de métal + couches éventuelles de calorifugeage),

$$T_{p1} = \frac{DQEAF}{A_1 \cdot HA} + T_o, \text{ et}$$

$DQEAF = f(T_{p1}, T_o)$  (13), la fonction  $f$  résultant de l'emploi de la norme Belge NBN 234 mise sous forme analytique,

etc...

La résolution des équations (9), (10), (11), (12) ... par méthode itérative permet d'obtenir simultanément les valeurs des flux de chaleur, des coefficients d'échange et des températures de parois, et la température d'eau quittant le foyer TEF.

### 1.2.3. Transferts thermiques dans l'échangeur

L'échangeur est supposé opérer d'une manière "méthodique" entre les températures de gaz  $T_{ech}$ ,  $T_f$ , et les températures d'eau TEF, TS (voir figure 1).

Les écarts de températures entre l'eau et les gaz aux deux extrémités sont caractérisés par leur moyenne logarithmique

$$\delta\theta = \frac{(T_{ech} - TEF) - (T_f - TS)}{\log_e \frac{T_{ech} - TEF}{T_f - TS}}$$

#### a/ Transfert global et transfert à l'eau

Le transfert entre les gaz de combustion et l'ensemble des parois internes de l'échangeur est fourni par le bilan enthalpique :

$$\dot{Q}_{ech} = \left[ \Delta H_g \right]_{T_{ech}}^{T_f} = DQGEE + DQGAE \quad (14)$$

Quant à la puissance calorifique transmise aux parois humides, elle est telle que :

$$DQGEE = A_2 \cdot HECH \cdot \delta\theta, \quad (15)$$

$A_2$  étant l'aire de captation et HECH le coefficient de transfert entre gaz et eau.

#### b/ Loi de variation du coefficient d'échange gaz-eau

On admet que HECH est lié d'une part au débit massique  $Q_g$  des gaz de combustion, et d'autre part à leur température effective définie par l'expression :

$$TGE = \frac{TEF + TS}{2} + \delta\theta \quad (16)$$

Pour tenir compte de l'évolution due à  $Q_g$ , on s'est basé sur des travaux effectués à l'IFP sur un générateur de type commercial [10]. Le terme correctif dû à la température a été tiré des travaux de GANAPATHY [8] se rapportant à des écoulements gazeux au travers des nappes de tubes.

Pour des conditions de fonctionnement hors de celles du calage, on pose ainsi :

$$HECH = (HECH)_{CAL} \cdot \left[ \frac{Q_g}{Q_{g,CAL}} \right]^{0,6} \cdot \left[ \frac{T_{GE}}{T_{GE,CAL}} \right]^{0,35} \quad (16)$$

### c/ Bilans thermiques relatifs à l'eau et aux parois de l'échangeur

On écrit un ensemble d'équations énergétiques dont la résolution par méthode itérative permet d'atteindre :

- la puissance utile transmise à l'eau PUECH ;
- les pertes par les parois humides DQAE et celles par les parois sèches DQAE ;
- la température de l'eau en sortie de chaudière TS ;
- la température des fumées évacuées T<sub>f</sub>.

Aux expressions (14), (15), (16), on adjoint ainsi des relations du type :

$$DQEE = PUECH + DQAE$$

avec PUECH = CW . QW (TS - TEF)

$$T_{p2} = \frac{DQAE}{A_2 \cdot HA} + T_o, \text{ et}$$

DQAE = f(T<sub>p2</sub>, T<sub>o</sub>), la fonction f résultant comme pour le foyer de l'adaptation de la Norme Belge NBN 224.

$$DQAE = ECHA \cdot A'_2 \cdot (T_{GE} - T_o)$$

avec 1/ECHA = 1/HGE + 1/HA + Σa/k  
et 1/HGE = 1/HECH - 1/HEAU - a/k

etc...

### 1.2.4. Bilan thermique complet de la chaudière

Finalement, pour un état d'isolation donné de la chaudière et pour des conditions d'exploitation fixées telles que :

- débit de combustible QFUEL,
- excès d'air e%,
- débit d'eau QW,
- température d'entrée de l'eau TE,

on obtient pour le fonctionnement continu les renseignements pratiques suivants :

- la puissance utile de la chaudière P<sub>u</sub> = PUF + PUECH,
- le rendement utile η<sub>u</sub> = P<sub>u</sub>/P<sub>f</sub>,
- la température d'eau finale TS
- la température des fumées T<sub>f</sub>
- les pertes par les fumées P<sub>f</sub> =  $\left[ \Delta h_g \right]_{T_o}^{T_f}$

- l'analyse détaillée des pertes par les parois sèches et humides.

### 1.2.5. Modalités pratiques de la simulation en régime continu

La simulation du fonctionnement continu fait l'objet de deux programmes distincts nommés CALAGE et CONTIN.

Le premier est réservé au calage préalable du modèle sur un ou plusieurs résultats d'expérience acquis sur plateforme d'essais ou sur site. Un résultat d'expérience représente une "condition de référence" caractérisée par un réglage de brûleur (débit de fuel et excès d'air), une puissance utile de chaudière, une température d'évacuation des fumées et une température des gaz de combustion à l'entrée de l'échangeur.

Le second programme exploite une condition de référence préalablement traitée dans le premier, avec le double objectif :

- de fournir une analyse détaillée du bilan thermique,
- d'extrapoler les performances du générateur opérant sous des conditions différentes de celles de référence.

### 1.3. Simulation du fonctionnement discontinu

Les calculs relatifs à cette séquence du modèle font l'objet du programme SIMULCH.

Le fonctionnement discontinu envisagé ici est provoqué par l'aquastat de la chaudière, qui opère entre 2 seuils de températures d'eau fixés par son réglage différentiel.

#### 1.3.1. Hypothèses de base

Pour simuler la charge calorifique "appelée", on agit sur le débit d'eau QW circulant dans la chaudière : cette manière de procéder est la plus proche de la réalité, où en général l'eau chaude est injectée dans le circuit de chauffage par l'intermédiaire d'une vanne 3 voies (figure 3).

La régulation de la chaudière s'opère en "tout ou rien" entre les niveaux de températures d'eau affichés TS1 (niveau bas, correspondant à la remise en route du brûleur) et TS2 (niveau haut, correspondant à la coupure du brûleur).

A un instant donné, l'état du mélange gazeux est caractérisé par sa température effective (T<sub>f</sub> dans le foyer, T<sub>GE</sub> dans l'échangeur) et par sa masse (MF dans le foyer, ME dans l'échangeur).

L'état du fluide caloporteur est défini par sa température moyenne (TEF ou TEE) dans chacun des 2 éléments de la chaudière, les masses en eau correspondantes étant WF et WE.

Les parois de la chaudière sont assimilées à des résistances thermiques pures. Mais en principe, au prix de calculs beaucoup plus longs, on peut dans le programme prendre en compte leur inertie thermique,

et les traiter comme des murs monodimensionnels.

### 1.3.2. Définition des coefficients d'échange internes

Pour des raisons d'ordre numérique, on est conduit à exprimer tous les échanges entre gaz et eau par des relations linéaires de la forme

$$\dot{Q} = H \cdot A \cdot (T_g - T_{\text{eau}})$$

$T_g$  s'apparentant à TGF ou à TGE.

Lorsque le brûleur est en fonctionnement, les valeurs des coefficients d'échange (HF dans le foyer, HECH dans l'échangeur) sont celles calculées en régime continu.

Lorsque le brûleur s'arrête, on a admis pour ces coefficients d'échange des lois de variation basées sur les considérations suivantes.

1°/ Dans le foyer, après un court laps de temps, HF s'apparente au coefficient de convection  $h_1$  et suit la loi d'évolution définie par la relation (6).

2°/ Dans l'échangeur, HECH suit la loi d'évolution définie par la relation (16).

3°/ La loi de décroissance du débit gazeux  $Q_g$  en fonction du temps est linéaire : elle s'étend ici sur une période de quelques secondes. La limite inférieure de  $Q_g$  constitue le "débit d'air de balayage" provoqué par le tirage de la cheminée. Ce débit à l'arrêt est fixé par l'expérience. Des essais effectués à IFP ont montré que, pour de petites chaudières domestiques, il était de l'ordre de 10 kg/heure.

Au cours de la mise en route du brûleur, on conserve les mêmes lois d'évolution que précédemment entre le débit de balayage et le débit gazeux établi.

### 1.3.3. Equations de base

A chaque instant, l'état thermodynamique du système est caractérisé par 6 variables :

- 4 variables pour les gaz TGF, TGE, MF et ME
- 2 variables pour l'eau TEF et TEE.

Pour les gaz, on applique dans le foyer et l'échangeur les lois d'équation d'état, de conservation de masse et d'énergie :

$$(p.V)_F = MF \cdot R \cdot TGF \quad (17)$$

$$\frac{dMF}{dt} = (\text{débit fuel} + \text{débit d'air}) - (\text{débit de transfert entre foyer et échangeur}) \quad (18)$$

$$d(MF \cdot U_F) = - d\dot{Q}_F + [\Delta H] \quad (19)$$

$U_F$  étant l'énergie interne spécifique des gaz dans le foyer, et  $[\Delta H]$  la différence entre les débits enthalpiques à l'entrée et en sortie de foyer, etc...

Pour l'eau, on applique la loi de conservation d'énergie dans le foyer et l'échangeur. On écrit ainsi :

$$WF \cdot CW \cdot d(TEF) = DQ_{GEF} - DQ_{EAF} - (TEF - TE) CW \cdot QW \quad (20)$$

$$WE \cdot CW \cdot d(TEE) = DQ_{GEE} - DQ_{EAE} - (TEE - TEF) CW \cdot QW \quad (21)$$

Le système d'équations étant mis en forme, il reste 6 équations différentielles du type :

$$dy_i = f(y_1 \dots y_i \dots y_6)$$

où les  $y_i$  sont les 6 variables caractéristiques définies ci-dessus.

Connaissant à chaque instant les valeurs de ces variables, leurs dérivées par rapport au temps et tous les débits calorifiques mis en jeu, on vérifie que les bilans thermiques sont respectés :

$$P_u = DQ_{GEF} + DQ_{GEE} - (DQ_{EAF} + DQ_{EAE}) \quad (22)$$

$$P_i = DQ_{GEF} + DQ_{GEE} + DQ_{GAF} + DQ_{GAE} + [\Delta H_g]_{T_0}^{T_f} \quad (23)$$

### 1.3.4. Renseignements pratiques fournis par la simulation

Tous les débits calorifiques étant intégrés au cours des calculs, on en déduit les rendements utiles du foyer, de l'échangeur et de la chaudière durant un cycle de fonctionnement, et les pertes correspondantes par les parois et les fumées.

En outre, le programme calcule pour un régime cyclique établi :

- la durée d'un cycle ;
- la fraction du temps de marche du brûleur dans le cycle ;
- la consommation de combustible par cycle.

Pour obtenir ces résultats à différentes charges de la chaudière, on peut faire varier soit le débit d'eau  $QW$  dans le générateur, soit la température d'entrée d'eau (dite de retour)  $TE$ , soit éventuellement ces deux paramètres pour un réglage donné de l'aquastat.

## II - EXEMPLES D'APPLICATION DU MODELE

Les exemples qui suivent se rapportent à deux chaudières de chauffage domestique qui ont été essayées en laboratoire (parmi 14 autres) au cours de l'Etude coopérative mentionnée précédemment [1], [2]. Ces deux appareils, repérés B et E, ont une puissance utile nominale de l'ordre de 29 kW (25 th/h).

La chaudière B est en acier avec ballon d'eau sanitaire incorporé. La chaudière E, sans production d'eau chaude intégrée, est en fonte et a pour particularité d'être munie d'un foyer briqueté.

Le combustible utilisé ici est du fuel-oil domestique, distillat pétrolier ayant les caractéristiques

moyennes suivantes :

$$C = 86 \%, H = 13,5 \%, S = 0,5 \%$$

$$PCI = 42,8 \text{ MJ/kg (10 250 kcal/kg)}.$$

Dans les cas traités, la puissance appelée (ou charge) est provoquée uniquement par les besoins en chauffage. Nous allons examiner l'influence d'un certain nombre de paramètres d'ordre pratique sur les performances en nous appuyant sur la simulation mathématique, et en comparant dans la mesure du possible les résultats à ceux tirés de l'expérience.

### II.1. Influence du débit de fuel

Sur la figure 4 sont reportés les bilans thermiques obtenus en régime continu pour des débits de fuel passant de 3,13 à 1,93 kg/h sur la chaudière E.

Au banc d'essais, cette variation de débit du brûleur a été obtenue par changements successifs de gicleurs. Les performances calculées l'ont été à partir d'un calage (CAL) du modèle effectué sur l'essai à débit maximal.

Les rendements théoriques apparaissent ici être quelque peu inférieurs aux rendements expérimentaux, et on voit que les différences sont imputables aux pertes par les parois. En dehors des imperfections inhérentes à toute simulation mathématique et auxquelles ce modèle n'échappe pas, signalons que sur les plates-formes d'essais les incertitudes d'appréciation directe des rendements utiles ont été chiffrées aux environs de  $\pm 2 \%$ .

On remarque immédiatement que le rendement utile tend à augmenter lorsque le débit de fuel diminue. Bien entendu, ceci est dû en grande partie à la diminution de chaleur sensible emportée par les fumées. Mais il faut signaler que le rendement de foyer lui-même augmente, comme le laisse prévoir la relation de corrélation (7) du paragraphe I.2.2.

En effet, on peut montrer que  $\eta_f$  est une fonction décroissante de  $D'$ . Lorsque dans la chambre de combustion le rayonnement est le mode de transfert prépondérant (ce qui est le cas ici où le rayonnement intervient pour plus de 70 %), la densité de feu réduite  $D'$  décroît avec  $P_1$ , ce qui contribue à augmenter le rendement du générateur.

L'accroissement du rendement s'accompagne ici d'une très nette diminution de la température des fumées évacuées, comme le montre la figure 5. On notera d'ailleurs ici la très bonne concordance existant entre l'expérience et le calcul.

Cette notion de température de fumées revêt une grande importance pratique. En effet, si une température "basse" est gage de bon rendement, elle peut être également source d'ennuis du fait des condensations possibles dans le conduit de cheminée quand on atteint le point de rosée acide. Pratiquement, sur les installations de chauffage domestique, on évite de descendre au-dessous de 200°C en sortie de chaudière. Dans cette optique, l'emploi du modèle est particulièrement efficace pour prévoir le débit calorifique minimal admissible sur un générateur donné. Ceci est illustré sur la figure 6 : des calculs systématiques effectués sur la chaudière B ont montré que, sous prétexte d'augmenter son rendement en diminuant sa puissance nominale (dans le cas d'une surpuissance notoire de l'installation de chauffage par exemple), on ne pourrait songer à descendre au-dessous d'un réglage de brûleur correspondant à environ 1,3 kg/h de fuel. Signalons d'ailleurs, que dans la pratique, on ne trouve pas de brûleurs à pulvérisation mécanique et air soufflé opérant au-dessous de 1,4 kg/h.

La figure 7 se rapporte à l'évolution du rendement de la chaudière B opérant en régime discontinu pour 2 réglages de débit du brûleur : 3,04 (débit nominal) et 2 kg/h (débit réduit). On constate que là encore, pour une puissance appelée  $P_u$  ou fraction de charge  $\alpha$  donnée, le rendement augmente quand on réduit le débit de fuel au brûleur.

Le calcul paraît ici devoir surestimer les rendements expérimentaux : mais il faut savoir qu'au cours de tels essais, il est difficile de maintenir constants les paramètres de réglage du brûleur (débit de combustible et excès d'air), et la température moyenne de l'eau.

L'allure de ces courbes de rendement est tout-à-fait caractéristique de celle rendant compte des performances d'une chaudière fonctionnant en régime "tout ou rien". On notera que la décroissance du rendement est particulièrement marquée à faible charge, au-dessous de 25-30 % pour cette chaudière. Le détail des pertes est fourni sur la figure 8. On remarquera que les pertes par les parois, qui varient assez peu en valeur absolue avec la puissance appelée  $P_u$ , prennent de ce fait une importance relative croissante quand la charge de la chaudière diminue. D'où l'intérêt de choisir un générateur dont la puissance maximale ne soit pas exagérément au-delà des besoins thermiques réels, sous prétexte de se ménager une réserve de puissance.

Actuellement, pour tenir compte des besoins instantanés d'eau chaude sanitaire en maison individuelle, on préconise d'opter pour une puissance installée supérieure d'environ 30 % à la puissance de chauffage nécessaire par grand froid.

### II.2. Influence de l'excès d'air

La réduction de l'excès d'air est le moyen d'action le plus souvent préconisé pour diminuer la consommation de combustible d'un générateur de chaleur.

La figure 9 montre le gain de rendement qu'on serait susceptible d'obtenir sur la chaudière B (en fonctionnement continu) en passant d'un excès d'air de 60 % à un excès d'air de 10 % : gain d'environ 1 point par tranche de 10 %.

Le modèle permet d'explicitier ici les phénomènes mis en jeu. On peut en effet faire les remarques suivantes.

1°/ Le rendement du foyer augmente, bien que la température des gaz le quittant ( $t_{ech}$ ) augmente également ; la raison fondamentale de cet accroissement de rendement est l'augmentation de la température adiabatique de combustion  $T_{ad}$ , qui contribue à diminuer la densité de feu réduite  $D'$ , donc à accroître le rendement  $\eta_f$  donné par la relation de corrélation (7).

2°/ Par contre, le rendement de l'échangeur croît avec l'excès d'air : ceci est dû à l'amélioration du coefficient de transfert, consécutive à une augmentation du débit massique des gaz (relation (16) du paragraphe I.2.3.), bien que leur température  $t_{ech}$  diminue.

3°/ Finalement, du fait de la part prépondérante prise par le foyer dans le bilan thermique de la chaudière, c'est son accroissement de rendement avec la diminution de l'excès d'air qui conditionne celui de l'appareil.

Rappelons que sur les chaudières de chauffage domestique pavillonnaires qui sont démunies par

principe de systèmes de régulation sophistiqués, on évite généralement de régler le brûleur au-dessous de 20 % d'excès d'air, ceci afin de se ménager une marge de sécurité quant à la qualité de la combustion.

### II.3. Influence de la température de l'eau

Un moyen préconisé pour améliorer le rendement d'exploitation, est de réduire la température de l'eau de chauffage.

Par le calcul, nous avons abaissé de 20°C la température de l'eau circulant dans la chaudière E. Les figures 10 et 11 montrent que, dans ces conditions, la réduction consécutive des pertes pariétales permet d'accroître d'une manière notable le rendement utile. Par exemple, pour une charge de 30 %, celui-ci passe de 75 à 78 %, soit une réduction de consommation en fuel de l'ordre de 4 %.

En dehors des problèmes propres à l'adaptation des émetteurs (radiateurs) aux "basses" températures du fluide caloporteur, l'abaissement de la température a de toute manière une limite : le retour de l'eau à la chaudière doit, dans toute la mesure du possible, demeurer supérieur au point de rosée humide des gaz de combustion (de l'ordre de 45°C avec le fuel envisagé ici).

En ce qui concerne l'emploi du modèle, on notera sur la figure 10 la très bonne concordance existant entre points calculés et points expérimentaux. Il faut souligner que dans le cas envisagé ici, les conditions opératoires au banc d'essais s'étaient maintenues particulièrement constantes et proches des conditions de calcul.

### II.4. Influence du différentiel de l'aquastat

L'influence éventuelle du différentiel de l'aquastat équipant la chaudière est particulièrement difficile à mettre expérimentalement en évidence : des fluctuations extérieures incontrôlables, susceptibles d'être rencontrées sur un banc d'essais, peuvent en effet masquer un phénomène aux proportions modestes.

Par le calcul, nous avons envisagé trois cas pratiques correspondant à des différentiels respectivement égaux à 8, 5 et 3°. On a simulé le fonctionnement de la chaudière B opérant à environ 1/4 de sa puissance nominale. Les principaux résultats de calcul sont regroupés dans le tableau ci-dessous.

#### FONCTIONNEMENT DISCONTINU

Chaudière B -  $e = 35\%$  -  $Q_{FOD} = 3,04 \text{ kg/h}$  -  $t_E = 60^\circ\text{C}$

Réglage Aquastat	Durée d'un cycle (s)			Consom. FOD (kg/h)	Énergie utile (kWh)	Pertes pa- rois (kWh)	Pertes fu- mées (kWh)	$\eta_u$ (%)
	marche brûleur	arrêt brûleur	totale					
72-80	175	461	636	0,832	7,44	0,81	1,73	74,8
75-80	134	344	478	0,851	7,57	0,82	1,76	74,8
77-80	97	254	351	0,841	7,47	0,82	1,74	74,7

Nota : Les bilans thermiques sont rapportés à 1 h de fonctionnement cyclique.

On ne peut distinguer de différences bien significatives entre les performances, malgré les durées de cycles différant sensiblement d'un réglage à l'autre (correspondant à 6 allumages/heure dans le 1er cas et 10 dans le 3è). Tout au plus peut-on remarquer que le niveau moyen de température d'eau tend à augmenter quand le différentiel diminue, et qu'on peut s'attendre de ce fait à un accroissement des pertes pariétales. Mais ce dernier phénomène ne pourrait vraiment être sensible que sur des chaudières mal calorifugées.

Pratiquement, le différentiel des aquastats équipant les chaudières de chauffage domestique se situe entre 5 et 10°C.

### II.5. Influence du calorifugeage

Le calorifugeage est une caractéristique d'équipement ayant une grande importance sur le rendement d'exploitation du générateur.

Par le modèle, nous avons étudié l'influence de l'état d'isolation en fonctionnement continu pour différents débits de fuel, en opérant sur la chaudière B (bien représentative en 1977 de la qualité courante d'isolation rencontrée sur ce type d'appareil).

On a considéré 3 états d'isolation différents : le calorifugeage d'origine, l'absence totale de calorifugeage, et un "super calorifugeage" consistant en l'adjonction à l'équipement commercial d'une couche supplémentaire de 40 mm de laine de verre sur toutes les surfaces.

#### II.5.1. Influence sur le rendement

L'examen de la figure 12 permet de faire deux constatations essentielles.

1°/ Un calorifugeage très poussé permet d'escompter des gains sensibles par rapport aux performances initiales : 3 points de rendement jusque vers 2,4 kg/h, 4 points au débit de 1,4 kg/h.

2°/ La variation du rendement avec le débit de fuel est d'autant moins sensible que la chaudière est moins bien calorifugée.

#### II.5.2. Analyse détaillée des pertes par les parois

L'analyse détaillée des pertes par les parois, rendue possible par la simulation mathématique, permet de mettre en évidence les rôles respectifs joués par les surfaces humides et sèches dans le bilan des pertes. Sur la chaudière B envisagée ici, les surfaces sèches représentent 11 % de la surface totale en contact avec l'ambiance.

Sur la figure 13, on peut faire les observations suivantes.

1°/ les pertes totales par les parois sont fortement influencées par l'état d'isolation, et elles croissent d'autant plus vite avec la charge (celle-ci étant ici conditionnée par le débit de fuel) que le calorifugeage est moins soigné.

2°/ Pour un calorifugeage donné, la loi de variation des pertes aux parois est essentiellement régie par celle des parois sèches, les pertes par les parois humides variant très peu. Ceci est dû au fait que lorsque la charge croît en régime continu, le niveau moyen des températures internes des gaz augmente, d'où

une élévation de température des parois non irriguées par l'eau.

3°/ Les pertes totales aux parois ne peuvent être considérées comme étant pratiquement constantes avec la charge que dans le cas du calorifugeage très poussé, qui atténue fortement l'effet dû aux parois sèches.

### II.5.3. Influence sur la température et les pertes par les fumées

La figure 14 montre que l'amélioration du calorifugeage est susceptible de provoquer une augmentation décelable de la température des fumées (donc les pertes par chaleur sensible), bien que le rendement de la chaudière augmente.

Cet paradoxe apparent, confirmé par l'expérience, trouve son explication dans l'analyse des phénomènes thermiques internes à la chaudière. Le calcul montre en effet qu'une forte diminution des pertes par les parois imprime aux gaz de combustion un surcroît d'enthalpie qui ne se transmet pas intégralement à l'eau, du fait des limitations dues aux coefficients d'échange.

### II.6. Calcul de la consommation d'entretien

Si on rapporte les pertes totales (fumées + parois) exprimées en valeur absolue à la charge appelée (ou puissance utile équivalente) en fonctionnement discontinu, on trouve une relation pratiquement linéaire illustrée sur les figures 15 et 16 pour les chaudières B et E.

Cette propriété de linéarité, largement confirmée par l'expérience [1], [2], provient du fait que :

- les pertes par les parois humides sont pratiquement constantes,
- les pertes par les parois sèches et par les fumées sont sensiblement proportionnelles au temps de marche du brûleur.

Lorsque la demande en chauffage devient nulle ( $P_u = 0$ ), la chaudière fonctionne en régime dit d'"entretien" : le brûleur ne se met en route que pour maintenir l'eau à la température de consigne de l'aquastat. La consommation de fuel correspondante  $C_0$ , qui ne sert qu'à compenser les pertes de l'appareil, est une notion intéressante à connaître : elle permet de juger de la qualité du générateur, et en particulier de celle de son calorifugeage. La mesure prévue dans la nouvelle norme française d'essais de chaudière [11], est très délicate. On doit rechercher un réglage d'aquastat permettant de maintenir à une valeur imposée l'écart entre la température moyenne de l'eau de la chaudière et la température ambiante (cet écart est de l'ordre de 50° dans la norme précitée). Pour obtenir une précision suffisante dans la mesure des consommations, l'essai sur plate-forme doit se dérouler sur une période proche de 24h, et durant cette période la cellule d'essais doit être maintenue à une température aussi constante que possible.

Le modèle permet d'estimer a priori la consommation d'entretien.

En se reportant à la figure 3, on voit que le régime d'entretien correspond à une circulation d'eau chaude s'établissant d'une manière naturelle (par thermo-siphon) dans la chaudière, la vanne 3 voies étant complètement fermée du côté circuit de chauffage. On entre dans le modèle mathématique en posant que ce débit d'eau est très faible (on a pris dans les exemples cités 1 % du débit nominal), et on prend pour température de retour TE celle correspondant à la plage inférieure de l'aquastat (consigne TS1).

On donne ci-dessous les résultats obtenus à partir des chaudières B et E.

Régime d'entretien - Calculs effectués avec un débit d'eau interne de 10 kg/h

Chaudière	Réglage brûleur		Réglage aquastat		$t_A$ (°C)	$\Delta$ air eau (°)	Durée du cycle (s)			$C_0$ (kg/h)
	$Q_{FOD}$ (kg/h)	e (%)	TS1 (= $T_p$ )	TS2			marche brûleur	arrêt brûleur	totale	
B	3,035	35	75	80	25	51	149	4 957	5 106	0,089
E	3,13	25	85	90	20	66	26	700	726	0,114

L'écart  $\Delta$  air eau correspond à la différence  $t_m - t_A$ , avec  $t_m = \left( \frac{TS1 + TS2}{2} \right) - TE$ .

Les consommations d'entretien reportées ci-dessus correspondent à des pertes respectivement égales à : 1,03 kWh (882 kcal/h) pour la chaudière B et 1,31 kWh (1125 kcal/h) pour la chaudière E.

En se reportant aux figures 15 et 16, on remarque que ces pertes au voisinage de la puissance nulle sont supérieures à celles qu'on obtiendrait en prolongeant les droites au-delà du point a. Cela s'explique par le fait qu'en régime d'auto-entretien, pour un réglage donné de l'aquastat, la température moyenne de l'eau est prise supérieure à celle du fonctionnement normal : ainsi par exemple pour la chaudière B,  $t_m = 68,8^\circ\text{C}$  en fonctionnement normal (avec  $t_p = 60^\circ\text{C}$ ) contre  $t_m = 76,3^\circ\text{C}$  en régime d'entretien (avec  $t_p = 75^\circ\text{C}$ ).

Cette discontinuité de la relation linéaire entre pertes et puissance utile au voisinage de la puissance nulle a été particulièrement bien mise en évidence, sur le plan expérimental, par SCHLIENGER et THENARD [12]. Pour parvenir à l'ordonnée d'origine de la droite, les auteurs préconisent d'effectuer l'essai d'auto-entretien "avec une consigne d'aquastat correspondant aux environs des 2/3 de l'écart de température entre la consigne d'aquastat de la chaudière en marche continue et la température ambiante".

La définition précise de la droite étant ainsi obtenue par deux points correspondant d'une part au régime nominal et d'autre part au régime d'entretien réajusté, on peut alors expliciter le rendement de chaudière par une expression pratique de la forme :

$$\eta_d = \eta_c \left( 1 - \frac{1 - m}{m} \cdot c \right) \quad (24)$$

m étant le taux de marche du brûleur, et c un coefficient d'entretien thermique défini par l'expression

$$c = \frac{C_0}{Q_{FOD}}$$

### CONCLUSIONS

Un modèle mathématique a été créé à l'Institut Français du Pétrole, dans le cadre d'une Etude coopérative menée sur les petites chaudières de chauffage domestique.

Pour l'établir, on s'est appuyé sur les résultats expérimentaux obtenus sur plates-formes d'essais. Ce modèle n'est pas un modèle de conception, mais un modèle d'exploitation. Il permet d'étudier

le comportement d'un générateur donné sous l'influence de divers paramètres tels que : réglage du brûleur (débit de fuel et excès d'air), état d'isolation des parois, réglage de l'aquastat, et ceci à partir de renseignements fournis par un essai effectué en régime continu, ou tirés éventuellement du catalogue constructeur. En particulier, on peut suivre d'une manière plus détaillée et plus fine que par l'expérience la répartition de l'énergie introduite entre énergie utile et pertes, et en tirer les conséquences pour améliorer les conditions d'exploitation ou orienter une nouvelle conception.

La simulation du fonctionnement continu peut s'effectuer indépendamment de celle du fonctionnement discontinu, le modèle ayant été préalablement calé sur un résultat expérimental.

Cette possibilité permet ainsi d'explorer rapidement l'influence d'un ou plusieurs paramètres sur les performances en régime continu, et de réserver la simulation du régime discontinu - beaucoup plus longue en temps calcul - à l'étude de conditions sélectionnées.

Dans le cadre de l'IFP, un emploi caractéristique de ce modèle concerne actuellement l'élaboration d'un ensemble de données reliant la consommation à la puissance utile pour différentes conditions externes, ces données devant être utilisées ensuite dans un modèle de bâtiment rendant compte du bilan énergétique annuel.

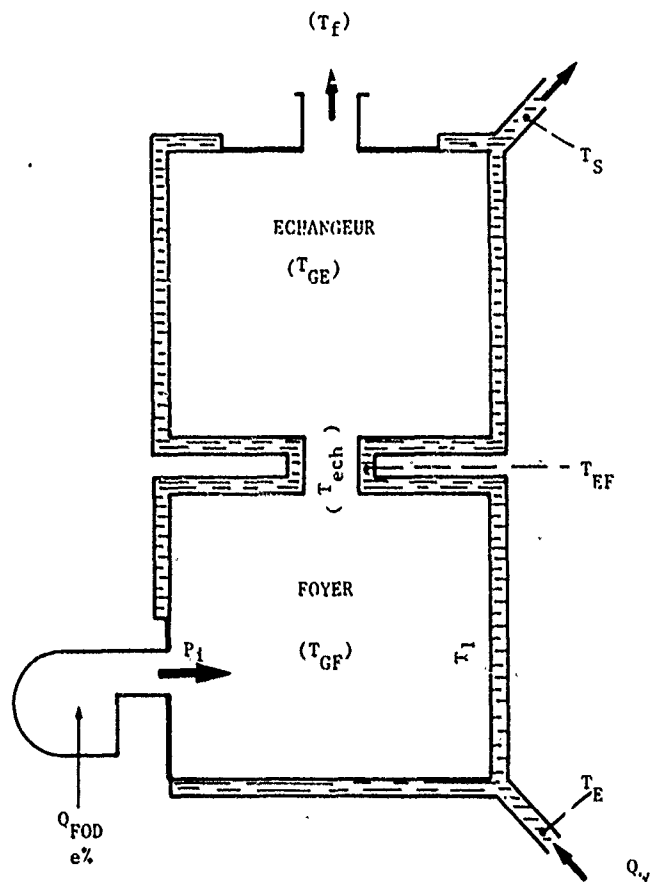
On envisage également, sur la base d'expérimentations nouvelles, l'extension du modèle aux chaudières de plus fortes capacités que celles considérées ici : quelques centaines de kW, domaine du chauffage collectif ou industriel. L'un des objectifs de cette extension est l'étude fine des avantages respectifs des marches tout ou rien et modulante.

## BIBLIOGRAPHIE

- [1] S. GAUFFIER, F. MAUSS, E. PERTHUIS et J.P. SCHLIENGER  
 "Journée d'étude sur l'utilisation rationnelle du pétrole pour le chauffage".  
 Table ronde N° 3 (Rendement à charge variable des petites chaudières). A.F.T.P. Paris décembre 1976  
 pages 101-131.
- [2] Idem. A.I.C.V.F., Paris, avril 1977
- [3] J.P. LE BRETON  
 "Transfert de chaleur dans les foyers industriels"  
 Thèse Faculté des Sciences Université Rouen, février 1977
- [4] P. ANGLESIO  
 "Attuali possibilita di valutazione dello scambio termico in focolai di caldaie per riscaldamento"  
 Atti E Rassegna Tecnica Società ingegneri e architetti in Torino. N. Serie A 32, N° 5-8, Maggio-Agosto 1978, p. 109-115
- [5] H.C. HOTTEL, A.F. SAROFIM  
 "Radiative Transfer"  
 Mac Graw - Hill Book Company, New York 1967, chapter 7-8
- [6] T.R. JOHNSON, J.M. BEER  
 "4th Symposium on Flames and Industry"  
 Paper N°4 (zone method analysis of radiant heat transfer : a model for luminous radiation). The  
 Institute of Fuel, London 1972
- [7] F. MAUSS, E. PERTHUIS  
 "Transferts thermiques sur foyers expérimentaux".  
 Revue Institut Français du Pétrole, vol. XXV - N°1, 1970, p. 56-88
- [8] V. GANAPATHY  
 "Quick Estimation of Gas heat Transfer Coefficients".  
 Chemical Engineering, September 13, 1976, p. 199-202
- [9] INSTITUT BELGE DE NORMALISATION  
 "Méthode d'essai des chaudières de chauffage central".  
 NBN 234, Bruxelles 1957
- [10] F. MAUSS, E. PERTHUIS  
 "Transferts thermiques dans les chaudières à eau chaude".  
 Revue Institut Français du Pétrole, Vol XXXIII, N° 7-8, 1968, p. 988-1022
- [11] ASSOCIATION FRANCAISE DE NORMALISATION  
 "Chaudières automatiques fonctionnant aux combustibles liquides, équipées de brûleurs  
 à pulvérisation"  
 Projet AFNOR E 31-353, Paris 1976
- [12] J.P. SCHLIENGER, P. THENARD  
 "Rendement moyen d'une chaudière de chauffage domestique"  
 Doc. SHELL FRANCAISE, CCAE Pth/EB N° 13/79, Centre de Recherches de Grand-Couronne, mars 1979



## SCHEMA DE CHAUDIERE (Programmes CONTIN et SIMULCH)



## LEGENDE

- surface sèche
- == surface humide

NOTA- Pour simplifier le schéma,  
on n'a pas représenté de  
surface réfractaire

fig . 1

COEFFICIENTS DE TRANSFERT ET FLUX DE CHALEUR

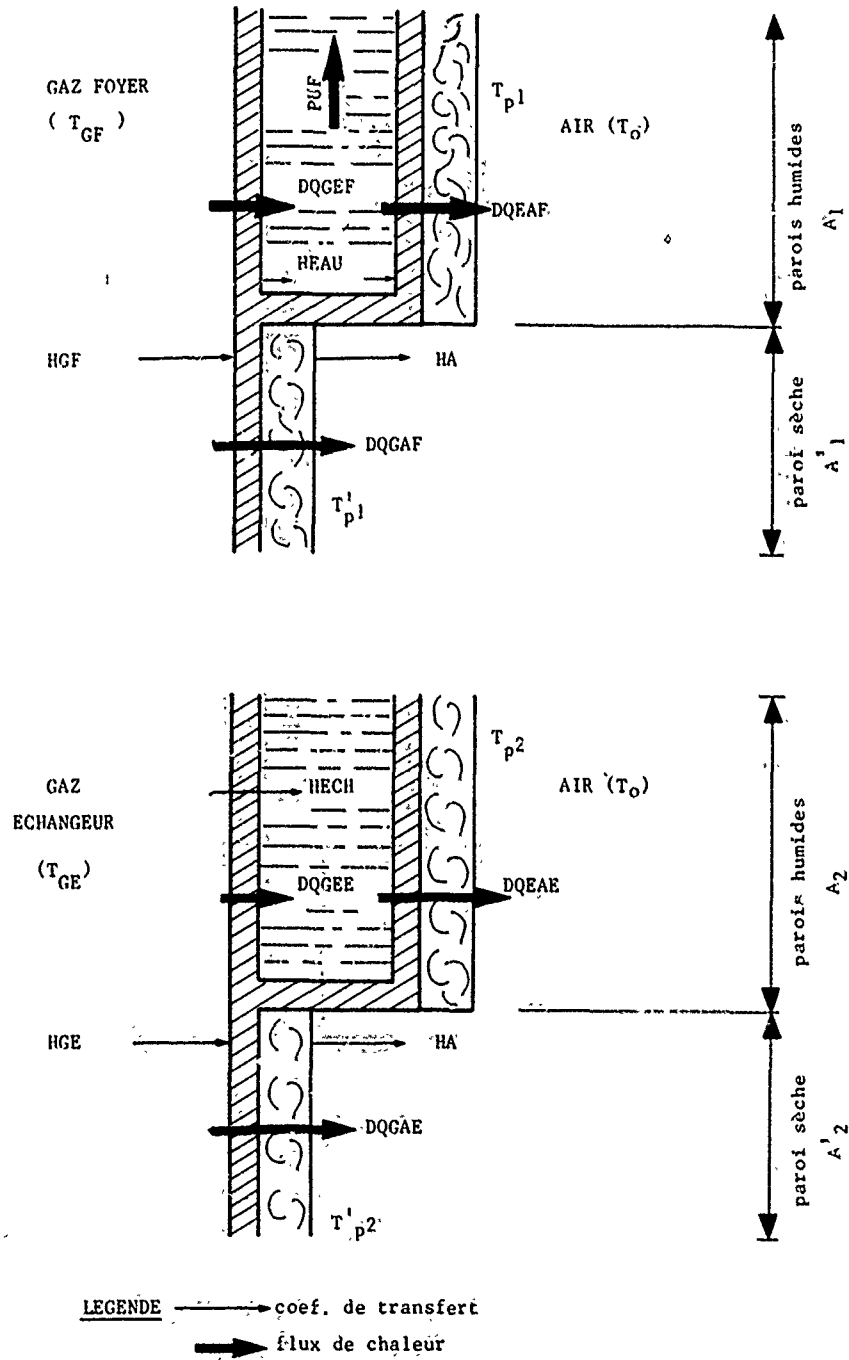
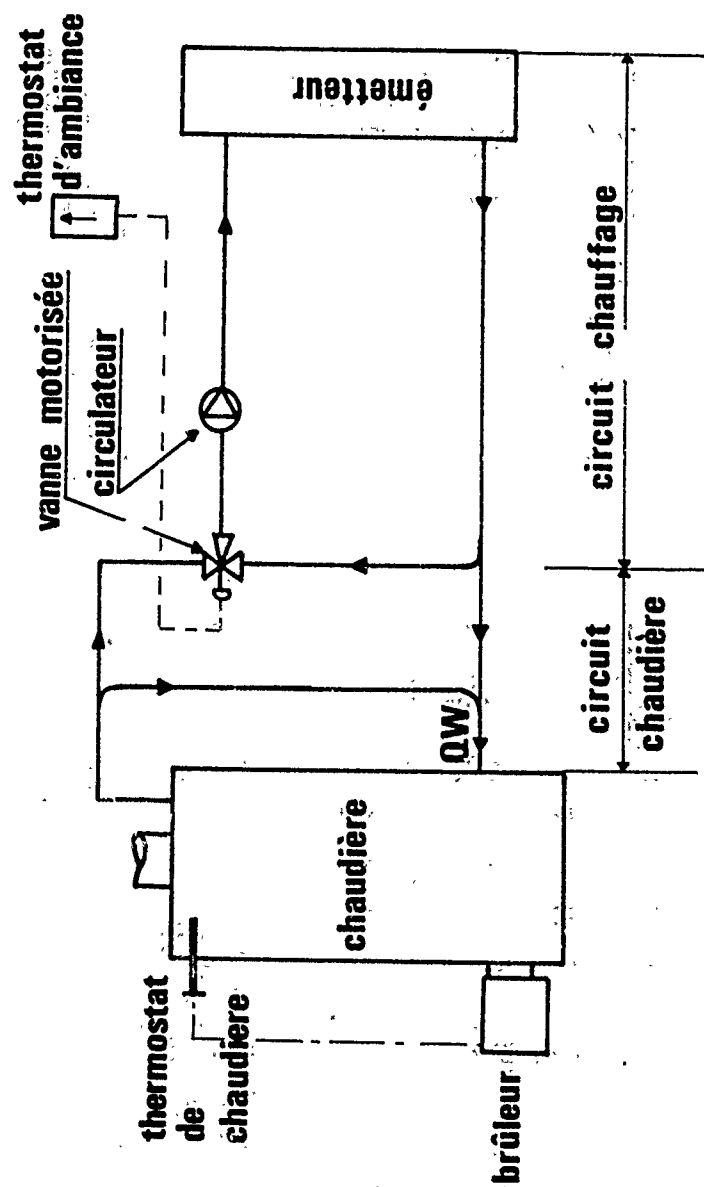


fig. 2



**Fig.3 - SCHEMA D'UNE INSTALLATION DE CHAUFFAGE PAR EAU CHAUDE**

**FUNCTIONNEMENT CONTINU - Influence du débit de fuel sur la température des gaz évacués**

Caudière E briquetée -  $\phi = 20$  à 25 %

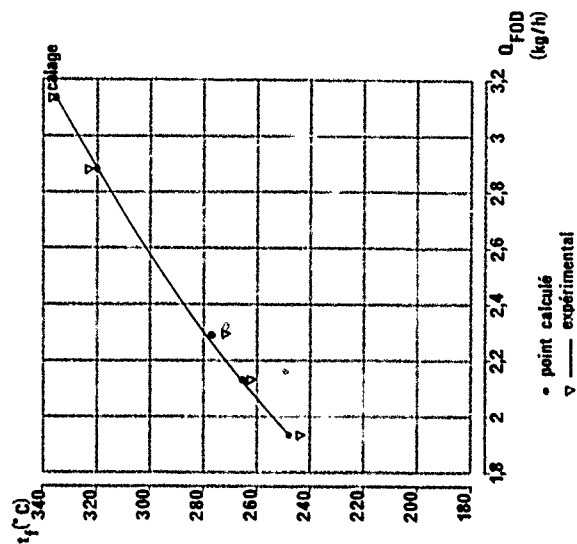


Fig. 5

**FUNCTIONNEMENT CONTINU - Influence du débit de fuel sur le bilan thermique**

Caudière E briquetée -  $\phi = 20$  à 25 % -  $t_E = 62^\circ\text{C}$

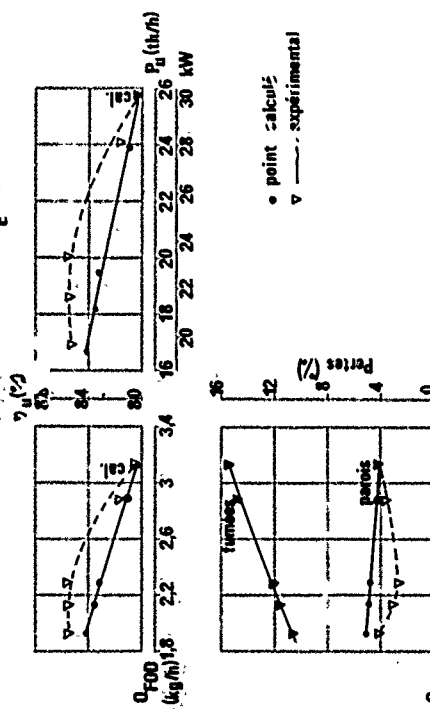


Fig. 4

**FUNCTIONNEMENT CONTINU - Influence du débit de fuel sur la**  
**température des gaz évacués**

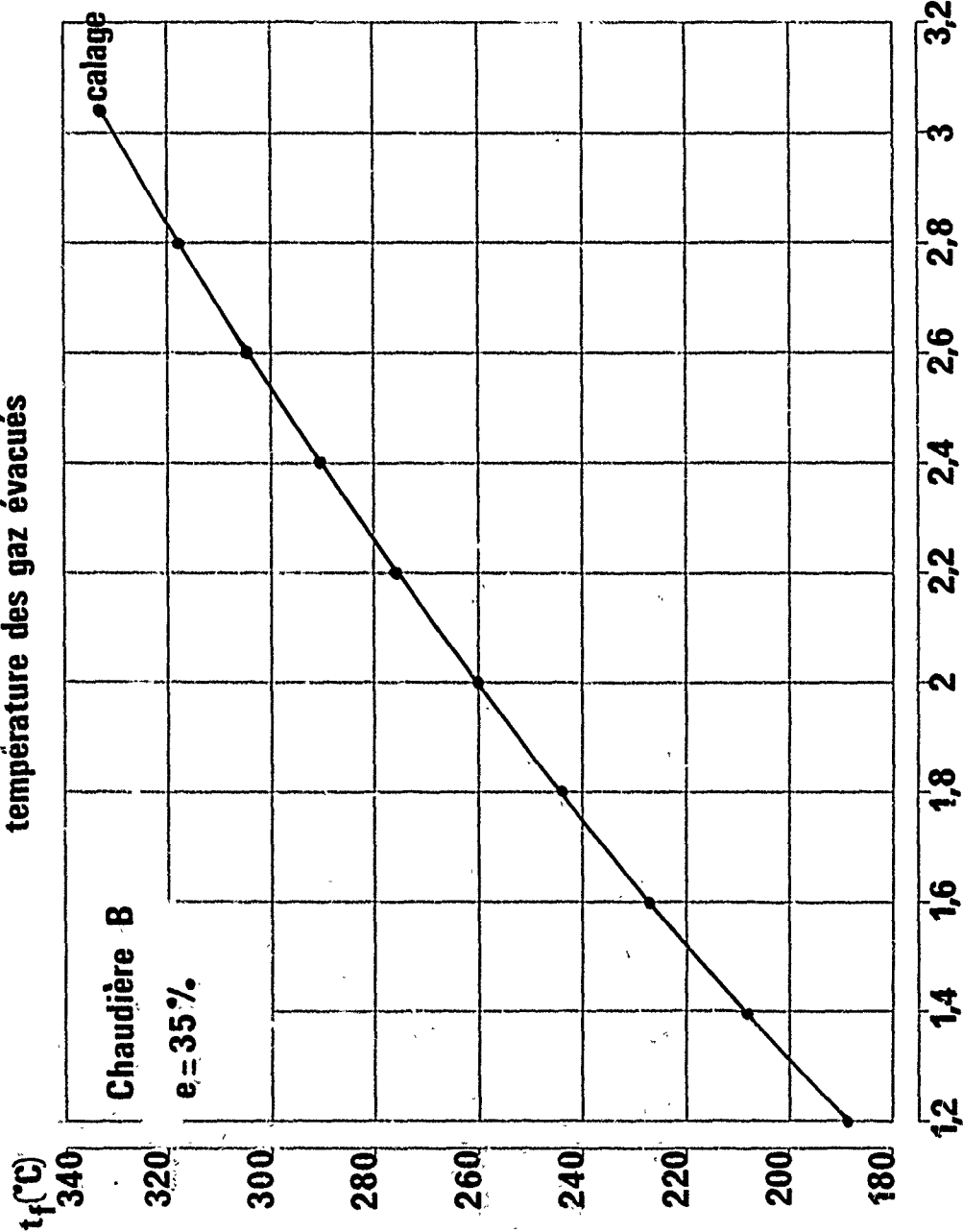


Fig. 6

 $Q_{FOD}$   
(kg/h)

# **FUNCTIONNEMENT DISCONTINU - Evolution des pertes suivant la charge**

Chaudière B,  $e=35\%$ ,  $t_E=60^\circ\text{C}$ , Réglage aquastat:  $75-80^\circ\text{C}$

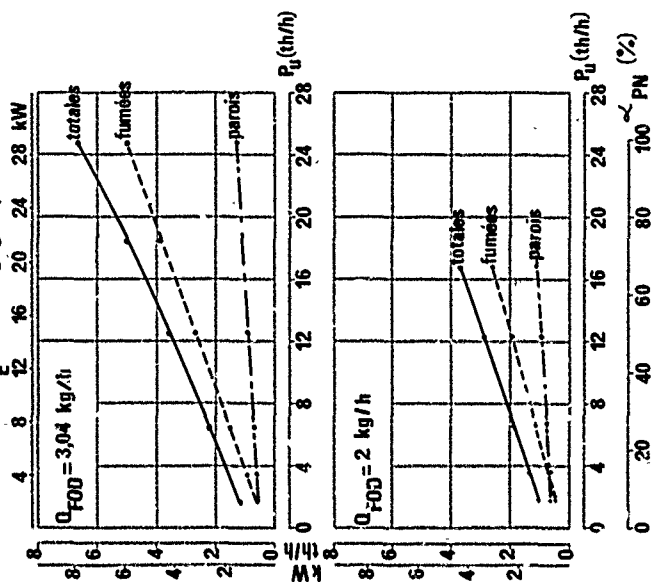


Fig. 8

# **FUNCTIONNEMENT DISCONTINU - Evolution du rendement suivant la charge et le débit de fuel**

Chaudière B,  $e=35\%$ ,  $t_E=60^\circ\text{C}$ , réglage aquastat:  $75-80^\circ\text{C}$

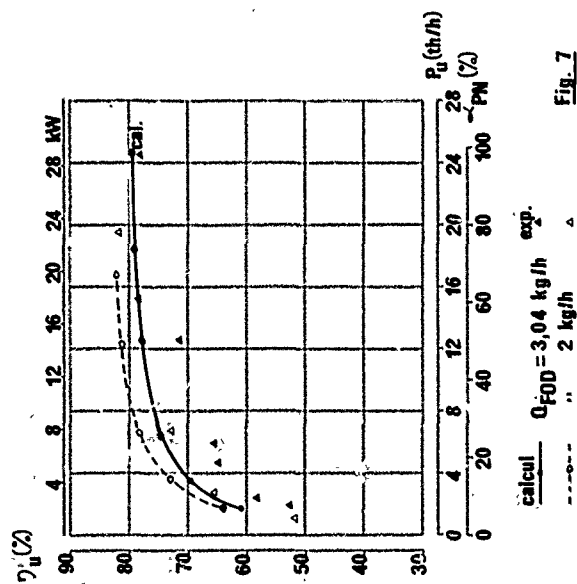
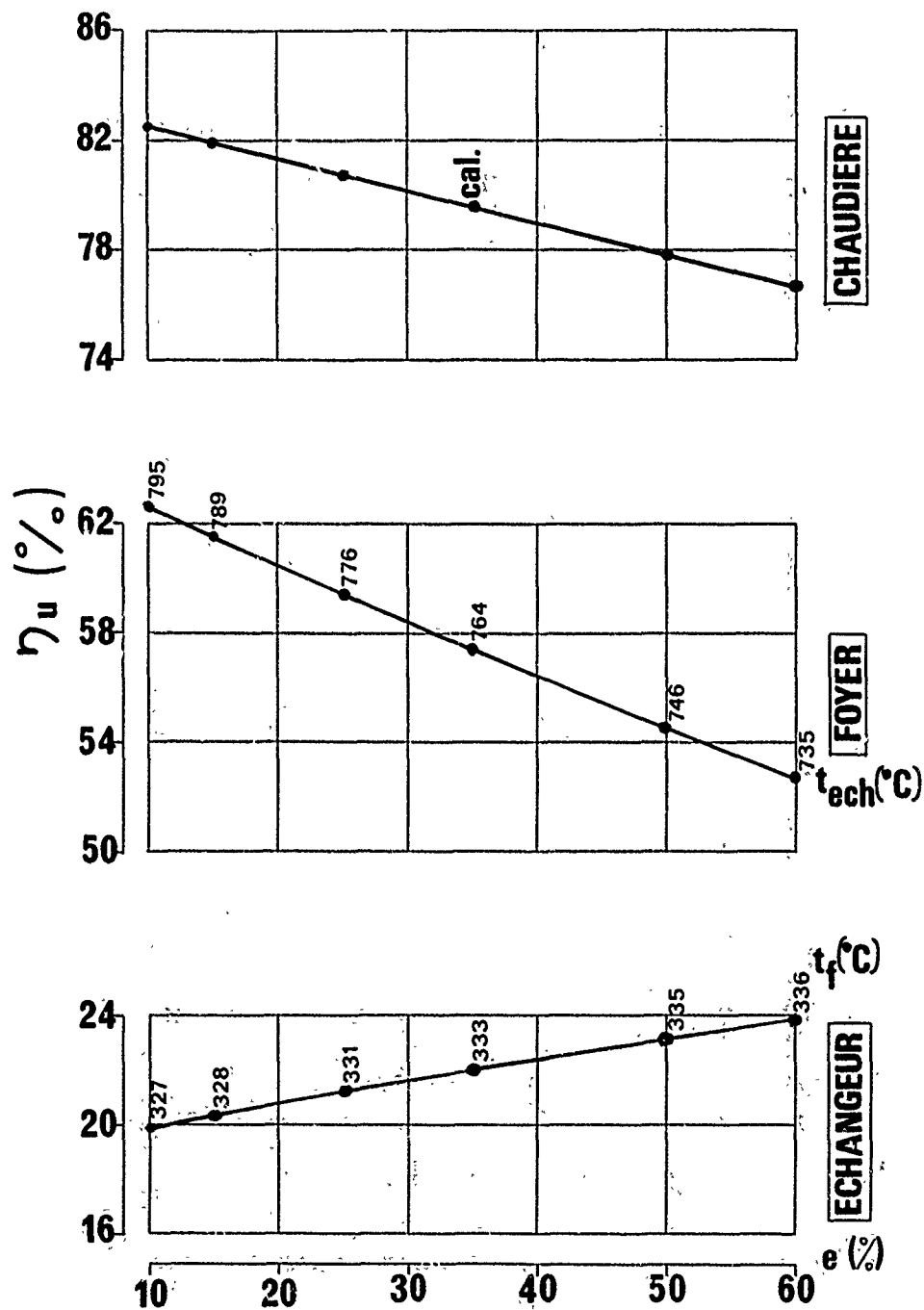


Fig. 7

# **FONCTIONNEMENT CONTINU - Influence de l'excès d'air sur les rendements utiles**

Chaudière B -  $Q_{FOD} = 3,04 \text{ kg/h}$



**Fig. 9**

FONCTIONNEMENT DISCONTINU - Pertes relatives en fonction de la charge et de la température d'eau

Chaudière E briquetée,  $Q_{FOD} = 3,13 \text{ kg/h}$ ,  $e = 25\%$

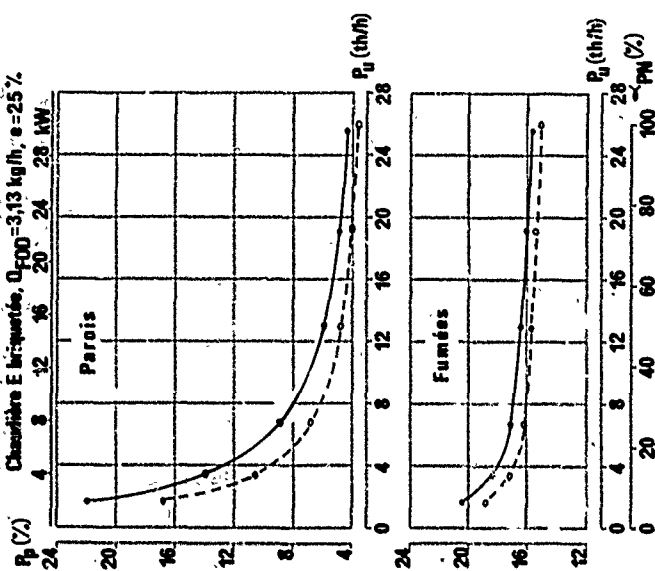


Fig. 11

FONCTIONNEMENT DISCONTINU - Evolution du rendement suivant la charge et la température d'eau

Chaudière E briquetée,  $e = 25\%$ ,  $Q_{FOD} = 3,13 \text{ kg/h}$

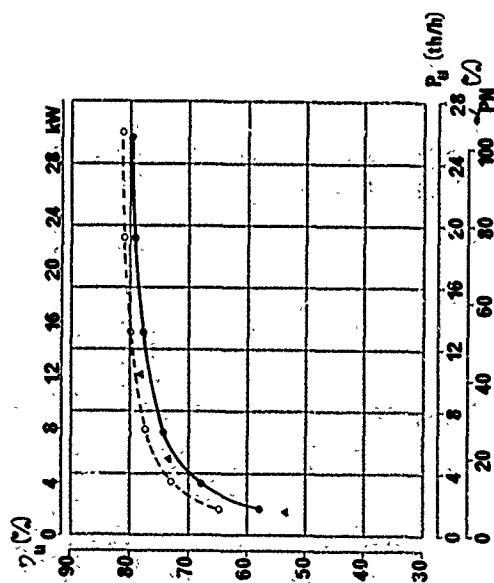


Fig. 10

exp. calcul  $t_E = 70^\circ\text{C}$  - aquastat 85-90°C  
 " " 51°C " 66-71°C



# **FUNCTIONNEMENT CONTINU - Influence du calorifugeage sur les pertes aux parois**

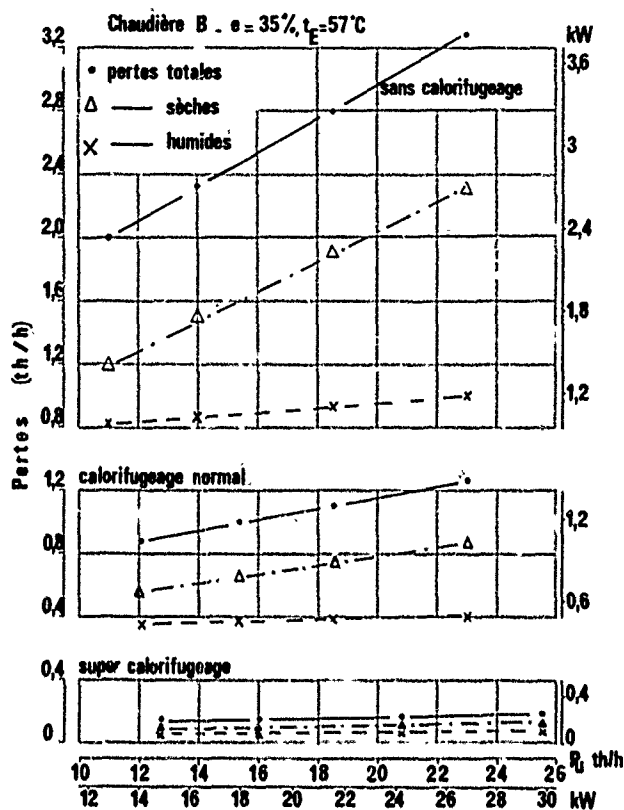


Fig. 13

# **FUNCTIONNEMENT CONTINU - Influence du calorifugeage sur la température des gaz évacués**

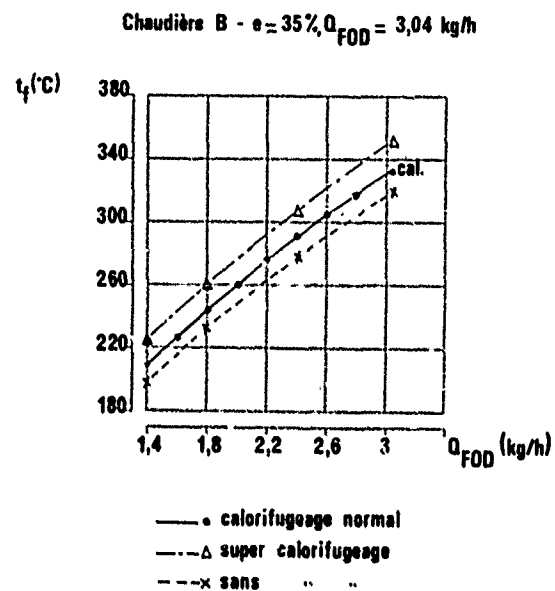


Fig. 14

# **FUNCTIONNEMENT CONTINU - Influence du calorifugeage sur le rendement utile**

Chaudière B -  $\epsilon = 35\%$ ,  $t_E = 57^\circ\text{C}$

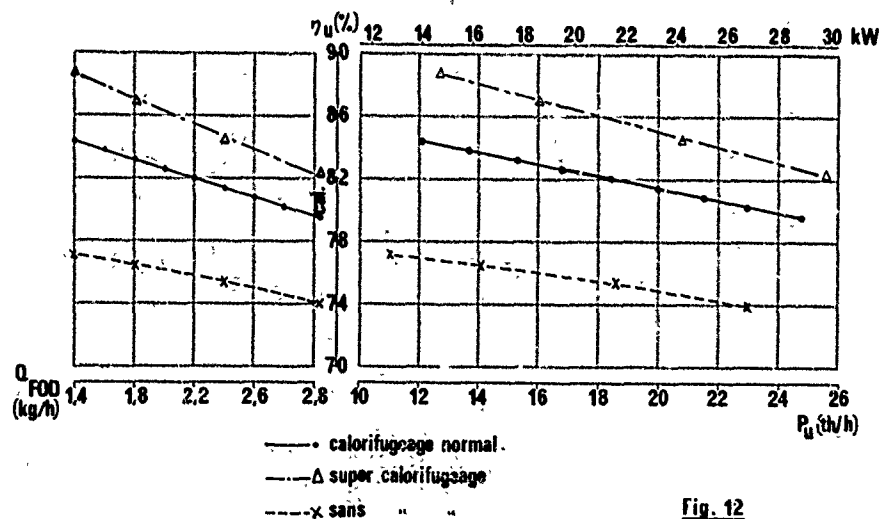
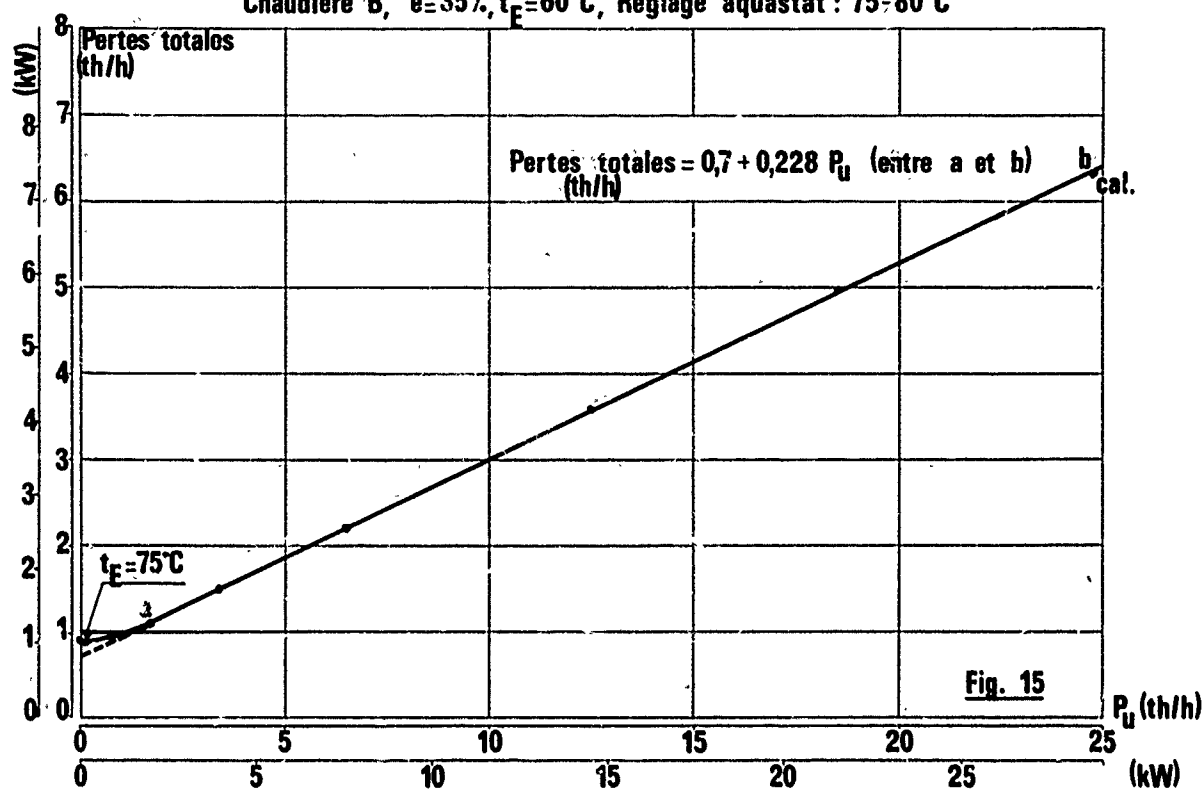


Fig. 12

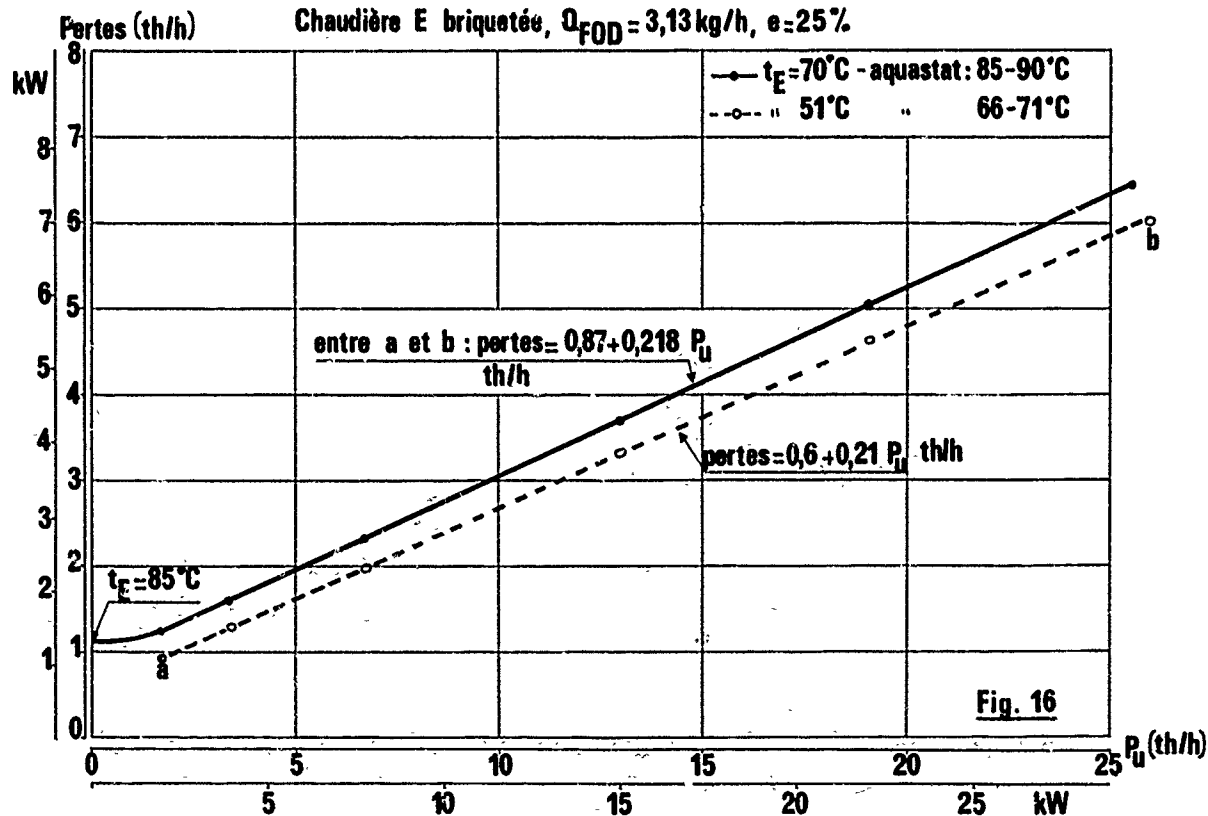
# **FUNCTIONNEMENT DISCONTINU - Evolution des pertes totales suivant la charge**

Chaudière B,  $e=35\%$ ,  $t_E=60^\circ\text{C}$ , Réglage aquastat :  $75-80^\circ\text{C}$



# **FUNCTIONNEMENT DISCONTINU - Evolution des pertes totales suivant la charge**

Chaudière E briquetée,  $Q_{FOD}=3,13\text{ kg/h}$ ,  $e=25\%$



## DISCUSSION

A.Ivernel, Fr

- (1) Disposez-vous de gicleurs à débit variable pour adapter la puissance thermique au besoin thermique de l'installation?
- (2) Pouvez-vous comparer les coûts d'un calcul à ceux d'un essai?

Réponse d'Auteur

- (1) On ne dispose pas de gicleurs à débit variable dans cette gamme de petites puissances. Ce type d'atomiseur se rencontre à partir de débits représentant quelques dizaines de kg/h de fuel.
- (2) Dans les conditions propres à IFP, on peut estimer un rapport des coûts de 1 à 8 en faveur du modèle, pour l'établissement d'une courbe complète de rendements. Cette estimation est basée sur un temps de calcul de l'30 et une expérimentation de 6 journées-technicien.

J.B.Michel, Ne

Une des méthodes suggérée par les agences s'occupant d'économies d'énergie pour ce type de chaudières est de récupérer complètement la chaleur sensible des fumées. Par exemple, la Compagnie Hollandaise "GASUNIE" à Groningen a construit une petite chaudière pilote avec un cycle séparé de circulation d'eau autour de la cheminée et avec récupération également de l'eau condensée. Est-ce que votre modèle pourrait tenir compte de ceci?

Réponse d'Auteur

Le modèle pourrait très probablement s'adapter à ce genre de situation. En particulier, la température de l'eau à l'entrée de la chaudière est un paramètre d'exploitation pouvant varier. Il faudrait ajouter un puits de chaleur dans le circuit échangeur.

Sur le plan strictement pratique, nous supposons que la condensation de l'eau des gaz de combustion doit poser de sérieux problèmes de corrosion pour les surfaces métalliques.

## A CHEMICAL REACTOR MODEL AND ITS APPLICATION TO A PRACTICAL COMBUSTOR

W. Krockow, and B. Simon  
Motoren- und Turbinen-Union München GmbH  
Dachauer Straße 665  
D 8000 München 50, Germany

E.C. Parnell  
Rolls Royce Ltd., Aero Division  
PO Box 3, Filton  
Bristol BS127QE, England

## SUMMARY

A computer model of a combustion chamber is presented, which in its approach is based on chemical reactors. The reactive flow field of the combustor primary zone is divided into elements (vortices) with different mixture ratios and residence times. The variations in concentration in each element are calculated by means of a detailed kinetic reaction mechanism, in which the decomposition of the fuel to carbon monoxide and hydrogen is described by a "one-step-quasi-global" reaction rate. Each element born in the primary zone of the combustor reacts according to its residence time and is subsequently followed on its way through the remaining zones of the combustor by the computer, with discrete amounts of air being added corresponding to the boundary conditions in the combustor.

Idealization of the model (normal distribution) is supported by measurement of the gas concentration at the outlet from the primary zone of a vaporiser-annular combustion chamber. Comparison between the calculated primary zone and outlet concentrations of  $\text{NO}_x$ , CO and unburned hydrocarbons and the measurements show very good agreement.

## SYMBOLS

AFR	-	air-fuel ratio	$Q_r$	kJ	recirculating enthalpy
C	-	normalizing factor	S	-	mixing parameter
EI	$\frac{g}{kg F}$	emission index	T	K	temperature
g	-	maximum number of equivalence ratios	t	s	time
$H_i$	kJ	enthalpy of the inlet fuel-air mixture	WSR	-	well stirred reactor
i	-	maximum number of equivalence ratios	x	m	axial position
n	-	maximum number of residence times	$\eta$	%	efficiency
P	bar	total pressure	$\psi(t)$	-	residence time distribution function
PFR	-	plug flow reactor	$\tau$	s	mean residence time
PSR	-	perfectly stirred reactor	$\phi$	-	equivalence ratio
$Q_i$	$\frac{kJ}{kmol}$	reaction enthalpy of the species i	Index F		fuel
$Q_c$	kJ	heat of combustion			

## 1. INTRODUCTION

The physical and chemical processes occurring in the interior of a gas turbine engine combustion chamber are of a rather complex nature. The flow, because liquid fuel is normally used, is two-phase, highly turbulent and subject to recirculation. Superimposed on the flow process are phase change, mixing and chemical processes which because of their interaction cannot appropriately be discussed separately.

To the engineer the combustion chamber is a rather difficult engine component to predict theoretically considering that minor changes of the flame tube will often have large consequences. More familiarity with all the physical and chemical processes, therefore, will no longer be sufficient to properly interpret test results or to predict the combustion performance when boundary conditions, i.e. the flame tube shape, porting and inlet conditions

are changed.

The engineer must therefore be provided with a computer model to assist in the assessment of the combustion chamber. Such a model will necessarily also be subject to certain limitations and simplifications regarding the physical and chemical processes.

At this time there are two major approaches being used for the description of the overall process in the flame tube:

- flow field models
- reactor models.

With flow field models a complete description of the three-dimensional temperature, concentration and velocity fields is sought.

The advantage afforded by the flow field model is that the combustion chamber is locally resolved for computation not only for mean values but also for local quantities at any place in the flame tube. This permits determination, not only of the combustion efficiency profile and pollutant concentration but also of the pattern factor. The model is also better suited for computing wall temperatures and designing wall cooling configurations.

The attendant penalties are these:

The interaction of turbulence and combustion are difficult to describe and there is therefore still some doubt.

The mathematical effort going into the description of recirculating 3-D flow fields is very great. Therefore a complex kinetic mechanism is generally omitted to keep computer times from becoming excessive. Nor is the evaporation of the fuel normally considered, but if it is, then only by a rather general formula which is difficult to integrate into the model and which permits no interaction between the liquid and the gaseous phases.

These disadvantages limit the usefulness of the flow field model to computational verification of simple experimental combustion chambers.

The reactor models eliminate these difficulties in that they resolve the combustion chamber into a number of chemical reactors. The properties of the reactors are selected to suit the flow and mixing conditions of the zones they represent. Suitable coupling of the reactors one with the other will additionally adapt the model to actual combustion chamber flow conditions.

The merits of the reactor model are obvious. Since they require less computation, a comprehensive kinetic mechanism can be incorporated into the model to be available when needed, e.g., to predict the emission of pollutants from the combustion chamber. In practical work, then, reactor models have proved their worth in the prediction of harmful emissions (Ref. 1 to 4).

## 2. DESCRIPTION OF MODEL

### 2.1 COMBUSTION CHAMBER MODEL

The combustion chamber model which has been developed subdivides the flow field of the combustion chamber primary zone as shown by Fletcher and Heywood (Ref. 1) into elements (eddies) of varying fuel/air mixture ratios and residence times. The massflow content of the various elements are obtained from two statistical distribution functions.

The equivalence ratios are computed from the following distribution function

$$f(\phi) = C \exp \left\{ -\frac{1}{2} \left( \frac{\phi - \bar{\phi}}{\sigma} \right)^2 \right\}$$

corresponding to a Gaussian normal distribution.

The residence times are determined by the function.

$$\psi(t) = 1 - \exp(-t/\tau)$$

which indicates the residence time distribution in a PSR (Fig. 1).

Fletcher et al. developed their model only for predicting  $\text{NO}_x$  in an engine combustion chamber, and as a first approximation they separated the mechanism of  $\text{NO}_x$  formation from the main combustion reactions and assumed the combustion products as well as radicals to be in equilibrium. The present model, however, is not merely to compute the  $\text{NO}_x$  emission of an engine combustion chamber but to determine the entire performance, which makes it necessary to consider also carbon monoxide, unburnt hydrocarbons, hydrogen and radicals.

For each individual eddy resulting from the distribution function of the mixture ratios and from the distribution function of the residence times in the primary zone of the combustion chamber, a detailed reaction kinetic study of the combustion process is made. Fig. 2 shows how the elements formed in the primary zone of the combustion chamber will, in the model, continue through the succeeding combustion chamber zones until they reach the exit.

The elements issuing from the primary zone exhibit various concentrations, temperatures and densities resulting from varying residence times and fuel-air ratios. Each of these elements will then pass through the succeeding combustion chamber zones, where discrete amounts of air are mixed in, in accordance with the flame tube shape and porting. For better identification, each element has three indices (see Fig. 2).

The first index refers to the equivalence ratio  $\phi$ , where the maximum number of equivalence ratios is  $i$ . For each mixture ratio there exists a maximum number  $n$  of elements each having spent a different lifetime (second index). In this a low index reflects a short life, and vice versa. The third index stands for the axial location at which the element happens to be at the moment. The exit from the primary zone is indicated by 0, with the succeeding axial locations being serially numbered from 1 to  $g$ . The condition and the location of the element 5, 12, 4, for example is interpreted as follows: In the primary zone the element had the equivalence ratio  $\phi_5$  and a residence time in that area of  $\tau_{12}$  seconds. It is now in the mixing zone in location 4. Its instantaneous equivalence ratio is a function of  $\phi_5$  and the airflow distribution, because on its way through the preceding axial positions  $x_1 - x_3$ , as much secondary air had been added as corresponds to its own fraction of the entire mass flow. Its instantaneous life time is a function of its previous residence time  $\tau_{12}$  in the primary zone plus the time it needed to flow from the primary zone exit  $x_0$  to the position  $x_4$ . In this manner every condition of each element in the entire combustion chamber depends only on a probability function of the mixing ratios and residence times in the primary zone, and of the configuration of the combustor.

This identification has been chosen because of computational convenience, and the method produces the following computing operation. A beginning is made with the element 1, 1, 0, which is the least element with the shortest residence time in the primary zone. Relative to the reaction kinetic computation this is to say that the concentration changes are computed for an equivalence ratio  $\phi$  from the time  $t = 0$  to  $\tau_1$ . Upon leaving the primary zone the kinetics are computed for each element until it issues from the combustion chamber, with its concentrations changing as a result of chemical reactions and of the continuous addition of air. The instantaneous concentration, temperature, density and combustion conditions of the element at the respective axial positions are multiplied by a weighting factor (mass fraction) and stored.

After the element 1, 1, 0 has left the combustion chamber as the element 1, 1,  $g$  the computation is continued using the element 1, 2, 0. For this element it is only necessary to compute between  $\tau_1$  and  $\tau_2$  since the time  $\tau_0$  to  $\tau_1$  has already been considered for the first element, which had the same equivalence ratio.

After the time  $\tau_2$  the element will leave the primary zone and will be computed all the way through to the combustion chamber exit, with its axial conditions being weighted, added to the preceding result and stored. When all primary zone elements of equal mixture

ratio have been computed, the kinetic computation begins at the time  $t = 0$  with the first element of a new fuel/air ratio. Using the present example this is to say that when element 1, 1, 0 has been computed down to element 1,  $n$ ,  $g$ , the computation will start again with the element 2, 1, 0. The further operation is analogous to all elements having an primary zone equivalence ratio of  $\phi_1$ .

## 2.2 THE RECIRCULATION MODEL

Air and fuel are generally supplied to the combustion chamber at conditions below the spontaneous ignition limit. This makes it difficult to start a kinetic computation. Sometimes equilibrium assumption is used to start the reaction while other authors,

Ref. 5, for example, allow temperatures above the spontaneous ignition temperature. In the model developed here it has been attempted to simulate the physical process of combustion being stabilised by the recirculation of hot gas. As will become clearly apparent from Fig. 3, taken from Ref. 8, an element of fuel and air entering the primary zone of the combustion chamber will mix with the recirculating exhaust gas, so that the mixture will ignite. This is equivalent to an enthalpy allowance  $Q_r$  in Fig. 3. When the element has ignited and the heat  $Q_c$  has been released, the element will recirculate and in turn become a source of ignition for other incoming elements, where it again relinquishes the previously received enthalpy  $Q_r$ . Using this ignition model it becomes possible to do reaction kinetic combustion computations for all combustion chamber inlet temperatures.

## 2.3 THE REACTION KINETIC MODEL

The reaction kinetic model illustrated in Table 1 consists of a one step quasi global reaction rate for the decomposition of the fuel into carbon monoxide and hydrogen in accordance with Edelman (Ref. 6), of an oxidation equation of the carbon monoxide into carbon dioxide, of a set of water gas reactions, and of the expanded Zeldovich mechanism for the description of nitric oxide formation. The vaporisation of fuel is described by an equation analogous to the chemical reaction equations. Table 1 also contains the constants of this equation which are taken from Ref. 7. It will be readily possible to expand the reaction kinetic model, if circumstances require it.

## 2.4 PROGRAM OUTPUT

In order to give an idea of the capacity of the computer model developed, let us here by way of example compute a highly loaded annular vaporizer combustion chamber. The following inlet conditions were selected:

$$\begin{aligned} p &= 15 \text{ bar} \\ T &= 673 \text{ K} \\ \text{AFR} &= 42/1 \end{aligned}$$

Fig. 4 illustrates the contour of this annular combustion chamber, below which are plotted along the centerline of the chamber the mole fraction of all components considered in the computation. Inasmuch as the primary zone is considered a WSR, the concentrations of the various components shown at the primary zone exit in Fig. 4 will apply to the entire primary zone.

The primary zone exit is characterised by large quantities of  $\text{H}_2\text{O}$ ,  $\text{CO}_2$ ,  $\text{CO}$  and  $\text{H}_2$ , with their concentrations all of the same order of magnitude. The radical concentrations, such as  $\text{O}$ ,  $\text{H}$  and  $\text{OH}$  are of a lower value.

Immediately downstream of the primary zone further oxidation reactions take place and reduce carbon monoxide, hydrogen and unburnt fuel, causing water and carbon dioxide to form. The  $\text{NO}$  content, too, slightly rises in this intermediate area and is indicative of the temperature rise in this zone.

Downstream of the large mixing zone holes changes in concentration will be caused by dilution. Only radicals and unburnt fuel will still continue to react.

### 3. COMPARISON BETWEEN MEASUREMENT AND COMPUTATION

#### 3.1 DESCRIPTION OF TEST PROCEDURE

In order to arrive at a comparison between values computed by the above method and experimental results, rig tests were carried out on an annular combustor, in which both air/fuel ratio and combustion efficiency distributions were derived. A general arrangement of the combustor is shown in Fig. 5, and only a brief description is given here as this type is fully described in Ref. 9.

The fuel, which is supplied to the combustor at a low pressure, together with some air is injected into a number of "vaporisers" via fuel tubes which are bifurcated at the outlets to inject equal amounts of fuel into each arm through metering orifices. The mixture strength is arranged to be much too rich for combustion to take place inside the vaporiser. The mixture is heated by virtue of the vaporisers being immersed in the burning zone and then exhausted upstream which supports the recirculation for the fundamental stabilisation of the process. Further air for combustion is then introduced through primary air ports, a percentage of which recirculates upstream. The remaining air is injected through a series of film cooling rings and a single row of ports, the latter providing the air for the mixing process, prior to the gases entering the turbine.

The two traverse planes considered in this report are shown in Fig. 5. Plane AA is conventionally considered as the primary zone exit, and BB as the combustor outlet. The probe used for gas sampling at plane AA was a single point water cooled one, mounted at the combustor outlet and protruding into the chamber. The traversing arrangement allowed circumferential movement as well as radial, and the majority of tests were carried out at 7 radial positions, each at a centre of equal area, over a 180° sector. From previous tests it had been shown that this size of sector was representative of the whole annulus. The probe was traversed continuously, the output being recorded on a multi-channel UV recorder. From the traces obtained, values were read off every 6° circumferentially.

For the exit traverse a 5 point water-cooled gas sampling probe was used, all the points being connected together. A 360° continuous traverse was carried out, a complete sweep taking about 9 minutes.

#### 3.2 ANALYSIS EQUIPMENT

##### a) PRIMARY ZONE

A diagrammatic circuit layout for primary zone analysis is shown in Fig. 6, with instrumentation identification in Fig. 6a. The sample is brought from the water cooled probe to the equipment through a steam heated line, dividing into 2 streams, X and Y. Sample X is used for the direct measurement of CO<sub>2</sub> after drying, and CO after drying and CO<sub>2</sub> removal. Sample Y gives the total CO<sub>2</sub> (dry) produced from the sample, combustion having been completed by passing it through a furnace. Additional air is added as necessary to give complete combustion, this being monitored on the CO IRGA, which should read zero. Measurements are made of the added air flow, the total flow after the furnace and the added flowmeter delivery pressure. After corrections for differences in added and total flowmeter downstream pressures and for volume changes caused by combustion reactions in the furnace, the sample dilution can be estimated and hence, using the furnace CO<sub>2</sub> concentration, the sample fuel/air ratio.

A "burnt" fuel/air ratio proportional to the combustion CO<sub>2</sub> and CO values is calculated, allowing the combustion efficiency to be computed as 100  $\left( \frac{\text{"burnt" fuel/air ratio}}{\text{fuel/air ratio}} \right) \%$

##### b) COMBUSTOR OUTLET

The arrangement used for combustor outlet analysis is basically that laid down by the Environmental Protection Agency and published in the Federal Register Vol. 43 No. 58, Fig. 1. Separate measurements can be made on samples from both stationary and traversing probes of CO<sub>2</sub>, CO, total hydrocarbons, NO<sub>x</sub>, NO and smoke content, permitting cal-



ulation of component emission indices combustion efficiency and fuel/air ratio.

### 3.3 TEST CONDITIONS

For the comparison of measured and calculated values considered in this paper, the following test conditions were used:

Combustor inlet temperature	773 K
Overall air/fuel ratio	38.5/1
Combustor outlet pressure	Atmospheric

At this condition both the primary zone outlet and combustor outlet planes are presented. Tests were also carried out under high pressure conditions, but as primary zone traverses were not possible under those conditions, these results are unsuitable for comparison with calculated values.

### 3.4 EXPERIMENTAL RESULTS

#### ATMOSPHERIC OUTLET PRESSURE

The air/fuel ratio and combustion efficiency distributions at the primary zone outlet are shown in Figs. 7 and 8 respectively. As well as the circumferential variations, the mean radial values are also included.

As can be seen there is a very wide range of values at this particular plane, indicating that there is still a considerable amount of mixing and combustion still to take place further downstream. As might be expected the more efficient areas are in general those with the weakest air/fuel ratio.

At the outlet plane mean values of air/fuel ratio, combustion efficiency, and emission indices for CO and CH<sub>4</sub> were obtained. These are compared with calculated values in a following paragraph.

### 3.5 COMPARISON OF CONCENTRATIONS AT PRIMARY ZONE EXIT

The measurements made of local AFR's at the exit of the primary zone, which produced the contours of Fig. 8, permit the assumptions made in the computer model to be verified. The most important of these is that of a Gaussian normal distribution of the mixture ratios in the primary zone. Fig. 9 is a statistical analysis of the AFR's measured in the form of a cumulative function. It shows that the proposition of a normal distribution of the mixture ratios actually holds true and, thus, that the assumption in the model agrees very well with the facts. The mixture ratios were computed from the measured concentrations of carbon monoxide, carbon dioxide and unburnt hydrocarbons, so that for these components a comparison could be made with the computation.

Shown for comparison in Table 2 are the measured and the computed concentrations of carbon monoxide, of unburnt hydrocarbons and the combustion efficiency. This comparison is considered good in view of the difficult job of establishing a combustion chamber computer model. The fact that in the case of unburnt hydrocarbons the difference between measurement and computation is less than a factor of 2 is especially significant, for it is the unburnt hydrocarbons which because of the high reaction rates are the most difficult to predict.

### 3.6 COMPARISON OF COMBUSTOR EXIT CONCENTRATIONS

The measurements at the combustion chamber exit were taken on the same unit that had previously been used for primary zone investigation.

Fig. 10 as Fig. 4 shows the computed profile of concentrations along its whole axis.

Plotted on this diagram for comparison are the measured concentrations of CO and UHC at the primary zone exit and at the end of the combustion chamber. Agreement is good, with the comparative values again listed in Fig. 10.

While in these tests no readings were taken of NO emission, they are known for this combustion chamber to be  $EI_{NO} = 35 \text{ g}_{NO}/\text{kg}_F$  at the combustion chamber exit measured at 15 bar.

Using the variation of NO emission with pressure of

$$EI_{NO} \propto p^{0.5}$$

an index of  $9 \text{ g}_{NO}/\text{kg}_F$  is determined for atmospheric conditions, which agrees well with the computed figure.

#### 4. POSSIBILITIES OF THE PROCEDURE

##### 4.1 EFFECT OF HOMOGENEITY

The degree of homogeneity of the primary zone in the model is controlled by the S-parameter, which is a measure of the width of the previously mentioned Gaussian distribution function. For all computations made so far a value of  $S = 0.5$  had been selected. This value had resulted from the measurement of the fuel/air distribution at the primary zone exit.

It is of considerable importance to the assessment of the computer model that this value of the S-parameter gives the best comparison with the test results for all components and that it is not necessary to select a different S-parameter for each component.

In a combustion chamber computer model the selection of a mixing parameter S as it had originally been defined in Ref. 4 and has here been further developed, provides a great advantage in that effects caused by variation in the mixing quality can be generally predicted. An improved injection system (e.g. air blast atomizer) or an increased flame tube pressure loss will obviously produce a more homogeneous mixture in the primary zone. Calculations using a better, i.e. a smaller value of S will thus be able to predict combustion concentrations for more homogeneous conditions.

For the reference combustion chamber, where the best agreement of computed with measured emission values both in the primary zone and at the combustion chamber exit resulted from an S-parameter of 0.5, the effect of the mixing quality has been shown in Fig. 11a - c for nitric oxide, carbon monoxide and unburnt hydrocarbons (in the form of  $C_8H_{16}$ ). With the combustion chamber configuration selected here, the emissions are reduced, as the mixing quality improves.

In the case of NO, with an improvement in homogeneity from  $S = 0.5$  to  $S = 0.3$ , the reduction is not very large, but is much greater for CO and UHC.

The curves of Fig. 11a - c are merely meant to serve as an example for the possible applications of the combustion chamber computer program. They do not apply generally, because at other flow distributions or combustion chamber conditions the curves may well be different in shape as well as quantitatively. This has been confirmed by a large number of calculations.

##### 4.2 EFFECT OF GEOMETRIC CHANGES

The computer process will also be able to estimate the effect of a change in air distribution. In Figs. 12a,b, the dilution holes have been divided into two rows, having the same total effective area as previously. They compare axial concentrations, temperature and combustion efficiency profiles for the old and the modified combustor.

This modification clearly causes the temperature profile to flatten out at a lower final value, which is accompanied by a lower combustion efficiency (Fig. 12a). Carbon monoxide and unburnt hydrocarbons are quenched earlier than with the reference configuration, which raises the concentration at the combustion chamber exit of both components (Fig. 12b). Nitric oxide responds in the opposite fashion, its final concentration being clearly below that of the reference configuration.

The production of NO is stopped in the zone between the row of primary holes and mixing holes. The concentration of the primary zone exit is merely diluted. This example reflects known phenomena, such as the opposite CO-NO response, the effect of temperature on NO, etc., which emphasises the general accuracy of the model.

#### 4. PARAMETERS AFFECTING THE COMBUSTION EFFICIENCY

Evaluation of the computed results relative to the axial profile of combustion efficiency or to the components affecting combustion efficiency provides interesting and generally applicable information.

From the computed concentrations of the components the combustion efficiency can be determined using the relationship

$$\eta [\%] = 100 - 0.1 \sum EI_i Q_i / Q_F$$

where  $Q_i$  are the calorific values of the components  $i$  and where  $Q_F$  is the calorific value of the fuel. Fig. 13 shows how much the various components  $i$  will affect the total combustion efficiency.

The values

$$\frac{\Delta \eta_i}{\Delta \eta} = \frac{EI_i Q_i}{\sum EI_i Q_i}$$

are plotted along the combustion chamber axis.

In the primary zone it is the unburnt hydrocarbons and the carbon monoxide which mainly affect the combustion efficiency, with hydrogen contributing a moderate 14 %, all other components being negligible. These effects change considerably towards the end of the combustion chamber. Carbon monoxide and hydrogen contribute to the loss in efficiency  $\Delta \eta$  to the same degree as in the primary zone, whereas the unburnt hydrocarbons are now less important. The effects of OH radicals and O atoms, which have not yet recombined at the combustion chamber exit, are increasing. Since in gas analysis the combustion efficiency at the combustion chamber exit can generally be determined only by means of the unburnt hydrocarbons and carbon monoxide, approximately 50 % of incompletely oxidated components are thus neglected.

#### 5. CONCLUSION

It can be shown that the proposal by Fletcher and Heywood, Ref. 1, to represent an heterogeneous reacting combustion chamber primary zone by using a probability function of the mixture ratios and a probability function of the residence times can also be applied to the calculation of the carbon-monoxide emission and unburnt hydrocarbons. To achieve this the proposal in Ref. 1 had to be further extensively developed. A new model for the recirculating of energy and exhaust gas would have to be developed to make available the proper starting conditions for a detailed reaction kinetic mechanism which would have to contain an equation which considers the vaporization of the fuel. During the development of the method it clearly became apparent that the transition from the primary zone (the WSR) to the downstream combustion chamber zones (the PSR's) has to be simulated differently from Ref. 1. It was necessary to follow every individual element generated in the combustion chamber primary zone through the combustion chamber to the exit and to add to it discrete air quantities in accordance with the combustion chamber configuration and inlet conditions.

The comparison of the calculated and the measured concentrations at the exit of the primary zone and at the exit of the combustion chamber showed good agreement, this agreement being arrived at with one mixing parameter for all components which were investigated.

Sample calculations show that this combustion chamber calculation method is able to effectively assist the combustion engineer in the development of a combustion chamber, as it enables predictions to be made of the effect of geometric modifications on the combustion characteristics of the combustion chamber.

## 6. REFERENCES

- 1 Fletcher, R.S.  
Heywood, J.E.      A Model for Nitric Oxide Emissions from Aircraft Gas Turbine Engine  
AIAA 9th Aerospace Sciences Meeting, New York, Jan.25-27, 1971
- 2 Hammond, D.D.  
Mellor, A.M.      Analytical Calculation of the Performance and Pollutant Emissions of Gas Turbine Combustors  
AIAA Paper No. 71-711
- 3 Moissier, A.M.  
Roberts, S.A.      Low Power Turbopropulsion Combustor Exhaust Emissions  
Vol. III Analysis, AFAPL-TR-73-36 (1973)
- 4 Swithenbank, J.  
Turan, A.  
Felton, P.G.      Progress in Modelling Combustors  
HIC 303 Sheffield University
- 5 Aceto, L.D.  
Kollrack, R.      Primary Zone Carbon Monoxide Levels for Gas Turbines,  
Part I Premixed Comb.  
AIAA Journal, Vol. 12 (1974) Nr. 4
- 6 Edelman, R.B.  
Fortune, O.F.      A Quasi Global Chemical Kinetic Model for the Finite Rate Combustion of Hydrocarbon Fuels with Application to Turbulent Burning in Hypersonic Engines and Nozzles  
AIAA Paper No. 69-86 (1969)
- 7 Adelman, H.G.  
Browning, L.H.  
Pefley, R.K.      Predicted Exhaust Emissions from a Methanol and Jet Fueled Gas Turbine Combustor  
AIAA Paper No. 75-1266
- 8 Waldmann, C.H.  
Wilson, R.R.  
et al.      Analysis of the Kinetic Mechanism of Methane-Air Combustion with Pollutant Formation  
Western States Section/The Comb. Inst., 1974 Spring Meeting Pullman, May 6-7, 1974
- 9 Parnell, E.C.  
Williams, M.R.      A Survey of Annular Vaporising Combustion Chambers  
11th Symp. on Comb. and Heat Transfer in Gas Turbine Systems, Cranfield Inst. of Technology, 1969

## ACKNOWLEDGEMENT

The authors wish to thank their respective management for permission to publish this paper and also their colleagues for assistance in its production.

Part of work reported was financed by the Bundesministerium der Verteidigung under ZTL-contract MTU 4.12.

Reaction Equation	A	$\alpha$	E
Fuel Vaporisation $(C_a H_b)_{\text{liquid}} \rightarrow (C_a H_b)_{\text{gas}}$	$2 \cdot 10^5$	0	9930
Chemical Reactions $C_a H_b + \frac{a}{2} O_2 \rightarrow a CO + \frac{b}{2} H_2$		see Ref. 6	
$CO + OH \rightleftharpoons CO_2 + H$	$5,60 \cdot 10^{11}$	0.	1080
$OH + H_2 \rightleftharpoons H + H_2O$	$2,19 \cdot 10^{13}$	0.	5150
$O_2 + H \rightleftharpoons OH + O$	$2,24 \cdot 10^{14}$	0.	16800
$O + H_2 \rightleftharpoons OH + H$	$1,74 \cdot 10^{13}$	0.	19450
$O + H_2O \rightleftharpoons OH + OH$	$5,75 \cdot 10^{13}$	0.	18000
$H + H + M \rightleftharpoons H_2 + M$	$5,00 \cdot 10^{18}$	-1,15	0.
$O + O + M \rightleftharpoons O_2 + M$	$4,70 \cdot 10^{15}$	-0,28	0.
$O + H + M \rightleftharpoons OH + M$	$5,30 \cdot 10^{15}$	0.	-2780
$H + OH + M \rightleftharpoons H_2O + M$	$1,17 \cdot 10^{17}$	0.	0.
$O + N_2 \rightleftharpoons NO + N$	$6,19 \cdot 10^{13}$	0,10	75241
$N + O_2 \rightleftharpoons NO + O$	$6,43 \cdot 10^9$	1,0	6250
$N + OH \rightleftharpoons NO + H$	$2,80 \cdot 10^{13}$	0.	0.

with  $K = A \cdot T^{\alpha} \exp(-E/RT)$   
Units in cal, K, mol, sec, cm

Table 1: Reaction Kinetic Mechanism

	Measurement	Calculation
$EI_{CO} \quad g_{CO}/kgF$	585	648
$EI_{UHC} \quad g_{UHC}/kgF$	317	212
$EI_{NO} \quad g_{NO}/kgF$	NA**	9.1
* $\eta \quad \%$	54.5	55.2

\*\*Not Available

\* For determination of combustion efficiency the following formulas were taken:

$$\text{Measurement: } 100 - \eta = 0.1 EI_{UHC} + \frac{EI_{CO}}{42.5}$$

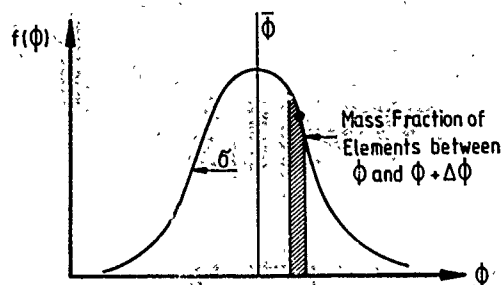
Calculation: Formula given in text regarding all unburnt species  
(Chapter 4)

Table 2: Comparison of Measured and Computed Values at Primary Zone Exit

## Equivalence Ratio Distribution Function

$$f(\phi) = C \exp \left[ -\frac{1}{2} \left( \frac{\phi - \bar{\phi}}{\sigma} \right)^2 \right]$$

C = Normalizing Factor

S =  $\sigma/\bar{\phi}$  Mixing Parameter

## Residence Time Distribution Function

$$\psi(t) = 1 - e^{-t/\tau}$$

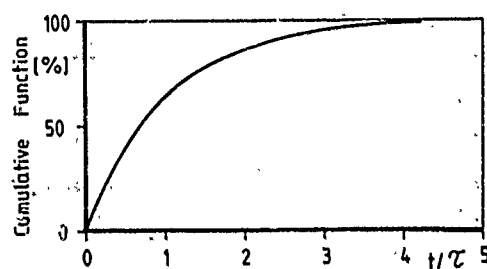
 $\tau$  Mean Residence Time

Fig. 1: Distribution Curves for Massfraction and Residence Time

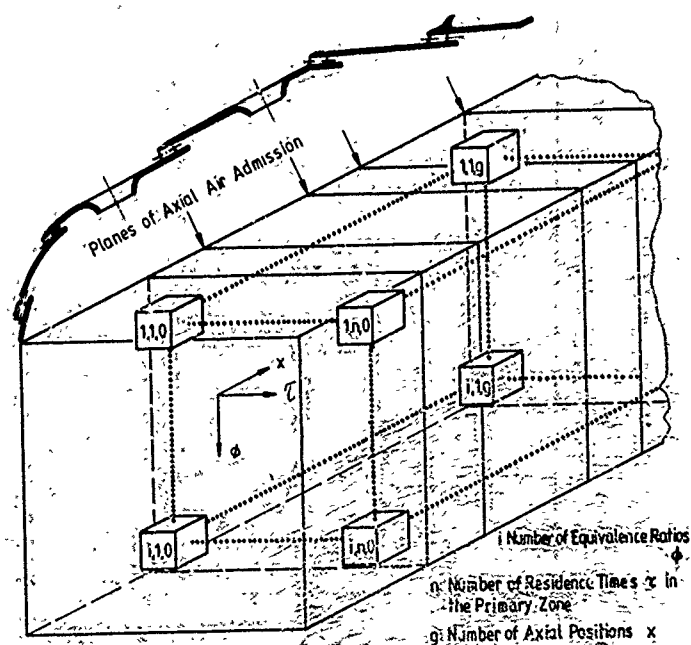


Fig. 2: Combustor Model

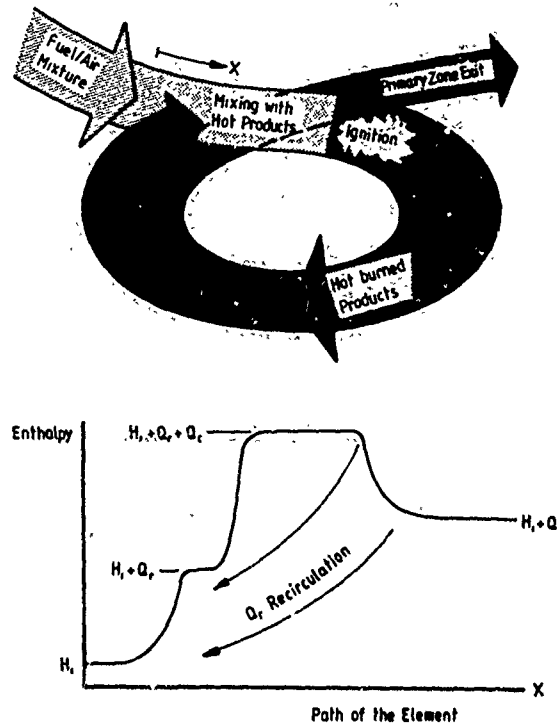


Fig. 3: Physical Explanation of Recirculation and Interchange of Enthalpy

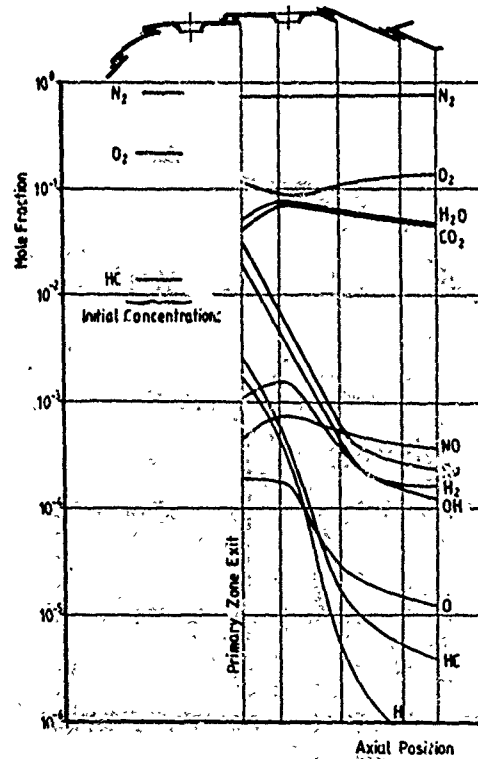


Fig. 4: Axial Profile of Species Concentration (AFR = 42,  $p = 15$  bar,  $T = 673$  K)

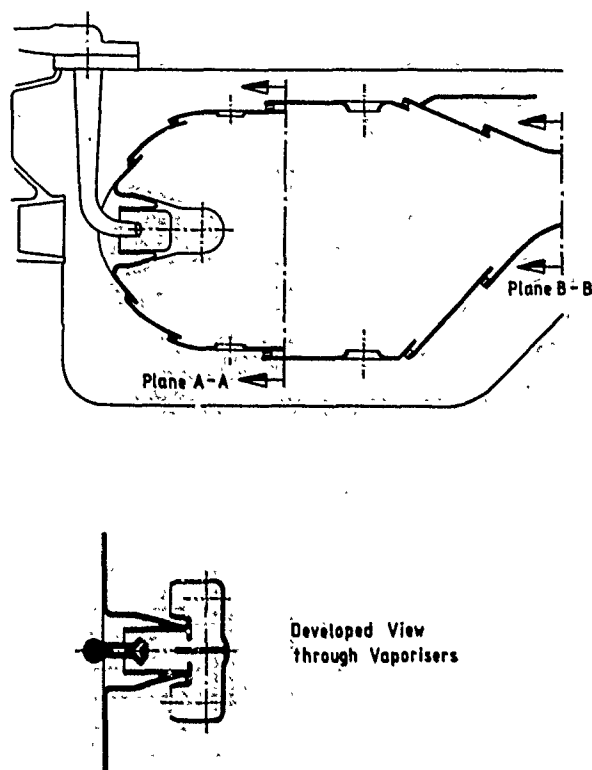
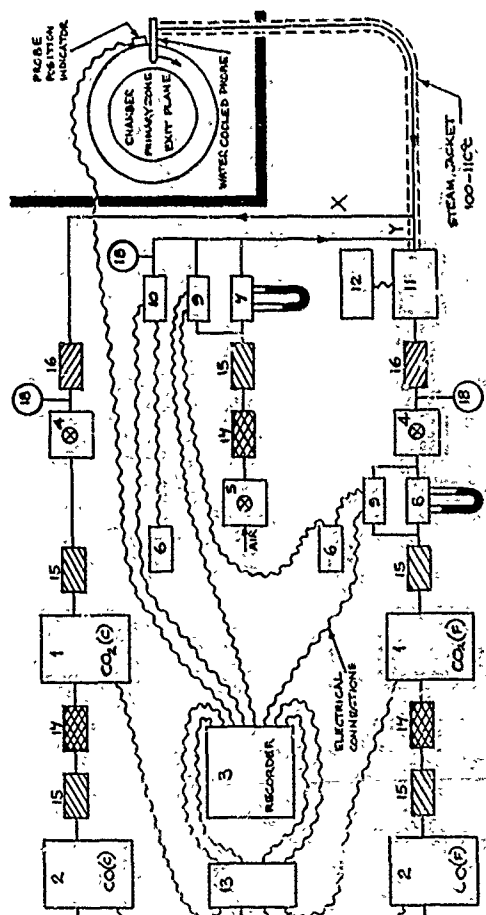


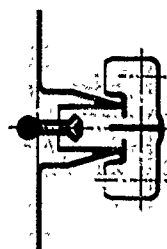
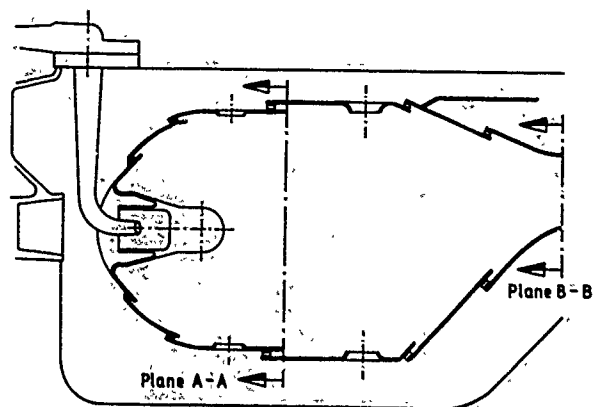
Fig. 5: General Arrangement of the Combustor



1	CO <sub>2</sub> Infrared gas analyser
2	CO Infrared gas analyser
3	12 channel UV recorder
4	Sample pump
5	Added air pump
6	Transducer converter
7	Capillary flowmeter (Added)
8	Capillary flowmeter (Total)
9	Differential pressure transducer
10	Absolute pressure transducer
11	Combustion furnace
12	Furnace power supply and temperature controller
13	Circuitry - signal damping and sensitivity adjustment
14	Parameter
15	Drying tube containing CaCl <sub>2</sub> and Mg (ClO <sub>4</sub> ) <sub>2</sub>
16	Drying tube containing CaCl <sub>2</sub>
17	CO <sub>2</sub> absorbent tube containing soda lime
18	Pressure gauge

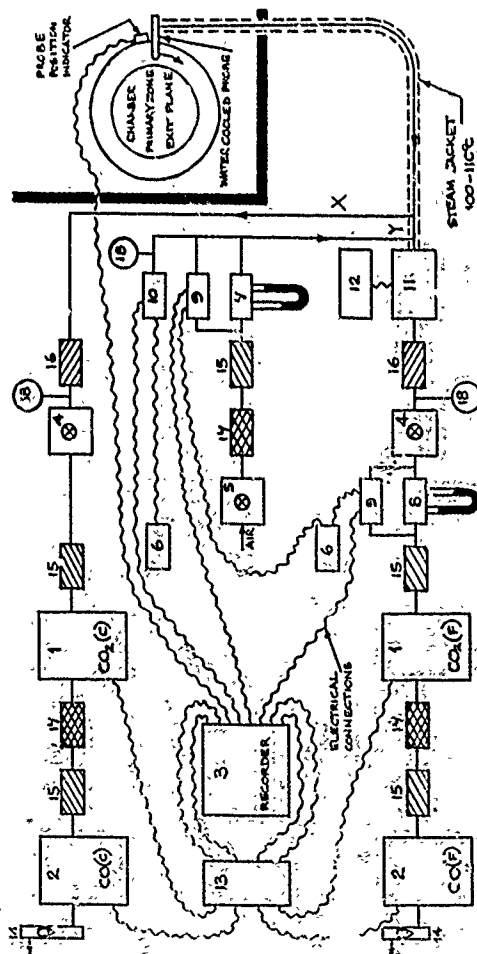
Fig. 6a: Identification of Numbered Items in Figure 6





Developed View  
through Vaporizers

Fig. 5: General Arrangement of the Combustor



1	CO <sub>2</sub> Infrared gas analyser
2	CO Infrared gas analyser
3	12 channel UV recorder
4	Sample pump
5	Added air pump
6	Transducer converter
7	Capillary flowmeter (Added)
8	Capillary flowmeter (Total)
9	Differential pressure transducer
10	Absolute pressure transducer
11	Combustion furnace
12	Furnace power supply and temperature controller
13	Circuitry - signal damping and sensitivity adjustment
14	Rotameter
15	Drying tube containing CaCl <sub>2</sub> and Mg (ClO <sub>4</sub> ) <sub>2</sub>
16	Drying tube containing CaCl <sub>2</sub>
17	CO <sub>2</sub> absorbent tube containing soda lime
18	Pressure gauge

Fig. 6a: Identification of Numbered Items in Figure 6

Fig. 6: Diagrammatic Circuit Layout for Primary Zone Analysis

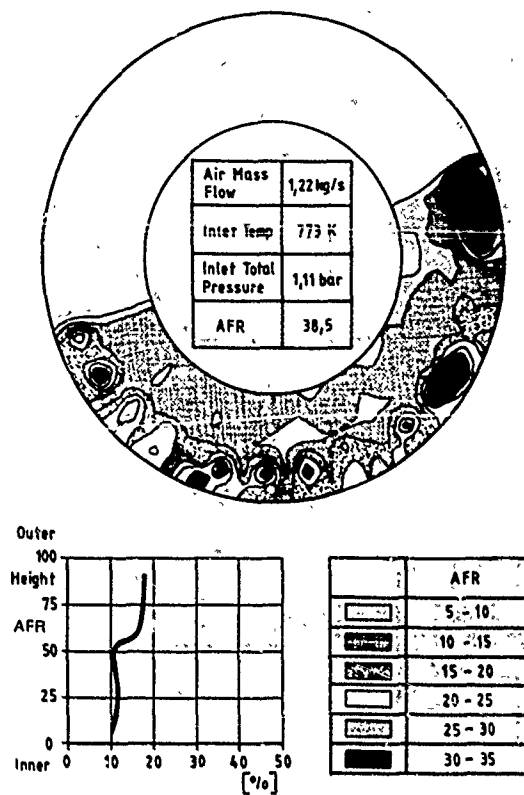


Fig. 7: Measured Air/Fuel Ratio Distribution at the Primary Zone Outlet

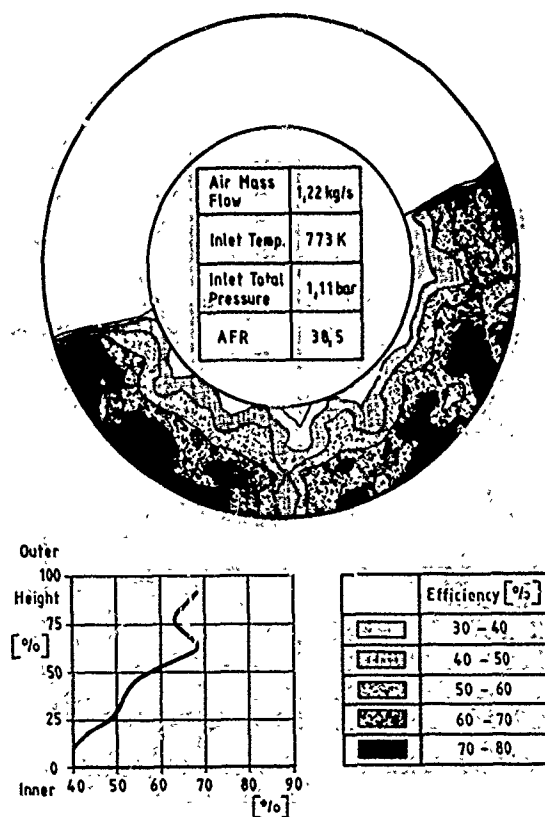


Fig. 8: Measured Combustion Efficiency Distribution at Primary Zone Outlet

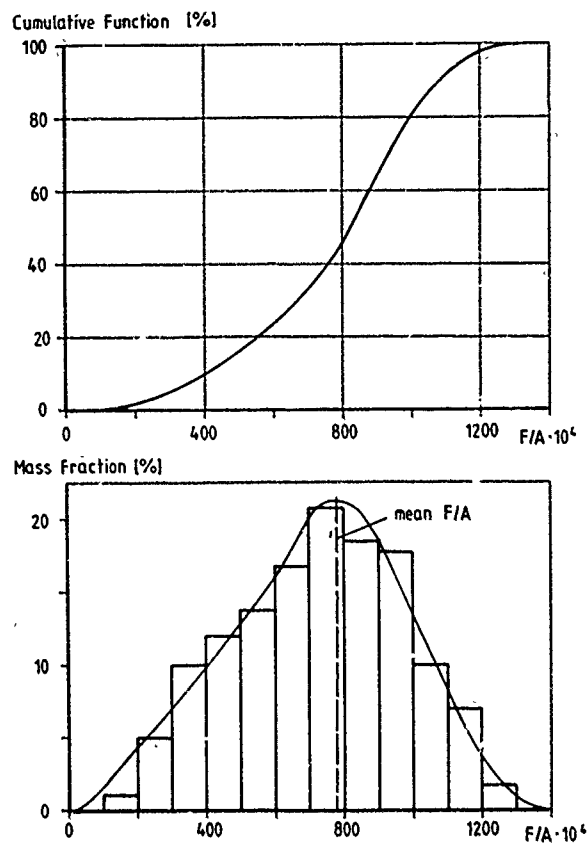


Fig. 9: Measured Fuel/Air Distribution Curves at Primary Zone Outlet

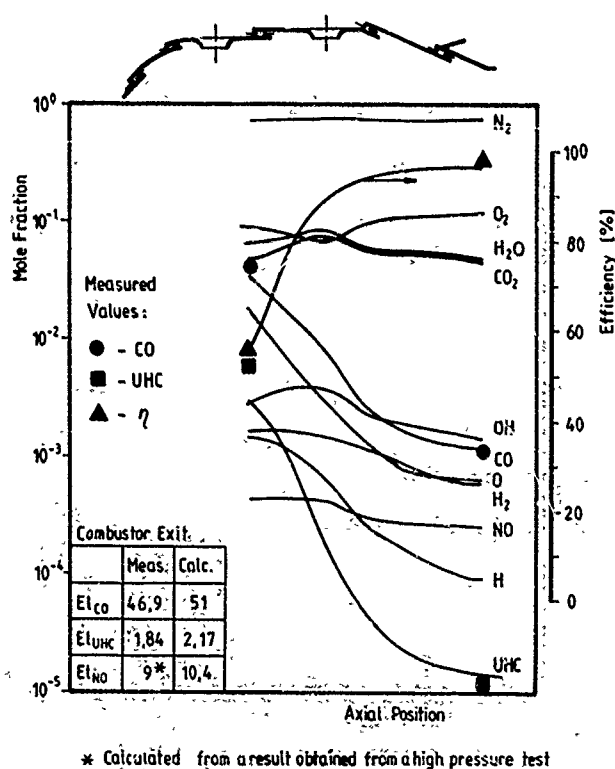


Fig. 10: Comparison of Measured and Computed Concentrations

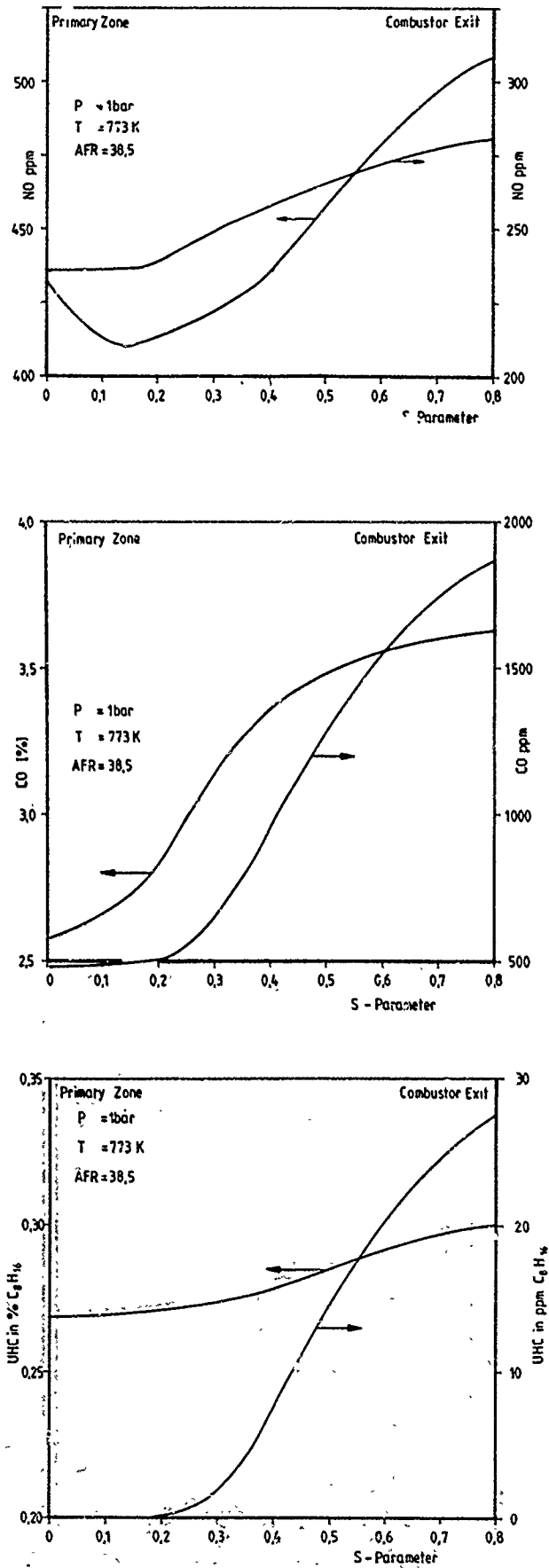


Fig. 11a - c: Influence of Homogeneity on NO, CO and UHC

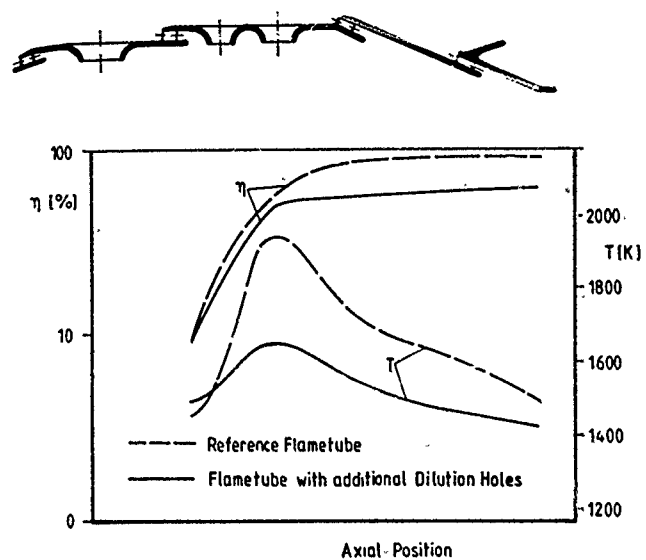


Fig. 12a: Influence of Additional Holes on Temperature and Efficiency

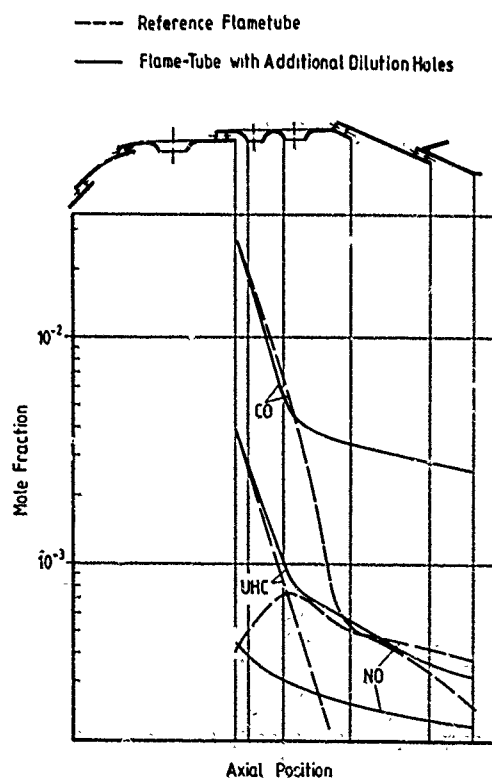


Fig. 12b: Influence of Additional Holes on Axial Concentrations

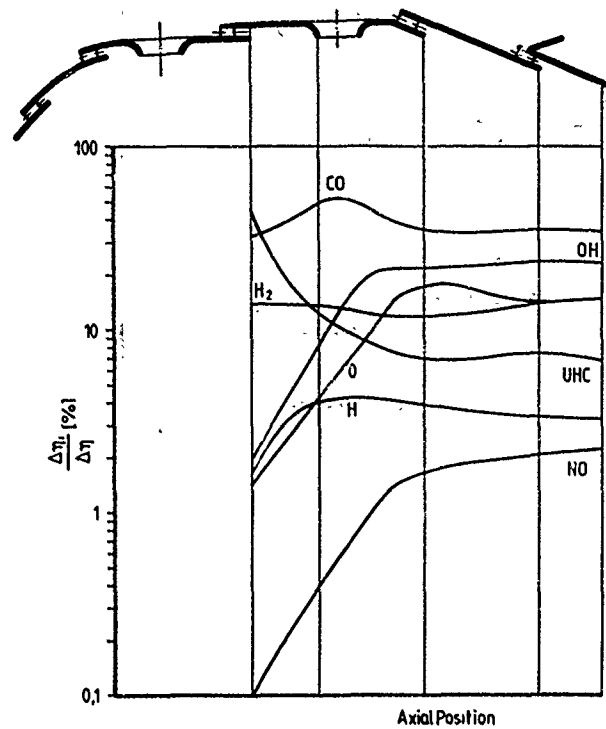


Fig. 13: Fraction of Efficiency Loss of Different Energy Containing Species

## DISCUSSION

P. Gastebois, Fr

Comment modélisez-vous l'introduction de l'air de dilution? Est-ce un mélange brutal ou introduisez-vous une loi de mélange entre l'air de dilution et les gaz en combustion?

Author's Reply

We did not make an infinite mixing assumption for the dilution and cooling air. We look for the data of the air distribution from a previous aerodynamic calculation and used a mixing law according to the equation:

$$m_j = [(x - x_j)/(x_M - x_j)]^{0.5} M_j$$

$M_j$  total air in the plane (e.g. dilution air)  
 $x$  axial position downstream of the injection plane  
 $x_j$  axial position of the injection plane  
 $x_M$  mixing length of the jets  
 $m_j$  mixed fraction of air at position  $x$

The mixing length  $x_j$  was taken from previous water model tests.

Comment by D.T. Pratt, US

The coalescence/dispersion model for reacting, segregated flow described in Paper 15 was devised in part, to overcome the difficulties of the Fletcher-Heywood " $\sigma$ "-model which is the basis of this paper.

The advantages are the following:

- (1) Fuel and air need not be premixed and  $\sigma$ -distributed.
- (2) No *a priori* assumption w.r.t. residence-time distributions need be made.
- (3) No special assumptions to effect recirculation-ignition problems are required.
- (4) No additional computational work is required.
- (5) A single parameter ( $\beta$  vs  $\sigma$ ) controls *both* FIA mixing distribution, recirculation-ignition, and decaying exponential residence time distribution *all* of these advantages are gained by using a stochastic (C/D) vs a deterministic ( $\sigma$ ) model!
- (6) Flame extinction (blowout) may be predictable.

J.B. Michel, Ne

What was the nitrogen content of the fuel that you utilized and did you take into account the fact that you did not have a mechanism for "NO fuel" formation? Do you believe that your predictions of  $\text{NO}_x$  are realistic?

Author's Reply

As the fuel which was used for the experimental tests had no nitrogen content, there was no need to account for a "NO fuel" formation mechanism. But some other results from reaction kinetic calculations using the assumption, that the fuel bound N is present as free N atoms in the hydrocarbon decomposition phase showed the same trends as those from published tests.

The  $\text{NO}_x$  predictions showed good agreement with measurements taken from a high pressure test and scaled down to atmospheric conditions by the well known pressure dependence (see Figure 10).

S. Wittig, Ge

Did you perform a sensitivity analysis of your model with respect to the reaction kinetics? Is the resulting axial temperature profile in agreement with selective measurements?

Author's Reply

We did not perform a sensitivity analysis with respect to the reaction kinetics except for the vaporisation equation which has been included in the kinetics. Calculations showed, that this equation affects the unburnt hydrocarbons with increasing combustor inlet pressure.

The mean exit temperature is in agreement with the measurements, but it is not possible to measure temperatures by thermocouples inside the combustor. Nevertheless the agreement of primary zone efficiencies also reflect a temperature agreement.

# SEMI-EMPIRICAL CORRELATIONS FOR GAS TURBINE EMISSIONS, IGNITION, AND FLAME STABILIZATION

by

A. M. Mellor  
Professor  
The Combustion Laboratory  
School of Mechanical Engineering  
Purdue University  
West Lafayette, Indiana 47907, U.S.A.

## SUMMARY

For operating conditions where the fuel evaporation rate is fast compared to the fuel vapor/air mixing rate, a characteristic time model has been formulated to predict gaseous emissions and efficiency in terms of combustor inlet conditions and geometry. The model, which involves kinetic and fluid mechanic times, has been used to design low  $\text{NO}_x$  burners, and study of several different conventional engine combustors suggests that the correlation may be universal. A related model, which includes a fuel droplet evaporation time, is being validated with data from laboratory combustors for spark ignition and lean flame stabilization. The preliminary application of this latter model to engine situations is described.

## LIST OF SYMBOLS

A	surface area of spark kernel at the quenching distance
a	empirical constant
B	mass transfer number for evaporation
$c_{pa}$	ambient specific heat at constant pressure
D	disc diameter
$D_{bo}$	Damköhler number at blowout
$D_{co}$	Damköhler number for CO oxidation
$D_{no}$	Damköhler number for NO formation
d	tube diameter
$d_{comb}$	combustor diameter at quench location
$d_o$	Sauter mean diameter of fuel spray
$d_q$	quenching distance
$E_{min}$	minimum spark ignition energy
EI	emissions index (g pollutant/kg fuel)
$k_a$	ambient thermal conductivity
$\ell_{co}$	effective CO quench length $(\ell_{co,quench}^{-1} + d_{comb}^{-1})^{-1}$
$\ell_{i,quench}$	air addition site where species i quenches
$\ell_{no}$	effective NO quench length $((\ell_{no,quench}/\cos\theta)^{-1} + d_{comb}^{-1})^{-1}$
$\ell_{pri}$	length from fuel injector to primary air penetration jets
$\dot{m}_a$	combustor air flow rate
$\dot{m}_{apz}$	primary zone air flow rate
P	combustor inlet pressure
$Q_i$	lower heating value of species i
R	universal gas constant
r	correlation coefficient
T	absolute temperature
$\bar{T}$	mean temperature $(.5T_{in} + .5T_\phi)$
$T_{co}$	CO oxidation temperature $(.85T_{in} + .15T_\phi)$



$T_{in}$	inlet air temperature
$T_{\eta}$	efficiency oxidation temperature $(.9T_{in} + .1T_{\phi})$
$T_{\phi}$	burned gas temperature at equivalence ratio $\phi$
$T_{\phi=1}$	adiabatic stoichiometric flame temperature
$V$	mixture velocity in spark gap
$V_{ann}$	air velocity in plane of flameholder
$V_i$	fuel injection velocity
$V_{ref}$	reference velocity at maximum combustor cross-sectional area
$V_{\phi=1}$	velocity estimate in NO forming region
$\alpha$	ambient thermal diffusivity
$\beta$	effective evaporation coefficient
$\Delta T_{\phi=1}$	stoichiometric temperature rise
$\eta_c$	combustion efficiency
$\theta$	air swirler vane angle
$\rho_a$	ambient density
$\sigma_y$	standard deviation from least squares fit
$\tau_{co}$	characteristic time for CO oxidation
$\tau_{eb}$	characteristic time for fuel evaporation
$\tau'_{eb}$	$(\tau_{eb}/T_{in})$
$\tau_{fi}$	characteristic time for fuel injection
$\tau'_{fi}$	$(\tau_{fi}/T_{in})$
$\tau_{hc}$	characteristic time for fuel ignition delay
$\tau'_{hc}$	$(\tau_{hc}/T_{in})$
$\tau_{no}$	characteristic time for NO formation
$\tau_{sl}$	characteristic time for heat conduction
$\tau_{sl,co}$	CO oxidizing eddy lifetime
$\tau_{sl,no}$	NO forming eddy lifetime
$\tau_{\eta}$	kinetic time for combustion efficiency
$\phi$	overall equivalence ratio
$\phi_t$	prechamber equivalence ratio

## 1. INTRODUCTION

Gas turbine combustor design engineers would find extremely useful quantitative models for combustion efficiency, emissions, flame stabilization, smoke and radiation, ignitability and altitude relight, and exit temperature traverse quality. Air loading correlations have frequently proven convenient for some of these performance parameters when combustors are of dissimilar scales but identical geometry and when mixing of fuel vapor with air occurs more slowly than the rate of fuel evaporation (i.e., aviation specification fuels with properly designed atomizers). Lefebvre and co-workers (1,2) give examples of these scaling parameters, which currently are in wide use by industry, for combustion efficiency and the blowoff limit.

However, both the current interest in low emissions combustors of exotic geometry (3) and the de-graded fuels to be available in the future (4) require extrapolations of these models, and in some cases applications to situations for which they were never intended. Thus there is substantial reason to develop new correlations and calculational procedures which include more explicitly the effects of combustor design and fuel properties.

About ten years ago, in response to a growing concern over aircraft air pollution, a number of chemical reactor network models were constructed (5,6). Chemical kinetics were emphasized since it was known that the pollutants were not in local equilibrium in the combustor exhaust plane, and the fluid mechanics were modeled via series or parallel flow modules consisting of perfectly or partially stirred, and plug flow reactors. The fuel spray in its liquid form was usually ignored. Generally speaking, the models were too

coarse to correlate and predict gaseous emissions (6).

More recently, the research community has shown feasible the use of multi-dimensional turbulent, elliptic, reacting flow codes, some two-phase because the liquid fuel injection is modeled. The interested reader is referred to (7) for a recent review and to (8) - (16) for the latest work; additional approaches have been discussed at the present Symposium. Usually limited to predictions of gaseous emissions, efficiency, and pattern factor, such detailed models are expected at best to provide insight into the nature of the complex flow in turbine engine combustors. Qualitative trends may be predicted as well, but quantitative agreement would most likely be fortuitous, a result of oversimplification of the spray, turbulence, and chemistry submodels, the frequent ignorance of the proper treatment of submodel interactions, computer size limitations, and numerical inaccuracies (7). It is interesting to note that hybrid models, combinations of the chemical reactor and finite difference approaches, are expected by some workers to be potentially more useful (8,9,17).

Although progress with these detailed codes has been rapid and encouraging, for near term applications more simple and less expensive techniques are also desirable for design purposes. The characteristic time approach (6), the subject of the present paper, represents one method in this category; developed from study of simplified bluff-body stabilized flames for spark ignition, lean flame stabilization, gaseous emissions, and combustion efficiency, it is extendable to practical hardware as well. Brief descriptions of model derivation and applications to date will be presented in the following sections.

## 2. CHARACTERISTIC TIME APPROACHES

The identification of important time scales characteristic of chemically reacting flows has been utilized by many investigators. For example, Damköhler (18) considered flame stabilization, Karlovitz et al. (19) turbulent premixed flames, and several workers have applied these ideas to gas turbine combustion (20-24). The concept involves identification of relevant subprocesses (fuel evaporation, turbulent mixing, and chemical kinetics) where for quantitative applications the characteristic times must be evaluated in the flow region responsible for the phenomenon of interest. This region for ignition is easily identified as the spark gap. In a conventional combustor, the stoichiometric contour in the shear layer between the recirculation zone and the main flow is important to both NO formation and flame stabilization, whereas the leaner regions near the combustor walls determine CO and HC emissions and thus combustion efficiency (6).

The characteristic times in current use are defined in Table 1; there has been extensive development of their particular forms, which will be discussed in the following sections, since their original formulation (6). For cases where fuel evaporation is non-negligible, a mean spray droplet lifetime is evaluated as the Sauter mean diameter squared divided by the fuel evaporation coefficient modified for forced convection. The latter is evaluated for conditions expected to be typical of the combustor primary zone, where the spray evaporates, and includes the dependence on fuel volatility. The mean diameter is primarily a function of fuel viscosity. Thus changes in fuel properties or injector are reflected in the quantity  $\tau_{eb}$ , the fuel droplet lifetime.

TABLE 1. Characteristic Times for Ignition, Combustion, and Pollutant Formation in Two-phase Turbulent Flow

Time	Symbol	Simplified Combustors	Turbine Combustors
<u>Liquid Fuel Evaporation:</u>			
Fuel Droplet Lifetime	$\tau_{eb}$	$d_o^2/\beta$	$d_o^2/\beta$
<u>Turbulent Mixing:</u>			
Eddy Dissipation Time for Injected Fluid	$\tau_{fi}$	$V_f \tau_{eb}/V_{ann}$	?
Eddy Dissipation Time in the Shear Layer where NO forms	$\tau_{sl,no}$	$D/V_{\phi=1}$	$l_{no}/V_{\phi=1}$
Eddy Dissipation Time in the Shear Layer where CO and HC Oxidize	$\tau_{sl,co}$	$D/V_{ann}, (D-d)/V_{ann}$	$l_{co}/V_{ref}$
Conductive Heat Transfer Time (Stagnant Mixture)	$\tau_{sl}$	$A/\alpha$	-
<u>Chemical Kinetics:</u>			
NO Formation Time	$\tau_{no}$ (msec)	$10^{-12} \exp(135 \text{ kcal/mole}/RT_{\phi=1})$	$10^{-12} \exp(135 \text{ kcal/mole}/RT_{\phi=1})$
CO Oxidation Time	$\tau_{co}$ (msec)	$10^{-1} \exp(3.1 \text{ kcal/mole}/RT_{co})$	$10^{-3} \exp(10.76 \text{ kcal/mole}/RT)$
Fuel and CO Oxidation Time	$\tau_n$ (msec)	$10^{-2} \exp(4.5 \text{ kcal/mole}/RT_n)$	$10^{-2} \exp(4.5 \text{ kcal/mole}/RT_n)$
Fuel Ignition Delay Time	$\tau_{hc}$ (msec)	$10^{-4} \exp(21 \text{ kcal/mole}/RT)/\phi$	$10^{-4} \exp(21 \text{ kcal/mole}/RT)/\phi$

Several fluid mechanic times have been found important. The quantity  $\tau_{fi}$  is associated with fuel injection, while the various  $\tau_{sl}$ 's in Table 1 are related to large scale mixing in the shear layer as determined by the air addition scheme along the combustor liner. For simplex pressure atomizers, the fuel penetration time  $\tau_{fi}$  is evaluated as the product of the initial fuel injection velocity and the droplet lifetime, normalized by some air velocity; for the laboratory flames, the air velocity in the plane of the flameholder ( $V_{ann}$ ) is used.

In both the simplified and practical combustors, as noted above CO (and unburned hydrocarbons, HC) and NO are found to originate in differing regions of the flames. Thus two mixing times are required, one for

each species. Both are defined in terms of a significant length, a function of combustor geometry, and a characteristic velocity, given by the combustor inlet conditions. Particulars will be reviewed in the sections to follow. Last, for the special case of ignition in quiescent sprays  $\tau_{s2}$  has been defined as a heat conduction time, the ratio of the surface area of the spark kernel evaluated at the quenching distance to the thermal diffusivity of air.

Four kinetic times, all in Arrhenius form, have been found useful. They describe the rates of NO formation ( $\tau_{NO}$ ), CO oxidation ( $\tau_{CO}$ ), fuel and CO oxidation lumped to correlate combustion efficiency ( $\tau_n$ ), and an ignition delay time for flame stabilization ( $\tau_{hc}$ ). This last time includes the equivalence ratio explicitly since at the lean limit the rate is expected to be first order in fuel concentration. The activation energies and choice of reaction temperatures for all of the kinetic characteristic times are determined from combustor inlet temperature variations; the pre-exponential factors are chosen so that the kinetic times are of order of msec. Note that these kinetic times are primarily a function of combustor inlet conditions, overall equivalence ratio, and fuel heating value.

Thus fuel properties, combustor geometry and inlet conditions are all included in the characteristic time model. Appropriate combinations of these times should therefore correlate the spark ignition and lean blowout limits, CO and NO emission indices (g pollutant/kg fuel), and combustion efficiency. Note that all of the characteristic times are chosen only to include the expected trend with a variation in fuel, combustor, or cycle design, and of course are not exact quantities. Hence qualitative trends can be encompassed in the model, but experimental data are required to quantify the model, which is thus semi-empirical. As noted previously, success requires recognition of that portion of the combustor flow limiting to the phenomenon of interest. In the following sections we chart progress in model validation.

### 3. SPARK IGNITION AND FLAME STABILIZATION

The stabilization of premixed turbulent flames can be thought of in terms of the relevant Damköhler number a constant in the limit; specifically, for Damköhler number taken as the ratio of a turbulent mixing time to an ignition delay time, the limit is defined when the ratio equals unity:

$$D_{bo} \equiv \tau_{sl,co} / \tau_{hc} \begin{matrix} > 1 \text{ stable} \\ < 1 \text{ unstable} \end{matrix} \quad (1)$$

This criterion simply states that the residence time (replaced by a turbulent fluid mechanic time following Spalding (25)) precisely equals the fuel ignition delay time at the limit. Recognizing that neither of these characteristic times can be estimated exactly in a combustor, Eq. (1) is replaced by the limit equation

$$\tau_{sl,co} \sim \tau_{hc} \quad (2)$$

Zukoski and Marble (20), and more recently Altenkirch and Mellor (24), have argued that both times in Eq. (2) must be evaluated in the shear layer between the fresh air and the recirculating fuel/burned gas mixture. Zukoski (26) further discusses Eq. (2) for two-dimensional and axisymmetric flows; we limit our attention here to the latter case. Note that  $\tau_{hc}$  must be evaluated at the highest flame temperature attainable in the flame, since the corresponding physical regions of the flow will be the last to extinguish.

#### a. Premixed Turbulent Flames (Afterburners) - Lean Blowoff

Plee and Mellor (27) have used premixed turbulent flame stabilization data obtained by Ballal and Lefebvre (28), for the bluff-body flameholder depicted in Fig. 1A, to quantify Eq. (2). For inlet temperature variations from 300 to 575 K with gaseous  $C_3H_8$  as fuel the apparent activation energy in  $\tau_{hc}$  was found to be 21 kcal/mole. Acceleration of the reactants as they flow past the recirculation zone was accounted for by a density (i.e., temperature) correction to the velocity in the plane of the flameholder  $V_{ann}$ , so that

$$\tau'_{sl,co} = (D/V_{ann}) (T_{in}/T) \quad (3)$$

$$\tau_{hc} = 10^{-4} \exp\{21 \text{ kcal/mole}/RT\}/\phi \text{ msec} \quad (4)$$

and the blowoff limit condition becomes

$$\tau_{sl,co} \sim \tau_{hc} (T/T_{in}) \equiv \tau'_{hc} \quad (5)$$

In the above  $D$  is flameholder diameter (a measure of the length of the recirculation zone), and  $T_{in}$  is inlet temperature of the premixed reactants. As was noted the kinetic temperature  $T$  in Eq. (3) through (5) must be evaluated at the maximum temperature available in the system, so it is taken as the adiabatic flame temperature at the approach equivalence ratio  $\phi$ .

The blowoff limit correlation is shown in Fig. 2 for the premixed data of Ballal and Lefebvre (28). The limit equation given in the figure is

$$\tau_{sl,co} = 2.11 \tau'_{hc} - 0.46 \quad (6)$$

where  $T$  and  $\phi$  are evaluated just prior to blowoff. Operation at conditions above the least squares line is stable, and in Fig. 2 it is shown how one can approach the limit by either increasing the inlet velocity or decreasing the equivalence ratio. The quantity  $r$  is a correlation coefficient ( $r = 1.00$  is perfect), and  $\sigma_y$  is the standard deviation (27).

Note that correlation (6) does not include the approach flow turbulent intensity explicitly, as do other correlations (28). Most likely some of the scatter of Fig. 2 is due to neglect of intensity variations, but since turbulence parameters are rarely known in the practical case, a direct correlation in terms of inlet velocity  $V_{ann}$  is preferred. Also, turbulence-chemistry interactions (26) are ignored since

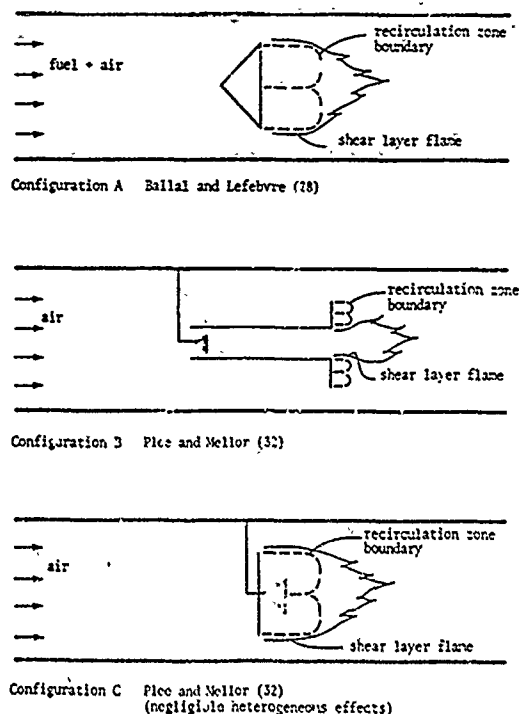


Figure 1. Schematic of three simplified bluff body stabilized flames.

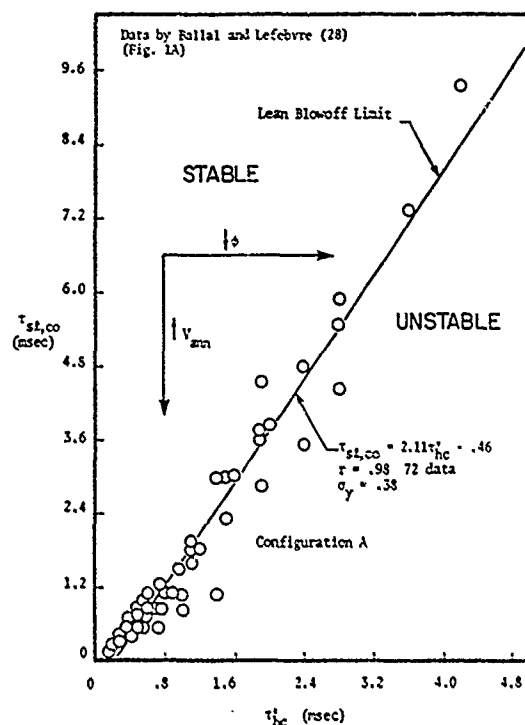


Figure 2. Characteristic time correlation for lean blowoff in a bluff body stabilized flame burning gaseous propane (Fig. 1A).

fluid mechanics and reaction rates are treated separately in Eq. (6). Because the apparent activation energy is determined empirically, perhaps its value reflects these interactions since it is different from pure kinetic values defined in a similar spirit (29,30,31). In any case Eq. (6) provides a design tool which incorporates variations in flameholder geometry and inlet conditions.

#### b. Partially Prevaporized and Premixed Flames (Prechamber Combustors) — Lean Blowoff

For Configuration B of Fig. (1), data obtained by Plee and Mellor (32) have also been correlated (27). Fuels tested were liquid  $C_3H_8$ , which flash evaporates at the inlet conditions, and Jet A, which partially evaporates in the fuel preparation tube, designed to minimize the possibility of flashback (33). The presence of liquid fuel was found to narrow the lean limit due to the time required for evaporation; therefore Eq. (5) becomes (27)

$$\tau_{sl,co} \sim \tau_{hc}' + a\tau_{eb}' (T/T_{in}) \quad (7)$$

$$\sim \tau_{hc}' + a\tau_{eb}' \quad (8)$$

where the quantity  $a$  must be determined empirically. Eq. (7) and (8) imply that the fuel must partially evaporate before the homogeneous kinetics can lead to ignition.

The characteristic length for Configuration B is disc diameter less tube diameter, and  $\tau_{hc}$  is defined by Eq. (4) with  $\phi$  the tube equivalence ratio ( $\phi_t$ ) and  $T$  the mean of  $(T_{\phi_t} + T_{in})$  or  $(T_{\phi=1} + T_{in})$  for  $\phi_t > 1$ ;  $\tau_{eb}$  is given in Table 1. A result similar to that shown in Fig. 2 is given by Plee and Mellor (27) with the correlation

$$\tau_{sl,co} = 2.24 (\tau_{hc}' + 0.011\tau_{eb}') + 0.06. \quad (9)$$

Note that the empirical value of the constant  $a$  in Eq. (9) has no physical significance since the characteristic times are only order-of-magnitude estimates; however, liquid fuel properties and injector design are not implicitly included in the model via  $\tau_{eb}$ .

#### c. Liquid Fueled Turbulent Diffusion Flames with Negligible Fuel Penetration (Conventional Combustors) — Lean Blowoff

Plee and Mellor (32) have in addition reported data for Configuration C in Fig. 1. In the case where fuel penetration is negligible (upper flame of Fig. 3), the flame is mixing controlled, that is, the rate of mixing of fuel vapor with air, rather than the evaporation rate of liquid fuel, determines the heat release rate (34). This is the situation usually encountered in practical conventional combustors burning aviation specification fuels with proper injection techniques (35). Kinetics, of course, influence the mixing dominated flame. If  $T$  in Eq. (4) is taken as the adiabatic stoichiometric flame temperature  $T_{\phi=1}$  (the maximum temperature in a diffusion flame) and  $\phi$  the overall equivalence ratio at blowoff, then the limit is shown in Fig. 4 and given by

$$\tau_{sl,co} = 1.47 (\tau_{hc}' + 0.011\tau_{eb}') + 0.08. \quad (10)$$

Note the similarities of Eq. (9) and (10). In fact all three configurations of Fig. 1 can be correlated

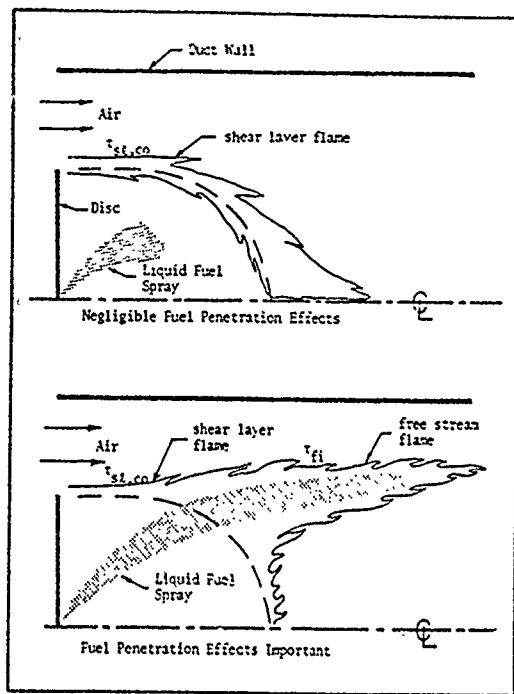


Figure 3. Burner schematic illustrating the effect of fuel penetration on flame structure.

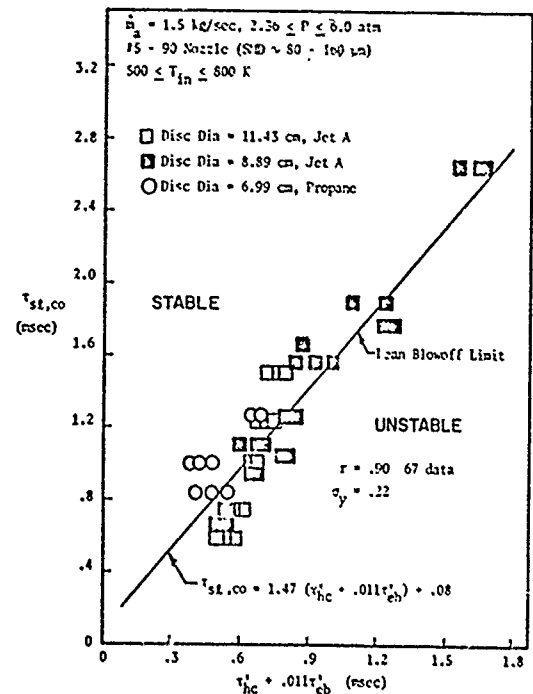


Figure 4. Characteristic time correlation for data obtained on the disc-in-duct (Fig. 1C) flameholder (negligible fuel penetration effects).

together: the result is shown in Fig. 5 with the universal correlation

$$\tau_{sl,co} = 1.82(\tau'_{hc} + 0.011\tau'_{eb}) + 0.04 \quad (11)$$

where the terms used in  $\tau_{sl,co}$  depend on flameholder design and those in  $\tau'_{hc}$  on the nature of the flame (premixed, partially pre-vaporized and pre-mixed, or unmixed liquid fuel and air).

Eq. (11) gives the lean blowoff limit in terms of "variations in pressure, inlet temperature, reference velocity, flameholder geometry, housing diameter, fuel type, and injector size . . . Knowledge of the flameholder configuration inlet conditions and atomization determines  $\tau_{sl}$  and  $\tau'_{eb}$ ; from these,  $\tau'_{hc}$  can easily be computed that is a function of the inlet conditions and the blowoff equivalence ratio. The blowoff velocity is also calculated in a similar fashion if the geometry, pressure, inlet temperature, atomization, and equivalence ratio are given. In addition, the correlation can predict simple flameholder modifications necessary to optimize flame stabilization for a given operating condition (27)."

#### d. Liquid Fueled Turbulent Diffusion Flames with Strong Fuel Penetration - Lean Blowoff

For Configuration C of Fig. 1 with fuels of lower volatility or higher viscosity than Jet A, fuel penetration alters the structure of the flame to the case shown in the lower portion of Fig. 3, particularly for the smaller disc diameters (27,32). Increased flame length associated with the fuel penetration enhances the stability of the combustion process. Plee and Mellor (27) have shown that inclusion of  $\tau'_{fi}$ , with all other terms defined as in Section 3.c above, collapses these data as well, where

$$\tau'_{fi} = V_f \tau_{eb}/V_{ann} \quad (12)$$

$$\tau'_{fi} = \tau_{fi} (T/T_{in}). \quad (13)$$

Here  $V_f$  is the initial fuel injection velocity estimated from empirical information provided by Crowe (36). The fuel penetration effect has been shown important when the ratio  $(\tau'_{fi}/\tau_{sl})$  is greater than ten (27).

The final complete correlation is shown in Fig. 6 with the limit equation

$$\tau_{sl,co} + 0.12\tau'_{fi} = 2.12(\tau'_{hc} + 0.011\tau'_{eb}) + 0.095. \quad (14)$$

For negligible fuel penetration ( $\tau'_{fi} \approx 0$ ), Eq. (14) compares favorably to Eq. (10) and (11), and for premixed systems ( $\tau'_{eb} = \tau'_{hc} = 0$ ) Eq. (14) is nearly identical to Eq. (6). The fuels utilized to develop Eq. (14) included JP-4, Jet A, DF-2, and Jet A blended with a small amount of lubricating oil to give an increased end boiling point (27); more recently model predictions for unleaded gasoline, JP-10, No. 4 and No. 6 oils have been validated with Configuration C of Fig. 1 (37). These flames, with strong fuel penetration effects, are thought to be approaching the other limit in spray combustion, where the fuel evaporation rate determines the heat release rate.

The fuel penetration effect is not anticipated to occur in conventional combustors operating with aviation specification fuels. Thus Eq. (14) with  $\tau'_{fi} = 0$  has been used for blowoff data (38) for the T-63 conventional combustor (39). Using the definition of  $\tau_{sl,co}$  given in Table 1 for practical combustors

$$\tau_{sl,co} = \lambda_{co}/V_{ref} \quad (15)$$

where

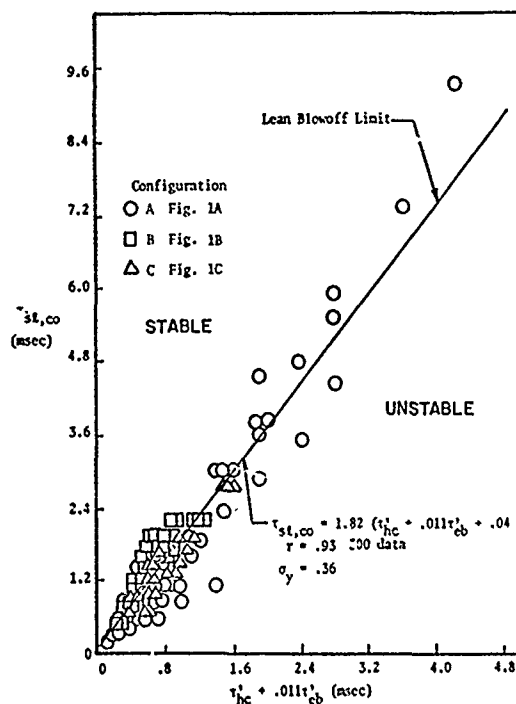


Figure 5. Complete characteristic time correlation for inlet, geometry and fuel variations on three simplified bluff body stabilized flames (negligible fuel penetration effects).

$$\ell_{co}^{-1} = \ell_{pri}^{-1} + d_{comb}^{-1}$$

(see (35)),  $\ell_{pri}$  is the distance from the fuel injector to the centerline of the primary air penetration holes at combustor diameter  $d_{comb}$ , and  $V_{ref}$  is reference velocity, Eq. (14) with  $\tau_{eb}$  also taken as zero was used to compute the three points to the left of the limit in Fig. 7 for Diesel fuel 2, Jet A, and JP-4, respectively.

Then, using estimates of Sauter mean diameter  $d_0$  given by Moses (38) and Eq. (11) including the  $\tau_{eb}$  term, the points to the right of the limit in Fig. 7 were established. Note that the ordering of the fuels is now reversed. Clearly, reasonable choices of  $d_0$  for each fuel could be selected which would align all three fuels exactly with the lean limit Eq. (14). Hence one problem in application of the characteristic time model to practical combustors appears: Sauter mean diameter is required in some cases at the engine operating point (elevated temperatures and pressures), a number not usually available.

However, Eq. (14) with  $\tau_{fi} = 0$  is recommended for engine applications; a preliminary model test is shown in Fig. 7. Further model validation will proceed with additional turbine combustor blowoff data.

#### e. Stagnant Sprays - Spark Ignition

Construction of a related model for spark ignition is in progress (40). First efforts have involved minimum ignition energy data obtained by Ballal and Lefebvre (41) for quiescent sprays of several fuels. Recognition that to first order the ignition of a spray is evaporation limited (42) greatly simplifies model development.

Starting with Eq. (8) without the velocity correction due to combustion (the mixture is stagnant),

$$\tau_{sl} \sim \tau_{hc} + a\tau_{eb} \quad (17)$$

Neglecting kinetics in favor of evaporation means

$$a\tau_{eb} \gg \tau_{hc} \quad (18)$$

so that the spark ignition limit is given by

$$\tau_{sl} \sim \tau_{eb} \quad (19)$$

where  $\tau_{sl}$  must be redefined for a stagnant mixture; the heat source is now the spark rather than an adjacent recirculation zone.

Heat loss by conduction, as opposed to turbulent convection, will compete with the heat addition from

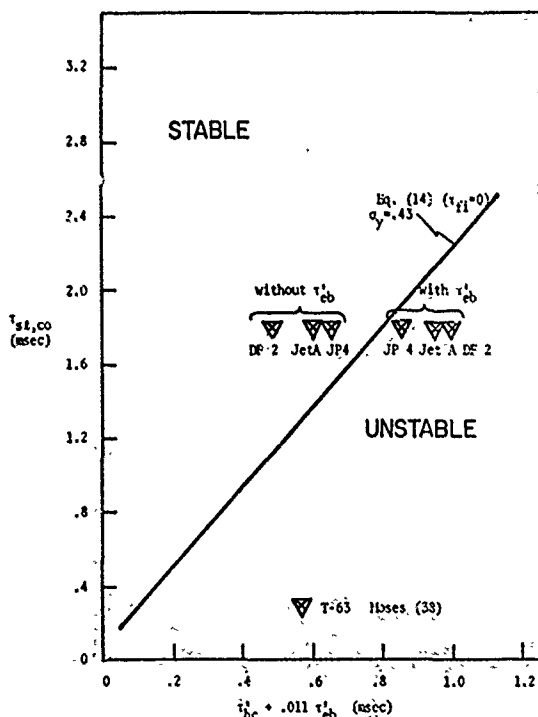


Figure 7. Application of flame stabilization model to conventional combustors.

the spark which drives the evaporation (40). Hence  $\tau_{sl}$  for this special case is given by

$$\tau_{sl} = \pi d_q^2 \rho_a c_{pa} / k_a \quad (20)$$

where  $d_q$  is quenching distance related to minimum spark ignition energy  $E_{min}$  via

$$d_q = \{E_{min} / \frac{\pi}{6} \rho_a c_{pa} \Delta T_{\phi=1}\}^{1/3} \quad (21)$$

Other properties which appear are ambient gas density ( $\rho_a$ ), specific heat ( $c_{pa}$ ), and thermal conductivity ( $k_a$ );  $\Delta T_{\phi=1}$  is the adiabatic stoichiometric temperature rise associated with the droplet or spray diffusion flame after ignition.

One other modification to Eq. (19) is required. What limits ignition is the vapor phase concentration of fuel vapor, which can be increased by decreasing  $\tau_{eb}$ . However, increasing the total number of droplets by increasing the equivalence ratio will also increase the spray evaporation rate linearly. This effect is included by altering the  $\tau_{eb}$  term so that the ignition limit becomes

$$\tau_{sl} \sim \tau_{eb} / \phi \quad (22)$$

If the quantity  $d_q$  is computed from the data reported by Ballal and Lefebvre (41), and Eq. (22) is tested, then Fig. 8 results. Excluding for the moment the flagged data (the points near the origin are data with symbols omitted for clarity) the fit is linear and the y-intercept is near zero, as predicted by the model, with the ignition limit given by

$$\tau_{sl} = 14.2 \tau_{eb} / \phi + 2.29 \quad (23)$$

How changes in spark energy, Sauter mean diameter, and fuel volatility (B, the transfer number) affect a stable operating point are shown in Fig. 8.

Fig. 9 demonstrates the correlation in terms of  $E_{min}$  versus  $\phi$  for one fuel (dashed lines are from Eq. (23)) and explains the deviation of the flagged data from the fit in Fig. 8. All of these points are for the lowest equivalence ratios, which tend to negate Eq. (18). Thus the kinetic time for ignition must be evaluated and included in a complete model; this work is currently underway. In addition, preliminary studies of data for flowing sprays with the conventional definition of  $\tau_{sl}$  ( $d_q/V$ ), neglecting kinetics, show similar agreement as in Fig. 8 (43). Of course, turbine combustor model evaluation is the eventual goal.

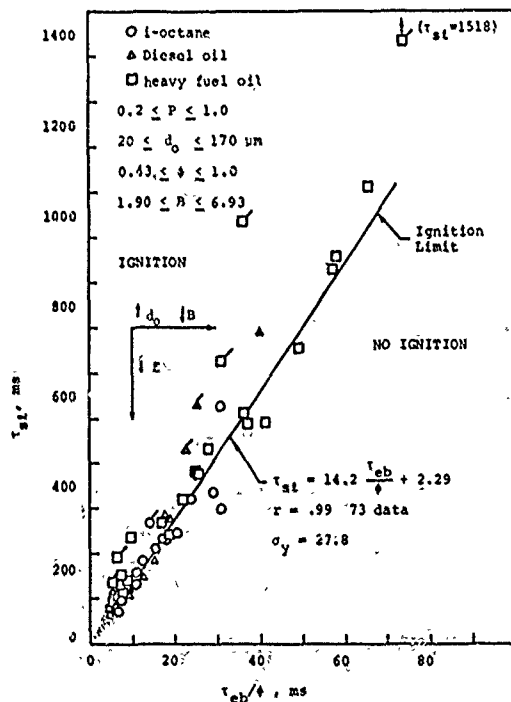


Figure 8. Characteristic time correlation for the ignition of quiescent fuel sprays (data from Ballal and Lefebvre (41)).

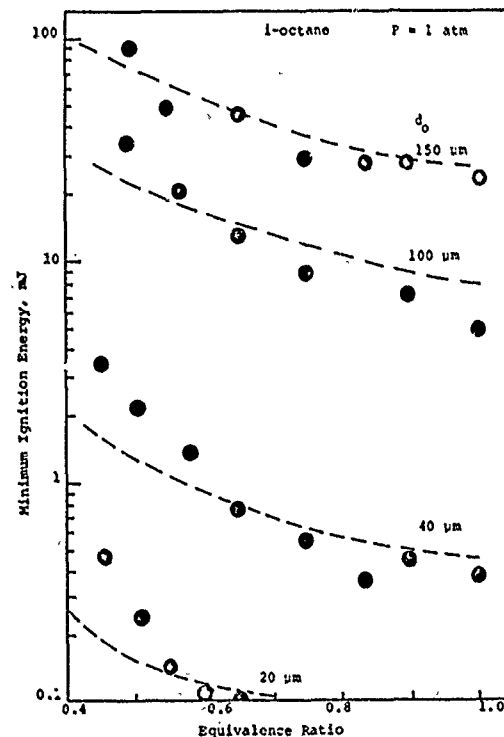


Figure 9. Minimum ignition energy of quiescent mixtures for various drop sizes (data from Ballal and Lefebvre (41)).

#### 4. EMISSIONS AND EFFICIENCY

In the area of gaseous emissions, and to a lesser extent combustion efficiency, considerably more experience has been obtained with the characteristic time approach for flames as in the upper portion of Fig. 3 (34) and for conventional combustors (34,44,45,46,47). For the second flame in Fig. 3 and for configuration B of Fig. 1, seeking similar correlations is an area of active research (48).

For nitric oxide in mixing controlled situations it can be shown (34,47) that the  $NO_x$  emission index (g as  $NO_2$ /kg fuel) will scale linearly with the relevant Damköhler number:

$$NO_{x,EI} \sim D_{no} = \tau_{sl,no} / \tau_{no} \quad (24)$$

Eq. (24) states that an increase in NO-forming eddy lifetime ( $\tau_{sl, no}$ ) will increase NO emissions linearly. The inverse dependence on  $\tau_{no}$  reflects that increases in  $T_{\phi=1}$  (Table 1), which decrease  $\tau_{no}$ , also increase  $NO_xEI$ .

It is the formation of NO which must be quenched in gas turbine combustors, whereas CO (and HC) is limited by quenching of its oxidation reactions. Thus the functional dependence of COEI is the inverse to that for  $NO_xEI$  (34):

$$COEI \sim D_{co}^{-1} = \tau_{co} / \tau_{sl, co} \quad (25)$$

Here long eddy lifetimes and high temperatures decrease CO (and HC) emissions.

If CO and HC concentrations are proportional to one another over the range of data to be correlated, then it can be shown that (48)

$$100 - \eta_c(\%) \sim D_{\eta}^{-1} = \tau_{\eta} / \tau_{sl, co} \quad (26)$$

where combustion efficiency  $\eta_c$  is obtained from (49)

$$100 - \eta_c(\%) = \{ (COEI)Q_{co} + (HCEI)Q_{hc} \} / 10Q_{fuel} \quad (27)$$

The Q's are the lower heating values of the indicated species.

Finally, for cases where fuel penetration is important, no fuel independent correlation has yet been achieved (48). Although this case may not be significant in gas turbine applications, it can represent the situation in boilers utilizing residual oil or pulverized coal.

#### a. Liquid Fueled Turbulent Diffusion Flames with Negligible Fuel Penetration (Configuration 1C) - Emissions and Efficiency

Probing of the flame shown schematically at the top of Figure 3 (50) demonstrated that CO (and HC) quench at the outer but leading edge of the shear layer, while NO forms on the centerline of the flame downstream of the recirculation zone. Consequently the eddy lifetimes were taken as

$$\tau_{sl, co} = D / v_{ann} \quad (28)$$

and

$$\tau_{sl, no} \sim D / v_{\phi=1} \quad (29)$$

where

$$v_{\phi=1} = \frac{1}{2} v_{ref} \{ 1 + T_{\phi} / T_{in} \} \quad (30)$$

As before, the kinetic times were determined from inlet temperature variations, and slightly different definitions from those of Table 1 were used in this early work (34). Here  $T_{\phi}$  is the burned gas temperature at the overall equivalence ratio  $\phi$ .

For liquid  $C_3H_8$  as fuel the NO and CO correlations are shown in Fig. 10 and 11, respectively; both curves are linear as the model predicts. Note also the near zero y-intercepts and the good correlation coefficients. A similar combustion efficiency correlation for the mixing controlled case is shown in Fig. 12, for several additional fuels (48). In the latter case  $\tau_{\eta}$  is given in Table 1, where

$$\tau_{\eta} = 3.9T_{in} + 0.1T_{\phi} \quad (31)$$

The respective least squares fits are

$$NO_xEI = 0.68\tau_{sl, no} / \tau_{no} + 0.36; \quad (32)$$

$$COEI = 17.9\tau_{co} / \tau_{sl, co} + 3.4; \quad (33)$$

$$100 - \eta_c(\%) = 2.4\tau_{\eta} / \tau_{sl, co} - 1.69. \quad (34)$$

For negligible fuel penetration these equations give emissions and efficiency in terms of inlet conditions, flameholder geometry, and fuel heating value. They have been utilized to design the optimal disc-in-duct burner configuration which exhibits minimal CO emissions (34).

#### b. Liquid Fueled Turbulent Diffusion Flames with Negligible Fuel Penetration (Conventional Combustors) - Emissions

Considerable utilization of the characteristic time model has occurred for gaseous emissions from conventional combustors (6, 35, 44, 45, 46, 47). The most recent work (46) has dealt with the Pratt and Whitney JT9D and shown that identical correlations can be obtained with the combustors analyzed previously, the GT-309 vehicular and T-63 helicopter burners.

For most cases droplet evaporation can be assumed rapid compared to the kinetics and air/fuel vapor mixing (35, 44); hence  $NO_x$  and CO emissions are expected to correlate with Eq. (24) and (25). The definitions of the kinetic and mixing times are given in Table 1, but the mixing times differ from those of Configuration 1C due to the more complicated geometry of the gas turbine combustor (46). Here best correlations are obtained with

$$\tau_{no}^{-1} = (\tau_{no, quench} / \cos\theta)^{-1} + d_{comb}^{-1} \quad (35)$$



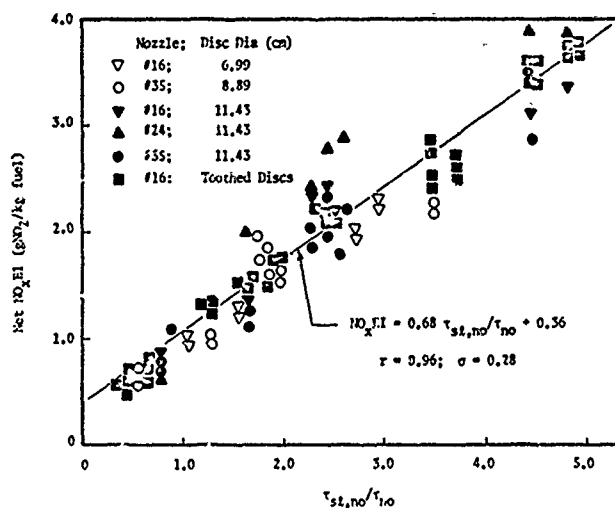


Figure 10.  $\text{NO}_x \text{EI}$  versus  $\tau_{sl,no}/\tau_{no}$  (propane fuel)

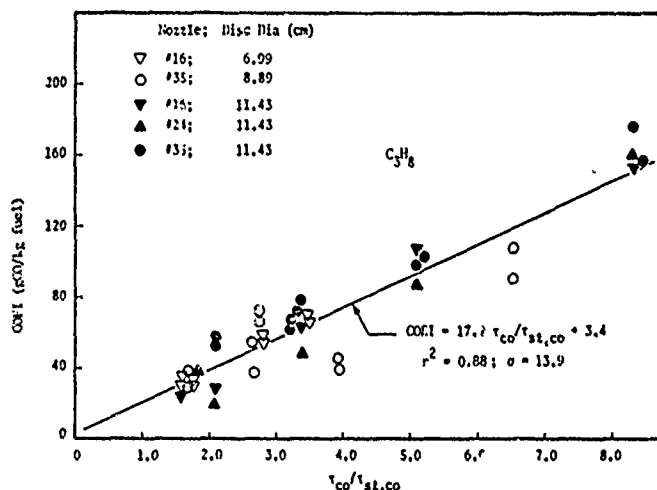


Figure 11. COEI versus  $\tau_{co}/\tau_{sl,co}$  (circular discs)

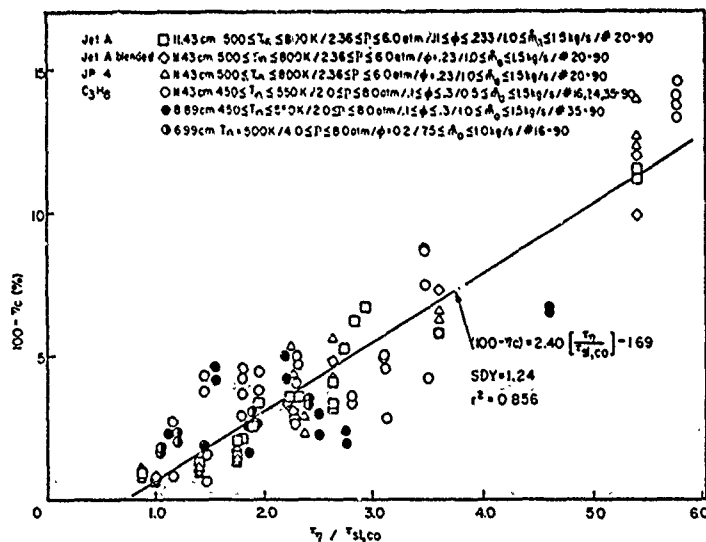


Figure 12. Combustion inefficiency correlation for mixing controlled disc stabilized flames.

$$\ell_{co}^{-1} = \ell_{co,quench}^{-1} + d_{comb}^{-1} \quad (36)$$

The quench lengths  $\ell$  represent distance from the fuel injector to an air addition site, as in Eq. (16). For NO this is usually associated with the secondary holes, but for CO generally moves to upstream locations as engine power is reduced (35,44,46). The angle  $\theta$  is that of any air swirler (46). Reference velocity  $V_{ref}$  is defined in terms of maximum combustor cross-sectional area, and

$$V_{\phi=1} = (\dot{m}_{apz}/\dot{m}_a)(T_{\phi=1}/T_{in})V_{ref} \quad (37)$$

Here  $(\dot{m}_{apz}/\dot{m}_a)$  is the fraction of total air flow estimated to pass through the primary zone (46).

The  $\text{NO}_x$  correlation for all three combustors is shown in Fig. 13; the least squares fit is

$$\text{NO}_x \text{EI} = 4.32\tau_{sl,no}/\tau_{no} + 0.46 \quad (38)$$

with correlation coefficient  $r = 0.98$ . For CO, a surface area correction is required for the annular combustor, and brings the three correlations together with an approximate slope of thirty-five (46).

It should be noted that the combustor inlet conditions differ for these three engines, and that geometries and injectors vary as well. In addition, with the exception of the T-63 CO emissions (35), the above correlations collapse fuel volatility and viscosity variations from JP4 to DF2. Consequently, for the correlation of additional conventional combustors operating with aviation specification fuels, the following expressions are recommended (46):

$$\text{NO}_x \text{EI} = 4.5\tau_{sl,no}/\tau_{no} \text{ (g NO}_2\text{/kg fuel)}; \quad (39)$$

$$\text{COEI} = 35\tau_{co}/\tau_{sl,co} \text{ (g CO/kg fuel)}. \quad (40)$$

Hammond (45) has verified the predictive ability of the characteristic time model. His results are shown in Fig. 14 and 15. For geometry modifications A and B,  $\text{NO}_x$  is predicted to within one standard deviation; predictions for CO are somewhat too high. At idle both modifications suffered from blow-out, which has subsequently been explained using the model of Section 3 (39).

## 5. SUMMARY AND CONCLUSIONS

It remains to validate the models for lean blowoff, combustion efficiency and spark ignition for engines, as has been accomplished for gaseous emissions. For efficiency, penalties associated with alternative fuels are of particular interest (48). In addition, advanced gas turbine combustors featuring staging and or premixing/prevaporizing are next for emissions modeling. It is hoped that the characteristic time model will continue to prove a useful interim design tool for combustor designers (45).

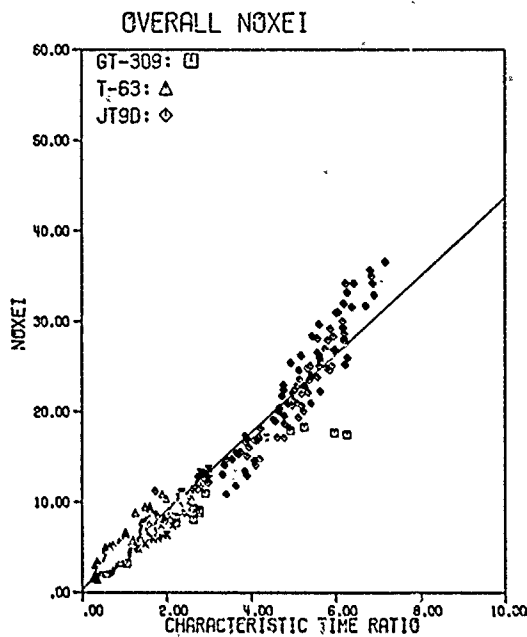


Figure 13. Universal correlation for  $\text{NO}_x$  emissions from conventional combustors.

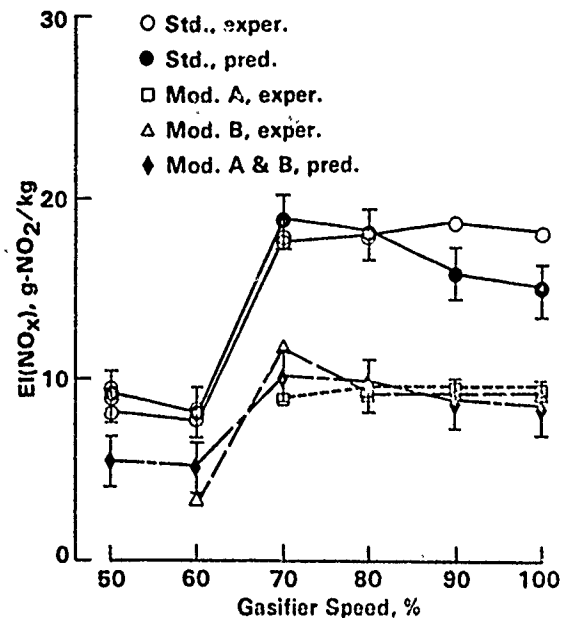


Figure 14. Comparison of predicted and experimental  $\text{EI}(\text{NO}_x)$  versus gasifier speed (from Hammond (45)).

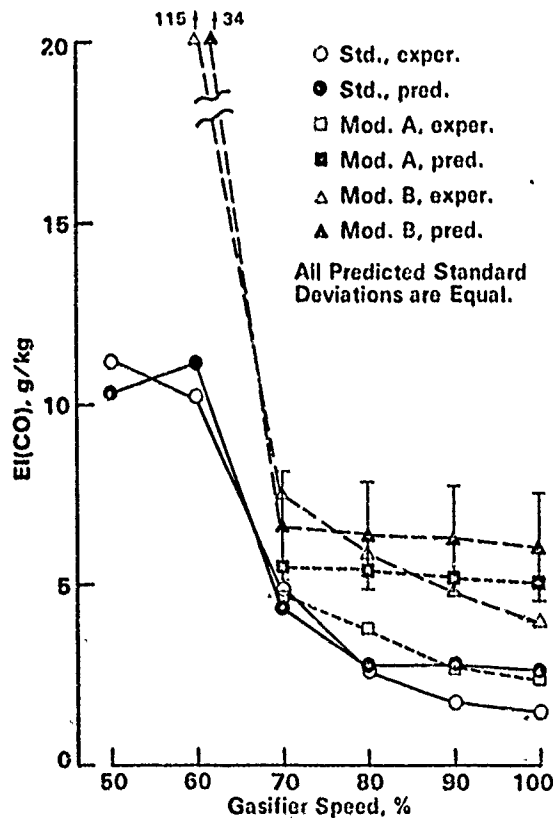


Figure 15. Comparison of predicted and experimental  $\text{EI}(\text{CO})$  versus gasifier speed (from Hammond (45)).

#### 6. REFERENCES

1. Greenhough, V. W. and Lefebvre, A. H., "Some Applications of Combustion Theory to Gas Turbine Development," Sixth Symposium (International) on Combustion, New York, Reinhold, 1957, pp. 858-869.
2. Lefebvre, A. H., College of Aeronautics, Cranfield, "Theoretical Aspects of Gas Turbine Combustion Performance," 1966, Note Aero No. 163.
3. Jones, R. E., Diehl, L. A., Petrash, D. A. and Grobman, J., "Results and Status of the NASA Aircraft Engine Emission Reduction Technology Programs," 1978, NASA TM 79009.

4. Longwell, J. P., "Synthetic Fuels and Combustion," Plenary Lecture, Sixteenth Symposium (International) on Combustion, Pittsburgh, The Combustion Institute, 1977, pp. 1-15.
5. Mellor, A. M., "Current Kinetic Modeling Techniques for Continuous Flow Combustors," Emissions from Continuous Combustion Systems, New York, Plenum Press, 1972, pp. 23-53.
6. Mellor, A. M., "Gas Turbine Engine Pollution," Pollution Formation and Destruction in Flames, Vol. I of Progress in Energy and Combustion Science, Chigier, N. A., Editor, Oxford, Pergamon, 1976, pp. 111-133.
7. Mellor, A. M., "Turbulence Combustion Interaction Models for Practical High Intensity Combustors," Presented at Seventeenth Symposium (International) on Combustion, 1978.
8. Swithenbank, J., Turan, A. and Felton, P. G., "Three-dimensional Two-phase Mathematical Modeling of Gas Turbine Combustors," Project SQUID Workshop on Gas Turbine Combustor Design Problems, 1978.
9. Harsha, P. T. and Edelman, R. B., "Application of Modular Modeling to Ramjet Performance Prediction," 1978, AIAA Paper No. 78-944.
10. Novick, A. S., Miles, G. A. and Lilley, D. G., "Numerical Simulation of Combustor Flow Fields," 1978, AIAA Paper No. 78-949.
11. Mongia, H. G. and Smith, K., "An Empirical/Analytical Design Methodology for Gas Turbine Combustors," 1978, AIAA Paper No. 78-998.
12. Jones, W. P. and Priddin, C. H., "Predictions of the Flow Field and Local Gas Composition in Gas Turbine Combustors," Presented at Seventeenth Symposium (International) on Combustion, 1978.
13. Novick, A. S. and Miles, G. A., "Modeling Parameter Influences in Gas Turbine Combustor Design," 1979, AIAA Paper No. 79-0354.
14. Bruce, T. W., Mongia, H. C. and Reynolds, R. S., "Combustor Design Criteria Validation. Vol. I. Element Tests and Model Validation," 1979, USARTL-TR-78-55A.
15. Mongia, H., Reynolds, R., Coleman, E. and Bruce, T., "Combustor Design Criteria Validation. Vol. II. Development Testing of Two Full-scale Annular Gas Turbine Combustors," 1979, USARTL-TR-78-55B.
16. Mongia, H. C. and Reynolds, R. S., "Combustor Design Criteria Validation. Vol. III. User's Manual," 1979, USARTL-TR-78-55C.
17. Felton, P. G., Swithenbank, J. and Turan, A., Sheffield University, "Progress in Modelling Combustors," 1977, HIC 300.
18. Danköhler, G., "Einflüsse der Strömung, Diffusion und des Wärmeüberganges auf die Leistung von Reaktionsöfen," Z. Elektrochem, 42, 1936, pp. 846-862.
19. Karlovitz, B., Denniston, D. W., Jr., and Wells, F. E., "Investigation of Turbulent Flames," J. Chem. Phys 19, 1951, pp. 541-547.
20. Zukoski, E. E. and Marble, F. E., "Experiments Concerning the Mechanism of Flame Blowoff from Bluff Bodies," Proc. Gas Dynamics Symposium on Aerothermochemistry, Northwestern Univ., 1956, pp. 205-210.
21. Mellor, A. M., "Simplified Physical Model of Spray Combustion in a Gas Turbine Engine," Comb. Sci. Tech. 8, 1973, pp. 101-109.
22. Gouldin, F. C., "Controlling Emissions from Gas Turbines - the Importance of Chemical Kinetics and Turbulent Mixing," Comb. Sci. Tech. 7, 1973, pp. 33-45.
23. Vranos, A., "Turbulent Mixing and NO<sub>x</sub> Formation in Gas Turbine Combustors," Comb. Flame 22, 1974, pp. 253-258.
24. Altenkirch, R. A. and Mellor, A. M., "Emissions and Performance of Continuous Flow Combustors," Fifteenth Symposium (International) on Combustion, Pittsburgh, The Combustion Institute, 1974, pp. 1181-1189.
25. Spalding, D. B., "Mixing and Chemical Reaction in Steady Confined Turbulent Flames," Thirteenth Symposium (International) on Combustion, Pittsburgh, The Combustion Institute, 1971, pp. 649-657.
26. Zukoski, E., "Afterburners," Chapt. 21 in The Aerothermodynamics of Aircraft Gas Turbine Engines, 1978, AFAPL-TR-78-52.
27. Plee, S. L. and Mellor, A. M., "Characteristic Time Correlation for Lean Blowoff of Bluff-body-Stabilized Flames," Combust. Flame 35, 1979, pp. 61-80.
28. Ballal, D. R. and Lefebvre, A. H., "Weak Extinction Limits of Flowing Turbulent Mixtures," ASME Paper No. 78-GT-144, 1978, to be published in ASME Transactions.
29. Engleman, V. S., Edelman, R. B., Bartok, W. and Longwell, J. P., "Experimental and Theoretical Studies of NO<sub>x</sub> Formation in a Jet-stirred Combustor," Fourteenth Symposium (International) on Combustion, Pittsburgh, The Combustion Institute, 1973, pp. 757-765.

30. Dryer, F. L. and Glassman, I., "Combustion Chemistry of Chain Hydrocarbons," Alternative Hydrocarbon Fuels: Combustion and Chemical Kinetics, New York, AIAA, 1978, pp. 255-306.
31. Edelman, R. B. and Harsha, P. T., "Some Observations on Turbulent Mixing with Chemical Reactions," Turbulent Combustion, New York, AIAA, 1978, pp. 55-102.
32. Plee, S. L. and Mellor, A. M., "Flame Stabilization in Simplified Prevaporizing, Partially Vaporizing, and Conventional Gas Turbine Combustors," AIAA J. Energy 2, 1978, pp. 346-353.
33. Plee, S. L. and Mellor, A. M., "Review of Flashback Reported in Prevaporizing/Premixing Combustors," Combust. Flame 32, 1978, pp. 193-203.
34. Tuttle, J. H., Colket, M. B., Bilger, R. W. and Mellor, A. M., "Characteristic Times for Combustion and Pollutant Formation in Spray Combustion," Sixteenth Symposium (International) on Combustion, Pittsburgh, The Combustion Institute, 1977, pp. 209-219.
35. Mellor, A. M., "Characteristic Time Emissions Correlations: The T-63 Helicopter Gas Turbine Engine," AIAA J. Energy 1, 1977, pp. 257-262.
36. Crowe, C. T., "A Computational Model for the Gas-droplet Flow Field in the Vicinity of an Atomizer," Western States Section/Combustion Institute Paper No. 74-23, 1974.
37. Leonard, P. A. and Mellor, A. M., Unpublished data.
38. Moses, C. A., "Studies of Fuel Volatility Effects on Turbine Combustor Performance," Paper presented at the 1975 meeting, Central States Section/The Combustion Institute.
39. Plee, S. L., "Characteristic Time Model for Flame Stabilization in Simplified Continuous Combustion Systems," Ph.D. Thesis, School Mech. Eng., Purdue University, 1978.
40. Peters, J. E. and Mellor, A. M., "An Ignition Model for Quiescent Fuel Sprays," Central States Section/The Combustion Institute Paper No. CSS/CI-79-14; submitted to Combust. Flame, 1979.
41. Ballal, D. R. and Lefebvre, A. H., "Ignition and Flame Quenching of Quiescent Fuel Mists," Proc. Roy. Soc. A London 364, 1978, pp. 277-294.
42. Lefebvre, A. H., Mellor, A. M. and Peters, J. E., "Ignition/Stabilization/Atomization - Alternative Fuels in Gas Turbine Combustors," Alternative Hydrocarbon Fuels: Combustion and Chemical Kinetics, New York, AIAA, 1978, pp. 137-159.
43. Peters, J. E. and Mellor, A. M., Unpublished data.
44. Mellor, A. M., "Characteristic Time Emissions Correlations and Sample Optimization: GT-309 Gas Turbine Combustor," AIAA J. Energy 1, 1977, pp. 244-249.
45. Hammond, D. C., Jr., "Evaluating Characteristic Time Emissions Predictions for Three Vehicular Gas Turbine Combustors," AIAA J. Energy 1, 1977, pp. 250-256.
46. Mellor, A. M. and Washam, R. M., "Characteristic Time Correlations of Pollutant Emissions from an Annular Gas Turbine Combustor," ASME Paper No. 79-GT-194; AIAA J. Energy, in press, 1979.
47. Washam, R. M. and Mellor, A. M., "Correlation Technique for Ambient Effects on Oxides of Nitrogen," AIAA J. Aircraft, in press, 1979.
48. Schmidt, D. A. and Mellor, A. M., "A Characteristic Time Model for Combustion Inefficiency from Alternative Fuels," AIAA Paper No. 79-0357; AIAA J. Energy, in press, 1979.
49. Blazowski, W. S. and Henderson, R. E., "Aircraft Exhaust Pollution and its Effect on the U.S. Air Force," AFAPL-TR-74-64, 1974.
50. Tuttle, J. H., Shisler, R. A. and Mellor, A. M., "Investigation of Liquid Fueled Turbulent Diffusion Flames," Comb. Sci. Tech. 14, 1976, pp. 229-241.

#### 7. ACKNOWLEDGEMENTS

Funding for the development of the characteristic time model has been provided by the U.S. Army Tank-Automotive Research and Development Command (P. Machala and A. Jaeger, technical monitors), the Environmental Protection Agency (R. Munt, technical monitor), the Air Force Office of Scientific Research (B. T. Wolfson, technical monitor), the Army Research Office (J. Murray, technical monitor), General Motors Corporation (J. S. Collman and P. Vickers, technical monitors), Ford Motor Company (W. Wade, technical monitor), and the General Electric Company (C. Wilkes, technical monitor), to all of whom the author expresses his gratitude. Preparation and presentation of this paper were made possible under Contract F33615-77-C-2069 with the Air Force Aero Propulsion Laboratory (R. E. Henderson, technical monitor). The United States Government is authorized to reproduce and distribute reprints for governmental purposes notwithstanding any copyright notation hereon.

COMBUSTION MODELLING WITHIN GAS TURBINE ENGINES,  
SOME APPLICATIONS AND LIMITATIONS.

J. Odgers.  
Université Laval  
Québec, Canada.

ABSTRACT

A review is given of some of the more pertinent models postulated to describe the performance of gas turbine combustors. Six different design/development stages are considered - (a) the initial sizing of a combustor, (b) the initial development testing, (c) primary zone modelling, (d) secondary zone modelling, (e) dilution zone modelling, (f) changes due to the alteration of ambient conditions. The models are assessed in scope plausibility, experimentally, and in terms of time and economic justification. For (a) it is suggested that a zero-dimensional model will suffice, as also for (b). Item (c) will probably require a three-dimensional model; (d) and (e) will probably suffice with a one - or two-dimensional model. For item (f) a zero-order model might well be satisfactory. If it can be produced with sufficient accuracy, a single complex (probably three-dimensional) model could adequately describe all items, (a) to (f). A short discussion deals with the need of future data, and the paper recommends the type of models which may be used currently, and those which are likely to be used in the future.

1. INTRODUCTION.

It is about thirty years since the potential of gas turbine manufacture began to make itself felt as a major industry. Due to the high degree of technology, it immediately became obvious that the development of new combustion systems would be expensive and time consuming. Hence a search began for an understanding of the combustion processes so that modelling procedures could be instituted. Most of the earlier parameters involved some form or other of Mach number scaling, since this involved most of the variables of importance to performance. Further, Mach number correlated with the pressure drop across the combustor, which in turn, was a function of the engine efficiency. Droplet evaporation characteristics were also explored, but it was generally conceded that the droplets had but little overall effect providing that the size was small (about 80 to 100 microns). Later, parameters were introduced based upon global reactions within 'perfectly stirred reactors' (PSR's). An aspect, appreciated, but still very imperfectly understood, is the very complex mixing process between air, fuel and products of reaction. The demand for a long life engine has emphasised the need to better the knowledge of the heat transfer processes within the combustor and the requirement for improved materials of construction.

As the years progressed, engineering 'know-how' enabled combustors to be made which operated with high combustion intensities, and in recent years it has been recognised that the combustion processes might limit the combustor size at some conditions, whereas previously aerodynamics were always assumed to be the limiting factor. Simultaneously with the progress in engineering, the chemistry of flames has become better known, and many of the individual reactions which comprise the process of the combustion of hydrocarbons have been investigated and their rate constants determined with fair accuracy. Recently, physicists have produced comprehensive mixing theories. Thus many of the individual bricks are now available to produce a comprehensive model. It remains only to invent a technique to bind them together. The cement exists in the form of large computers which are capable of solving the complex equations.

The net result is that, whereas twenty years ago the engineer had to 'make do' with elementary and limited correlations, today he is faced with a multitude of models ranging from simple zero-order ones to complex three-dimensional ones combining all possible aspects of evaporation, mixing and kinetic considerations, both with and without simultaneous heat transfer.

From an engineering viewpoint, the justification of a model is, to a large measure, based upon -

- (a) Does it predict sufficiently accurately?
- (b) How much time is needed to obtain a solution?
- (c) How easy is it to understand the result, and what are the possible implications?
- (d) What is the financial cost of the solution?

Generally (a) and (d) are the most important, but some of the proposed models are now so complex that the average engineer has difficulty in understanding them, and very rightly he seeks an expert to act as consultant. Unfortunately, sometimes the consultant has a problem in appreciating exactly what the engineer requires from the model. The net result is a certain amount of confusion whereby the reputations of both engineer and consultant (or the model), may suffer.

Therefore, what is needed is an appreciation of the types of model available and their possible application(s), the latter often depending upon the state of the development of the combustor. As an example, unless it was a perfect model, there would be little point to use a complex three-dimensional model for the initial sizing of the combustor. Such a model would, however, be very appropriate to the specification of the primary zone conditions, and their effects upon wall temperatures.

It is the intention of these notes to give some aid in this type of selection and to indicate, where possible, the known accuracy of the model suggested and its limitations.

## 2. MODELS AVAILABLE.

There are so many models available that it is impossible to review all of them in a paper such as this. The ones mentioned here are those of which the author has had some personal experience and/or those which have some measure of popularity. The models will be classified as 0 -, 1 -, 2 -, and 3 - dimensional, plus a single model specifically aimed at furnaces but of possible application to gas turbine combustors. The classification is not ideal, and some overlapping occurs, but it is convenient.

### 2.1 Zero - Dimensional Models.

This type of model treats the entire reaction zone as a single unit, and it is typified by the perfectly stirred reactor (PSR) in which velocities, temperatures, heat flux densities and compositions are uniform throughout the zone. An approach to such an ideal system was made by Longwell et al [1] using their well stirred reactor. This exhibited most of the characteristics described by Bragg [2], Avery et al [3] and Vulis [4]. The derived rate equations are simple, but the accuracy depends upon the approach to homogeneity. Therefore, they are not directly applicable to systems where the mixing processes are predominant. Essenhigh [5] and Swithenbank [6] have attempted to correct for unmixedness, and for a single reactor their results are in fair accord with experimental measurement.

The original Longwell model purported to do no more than to describe blow-out phenomena, and to a lesser degree, the fractional oxygen consumption efficiency of the equipment. The performance was related to the equation (lean mixtures of air and iso-octane)

$$\frac{N}{VP^n} = \frac{4,76k}{R_1^n} \frac{e^{-E/R_2T}}{T^{n-0,5}} \frac{[2\phi(1-\epsilon)]^f (1-\phi\epsilon)^{n-f}}{\phi\epsilon[4,76+\phi(1,36-\epsilon)]^n} \quad (1)$$

The units for equations (1) and (2) are -

N mol/s	E cal/mol	$R_1$ (0,082) l.atm/(mol.k)
V l	C K	$R_2$ (1,987) cal/(mol.k)
P atm	T K	

Oders et al [7 to 12] experimented with a spherical combustor in an attempt to relate its performance to that of real combustors. In [7 to 9] the various practical aspects were examined over a wide range of conditions. Later [10] these results, and those of other workers, were analysed and an equation was obtained which described all the data.

$$\frac{N}{VP^n} = \frac{1,29 \cdot 10^{10} (m^*+1) [5(1-y_c)]^\phi (\phi-y_c)^\phi e^{-C/T}}{0,082^2 y_c [5(m^*+1)+\phi+y_c]^{2\phi} T^{2\phi-0,5}} \quad (2)$$

Using Eqn. (2) as a basis, the stability and combustion efficiency performance of a number of real combustion chambers [11] was correlated (for weak mixtures in the primary zone) by -

$$\eta = 0,911 \log_{300}^V + 4,01n - 1,097 + D' \quad (3)$$

Equation (3) may be used to predict the performance of a combustor at any condition; the one curve is unique for a wide range of air/fuel ratios, inlet temperatures and pressures. For a totally unknown chamber, it is only necessary to obtain a value of the constant  $D'$  by experiment. This may not be in the near future, since recent work at Laval University suggests that  $D'$  may be related to the combustor pressure loss. Kretschmer et al [12] have shown that Eqn. (2) may be used to predict effects due to changes in ambient conditions, including the prediction of  $NO_x$ .

Using a somewhat similar theoretical basis, Greenhough and Lefebvre [13] derived a loading parameter similar to that of Longwell, which they showed to be applicable to aircraft combustors. For a given chamber, at a fixed air/fuel ratio, the efficiency and stability may be expressed by plotting the value of  $\theta$  against the efficiency, where  $\theta$  is given by Eqn. (4). The disadvantage of the  $\theta$  parameter is that a curve has to be made experimentally for each operating air/fuel ratio.

$$\theta = \frac{ADP^{1,75}}{m} \cdot e^{T/b} \quad (4)$$

The units for equation (4) are -

A $iv^2$	m lb/s	$b$ (=300) K
D in	T K	

An important feature of the  $\theta$  curve is the plateau of high efficiencies at low loadings. Many workers have used a 'safe' value of this parameter (say  $\theta = 10^6$ ) to size a new combustor.

A major disadvantage of all the above models is their inability to predict the amounts of the pollutants ( $CO$  &  $HC$ ). This has been overcome to some extent by the use of empirical curves which relate the pollutant concentration to the efficiency, but the technique is of limited application and not very accurate.

For a system which is not limited by mixing, it ought to be possible to predict pollutants if the chemical kinetics are fully known. A large number of publications are available on this topic, and typical

examples are given in [14 to 18]. Generally the reaction is thought of as being a two-stage process, the breakdown of the hydrocarbon being followed by the combustion of the resultant carbon monoxide. The first reaction is fast compared with the second, and hence it is the kinetics of the CO burning that limit the overall process and the amounts of pollutants produced. Reaction schemes have been proposed ranging from about 8 reactions to 40 or more. The number of reactions selected appears to be a function of the size of computer available. Models of this type have been used to predict the performance of PSR's with fair success, but only over a limited range of conditions. As an example, Hammond and Mellor [19] applied such a scheme to a reactor burning a propane/air mixture. They could only obtain viable solutions over the range  $\phi = 0.9$  to  $\phi = 1.2$ , but within these limits theory and experiment agreed quite well. Similar schemes have been used by others (See review [20]) but the models appear to be limited in application and exhibit large errors when used to predict the performance of any of the other systems.

## 2.2 One-Dimensional Models.

Although not so simple as the zero-dimensional models, the one-dimensional models are still relatively simple, and the calculations are cheap to do. Heat flux and species may be predicted, but a knowledge of fluid flow and chemical heat release will then be required as input to the model. However, the use of this concept enables one to depart from the PSR to one which is mixing limited, or reaction limited, or both (well-stirred reactor, WSR).

Typical of a simple reaction scheme is that of Essenhigh [5] which is applied to the analysis of an adiabatic flame, using a PSR approach. The flame is divided into a series of cells, each of which is regarded as a PSR fed by the preceeding cell and feeding the succeeding one. The analysis yields a pair of algebraic equations, conveniently in finite difference form. The solution gives temperature or concentration profiles as a function of distance or time, for the various input conditions. The theory gives a rational solution to the problem, but to date it has not been thoroughly tested against practical measurements.

Contrary to the above, Hottel et al [21] assume that combustion occurs so rapidly that the gas temperature at the burner end (of a furnace) is the adiabatic flame temperature. It is also assumed that the net radiative flux in the gas flow direction is negligible compared with that normal to it. Thus it is possible to predict the local flux density along the x-axis.

The module approach circumvents the requirement of a detailed analysis of the microstructure by breaking the chamber into separate zones, each of which is assumed to behave in a predictable manner. In the short term, this kind of prediction may yield a much more valuable correlation than any of the techniques previously discussed. Also, by a judicious choice of zones, modules may be selected which will represent, fairly accurately, a three-dimensional system.

Swithenbank [22] has attempted to model a turbojet combustor. The primary zone is represented by three modules, a pair of WSR's coupled by a plug-flow reactor (PFR). The volumes are calculated from jet entrainment theory, the total volume of the primary zone having been assessed previously by some independent method. The volumes of the various reactors are estimated on the assumption of uniform gas density; the swirler and recirculation volumes are ratioed according to their mass flows; that of the primary is considered to be symmetrical about the primary orifices. The secondary zone has two modules, a WSR followed by a PFR. The volume of the WSR is obtained by the assumption that it is symmetrical about the secondary zone holes, with its upstream boundary abutting the primary zone. The dilution stirred reactor is supposed symmetrical about the dilution holes, and of a volume which is ratioed in proportion of its mass flow to that of the secondary zone. Between the secondary WSR and the dilution WSR, the resultant volume is taken as being the secondary PFR. The plug flow module of the dilution zone is taken as that between the downstream end of the dilution WSR and the exit of the combustor. Thus, for each module, the mass flow, volume and residence time have been defined, and this may be used to predict the composition leaving each module (providing there is a suitable reaction scheme). The output of one module becomes the input of the next, although within the primary zone an iterative calculation must be used since there is recirculation from one zone to another. Temperature traverses in a real combustor were quite closely predicted using this model, but extensive testing has not been attempted.

So far, the models examined have assumed that the influence of fuel droplets is negligible. It is obvious that a more complete analysis could be made if the fuel droplet size and distribution were incorporated together with evaporative effects. In this respect Mellor's proposal [23] is of some interest. The 'modules' are characterised by residence times, each time serving a particular region defined within the combustor. Mellor defines five such times - (i) the fuel drop lifetime, (ii) the eddy dissipation time for the injected fluid (this represents small scale turbulent mixing near to the fuel injector in the recirculation zone), (iii) the eddy dissipation time in the shear layer (this represents the large scale turbulent mixing of fresh air and the recirculated burned gas), (iv) the fuel ignition and burning time (representing the time for homogeneous combustion of the fuel), and (v) the NO formation time. The approach is very promising and could well yield very useful results, providing that the various residence times can be defined with sufficient precision so that they may be used over a wide range of conditions and geometries. To date, not a great deal of analysis has been experimentally investigated, but that which has is apparently in fair agreement with the predictions. NOx and CO exhaust-plane emissions have generally correlated well with their respective time functions, except when fuel atomisation was poor. The results also confirm the theory that the homogeneous combustion time and the ignition delay times are much shorter than either the droplet evaporation times or the mixing times.

One dimensional models have proved to be popular for the prediction of NOx, largely due to the way that the rate of formation depends so largely upon temperature. As an example Heywood et al [24] took the secondary zone of a combustor and treated it as a one-dimensional model with instantaneous mixing of the secondary air. Calculated values of NOx were about the same value as those from aircraft engines. Hung [25 & 26] suggests a diffusion limited model that predicts NOx within gas turbine combustors, including the use of nitrogen-containing fuels and the effects of water injection etc. The primary

zone is assumed to have a flow pattern similar to that described by Clarke [27], such that the three dimensional effect can be accounted for by the use of a quasi-one-dimensional model. For the swirler, the core radius of the reverse flow is determined in order to provide a boundary for the recirculation zone. Kollack and Aceto [28] studied the effects of recirculation in a combustor using a computer programme which simultaneously solved the chemical kinetic, thermodynamic, and gas dynamic equations for a premixed one-dimensional recirculation system. The effect of hot gas recirculation was to form NOx at an earlier stage but to about the same maximum as the unrecirculated case. Cold gas could reduce the NOx by an order of magnitude.

### 2.3 Two-Dimensional Models.

These models predict with x-y coordinates and are suitable for systems (such as a gas-turbine combustor) where axis-symmetric flows prevail. The problem is simplified if the flow is uni-directional and without recirculation, such as a simple, confined turbulent diffusion flame. The Patanker-Spalding technique has been used to solve this problem [29]. The problem appears simple, but the flows are still very complex, and an adequate digital computer is required. Adequate modelling of the following features is required - (i) turbulence, (ii) reaction rate, (iii) radiation chemical kinetics (sometimes) and (iv), possible two-phase effects. The Gemix Computer Code is available to solve the problem, by which six simultaneous differential equations are solved for velocity, turbulence energy, turbulence scale, stagnation enthalpy, fuel concentration, and concentration fluctuations. Unfortunately, aircraft combustors exhibit recirculation, and this means that iterative procedures must be used instead of marching integration. For a relatively simple axis-symmetric furnace, computations of this kind have shown good qualitative agreement with the experimentally determined features. A more complicated procedure is available for a system having pre-vaporised fuel injected with swirling air into a film-cooled combustor [30]. The models employed for this scheme utilised turbulence, concentration fluctuations, radiation, a simple combustion kinetic scheme, and NOx kinetics. The computer code used was EASI (steady state model), and qualitative agreement was obtained with the experimental data. The difference was attributed in part to the fact that the combustor was only partially axis-symmetric. Platt [31 & 32] has published a computer programme for the calculation of steady-flow, homogeneous reaction kinetics. It is implied that this would improve the Spalding-Gosman predictions with respect to chemical kinetics. Recently, Spalding et al [33] have published predictions of the hydrodynamic and thermodynamic properties of flow relevant to a jet-engine after-burner. The flow was two-dimensional, axis-symmetric, unsteady, compressible, and chemically reacting. A fuel spray analysis was included. It is claimed that the numerical solution procedure gave a useful tool for investigating the 'buzz' in the engine after-burner.

### 2.4 Three-Dimensional Models.

These should be the 'all-can-do' models which, if sufficiently accurate, should yield perfect predictions throughout the combustor. Currently, the known models predict species, concentrations, temperatures and velocities at any point within the combustor. It is possible to include the prediction of flame radiation and wall temperatures (with and without film cooling) at the price of a more complicated programme. The major problems preventing the general introduction of these models are -

- (i) Assumptions involving flow and turbulence predictions may not be correct,
- (ii) reaction kinetics may not be correct,
- (iii) factors governing carbon formation are not known, and this affects the accuracy of flame radiation predictions,
- (iv) for accurate prediction, a large number of points is required (i.e. fine mesh). This increases the computer time and cost,
- (v) a specialist engineer/programmer is needed or else the work must be given to a consultant,
- (vi) a large computer must be available.

From this it might seem that the chance of a satisfactory three-dimensional programme would be remote. However, considerable progress has been made and several models exist which demonstrate the correct trends of conditions within the combustor. Perhaps the most comprehensive is that of Spalding [34]. This uses a finite difference computational procedure to predict quantitatively the local flow, heat transfer and combustion processes inside a three-dimensional can combustor, where the flow is swirling and recirculating. A gaseous fuel system was employed. The process required the numerical solution of twelve simultaneous differential equations in finite difference form. It is claimed that the system will compute economically and thereby substantially reduce the experimental portion of the development time. Although the results given were not verified experimentally, it was noted that the physical models used had all been shown to be valid in simpler two - and three - dimensional situations and that the procedure now seemed to be ready to be employed within industry.

### 2.5 Miscellaneous Models:

Several models exist which do not readily fall into any of the above categories. Of the ones examined, only one seemed to be of significance. This model was developed specifically for furnaces, but the results are so interesting that it would seem logical to test the method against the performance of a gas turbine. The model is that of Magnusson et al [37], and it relates the rate of combustion to the rate of eddy dissipation of turbulent eddies. The rate of reaction is expressed by the mean concentration of a reacting species, the turbulent kinetic energy and the rate of dissipation of the turbulent kinetic energy. It differs from other models in that it does not call for prediction of fluctuations of reacting species, and, additionally, it is applicable to both premixed and diffusion flames. A very interesting feature is that the model can be used to predict soot formation and combustion in turbulent flames. The theory was tested by computing the behaviour of seven flames representing turbulent diffusion flames, premixed turbulent enclosed flames, combined premixed/diffusion flames, and turbulent diffusion sooting flames. In all cases close correlation was obtained between prediction and experiment.



## 2.6 Wall Cooling.

Most combustion models do not take wall cooling into account and those that do regard it as an additional complication to an already complex model. Thus, only the two- and three-dimensional models of Spalding and co-workers attempt to make these predictions in conjunction with the combustor model. More generally, the combustor predictions are used to estimate the local gas conditions, and these are then utilised with a separate film cooling correlation. A number of wall temperature prediction techniques exist, [38 to 40] for example, which give reasonably satisfactory predictions. Basically, all of them use the same equations, modified according to the whims of the user, and there seems little to choose in the accuracy of predictions. These latter range from  $\pm 20$  to  $\pm 40$ K, depending upon conditions. The simple models appear to give about the same precision as the complex ones.

## 3. WHICH MODEL ? AND WHEN ?

One of the major problems, confronting anyone trying to assess the accuracy of a model, is that most authors justify their parameter solely against their own experimental work. Also, because of publication difficulties, the data are not usually given in sufficient detail to enable them to be used to check the parameters of other workers. Add to this that certain computer programmes are limited by propriety rights, and the difficulties of comparing one model with another become obvious. To complicate the matter further, the economics of the calculation are sometimes a restricting factor, as is also the specialised knowledge required to solve some of the more complex programmes. It is not, therefore, surprising that the following assessment must have reservations, and that no clear-cut picture will emerge.

The only models which have been tested at all comprehensively are the simple empirical and semi-empirical ones. An attempt will be made to indicate their accuracy, so that the proposers of future complex models will have at least a target which they must surpass. This is not to denigrate the complex models from a scientific viewpoint, but the engineer must keep constantly in mind that his product must be economic; for the same accuracy, a cheap model is 'better' than a complex expensive one.

### 3.1 Initial Sizing of the Combustor.

A combustor has been selected which was developed to meet Condition 1, Table I, as its design point. To indicate what happens if a number of design conditions have to be met (instead of one), three new 'design' conditions have been added.

TABLE I.

Cond. No.	$\dot{m}_a$ kg/s	$T_2$ K	$P_2$ $10^5$ Pa	$\Delta P/P$	$Ma$	$\dot{m}_f$ kg/s	$\phi_{pz}$
1*	4,67	476	4,05	0,05	0,056	0,0778	1,0
2	10,06	641	10,13	0,05	0,056	0,1677	1,0
3	17,97	803	20,26	0,05	0,056	0,2295	1,0
4	0,74	300	1,01	0,0125	0,028	0,0082	0,67

\* Original design point.

Five different (all simple) correlation parameters have been selected to determine the size, based upon either aerodynamic or combustion performance characteristics. The relationships are well known, but they have been rearranged in SI units.

#### (i) Mach Number Relationship. [35]

$$Ma = 14,3 \frac{\dot{m} \sqrt{T}}{AP} \quad (5)$$

#### (ii) Pressure Loss Relationship. [36]

$$A = 59 \frac{\dot{m}_a \sqrt{T}}{P} \left( \frac{P}{\Delta P} \right)^{0,5} \quad (6)$$

#### (iii) Bragg's Relationship. [41]

$$A = 0,01621 \frac{\dot{m}_f \sqrt{T}}{P} \left( \frac{P}{\Delta P} \right)^{0,5} \quad (7)$$

#### (iv) Theta Parameter. [13] (=99%)

$$AD = 1,88 \cdot 10^8 \left( \frac{\dot{m}_a}{P^{1,75}} \right) e^{T/b} \quad (8)$$

#### (v) Odgers-Carrier Parameter. [11] (=99%)

$$d = 3745 (300/T)^{0,411} (\dot{m}_f/P)^{0,333} \quad (9)$$

This latter parameter is specific to  $\phi = 1,0$  in the primary zone. For any other value of  $\phi$ , Eqn. (3) must be used.

It is important to realise that at least two of the above parameters must be used (one aerodynamic and one combustion). In the Laval Laboratories all five are employed. The results given by the above equations, for the conditions of Table I, are given in Table II. It is interesting that both Eqns. (8 & 9) predict the need for a larger chamber to meet the combustion efficiency of 99% implicit in the values selected for these equations. In fact, if the final real chamber dimensions are inserted into the original version of Eqn. (9) (i.e. Eqn. 3), then for condition 4, the predicted efficiency of 93% is in fair accord with the measured value of 91%. The results of Table II clearly demonstrate the need to consider all the running points as design points. The days of designing to meet a single 'critical' condition are past. The demand of very high combustion efficiencies at idling conditions (to meet environmental requirements) requires a very critical look at the initial sizing procedure.

TABLE II

Cond. No.	Eqn. No.	5*	6	7	8	9
	Value					
1	A m <sup>2</sup>	0,0642	0,0662	0,0308	0,0843	0,0713
	D m	0,286	0,290	0,198	0,328	0,301
	d m	0,228	0,232	0,139	0,262	0,241
2	A m <sup>2</sup>	0,0642	0,0662	0,0308	0,0483	0,0274
	D m	0,286	0,290	0,198	0,206	0,187
	d m	0,228	0,232	0,139	0,165	0,150
3	A m <sup>2</sup>	0,0642	0,0662	0,0308	0,0153	0,0274
	D m	0,286	0,290	0,198	0,140	0,130
	d m	0,228	0,232	0,139	0,112	0,104
4	A m <sup>2</sup>	0,0642	0,0662	N/A	0,0943	0,172#
	D m	0,286	0,290		0,347	0,468#
	d m	0,227	0,232		0,277	0,374#

\* This is the actual size of the combustor which was based upon a casing Mach number=0,056.

# 'Idling' conditions based upon Eqn. (3).

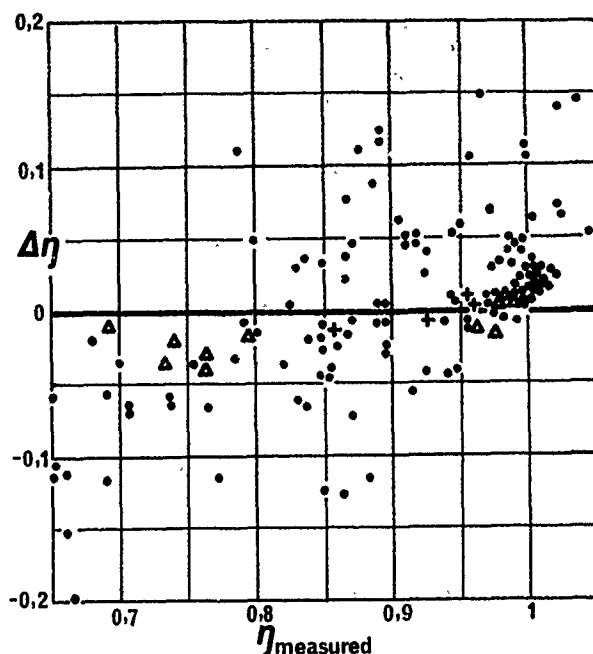
### 3.2 Initial Combustor Development.

It does not come within the province of this paper to discuss flow visualisation experiments and their value to the engineer, but it is assumed that these studies will have been carried out and that the results would have indicated that (a) the flow pattern was satisfactory, (b) the film cooling jets appear satisfactory, (c) jet penetrations into the various zones are satisfactory, and (d) the primary and recirculation zone volumes are well defined. The combustor pressure loss will also have been measured and found satisfactory.

Following this, atmospheric testing will be done to verify the combustor performance at ground level and to forecast its performance at other conditions. The ideal model would predict ignitability, combustion efficiency, exhaust traverse quality, type and quantity of pollutants, and blow-out characteristics. An indication that the flame-tube wall temperatures are satisfactory would also be useful. All this could be done with a satisfactory three-dimensional model, but at present no proven one exists which is both accurate and cheap. How accurate must it be? Obviously combustion efficiencies must eventually predict to better than 1%; the other topics are less critical providing that the operating characteristics are superior to those demanded. They should at least be better than the simple models cited below.

Equation (3) may be used to predict combustion efficiencies at all conditions providing that the constant D' has been first established. Theoretically only a single efficiency determination is needed to establish D'. In practice the mean of four determinations provides a much more reliable figure. At least two measurements should be made of efficiencies in excess of 99%, and at least one of the order of 90%. The efficiencies need to be accurate and demand the use of gas analysis; pyrometric techniques are simply not accurate enough.

For the following example, a combustor was run at atmospheric pressure but at four different conditions. The value of D' was assessed at 0,336. The combustor was then run over a wide range of conditions (A/F 216 to 34, P<sub>2</sub> 0,34 to 7,66 atm, T<sub>2</sub> 243 to 545K). The predicted and measured efficiencies are indicated in Fig. (1). It is obvious that the gas analysis results agree with the predictions better than do the pyrometric values. Earlier analysis [11] indicated that the latter could have errors of  $\pm 5\%$ . More recent work suggests that Eqn. (3) will predict within  $\pm 2\%$  at low efficiencies (say 80 to 90%) and better than 1% at high efficiencies (say 99%). Eqn. (3) may also be used to indicate the blow-out curve for a combustor. For a PSR flame extinction seems to occur at a relatively constant flame temperature, of the order of 1500K. In a real combustor, due to mixing and droplet evaporation, the temperature is somewhat lower. Equation (3) has a very steep fall off toward  $\eta = 0$ , at an efficiency of 60%. This value of  $\eta$  may be inserted into Eqn. (3) and assumed to give blow-out loadings.



- ◆ Points used to define D'.
  - ▲ Efficiencies determined by gas analysis.
  - Efficiencies determined by pyrometry.
- $\Delta\eta = \eta_{\text{measured}} - \eta_{\text{predicted}}$

Fig. 1. Prediction of Combustion Efficiencies Using Equation (3).

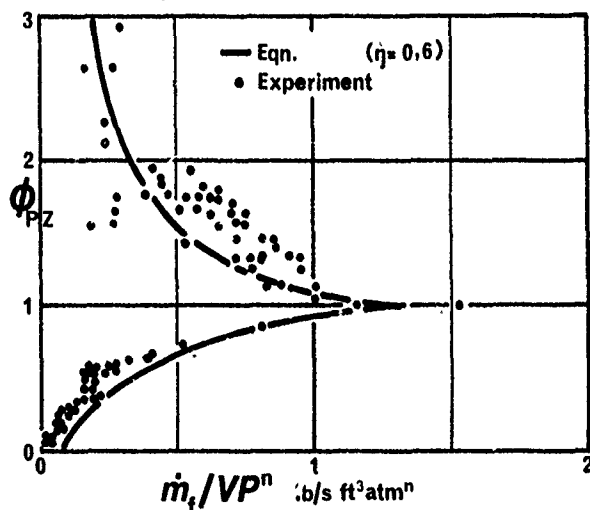


Fig. 2. Prediction of Blow-out Using Eqn. (3)

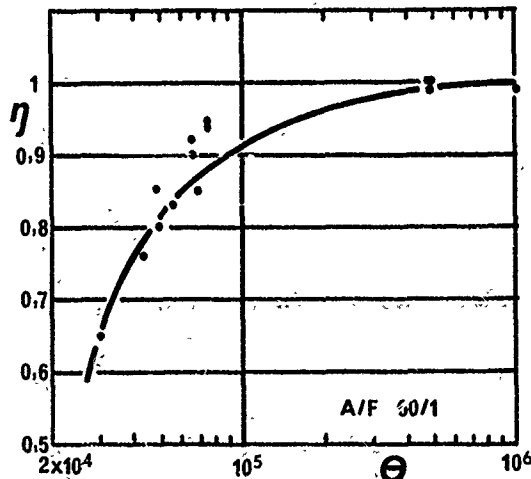


Fig. 3 Prediction of Efficiency, Theta Parameter.

Figure 2 compares the predictions with experimental results. As a general indication the prediction is satisfactory, but there is considerable room for improvement. To the best knowledge of the author, no prediction technique exists which will predict ignition limits. Of course, if the system was perfect, the ignition and stability limits would coincide. For the particular can used here, a rough approximation to the ignition limits was achieved by putting  $\eta = 90\%$  in Eqn. (3). This could well be circumstantial.

An alternative to the use of Eqn. (3) is to use the  $\theta$  correlation (Eqn. 4). This, however, requires more experiments, since three or four points are required to establish each curve for a single operating air/fuel ratio. Typical results, for the same chamber as above, are shown in Figs. 3 and 4. The A/F = 60/1 points show much less scatter than those for A/F = 100/1. This might be indicative of the need to assume a variable reaction order, as per Eqn. (3). As before, the fall-off in efficiency may be used to predict blow-out. The accuracy of prediction is about the same as that given by Eqn. 3.

Both of the above techniques predict efficiency at the exhaust. If pollutants are required, either an alternative parameter must be sought, or some estimate may be made by assuming that the ratio of CO to HC varies in the same way as the measured values used to define the correlation equation. If the combustion efficiency is in excess of 99.5%, the exercise becomes academic. For the prediction of NOx, the curve of Kretschmer [12] may be used, or that of Lipfert [42] or most other simple correlations.

An indication as to the film cooling may be obtained from the following equation (empirical) developed at Laval University.

$$\% \text{Film Cooling} = 0.1 T_1 - 30 \quad (\pm 10\%) \quad (10)$$

An equation which predicts (very approximately) the traverse quality is -

$$Q = (73.85 - 138.5 \Delta P/P) - 27L/d \quad (11)$$

$$Q = \frac{T_{\text{max}} - T_{\text{mean}}}{\text{Mean Temp. Rise}} \quad (11a)$$

Both Eqns. (10 & 11) are relevant to conventional combustors with conventional fuel systems. There are indications that neither apply (for instance) to air-blast fuel injection systems. The accuracy of prediction for both equations is not satisfactory, and better correlations should be sought. They are only a guide, and should be accepted as such.

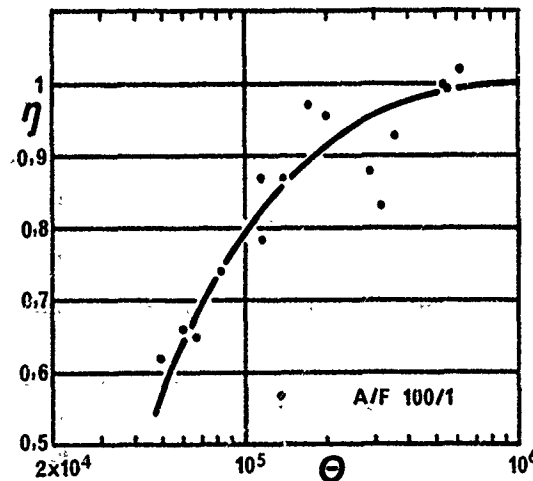


Fig. 4 Prediction of Efficiency, Theta Parameter.

It is obvious that there is room for improvement for all the above techniques. They are given here (a) because they are 'better than nothing', and (b) they give an idea of the accuracy which must be bettered by any replacement correlations. Assuming that the combustor design has proved to be satisfactory at this stage, the next phase is to examine the performance of the individual zones of the combustor.

### 3.3 Primary Zone Model.

Any model for use in the primary zone should predict one or more of the following -

- (i) flame temperature distribution.
- (ii) flame emissivity.
- (iii) local air/fuel and composition.
- (iv) local gas velocities.
- (v) combustor wall temperatures.
- (vi) flame stability.
- (vii) carbon formation and consumption.

There are no simple models which will predict accurately within this zone. Crude, empirical models exist which give some idea of the mean gas temperature and emissivity, hot gas velocity and cooling jet velocity. Thus, an appraisal of the wall temperature can be made which, strangely enough, is often sufficiently accurate for engineering purposes. Again, these predictions, and the observed accuracy, represent a target for the more refined techniques.

For the sole purpose of wall temperature prediction, the following empirical equations have been developed at Laval University. They relate to the various mean hot gas temperatures.

$$T_r = T_a + \eta_r \Delta T_\theta = 1 \quad (12)$$

$$\eta_r = 0,56 + 0,44 \tanh [1,5475 \times 10^{-3} (T_a + 108 \ln P_a - 1863)] \quad (12a)$$

$$T_{pz} = T_a + 0,5 \eta_{pz} (\Delta T_\theta = 1,0 + \Delta T_{pz}) \quad (13)$$

$$\eta_{pz} = 0,71 + 0,29 \tanh [1,5475 \times 10^{-3} (T_a + 108 \ln P_a - 1863)] \quad (13a)$$

$$T_{out\ pz} = T_a + \eta_{pz} \Delta T_{pz} \quad (14)$$

The high values ascribed to these equations are excused by the importance of flame radiation in the zone. Based upon the experimental information available it is estimated that the flame temperatures predicted in this way have the following accuracy -

- + 100K at conditions of low efficiency
- + 50K at conditions of high efficiency

The heat transfer equations used to calculate the wall temperature are due to Lefebvre et al [43]-

$$R_1 = S \left[ \frac{1-e_w}{2} \right] e_g T_g^{1,5} [T_g^{2,5} - T_{w1}^{2,5}] \quad (15)$$

$$C_1 = 0,017 \left[ \frac{\lambda_c}{\mu_c} \right]^{0,8} \left[ \frac{\dot{m}_c}{A_c d_c^{0,2}} \right] [T_c - T_{w1}] \quad (16)$$

$$R_2 = 0,4 S [T_{w2}^4 - T_a^4] \quad (17)$$

$$C_2 = 0,02 \left[ \frac{\lambda_a}{\mu_a} \right]^{0,8} \left[ \frac{\dot{m}_a}{A_a d_a^{0,2}} \right] [T_{w2} - T_a] \quad (18)$$

$$K_{12} = \frac{\lambda_w}{\mu_w} (T_{w1} - T_{w2}) \quad (19)$$

$$R_1 + C_1 = R_2 + C_2 = K_{12} \quad (20)$$

The emissivity equation is also that of Lefebvre -

$$e_g = 1 - \exp. [-0,286 P \text{Lu}(f_1)^{0,5} T_g^{-1,5}] \quad (21)$$

However, the luminosity equation has been derived in this laboratory, based upon the data given in [43 to 45].

$$\text{Lu} = 0,0691 (C/H - 1,82)^{2,71} \quad (22)$$

The film cooling expression is that of Odgers and Winter [46]

$$\frac{T_g - T_w}{T_g - T_c} = f \left\{ K \left[ \frac{\dot{m}_c A_c}{\dot{m}_g A_g} \right]^{0,8} \left[ \frac{T_g}{T_c} \right]^{0,6} \frac{x^{0,8}}{s} \right\} \quad (23)$$

Using the above equations and the appropriate film cooling correlation (depending upon the geometry of the film cooling device), the wall temperatures may be predicted in the primary zone with an accuracy of not less than  $\pm 50K$ . A typical result is given in Fig. 5. The above accuracy cannot be guaranteed for air-blast or similar systems.

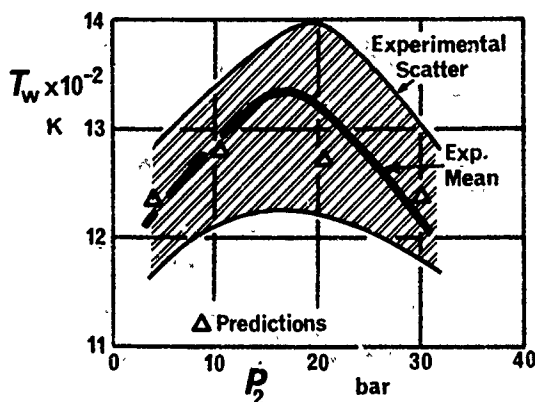


Fig. 5 Wall Temperature Predictions.

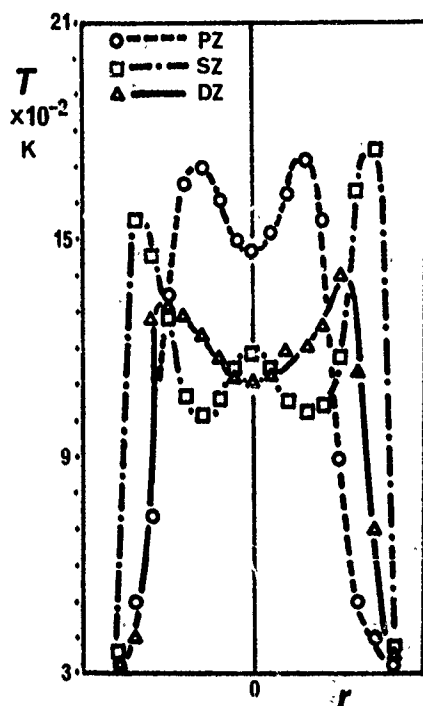


Fig. 6 Zone Temperatures in an Aircraft Combustor.

In order to provide the necessary detail, the complexity of the primary zone demands a two- or a three-dimensional model. Those of Spalding and Co. are of considerable interest, as also that of [37]. It seems very doubtful that any of the modular techniques would give the required structural detail. It would be of considerable interest to compare some of these models and their corresponding predictions. It should now be possible to provide the experimental data required to fully test such techniques. Gas analysis methods now exist which will provide the required composition data, and the Pulse Thermo-couple developed by Kretschmer has been shown to be an accurate and fast way of evaluating the temperature distribution [47]. A typical set of traverse data through an aircraft combustor is shown in Fig. 6. The values were obtained by sampling through the air admission holes; samples between holes show a somewhat different pattern. The temperatures measured agree closely with those given by detailed gas analyses, although the latter show the fuel efficiency to be quite low. Indications are that the fuel efficiency in the primary zone is of the order of 50%. These results support the assumption that hydrocarbons are the result of mixing inefficiency and the remaining species are kinetic limited. It has been shown [48] that even completely premixed air and fuel yield considerable amounts of hydrocarbons when combusted in a typical primary zone. This would cause considerable difficulty to the 'mixing limited' enthusiasts.

### 3.4 Secondary Zone Model.

This is the region where the combustion is sensibly completed and the model should forecast -

- (i) gas temperature distribution
- (ii) local A/F and species distribution
- (iii) gas velocity distribution
- (iv) wall temperature distribution.

The flows in this zone are still complex, and it is suggested that the same models be used in this region as for the primary zone. A few gas analysis measurements suggest that Eqn. (3) will reasonably predict the efficiency at the exit of this zone. Other than this, the only model used extensively is one to predict wall temperatures. This is identical in procedure to that outlined in Para. 3.3, except that the mean gas temperatures are estimated (at Laval) by the following empirical equations.

$$T_{in_{sz}} = T_{out_{pz}} \quad (24)$$

$$T_{out_{sz}} = T_2 + \eta_{sz} \Delta T_{\phi=pz} \quad (25)$$

$$T_{mean_{sz}} = \frac{T_{in} + T_{out}}{2} \quad (26)$$

The simple model predicts wall temperatures with an accuracy of  $\pm 30K$ .

### 3.5 Dilution Zone Model.

For the simple model to predict the wall temperatures, the procedure is as before but with gas temperatures given by -

$$T_{in_{dz}} = T_{out_{sz}} \quad (27)$$

$$T_{out_{dz}} = T_2 + \eta_{dz} \Delta T_{\phi=pz} \quad (28)$$

$$T_{mean_{dz}} = \frac{T_{in} + T_{out}}{2} \quad (29)$$

The accuracy is again  $\pm 30K$ .

Obviously the complex model used to predict conditions in the primary and secondary zones could also be used for this zone. However, if it can be definitely established that combustion is sensibly completed within the secondary zone, then the possibility of a much simpler model is obvious.

### 3.6 Changes in Ambient Conditions.

If it can be avoided, there seems to be little point in using a complex model for this purpose. The problem is simplified to some extent by the fact that the performance of the combustor is already known at some 'near' condition. Hence, it is usually possible to utilise some type of 'scaling factor' Kretschmer [12] suggests several such. An example of the predicted and measured changes in efficiency, due to increased inlet temperature, is given in Fig. 7. The agreement is satisfactory, but the method gives no indication of the contribution of the individual pollutants. These have to be assessed from a prior knowledge of the combustor characteristics at other conditions.

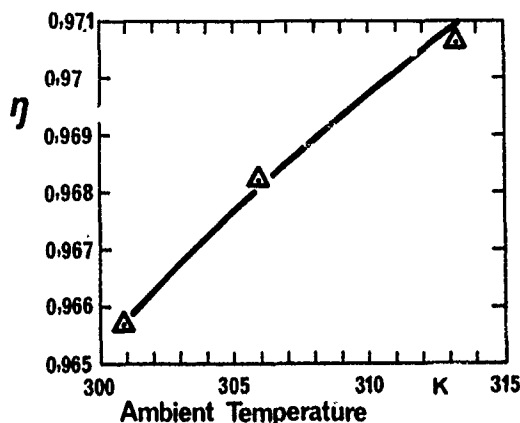


Fig.7 Effects of Ambient Temperature upon Combustion Efficiency.

(a) combustor conditions (b) steam and water injection (c) the presence of nitrogen in the fuels (d) ambient changes and (e) changes in combustor geometry. The claims are supported by experimental evidence, and the technique is worthy of further consideration.

Kretschmer's techniques will also predict NOx changes fairly accurately. Marzeski et al [49] specifically examine the effects of ambient changes upon emissions at idling conditions. They give formulae for changes in HC and NOx, but report a failure when attempting the prediction of CO. There seems to be a possibility of using this work in conjunction with that of [12] in order to obtain a full range of predictions at all conditions.

### 3.7 Prediction of Oxides of Nitrogen.

NOx has assumed such a significance in the field of pollution that it seems reasonable to consider models specific to its prediction. The published literature is so enormous that a full review here is not possible. Comment will be reserved to those papers which, in the author's opinion, have widespread application. For approximate estimates, the correlations of Kretschmer [12] and Lippfert [50] are adequate. The model of Hung [25 & 26] is more sophisticated and is claimed to predict accurately the effects of

## 4. DISCUSSION

It must be concluded that there is no model available which will satisfactorily take into account all the variables which occur in the operation of gas turbine combustors and predict the performance with sufficient accuracy. A number of models exist of limited application, and others encourage further investigation since they have the prospect of more general usage. Whilst work to date has shed light on the general understanding of the combustion processes, the situation is that there is still no model capable of catering for the predictive requirements of real combustors.

A major reason for this is the absence of accurate experimental data within the combustors which would enable any theory to be comprehensively tested. What is required (say) is measured data from five combustors operated over a range of conditions. For each combustor there would be a 'map' of the primary, secondary and dilution zones giving detailed distributions of (a) temperature (b) species (c) gas emissivity (d) velocities (e) fuel droplet sizes and placement (f) carbon measurements and (g) wall temperature measurements. The chambers should be selected so as to include geometry variations, conventional fuel injection, air-blast injection, pre-vapourised fuel and premixed fuel/air.

It is realised that this would be an expensive project, but the end-result would be to possess a set of data sufficient to test any proposed theory. The desire for an adequate model is now so strong that it ought to be possible to set up a national, or even an international, committee to standardise the techniques of measurement, obtain the necessary funds and to place the work in approved laboratories. If the results led to a satisfactory 'universal' model, the savings in development time would more than amply repay the cost of the work, as well as assisting in the understanding of the complex phenomena of combustion within a real system. It is further believed that any model developed for the gas turbine combustor could have widespread application to other continuous flow combustion systems such as furnaces and domestic heating equipment.

### NOMENCLATURE

A	Outer casing reference area	m <sup>2</sup>
a	Flame tube reference area	m <sup>2</sup>
b	Constant depending upon A/F (see 13)	K
C	= E/R	K
D	Outer casing reference diameter	m
D'	Constant	-
d	Flame tube reference diameter	m
E	Activation energy	J/mol
e	Emissivity	-
f	Reaction order for fuel	-
f	Fuel/air ratio (by mass) Eqn. (21)	-
K	Constant	-

# NOMENCLATURE (Cont'd)

k	Any constant	-
L	Length of dilution zone	m
Lu	Flame luminosity	-
Ma	Mach number	-
m	mass flow	mol/s
m*	Ratio mols inerts/mols oxygen	-
N	Mass flow	mol/s
n	Overall reaction order	-
O/F	Oxygen/fuel ratio (mass or volume)	-
P	Pressure	Pa (atm)
Q	Traverse quality	-
q	Velocity head	Pa
R	Gas constant	J/(mol.K)
S	Radiation constant ( $5,667 \times 10^{-8}$ )	W/(m <sup>2</sup> .K <sup>4</sup> )
s	Slot thickness	m
T	Temperature	T
V	Volume	m <sup>3</sup> (l)
x	Distance from film cooling slot	m
ΔP	Pressure drop	Pa
ΔT	Theoretical temperature rise	K
ε	Fractional oxygen consumption efficiency	-
θ	Parameter, see: Eqn. (4)	-
λ	Gas conductivity	W/(m.K)
μ	Gas viscosity	kg/sm Pa.s
ψ	Fuel loading, see Eqn. (3), Ref. 11	kg/(s.m <sup>3</sup> Pa <sup>n</sup> )
η	Combustion efficiency	-
¶	Parameter = log log (1/η)	-
Π	Engine Compression Ratio	-

## SUFFIXES

a	inlet air (or amount of air in outer casing at any point.
c	film cooling
dz	dilution zone
f	fuel
g	hot gas or flame gas
i	at inlet conditions
m	mass
pz	primary zone
r	recirculation zone
ref	reference point
sz	secondary zone
v	volume
w	wall
1	referred to within combustor
2	referred to outer casing

## REFERENCES

1. Longwell, J.P. & Weiss, M.A., "High Temperature Reaction Rates in Hydrocarbon Combustion", I. & E.C. 47, No. 8, p. 1634.
2. Bragg, S.L., British Aeronautical Research Council, "Application of Reaction Rate Theory to Combustion Chamber Analysis", 1953, Paper No. 16170.
3. Avery, W.H. & Hart, R.W., "Combustor Performance with Instantaneous Mixing", I. & E.C., 45, No. 8, 1953, p. 1634.
4. Vulis, L.A., "Thermal Regions in Combustion", New York, Mc Graw Hill, 1961.
5. Essenhigh, R., "An Introduction to Stirred Reactor Theory Applied to Design of Combustors, Combustion Technology", Pennsylvania, State University, Some Modern Developments, 1973.
6. Swithenbank, J., Poll, I. & Vincent, M.W., "Combustion Design Fundamentals", 14th Symposium (Int.) on Combustion, Combustion Institute, 1973, p. 627.
7. Clarke, A.E., et al, "Combustion Stability in a Spherical Combustor", 7th Symposium (Int.) on Combustion, Butterworth, 1959, p.664.
8. Clarke, A.E., et al, "Further Studies of Combustion Phenomena in a Spherical Combustor", 8th Symposium (Int.) on Combustion, Williams & Wilkins, 1962, p. 982.
9. Clarke, A.E., et al, "Combustion Processes in a Spherical Combustor", 10th Symposium (Int.) on Combustion, Combustion Institute, 1965, p. 1151.
10. Kretschmer, D. & Odgers, J., "Modelling of Gas Turbine Combustors - A Convenient Reaction Rate Equation", ASME, J. Eng. for Power, July 1972, p. 173.

# REFERENCES (Cont'd)

11. Odgers, J. & Carrier, C., "Modelling of Gas Turbine Combustors - Consideration of Combustion Efficiency and Stability", Trans. ASME, J. Eng. Power, April 1973, pp. 105-113.
12. Kretschmer, D. & Odgers, J., "Modelling of Combustors - The Effects of Ambient Conditions Upon Performance", ASME, Paper No. 73-WA/GT-6, 1973.
13. Lefebvre, A.H. & Greenhough, V.W., "Some Applications of Combustion Theory to Gas Turbine Development", 6th Symposium (Int.) on Combustion, Reinhold Publishing Corp., 1957, p. 858.
14. Osgerby, I. T., "Literature Review of Turbine Combustion Modelling and Emissions", AIAA Journal, Vol. 12, No. 6, June 1974, pp. 743-754.
15. Edelman, R. & Economos, C., "A Mathematical Model for Jet Engine Combustor Pollutant Emissions", AIAA/SAE, 7th Propulsion Joint Specialist Conference, Paper No. 71-714, June 1971.
16. D'Souza, M.V. & Karim, G.A., "An Analytical Study of Methane Oxidation in a Steady - Flow Reactor", Comb. Science & Tech., 3, 1971, p. 83.
17. Edelman, R.B. & Fortune, O., "A Quasi-Global Chemical Kinetic Model for the Finite Rate Combustion of Hydrocarbon Fuels", AIAA, Paper 69-86, 1969.
18. Kennedy, I.A., "Modelling of Combustion Chambers for Predicting Pollutant Concentrations", ASME, Paper No. 74-HT-NN, 1973.
19. Hammond Jr., D.C. & Mellor, A.M., "Analytical Calculations for the Performance and Pollutant Emissions of the Gas Turbine Combustors", revised version of AIAA, Paper No. 71-711, Comb. Science Tech., 4, 1971, p. 101.
20. Odgers, J., "Current Theories of Combustion within Gas Turbine Chambers", 15th Symposium (Int.) on Combustion, Combustion Institute, 1974, p.1321.
21. Hottel, H.C., "Radiative Transfer", Mc Graw Hill, 1967.
22. Swithenbank, J., Poll, I. & Vincent, M.W., "Combustion Design Fundamentals", 14th Symposium (Int.) on Combustion, Combustion Institute, 1973, p. 627.
23. Mellor, A.M., Bilger, R.W., Shisler, R.A. & Tuttle, J.H., "Emissions from Aircraft Fuel Nozzle Flames", Report No. PURDU-CL-75-04, July 1975.
24. Heywood, J. B., "Gas Turbine Combustor Modelling for Calculating Nitric Oxide Emissions", AIAA, Paper No. 71-7112, 1971.
25. Hung, W.S.Y., "An Experimentally Verified NOx Emission Model for Gas Turbine Combustors", ASME, Paper No. 75-GT-71, 1975.
26. Hung, W.S.Y., "A Diffusion Limited Model that Accurately Predicts the NOx Emissions from Gas Turbine Combustors Including the Use of Nitrogen Containing Fuels", ASME, Paper No. 75-Pwr-11, Nov. 1975.
27. Clarke, J.S., "The Relation of Specific Heat Release to Pressure Drop in Aero-Gas-Turbine Combustion Chambers", Proc. IME-ASME, Conf. on Combustion, 1955, p. 354.
28. Kollrack, R. & Aceto, L.D., "Recirculation Effects in Gas Turbine Combustors", 95th Winter Annual Meeting of the ASME, Paper No. 74-WA/FT-3, Nov. 18, 1974.
29. Patankar, S.V., "Heat and Mass Transfer in Boundary Layers", London Intertext Books, 1970.
30. Spalding, D.B., "Numerical Computation of Practical Combustion Chamber-Flows", AGARD-CP-164, Paper No. 1-1, 1974, p. II-1.
31. Pratt, D.T., Washington State University, Dep. Mech. Eng., "PSR-A Computer Program for Calculation of Steady Flow homogeneous Combustion Reaction Kinetics", 1974, Bulletin 336.
32. Pratt, D.T., "Mixing and Chemical Reaction in Continuous Combustion", Prog. Eng. Combust. Sc. Vol. 1, 1976, p. 1.
33. Spalding, D.B., Pratt, D.T., Elgobashi, S. & Srivatsa, S.K., "Unsteady Combustion of Fuel Spray in Jet-Engine Afterburners", ISABE, Munich, March 1976, p. 447.
34. Spalding, D.B. & Serag-Eldin, M.A., "Prediction of the Flow and Combustion Processes in a Three-Dimensional Combustion Chamber", ISABE, Munich, March 1976, 489.
35. Lewitt, E.H., "Hydraulics", Pitman, 1923.
36. Rouse, H., "Elementary Mechanics of Fluids, Wiley, 1946.
37. Magnussen, B.F., "On Mathematical Modelling of Turbulent Combustion with Special Emphasis on Soot Formation and Combustion", 16th Symposium (Int.) on Combustion, 1976.



2315

REFERENCES (Cont'd)

38. Spalding, D.B., " Prediction of Adiabatic Wall Temperatures in Film Cooling Systems", AIAA Journal, Vol. 3, No. 5, May 1965, p. 966.
39. Sturgess, J., "Correlation of Data and Prediction of Effectiveness from Film Cooling Geometries of a Practical Nature", Cranfield Int'l Prop. Symposium, 1969.
40. Papell, S.S. & Trout, A.M., "Experimental Investigation of Air Film Cooling Applied to an Adiabatic Wall by Means of an Axially Discharging Slot", NASA, Tech. Note D-9.
41. Bragg, S.L., Paper to the Combustion and Fuels Committee of the ARC, "Application of Reaction Rate Theory to Combustion Chamber Analysis", Sept. 1953.
42. Lipfert, F.W., "Correlation of Gas Turbine Emission Data", ASME, Paper No. 72-GT-60, 1972.
43. Lefebvre, A.H. & Herbert, M.V., "Heat Transfer Processes in Gas Turbine Combustion Chambers", Proceedings of the Institute of Mechanical Engineers, Vol. 174, No. 12, 1960, p. 463.
44. Marsland, J., Odgers, J. & Winter, J., "The Effects of Flame Radiation on Flame-Tube Metal Temperatures", 12th Symposium (Int.) on Combustion, Combustion Institute, 1969, pp. 1265-1276.
45. Lefebvre, A.H. & Herbert, M.V., "Heat Transfer Processes in Gas Turbine Combustion Chambers", Proceedings of the Institute of Mechanical Engineers, Vol. 174, No. 12, 1960, p. 463.
46. Odgers, J., "Lucas Gas Turbine", Nov. 1963, Rep. No. B48314, (Unpublished Work).
47. Kretschmer, D., Odgers, J. & Schlader, A.F., "The Pulsed Thermocouple for Gas Turbine Application", ASME, Paper No. 76-GT-1, April 1976.
48. Roy, P., Schalder, A.F. & Odgers, J., "Premixed Combustion in a Baffle Combuster and the Effect of Steam Injection", ASME, Paper No. 74-GT-8, 1974.
49. Marzeski, J.W. & Blazowski, W.S., "Ambient Temperature and Pressure Corrections for Aircraft Gas Turbine Idle Pollutant Emissions", ASME, Paper No. 76-GT-130, 1976.
50. Lipfert, F.W., "Correlation of Gas Turbine Emission Data", ASME Paper No. 72-GT-60, 1972.

W.Krockow, Ge

As you referred to my paper, comparing your temperature distribution with the presented AFR distribution in my paper, I must point out, that this comparison is invalid because I made a statistical distribution while you presented a local distribution. You can do a comparison if you plot the mass fraction of equal temperature containing areas above temperature.

Author's Reply

I thank Dr Krockow for his correction and will examine our data in the light of his remark. My point was that it seems unlikely that all flame tube geometries could be represented by the same distribution.

D.C.Dryburgh, UK

I should like to comment on Prof. Odgers talk and say a word in defence of large models.

- (1) We are having to consider much more complex flame tubes and we never know with models whether the correlations are still valid.
- (2) I agree with Prof. Odgers that it is probably unlikely that any single model will do everything.
- (3) Models have an important role in giving improved understanding of what is going on in the flame tube. We have used a 3-D model to look on the complex 3D flow near a swirl injector in an annular flame tube and the flow is very complex and impossible to guess. The details are needed by the combustion engineer developing the flame tube. Having got to this stage it is worth while extending the model to calculate the chemistry and the efficiency.

Author's Reply

With regard to the first point, I agree that it is unwise to use simple models outside the range of conditions for which they were established but my experience with several larger models is that they appear even more sensitive to extrapolation.

The third item is well put. I had hoped that during my presentation that I had expressed that the complex model does indeed describe phenomena which is beyond the scope of the simple model. However, this does not alter my belief that, currently, the simple model offers more to the design engineer and will do so for some time to come.

D.T.Pratt, US

Remember those 2 famous words:

- (1) Enrico Fermi (on the 20th anniversary of quantum mechanics): "We are still confused, but on a higher level".
- (2) Another quote: "Garbage in, Garbage out" holds as well for slide rules as for computers!

Author's Reply

It is difficult to make a response to these quotations except to say that I could not help but agree with them as statements.

Comment by D.T.Pratt, US

In context (p.25-4, § 2.3), Reference 31 and 32 should be:

- |                                  |  |
|----------------------------------|--|
| 31. Pratt, D.T.                  | <i>Calculation of Chemically Reacting Flows with Complex Chemistry</i> , in Studies in Convection, Vol.2, B.E.Launders, Ed., Academic Press, 1977.   |
| 32. Pratt, D.T.<br>Wormeck, J.J. | <i>CREK - A Computer Program for Calculation of Combustion Reaction Equilibrium and Kinetics in Laminar or Turbulent Flows</i> - Washington State University Report WSU-ME-TEL-76-1, 1976. |

S.Wittig, Ge

"Accuracy" as defined seems not always to have highest priority in this phase of modelling. Even in the relatively simple case (see 3.5) of the dilution zone, simple correlations will be insufficient in really understanding the effects of various parameters. The need for more advanced detailed models in aiding the designer seems to be clearly established.

Author's Reply

As I said in my presentation, the accuracy of the simple models is not yet sufficient, but it seems to be often better than the complex models. Phenomenologically, the latter produce a better description but it is my impression that in the immediate future the combustion engineer will have to rely on empirical or semi-empirical models. I do not see the complex models being available (with sufficient quantitative accuracy) within the next five to ten years.

10-1

" ETUDE DE L'AERODYNAMIQUE D'UNE CHAMBRE DE COMBUSTION

EN VUE D'UNE MODELISATION SEMI-EMPIRIQUE"

*par Patrick HEBRARD et Philippe MAGRE*

Office National d'Etudes et de Recherches Aérospatiales

92320 - Châtillon-sous-Bagneux (FRANCE)

---ooOoo---

La prévision des performances de la combustion et de la formation des espèces polluantes dans les foyers de turbomachine, nécessite une méthode de calcul qui tienne compte de tous les phénomènes qui se produisent dans les différentes parties du foyer.

Parmi ceux-ci les effets de l'aérodynamique des gaz, souvent les plus méconnus, sont nécessaires pour étayer les méthodes de modélisation des chambres de combustion par une combinaison de foyers élémentaires. Il faut pouvoir décrire l'organisation de ceux-ci ; c'est-à-dire : emplacement, nature, volume, répartition des débits, connection entre chacun d'eux. C'est pourquoi des expériences ont été conduites simultanément dans des maquettes de chambre de combustion fonctionnant à chaud et à froid. Ces expériences ont pour but de :

- caractériser l'aérodynamique de la chambre de combustion (visualisations en tunnel hydrodynamique et mesures de vitesse sur modèle aérodynamique) ;
- mesurer les temps de séjour dans le tube à flamme par thermodilution (aérodynamique) et par suivi de particules (tunnel hydrodynamique) ;
- déterminer l'efficacité de combustion et la production des espèces polluantes en fonction du régime.

L'utilisation de ces résultats pour l'élaboration du modèle monodimensionnel par foyers élémentaires permet de calculer la fonction de distribution des temps de séjour en sortie des réacteurs élémentaires et en particulier de la zone primaire. Les performances globales du foyer sont également prédites. L'accord entre les résultats des calculs et des expériences avec et sans combustion est satisfaisant vu la simplicité des hypothèses de départ.

"AERODYNAMIC STUDY OF A COMBUSTION CHAMBER  
WITH A VIEW TO ITS SEMI-EMPIRICAL MODELLING

The prediction of combustion performance and of polluting species formation in turbomachine combustors requires a calculation method that takes into account all phenomena taking place in various parts of the combustion chamber.

Among these, aerodynamic effects, often very poorly known, must be introduced to justify modeling methods based on a combination of elementary combustors ; these methods rest on a correct description of their features and their relationships : location, nature, volume, flowrate distribution, connexions.

To this end, experiments were carried out on a combustor model, both without and with combustion, with a view to :

- characterize the combustor aerodynamics, by visualizations in the water tunnel and velocity measurements on an aerodynamic model,
- measure residence times in a flame tube by thermodilution (aerodynamics) and particle dynamics (water tunnel),
- determine the combustion efficiency and the polluting species production for each regime.

Using these results for the development of a one-dimensional model of elementary combustors makes it possible to calculate the distribution function of residence time in all elementary reactors, especially in the primary zone. The overall performance of the combustor can also be predicted. The agreement between calculated and experimental results is satisfactory if we consider the simplicity of the assumptions on which the model is based.

# NOTATIONS

$C_p$	Chaleur massique à pression constante
$C_e(t), C_d(t)$	Concentration en fonction du temps d'un traceur à l'entrée ou à la sortie du foyer.
$f(t)$	Fonction distribution des temps de séjour
$F(t)$	Fonction répartition des temps de séjour
$k_i$	Débit de kérosène dans le foyer élémentaire n° i
$M_x, M_y$	Quantité de mouvement suivant X et Y du jet primaire
$n_{O_2}, n_H$	Nombre de moles du constituant par unité de masse du mélange.
$p_e$	Pression à l'entrée de la chambre de combustion
$q_i$	Débit d'air dans le foyer élémentaire n° i
$Q$	Débit d'air total dans le foyer.
$Q_1$	Débit d'air dans les orifices primaires.
$Q_2$	Débit d'air dans les orifices de dilution.
$Q_c$	Débit d'air dans les cannes (Maquette B).
$Q_f$	Débit d'air dans les films des cannes (maquette B).
$Q_{fc}$	Débit d'air en fond de chambre (Maquette B).
$Q_F$	Débit d'air dans un film de refroidissement.
$Q_P$	Débit d'air primaire ne participant à aucune recirculation dans la zone primaire
$Q_{R1}$	Débit d'air primaire recirculant en fond de chambre.
$Q_{R2}$	Débit d'air primaire recirculant latéralement.
$Q'_{R2} = Q_{R2} + Q_F$	
$T, T_e$	Température - température à l'entrée du foyer.
$V = \sum_i \frac{V_i}{V_j}$	Volume du réacteur élémentaire n° i. Volume total du foyer.
$V_{ext}$	Vitesse dans le jet primaire. Vitesse de l'air entre le carter et le tube à flamme.
$X, Y, Z$	Coordonnées dans la zone primaire.
$\Delta_1 Q, \Delta_2 Q$	Enthalpies de réaction.
$\beta$	Fraction de débit entraîné
$\varphi$	Richesse global du foyer
$\eta$	Efficacité de combustion
$\theta_m$	Angle moyen du jet primaire.
$\pi, \psi$	Fractions de débit.
$\tau = \frac{Q_{R1} + Q'_{R2}}{Q_1 + Q_F}$	Taux de recirculation global (mesuré avec combustion).
$\tau' = \frac{Q_{R1}}{Q_1}$	Taux de recirculation en fond de chambre.
$\tau_f$	Constante de temps des fils de chauffage
$\tau_A, \tau_{Am}$	Temps de séjour moyen - Temps de séjour moyen mesuré.
$\Omega = \frac{Q}{p_e V C_{300}^{1/3}}$	Facteur de charge du foyer.

## 1 - INTRODUCTION

La prévision des performances des foyers de turbomachine tant du point de vue de l'efficacité de combustion que de la pollution exige [1,2] exige une technique de modélisation suffisamment précise et réaliste pour tenir compte des divers phénomènes dans chaque partie du foyer.

Parmi les méthodes de modélisation [3], on peut distinguer deux groupes principaux :

- le premier consiste à représenter chacune des régions principales du foyer par une succession de réacteurs chimiques élémentaires [4-5-6]. On peut prédire alors le comportement global du foyer ou même effectuer une optimisation de ses performances [4].

- selon le second groupe de méthodes, on étudie dans le détail chaque région principale du foyer : ainsi la zone primaire n'est plus considérée comme un ou plusieurs réacteurs élémentaires mais comme une zone de combustion turbulente dans un écoulement tridimensionnel [7-8-9-10-11].

La validation de ces modèles nécessite l'expérimentation de diverses chambres de combustion. En particulier, la mise en oeuvre de modèles monodimensionnels (succession de réacteurs élémentaires) demande une bonne connaissance de la dynamique des gaz dans le foyer. Ainsi il est nécessaire d'avoir des informations concernant les réacteurs élémentaires : emplacement, volume, temps de séjour, etc...

Dans ce but, une série de maquettes (figure 1) a été essayée. La zone primaire d'un foyer de turbomachine A a été matérialisée sous forme de montages pouvant répondre à différentes utilisations :

- maquettes ou demi-maquettes fonctionnant en air froid pour des mesures de vitesse, de turbulence, de temps de séjour par thermodilution.
- demi-maquettes placées en tunnel hydraulique afin de visualiser l'écoulement et d'y mesurer les temps de séjour par comptage de particules et traitement du signal vidéo.
- maquette complète étudiée avec combustion (relevé des performances en fonction du régime ; analyse de la combustion par sondages à l'intérieur du foyer).

Ces diverses expériences ayant donné des résultats jugés trop liés à un type particulier de chambre, ceux-ci ont été poursuivis dans un foyer B (figure 1), cette chambre B est dérivée de A mais en diffère par :

- le fond de chambre qui est raccourci,
- la présence de cannes à prévaporisation qui remplacent les injecteurs de carburant situés dans les orifices primaires de A.
- Les orifices primaires qui sont réduits de manière à conserver le débit primaire malgré l'introduction d'air par les cannes à prévaporisation.

Le but de cette étude ne consiste pas à optimiser ni une chambre de combustion particulière ni un modèle de calcul. Au contraire, on utilise un modèle volontairement simple dont la définition s'appuie sur les caractéristiques aérodynamiques effectives des écoulements étudiés.

A partir des résultats expérimentaux recueillis dans les chambres A et B, une modélisation monodimensionnelle a été élaborée pour chacune d'elles. Les différences entre ces deux chambres et leurs performances sont discutées ainsi que les résultats de la modélisation.

## 2.- ETUDE EXPERIMENTALE SANS COMBUSTION

### 2.1- Moyens d'essai

Bien que ne permettant pas de présenter l'ensemble des phénomènes intervenant dans les écoulements avec changement de densité et cinétique chimique, les études par simulation sur modèles fonctionnant à froid constituent un outil précieux pour la compréhension de l'aérodynamique interne des chambres de combustion. Plusieurs études ont déjà confirmé la similitude entre écoulements avec et sans combustion à condition que les nombres de Reynolds fondés sur les conditions d'entrée soient comparables [12-13-14]. Plusieurs maquettes semblables à celles étudiées en combustion ont donc fait l'objet d'essais sur les deux installations suivantes :

- un tunnel hydrodynamique
- une veine aérodynamique

#### 2.1.1- Tunnel hydrodynamique -

Sur un tunnel hydrodynamique semblable à celui utilisé par H. WERLE [15], nous avons mis en oeuvre des techniques classiques de visualisation (filets colorés, bulles d'air ou d'hydrogène par électrolyse) pour préciser la configuration de l'écoulement. Les visualisations qualitatives sont complétées sous un aspect quantitatif, spécialement utilisé pour les mesures de temps de séjour par comptage de microparticules neutres vis à vis de l'écoulement [16-18]. Les techniques mises en oeuvre qui font appel au traitement de signaux vidéo résultant des enregistrements des divers essais, sont largement discutés dans les références [16 et 20].

#### 2.1.2- Veine aérodynamique

La veine aérodynamique sur laquelle peuvent être montées plusieurs types de maquettes [19] permet d'effectuer des cartographies tridimensionnelles de vitesse à partir d'un fil chaud tournant selon une technique mise au point au CERT [17]. Les cartographies de vitesse sont complétées par des mesures de fonction de répartition de temps de séjour obtenues par une technique originale de traceur thermique par thermodilution [19]. Cette technique dont le principe est représenté à la figure 2 associe un chauffage de l'écoulement par impulsions électriques calibrées sur des fils thermorésistifs, une mesure de fluctuations de température par fil chaud à faible taux de surchauffe et un échantillonnage par moyenne numérique.

## 2.2- Résultats qualitatifs sur les visualisations

Compte tenu de la complexité et du caractère fortement tridimensionnel de l'écoulement dans la zone primaire, les visualisations sont indispensables pour permettre d'interpréter les diverses mesures (vitesse, temps de séjour, etc...) effectuées en parallèle. Elles permettent aussi de voir rapidement l'effet dû à une modification (géométrique ou cinétique) sur l'ensemble de l'écoulement.

La configuration de base A' est la configuration sans canne et avec fond de chambre allongé ; on étudie ensuite l'influence due à une modification de ces derniers points.

De nombreuses visualisations par filets colorés ont conduit à la description suivante de l'écoulement. Cette représentation qui montre le caractère fortement tridimensionnel de l'écoulement contraste singulièrement avec les schématisations habituelles (jet et tourbillon importants en fond de chambre). Les jets primaires pénètrent dans la chambre en créant un double système de tourbillons :

- Latéralement, une paire de tourbillons d'axe OX, qui sont le siège de vitesses élevées, s'étendent jusqu'à la dilution et remontent en partie au fond de chambre (figures 3 et 4). Le caractère fortement instable de leur surface de contact se traduit par une alimentation alternative entre ces derniers.

- par un léger mouvement hélicoïdal en amont, ces tourbillons font recirculer, en fond de chambre, une partie  $Q_{R1}$  du débit primaire  $Q_1$ . Ce débit  $Q_{R1}$  se retrouve en partie dans un tourbillon de petite taille d'axe OZ assurant la continuité avec le précédent (tourbillon en fer à cheval).

- Le reste du débit  $Q_{R1}$  alimente une partie du fond de chambre de façon instationnaire au voisinage du plan de symétrie entre orifices ( $Z \approx \pm 30$ ).

- Dans leur partie latérale et aval, les tourbillons d'axe OX sont alimentés par la fraction  $Q_{R2}$  du débit primaire et traversés en leur cœur par le débit  $Q_{R1}$  venant du fond de chambre.

Enfin une partie  $Q_p$  du débit primaire va directement vers la dilution quasiment sans mélange avec le reste de l'écoulement primaire.

Ces divers commentaires doivent être complétés par les deux remarques suivantes :

- Il est évident que le passage entre  $Q_{R1}$ ,  $Q_{R2}$ ,  $Q_p$  est plus continu qu'il n'apparaît dans la description précédente mais cette dernière a déjà été effectuée dans l'optique d'une modélisation par combinaison de réacteurs élémentaires alimentés de façon discrète par différents débits.

- Une part importante du fond de chambre (figure 3) ne participe pratiquement pas à l'écoulement et peut être considérée comme une zone quasi-morte. Ceci nous a conduit à réduire le volume de ce dernier dans la seconde maquette B.

En dehors de celle portant sur le volume du fond de chambre, la seconde modification envisagée concerne la simulation des cannes à pré vaporisation. De nombreux essais ont été effectués à divers débits en modifiant les deux paramètres suivants :

- débit des cannes =  $Q_c/Q_1$  (de 0 à 40 %),
- position des cannes par rapport aux orifices primaires.

Un des rôles des cannes étant d'améliorer la recirculation du fond de chambre, on a donc effectué une étude systématique permettant de positionner ces dernières de façon à obtenir dans tous les cas de fonctionnement un débit  $Q_c$  alimentant le fond de chambre. Les résultats de ces essais [18] ont conduit à faire déboucher ces dernières au 1/3 amont des orifices primaires.

Qualitativement, on ne remarque pas de différence notable avec les cas sans canne si ce n'est sur le fond de chambre, point sur lequel nous reviendrons par la suite (temps de séjour).

## 2.3- Mesures de vitesse et répartition des débits

### 2.3.1- Mesures de vitesse

A la figure 5 sont présentés quelques résultats significatifs sur les mesures de direction de vitesse dans la zone primaire obtenues dans le cas suivant :

configuration A  
débit total 0,25 kg/s.

On y retrouve plusieurs éléments obtenus par visualisation (par exemple : tourbillons latéraux importants avec mouvement hélicoïdal).

Un paramètre important pour la modélisation, étant la part de débit ( $Q_{R1}$ ) recirculant en fond de chambre mais en ressortant ensuite (par opposition au débit entraîné qui reste dans la zone de recirculation), nous avons cherché à le mesurer.

### 2.3.2- Mesure de $Q_{R1}$

Deux méthodes complémentaires ont été employées pour cette mesure :

#### a) à partir des sondages de vitesse [19]

La première méthode consiste à déterminer à partir des cartographies de vitesse et de sa "trace" dans le plan  $Y = 0$ , la surface de séparation entre les deux fractions de débits suivantes :

$$Q_{R1} = \tau' Q_1$$

et  $(1 - \tau') Q_1$

Les résultats de ces mesures, correspondant à la maquette A, sont présentés à la figure 6 en fonction des paramètres géométriques ( $h/H$  ou  $\theta_m$ ) et cinématiques ( $V_T$ ).

#### b) à partir des temps de séjour

Dans le cas où, comme pour la maquette B', le volume occupé en fond de chambre par l'écoulement est connu, la mesure de  $\bar{\tau}_f$  (temps de séjour moyen en fond de chambre) permet d'accéder à  $Q_{R1}$ .

$$\overline{C}_1 = \frac{V_1}{Q_{R1} + Q_C}$$

On mesure de façon semblable  $Q_{R2}$  par :

$$\overline{C}_2 = \frac{V_2}{Q_{R1} + Q_{R2} + Q_C}$$

Les essais obtenus sur un banc hydraulique (§ 242) sont présentés à la figure 7 pour  $0 \leq Q_C/Q_1 \leq 35\%$ .

Les valeurs pour  $Q_C = 0$  sont compatibles avec les essais précédents, ce qui confirme l'existence d'un volume mort en fond de chambre dans le cas de la maquette A'. On notera avec intérêt les évolutions de  $Q_{R1}$ ,  $Q_{R2}$ ,  $Q_P$  avec  $Q_C/Q_1$ .

#### 2.4- Mesures de temps de séjour

Pour compléter les essais en vue de parfaire la modélisation, nous avons cherché à déterminer la fonction de distribution de temps de séjour  $f(t)$  (ou  $F(t)$  fonction de répartition) en divers point du foyer. La technique, classique dans son principe, consiste à injecter en entrée une faible concentration  $C_e(t)$  d'un traceur que l'on détecte en sortie ( $C_s(t)$ ); on montre aisément que dans ce cas [21]

$$C_s(t) = \int_0^t C_e(t-t') f(t') dt'$$

Sur ce principe et compte tenu des impératifs liés à ces essais (emplacement, temps de réponse...), nous avons mis en oeuvre deux techniques originales de mesure.

##### 2.4.1- mesures sur banc aérodynamique

La technique par thermodilution dans laquelle  $C_e(t)$  correspond à un échelon descendant permet donc d'obtenir rapidement, en un point quelconque du foyer, la fonction de répartition de temps de séjour  $F(t)$  entre l'entrée de la zone primaire et le point de mesure par :

$$F(t) = 1 - C_s(t)$$

Bien qu'effectuées pour différentes vitesses, les mesures ne sont présentées que pour le cas  $V_j = 25$  m/s. Cette valeur correspond à un optimum compte tenu du niveau du signal de température à mesurer et du rapport entre le temps de séjour moyen et la constante du temps des fils de chauffage de l'écoulement.

##### 2.4.1.1 - Mesures en aval de la zone primaire

Pour tous les points situés en aval et dans la zone de dilution, les courbes de décroissance en température sont semblables et présentent les caractéristiques suivantes (fig. 8).

- 1/ aux premiers instants suivant le refroidissement, la température conserve la valeur initiale  $T_c$  pendant une durée  $\Delta t_0$  dépendant du point de mesure,
- 2/ vient ensuite une zone de transition de 10 à 20 ms,
- 3/ enfin, suit une zone de décroissance plus ou moins exponentielle dont la constante de temps mesurée, pratiquement indépendante du point de mesure, vaut sensiblement 155 ms (valeur exacte : 115 à 120 ms) (y compris la zone de transition).

##### Interprétation

Les courbes de décroissance en température comportent deux types d'informations concernant d'une part, la fonction de répartition de temps de séjour en sortie de zone primaire et d'autre part, la nature de la zone de dilution.

En effet, la fraction du signal correspondant aux portions (2) et (3) ainsi qu'à une partie de la zone (1), est caractéristique de la fonction de distribution de temps de séjour en sortie de zone primaire. Ce signal, arrivant à l'entrée de la zone de dilution est ensuite translaté dans cette dernière, sans déformation et sur une durée dépendante de la distance du point de mesure à l'entrée.

Ce résultat est confirmé par le tracé (fig. 8) de  $\Delta t_0$  en fonction de l'abscisse. Après une zone de transition localisée au niveau des orifices de dilution, ces courbes quasiment linéaires dans la zone de dilution ont une pente dont la valeur

$$\frac{dX}{d\Delta t_0} \approx 3,4 \text{ m/s}$$

semble tout à fait compatible avec la vitesse moyenne de l'écoulement (3,1 m/s) dans cette zone et conduisent à modéliser la dilution comme un réacteur de type piston.

##### 2.4.1.2 - Mesures en sortie et dans la zone primaire

Les courbes de décroissance en température (fig. 9) sont semblables aux précédentes mais ici  $\Delta t_0$  et  $\Delta t_c$  dépendent du point de mesure. En sortie de zone primaire, les écarts entre courbes y montrent bien le caractère inhomogène de l'écoulement :

- Résultats identiques dans les tourbillons latéraux ( $Z \sim 10$  à 15)

- Dans le plan de symétrie  $Z = 0$  des relevés différents correspondant à des trajets d'écoulement différents (la fraction de  $Q_p$  interceptée se traduisant par une diminution de  $\Delta t_{0m}$ , augmente vers la zone d'impact des jets  $Y \sim 0$ ).

On retrouve cette disparité dans la zone primaire :

- temps de séjour moyen très variable (200 ms en fond de chambre, 140 ms à 170 ms latéralement, 100 ms à 140 ms en aval des jets (fig. 9)).

- courbes iso  $\Delta t_0$  (fig. 10) permettant de retrouver la présence de tourbillons latéraux (coupe B - B') et la convergence de l'écoulement entre orifices en fond de chambre (coupe A-A').

Ces quelques résultats montrant l'impossibilité d'une modélisation de la zone primaire sous forme d'une combinaison simple de réacteurs élémentaires, nous ont conduit à compléter ces mesures, sur banc hydraulique par comptage de particules.

#### 2.4.2 - Mesures sur banc hydraulique

Dans ce cas, la mesure se fait en comptant, au moyen des techniques décrites en [20], les temps de séjour pour un nombre significatif, (200 à 500 suivant les essais), de particules neutres par rapport à l'écoulement dont on peut modifier le point d'injection.

Les mesures sont effectuées aux points suivants :

- sortie de fond de chambre,
- sortie de zone primaire.

Après avoir vérifié l'évolution des temps de séjour suivant une loi  $\tau \sim Q^{-1}$  en fonction du débit  $Q$ , on présente les principaux résultats correspondants au cas d'écoulement suivant :

$Q_1 = 50 \text{ cm}^3/\text{s}$  par orifice primaire

##### 2.4.2.1 - Mesures en sortie de fond de chambre

Dans le cas  $Q_c = 0$ , les résultats présentés figure 11 conduisent à adopter pour le fond de chambre un réacteur homogène (ceci est possible puisque la sortie et l'entrée en sont confondus).

Dans le cas  $Q_c \neq 0$  pour tenter de préciser ce point, nous avons complété chaque mesure par un suivi de la particule au moyen de la caméra vidéo de façon à associer à chaque temps de transit, un trajet de particule. Les trajets caractéristiques sont schématisés à la figure 12 sur laquelle on peut distinguer :

- Les particules entraînées par le jet des cannes et faisant un (ou plusieurs) aller et retour au fond de chambre au voisinage du plan  $z = 0$ . Les courbes donnant  $f(t)$  pour ces seules particules sont caractéristiques de réacteurs piston avec une certaine diffusion (fig. 12).
- Les particules entraînées par les tourbillons latéraux en fond de chambre au voisinage du plan  $z = \pm 30$ .

L'examen des courbes conduit donc, dans ce cas, à identifier un réacteur piston suivi d'un foyer homogène (fig. 12).

Remarque : Cette analyse conduirait à une modélisation assez fine qui a été ensuite simplifiée dans le but de ne pas être trop particulière à ce type de foyer. D'autre part, certaines configurations (par exemple avec retour) ne sont pas modélisables actuellement.

##### 2.4.2.2 - Mesures en sortie de réacteur latéral

Les courbes correspondant au réacteur latéral se présentent toutes de la même façon avec un temps de transit (l'entrée et la sortie ne sont plus confondues) et une courbe exponentielle. On le modélise donc par un foyer homogène en série avec un réacteur piston (Fig. 13).

Notons aussi que dans ce cas, on ne trouve aucune différence significative sur les temps de séjour suivant que les particules employées viennent :

- soit du fond de chambre avec le débit  $Q_{R1} + Q_c$ .
- soit latéralement avec le débit  $Q_{R2}$ .

Ce point, important au niveau de la modélisation, montre donc que l'ensemble des particules traverse ce réacteur avec un débit moyen  $Q_{R1} + Q_{R2} + Q_c$ .

##### - Mesures en aval du jet

Dans ce cas, les courbes non présentées ici [18] sont caractéristiques d'un réacteur piston comportant une légère diffusion.

Ainsi cet ensemble de mesures : répartition des débits, fonction de distribution de temps de séjour et valeur moyenne sert à définir l'emplacement, le volume, la nature et la répartition des débits des réacteurs élémentaires utilisés dans la modélisation (§ 4.2).

### 3. ETUDE EXPERIMENTALE DE LA COMBUSTION

#### 3.1 - Moyens d'essais

On dispose de deux maquettes représentant les chambres de combustion A et B (Fig. 1). Pour chacune de ces deux maquettes la répartition des débits, estimée par les rapports de surfaces effectives de passage, s'effectue comme suit :

- |                          |        |
|--------------------------|--------|
| - air primaire           | 28,2 % |
| - air de dilution        | 39,2 % |
| - air de refroidissement | 32,6 % |

La différence essentielle entre les deux maquettes réside dans la géométrie de la zone primaire. En particulier, le choix de la position des cannes à pré vaporisation a été optimisée en fonction de visualisations en canal hydraulique et des résultats de mesures d'efficacité de combustion obtenus pour différentes positions des cannes par rapport aux orifices primaires.

Les conditions d'essais des deux maquettes A et B sont les suivantes :

- débit d'air total dans le foyer  $350 \text{ g/s} \leq Q \leq 700 \text{ g/s}$
- température de l'air à l'entrée du foyer  $300 \text{ K} \leq T_e \leq 700 \text{ K}$
- pression à l'intérieur du foyer  $p_e = 1 \text{ bar}$
- richesse global du foyer  $\varphi < 0,3$



Les conditions d'essai sont contrôlées en temps réel pendant les essais. Pour divers régimes du foyer, et en diverses positions de sondage à l'intérieur de la chambre (fig.1), on prélève les produits de combustion dans une petite bouteille. Ces échantillons sont analysés par chromatographie en phase gazeuse. Un premier chromatographe permet de doser le gaz carbonique et le méthane. Un second chromatographe sépare oxyde de carbone, azote et oxygène tandis qu'un troisième isole l'hydrogène. L'analyse des oxydes d'azote est réalisée au moyen d'un appareil classique à chimiluminescence.

Deux types d'expériences ont été conduites dans ces chambres de combustion. Des expériences décrivent l'état du foyer du point de vue des espèces chimiques pour un régime de fonctionnement particulier. Cette série d'expériences a été réalisée dans la maquette A et reprise d'une manière plus détaillée dans la maquette B. La seconde série d'expériences avait pour but d'évaluer le fonctionnement global de la chambre de combustion A. Pour différents régimes - c'est-à-dire différents points de fonctionnement caractérisés par  $Q$ ,  $T_e$  et  $\varphi$  - on relève des efficacités de combustion, niveaux de pollution en des positions caractéristiques à l'intérieur du foyer (entrée et sortie de la zone primaire, sortie du foyer).

### 3.2 - Analyse de la combustion à l'intérieur de la chambre

Les points de sondage à l'intérieur du foyer (fig.1) sur toute l'envergure de celui-ci sont choisis en fonction des résultats des visualisations. Ainsi les positions 1, 2, 3 correspondent au fond de la chambre, les points 4, 5 et 6 à l'aval des orifices primaires et la position 7 à la sortie du foyer.

Le régime pour lequel les sondages ont été effectués correspond à l'adaptation de la chambre de combustion A ( $Q = 530$  g/s ;  $T_e = 545$  K ;  $\varphi = 0,226$ ). En vue de comparer les résultats dans les chambres A et B, ce régime a été conservé pour les essais dans la maquette B.

Les sondages effectués en fond de chambre position 2 ne permettent pas de déceler une organisation très nette de l'écoulement. L'alimentation alternée des tourbillons occupant cette région par le débit  $Q_{R1}$  peut expliquer cette absence d'organisation. La richesse y est toujours plus grande que 1 et le degré d'avancement de la combustion inférieur à 0,5.

En aval de la zone primaire, le plan de symétrie du foyer ( $Y = 0$  ; position 5) et le plan contenant les axes des tourbillons latéraux ( $Y = \pm 15$  ; position 4 et 6) sont explorés. Après avoir vérifié la symétrie du foyer pour les positions 4 et 6, on peut voir sur la figure 14 que l'écoulement est maintenant bien organisé autour des jets d'air primaire. En effet, la périodicité de la richesse est la même que celle de l'injection du carburant qui se situe au niveau des orifices primaires des chambres A et B. Le choix du point de fonctionnement du foyer ( $\varphi = 0,22$ ) comme étant le point d'adaptation de la chambre A est justifié par le fait que l'on retrouve bien une richesse moyenne proche de 1 à la sortie de la zone primaire. On retrouve également que le débit  $Q_c$  a modifié l'adaptation de la chambre B puisque la richesse moyenne n'est plus que 0,61. En recalculant les rapports des débits d'air évalués à ce niveau pour les configurations A et B, on obtient  $\frac{(Q_{R1} + Q_c + Q_{R2} + Q_{R3} + Q_{R4})_B}{(Q_{R1} + Q_{R2})_A} = 1,48$  qui est de l'ordre du rapport  $\frac{Q_A}{Q_B} = 1,64$  ( $Q_F$  est le débit dans un film de refroidissement de la chambre,  $Q_g$  dans celui de la canne et  $Q_{g1}$  le débit dans le fond de la chambre B - voir modélisation § 4.2).

Les relevés effectués en position 5 (fig. 15) donnent des résultats très différents de ceux de la position 4. Cette partie du foyer est, en effet, directement alimentée par la fraction des jets primaires non carburée et ne recirculant pas ( $Q_p$ ) : La richesse moyenne n'est plus que de l'ordre de 0,1 pour les deux chambres A et B. De plus la richesse étant minimale dans l'axe des jets primaires, on peut dire que le carburant présent à cet endroit est amené par diffusion issue de tourbillons latéraux et non par convection à partir des orifices primaires.

### 3.3 - Influence du régime sur le fonctionnement de la chambre

Ces expériences avaient pour but de déterminer l'effet du régime sur les performances du foyer (rendement, pollution). Ainsi pour chaque point de fonctionnement du foyer, on relève les valeurs moyennes des concentrations sur une traversée aux points 2, 4 et 7 de la maquette A, ce qui permet d'atteindre le degré d'avancement de la combustion. Des relevés du même genre ont également été effectués sur la maquette B mais d'une manière moins systématique. La figure 16 montre l'effet de la richesse sur l'inefficacité de combustion. Ces résultats expérimentaux qui présentent une dispersion importante en raison des hétérogénéités à l'intérieur du foyer sont comparés aux prédictions d'un calcul (voir § 4.3).

L'évolution des oxydes d'azote en fonction de la richesse (fig. 17) s'interprète assez facilement. L'accroissement du NO avec la richesse dure jusqu'à une richesse voisine de celle de l'adaptation ( $\varphi = 0,22$ ). Au-delà de cette valeur NO décroît tandis que  $NO_2$  continue de croître. Cet accroissement s'explique par l'apport d'air de dilution à l'aval de la zone primaire : le NO continue de s'oxyder en  $NO_2$ .

## 4. MODELE MONODIMENSIONNEL DE FOYER

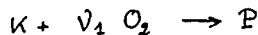
### 4.1 - Principe de la modélisation

Les résultats présentés et discutés dans les paragraphes précédents ont permis des recoupements qualitatifs avec les essais en aérodynamique pure. Dans le but d'avoir une interprétation quantitative du comportement du foyer, une modélisation simple a été entreprise. Ce type de modélisation qui consiste à représenter le foyer par une série de foyers élémentaires s'appuie sur l'ensemble des renseignements acquis au cours des visualisations, mesures aérodynamiques, etc... En effet, la discrétisation de la chambre de combustion en réacteurs élémentaires est facilitée par les visualisations en tunnel hydraulique qui ont localisé les zones de recirculation. Les mesures de temps de séjour ont permis de déterminer la nature des réacteurs élémentaires (homogène ou de type piston). De même le choix de la répartition des débits dans ces réacteurs est la conséquence des mesures de taux de recirculation.

Cette modélisation semi-empirique s'appuie sur les travaux de R. BORGHI [4]. Rappelons-en brièvement le principe général : on représente la chambre de combustion par une suite de  $n_r$  réacteurs chimiques de volumes variables. On peut introduire dans chacun de ces foyers des entrées d'air ou de carburant qui simulent dilution, cannes à pré vaporisation... On peut calculer les conditions d'entrée du  $i^{\text{ème}}$  réacteur à l'aide des conditions de sortie du réacteur  $(i-1)$  et des conditions de l'alimentation en air,  $q_i$ , et en carburant  $k_i$  de ce  $i^{\text{ème}}$  réacteur. Il suffit d'écrire les bilans énergétiques et de masse. Le  $i^{\text{ème}}$  réacteur est caractérisé par  $q_i$ ,  $k_i$ ,  $T_{e_i}$  température d'entrée, et  $V_i$  le volume du réacteur. Le problème consiste à déterminer le degré d'avancement de la combustion  $\xi_i$  atteint dans chacun de réacteurs pour un temps de séjour donné

$$t_{s_i} = \frac{\rho V_i}{\sum (q_i + k_i)} \quad (\text{avec } \sum q_i = Q)$$

Les phénomènes de combustion et de pollution dans le foyer sont schématisés par deux réactions chimiques



Les lois de production utilisées dans le calcul sont :

- pour la réaction énergétique [30] :

$$\text{et } W_1 = 0,2 T^2 (\rho n_{O_2}) (\rho n_K) \exp\left(-\frac{7500}{T}\right)$$

L'accroissement de température provoqué par la combustion est égal à :

$$T_s - T_e = \frac{\Delta_1 Q}{C_p} \xi$$

$$\text{où } \xi = n_{r_s} - n_{r_e} + \frac{\Delta_2 Q}{\Delta_1 Q} (n_{N_2 s} - n_{N_2 e})$$

$$\text{et } \Delta_1 Q = 4,5 \cdot 10^6 \text{ J/mole}$$

$$C_p = 1000 \text{ MKs}$$

- pour la réaction de pollution (mécanisme de Zeldovitch)

$$W_2 = 6 \cdot 10^{12} (\rho n_{N_2}) (\rho n_{O_2})^{0,5} \exp\left(-\frac{67500}{T}\right)$$

$$\Delta_2 Q = -1,8 \cdot 10^5 \text{ J/mole}$$

La méthode de calcul de  $\xi$  et des produits polluants est indiquée par R. BORGHI dans [4].

#### 4.2 - Application aux foyers étudiés

L'ensemble des expériences en air froid et en tunnel hydrodynamique conduit à un modèle différent pour chaque chambre A ou B. Ces modèles sont décrits figure 18 pour l'emplacement des réacteurs et figure 19 pour la répartition des débits.

La zone primaire de la maquette A est divisée en trois réacteurs élémentaires. Le débit d'air primaire  $Q_1$  se partage comme suit :

-  $Q_{R1}$  qui alimente le réacteur 1 (celui-ci recevant de plus le carburant)

-  $Q_{R2}$  qui constitue une partie du débit total  $Q'_{R2}$  alimentant le réacteur 3 ( $Q'_{R2} = Q_{R2} + Q_F$ ).

-  $Q_p$  qui ne participe pas à la recirculation dans la zone primaire va directement dans le réacteur 4.

Ce réacteur 4 constitue le premier élément de la zone de dilution. Il reçoit un débit  $Q_p + Q_2/2 + Q_F$  ( $Q_2$  débit total de l'air de dilution). Le réacteur 5, deuxième élément de la zone de dilution reçoit  $Q_2/2 + Q_F$  tandis que le réacteur piston 6 n'est plus alimenté que par le dernier film de refroidissement. Les résultats des mesures de temps de séjour (fig.8) justifient l'assimilation du réacteur 6 à un réacteur piston.

Le choix de  $Q_{R1}$  ayant été déterminé par les mesures de  $\tau' = \frac{Q_{R1}}{Q_1}$ ,  $Q_{R2}$  restait à définir. Un taux de recirculation global  $\tau = \frac{Q_{R1} + Q_{R2}}{Q_1 + Q_F}$  a été évalué indirectement lors des essais avec combustion.

Cette méthode basée sur la propriété de l'eau de réduire les oxydes d'azote dans une chambre de combustion est exposée dans [19]. La valeur de  $\tau$  retenue pour la modélisation est 0,7 tandis que  $\tau' = 0,36$ . Cette valeur  $\tau = 0,7$  est compatible avec celle de  $\frac{Q_{R1} + Q_{R2}}{Q_1 + Q_F}$  estimée pour  $Q_c/Q_1 = 0$  (fig.7). Les volumes sont déduits de la répartition du débit et des temps de séjour mesurés.

La modélisation de la chambre B est plus complexe. La présence des cannes modifie non seulement les débits  $Q_{R1}$ ,  $Q_{R2}$  et  $Q_p$  mais aussi la disposition et la nature des réacteurs dans la zone primaire. Le réacteur piston 1 et le réacteur homogène 2 simulent le fond de la chambre. Le réacteur 1 est traversé par  $Q_c$ , débit canne, augmenté de la fraction  $\pi$  de  $Q_{R1}$  ( $\pi = 1/3$ ) et du carburant. Le réacteur 2 reçoit  $Q_2 + Q_{R2}$  et la fraction  $(1 - \pi)$  de  $Q_{R1}$ . Le débit alimentant 3 est constitué de  $Q'_{R2} = Q_{R2} + Q_F$ . Ce réacteur est suivi d'un réacteur piston 4. Les réacteurs suivants sont identiques à ceux de la chambre A.

Cependant, cette modélisation retenue pour l'étude de la combustion présente des différences par rapport à la modélisation originelle sans combustion, en plus de la présence des débits  $Q_1$ ,  $Q_2$  et  $Q_F$ . Ainsi, on n'a pas tenu compte du débit entraîné  $\beta (Q_c + \pi Q_{R1})$  dans le réacteur 1 ( $\beta = 1/6$  d'après les mesures de temps de séjour). De plus, dans la modélisation avec combustion, on a simpli-

fié la répartition des débits en fixant  $\psi = 1$ . En fait, pour prendre en compte la valeur réelle  $\psi = 0,6$ , il suffit de choisir les volumes des réacteurs 1 et 2 en accord avec les temps de séjour mesurés effectivement pour  $\psi = 0,6$ .

Il est possible de retrouver la fonction de transfert qui calcule la distribution des temps de séjour en aérodynamique pure dans le foyer A à l'aide d'une modélisation différente légèrement de celle avec combustion (fig. 19):

- un réacteur fictif simule la constante de temps des fils de chauffage utilisés pour la mesure des temps de séjour (§ 2.4.1).

- le réacteur 1 - 2 remplace les réacteurs 1 et 2 du cas avec combustion.

- le réacteur 3 est suivi maintenant d'un réacteur piston 3'

- le réacteur piston 4' reçoit le débit  $Q_p$  qui, dans le cas avec combustion, alimentait sans intermédiaire la zone de dilution.

Les résultats du calcul sont comparés aux expériences effectuées à la sortie de la zone primaire (fig. 20) : l'accord satisfaisant démontre que le découpage de la zone primaire en foyers élémentaires peut représenter la chambre de combustion A.

#### 4.3 Résultats des calculs

L'étude de la stabilité du foyer a été entreprise avec les modèles de chambre A et B et les résultats numériques et expérimentaux sont comparés sur la figure 21. L'accord pour le foyer A est bon mais un peu moins satisfaisant pour B quoique la tendance soit correctement prédite (richesse limite d'extinction pauvre pratiquement constante avec le régime). Ceci constitue une nouvelle justification a posteriori des modélisations retenues. En effet, ce sont les réacteurs numérotés 1 dans la modélisation de la figure 19 (réacteur homogène pour A et piston pour B) qui conditionnent ces limites d'extinction. De plus, l'utilisation des valeurs  $Q_{R1}$  et  $Q_C + \pi Q_{R1}$ , trouvées lors des essais à froid, comme débits alimentant les réacteurs 1 de A et B n'est pas irréaliste.

La prédiction des performances globales du foyer est donnée figure 16 pour ce qui concerne l'influence de  $\psi$  sur l'efficacité de combustion à l'entrée, sortie de la zone primaire et sortie du foyer. Dans ces deux cas de chambre de combustion, on constate un bon accord pour l'entrée de la zone primaire. Les résultats sont moins satisfaisants en sortie de la zone primaire. La modélisation de la chambre B qui est pourtant plus fine que celle utilisée pour A (pas de réacteur piston en sortie du réacteur 3) ne donne pas des résultats meilleurs. La raison de cette dispersion doit être cherchée au niveau des hypothèses introduites pour les réactions chimiques. Ces hypothèses sont insuffisantes pour prédire mieux que des tendances. Ceci est encore plus net pour la prédiction des oxydes d'azote (fig. 17) où le mécanisme de Zeldovitch ne peut prendre en compte la formation des oxydes d'azote à faible richesse. Malgré ce défaut, qui pourra être éliminé par introduction d'une cinétique chimique plus complète et réaliste, la technique de modélisation adoptée permet de reproduire fidèlement les tendances de comportement de chambre de combustion de types différents. Ainsi l'amélioration de performances en passant de A à B est bien rendue par cette modélisation au prix d'un calcul simple et d'hypothèses limitées étayées par des expériences.

#### 5. CONCLUSION

Dans le but de valider un modèle particulièrement simple de chambre de combustion, deux ensembles d'expériences ont été conduits sur des maquettes schématiques fonctionnant avec ou sans combustion. Les principaux résultats sont les suivants :

Les visualisations hydrodynamiques complétées ensuite par les cartographies de vitesses ont conduit à une description relativement fine de l'aérodynamique dans la zone primaire. En particulier, on a mis en évidence le double système tourbillonnaire alimentant la zone primaire d'une part en fond de chambre, d'autre part latéralement. La répartition du débit primaire dans les différentes zones a pu être évaluée ainsi que l'influence de divers paramètres (angle de jets, débit et position des cannes à pré vaporisation).

Ces mesures ont été complétées, toujours à froid, par des mesures, en tout point de la chambre, de fonction de répartition des temps de séjour obtenus par diverses techniques.

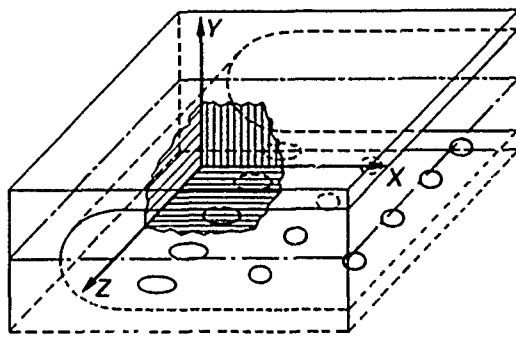
La comparaison avec les essais en combustion a été effectuée en estimant dans ce cas le débit recirculé ainsi que de nombreux prélèvements ( $NO$ ,  $NO_2$ ,  $CO$ ,  $CO_2$ ,  $N_2$ ,  $O_2$ ) en divers points choisis en fonction de l'aérodynamique. Dans ce dernier cas aussi, on a pu évaluer l'évolution des performances du foyer avec le régime.

Le modèle monodimensionnel utilisé, qui diffère par certains points des schémas habituellement employés, a donc été élaboré à partir de ces diverses données expérimentales. Le modèle permet aussi de calculer les performances globales du foyer ainsi que les fonctions de distribution de temps de séjour en sortie de réacteurs élémentaires. Bien que le modèle utilisé soit volontairement simplifié, en particulier pour l'aérodynamique (il ne prend pas en compte tous les résultats obtenus en particulier le taux de débit entraîné) et la chimie (oxydes de carbone et  $NO$  précoce), les résultats obtenus sont en bon accord. Cependant, une telle modélisation s'est appuyée sur l'analyse de l'écoulement faite au préalable. Il est probable que pour étudier une autre chambre, il faudrait refaire cette étude ; en particulier, la présence d'injecteurs aérodynamiques ("swirler") changerait la dynamique des gaz. Pour s'affranchir de cette analyse aérodynamique, il faut faire des calculs tridimensionnels beaucoup plus compliqués tels que ceux actuellement développés à l'ONERA [ 11 ].

# REFERENCES

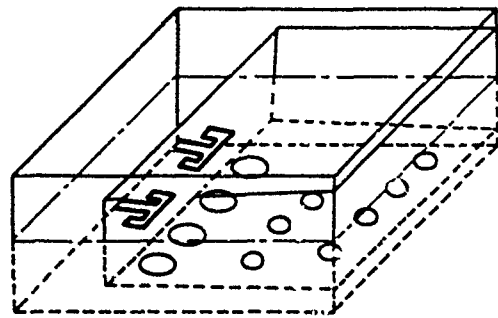
- [1] A. QUILLEVERE - "Developpement des chambres de combustion à haute intensité" AGARD Conference Proceedings n° 34- "Advanced Components for turbojet Engines" - Sept. 68 - Toulouse.
- [2] A.M. MELLOR - "Gas Turbine Engine Pollution" "Progress in Energy Combustion Science" - 1976 Vol. 1 p. 111-133 - Pergamon Press.
- [3] J. ODGERS - "Combustion modeling within gas turbine engines" - AIAA - 15 th Aerospace Sciences Meeting, Los Angeles (24-26 january 1977).
- [4] R. BORGHI - "Etude théorique de l'optimisation de la combustion dans les foyers de turbomachine" Acta Astronautica, vol. 1 (1974) p. 667-685.
- [5] W. S. Y. HUNG - "An experimentally verified NOx emission model for gas turbine combustion" - ASME Paper 75 - GT - 71
- [6] J. SWITHENBANK, I. POLL, M.W. VINCENT, D.D. WRIGHT - "Combustion design Fundamentals" 14th symposium (International) on combustion-p.627.
- [7] A.S. NOVICK, G.A. MILES, D.G. LILEY - "Numerical simulation of combustion flow fields : a primitive variable design capability" - Journal of Energy - vol. 3 - n° 2 - March-April 1979-p.95-105
- [8] W.P. JONES, W.C. CLIFFORD, C.H. PRIDDIN, R. de CHAIR- "A comparison between predicted and measured species concentrations and velocities in a research combustor" - Symposium AGARD sur les hautes températures dans les turbomachines - 19 - 23 septembre 1977 Ankara
- [9] M. A. SERAG ELDIN, D.B. SPALDING - "Prediction of the flow and combustor processes in a three dimensional combustor chamber" - Imperial college of science and technology HTS/76/3- Février 76.
- [10] A. ELLAIL, A.D. GOSMAN, F.C. LOCKWOOD, I.E.A. MEGAHED- "Description and validation of a three dimensional procedure for combustion chamber flows" - Journal of Energy - Vol. 2 - n° 2 - March-April 1978 - p. 71-80
- [11] F. HIRSINGER, H. TICHITSKY - "Modélisation de zones de combustion en régime instationnaire" AGARD - 54th (B) Specialists' Meeting on combustor Modelling - Cologne 1979.
- [12] A.J. GERRARD - "Utilisation des modèles hydrauliques pour l'étude de l'écoulement des fluides dans un groupe moteur et une chambre de combustion" N.T. Hispano-Suiza 21.6.66.
- [13] E.F. WINTER et al - "Apparatus and technique for the application of a water flow system to the study of aerodynamic system" - British journal of applied physics. Juillet 1956.
- [14] KENNEDY - "Ramburner flow visualizations studies" 11th JANNAF Combustion Meeting - vol. 2 Pasadena Sept. 74.
- [15] H. WERLE - "Le tunnel hydrodynamique au service de la recherche aérospatiale" - Publication ONERA n° 156 (1974)
- [16] A. GIOVANNINI, P. HEBRARD - "Etudes fondamentales d'écoulements dans les foyers de turbomachine" Rapport CERT n° 3/2062 - DERMES avril 1978.

- [17] P. DAUGA - "Anémométrie à fil chaud. Méthodes de mesure directionnelles" - Thèse (Toulouse 1975).
- [18] C. LE MENAHEZ, A. MIR - "Aérodynamique d'une chambre de combustion" - Etude approfondie - ENICA Toulouse (1978).
- [19] P. HEBRARD, P. MAGRE, G. COLLIN - "Analyse et modélisation de l'écoulement dans un foyer de turbomachine" - La Recherche Aérospatiale n° 1978-5.
- [20] A. GIOVANNINI, P. HEBRARD, G. TOULOUSE - "Quantitative results of flow visualisations by treatment of video signal" Euro Mech (août 79) - Technics of sizing and tracking particles.
- [21] J.M. BEER et K.B LEE - "The effect of the residence time distribution on the performance and efficiency of combustors" 10th symposium on combustion (1965) p. 1187 à 1202.
- [22] W. BARTOK, J.E. HEATH et M.A. WEISS - "Mixing in a jet stirred reactor" - A.I. Ch. E. Journal vol. 6 - n° 4 (déc. 1960) - p. 685 à 687.
- [23] S. TR. RAO, J. KUO et RH. ESSENHIGH - "Characterisation of stirring factor by cold-model simulation" - ASME - 4° National incinerator conference (Mai 1970). Cincinnati p. 314 à 326.
- [24] S. TR. RAO et RH. ESSENHIGH - "Experimental determination of stirring factors generated by straight and swirling jet in isothermal combustion-chamber models." 13° symposium combustion (1971) p. 603 à 615.
- [25] H.C. HOTTEL, G.C. WILLIAMS, G.A. MILES - "Mixedness in the well stirred reactor" - 11° symposium on combustion (1966) p. 771 à 778.
- [26] T. A. BOVINA - "Studies of exchange between re-circulation zone behind the flame-holder and outer flow" - 7° symposium on combustion - p. 692 à 696 - 1958)
- [27] G. WINTERFELD - "On process of turbulent exchange behind flame-holders" - 10° symposium on combustion (1966) p. 1265 à 1275.
- [28] H.A. BECKER, H.C. HOTTEL et WILLIAMS - "Characterisation of concentration fluctuations in a turbulent jet by the scattered light technique" - Paper n° 17 d - 56° Annual Meeting of the A.I. Ch.E. (1963).
- [29] O. LEVENSPIEL - "Chemical Reactions Engineering" John Wiley et Sons (1962).
- [30] J. DUTERQUE, R. BORGHI - "Combustion du propane dans un foyer homogène" - La Recherche Aérospatiale n° 1975-6 - p. 347-357



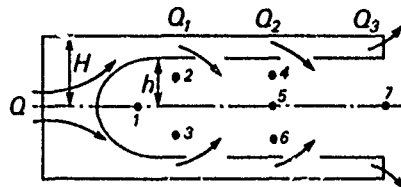
Maquette A

—— 1/2 maquette sans combustion



Maquette B

----- et — maquette complète avec combustion



Réglages possibles

$Q, Q_1/Q, Q_2/Q, Q_3/Q, h$

. positions des sondes de prélèvement

Fig. 1 - Schémas des maquettes

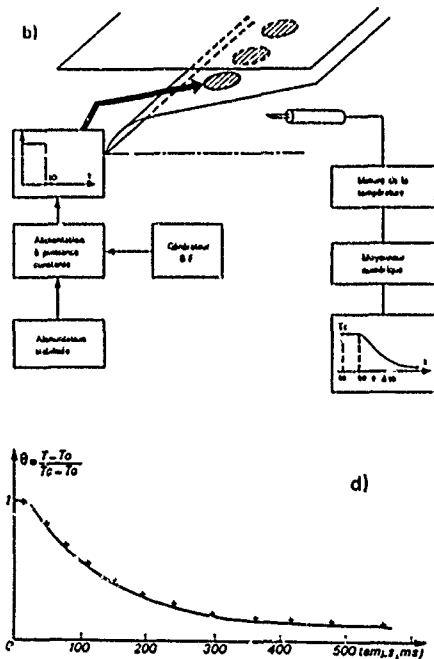


Fig. 2 - Mesure des temps de séjour : principe

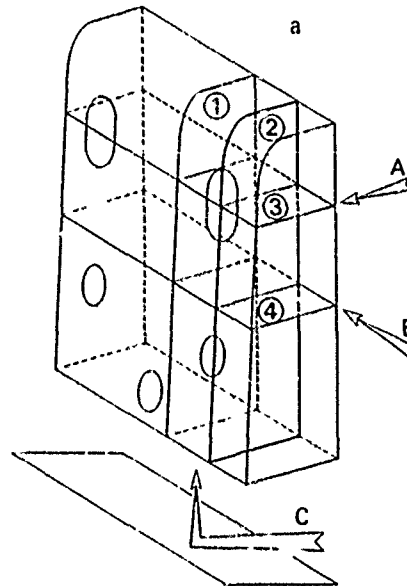
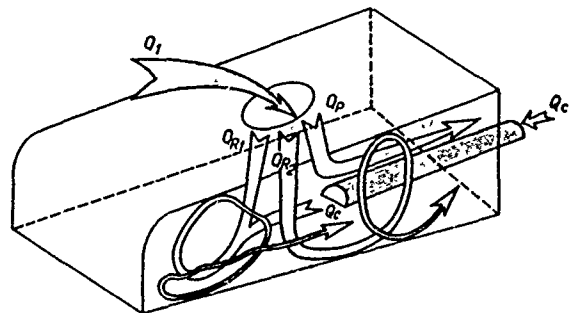


Fig. 3 - Visualisations dans le tunnel hydraulique

a) Schéma de la maquette  
b) Vue B, éclairage 2

c) Vue C, éclairage 3  
d) Vue A, éclairage B



$Q_1$  : Débit des orifices primaires  
 $Q_{R1}$  : Débit recirculé en fond de chambre  
 $Q_{R2}$  : Débit recirculé latéralement  
 $Q_p$  : Débit allant directement vers la dilution  
 $Q_c$  : Débit des cannes

Fig. 4 - Répartition des débits dans la zone primaire

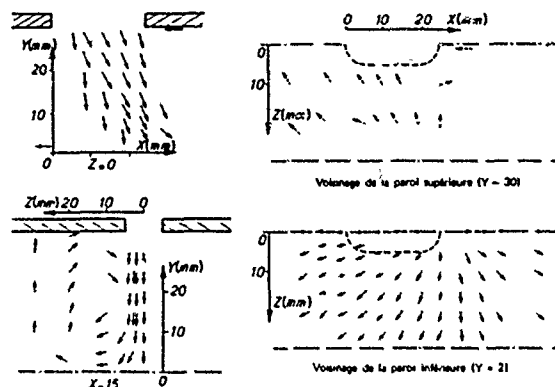


Fig. 5 - Direction de la vitesse dans la zone primaire

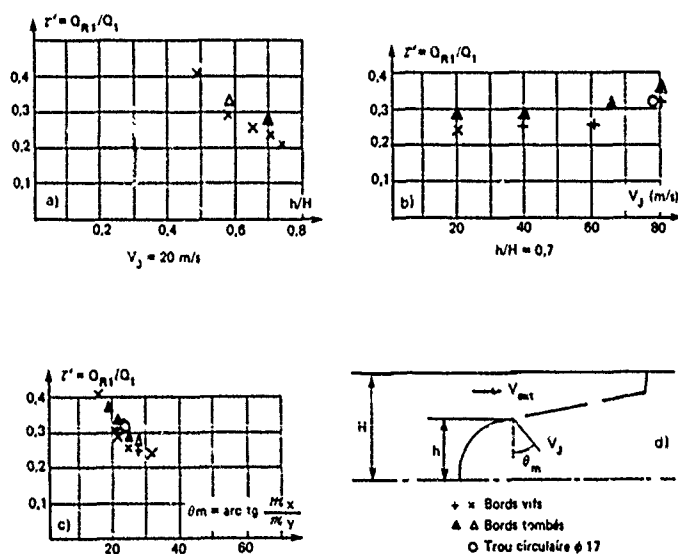


Fig. 6 - Mesure du débit recirculé  $Q_{R1}$

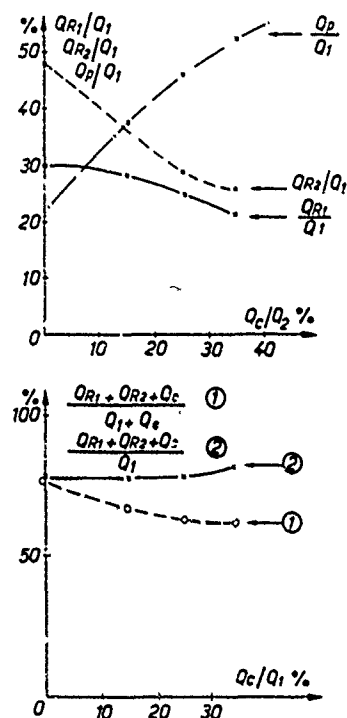


Fig. 7 - Influence du débit des cannes sur la répartition des débits

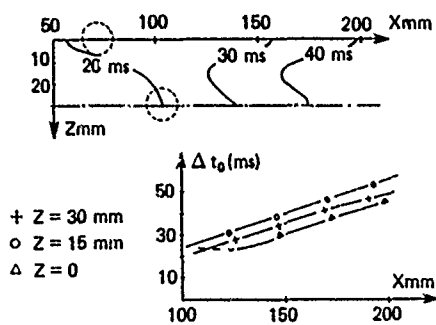
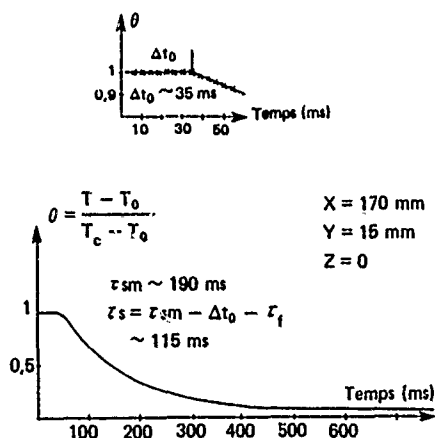


Fig. 8 - Temps de séjour. Mesures dans la zone de dilution

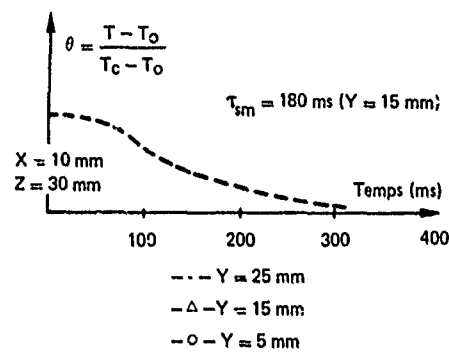
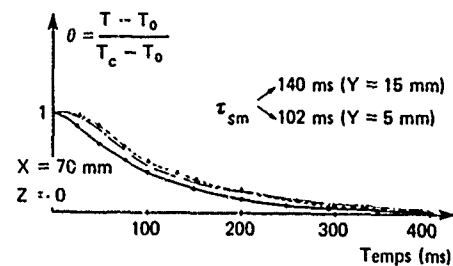
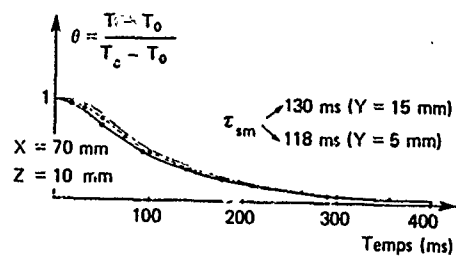


Fig. 9 - Temps de séjour. Mesure à la sortie et dans la zone primaire

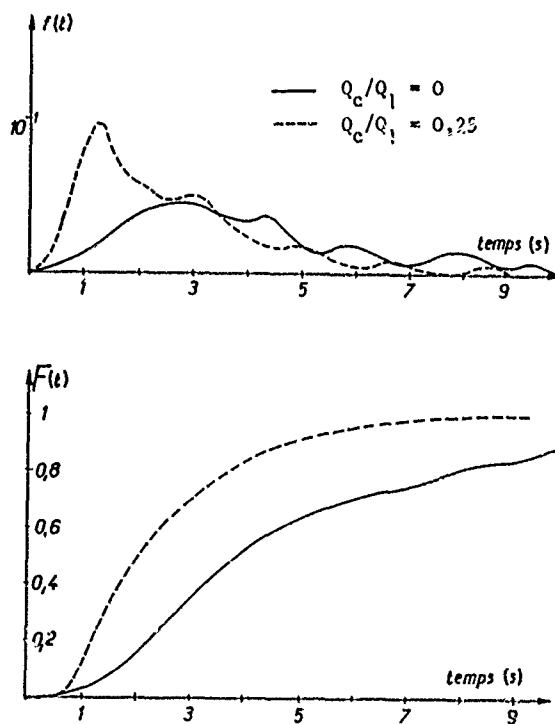


Fig. 11 - Mesure du temps de séjour en fond de chambre. Influence du débit des caunes

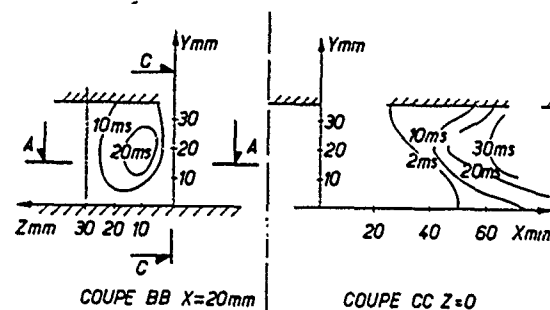
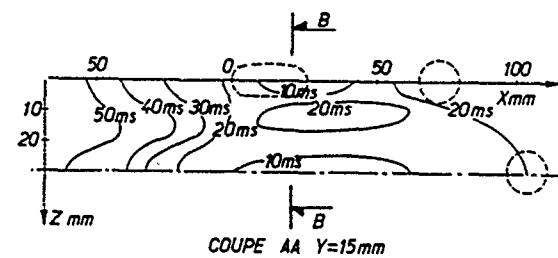


Fig. 10 - Temps de transit.  
Mesure dans la zone primaire

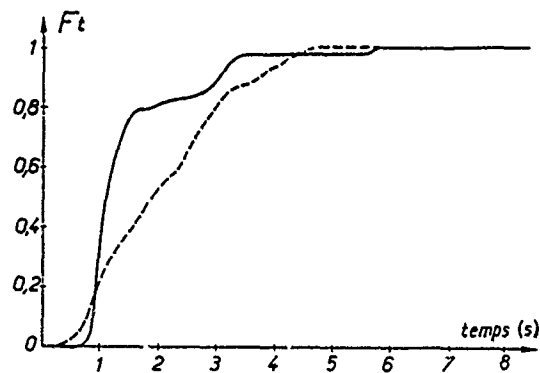
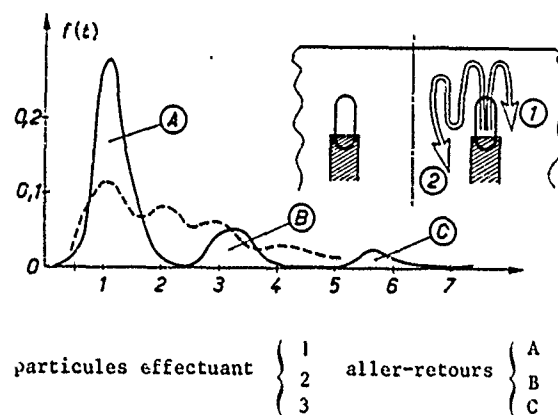


Fig. 12 - Mesure des temps de séjour  
en fond de chambre  $Q_c/Q_1 = 25\%$



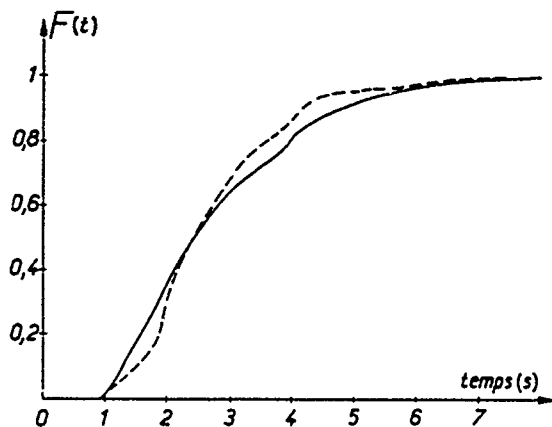
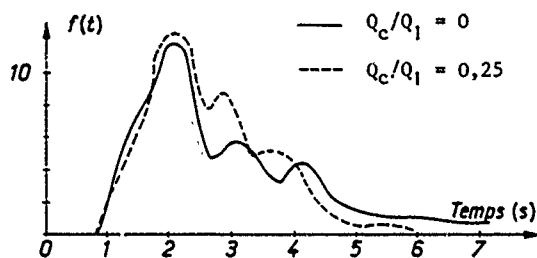


Fig. 13 - Mesure du temps de séjour dans le réacteur latéral. Influence du débit des cannes

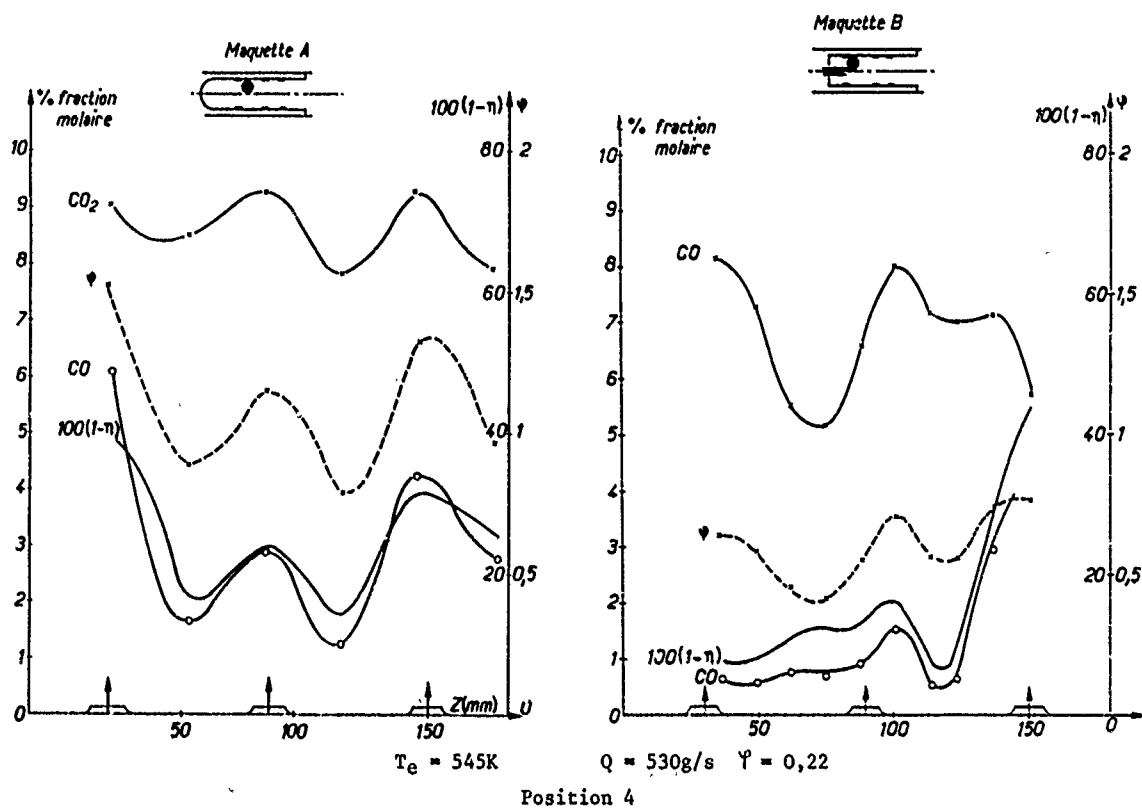


Fig. 14 - Sondages à la sortie de la zone primaire

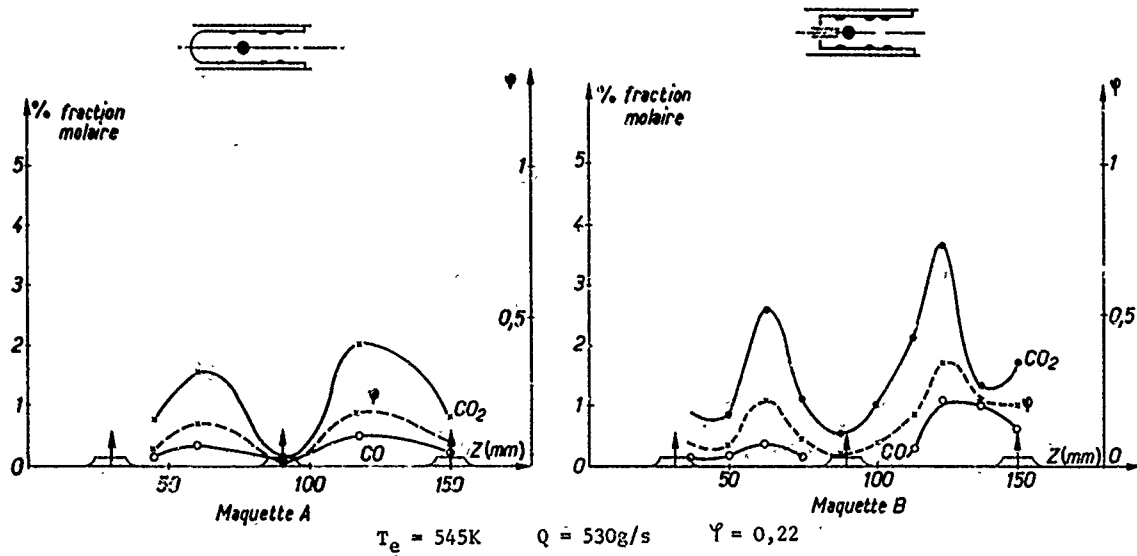


Fig. 15 - Sondages à la sortie de la zone primaire

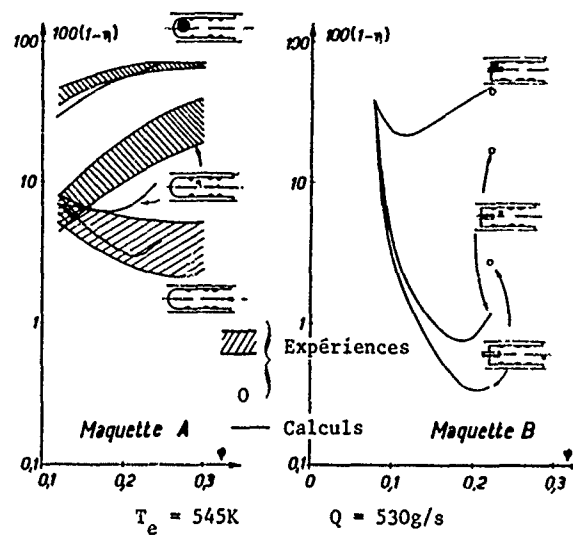


Fig. 16 - Inefficacité de combustion. Effet de la richesse

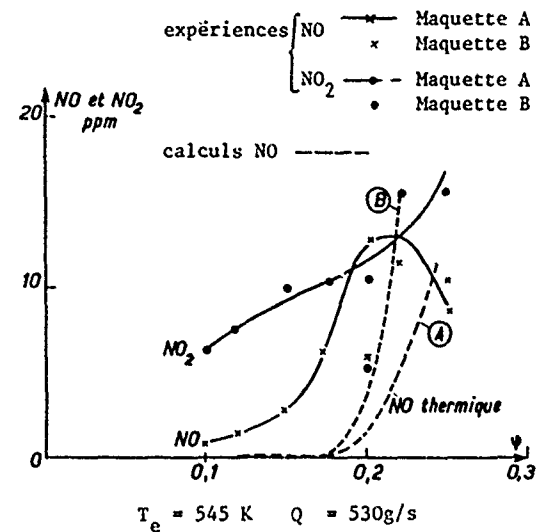
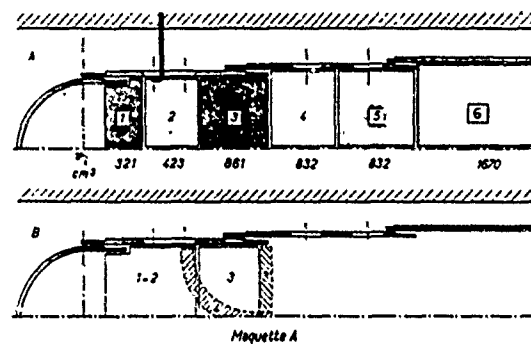


Fig. 17 - Oxydes d'azote en sortie du foyer



avec combustion

sans combustion

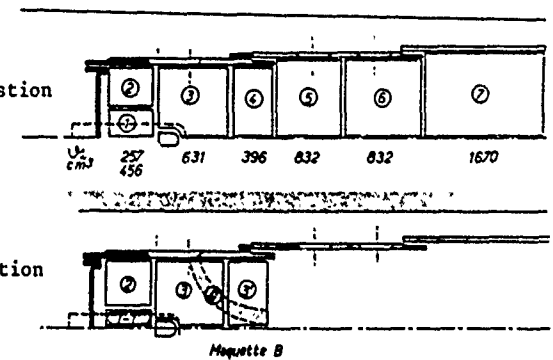
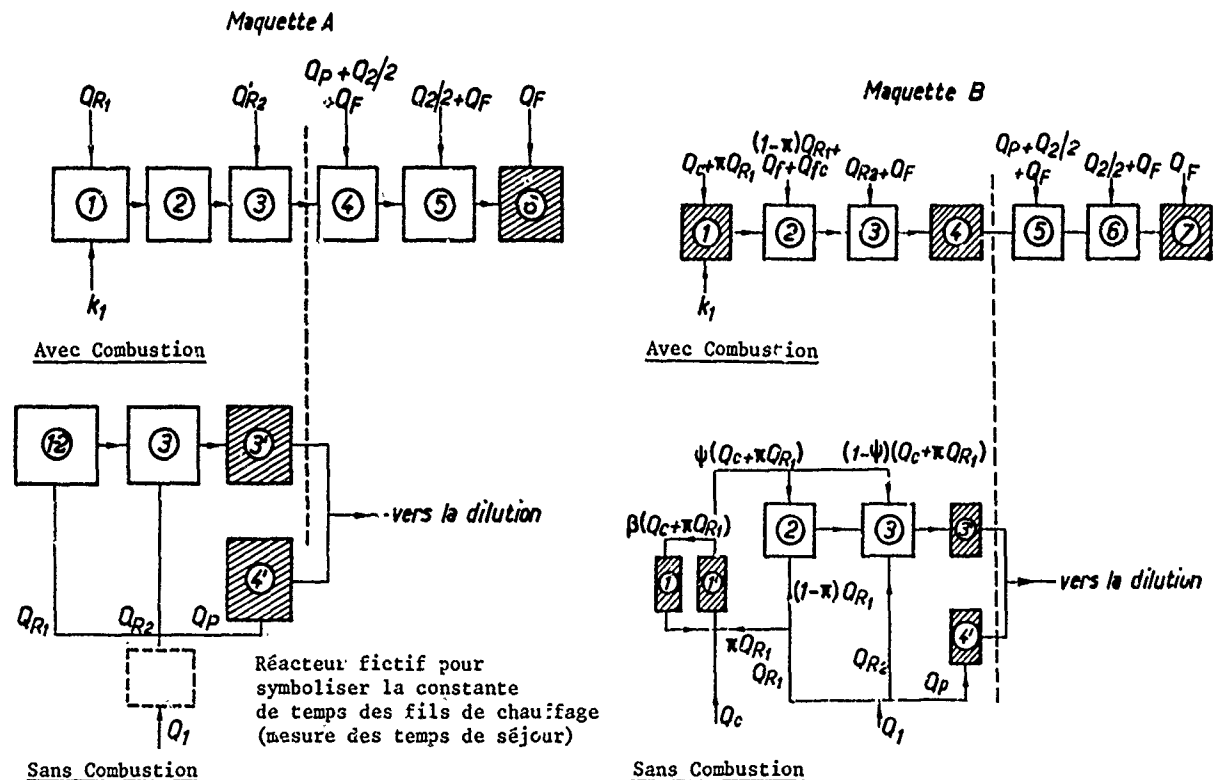


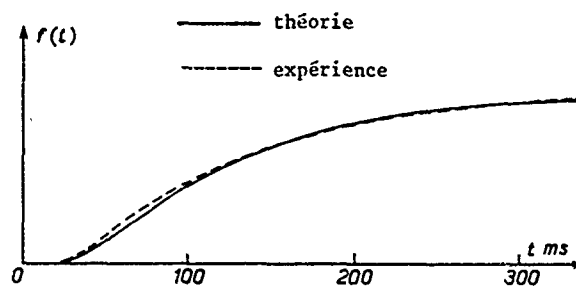
Fig. 18 - Modélisation monodimensionnelle - Discretisation du foyer



□ Réacteur homogène

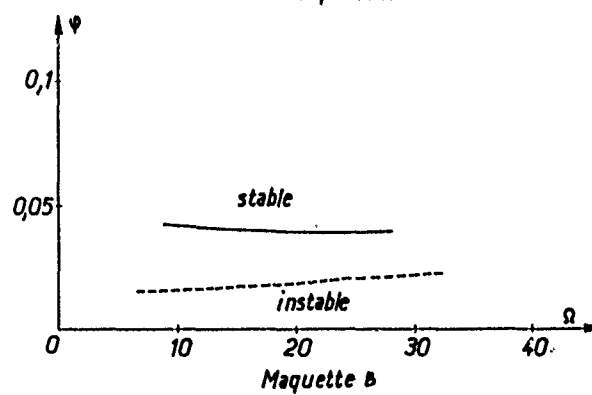
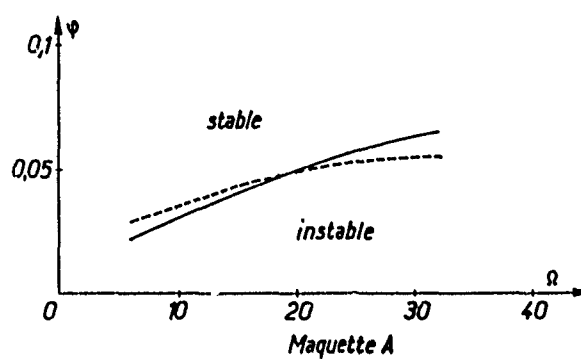
▨ Réacteur piston

Fig. 19 - Modélisation monodimensionnelle. Répartition des débits



Maquette A

Fig. 20— Distribution des temps de séjour



$$\text{Facteur de charge du foyer } \Omega = \frac{Q}{P_e V_e (T_e/500)}$$

— Expériences      - - - - - Calculs

Fig. 21— Stabilité du foyer

**D.C.Dryburgh, US**

I would like to link this paper with Professor Odgers' paper and the remarks I was making in defence of complex models. I was very delighted by these beautiful flow visualisations. The remark I would really like to make, is that if you have got a good aerodynamic model that will reproduce these results you can use that model to quantify the pictures that we got. We saw, that when you injected the dye into different points in a particular hole the flow went in different places; it behaves in completely different ways. If you can simulate that in a model and store the results you can do all sorts of things with such results. You can use it to predict your residence times, to fit in to the other plug flow and mixed reactors that you used. You can use a complex model as a starting point for all sorts of calculations. You can do the flow visualisation in great detail. If you have got the right sort of computer display facilities, you can look at your film from different points of view and use it to give people a good understanding of what is going on in the combustion chamber. It is one of the great attraction of a complex flow model. The other statement I would like to point out is that these models very often have to be done cold. Our experience has been that although the flow may not appear to change very greatly, when you light up a flame, there are some quite important changes which you obviously cannot predict by any flow visualisation techniques. So, I feel there are limitations to the use of water analogy.

**Réponse d'Auteur**

Nous n'avons pas pu présenter dans le détail les techniques expérimentales de visualisation. Le film présenté est qualitatif, mais comme vous avez pu voir, nous tentons aussi de faire de la visualisation quantitative. Pour chaque film réalisé nous disposons d'enregistrements sur magnétoscope des images vidéo, qui sont ensuite traitées par ordinateur. On peut alors obtenir soit des mesures de temps de séjour par suivi de particules, par colorimétrie. Il est aussi prévu de faire de la trajectographie.

Nous pensons effectivement qu'il n'est pas possible de montrer l'influence de la combustion. Malgré tout, les simulations à froid montrent, dans un premier temps et de manière qualitative, la configuration de l'écoulement. Et d'après notre expérience il n'y a pas de différence fondamentale (toujours d'un point de vue qualitatif) entre les cas avec ou sans combustion.

**W.Krockow, Ge**

Can you please comment on the possible wall influence on the residence time distribution you measured?

**Réponse d'Auteur**

Les résultats présentés sont obtenus sur une demi-maquette. Avant d'effectuer des mesures sur cette demi-maquette, deux séries de tests ont été effectués:

- comparaison, sur une maquette complète et une demi-maquette, des modules et direction des vitesses moyennes dans la zone primaire. Nous n'avons pas vu de différence fondamentale.
- comparaison également sur les mesures de temps de séjour moyen et de la fonction distribution de ces temps de séjour. Là aussi pas de différence notable entre les deux expériences.

Par contre les mécanismes d'interaction entre jets (battements) peuvent être modifiés selon qu'ils sont étudiés dans une demi chambre ou une chambre complète.

REPORT DOCUMENTATION PAGE																		
1. Recipient's Reference	2. Originator's Reference	3. Further Reference	4. Security Classification of Document															
	AGARD-CP-275	ISBN 92-835-0260-4	UNCLASSIFIED															
5. Originator	Advisory Group for Aerospace Research and Development North Atlantic Treaty Organization 7 rue Ancelle, 92200 Neuilly sur Seine, France																	
6. Title	COMBUSTOR MODELLING																	
7. Presented at	the Propulsion and Energetics Panel 54th(B) Specialists' Meeting, held at DFVLR, Cologne, Germany, on 3-5 October 1979.																	
8. Author(s)/Editor(s)	Various		9. Date February 1980															
10. Author's/Editor's Address	Varicus		11. Pages 392															
12. Distribution Statement	This document is distributed in accordance with AGARD policies and regulations, which are outlined on the Outside Back Covers of all AGARD publications.																	
13. Keywords/Descriptors	<table border="0"> <tbody> <tr> <td>Combustors</td> <td>Evaporation of fluids</td> <td>Flame oscillations</td> </tr> <tr> <td>Combustor models</td> <td>Turbulent diffusion flames</td> <td>Furnace performance</td> </tr> <tr> <td>Flow in combustors</td> <td>Ignition</td> <td>Combustion in boilers</td> </tr> <tr> <td>Gas kinetics of combustion</td> <td>Spray bars</td> <td>Afterburners</td> </tr> <tr> <td>Mixing of gases</td> <td>Flame stabilization</td> <td>Pollutant emissions</td> </tr> </tbody> </table>			Combustors	Evaporation of fluids	Flame oscillations	Combustor models	Turbulent diffusion flames	Furnace performance	Flow in combustors	Ignition	Combustion in boilers	Gas kinetics of combustion	Spray bars	Afterburners	Mixing of gases	Flame stabilization	Pollutant emissions
Combustors	Evaporation of fluids	Flame oscillations																
Combustor models	Turbulent diffusion flames	Furnace performance																
Flow in combustors	Ignition	Combustion in boilers																
Gas kinetics of combustion	Spray bars	Afterburners																
Mixing of gases	Flame stabilization	Pollutant emissions																
14. Abstract	<p>These Conference Proceedings contain the 24 papers presented at the AGARD Propulsion and Energetics Panel 54th (B) Specialists' Meeting on 'Combustor Modelling' which was held in Cologne, Germany, on 3-5 October 1979. The questions and answers after the presentation of each paper are included.</p> <p>The Specialists' Meeting was organized into five sessions: Survey (2 papers); Basic Phenomena (11 papers which were presented in two parts); Transient Phenomena and Instabilities (2 papers); Furnaces and Boilers (5 papers); and Gas Turbine Combustors and R/H Systems (4 papers).</p> <p>The meeting provided a forum during which the different models and methods used in turbine engine research and development could be compared. Even models used in non-aerodynamical circles were discussed.</p> <p>The aim of the meeting was to provide research scientists with knowledge on realistic types of combustor models and on experimental conditions under which the theoretical models are valid for practice, and to assist manufacturing engineers in the selection of adequate theoretical models. Whether the meeting achieved the aim will be assessed in a Technical Evaluation Report, to be published as AGARD Advisory Report AR-153.</p>																	

<p>AGARD Conference Proceedings No.275 Advisory Group for Aerospace Research and Development, NATO COMBUSTOR MODELLING Published February 1980 392 pages</p> <p>These Conference Proceedings contain the 24 papers presented at the AGARD Propulsion and Energetics Panel 54th (B) Specialists' Meeting on 'Combustor Modelling' which was held in Cologne, Germany, on 3-5 October 1979. The questions and answers after the presentation of each paper are included.</p> <p>The Specialists' Meeting was organized into five sessions: Survey (2 papers); Basic Phenomena (11 papers which</p> <p>P.T.O.</p>	<p>AGARD-CP-275</p> <p>Combustors Combustor models Flow in combustors Gas kinetics of combustion Mixing of gases Evaporation of fluids Turbulent diffusion flames Ignition Spray bars Flame stabilization Flame oscillations Furnace performance Combustion in boilers Afterburners Pollutant emissions</p>	<p>AGARD Conference Proceedings No.275 Advisory Group for Aerospace Research and Development, NATO COMBUSTOR MODELLING Published February 1980 392 pages</p> <p>These Conference Proceedings contain the 24 papers presented at the AGARD Propulsion and Energetics Panel 54th (B) Specialists' Meeting on 'Combustor Modelling' which was held in Cologne, Germany, on 3-5 October 1979. The questions and answers after the presentation of each paper are included.</p> <p>The Specialists' Meeting was organized into five sessions: Survey (2 papers); Basic Phenomena (11 papers which</p> <p>P.T.O.</p>	<p>AGARD-CP-275</p> <p>Combustors Combustor models Flow in combustors Gas kinetics of combustion Mixing of gases Evaporation of fluids Turbulent diffusion flames Ignition Spray bars Flame stabilization Flame oscillations Furnace performance Combustion in boilers Afterburners Pollutant emissions</p>
<p>AGARD Conference Proceedings No.275 Advisory Group for Aerospace Research and Development, NATO COMBUSTOR MODELLING Published February 1980 392 pages</p> <p>These Conference Proceedings contain the 24 papers presented at the AGARD Propulsion and Energetics Panel 54th (B) Specialists' Meeting on 'Combustor Modelling' which was held in Cologne, Germany, on 3-5 October 1979. The questions and answers after the presentation of each paper are included.</p> <p>The Specialists' Meeting was organized into five sessions: Survey (2 papers); Basic Phenomena (11 papers which</p> <p>P.T.O.</p>	<p>AGARD-CP-275</p> <p>Combustors Combustor models Flow in combustors Gas kinetics of combustion Mixing of gases Evaporation of fluids Turbulent diffusion flames Ignition Spray bars Flame stabilization Flame oscillations Furnace performance Combustion in boilers Afterburners Pollutant emissions</p>	<p>AGARD Conference Proceedings No.275 Advisory Group for Aerospace Research and Development, NATO COMBUSTOR MODELLING Published February 1980 392 pages</p> <p>These Conference Proceedings contain the 24 papers presented at the AGARD Propulsion and Energetics Panel 54th (B) Specialists' Meeting on 'Combustor Modelling' which was held in Cologne, Germany, on 3-5 October 1979. The questions and answers after the presentation of each paper are included.</p> <p>The Specialists' Meeting was organized into five sessions: Survey (2 papers); Basic Phenomena (11 papers which</p> <p>P.T.O.</p>	<p>AGARD-CP-275</p> <p>Combustors Combustor models Flow in combustors Gas kinetics of combustion Mixing of gases Evaporation of fluids Turbulent diffusion flames Ignition Spray bars Flame stabilization Flame oscillations Furnace performance Combustion in boilers Afterburners Pollutant emissions</p>

<p>were presented in two parts); Transient Phenomena and Instabilities (2 papers); Furnaces and Boilers (5 papers); and Gas Turbine Combustors and R/H Systems (4 papers).</p> <p>The meeting provided a forum during which the different models and methods used in turbine engine research and development could be compared. Even models used in non-aerodynamical circles were discussed.</p> <p>The aim of the meeting was to provide research scientists with knowledge on realistic types of combustor models and on experimental conditions under which the theoretical models are valid for practice, and to assist manufacturing engineers in the selection of adequate theoretical models. Whether the meeting achieved the aim will be assessed in a Technical Evaluation Report, to be published as AGARD Advisory Report AR-153.</p> <p>ISBN 92-835-0260-4</p>	<p>were presented in two parts); Transient Phenomena and Instabilities (2 papers); Furnaces and Boilers (5 papers); and Gas Turbine Combustors and R/H Systems (4 papers).</p> <p>The meeting provided a forum during which the different models and methods used in turbine engine research and development could be compared. Even models used in non-aerodynamical circles were discussed.</p> <p>The aim of the meeting was to provide research scientists with knowledge on realistic types of combustor models and on experimental conditions under which the theoretical models are valid for practice, and to assist manufacturing engineers in the selection of adequate theoretical models. Whether the meeting achieved the aim will be assessed in a Technical Evaluation Report, to be published as AGARD Advisory Report AR-153.</p> <p>ISBN 92-835-0260-4</p>
<p>were presented in two parts); Transient Phenomena and Instabilities (2 papers); Furnaces and Boilers (5 papers); and Gas Turbine Combustors and R/H Systems (4 papers).</p> <p>The meeting provided a forum during which the different models and methods used in turbine engine research and development could be compared. Even models used in non-aerodynamical circles were discussed.</p> <p>The aim of the meeting was to provide research scientists with knowledge on realistic types of combustor models and on experimental conditions under which the theoretical models are valid for practice, and to assist manufacturing engineers in the selection of adequate theoretical models. Whether the meeting achieved the aim will be assessed in a Technical Evaluation Report, to be published as AGARD Advisory Report AR-153.</p> <p>ISBN 92-835-0260-4</p>	<p>were presented in two parts); Transient Phenomena and Instabilities (2 papers); Furnaces and Boilers (5 papers); and Gas Turbine Combustors and R/H Systems (4 papers).</p> <p>The meeting provided a forum during which the different models and methods used in turbine engine research and development could be compared. Even models used in non-aerodynamical circles were discussed.</p> <p>The aim of the meeting was to provide research scientists with knowledge on realistic types of combustor models and on experimental conditions under which the theoretical models are valid for practice, and to assist manufacturing engineers in the selection of adequate theoretical models. Whether the meeting achieved the aim will be assessed in a Technical Evaluation Report, to be published as AGARD Advisory Report AR-153.</p> <p>ISBN 92-835-0260-4</p>

**AGARD**

NATO  OTAN

7 RUE ANCELLE · 92200 NEUILLY-SUR-SEINE  
FRANCE

Telephone 745.08.10 · Telex 610176

DISTRIBUTION OF UNCLASSIFIED  
AGARD PUBLICATIONS

AGARD does NOT hold stocks of AGARD publications at the above address for general distribution. Initial distribution of AGARD publications is made to AGARD Member Nations through the following National Distribution Centres. Further copies are sometimes available from these Centres, but if not may be purchased in Microfiche or Photocopy form from the Purchase Agencies listed below.

NATIONAL DISTRIBUTION CENTRES

**BELGIUM**

Coordonnateur AGARD - VSL  
Etat-Major de la Force Aérienne  
Quartier Reine Elisabeth  
Rue d'Everé, 1140 Bruxelles

**CANADA**

Defence Science Information Services  
Department of National Defence  
Ottawa Ontario K1A 0K2

**DENMARK**

Danish Defence Research Board  
Østerbrogades Kaserne  
Copenhagen Ø

**FRANCE**

O.N.E.R.A. (Direction)  
29 Avenue de la Division Leclerc  
92320 Châtillon sous Bagneux

**GERMANY**

Zentralstelle für Luft- und Raumfahrt-  
dokumentation und -information  
c/o Fachinformationszentrum Energie,  
Physik, Mathematik GmbH  
Kernforschungszentrum  
7514 Eggenstein-Leopoldshafen 2

**GREECE**

Hellenic Air Force General Staff  
Research and Development Directorate  
Holargos, Athens

**ICELAND**

Director of Aviation  
c/o Flugrad  
Reykjavik

**ITALY**

Aeronautica Militare  
Ufficio del Delegato Nazionale all'AGARD  
3, Piazzale Adenauer  
Roma/EUR

**LUXEMBOURG**

See Belgium

**NETHERLANDS**

Netherlands Delegation to AGARD  
National Aerospace Laboratory, NLR  
P.O. Box 126  
2600 A.C. Delft

**NORWAY**

Norwegian Defence Research Establishment  
Main Library  
P.O. Box 25  
N-2007 Kjeller

**PORTUGAL**

Direcção do Serviço de Material  
da Força Aérea  
Rua da Escola Politécnica 42  
Lisboa  
Attn: AGARD National Delegate

**TURKEY**

Department of Research and Development (ARGE)  
Ministry of National Defence, Ankara

**UNITED KINGDOM**

Defence Research Information Centre  
Station Square House  
St. Mary Cray  
Orpington, Kent BR5 3RE

**UNITED STATES**

National Aeronautics and Space Administration (NASA)  
Langley Field, Virginia 23365  
Attn: Report Distribution and Storage Unit

THE UNITED STATES NATIONAL DISTRIBUTION CENTRE (NASA) DOES NOT HOLD  
STOCKS OF AGARD PUBLICATIONS; AND APPLICATIONS FOR COPIES SHOULD BE MADE  
DIRECT TO THE NATIONAL TECHNICAL INFORMATION SERVICE (NTIS) AT THE ADDRESS BELOW.

PURCHASE AGENCIES

*Microfiche or Photocopy*

National Technical  
Information Service (NTIS)  
5285 Port Royal Road  
Springfield  
Virginia 22161, USA

*Microfiche*

Space Documentation Service  
European Space Agency  
10, rue Mario Nikis  
75015 Paris, France

*Microfiche*

Technology Reports  
Centre (DTI)  
Station Square House  
St. Mary Cray  
Orpington, Kent BR5 3RF  
England

Requests for microfiche or photocopies of AGARD documents should include the AGARD serial number, title, author or editor, and publication date. Requests to NTIS should include the NASA accession report number. Full bibliographical references and abstracts of AGARD publications are given in the following journals:

Scientific and Technical Aerospace Reports (STAR)  
published by NASA Scientific and Technical  
Information Facility  
Post Office Box 8757  
Baltimore/Washington International Airport  
Maryland 21240, USA

Government Reports Announcements (GRA)  
published by the National Technical  
Information Services, Springfield  
Virginia 22161, USA